THE ANALYSIS OF CONCRETE STRUCTURES INCLUDING THE EFFECTS OF WARPING RESTRAINT

by P. Waldron, B.Sc.

December, 1979

ABSTRACT

The increasing use of thin-walled concrete sections is largely attributable to the development of high performance materials and to improvements in construction techniques. Large warping displacements are a characteristic feature of these sections and, if restrained, can induce significant levels of additional stress. Under these circumstances, simple beam theory may no longer be sufficiently accurate for the analysis, and a more general approach will be required. Therefore, as an introduction, thin-walled beam theory is first developed for open, closed and multi-cellular sections subject to applications of mixed torsion. The relevance of this theory to box girder bridges is then examined by means of a parametric study of existing structures. The important geometrical properties of a range of typical sections are also established and presented in graphical form.

Fundamental equations governing the torsional behaviour of straight and curved members are expressed in terms of the applied loads and initial boundary conditions only. The longitudinal distribution of the various stress resultants, due to both uniformly distributed and concentrated loads, are then determined for the circular curved girder built-in at both ends. A total strain energy equation is derived for the general case, including the effects of bimoment and warping torsion, and is used to establish the flexibility matrix for straight and curved members. This enables the full stiffness matrix to be obtained numerically, forming the basis for a general analysis suitable for rapid solution by computer. Subsequently, this analysis has been used to analyse a prestressed concrete elevated road junction, the results from which have then been compared with those already available from an elastic model study.

The well established procedure whereby curved members are idealized as an assemblage of equivalent straight beams is investigated in detail. Possible errors caused by this approximation are estimated for members covering a wide range of geometrical properties. Further inaccuracies due to neglecting the effects of warping restraint are also quantified, and both sources of error are evaluated in the analysis of a three span continuous bridge of composite construction.

Finally, an advanced method of ultimate load analysis is proposed, based on a model which permits the formation of a corner mode of failure. Since the effects of warping restraint can now be accommodated, this enables simple open section beams to be analysed for the first time. Results from the proposed theory are subsequently compared with those from four reinforced concrete beams of open profile, the construction and testing of which are also briefly described.

CONTENTS

ACKNOWLEDGEMENTS   ii

INDEX OF FIGURES INDEX OF PLATES   vii

INDEX OF PLATES   xvi

INDEX OF TABLES   xvii

NOTATION   xix

1.   GENERAL INTRODUCTION   1

     1.1   STRUCTURAL ACTIONS ASSOCIATED WITH THIN-WALLED BEAMS 2

           1.1.1 Bending   2

           1.1.2 Torsion   2

           1.1.3 Distortion   7

           1.1.4 Transverse Slab Action   8

     1.2   CONCRETE STRUCTURES LOADED IN TORSION   9

           1.2.1 Box Girder Bridges   11

           1.2.2 The Shear Core   14

           1.2.3 Other Applications   20

     1.3   SCOPE OF THIS WORK   25

           1.3.1 Elastic Analysis   25

           1.3.2 Ultimate Load Analysis   30

     1.4   SIGN CONVENTIONS   34

           1.4.1 Co-ordinate Systems   34

           1.4.2 Stresses and Deformations   37

2.   THIN-WALLED BEAM THEORY   39

     2.1   INTRODUCTION   39

           2.1.1 Historical Review   40

INDEX OF FIGURES

PLATES

TABLES

NOTATION

A	Cross-sectional area
B	Bimoment
C_1, C_2, etc.	Constants
D	Force in one stirrup leg
E	Modulus of elasticity
F	Shear flow
G	Shear modulus; position of centroid
I_c	Central second moment of area
I_d	Torsional second moment of area
I_x, I_y, I_{xy}	Bending second moments of area
I_w	Warping moment of inertia (open sections)
$I_{\hat{w}}$	Warping moment of inertia (closed sections)
M	Bending moment
N	Direct force
P	Applied shear load
S	Shear centre position
S_w	Warping shear function (open sections)
$S_{\hat{w}}^-$	Warping shear function (closed sections)
T	Total torsion; applied torque
T_{sv}	St. Venant's torsion
T_w	Warping torsion
U	Total strain energy
V	Shear force
Z	Force in longitudinal steel
b	Breadth of section (between corner bars)
b_c	Breadth of concrete beam
b_s	Breadth of section between stirrups
c_{mn}	Connection matrix coefficients

e_x, e_y	Movement of shear centre
f	Dimensionless warping function
f_{mn}	Flexibility coefficients for curved members
g_{mn}	Flexibility coefficients for straight members
h_{mn}	Flexibility coefficients for equivalent straight members
h	Height of section (between corner bars)
h_c	Height of concrete beam
h_1, h_2	Defined in fig. 5.2
j	Torsional/bending stiffness ratio $\sqrt{GI_d/\Psi EI_x}$
k	Decay coefficient $\sqrt{\mu GI_d/EI_{\hat{w}}}$ or $\sqrt{GI_d/EI_w}$
k_1, k_2, etc.	Constants
n	Normal to peripheral co-ordinate, s
p	Perimeter of idealized section = $2(b + h)$; uniformly distributed load
r	Radius of curvature of shear axis
r_o	Radius of curvature of centroidal axis
s	Peripheral co-ordinate
t	Uniformly distributed torsion
u, v, w	Deformation system
x_o	Horizontal distance between shear centre and centroid
y_o	Vertical distance between shear centre and centroid
x, y, z	Cartesian co-ordinate system
α	Angle of crack inclination; general angle
β	Angle subtended by member (or half-member)
γ	Shear strain
δ	Wall thickness
$\Delta\tau_{sv}$	Secondary shear stress
Δ_x, Δ_y	Movement of centroid after cracking
ε	Axial strain
η	Dimensionless warping parameter $\dfrac{1}{1 + k^2 r^2}$

θ	Angular deformation; general angle
ℓ	Length of member
λ	Ratio of top/bottom steel yield forces; general angle
μ	Warping shear parameter $(1 - I_d/I_c)$
ν	Poisson's ratio
ξ	General angle
ρ	Radius of curvature
ρ, ζ, α	Cylindrical co-ordinate system
σ	Direct stress
Σ	Summation
τ	Shear stress
ϕ	Reduced angle of rotation
Φ	Total angle of rotation
Ψ	Dimensionless warping function $(1 - I_{xy}/I_x I_y)$
ω	Sectorial co-ordinate (open sections)
$\hat{\omega}$	Sectorial co-ordinate (closed sections)
Ω	Twice the enclosed area (2 bh)
C	Connection matrix
E	Equilibrium matrix
F	Curved member flexibility matrix
G	Straight member flexibility matrix
H	Equivalent straight member flexibility matrix
K	Complete member stiffness matrix
$\mathbf{K_{11}, K_{12}}$, etc.	Member stiffness sub-matrices
K'	**K** transformed (to system co-ordinates
$\mathbf{K^*}$	System stiffness matrix
$\mathbf{T_1, T_2}$	End 1, end 2 transformation matrices
T	Complete member transformation matrix
d	Complete member end displacement vector

$\mathbf{d}_1, \mathbf{d}_2$	End 1, end 2 displacement vectors
$\mathbf{d}_{1*}, \mathbf{d}_{2*}$	End 1, end 2 rigid-body displacement vectors
$\mathbf{d}'$	$\mathbf{d}$ transformed to system co-ordinates
$\mathbf{d}^*$	System displacement vector
$\mathbf{e}_2$	End 2 displacement vector for cantilever beam
$\mathbf{p}$	Complete member end-force vector
$\mathbf{p}_1, \mathbf{p}_2$	End 1, end 2, force vectors
$\mathbf{p}'$	$\mathbf{p}$ transformed to system co-ordinates
$\mathbf{p}^*$	System force vector
$\bar{\mathbf{p}}$	Vector of stress resultants

Subscripts

b, t	Bottom, top
c	Concrete; cracked co-ordinate system
s	Steel
sv	St. Venant
v	Shear
w	Warping
y	Yield
i, j, m, n	Designation of various coefficients
1, 2	Member ends
ρ, ζ, α	
x, y, z	
s, n, α	Various co-ordinate systems
s, n, z	

Superscripts

$'$ $''$ $'''$ iv	1st, 2nd, 3rd and 4th differentials with respect to the longitudinal member axis
*	System co-ordinates
t	Matrix transposition
-1	Matrix inversion

CHAPTER ONE

GENERAL INTRODUCTION

Only recently have reinforced and prestressed concrete structures been required to carry significant levels of torsion, often in combination with other forms of loading. Historically, the designer has been able to avoid or at least minimise the problem by selecting structural configurations in which loads were transmitted to the foundations by the actions of bending, shear and direct thrust alone. Alternatively, if this was not possible, a simple elastic analysis based on St. Venant's theory for pure torsion was generally adequate since members were typically solid or thick-walled in section.

For a variety of reasons these options are rarely available to-day. For example, the general arrangement of many modern structures is frequently such that the ability to withstand significant torsional loads is essential to the equilibrium of the system. In such cases, where a particular layout is necessary to enable the structure to perform its primary function or to satisfy difficult alignment requirements, there is often little opportunity for selecting an alternative configuration in which torsional effects may be safely neglected. Furthermore, with improvements in materials and construction techniques there has been a general tendency to reduce wall thicknesses in order to achieve a corresponding reduction in self weight. In these circumstances, it is no longer sufficient to simply use St. Venant's theory for the torsional analysis and the additional effects associated with thin-walled sections must also be considered.

1.1   STRUCTURAL ACTIONS ASSOCIATED WITH THIN-WALLED BEAMS

In general, any system of eccentric point loads may be reduced into its various component parts.   For the deformable thin-walled beam these essentially correspond to the actions of bending, torsion and distortion.   Consider the twin-cell box girder with side cantilevers, shown in fig. 1.1a, subject to a single point load P at an eccentricity e from the section centre.   The components of vertical shear force and torsional moment are readily determined from conditions of equilibrium (figs. 1.1b and c), whereas the various distortional loads form self-equilibrating systems and are not directly obtainable from considerations of statics alone (figs. 1.1 d and e).

1.1.1   Bending

The deformation and cross-sectional distribution of longitudinal stress due to pure bending, as calculated by simple beam theory, are shown in figs. 1.2b and 1.3a respectively.   While the errors introduced by neglecting shear deformation in this theory are generally acceptable for thick-walled and solid sections, this is frequently not the case for thin-walled members.   The effect of shear deformation in the plane of the flanges is to reduce the direct stress due to bending at positions away from the webs, as shown in fig. 1.3b, and is referred to as shear lag.   This behaviour may limit the effective width of the flanges for design purposes, especially when wide side cantilevers are employed, and result in a significant underestimation of the maximum direct stress at the top and bottom of the web elements.

1.1.2   Torsion

It must first be assumed that the member responds to the application of torsion by a rigid-body rotation of the entire section about the shear centre (fig. 1.2c), and may thus be considered in
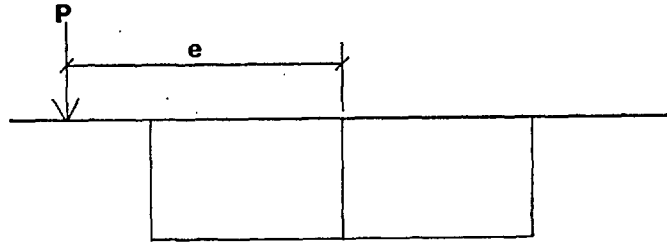
a. *Eccentric Load System*
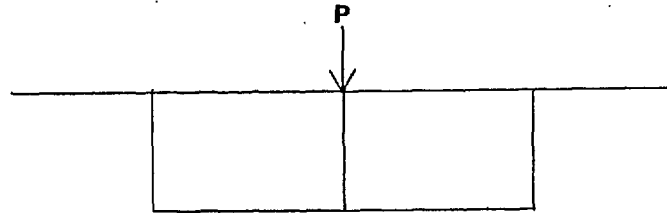
b. *Bending/Shear*
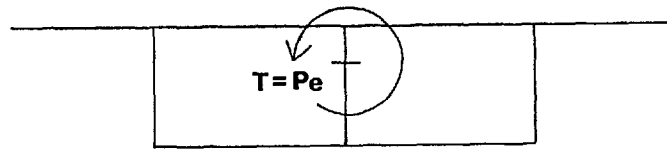
c. *Torsion*
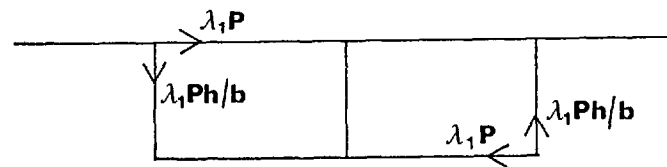
d. *Anti-symmetrical Distortion*
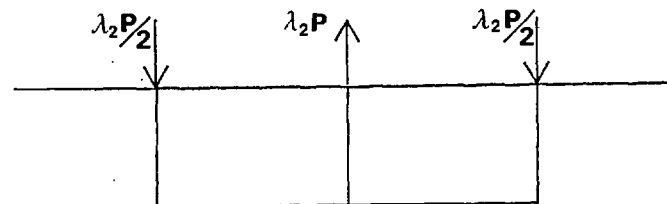
e. *Symmetrical Distortion*

Figure 1.1 *The Basic Structural Actions in a Typical Twin Cell Box Girder*
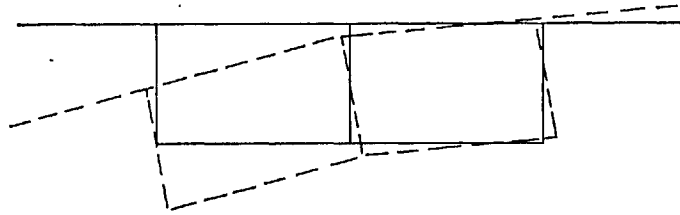
a. Overall Deformation
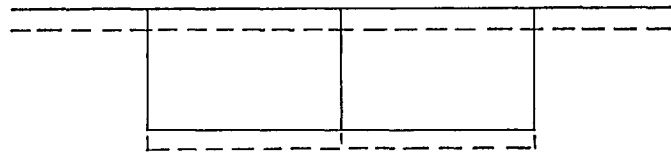
b. Bending
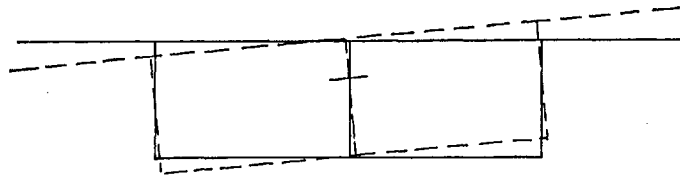
c. Torsion
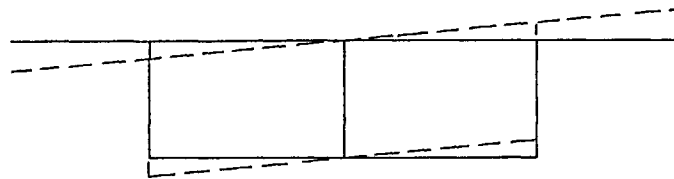
d. Anti-symmetrical Distortion
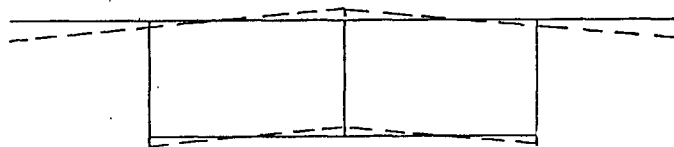
e. Symmetrical Distortion

Figure 1.2   Cross-sectional Deformations in a Typical Twin Cell
Box Girder
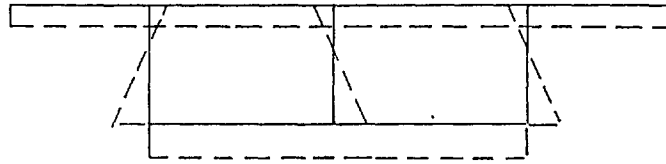
a. Bending
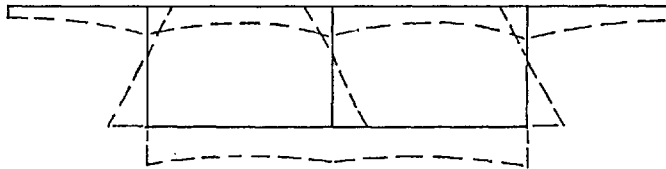
b. Bending with Shear Lag Effects
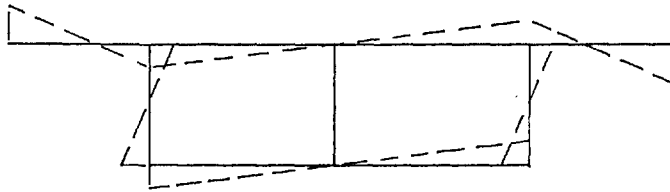
c. Warping Torsion
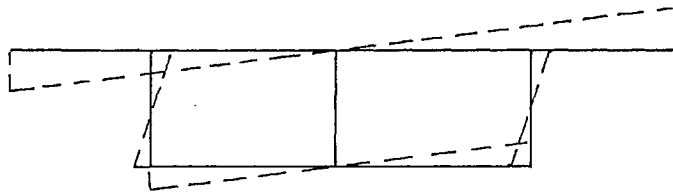
d. Anti-symmetrical Distortion
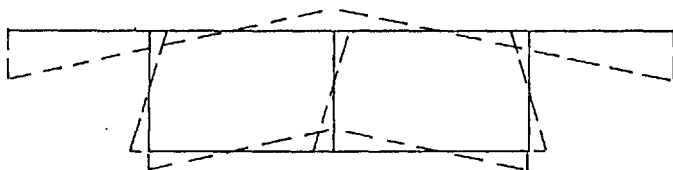
e. Symmetrical Distortion

Figure 1.3   Distribution of Longitudinal Direct Stress in a Typical
Twin Cell Box Girder

isolation from any distortional effects.   Since thin-walled members

are unlikely to possess sufficient transverse stiffness to prevent

distortion, an adequate number of diaphragms must usually be introduced

along the length of the beam.   Ideally, these should be infinitely

flexible in the direction of the member axis thereby permitting axial

displacements to occur without longitudinal restraint.

Under pure twist a system of circulatory shear stresses is

created in accordance with St. Venant's theory and in exactly the same

way as for solid and thick-walled sections.   In general, the out-of-

plane axial displacements (or warping displacements) corresponding to

this form of loading are characteristically larger for thin-walled

sections than for other configurations with similar overall dimensions.

However, since the transverse distribution of warping displacements is

identical at all positions along the beam, this does not result in the

formation of any longitudinal direct stresses.

On the other hand, if the axial displacements are in any way

restrained, a system of direct stresses is induced with the typical

cross-sectional distribution shown in fig.1.3c.   This constitutes a

system in equilibrium and has no resultant component of either direct

force or bending moment.   A complementary system of warping shear

stresses is also created which acts in conjunction with the St. Venant

shear stresses to resist the applied torsional moment.   Thus, while

the total torque at any section is readily obtainable in a statically

determinate structure, the longitudinal distribution of warping shear

stresses is always statically indeterminate and must be evaluated by

solving the fundamental differential equation governing torsional

deformation.

In longitudinally restrained thick-walled or solid sections,

only St. Venant's torsion need be considered to the exclusion of warping

torsion. In very thin-walled sections the opposite is generally true. While the latter case is never likely to be directly applicable to concrete structures, the continuing trend to thinner wall sections does mean that both components of torsion must frequently be taken into account in the analysis (denoted mixed torsion).

1.1.3   Distortion

In the preceeding discussion on torsional behaviour it has been necessary to adopt the concept of closed spaced diaphragms, rigid in their own plane but infinitely flexible in the direction of the longitudinal member axis. Thus, the structural section has been permitted to develop axial deformations and to undergo rigid-body rotations while maintaining its original cross-sectional profile. However, in practice, diaphragms do not correspond to this idealised form but are generally only located at the supports and at discrete points along the length of the member. The cross-section can therefore distort between diaphragm positions to a degree dependent upon the transverse flexibility of the section and the distance from a point of effective restraint.

The two basic modes of distortion to be found in twin cell box girders are shown in figs. 1.1d and e. The anti-symmetrical mode represents torsional distortion and is possible when torsion is applied to a deformable section. Alternatively, the symmetrical mode develops under certain transverse distributions of load and is denoted transverse bending distortion.

Apart from the flexural deformations of the individual wall elements (shown in figs. 1.2d and e), the cross-section is also subject to the formation of axial warping displacements. Since the distortional deformation along the beam is necessarily variable between points of

restraint, the warping displacements are no longer constant and
additional direct stresses are developed with the transverse distribution
shown in figs. 1.3d and e. These systems of direct stress are self-
equilibrating in the same way as those due to torsional warping and do
not influence the other stress resultants. Furthermore, the complemen-
tary shear stresses associated with distortional direct stresses are
also self-equilibrating and have no internal resistive effect on the
applied torsional moment. However, they do combine with those shear
stresses due to both St. Venant and warping torsion to further compli-
cate the final stress distribution in the various structural elements.

1.1.4   Transverse Slab Action

The application of point or patch loading, usually to the
top flange, introduces deformations which result in further cross-
sectional distortions. An infinite number of such systems are
possible but do not constitute independent distortional modes in
the sense of those discussed in §1.1.3 and may be considered separately.
While the transverse effects due to these loads are essentially local
and disappear rapidly at positions away from the point of application,
the transverse stresses induced are often substantial and can signif-
icantly influence the direct stresses in the direction of the long-
itudinal beam axis due to Poisson's ratio effects.

1.2   CONCRETE STRUCTURES LOADED IN TORSION

Whereas the problems associated with torsional loads have been largely avoided in the design of concrete structures, this has not been the case in other industries. In particular the aircraft designer has always been confronted with the need to provide sub-stantial torsional stiffness in wing and fuselage sections in order to effect an economic design of minimum weight. While space-frame structures, *e.g.* the bi-plane wing, are generally more efficient in resisting bending and direct stresses, the closed box section is usually lighter where shear and torsional loads predominate. Indeed, the rapid development of the monocoque configuration in the early 1930's was a direct consequence of the relatively higher torsional loads induced by greater speed. This is generally regarded as the first significant use of thin-walled sections subject to combined loads, although the automobile, ship building and steel construction industries were also quick to adopt this form of construction for similar reasons.

To simplify the analysis, sections were generally idealised into a series of direct stress-carrying members (stringers or booms), concentrated at discrete points around the perimeter. These were then connected by thin membranes which were assumed to be capable of trans-mitting shear forces only. The close resemblance of this idealisation to the actual practice of fixing longitudinal stiffeners to the continuous shear walls, together with improvements in welding and fabrication techniques, undoubtedly encouraged the rapid acceptance of these methods.

In recent years those industries with experience in the use of thin-walled structures have been well placed to take full advantage of

modern theoretical and analytical techniques to improve the efficiency of their designs. On the other hand, concrete structures have traditionally been constructed from thick-walled or solid members and the problems associated with thin-walled sections are not generally well understood. However, gradual improvements in material performance and construction techniques have resulted in corresponding reductions in section thickness to the extent that thin-walled behaviour must now frequently be assumed.

Cross-sectional Configurations

For the purposes of torsional analysis, thin-walled sections may be conveniently separated into two major classifications. Those with cellular configurations are denoted *closed* sections and resist the application of pure torsion by the formation of constant shear flows around the periphery of the closed parts. The connectivity condition ensures that only relatively small warping displacements are created, and the stresses arising from warping restraint are correspondingly small and often local in effect.

On the other hand, the pure resistive shear stresses developed in *open* sections are linearly distributed across the wall thickness and result in large out-of-plane warping displacements at the free edges of the section. Moreover, warping restraint stresses can assume a greater significance in these sections and may substantially alter the stress distribution along the entire length of the beam. As a result of these differences, closed sections are favoured for most torsional applications except where practical considerations make this impossible.

The differences in behaviour between open and closed sections are also reflected in the different theoretical approaches adopted in

their respective analyses. However, in practice, most members comprise both open and closed parts and are referred to as *open/closed* sections. These include the large majority of thin-walled members used in structural engineering, *e.g.* box girder bridges with side cantilevers, and are generally treated as closed sections for the purposes of analysis since the torsional behaviour is predominantly governed by the closed part.

Undoubtedly, the two most common examples of thin-walled concrete structures are the box girder bridge and the shear core, used in the construction of tall buildings. These are examined in some detail throughout this work and, in general, cover all aspects of open, closed and open/closed behaviour. In the remainder of this section the significant features of these two structural forms are briefly introduced together with other less common examples of thin-walled concrete structures.

1.2.1   Box Girder Bridges

The concrete box girder has evolved into a highly efficient and aesthetically pleasing solution for medium and long span bridges, combining as it does, high flexural stiffness due to the well spaced flanges, and excellent torsional capacity due to the closed cell formation. Its development into the slender, thin-walled structure that we know to-day has been influenced by several important and inter-related factors. These include:

a.   advances in material technology and construction techniques (*e.g.* prestressing) which have enabled wall thicknesses to be greatly reduced,

b.   the need to accommodate increased traffic flow resulting in larger width/depth aspect ratios or, alternatively, in the introduction of wider side cantilevers,

c.   increases in effective span lengths due to the cost or

technical difficulties encountered in locating supports,

especially in urban areas, and

d.   the powerful computer-based analytical techniques now

available, which have resulted in a more complete under-

standing of the elastic behaviour of such structures.

While earlier, more conservative box girder designs employed configur-

ations which rendered warping and distortional effects negligible,

this is no longer the case and the thin-walled behaviour outlined in

§1.1 must often be taken into consideration.

Examples of the wide range of sections typically found in

practice are shown in fig. 1.4. These have been abstracted from a

feature survey of existing box girder bridges by Swann[102] and form

part of the parametric study of thin-walled section properties in

§2.5. While all of these basic configurations may be used throughout

the full range of spans suited to box girder bridges (typically 25-120m

but exceptionally 10-210m), each cross-sectional type is only really

a practicable solution for a narrow range of carriageway widths.

In general, the torsional capacity of the single cell box

girder is far in excess of that necessary to resist the total imposed

load at its greatest possible eccentricity. Thus, where extra width

is required, cantilevers are commonly provided thereby transforming

the section into the open/closed profile shown in fig. 1.4a. However,

since cantilever length is usually restricted to approximately 4 m,

in order to avoid excessive depth at the root, twin or multi-cellular

profiles must be employed where wider carriageways are required,

figs. 1.4b and c. Because of the relatively large formwork costs

associated with box sections, economies can often be effected by using
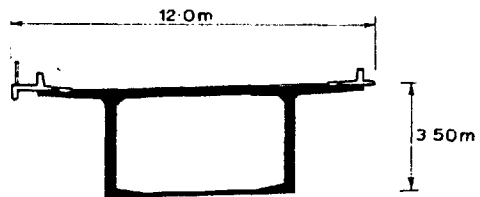
a.   Single Cell
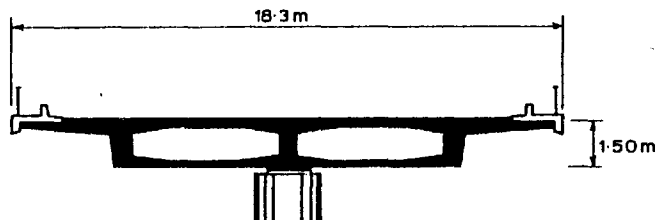
b.   Twin Cell
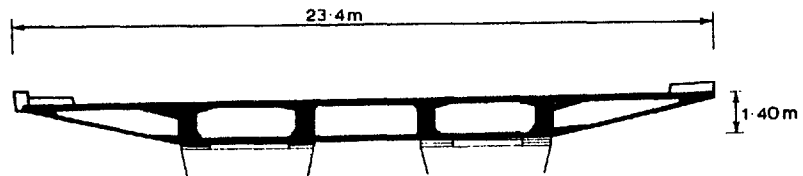
c.   Multi-cellular Section
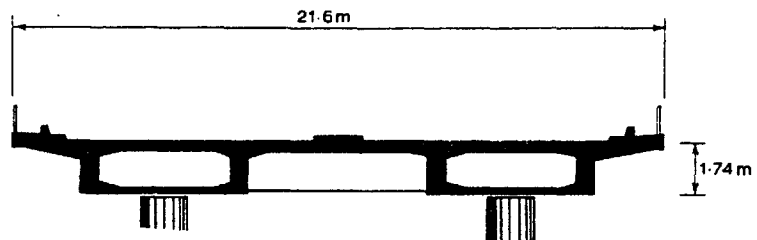
d.   Twin Spine, Single Cell
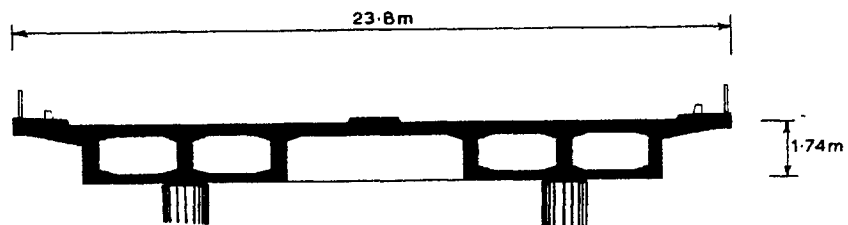
e.   Twin Spine, Double Cell

Figure 1.4   Typical Box Girder Configurations[102]

twin spine sections, figs. 1.4d and e, constructed in two halves

and joined together through adjacent cantilevers.   However, without

rigid connecting diaphragms at frequent intervals, transverse bending

distortion can be significant thus limiting the total torsional capacity

to the sum of that provided by the individual spines.

One type of box girder arrangement which merits particular

attention is the highly curved road bridge which is a characteristic

feature of most elevated motorway systems.   In such cases significant

torsion is likely to be induced by the self-weight of the structure

alone although, in practice, this will often be supplemented by

highly eccentric vehicular loading (due to wide side cantilevers) and

by irregular or skewed supports.   Since the radius of curvature is

usually greater that ten times the overall section width[102], such

structures are often idealized as equivalent striaght members for the

purposes of design.   However, where there are severe alignment

problems, *e.g.* at graded motorway intersections (plate 1.1), this ratio

can be reduced to the order of four.   In this case, the effects

curvature assume a greater significance and must be taken into account

in the analysis.

1.2.2   The Shear Core

This common form of thin-walled structure is almost invariably

constructed in reinforced concrete.   It has been widely employed in

the design of high-rise buildings, in order to provide the necessary

torsional and flexural resistance to wind and earthquake loadings, and

may be economically constructed by slip-forming methods, plate 1.2.

In order to fulfil a secondary function as a lift or service

shaft, openings are usually required at each level.   Where these are

large, *e.g.* plate 1.3, the structure is effectively transformed into

Plate 1.1   Graveley Hill Interchange, Birmingham.

Plate 1.2   National Westminster Tower, London.
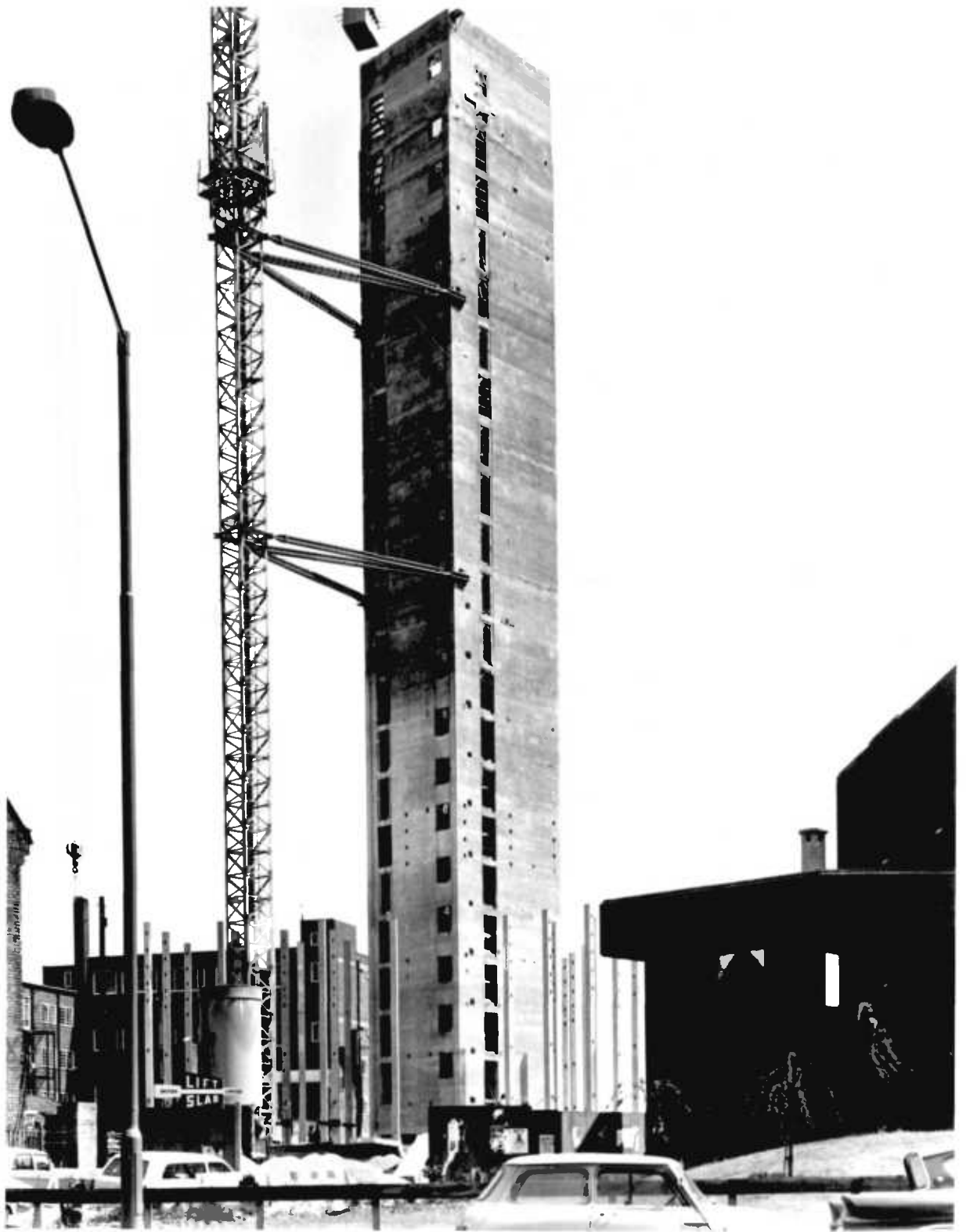
Plate 1.3   Dalton Tower, University of Aston, Birmingham.

an open section tube that is torsionally much weaker than the original
closed section, fig. 1.5a. As a result, when this structure is sub-
jected to applied torque, significant warping displacements occur
noticeably at the free edges of the section.   However, these are
fully restrained at the foundation level thereby creating substantial
and additional systems of direct and shear stress.   Furthermore, the
shear centre is now positioned well outside of the section and trans-
verse wind loads, even those symmetrically placed about the structure,
have a greatly increased torsional lever arm.

For these reasons, open tube configurations are avoided when-
ever possible.   Worked examples by Stafford Smith and Taranath[98],
substantiated by model tests, indicate that cross-beams provided at
each level, fig. 1.5b, can increase the torsional stiffness of a
typical structure by a factor of approximately four.   With this modi-
fication the section is transformed into a pseudo-closed profile and the
position of the shear centre is also significantly improved.
Alternatively, if headroom requirements make the provision of cross-
beams impossible, the restraining effects of fully connected floor
slabs alone may increase the torsional stiffness by up to 50%, fig. 1.5c.

The cross-sectional dimensions typically specified for such
structures and the type of loading to which they are subjected, makes
a full torsional analysis, including the effects of warping, essential.
Indeed, for shear cores of practical dimensions the vertical stresses
due to warping restraint are frequently of the same order as those
due to bending.   On the other hand, the effects of distortion can
invariably be neglected due to the excellent restraint provided by
the composite action of the floor slabs at each level.
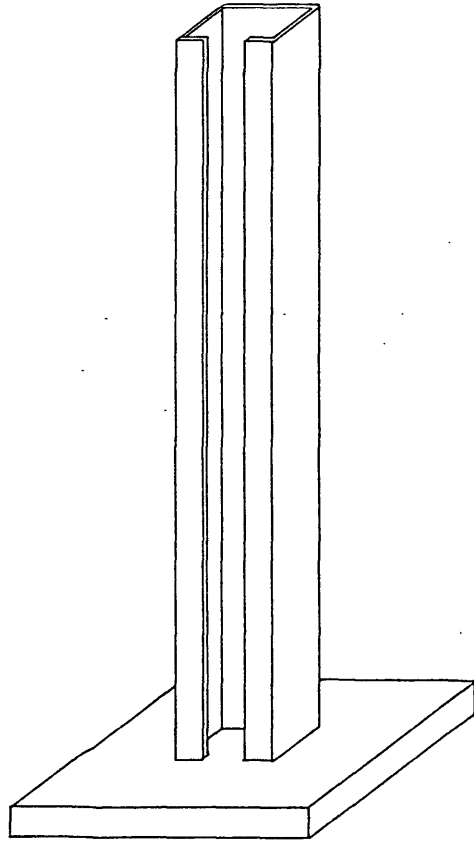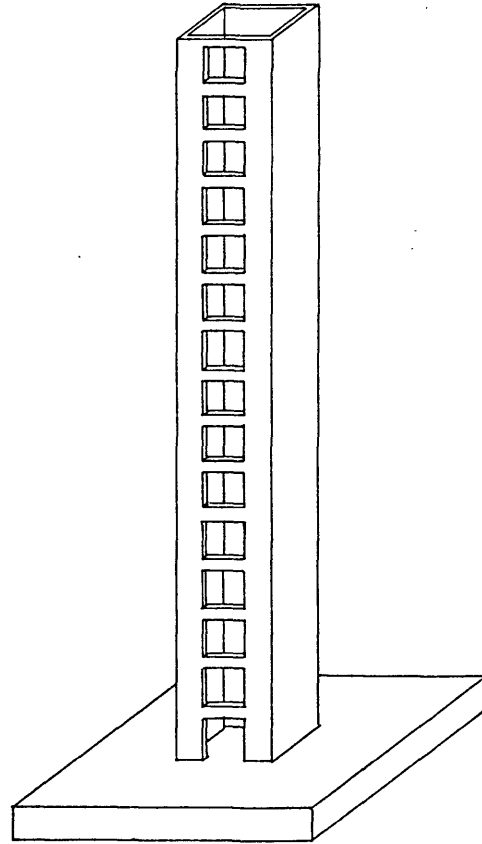
a. Open Section   b. Pseudo-closed Section   c. Open Section with Integral Floor Slabs
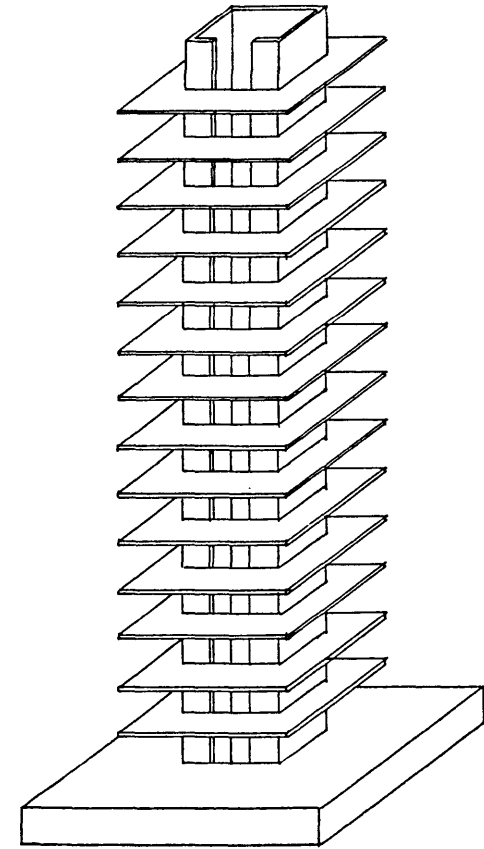
Figure 1.5 Typical Shear Core Arrangements

1.2.3   Other Applications

Apart from these two examples, structural concrete elements
subjected to substantial levels of applied torsion are becoming
increasingly common in all areas of civil and structural engineering.

For example, the box girder bridge is only a special appli-
cation of the hollow spine beam which is often employed as a general
solution for medium to long spans.   However, since the thin-walled
section is relatively expensive to construct, it is only really
practicable where self-weight or headroom restrictions are imposed, or
when the hollow configuration is required for carrying services, etc..

On the other hand, true open sections are rarely found in
practice due to their inherently poor torsional capacity.   Undoubtedly,
the shear core represents the most important form of open section,
although it has already been demonstrated that the addition of cross-
beams transforms the section into a more efficient pseudo-closed
profile.   Other applications, such as short span bridges and folded
plate roof structures, effectively respond to eccentric loading by the
action of transverse bending and are, therefore, not subject to
significant torsional distortion or warping restraint effects.

Marine Applications

Recently, there has been a substantial increase in the number
of structures designed for installation at sea and, in many cases,
concrete has been selected due to its well proven record on durability
in the marine environment.

Wave forces, by their very nature, are extremely variable in
magnitude and multi-directional in effect and can therefore impose
significant torsional loads often in combination with bending moment
and shear.   Indeed, recent innovations in the design of floating

breakwaters, fig. 1.6, and wave power devices, fig. 1.7, have depended exclusively on the excellent torsional capacity of the closed box section in order to perform their primary function. This is in direct contrast to more conventional structures, such as immersed tube tunnels, in which torsional loading is often only of importance before and during installation on to the sea bed.

A revival of interest is also being shown in the construction of concrete ships. Due to steel shortages, these were used extensively during both world wars and several recent proposals for liquid and bulk carriers are claimed to be viable by their designers[31]. The transportation of liquid nitrogen gas by these means would appear to be particularly attractive due to the excellent cryogenic behaviour of concrete, plate 1.4.

Solid Sections

Whereas the major part of this thesis relates only to the behaviour of thin-walled members, some solid structural elements are also required to resist substantial levels of applied torsion. Crane rails, cantilevered staircases and edge beams to shells and slabs are common examples. On occasions solid beams are also required to resist the additional torsional moments due to high curvature. However, due to the relatively high costs of construction, such applications are rare but include spiral ramps in multi-storey car parks and approaches to pedestrian overbridges, *e.g.* plate 1.5.

While the effects of warping and distortion are negligible in solid beams, much of the ultimate load analysis presented in Chapter 5 is equally valid for these members.
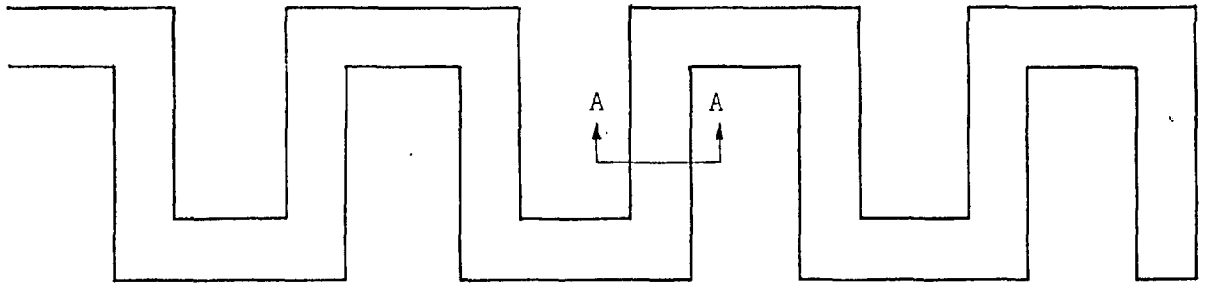
a. Rectangular Configuration
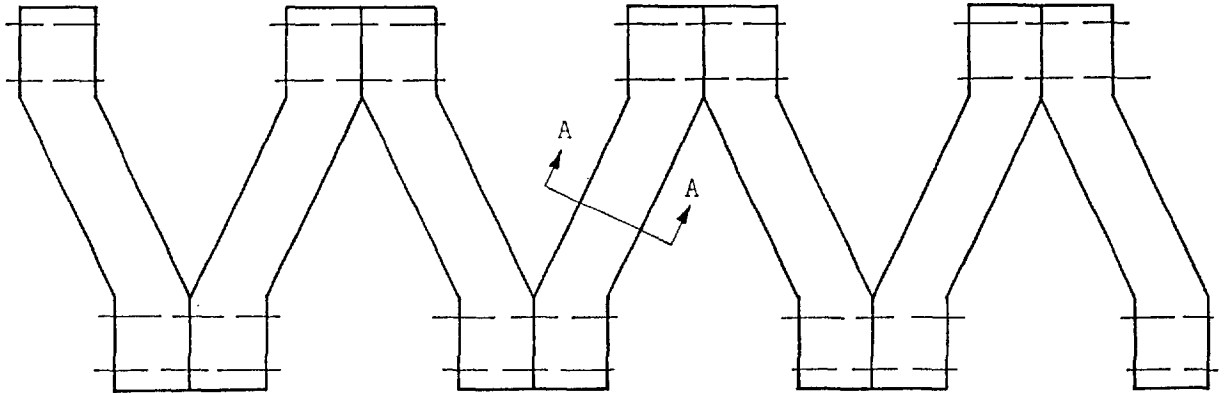
b. Zig-Zag Configuration
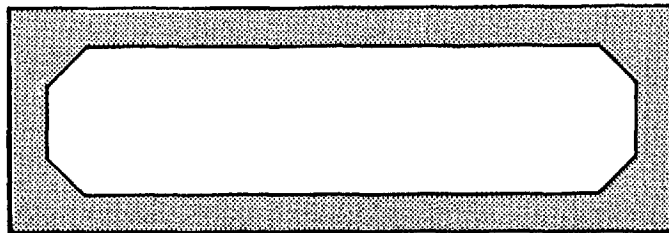
c. Typical Section A-A

Figure 1.6   Proposed Floating Breakwaters
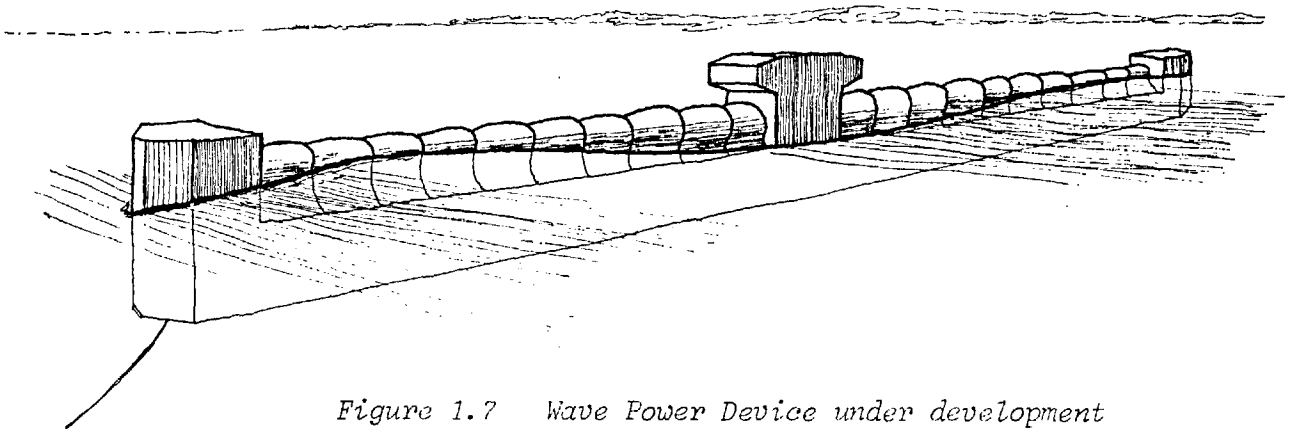
Figure 1.7   Wave Power Device under development
at Lancaster University

VOID/
BALLAST

BALLAST WATER

45cm CONCRETE

W.T. FLAT

20cm CONCRETE

RES
F.O.

LNG

LNG

VOID
SPACE

VOID
SPACE

60cm CONCRETE

CRYOGENIC INSULATION
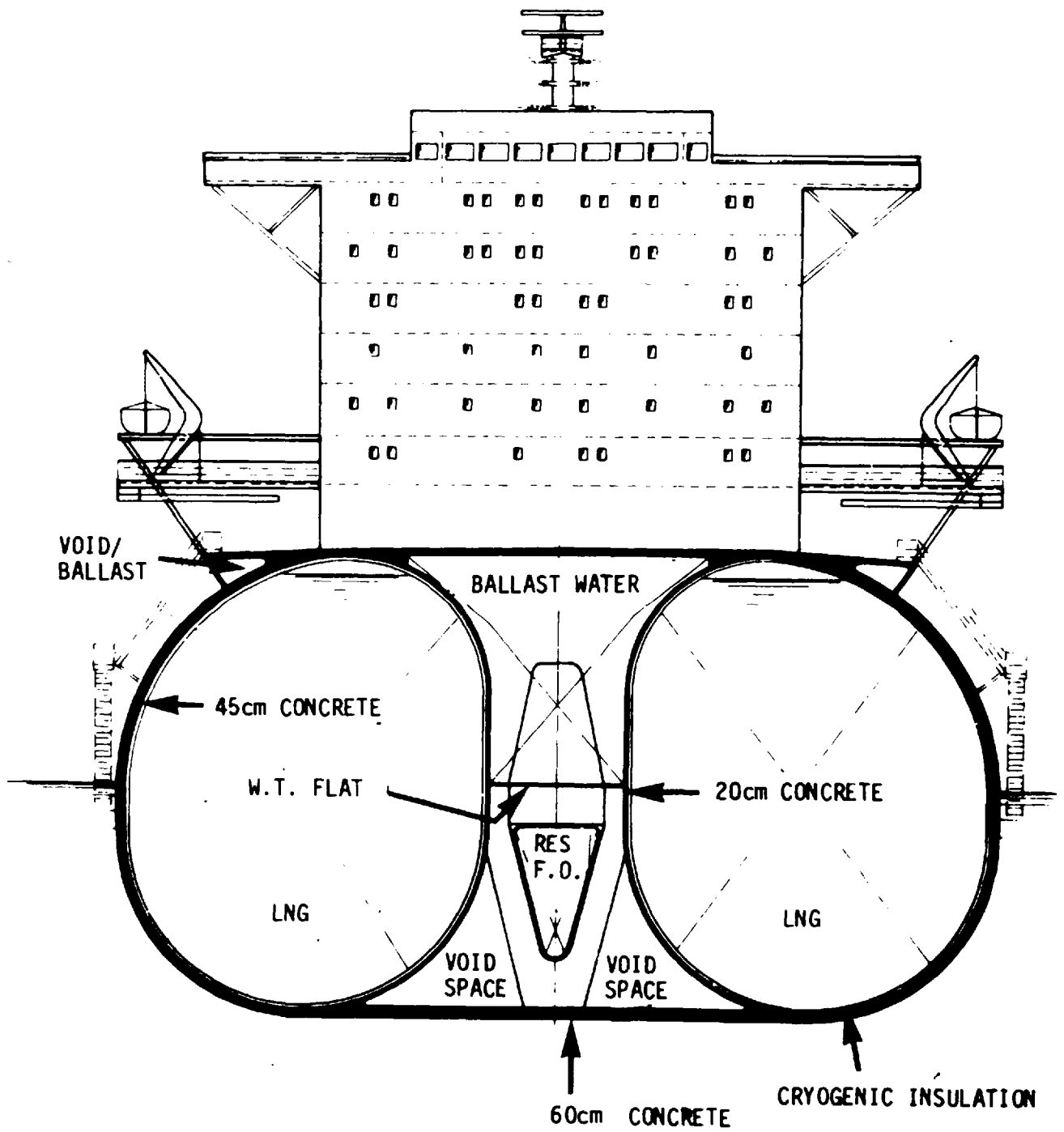
Plate 1.4   Proposed LNG Tanker (128 000 m³ capacity).
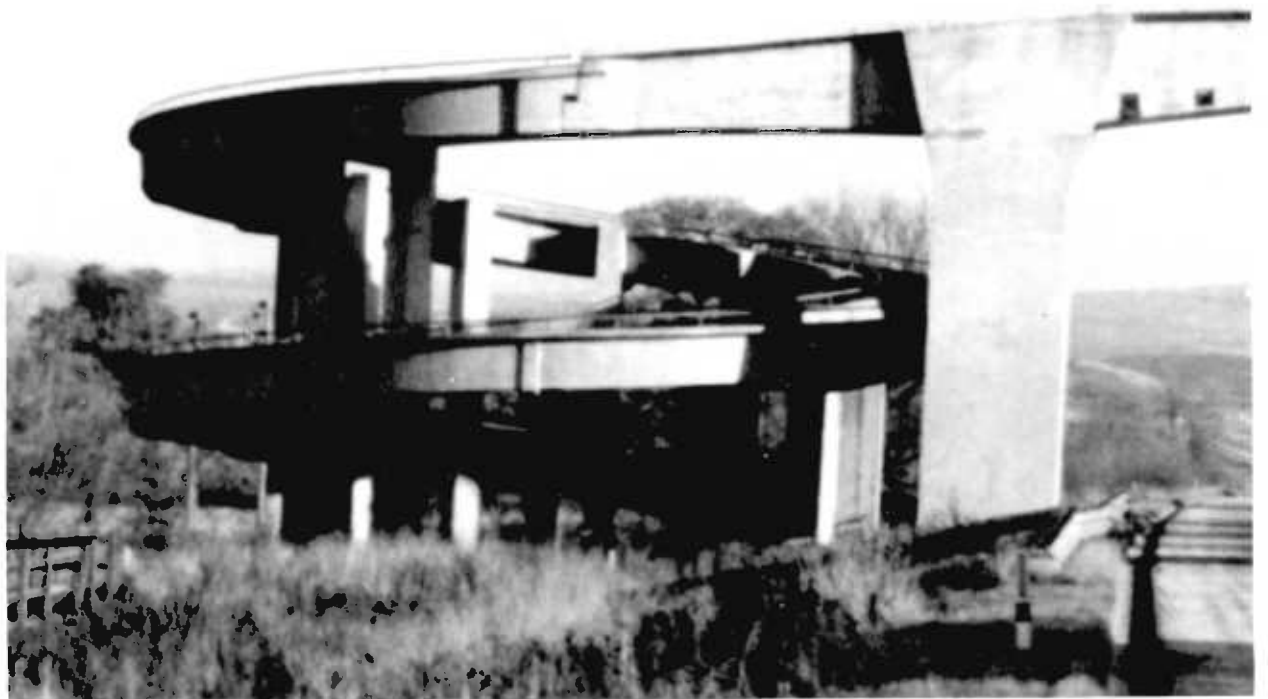
Plate 1.5   Approach to Motorway Overbridge (M4 near Swindon).

1.3   SCOPE OF THIS WORK

1.3.1   Elastic Analysis

The major part of this thesis is concerned with the elastic

analysis of curved, thin-walled box girder bridges. However, where

appropriate, the various derivations have also been reduced to a form

suitable for straight members.   Thus, the response of shear core

structures can also be investigated by the proposed method of analysis,

as can straight box girders or those with combined straight and curved

parts.

Structural Actions Considered

The basic requirement in the analysis of thin-walled sections,

in common with that for thick-walled and solid sections, is the

determination of the longitudinal distribution of direct and shear stress.

Therefore, while the additional transverse stresses due to distortional

bending and local slab action may be important in some instances, their

effect must be assessed separately and superimposed on the final

solution.

It has been shown in §1.1 that the stresses obtained from

simple beam theory and St. Venant's theory for pure torsion are

statically equivalent to the applied load system for all cross-

sectional configurations.   In the case of thin-walled beams,

additional direct and shear stresses are also created due to the other

basic structural actions, namely, warping torsion, distortion and

shear lag.   However, these are essentially self-equilibriating

systems and, if small, may be neglected without influencing the over-

all equilibrium of the structure.

Shear lag is basically regarded as a problem associated

with bending in the absence of torsion although it may also occur at

sections where significant direct stresses are formed due to warping restraint. Since it is caused by shear deformation in the flanges, it is particularly important in very thin-walled members (*e.g.* steel bridges) or in sections with well spaced webs and wide side cantilevers. However, in the discussion to his paper, Rowe[71] justifies neglecting shear lag in the analysis of single-cell, concrete box girders, while Maisel and Roll[70] state that the effects are also negligible in multi-cellular configurations, due to the more favourable disposition of the webs. This is particularly the case for longitudinally prestressed structures where the shear lag effects due to initial prestress directly oppose those due to subsequent bending. For these reasons shear lag has been neglected completely in this study although its effects may be superimposed, if necessary, in the same way as those due to transverse bending.

While the causes of warping torsion and distortion are very different, both actions result in modes of warping displacement which, when restrained, induce systems of self-equilibriating stresses. For an arbitrary, closed cross-section, idealized into n stringers and shear walls, Argyris and Dunne[7] found that there were (n - 3) such modes of self-equilibrating stress (denoted eigenloads) corresponding to (n - 3) possible modes of warping displacement. Furthermore, since each mode now has its own centre of twist, the shear centre can no longer be used to separate shear and torsional loads. Megson[74] likens the various eigenloads to the buckling loads corresponding to the different buckled shapes of an elastic strut. He further states that, in general, a good approximation is obtained by considering only the mode corresponding to the lowest eigenload.

Thus, for a particular structure and arrangement of loads, it is generally sufficient to consider either the effects of warping torsion or one of the distortional modes.   In this connection Maisel and Roll[70] have conducted a parametric study on 864 different geometrical configurations of rectangular, single cell, simply supported box girders based on typical dimensions of existing structures[102].   The spans varied from 30 m to 70 m and diaphragms were only located at the end supports.   One of the main conclusions drawn from this study states that it is generally inadvisable to neglect torsional warping stresses in comparison to those created by torsional distortion.   On the one hand, while this conclusion does not extend directly to multi-cellular configurations where distortion could possibly be significant, neither does it take any account of intermediate diaphragms which are commonly employed in box girder construction to help maintain the original cross-sectional profile.

Distortional effects have therefore been neglected from the subsequent analysis, although it will be shown later how transverse bending distortion can be accommodated where necessary.   It would appear that this simplification is entirely satisfactory for the large majority of concrete box girders and also for shear core structures where distortional restraint is provided by the composite action of the floor slabs.

Although distortion has been neglected, torsional warping often occurs in practice and can be caused by various factors.   These include:

a.   restraint provided by transverse diaphragms,

b.   restraint at a built-in end,

c.   the application of non-uniform torsion along the beam,

d.   a change of cross-section in torque loaded members,

and can create substantial direct and shear stresses in certain thin-walled sections. The cross-sectional configurations which are especially susceptible to the formation of warping restraint stresses are identified later in a parametric study of existing structures.

Structural Analysis

The methods available for the elastic analysis of box girder bridges are summarized in §3.1 and will not be discussed here in detail. Nevertheless, for thin-walled structures displaying high curvature, complex loading, variations in cross-section and complicated systems of restraint, the most useful methods of analysis are those for which the members can be idealized into a series of discrete structural elements. Although both the flexibility and stiffness methods are suitable for obtaining a solution to this problem, the necessary load/displacement relationships are not readily available for either straight or curved thin-walled beams and these must first be established.

The important structural actions to be considered in the analysis have been identified previously in this section and are basically those of pure torsion, longitudinal bending and warping restraint. While the distribution of total torque and bending moment may be simply obtained from a consideration of statics, the effects of warping restraint are always indeterminate and can only be evaluated by taking account of the general state of deformation in the member. To this end, the structural mechanics associated with thin-walled members are first developed in Chapter 2 from which the fundamental differential equations governing torsional deformation along the beam are derived for the various cross-sectional configurations. The solution of these equations then yields the longitudinal distribution of all the necessary stress resultants in terms of the section

properties and applied loads only, for any system of end restraint.

In Chapter 3 the equation of total strain energy has been derived in terms of the appropriate stress resultants and section properties only. By introducing the necessary quantities into this equation, and by integrating along the length of the beam built-in at one end, the flexibility matrix with the necessary four degrees of freedom has been established for both straight and curved members. Basically this is all that is required for obtaining a solution by the flexibility method although a different matrix formulation is needed for the more general stiffness approach. However, this is a complex problem for circular curved members, due to the interaction between the fundamental equations governing bending and torsional behaviour, and thus a stiffness matrix has only been derived here in explicit form for straight members. An alternative approach has been adopted for curved members whereby the stiffness matrix is obtained numerically by inverting the previously determined flexibility matrix and introducing the appropriate conditions of end equilibrium.

By developing the necessary load/displacement relationships for both straight and curved thin-walled beams, most structures may now be idealized by relatively few elements. In this case, it is no longer sufficiently accurate to represent uniformly distributed loading by discrete point loads at the junctions of the idealized beams, and the fixed-end stress resultants corresponding to the four degrees of freedom must be determined for all likely forms of applied loading. This has been achieved for applications of shear and torsion (both uniformly distributed and concentrated loads) by introducing the appropriate boundary conditions into the equations describing the various stress resultant and deformation terms, and solving these simultaneously.

Structural Idealization

The stiffness method, incorporating the features described
here, has subsequently been used in Chapter 4 to analyse two complex
box girders. Both structures are continuous over several supports
and comprise both straight and curved members. Due to the development
of the circular curved beam element (including warping restraint effects),
only a small proportion of the computational effort used by other methods
has been required, while the results obtained compare very favourably
with those from published experimental and theoretical studies.

Previously, highly curved structures like these could only
be analysed by the stiffness method if they were idealized into a
series of end-connected straight beams. Such an idealization only
approximates the actual geometry and is also inefficient in terms of
analytical effort due to the larger number of elements required.
Nevertheless, with the suites of programs readily available this
procedure is likely to remain attractive for some time to come. The
errors introduced by this idealization are therefore examined in some
detail in Chapter 4 by means of a computer-based parametric study covering
the wide range of cross-sectional properties typically found in civil
engineering structures. The errors associated with neglecting warping
restraint can be equally significant in some cases and these are also
investigated with the primary objective of defining the structural
configurations for which these effects should be taken into consideration.

1.3.2   Ultimate Load Analysis

The methods of analysis presented in the first part of this
thesis are only truly applicable to concrete structures in the elastic
range and are, therefore, limited by first cracking. This is part-
icularly the case for structures subject to combined loads since,

after cracking, the torsional stiffness generally reduces dispropor-
tionately in comparison to the bending stiffness (although prestressing
is often effectively employed to extend the range of elastic behaviour).
Furthermore, with the adoption of limit state design philosophy, there
has been an increasing emphasis on the ultimate load analysis of torque
loaded structures, and the analytical methods available for this
purpose are discussed in some detail in §5.1.

Closed and Solid Sections

Since the core of a solid beam is relatively ineffective at
the ultimate limit state, solid and hollow sections can usually be
analysed by the same general theory.   The space truss and ultimate
equilibrium methods have both been widely accepted in practice and,
in their original forms, are suitable for the analysis of under-
reinforced beams subject to combined bending and torsional moments.
Both methods are formulated from conditions of equilibrium only and,
given the same initial assumptions, will predict identical collapse
loads.   The accuracy of these theories has been well established by
extensive experimental investigations over the full range of torsion/
bending interaction, and they are now incorporated into many design
recommendations.

Various attempts to introduce the effects of shear into the
analyses have created certain anomalies, mainly due to the assumption
that failure will occur with the neutral axis parallel to one or other
of the beam faces.   For the general case of combined loading, this
assumption is not supported by observation and, therefore, in §5.3
an alternative ultimate load analysis is proposed.   This is based on
a space truss model in which the orientation of the compression zone
at failure is unrestricted, thus enabling the effects of shear to be
included in a more rigorous fashion.

The well documented results from an extensive series of pre-stressed concrete beam tests are already available[44] and these indicate that a corner failure is possible under certain combinations of applied torsion, bending and shear. Subsequently, these beams have been analysed by the proposed method, and the predicted collapse loads and the orientation of the neutral axis at failure compare favourably with the recorded results.

Open Sections

In their original form the ultimate load methods are further limited in that they can only accommodate St. Venant's torsion and do not include the effects of warping restraint. In closed sections, applied torque is resisted entirely by the formation of constant shear flows around the periphery, while the stresses created by warping restraint constitute a self-equilibriating system and have no resistive effect. Thus, although the distribution of shear flow is modified by the presence of warping restraint, the total torsional capacity remains unaffected. Furthermore the longitudinal stresses associated with warping restraint are also self-equilibriating and, while a certain amount of redistribution will undoubtedly take place, the collapse load is unlikely to be significantly reduced.

However, for thin-walled open sections this is not usually the case. If warping displacements are at all restrained, then warping shear stresses are created which act in combination with the St. Venant shear stresses to resist the applied torque. Indeed, since the warping shear stresses are constant across the wall thickness the torsional capacity of this component is often the more significant. This is particularly the case after cracking when the St. Venant torsional stiffness invariably undergoes a marked

reduction.   While the corresponding system of longitudinal direct stress is self-equilibriating (as is the case for closed sections), the effects are no longer secondary and must be taken into consideration in any analysis.

In §5.4 an advanced ultimate load method is proposed which has been developed from the stress analysis of cracked sections.   A theoretical study of the shear centre and centroidal positions after cracking has enabled certain simplifications to be introduced into this analysis, thus permitting a general interaction equation to be derived in a form similar to that for closed sections.   The proposed method has subsequently been applied to the analysis of four open section beams, the construction and testing of which are also briefly described. While it is impossible to verify the interaction equations over the full range without a more extensive series of tests, the application of the theory is demonstrated and the results are encouraging.

1.4   SIGN CONVENTIONS

The effects of warping stresses and their associated defor-
mations are not always obvious, especially when dealing with curved
beams or complex cross-sectional configurations.   It is, therefore,
imperative to define sign conventions and systems of co-ordinate axes
which are both logical and unambiguous in their interpretation.

1.4.1   Co-ordinate Systems

Straight Members

As usual, the horizontal, vertical and longitudinal directions
are represented by the x, y and z-axes, respectively, and the right-
handed Cartesian co-ordinate system, fig. 1.8, has been adopted through-
out.   The positive face of a cross-section is defined as that for which
the external normal is in the same direction as the positive z-axis.
This is the face considered in the analysis when the selected section
is within the span; the negative face is generally used for support
sections.

The intersection of the x and y-axes is usually taken as the
centroid of the section when considering bending or normal stresses
and as the shear centre for applications of pure or non-uniform torsion.
In cases of combined loads, or where the origin has been arbitrarily
chosen, the selected position is made clear in the text.

Curved Members

In the analysis of circular curved members, it is more
convenient to use a cylindrical co-ordinate system (ρ, ζ, α), fig. 1.9,
with its origin at the centre of curvature.   In this case, the
distance from the origin to the centroid and shear centre are denoted
by r_o and r respectively.   Clearly, the 'direction' of member
curvature is important and is defined here as positive when α is
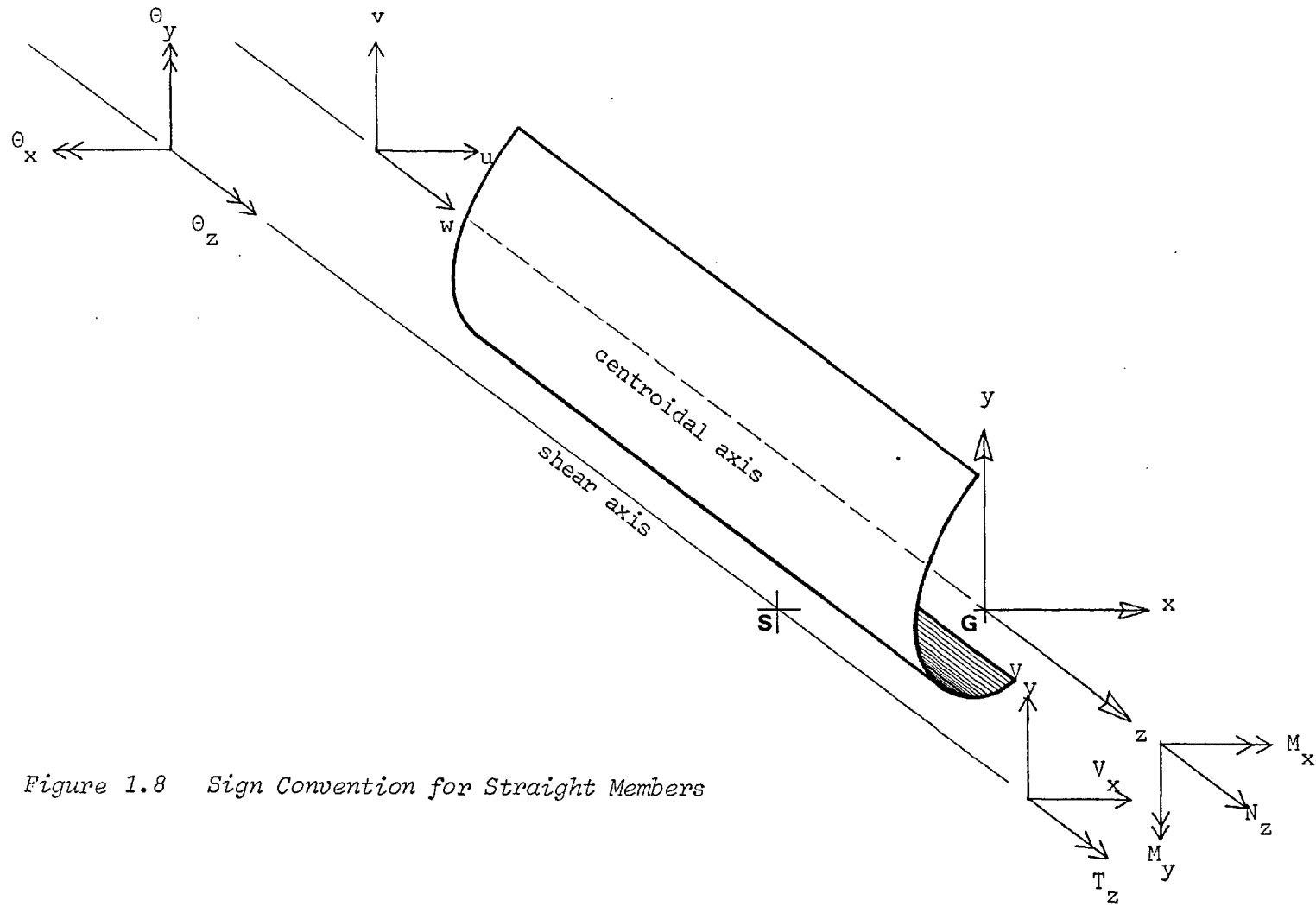
Figure 1.8   Sign Convention for Straight Members
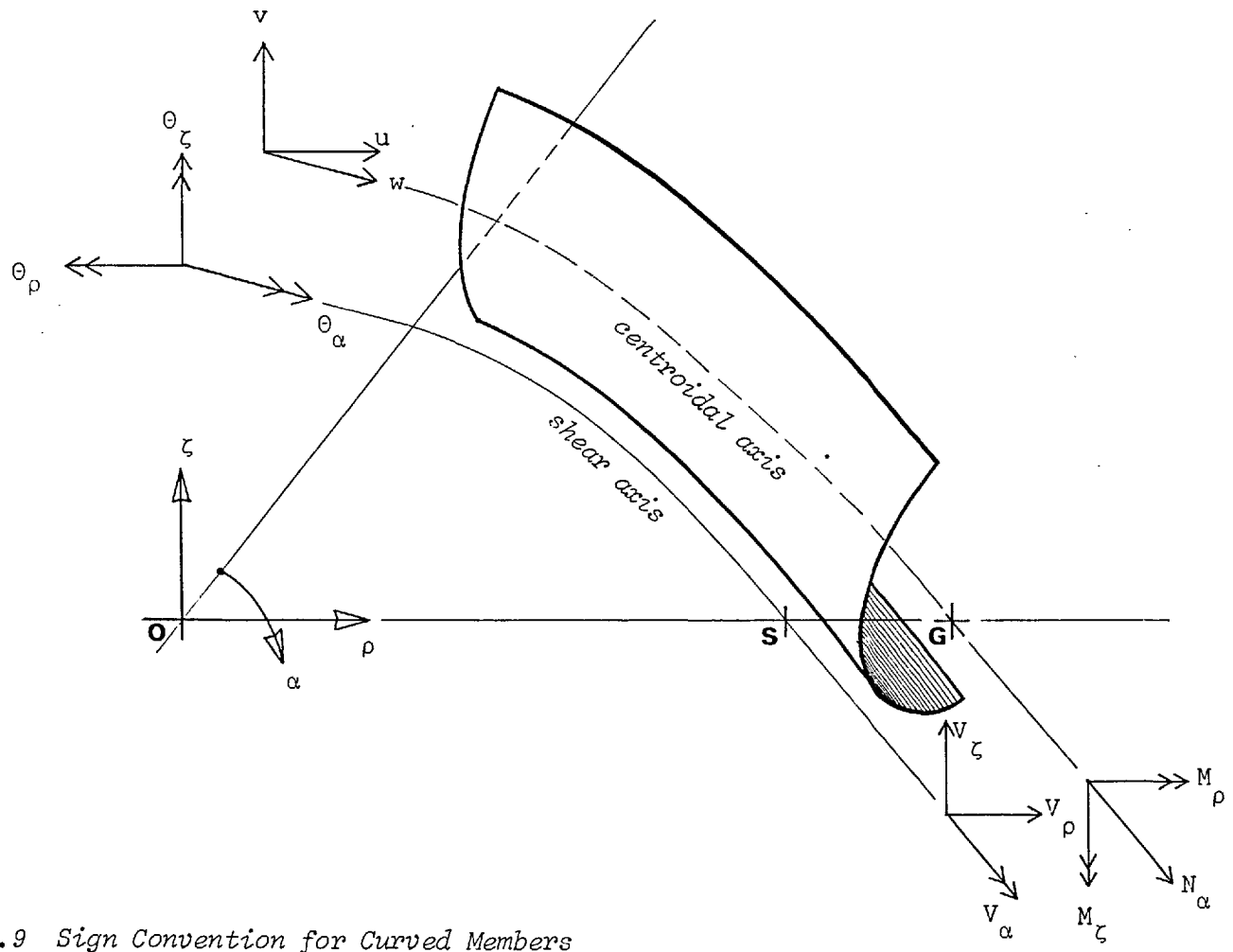
Figure 1.9 Sign Convention for Curved Members

- 37 -

increasing in a clockwise sense when viewed vertically downwards,
fig. 1.10a. The general effect of negative curvature (when α is
increasing in an anti-clockwise sense, fig. 1.10b) is to change the
direction of some of the force and deformation terms derived in
subsequent chapters. Where this occurs the sign corresponding to
negative curvature has been shown directly above that for positive
curvature.

In developing the basic thin-walled beam theory, a curvi-
linear co-ordinate system (α, s) has also been employed. The origin
of the s-axis may be taken at any convenient generator on the median
line of the section and is defined as positive when moving in a clockwise
direction about the shear axis with respect to the positive direction
of the longitudinal beam axis. These co-ordinate axes, stated in the
form (z, s), are also suitable for straight members where z is the
longitudinal beam axis, previously defined.

1.4.2   Stresses and Deformations

All deformations, stress resultants and externally applied
loads are positive quantities in the directions shown in figs. 1.8 and
1.9. In general, each quantity is suffixed to indicate the direction
of action, although these symbols have sometimes been omitted for
simplicity when the meaning is clear.

Any component of stress (on the positive face of the cross-
section) is regarded as positive if it acts in the positive direction
of its corresponding axis; otherwise it is negative. Therefore,
tensile stresses are always positive quantities regardless of the face
on which they act, as are shear stresses acting in the positive
direction of the peripheral co-ordinate s.

Warping Effects

Warping displacements and internal stress resultants due to warping restraint are derived in Chapter 2 for thin-walled beams of all cross-sectional configurations. These are expressed in terms of the various systems of co-ordinate axes, previously defined here, from which they derive their positive sense.

a. *Positive Curvature*   b. *Negative Curvature*
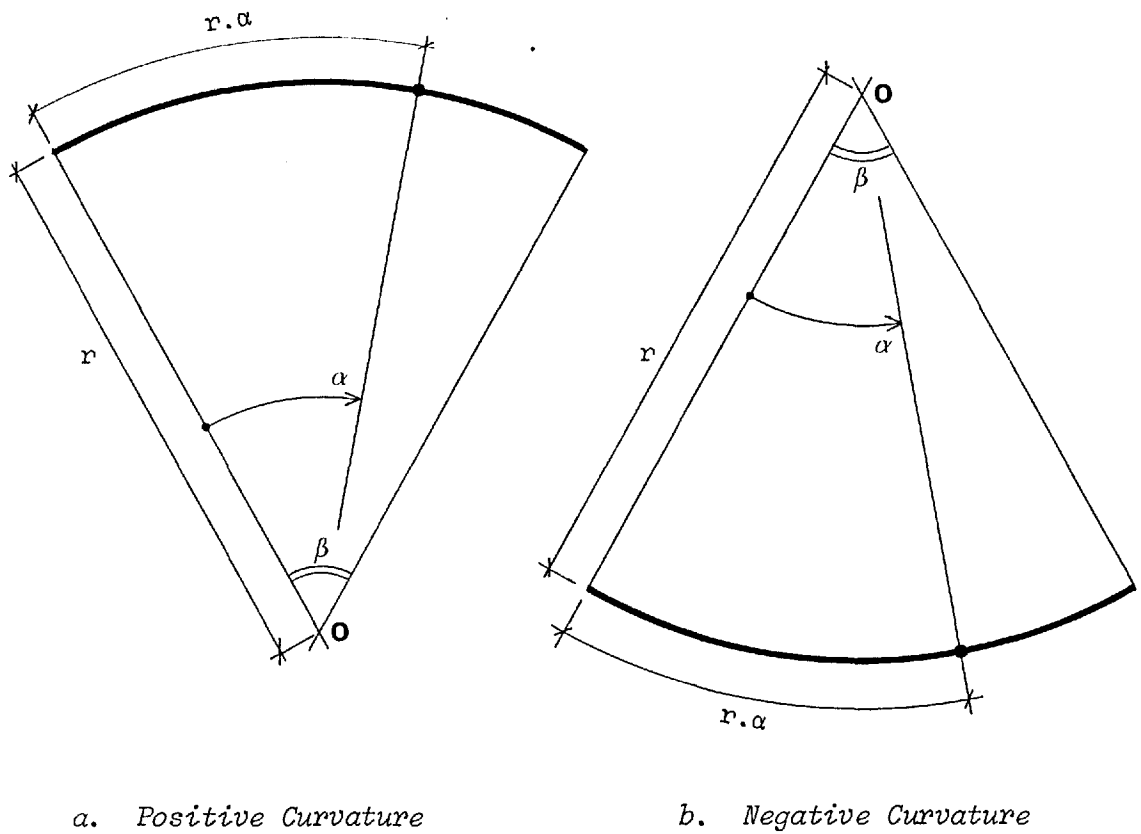
Figure 1.10 Direction of Curvature

CHAPTER TWO

THIN-WALLED BEAM THEORY

2.1   INTRODUCTION

The increasing use of thin-walled sections for structural

engineering applications is largely attributable to the development of

high performance materials and to improvements in construction

techniques.   However, the type of cross-section employed (*i.e.* open,

closed or multi-cellular) is generally determined by the requirements

of the particular structure and need not be the best suited to resist

the applied loading.   The different structural mechanics associated

with the various cross-sectional configurations are therefore con-

sidered here separately, although an approximation will later be

introduced to enable the subsequent development of analytical methods

to be equally applicable to all types of section.

This introductory chapter closely follows the work by

Dabrowski[25] and provides most of the basic expressions required later

in the thesis.   Wherever possible the same notation has been used to

avoid confusion although many of the formulae have had to be modified

in order to comply with the sign conventions defined in §1.4.

While Dabrowski includes the effects of member curvature in

the development of the fundamental equations, these effects are not

considered in the derivation of the basic structural mechanics which

are therefore equally applicable to both straight and curved members.

Recently, Konishi and Komatsu[53] have proposed a more rigorous treat-

ment of the structural mechanics of thin-walled sections in which

curvature effects are fully considered at every stage;   the resulting

modifications to the various cross-sectional and sectorial expressions

are summarized in Appendix 1.   Whether or not such a refinement is

warranted for curved girders of dimensions typically found in civil engineering practice is discussed more fully in Chapter 4 with reference to two complex road bridges.

2.1.1 Historical Review

St. Venant's original work on the twisting of circular and prismatic shafts was conducted in the middle of the last century, and is generally considered to be the first detailed theoretical treatment of the subject of pure torsion. By the beginning of this century the usefulness of his theory had been extended to include complex cross-sections by Prandtl's membrane analogy; Bredt had also introduced the concept of shear flow around the periphery of closed box sections. However, at this time, it was still not appreciated that the transverse distribution of shear could be significantly affected by restraint of warping displacements.

Timoshenko has been credited[50] with the discovery of warping torsion which he called *torsion with flange bending*; his observations were first published in 1905. Apart from notable contributions by Maillart and Eggenschwyler (1921), who introduced the concept of the shear centre, little work of any real consequence was published for a further twenty-five years.

Undoubtedly, much is owed to aeronautical engineers for the continued development of the subject. Wagner and Kappus proposed a general theory for open sections and Argyris and Dunne[7] introduced a theory for closed sections in which the member was idealised as an assemblage of shear walls and direct stress carrying elements. This work, including many other aspects relevant to aircraft engineering, has since been presented in books by Kuhn[55] and more recently by Megson[74].

The now celebrated book by Vlasov[109] has only been obtainable as a translation into English since 1961. However, it must have been available in Russia since the early 1940's and deals with the problem of mixed torsion in a quite exceptional way. It is generally recognized that Vlasov originated the use of *sectorial* co-ordinates and other terms which permitted thin-walled sections to be treated more logically as an extention of existing beam theory. The general formulation of the problem in these terms also enabled further theoretical developments to take place. Notable in this respect is the study by Benscoter[11] into the effects of shear deformation on the warping behaviour of closed sections. His assumptions regarding the nature of cross-sectional warping displacements have been widely accepted and allow a similar theoretical approach to be adopted for both open and closed sections.

Early work on curved girders was carried out by Unmanskii, although Dabrowski was first to derive the fundamental equations for non-deformable curved box girders, subject to non-uniform torsion, in 1965. A translation of more recent work by Dabrowski[25] deals with all aspects of curved girder analysis although the distribution of cross-sectional stresses is better covered by Konishi & Komatsu[53].

The generally poor understanding of the whole subject of mixed torsion by British engineers is largely explained by the dominance of foreign theoreticians (in particular Germans and East Europeans) and by the limited number of translations available. Although most recent work is still only to be found in isolated papers in the technical press, enthusiastic presentations of the subject in books by Kolbrunner and Basler[50] and by Zbirohowski-Koscia[122] (open sections only) are helpful.

Finally, while this is not intended as a thorough and complete bibliography on the subject of torsion, it does provide a summary of those engineers who have made significant contributions, some of whom are mentioned elsewhere in this thesis. At the same time it shows how thin-walled sections have only recently been treated as an extension to existing beam theory, especially in the case of curved members.

2.1.2   Sectorial Properties

Simple beam theory is effectively employed in the analysis of thick-walled and solid beams, subject to applications of direct force, bending moment and St. Venant's torsion. However, it is not sufficiently refined to explain the additional stresses created by warping restraint and in early work recourse to complex plate or shell theory was necessary. Vlasov's alternative approach proved much more attractive since he treated thin-walled, thick-walled and solid members as special cases of the same general theory. For this to be possible, he established new cross-sectional functions, denoted sectorial properties, to supplement those already used in simple beam theory.

It is possible, for example, to define the position of any point on the cross-section by the co-ordinates x, y, once the principal system axes have been established at the centroid. So, in exactly the same way, Vlasov created sectorial co-ordinates, ω (units: length^2), the distribution of which is determined from a knowledge of the shear centre position. By integrating this term and the square of this term over the entire cross-sectional area, it is also possible to calculate a sectorial shear function, S_w (units:length^4), and a warping moment of inertia, I_w (units:length^6), respectively. These

are directly analogous to the familiar shear functions S_x, S_y, and
second moments of area I_x, I_y, used in simple beam theory.

Stress Equations

If the doubly-symmetric section shown in fig. 2.1 is subject
to constant torque, then the member undergoes pure twist, fig. 2.1a.
This results in rigid-body rotations of the flanges together with a
transverse distribution of warping displacement which is identical at
any section along the length of the beam.   If at all restrained (fig.
2.1b), bending moments are created in the flanges which may be alter-
natively represented by the system of self-equilibrating end· forces, P,
shown in fig. 2.1c.   Such a system has no resultant direct force or
components of bending moment but may be expressed as a pair of equal and
opposite moments P.b, separated by the distance h, or by a pair of equal
and opposite moments P.h, separated by the distance b (fig. 2.1c).

This simple interpretation of the stress resultant due to
warping restraint has resulted in it being referred to as a *bimoment*
(units:force x $length^2$).   In this example the bimoment is equivalent
to the moment in one of the flanges multiplied by the distance between
them (*i.e.* B = P.b.h) and has the longitudinal distribution shown in
fig. 2.1d.   Shear stresses are also induced by warping restraint and
thus the total applied torque, T, is now resisted by a combination of
St. Venant torsion, T_{sv}, and warping torsion, T_w.   Although only
warping torsion exists at the fixed end, both components of torsion
are present elsewhere (fig. 2.1e) in a ratio which is dependent upon
the sectorial properties of the section and the distance from the point
of restraint.

It will be shown later in this chapter how the various terms
described here can be incorporated into the following normal and shear
stress equations:
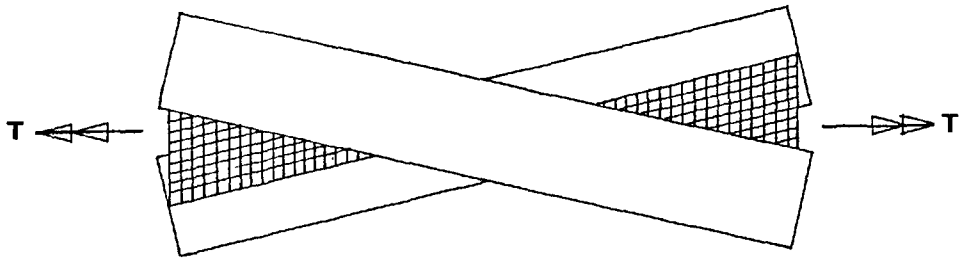
a. Pure Torsion
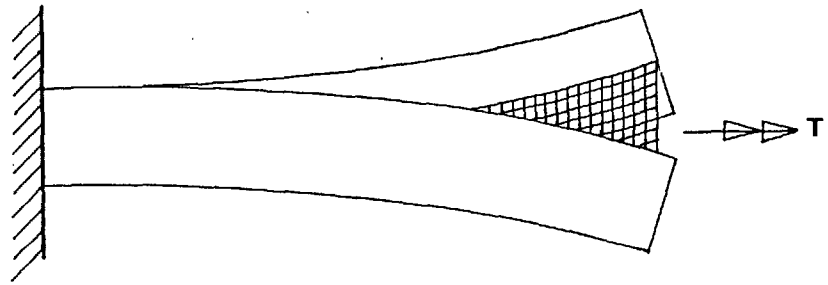
b. Restrained Torsion
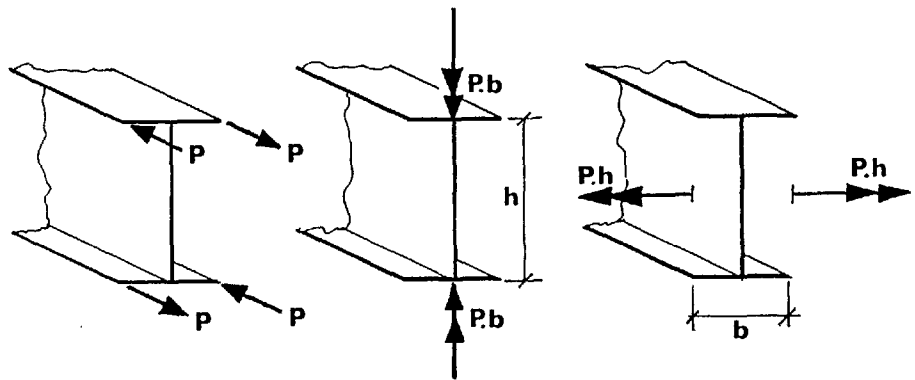
c. Representation of Bimoment
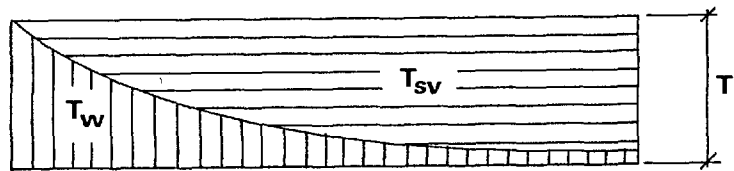
d. Distribution of Mixed Torsion
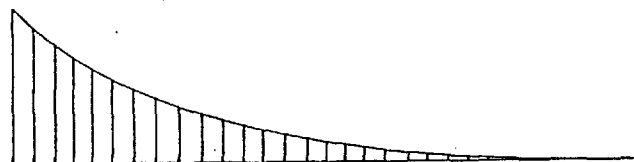
e. Bimoment Distribution

Figure 2.1   Typical I-Section Beam subject to Twist

$$\sigma = \frac{N}{A} + \frac{M_x \cdot y}{I_x} + \frac{M_y \cdot x}{I_y} + \frac{B \cdot \omega}{I_w}$$

and

$$\tau = \frac{V_y \cdot S_x}{\delta \cdot I_x} + \frac{V_x \cdot S_y}{\delta \cdot I_y} + \frac{2T_{sv} \cdot n}{I_d} - \frac{T_w \cdot S_w}{\delta \cdot I_w}$$

$\left.\right\}$ 2.1

By neglecting the last term in each equation, these are readily reduced to the form commonly used in simple beam theory.

Due to the connectivity conditions present in closed, open/closed and multi-cellular sections, the derivation of the various parameters for these configurations is somewhat different. In such cases the sectorial co-ordinate is denoted $\hat{\omega}$ while the warping shear function and moment of inertia are represented by the expressions $S_{\hat{w}}^{-}$ and $I_{\hat{w}}$ respectively. Any applied torque is now resisted entirely by St. Venant torsion in the form of constant peripheral shear flows and, although additional shear stresses (given by the derivative of the bimoment, B') are also present, they form a self-equilibrating system with zero resultant torsion. The direct and shear stress equations for sections with closed parts are thus given by

$$\sigma = \frac{N}{A} + \frac{M_x \cdot y}{I_x} + \frac{M_y \cdot x}{I_y} + \frac{B \cdot \hat{\omega}}{I_{\hat{w}}}$$

and

$$\tau = \frac{V_y \cdot S_x}{\delta \cdot I_x} + \frac{V_x \cdot S_y}{\delta \cdot I_y} + \frac{T}{\delta \cdot \Omega} - \frac{B' \cdot S_{\hat{w}}^{-}}{\delta \cdot I_{\hat{w}}}$$

$\left.\right\}$ 2.2

2.1.3 Assumptions

The kinematics of deformation associated with thin-walled beams are governed by an hypothesis which is more general than the Bernoulli hypothesis of plane cross-sections. In particular the section must be allowed to warp out of plane without undergoing cross-sectional distortion. In order to comply with this requirement in the development of the theory, it is necessary to adopt the concept of

closely-spaced diaphragms, rigid in their own plane but infinitely flexible in the direction of the longitudinal member axis. This assumption of zero distortion is never completely satisfied in practice, although for the large majority of concrete box girder bridges it does not lead to significant inaccuracies in the analysis.

In the subsequent development of thin-walled theory variations in stress and deformation across the wall thickness have been neglected. Clearly, for these simplifications to be acceptable, certain restrictions must be placed on the various cross-sectional dimensions. Vlasov defines a thin-walled beam as a structure having the form of a long, prismatic shell[70]. The shell thickness is small in comparison with any characteristic dimension of the cross-section while the cross-sectional dimensions are small compared with the overall length. He further states the following limiting criteria for which the theory is generally valid:

$$\frac{\text{shell thickness}}{\text{width or depth of cross-section}} \leqslant 0.1$$

and

$$\frac{\text{width or depth of cross-section}}{\text{length of shell}} \leqslant 0.1$$

From a parametric study of box girder structures[102] it is clear that the first of these criteria is not always satisfied, especially in respect of the web thickness/height ratio. However, it will be demonstrated in §2.5.3, in the case of an idealized single cell box girder with side cantilevers, that the assumption of thin-walled behaviour leads to an under-estimation of torsional stiffness of less than 10%, even for sections with web thickness/height ratios in excess of 0.3. Errors of a similar order are also apparent in a series of existing single cell concrete box girder bridges for which variations

in torsional stiffness have also been calculated.   These results indicate that disregarding the effects of secondary shear has only a small influence on the longitudinal distribution of the various stress resultants, although significant variations in the transverse distribution of both direct and shear stress are still possible. Kollbrunner and Basler[50], for example, suggest that the cross-sectional area should be less than one fifth of the area enclosed by the median line of the section if errors in the calculation of maximum shear stress are not to exceed 10%.   For box girders of approximately square cross-section, this requirement is similar to the first of those specified by Vlasov.   However, for rectangular sections with large aspect ratios, this criterion can require wall thickness/height ratios very much less than 0.1 and is a condition rarely satisfied in practice.   This subject has been further investigated in §2.5.3 for the series of existing structures previously mentioned.   Errors of 60-80% between the mean value of shear stress and the maximum value at the extreme fibre were common in these bridges, particularly in the support region of those structures displaying a variable cross-section.

With reference to the second of Vlasov's limiting criteria, Dabrowski[25] states that the theory is also suitable where the span length exceeds the cross-sectional breadth (as measured between the outer webs) by a factor of only three to four.   He considers this to be sufficient for thin-walled beam action to develop, thus extending the range of application of the theory to include the large majority of concrete box girder bridges.

2.2 OPEN SECTIONS

2.2.1 Pure (St. Venant) Torsion

The circular curved girder, shown in fig. 2.2a, is assumed to be simply supported, free from longitudinal restraint and subject to a constant torque, T, along its length.
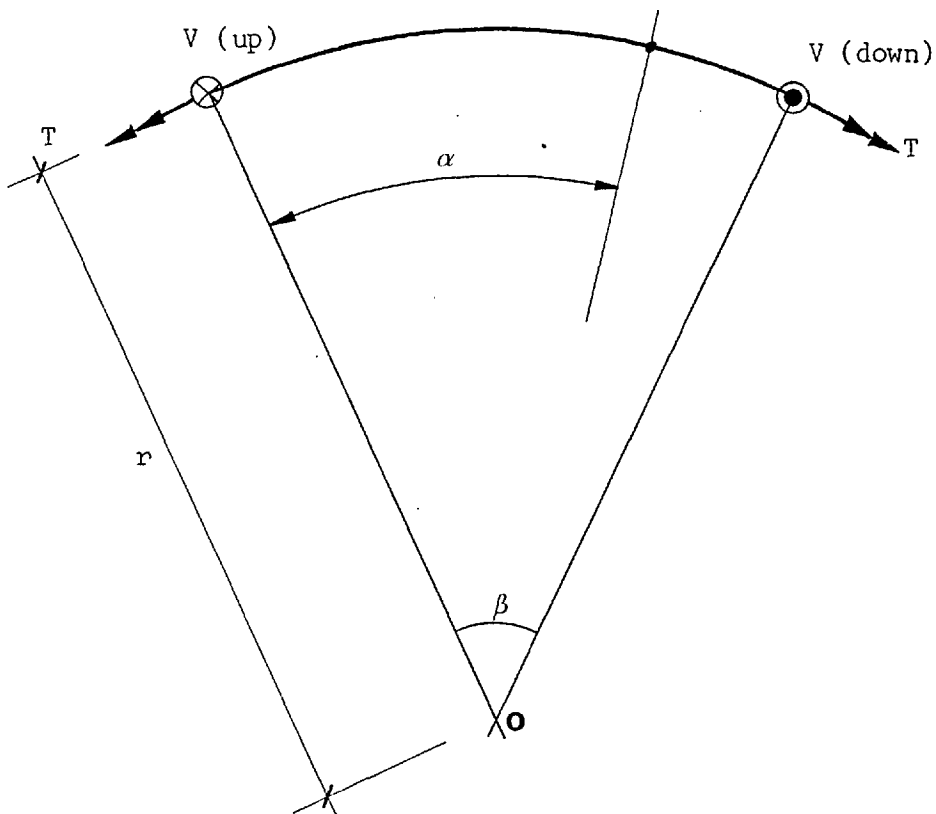
Figure 2.2a   The Circular Curved Girder subject to Pure Torsion

Equilibrium of the system is maintained by a pair of equal but opposite vertical shear forces, V, at the supports, of magnitude

$$V = T/r \qquad\qquad 2.3$$

and the distribution of torsion and bending moment along the beam
is given by

$$T_\alpha = T.\cos(\beta-\alpha) + Vr(1-\cos(\beta-\alpha)) = T$$

$$\text{and} \quad M_\alpha = -T.\sin(\beta-\alpha) + Vr.\sin(\beta-\alpha) = 0 \qquad \Big\} \quad 2.4$$

Now consider the positive face of the typical thin-walled
member, depicted in fig. 2.2b, in which the displacements in the tangential
and external normal directions have been denoted u_s and u_n, respectively.
Together with the longitudinal component, w, they form the displacement
system at any point (s, n) on the cross-section. At this stage, the
shear centre position, S, and the actual initial radius (s=0) are unknown
and must be arbitrarily selected as a basis for the analysis.
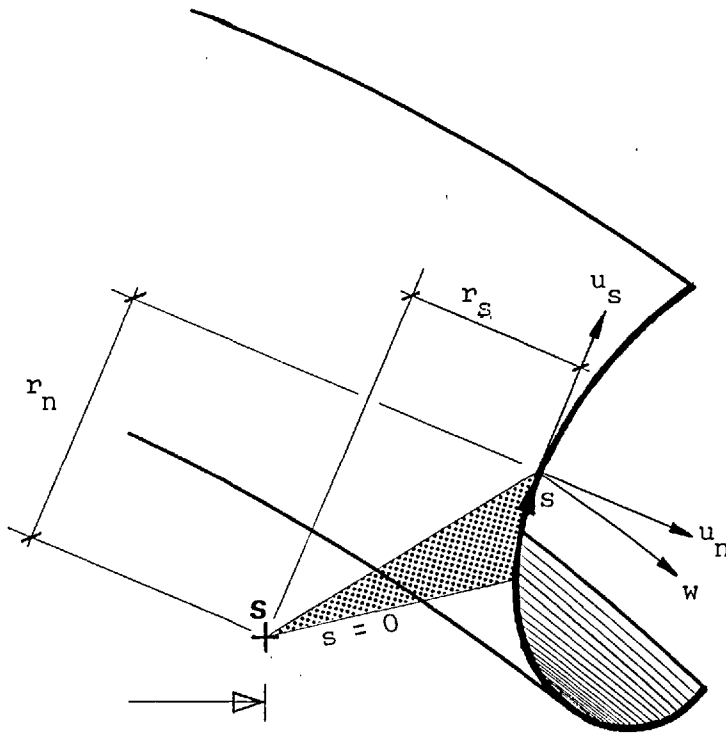
Figure 2.2b The Displacement System, u_s, u_n, w

Since the stress components σ_s, σ_n and τ_{sn} are zero at the free boundary edges of the section and are generally very small elsewhere, their effect has been neglected in the subsequent analysis. However, the three remaining components of strain may be expressed in terms of the newly defined displacement system, as

$$\left.\begin{array}{rcl} \varepsilon_\alpha & = & \dfrac{1}{r} \cdot \dfrac{\partial w}{\partial \alpha} \\[2mm] \gamma_{s\alpha} & = & \dfrac{\partial w}{\partial s} + \dfrac{1}{r} \cdot \dfrac{\partial u_s}{\partial \alpha} \\[2mm] \gamma_{n\alpha} & = & \dfrac{\partial w}{\partial n} + \dfrac{1}{r} \cdot \dfrac{\partial u_n}{\partial \alpha} \end{array}\right\} \qquad 2.5$$

and these equations are equally valid for open and closed sections, subject to all combinations of applied load.

For the special case of pure torsion, longitudinal warping is completely unrestrained and has an identical transverse distribution at any section along the beam. Accordingly, the first of eqns. 2.5 equates to zero with the result that no axial stresses are developed under this form of loading. It may also be shown[74] that $\gamma_{s\alpha}$ is zero on the median line of the section and that $\gamma_{n\alpha}$ is zero everywhere across the wall thickness. Noting, from fig. 2.2, that

$$\left.\begin{array}{rcl} \dfrac{1}{r} \cdot \dfrac{\partial u_s}{\partial \alpha} & = & \dfrac{r_s}{r} \cdot \dfrac{d\phi}{d\alpha} \\[3mm] \text{and} \quad \dfrac{1}{r} \cdot \dfrac{\partial u_n}{\partial \alpha} & = & \dfrac{r_n}{r} \cdot \dfrac{d\phi}{d\alpha} \end{array}\right\} \qquad 2.6$$

the two remaining expressions in eqn. 2.5 may be rewritten as

$$\left.\begin{array}{rcl} \gamma_{s\alpha} & = & \dfrac{\partial w}{\partial s} + \dfrac{r_s}{r} \cdot \dfrac{d\phi}{d\alpha} = 0 \quad \text{(on the median line)} \\[3mm] \text{and} \quad \gamma_{n\alpha} & = & \dfrac{\partial w}{\partial n} + \dfrac{r_n}{r} \cdot \dfrac{d\phi}{d\alpha} = 0 \quad \text{(everywhere)} \end{array}\right\} \qquad 2.7$$

Here, r_s and r_n represent the distance from the assumed shear centre

position to the tangent and external normal, respectively, and ϕ is

the reduced angle of rotation, given by

$$\phi = \Phi - v/r \qquad\qquad 2.8$$

Clearly, in straight beams the vertical displacement, v, of the shear

centre does not influence the rotation of the section and $\phi = \Phi$

(the total rotation).

By integrating eqn. 2.7, and observing that r_n is not a

function of n, we have

$$w_s = \frac{1}{r} \cdot \frac{d\dot\phi}{d\alpha} \int_o^s r_s \cdot ds + w_{so}$$

$$\left.\begin{array}{c}\end{array}\right\} \qquad 2.9$$

$$\text{and} \quad w_n = \frac{1}{r} \cdot \frac{d\dot\phi}{d\alpha} \cdot n \cdot r_n + w_{no}$$

where w_{so} and w_{no} are constants of integration equivalent to the

warping displacements at s = 0 and n = 0, respectively. There are,

therefore, two distinct but complementary forms of warping deformation.

The first of eqns. 2.9 represents the displacement profile on the median

line of the section only, while the second describes the distribution

across the wall thickness. The latter, denoted secondary warping, is

generally small for thin-walled members and is not discussed here

further.

By adopting Vlasov's definition of the sectorial co-ordinate,

thus:

$$\omega = \int_o^s r_s \cdot ds - w_{so}/\phi' \qquad\qquad 2.10$$

the expression for primary warping (the first of eqns. 2.9) may now

be written as

$$w = -\phi' \cdot \omega \qquad\qquad 2.11$$

where ϕ' represents the first derivative of the reduced angle of rotation, etc. The magnitude of the sectorial co-ordinate, ω (units : length^2), is equivalent to twice the shaded area shown in fig. 2.2 and is directly influenced by the initial choice of the centre of twist and the origin of the peripheral co-ordinate, s.

However, we are now in a position to determine the true location of these points, since a necessary condition for the free-flexural state of warping is that there should be no resultant bending moment or direct force at any section. Accordingly, we have

$$\int_A \sigma x.dA \quad = \quad \int_A \sigma y.dA \quad = \quad \int_A \sigma.dA \quad = \quad 0 \qquad\qquad 2.12$$

where the integrations are effective over the entire cross-sectional area. With σ determined from eqn. 2.11 and the first of eqns. 2.5, these conditions may be alternatively expressed as

$$\int_A \omega x.dA \quad = \quad \int_A \omega y.dA \quad = \quad \int_A \omega.dA \quad = \quad 0 \qquad\qquad 2.13$$

where the first two terms are sufficient to establish the true shear centre position and the third enables the initial radius to be selected such that $w_{so} = 0$ when $s = 0$. In this way the constant of integration in eqn. 2.10 is eliminated and the *principle* sectorial co-ordinate is given by

$$\omega \quad = \quad \int_o^s r_s.ds \qquad\qquad 2.14$$

where r_s is now measured from the true shear centre position and the origin of the peripheral co-ordinate system ($s = 0$) is taken to coincide with a point of zero warping displacement.

Indeed, the whole procedure is directly analogous to finding the centroid and the orientation of the principle neutral axes in the case of pure bending, and is examined in more detail in §5.

Now remembering that $\gamma_{n\alpha} = 0$, the only non-zero component of shear stress is given[74] by

$$\tau_{sv} = G.\gamma_{s\alpha} = 2Gn\phi' \qquad 2.15$$

This is linearly distributed across the wall thickness, as shown in fig. 2.3, and reaches a maximum value at the extreme fibres of the section, equivalent to:

$$\tau_{sv(max)} = \pm G\delta\phi' \qquad 2.16$$
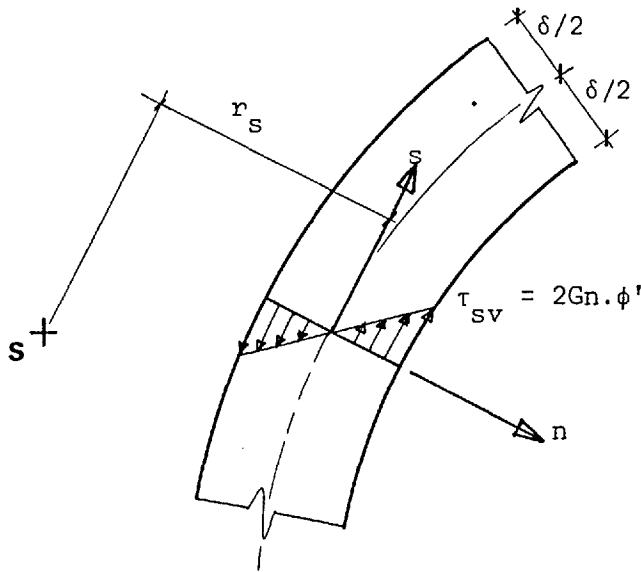
Figure 2.3   Distribution of St. Venant Shear Stress, τ_{sv}, *in Open Sections*

Finally, the torque, just as for straight members, may be expressed in the following general form:

$$T_{sv} = GI_d\phi' \qquad 2.17$$

where I_d, the second moment of area for pure torsion, is determined from

$$I_d = \frac{1}{3} \int_s \delta^3.ds \qquad 2.18$$

2.2.2   Non-Uniform (Warping) Torsion

If warping is prevented or partially restrained, the axial displacement at any point on the cross-section is no longer identical at all sections along the beam. The system of direct stresses, so formed, is determined by differentiating eqn. 2.11 with respect to the initially curved shear axis and substituting for w' in the first of eqns. 2.5, thus:

$$\sigma = E . \varepsilon_\alpha = - E \phi'' \omega \qquad\qquad 2.19$$

From this expression it is clear that the transverse distribution of longitudinal stress is directly proportional to the sectorial co-ordinate, ω, thereby inducing a complementary system of warping shear stresses here denoted τ_w.

By considering the equilibrium of the differential wall element r.dα, ds shown in fig. 2.4, the following relationship between the shear flow, F_w ($= \tau_w.\delta$), and the unit direct force, $\sigma.\delta$, is obtained:

$$\frac{1}{r} . \frac{\partial \sigma}{\partial \alpha} . \delta + \frac{\partial F_w}{\partial s} = 0 \qquad\qquad 2.20$$

After substitution for σ from eqn. 2.19 and integrating, this takes the form

$$F_w = E \phi''' \int_0^s \omega .ds + F_{wo} \qquad\qquad 2.21$$

However, if the integration is started at a free edge, the constant of integration, F_{wo}, is zero and eqn. 2.21 reduces to

$$F_w = E \phi''' S_w \qquad\qquad 2.22$$

where S_w is an additional sectorial function, given by

$$S_w = \int_0^s \omega\delta . ds \qquad\qquad 2.23$$
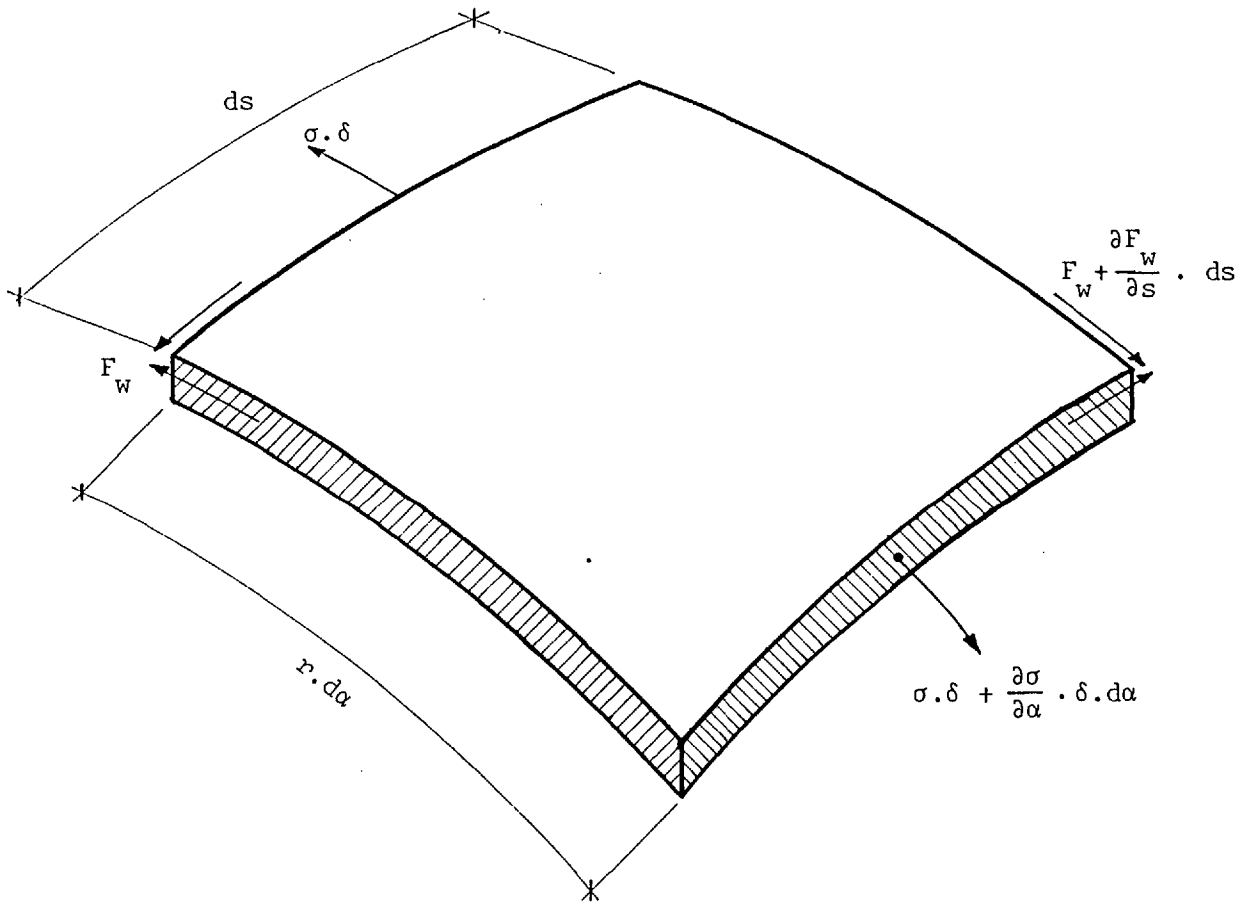
Figure 2.4   Differential Wall Element, r.dα,ds

Both sectorial parameters ω and S_w are functions of the

peripheral co-ordinate, s, and the transverse distribution of each

is depicted in fig. 2.5 for some typical open sections.

The bimoment, which is a measure of the magnitude of the

direct stress system created by warping restraint, may now be defined

as

$$B = \int_A \sigma\omega.dA \qquad\qquad 2.24$$
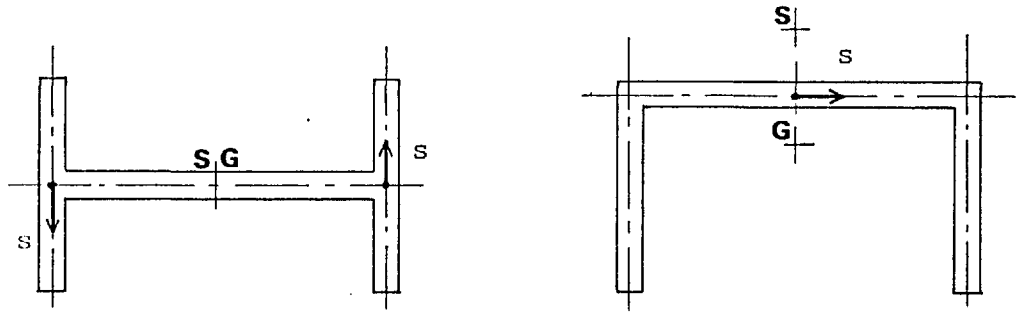
a. *Origin of Peripheral Co-ordinate,* s
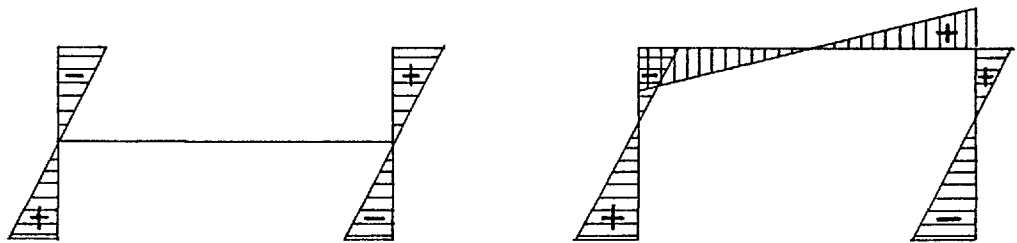
b. *Sectorial Co-ordinate,* ω
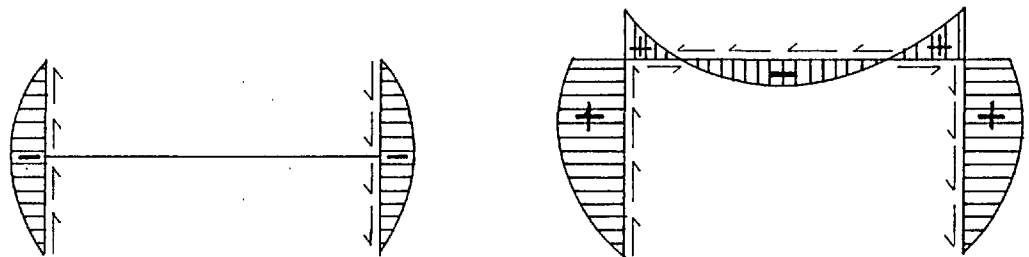
c. *Sectorial Shear Function,* S_ω

Figure 2.5   Transverse distribution of Sectorial Parameters
in Typical Channel and I-Sections

where, once again, the integration is taken over the entire cross-sectional area. On substitution for σ in this expression from eqn. 2.19, we have

$$B = - EI_w \phi''$$
<div align="right">2.25</div>

where I_w is referred to as the warping moment of inertia, and is given by

$$I_w = \int_A \omega^2 \, dA$$
<div align="right">2.26</div>

Now the component of shear stress, τ_w, induced by warping restraint, is clearly a function of S_w only (eqn. 2.22) and, in accordance with the simplifying assumptions made regarding secondary warping deformations, is constant across the wall thickness (fig. 2.6). By resolving the corresponding shear forces about the shear centre,
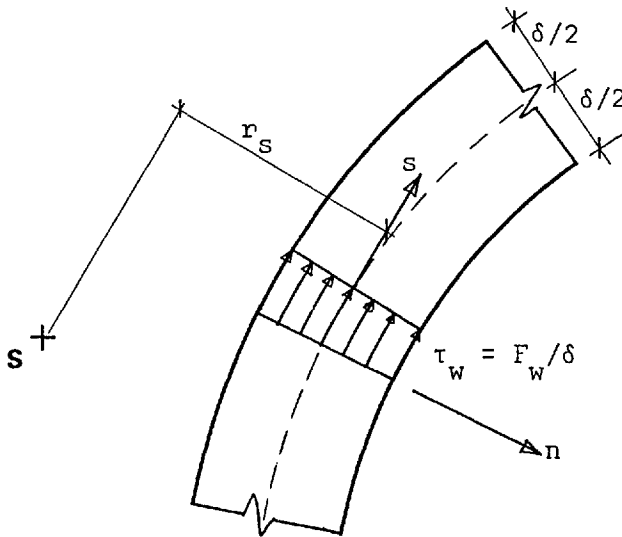
Figure 2.6 Distribution of Warping Shear Stress τ_w

the component of applied torque resisted by restrained warping is given by

$$T_w = \int_s F_w \cdot r_s \cdot ds$$
<div align="right">2.27</div>

which, on introduction of eqns 2.14 and 2.22, takes the form

$$T_w = E \phi''' \int_A S_w \cdot d\omega \qquad\qquad 2.28$$

By partial integration of this expression, in which it should be noted that $dS_w = \omega \cdot dA$, we have

$$T_w = - E I_w \phi''' \qquad\qquad 2.29$$

which is directly equivalent to B', the first derivative of the bimoment, defined in eqn. 2.25.

For the general case, ·the components of torsion due to pure and warping shear stresses are both present and must clearly equate with the total applied torque, T, such that

$$T = T_{sv} + T_w \qquad\qquad 2.30$$

However, it is also possible for torsional shear stresses to develop in the absence of any applied torque (e.g. the application of an external bimoment), in which case, $T_{sv} = - T_w$.

Stress Equations

By combining eqns. 2.15 and 2.17 (in the case of pure torsion) and eqns. 2.22 and 2.29 (for warping torsion), the shear stress distribution for mixed torsion is found to be

$$\tau = \tau_{sv} + \tau_w = \frac{2T_{sv} \cdot n}{I_d} - \frac{T_w \cdot S_w}{I_w \cdot \delta} \qquad\qquad 2.31$$

Similarly, by eliminating the term $E\phi''$ from eqns. 2.19 and 2.25, the transverse distribution of direct stress due to restrained warping may be expressed as

$$\sigma = \frac{B \cdot \omega}{I_w} \qquad\qquad 2.32$$

Clearly, these stress components are supplementary to those created by bending and direct force and the complete stress equations for thin-walled members of open section are given by eqn. 2.1.

2.2.3   Fundamental Equations

Consider the differential beam element shown in fig. 2.7 in which the torque, T, and uniformly distributed torsion, t, are applied about the shear axis, and the bending moment, M_x, and direct force, N, are applied about the centroidal axis. The abscissa and ordinate of the shear centre S, with respect to the centroid G, are denoted x_o and y_o, respectively.

By taking moments about the tangent to the curved shear axis and dividing by r.dα throughout, the following relationship is obtained:

$$T' + t + \frac{1}{r} (M_x - N.y_o) = 0 \qquad 2.33$$

Furthermore, by using eqns. 2.17 and 2.29, the total applied torque (from eqn. 2.30) may be expressed by a differential equation in terms of the reduced angle of rotation only, given by

$$T = GI_d \phi' - EI_w \phi''' \qquad 2.34$$

By differentiating this equation and substituting for T' in eqn. 2.33, the fundamental equation governing the twist of open sections is obtained, thus:

$$\phi^{iv} - k^2.\phi'' = \frac{1}{r.EI_w} \left(t.r + M_x - N.y_o \right) \qquad 2.35$$

In this expression the term k (units:length^{-1}) is called the decay function and represents the ratio of torsional stiffnesses, such that

$$k = \sqrt{\frac{GI_d}{EI_w}} \qquad 2.36$$

a. *Section*

b. *Plan*

$$T + \frac{\partial T}{\partial \alpha} \cdot d\alpha$$

$$M_x + \frac{\partial M_x}{\partial \alpha} \cdot d\alpha$$

$$N + \frac{\partial N}{\partial \alpha} \cdot d\alpha$$
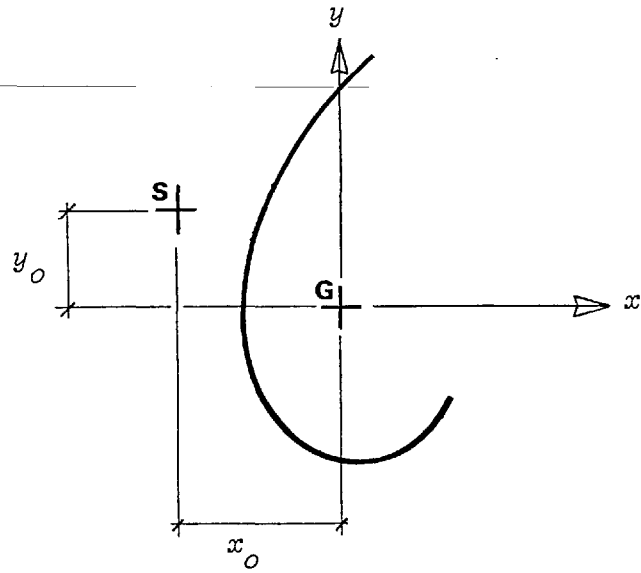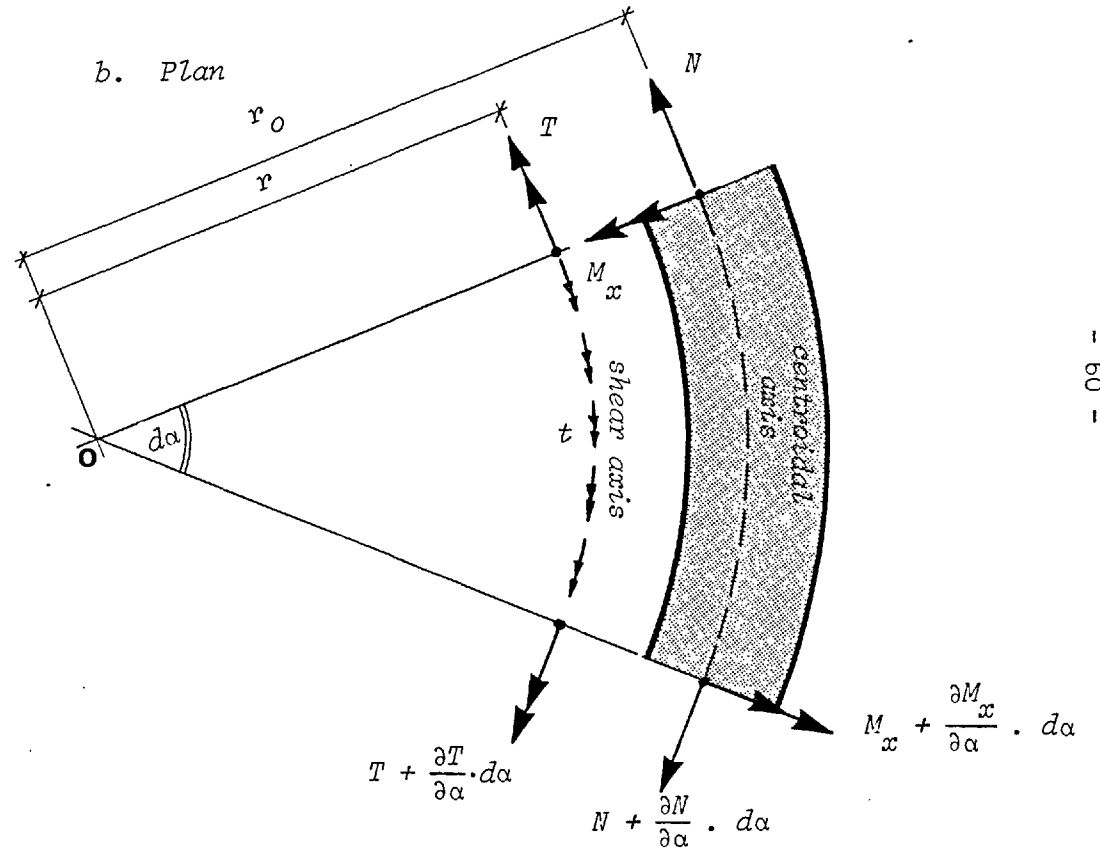
Figure 2.7   Differential Beam Element, r.dα

2.3   CLOSED AND OPEN/CLOSED SECTIONS

2.3.1   Pure (St. Venant) Torsion

In order to study the behaviour of this type of section under the application of pure torsion, an imaginary cut must first be made in the closed part. Shear stresses are developed in accordance with eqn. 2.15 and in exactly the same way as for open sections. They are linearly distributed across the wall thickness and are here denoted $\Delta\tau_{sv}$ (fig. 2.8a). In general, warping displacements of different magnitude will occur at the free edges of the cut and these must be equalised if the section is to be restored to its original form. This is achieved by applying a pair of equal but opposite shear forces at the imaginary cut with the result that a constant shear flow, F_{sv}, is formed around the entire perimeter of the closed part. The associated shear stresses, $\tau_{sv}(= F_{sv}/\delta)$, are constant across the wall thickness (fig. 2.8b) and the final distribution is shown in fig. 2.8c.

Clearly, the shear strain on the median line of the section is no longer zero and from the first of eqns 2.7, we now have

$$\gamma_{s\alpha} = \left(\frac{\partial w}{\partial s} + r_s.\phi'\right) = \frac{F_{sv}}{G.\delta} \qquad 2.37$$

where the shear deformation due to the vertical shear forces, V (from eqn. 2.3) has once again been neglected. By rearranging and integrating this expression the following relationship is obtained:

$$w_{s} - w_{so} = \int_{o}^{S} \frac{F_{sv}}{G.\delta} . ds - \phi' \int_{o}^{S} r_s.ds \qquad 2.38$$

in which the first integral only applies to the closed part of an open/closed section. Compatibility requirements are such that, on proceeding around the entire perimeter, there can be no resultant warping displacement, and accordingly
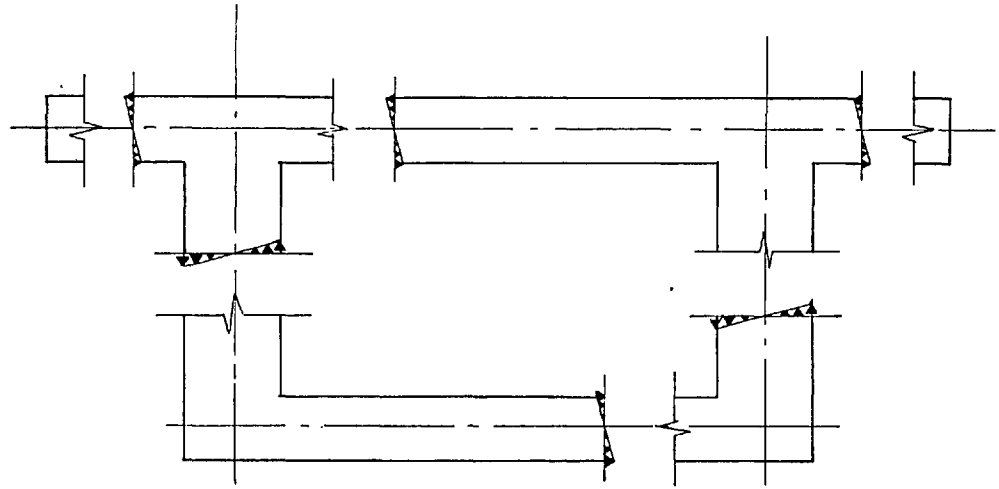
a. *Linearly Distributed Shear Stress*, $\Delta\tau_{sv}$
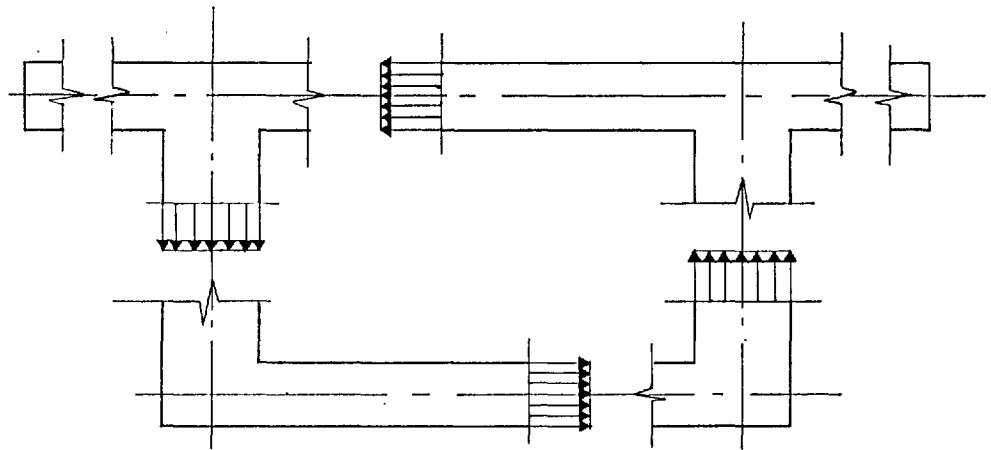
b. *Constant Distribution of Shear Stress in Closed Part*, τ_{sv}
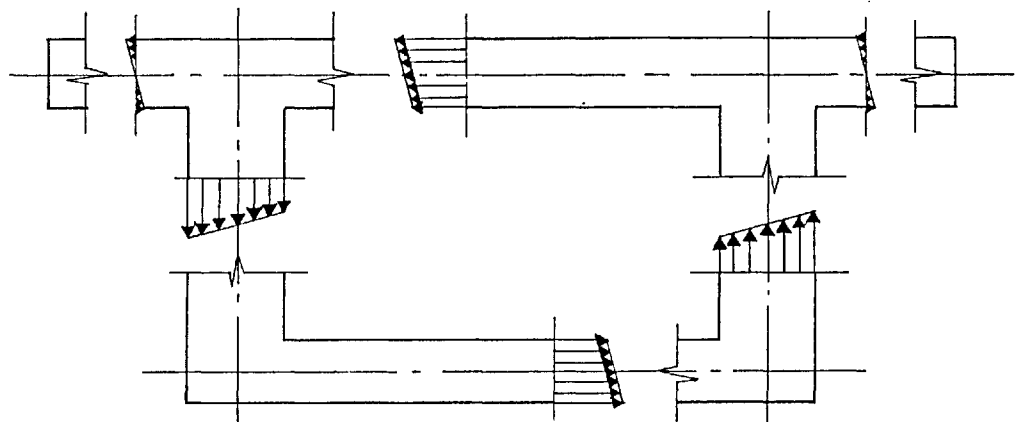
c. *Final Distribution of Shear Stress*, $\Delta\tau_{sv} + \tau_{sv}$

Figure 2.8   Distribution of Shear Stress in a Typical
              Single Cell Box Girder with Side Cantilevers

$$\oint \frac{F_{sv}}{G.\delta} \cdot ds - \phi'.\Omega = 0 \qquad\qquad 2.39$$

where Ω represents twice the enclosed area (or twice the enclosed area of the closed part of an open/closed section).

Now, by eliminating the constant shear flow, F_{sv}, from eqns 2.38 and 2.39, the relative warping displacement may be expressed in terms of the unit twist only, in the following way:

$$w_s - w_{so} = \phi'.\hat{\omega} \qquad\qquad 2.40$$

In this expression the term $\hat{\omega}$ is given by

$$\hat{\omega} = \omega - \frac{\Omega}{\oint \frac{ds}{\delta}} \int_o^s \frac{ds}{\delta} \qquad\qquad 2.41$$

and is called the *reduced* sectorial co-ordinate since it is equivalent to the sectorial co-ordinate, ω (calculated in accordance with eqn. 2.14), reduced by the second term which represents the shear deformation of the closed part of the section.

The true shear centre and the position of zero warping displacement may now be calculated in exactly the same way as for open sections. However, in this case the term ω in eqn. 2.13 must be replaced throughout by the reduced sectorial co-ordinate, $\hat{\omega}$. This then enables the principle sectorial co-ordinates to be determined and, by selecting $s = 0$ such that $w_{so} = 0$, eliminates the constant of integration from eqn. 2.40.

By taking moments about the shear centre, the torsional resistance is given by

$$T_{sv} = F_{sv} \oint r_s.ds + G \phi' \int_s \frac{\delta^3}{3} . ds \qquad\qquad 2.42$$

where the last term is due to the effect of the linearly distributed

shear stress, $\Delta\tau_{sv}$, which has been previously defined in eqns. 2.16 and 2.18. By substituting for the constant shear flow, F_{sv}, from eqn. 2.39 and noting that $\oint r_s \cdot ds = \Omega$, eqn. 2.42 may now be expressed in the following form:

$$T_{sv} = G\phi'\left[\frac{\Omega^2}{\oint\frac{ds}{\delta}} + \int_s \frac{\delta^3}{3} \cdot ds\right] \qquad 2.43$$

However, in practice, the error associated with neglecting the last term in brackets in this expression is small, in which case, from eqns 2.42 and 2.43, we have

$$T_{sv} = \Omega \cdot F_{sv} \qquad 2.44$$

and

$$T_{sv} = GI_d\phi' \qquad (2.17)$$

Here

$$I_d = \frac{\Omega^2}{\oint\frac{ds}{\delta}} \qquad 2.45$$

is the second moment of area for pure torsion for closed and open/closed sections. Eqn. 2.44 is better known as the Bredt-Batho formula[74] and the accuracy of the approximation is considered in greater detail in §2.5.3.

2.3.2   Non-uniform (Warping) Torsion

The warping displacement profile of a closed or open/closed section subject to pure twist is directly proportional to the sectorial function $\hat{\omega}$ (from eqn. 2.40). This term consists of the unit warping component, ω, as for open sections, reduced by the second term in eqn. 2.41 which is a measure of the shear deformation due to the connectivity requirements of the closed cell. When warping is restrained the shear stresses τ_w so produced have a modifying effect on the shear deformation term and it is no longer strictly correct to say $w_s = -\phi'.\hat{\omega}$, as is the case for pure torsion.

To avoid the theoretical complexities created by this interaction between warping stresses and shear deformation, Benscoter[11] assumed that the restrained warping displacements had an identical transverse distribution to those for pure torsion, but that they were no longer directly proportional to the unit twist, ϕ'. Having regard for this assumption eqn. 2.40 may now be rewritten as

$$w_s = -f'.\hat{\omega} \qquad\qquad 2.46$$

where the reduced angle of rotation, ϕ, has been replaced by a dimensionless warping function, f. Clearly, this is only an approximation to the true behaviour, but it has been widely accepted[25,38,70] and proven in the analysis of a large range of engineering structures.

The normal stress distribution and bimoment at a section, may now be defined as

$$\sigma = E.w_s' = -Ef''\hat{\omega} \qquad\qquad 2.47$$

and

$$B = \int_A \sigma\,\hat{\omega}.dA = -EI_{\hat{w}}.f'' \qquad\qquad 2.48$$

in which

$$I_{\hat{w}} = \int_A \hat{\omega}^2.dA \qquad\qquad 2.49$$

is the warping moment of inertia for closed sections.

The normal stresses, σ, due to warping restraint, induce additional shear flows, F_w, which are supplementary to the pure torsional shear flows, F_{sv}. Together their distribution is governed by equilibrium of the differential wall element shown in fig. 2.4. By eliminating σ from eqns. 2.20 and 2.47, and noting that

$$B' = -EI_{\hat{w}}f''' \qquad\qquad 2.50$$

we find that

$$F = F_{sv} + F_w = F_o - \frac{B'.S_{\hat{w}}}{I_{\hat{w}}} \qquad\qquad 2.51$$

in which the sectorial function, $S_{\hat{w}}$, for closed sections is given by

$$S_{\hat{w}} = \int_{0}^{s} \hat{\omega}.dA \qquad\qquad 2.52$$

In this instance the starting point for the integration cannot be selected at a free edge and generally $F_o \neq 0$. However, since the resultant of the total shear flow about the shear centre must be in equilibrium with the applied torque at a section, we have (from eqn. 2.51)

$$T = \oint F.r_s.ds = F_o \oint r_s.ds - \frac{B'}{I_{\hat{w}}} \int_s S_{\hat{w}}.r_s.ds \qquad 2.53$$

where the first term is only integrated around the closed part of the section. From this expression the initial shear flow F_o (at $s = 0$) is obtained, thus:

$$F_o = \frac{T}{\Omega} + \frac{B'}{\Omega.I_{\hat{w}}} \int_s S_{\hat{w}}.r_s.ds \qquad\qquad 2.54$$

and on substitution into eqn. 2.51 this yields the following relationship:

$$F = F_{sv} + F_w = \frac{T}{\Omega} - \frac{B'}{I_{\hat{w}}} . S_{\bar{\hat{w}}} \qquad\qquad 2.55$$

Here, the reduced sectorial function $S_{\bar{\hat{w}}}$ has been additionally defined as

$$S_{\bar{\hat{w}}} = S_{\hat{w}} - \frac{1}{\Omega} \int_s S_{\hat{w}}.r_s.ds \qquad\qquad 2.56$$

and its transverse distribution, together with those of the other sectorial parameters, is demonstrated in fig. 2.9 for a typical single cell box girder with cantilevers.

The total shear flow, F, in eqn. 2.55, may now be considered as comprising of two quite separate components. The first term is equivalent to the constant shear flow, F_{sv}, given by the Bredt-Batho formula (eqn. 2.44) and only occurs in the closed part of an open/closed section. The other term in eqn. 2.55 represents the secondary
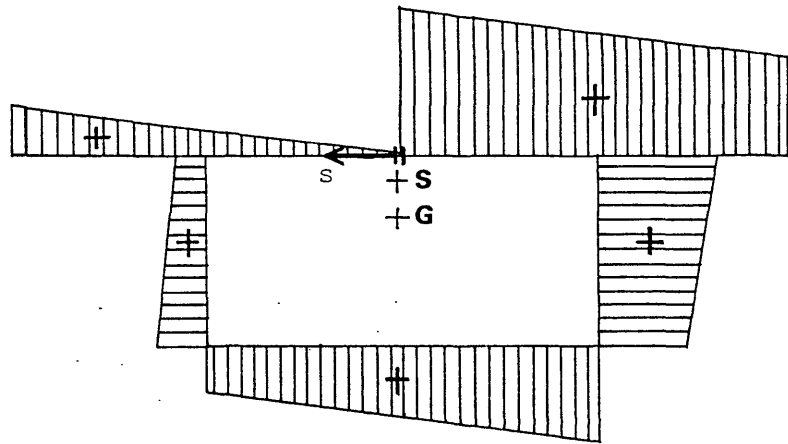
a. *Sectorial Co-ordinate,* ω
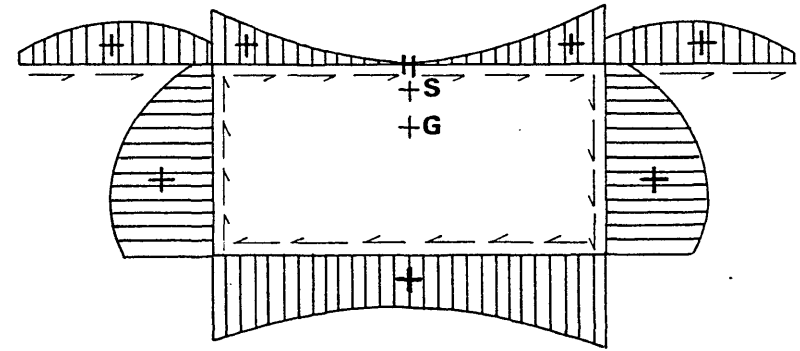
c. *Sectorial Shear Function,* $S_{\hat{\omega}}$
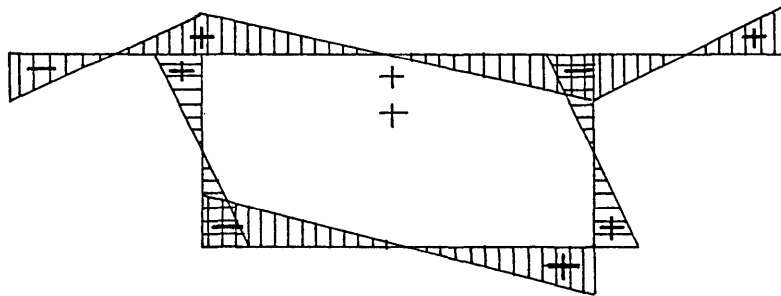
b. *Reduced Sectorial Co-ordinate,* $\hat{\omega}$
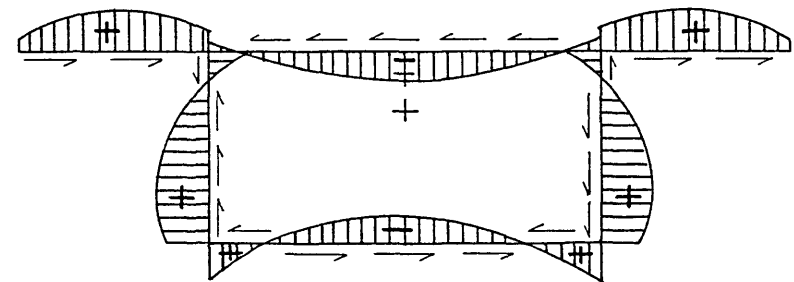
d. *Reduced Sectorial Shear Function,* $S_{\hat{\bar{\omega}}}$

Figure 2.9   *Transverse Distribution of Sectorial Parameters in Typical Single Cell Box Girder with Side Cantilevers*

shear flow, F_w, due to warping restraint. This extends over the entire cross-section and forms a self-equilibriating system with zero resultant torque.

Stress Equations

The total shear flow due to mixed torsion is constant across the wall thickness and the corresponding shear stress is simply obtained by dividing eqn. 2.55 by δ, thus:

$$\tau = \frac{T}{\Omega.\delta} - \frac{B'S_{\hat{w}}}{I_{\hat{w}}.\delta} \qquad 2.57$$

In the same way as for open sections, the direct stress component is derived directly from eqns. 2.47 and 2.48 and is given by

$$\sigma = \frac{B.\hat{\omega}}{I_{\hat{w}}} \qquad 2.58$$

When eqns. 2.57 and 2.58 are combined with the stress components due to bending and direct force, they provide the complete stress equations for thin-walled members of closed or open/closed section (eqn. 2.2).

2.3.3   Fundamental Equations

The shear strain relationship (eqn. 2.37), derived earlier for the case of pure torsion, is equally valid for mixed torsion and may be rewritten in the form

$$F = G\delta \left[\frac{\partial w_s}{\partial s} + r_s.\phi' \right] \qquad 2.59$$

Similarly, by integrating this expression around the entire perimeter of the closed part only, the connectivity condition (eqn. 2.39) is now given, in terms of the combined shear flow, F, by

$$\oint \frac{F}{G\delta} . ds = \Omega.\phi' \qquad 2.60$$

By using eqn. 2.55 to eliminate F from this expression, the following differential equation is obtained:

$$T = GI_d\phi' - EI_{\hat{w}}f''' \qquad 2.61$$

where use has been made of eqn. 2.50 and of the following geometric relationship:

$$\frac{I_d}{\Omega} \oint S_{\hat{w}}.\frac{ds}{\delta} = I_{\hat{w}} \qquad 2.62$$

However, by substituting for the warping displacement, w_s, from eqn. 2.46 (instead of from eqn. 2.40 for pure torsion) and noting the contents of eqn. 2.41, the total shear flow in eqn. 2.59 may be alternatively expressed as

$$F = G\left[(\phi' - f') \, r_s.\delta + \frac{\Omega.f'}{\oint \frac{ds}{\delta}} \right] \qquad 2.63$$

Once again, the applied torque at the section under consideration is obtained by resolving about the shear centre, thus:

$$T = \oint Fr_s.ds = G\left[(\phi'-f') \oint r_s{}^2.dA + \frac{\Omega.f'}{\oint \frac{ds}{\delta}} \oint r_s.ds \right] \qquad 2.64$$

This may be simplified and rearranged to give the following relationship:

$$\phi' = \mu f' + \frac{T}{GI_c} \qquad 2.65$$

where two new terms have been defined. The first is called the central second moment of area (units : length[4]) and is given by

$$I_c = \oint r_s{}^2.dA \qquad 2.66$$

in which the integration is carried out over the entire area of the closed part of the section only. The other term represents a dimensionless warping shear parameter of the following form:

$$\mu = 1 - \frac{I_d}{I_c} \qquad 2.67$$

where $0 < \mu < 1$

Now by substituting ϕ' from eqn. 2.65 into eqn. 2.61,
a differential equation is obtained in terms of the warping function,
f, only:

$$\mu T = \mu GI_d f' - EI_{\hat{w}} f'''$$ 2.68

On differentiation with respect to the longitudinal axis and on
consideration of the generally valid equilibrium condition (eqn. 2.33),
eqn. 2.68 may be expressed as:

$$f^{iv} - k^2.f'' = \frac{\mu}{r.EI_{\hat{w}}} \left[t.r + M_x - N.y_o \right]$$ 2.69

where the decay function, k, has been restated for closed and
open/closed sections, as

$$k = \sqrt{\mu \cdot \frac{GI_d}{EI_{\hat{w}}}}$$ 2.70

With the warping shear parameter, μ, equal to unity, eqn. 2.70
reduces to the form given in eqn. 2.36 for open sections. This express-
ion may therefore be considered as the general definition of the decay
function for all cross-sectional configurations. The function is also
frequently combined with the member length to form the dimensionless
product, $k\ell$, which is a more useful measure of the decay rate of warping
effects. Variations in this term and in the value of the warping
shear parameter are examined in §2.5.2 for a range of existing concrete
box girder bridges and for some typical open and closed sections.

2.4   MULTI-CELLULAR SECTIONS

Box girders of more than one cell display all the advantages associated with single cell configurations, namely, a very efficient distribution of stress throughout the cross-section, coupled with high flexural and torsional stiffness. They are frequently found in practice and enable the range of application of cellular structures to be greatly extended. However, while the structural mechanics governing the behaviour of these members are not significantly different from those of closed or open/closed sections, the situation is complicated by the fact that the shear flows in individual cells need no longer be identical.

2.4.1   Pure (St. Venant) Torsion

The relationship established in eqn. 2.60 simply ensures compatibility of warping displacements around the perimeter of closed sections. Here, it is restated as:

$$\phi' = \frac{1}{G\Omega_i} \oint_i F_{sv(i)} \cdot \frac{ds}{\delta_i} \qquad \qquad 2.71$$

where ϕ' refers to the unit twist of the complete multi-cellular section about the assumed shear centre, and the contour integral is taken around the entire perimeter of the ith cell only, the area of which is equal to $\Omega_i/2$ (fig. 2.10)
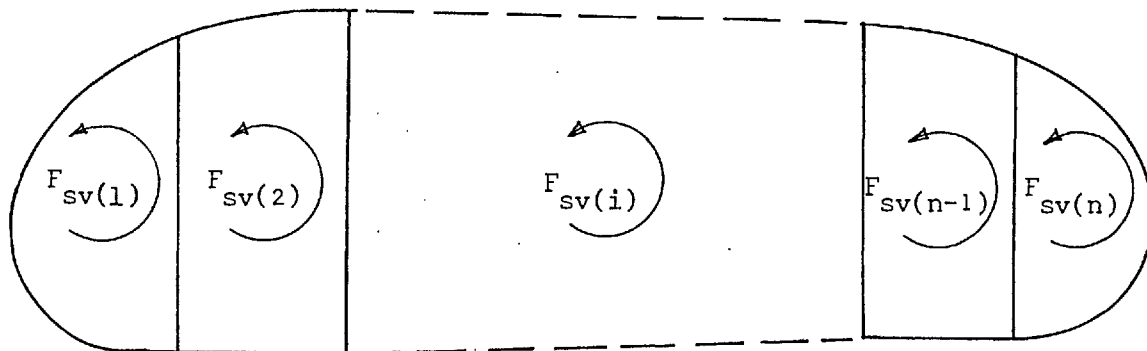
Figure 2.10   Idealised Multicellular Girder with n Cells

Under the application of pure torsion the shear flow, $F_{sv(i)}$, around each of the separate cells is constant and, consequently, the shear flow in any of the shared walls is equal to the difference of those in adjacent cells. If eqn. 2.71 is now applied successively to each of the cells shown in fig. 2.10, a series of n simultaneous equations is obtained of the general form:

$$\phi'G\Omega_i = -F_{sv(i-1)} \cdot \frac{s_{i-1,i}}{\delta_{i-1,i}} + F_{sv(i)} \cdot \oint_i \frac{ds}{\delta_i} - F_{sv(i+1)} \cdot \frac{s_{i,i+1}}{\delta_{i,i+1}} \qquad 2.72$$

in which $s_{i,i+1}$, $\delta_{i,i+1}$ are the length and thickness of the shared wall connecting cells i and i+1, respectively, etc. For a known value of applied torque, T, the equilibrium condition (in accordance with eqn. 2.44) is given by

$$T = \sum_{i=1}^{n} F_{sv(i)} \cdot \Omega_i \qquad 2.73$$

and this, together with the n expressions from eqn. 2.71, is sufficient to determine the unknown shear flows $F_{sv(i)}$ (i=1, n) and the reduced angle of rotation, ϕ'. Furthermore, the second moment of area for pure torsion may now be derived from the generally valid formula

$$I_d = \frac{T}{G\phi'} \qquad (2.17)$$

in the same way as for open and closed sections.

By expressing the warping displacement in the same general form as for closed sections, i.e.

$$w_s - w_{so} = - \phi' \cdot \hat{\omega} \qquad (2.40)$$

the reduced sectorial co-ordinate, $\hat{\omega}$, may now be derived from eqn. 2.38 directly, and is given by

$$\hat{\omega} = \int_o^s r_s \cdot ds - \frac{1}{\phi'} \cdot \int_o^s \frac{F_{sv(i)}}{G.\delta_i} \cdot ds \qquad 2.74$$

In this expression the first term is equivalent to the sectorial

co-ordinate ω (eqn. 2.14); where sufficient imaginary cuts have

been made to transform the member into an open section and where the

integral has been started at an arbitrarily selected initial radius

(s = 0). However, the integral in the second term of eqn. 2.74 must

be successively started at the cut position in each cell and the

shear flow used is that present in the cell under consideration.

Furthermore, at this stage it is unnecessary to solve for the reduced

angle of rotation, ϕ', from eqns. 2.71 and 2.72. By making ϕ' numerically

equal (say $\phi' = 1$) in both eqns. 2.72 and 2.74 its effect is eliminated

and eqn. 2.74 may be rewritten more simply in the form:

$$\hat{\omega} = \omega - \int_{o}^{s} \frac{F_{\overline{sv}(i)}}{G.\delta_i} \cdot ds \qquad 2.75$$

where $F_{\overline{sv}(i)}$ represents the unit shear flow, derived by putting
$\phi' = 1$ in eqn. 2.72.

With the reduced sectorial co-ordinate determined in this

way, the actual shear centre and the position of zero warping displace-

ment may now be established from eqn. 2.13, as for single sections.

2.4.2   Non-Uniform (Warping) Torsion

The direct stress and bimoment terms are identical to those

previously defined for single cell sections in eqns. 2.47 and 2.48,

respectively. However, the derivation of the reduced sectorial function

$S_{\overline{w}}$ is not as straightforward and must be calculated on a cell by

cell basis. From eqn. 2.55, we know that the secondary shear flow, F_w,

due to warping restraint is equivalent to

$$F_w = \frac{B'.S_{\overline{w}}}{I_{\hat{w}}} \qquad 2.76$$

and from eqns. 2.54 and 2.56 the function $S_{\widehat{W}}^{-}$ is given by

$$S_{\widehat{W}}^{-} = S_{\widehat{W}} - \frac{I_{\widehat{W}}}{B'}\left[F_{oi} - \frac{T_i}{\Omega}\right] \qquad 2.77$$

In this equation the term in brackets represents the total constant shear flow less that due to pure St. Venant torsion, in the ith cell. For simplicity this has been denoted F_i^{*}, such that by combining eqns. 2.76 and 2.77, we have

$$F_W = F_i^{*} - \frac{B'}{I_{\widehat{W}}} \cdot S_{\widehat{W}} \qquad 2.78$$

A further set of simultaneous equations may now be formulated in accordance with the connectivity condition (eqn. 2.72), but in which the shear flow is that due to warping torsion only. With F_W given by eqn. 2.78, the following expression is typical for the ith cell.

$$\phi'G\Omega_i = -F_{i-1}^{*} \cdot \frac{s_{i-1,i}}{\delta_{i-1,i}} + F_i^{*} \cdot \oint_i \frac{ds}{\delta_i} - F_{i+1}^{*} \cdot \frac{s_{i,i+1}}{\delta_{i,i+1}} - \frac{B'}{I_{\widehat{W}}} \cdot \oint_i \frac{S_{\widehat{W}}}{\delta_i} ds \qquad 2.79$$

where the twist, ϕ', is clearly different from that corresponding to the case of pure torsion (eqn. 2.72). Once more, the total torque T is determined by resolving the shear flow from eqn. 2.78 about the shear centre, but this must equate to zero since we are only considering the self-equilibriating shear flows, F_W. Therefore, we have

$$T = \oint F_W \cdot r_s \cdot ds = \sum_{i=1}^{n} F_i^{*} \Omega_i - \frac{B'}{I_{\widehat{W}}} \cdot \int_A S_{\widehat{W}} r_s \cdot ds = 0 \qquad 2.80$$

which together with eqn. 2.79 enables ϕ' and all the values of F_i^{*} (i = 1, n) to be calculated (for a unit value of $\frac{B'}{I_{\widehat{W}}}$).

With the scale factor $\dfrac{B'}{I_{\hat{w}}}$ again equal to unity, eqn. 2.77 reduces to

$$S_{\bar{w}} = S_{\hat{w}} - F_i^*$$
2.81

from which the function $S_{\bar{w}}$ is seen to equate to the readily obtainable sectorial function $S_{\hat{w}}$ reduced by the appropriate value of F_i^*.

2.4.3   Fundamental Equations

The fundamental equation governing the torsional behaviour of multi-cellular sections is identical to eqn. 2.69, derived for closed and open/closed single cell members.   The additional parameters I_c, μ and k are also determined from eqns. 2.66, 2.67 and 2.70, as before, although the range of numerical values typically found in multi-cellular sections differs greatly from other configurations and is discussed more fully in §2.5.2.

2.4.4   Curvature Effects

It is well established that the transverse distribution of direct stress in a curved member subject to pure bending is not only dependent upon the neutral axis position but is also a function of the distance from the centre of curvature.   Konishi and Komatsu[53] have recently investigated these effects with respect to thin-walled multi-cellular sections and have shown that member curvature also influences the distribution of the stresses due to warping restraint.   If these effects are to be taken into account in the analysis, the general stress equation for closed, thin-walled sections (eqn. 2.2) must be rewritten in the following form:

$$\sigma = \frac{R}{\rho}\left[\frac{N}{A} + \frac{M_x \cdot y}{I_x} + \frac{M_y \cdot x}{I_y}\right] + \frac{B \cdot \hat{\omega}}{I_{\hat{w}}}$$
2.82

where the various sectorial and geometrical functions have been redefined and are tabulated in Appendix 1.

2.5   PARAMETRIC STUDY OF ENGINEERING STRUCTURES

The design process usually adopted for box girder bridges, and other structures heavily loaded in torsion, is basically twofold. In this respect the process does not differ greatly from that employed for more conventional forms of construction and essentially consists of conceptual and detailed design stages.

Initial (Conceptual) Design

In this initial stage, the overall structural configuration must first be determined having regard for the purpose for which the structure is intended and for the prevailing site and ground conditions. In order that the most favourable structural material and method of construction may then be selected, consideration must be given to the time available for site work, future maintenance, general aesthetics and other environmental aspects, etc.. In general, the final solution will be that which satisfies all the above constraints at the least cost although, for this decision to be meaningful, several alternative proposals will often have to be approximately sized and costed for comparison and final selection by the client.

Final (Detailed) Design

With the general arrangement and appearance of the structure thus determined, the most suitable method of analysis must be selected having regard for the validity of any necessary assumptions and the desired accuracy of the final solution. A full analysis may then be undertaken for all the various design loads, and the levels of reinforcement and prestress determined accordingly.

Only at this stage will it become apparent whether or not the initial approximate sizing of the structure was adequate. If significant increases in concrete section are needed in overstressed

areas then a costly re-analysis might well be required.   Equally, in
structures where self-weight contributes a significant proportion of
the total design load, areas of understressed concrete will have to be
reduced to ensure an efficient solution.

2.5.1   Aids to Design and Analysis

Clearly, one of the most important areas in which the designer
requires assistance is in the initial selection of efficient structural
forms.   In this way, lengthy approximate analyses can be avoided
during the conceptual design stage and construction costs can be more
realistically appraised.   To meet this need, Swann[102] has produced an
international feature survey of existing concrete box girder bridges
in which data such as width, flange and web thicknesses, span, con-
struction costs, etc., are comprehensively evaluated.   This and
similar studies are widely used in practice and are invaluable in the
process of selecting the most efficient structural configuration.

However, once the cross-section and general arrangement have
been finalised, there is little further information available to the
analyst for determining the most suitable method of solution.   For
example, the computational effort can often be considerably reduced by
the introduction of certain simplifying assumptions although, for this
to be acceptable, an assessment must first be made of their likely
effect.   For the analysis of curved, concrete box girders in particular,
two of the most useful simplifications that can be made are (i). to dis-
regard thin-walled beam characteristics, and (ii). the representation of
member curvature by one or more equivalent straight beams.

Thin-walled Behaviour

The typical dimensions of hollow concrete members are such
that it is not always immediately clear whether or not thin-walled

behaviour should be assumed. The guidelines given in §2.1.3 are helpful in this respect although warping restraint stresses can be important in some configurations which do not apparently comply with these criteria. At the same time, certain members which are clearly thin-walled (*e.g.* circular or square sections with constant wall thickness) are not susceptible to significant warping of the cross-section, in which case the stresses due to axial restraint may safely be neglected.

However, a more reliable indication of the importance of warping restraint is available and is given in the form of the decay function, k, derived previously in eqns. 2.36 and 2.70 for open and closed sections, respectively. The length of the member is also an important consideration in this evaluation and it will be shown in §3.4.4 and §3.4.5 that warping restraint effects assume a greater significance in members in which the dimensionless parameter kℓ is small. The limiting value of this parameter, above which thick-walled beam analysis is adequate, is obviously dependent upon the accuracy of solution required but is, for example, given the numerical value of 10 in the Japanese Bridge Code[79].

Curvature Effects

A high degree of curvature is a common feature of many modern structures and can significantly influence the longitudinal and trans-verse distribution of the various stress resultants. While substantial savings in computation can be achieved by considering the curved member as an equivalent straight member for the purposes of analysis, this is only acceptable if the final solution is within the required degree of accuracy. When this is not the case, an alternative approach is possible whereby a series of end-connected straight beam elements is

used to represent the initial configuration. However, since an
infinite number of such elements is needed to model the original
structure exactly, it is desirable to establish the minimum number
required in order to achieve the necessary accuracy with the smallest
amount of computational effort.

The errors introduced by either of these structural idealiz-
ations have been evaluated in §4.4 for the wide range of sections
typically found in practice. However, where a large number of straight
beam elements is needed to adequately model a particular structure it
is envisaged that the curved beam element developed in Chapter 3 will,
in future, prove a more attractive alternative.

2.5.2   The Sectorial and Cross-sectional Properties of Structures

The errors most commonly introduced into the analysis of
concrete box girder bridges have been identified in the previous section.
These are due to neglecting curvature and warping restraint effects and
are discussed in detail in §4.4.1 and §4.4.2 respectively.   In both
cases a full error analysis has been undertaken and is presented in
terms of the various sectorial and cross-sectional properties. However,
for these to have some meaning, it is necessary to be able to identify
the structural configurations which are most affected and, for this
purpose, the properties of a range of existing structures and typical
sections are presented here.

Existing Structures

The feature survey by Swann[102] has provided the opportunity
for a detailed investigation of existing concrete box girder bridges.
Of the one hundred and seventy three bridges presented in the survey,
some clearly did not conform to the basic assumptions set out in
§2.1.3 on which the theory of thin-walled structures is based.   The

most common causes of disqualification were due to excessive thickness/ depth ratios in the webs, sections displaying variable overall depth along their length, or the apparent absence of diaphragms between spines of twin spine bridges.

Accordingly, only seventy structures were analysed in this study but these did include examples covering the full range of cross-sectional configurations shown in fig. 1.4. The various second moments of area I_x, I_y, I_{xy}, $I_{\hat{w}}$, I_d and I_c were calculated using a computer program developed and fully described by Pinkney[85], thus enabling the warping functions μ and k to be evaluated from eqns. 2.67 and 2.70 respectively. For this purpose, Poisson's ratio for concrete was assumed to be 0.15, from which we have

$$\frac{G}{E} = \frac{1}{2(1 + \nu)} = 0.435 \qquad\qquad 2.83$$

The ratio of bending and torsional stiffness, given by

$$j^2 = \frac{GI_d}{\Psi EI_x}, \qquad\qquad 2.84$$

has also been determined in this study as it is an important function in the subsequent error analyses.

The numerical values of k^2, j^2 and μ are given in Table 2.1 for the seventy sections considered in this investigation; the bridge reference numbers refer to those in the original study by Swann. In cases where the webs or flanges were thickened at the supports, only the mean values of the parameters calculated for the support and mid-span sections have been tabulated. The various quantities have also been plotted against minimum span length (in figs. 2.11 - 2.13) and highlight some interesting features which are discussed more fully in Chapter 6.

Bridge Ref.No.	Number of cells †	μ	j^2	$k^2 \times 10^{-2}\,\text{m}^{-2}$	ℓ_{min}(m)	$k\ell_{min}$
1	1	0.777	1.06	52.15	19	13.72
2	1	0.644	0.97	73.17	15	12.83
5	1*	0.592	0.96	35.98	18	10.74
6	1	0.839	0.95	38.92	25	15.60
7	4	0.605	1.33	15.97	27	10.79
9	5*IW	0.924	1.08	6.06	27	7.12
10	5 IW	0.843	0.95	7.48	27	7.38
11	2x1*	0.958	0.47	3.24	23	4.14
12	1	0.462	0.94	48.60	28	19.52
13	2	0.513	0.85	41.30	28	18.64
15	2*	0.843	1.25	13.55	21	7.74
19	2x1*	0.928	0.77	2.02	22	3.12
20	2x1	0.888	0.72	7.56	29	7.98
21	3	0.823	1.09	15.58	29	11.45
22	2x2	0.934	1.00	2.01	30	4.26
23	3*IW	0.787	0.78	36.20	24	14.40
26	2x1	0.928	0.93	2.30	31	4.71
27	1	0.579	1.04	37.93	31	19.09
28	1	0.851	0.84	14.08	32	12.01
29	1*	0.699	0.85	36.45	32	19.36
30	1	0.724	0.76	48.31	23	15.99
31	1	0.768	0.89	25.37	32	16.12
32	1*	0.811	0.93	37.95	20	12.31
33	2	0.775	1.01	23.06	18	8.65
36	2x1*	0.924	0.42	2.96	31	5.34
37	2x1*	0.960	0.33	1.58	29	3.64
38	3IW	0.877	0.80	54.20	15	11.00
39	1	0.785	0.97	21.01	18	8.25
40	1	0.669	0.88	35.46	18	10.72
42	2x1	0.973	0.79	1.60	20	2.52
43	1	0.678	0.93	43.18	21	13.80
44	1	0.797	0.67	29.77	33	18.01
45	1	0.519	0.72	32.19	26	19.86
46	1	0.290	0.61	50.39	35	24.85
47	2	0.769	1.21	31.88	22	12.42
50	3*	0.864	0.98	9.38	25	7.66
51	3*	0.832	1.07	12.46	34	12.00
53	1*	0.753	0.91	22.72	31	14.77
54	1	0.699	0.93	43.73	22	14.55
55	2*	0.834	0.97	14.83	29	11.16

Table 2.1   Sectorial Properties of Existing Concrete Box Girder Bridges[102]

Bridge Ref.No.	Number of cells†	μ	j^2	$k^2 \times 10^{-2} m^{-2}$	ℓ_{min}(m)	$k\ell_{min}$
58	1	0.644	0.97	59.36	27	20.80
59	1*	0.767	1.00	51.77	26	18.70
60	2	0.844	1.17	10.12	36	11.45
62	2x1*	0.944	0.77	3.80	31	6.04
63	2x1*	0.954	0.60	4.28	16	3.31
64	5	0.920	1.20	5.46	31	7.24
65	2x1*	0.942	0.64	2.95	27	4.64
66	2x1*	0.953	0.44	1.68	39	5.06
67	1	0.786	0.82	21.22	30	13.82
68	2*	0.766	0.93	11.78	33	11.31
70	2x1*	0.961	0.49	1.15	40	4.29
71	2x1*	0.959	0.73	2.10	27	3.91
73	1*	0.722	0.80	32.81	30	17.19
74	2x2*	0.966	0.98	0.98	25	2.13
75	1*	0.558	0.72	28.10	31	16.36
76	1*	0.789	0.82	26.07	33	16.85
82	1*	0.693	0.86	34.44	33	18.92
85	1*	0.674	0.76	32.46	20	11.39
89	1*	0.744	0.88	23.11	35	16.83
90	1	0.366	0.25	27.58	49	25.73
93	1*	0.579	0.94	22.68	31	14.74
94	1*	0.530	0.71	41.08	32	20.48
97	1*	0.526	0.65	23.10	39	18.74
103	1*	0.472	0.62	13.62	54	19.91
108	3*IW	0.492	0.96	8.74	53	15.70
112	1	0.300	0.65	30.08	58	31.81
117	2*	0.663	0.84	12.70	46	16.21
141	1	0.346	0.78	20.75	72	32.80
150	1	0.287	0.66	16.98	36	14.84
159	1*	0.257	0.56	11.17	63	21.15

† *Key to cross-sectional configurations*

n	n cell, single spine box girder
m x n	n cell, m spine box girder
*	variable cross-section
IW	inclined webs

Table 2.1 (contd.)   *Sectorial Properties of existing Concrete Box Girder Bridges*[102]
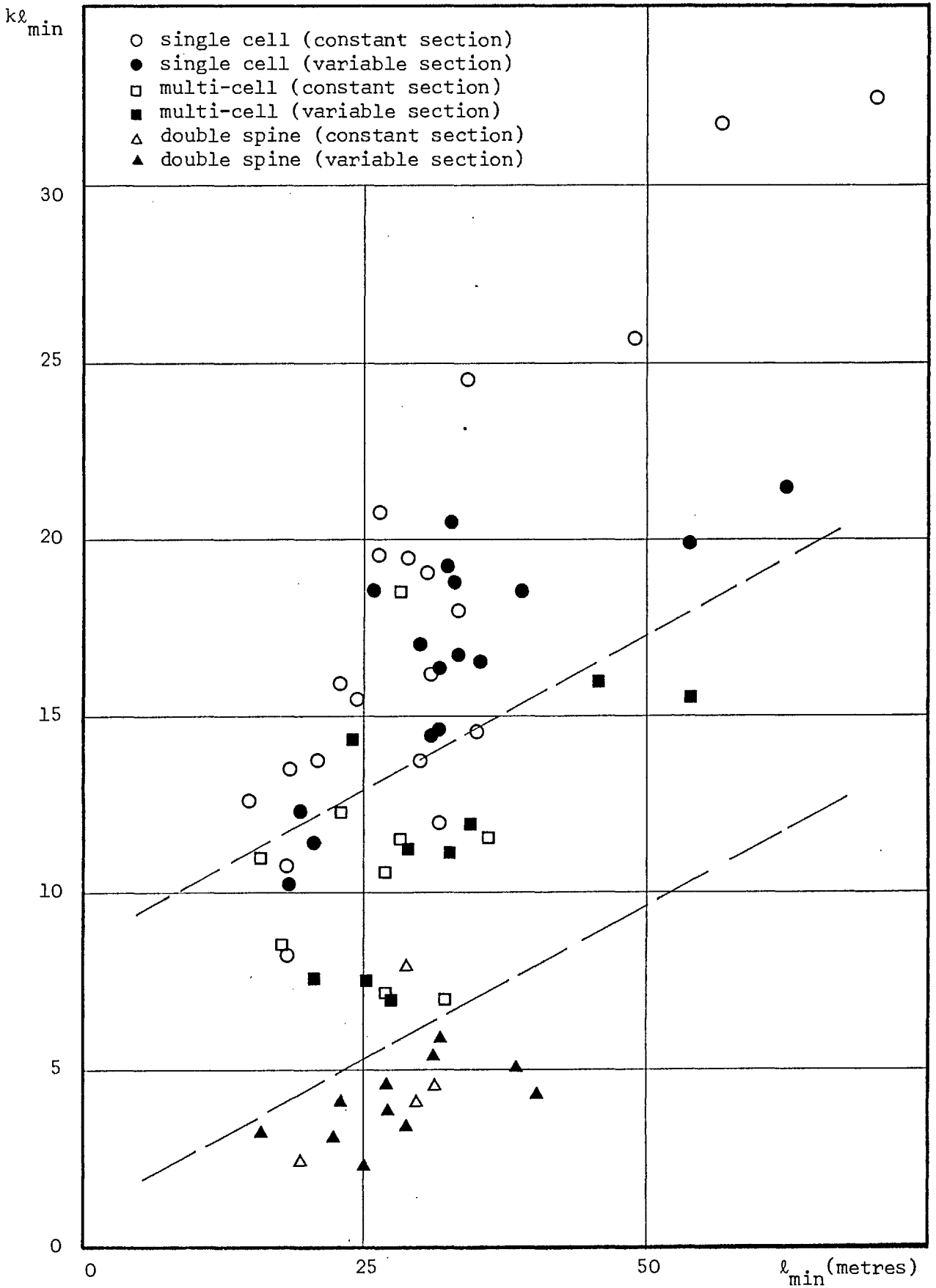
Figure 2.11 The Dimensionless Warping Parameter $k\ell_{min}$
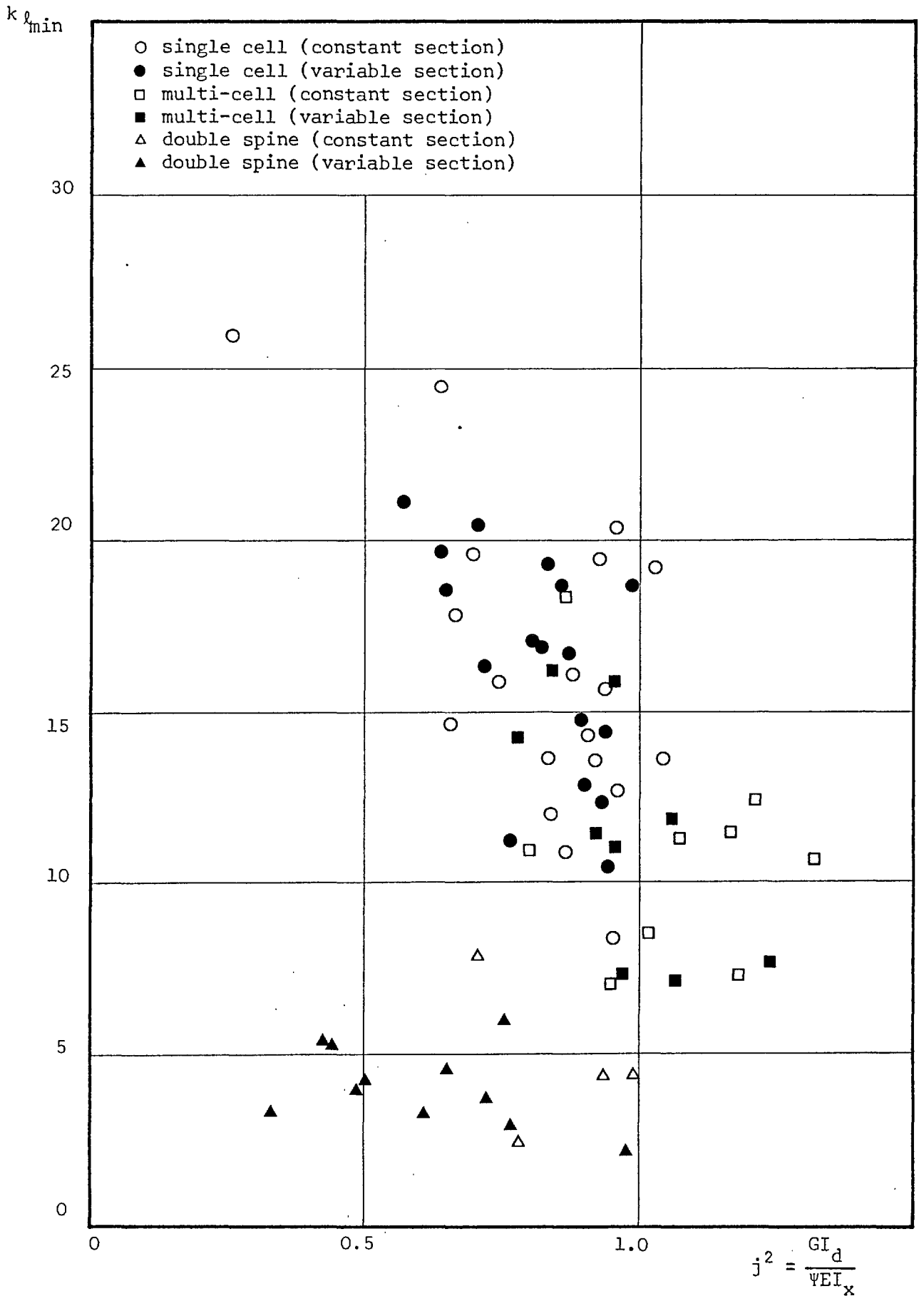
Figure 2.12 The Torsion/Bending Stiffness Ratio, j²
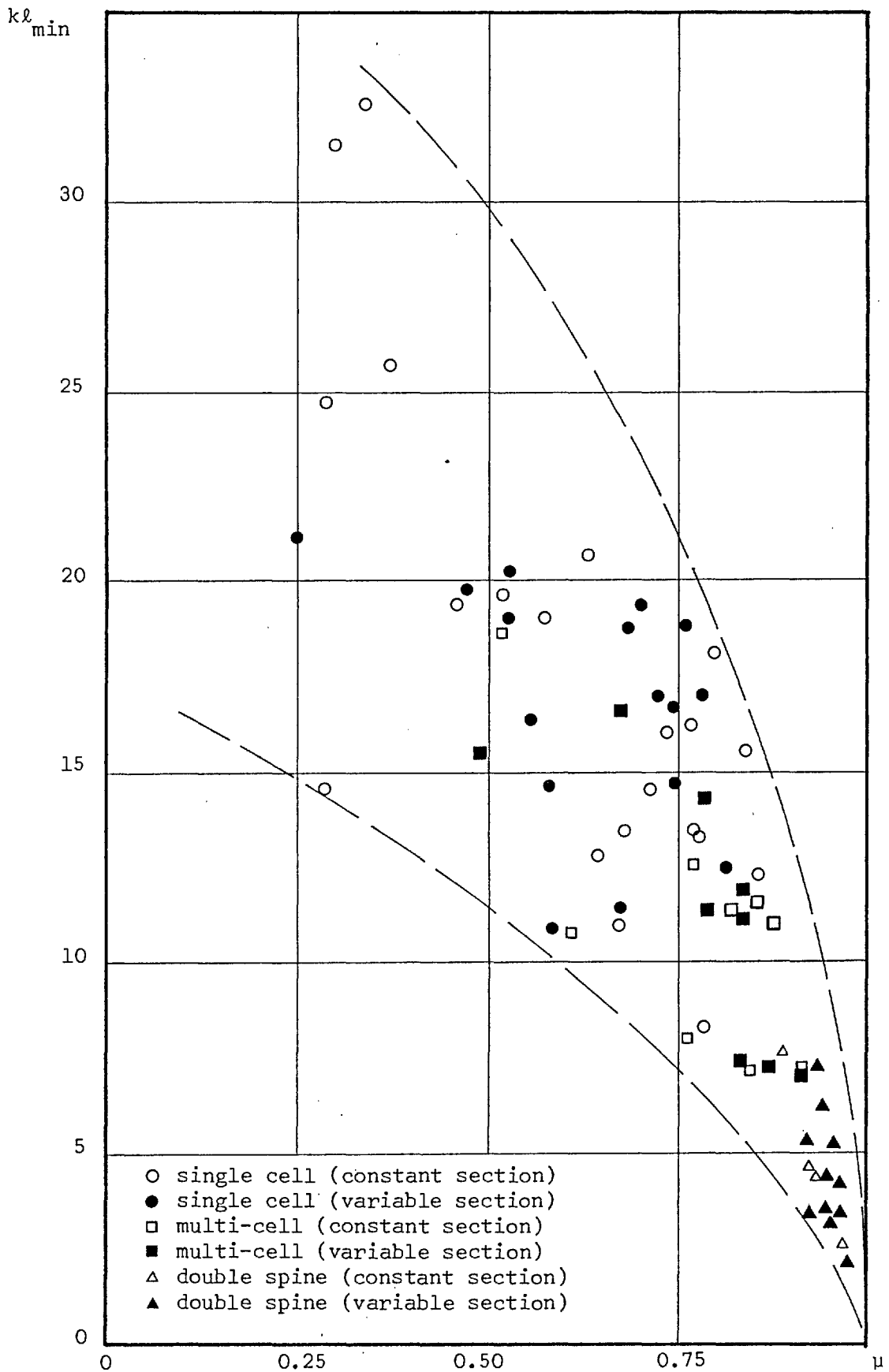
Figure 2.13   The Warping Shear Parameter, μ

Typical Sections

The study of existing concrete box girders is undoubtedly valuable but is restricted to bridge structures only. Therefore, in order to extend the usefulness of the error analyses presented in Chapter 4, a computer based investigation of the various sectorial properties of other structural sections has also been undertaken. Three basic configurations have been analysed, namely, the single cell box, channel section and I-section, and these are all commonly used for shear core and other general structural applications. The analysis has also been extended to include similar sections in which the top flange has been widened, as shown in fig. 2.14.

A large range of breadth/depth ratios are covered in the investigation although, for simplicity of presentation, only singly symmetrical sections have been considered in which the top flange is either equal to the section breadth or to twice the section breadth. The number of wall thickness/breadth ratios has been kept as large as possible and intermediate values can usually be interpolated with a sufficient degree of accuracy.

The parameters k^2, j^2 and μ are graphically presented in figs. 2.15 - 2.17 for the single cell box girder with and without cantilevers. However, the warping shear parameter μ is equal to unity for open sections and thus only k^2 and j^2 are shown in figs. 2.18 and 2.19 (for the channel sections) and in figs. 2.20 and 2.21 (for the I-sections). An additional error function has also been formulated for the six different cross-sections and is defined in the following way:

$$F_{max} = \left(\frac{I_x}{I_{\hat{w}}} \cdot \frac{\hat{\omega}}{y}\right)_{max} \quad \text{(closed sections)}$$

or

$$F_{max} = \left(\frac{I_x}{I_w} \cdot \frac{\omega}{y}\right)_{max} \quad \text{(open sections)}$$

2.85
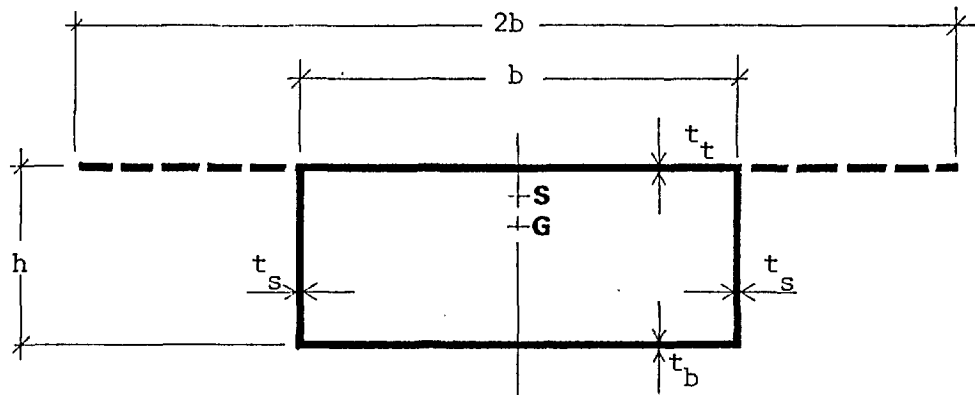
a. *Single Cell Rectangular Box*
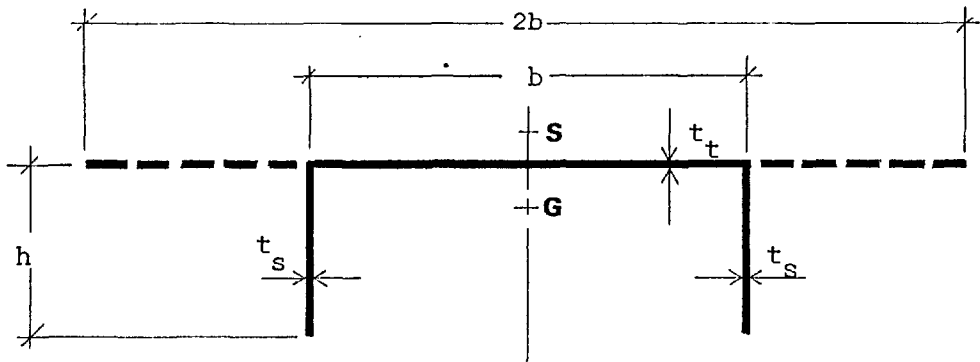
b. *Channel Section*
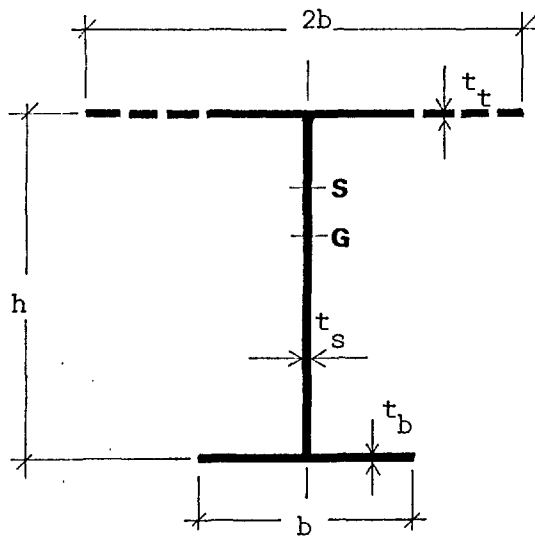
c. *I-Section*

Figure 2.14 Typical Sections considered in Parametric Study

These are presented in figs. 2.22 - 2.24 for the box, channel and

I-sections, respectively, and are subsequently used in §4.4.

2.5.3   Errors due to Variations in Shear Stress

In the derivation of the structural mechanics of closed thin-

walled sections, it has been assumed that the distribution of the

torsional shear stress is constant across the wall thickness and equal

to that on the median line of the section.   This is the distribution

of shear stress, τ_{sv}, shown in fig. 2.8b, which is created by the

connectivity requirements of closed sections and which neglects the

effects of the linearly distributed shear stresses, $\Delta\tau_{sv}$, shown in

fig. 2.8a.   With the basic dimensions of the existing concrete box

girder bridges studied in §2.5.2 readily accessible on the computer,

an opportunity existed for evaluating the errors introduced by this

assumption.   Only single cell sections have been investigated but

these made up just over half of the seventy bridges previously con-

sidered in the parametric study.

With the components of shear stress $\Delta\tau_{sv}$, τ_{sv} defined by

eqns. 2.16 - 2.17 and 2.44 - 2.45, the function used to describe the

error in maximum shear stress is given by

$$E_\tau = \frac{\Delta\tau_{sv}}{\tau_{sv} + \Delta\tau_{sv}} \times 100\% = \frac{\delta^2 \oint \frac{ds}{\delta}}{\Omega + \delta^2 \oint \frac{ds}{\delta}} \times 100\% \qquad 2.86$$

In this expression, the term δ (outside of the integral) is the maximum

wall thickness in the section;   this corresponded to the web thickness

in all the bridges investigated.   The error function has been plotted

in fig. 2.25 for the thirty-seven bridges studied and also for an

idealized cross-section in which the top and bottom flange thicknesses

are identical (and equal to half of the web thickness), and in which

the width of the cantilever is equal to half the width of the box.

Very large discrepancies between the maximum and mean values

of shear stress occured in most cases and are ample justification for

the initial limiting criteria outlined in §2.1.3 for thin-walled be-

haviour. None of the sections investigated fell within the 10% error

margin suggested by Kollbrunner and Basler[50] and, clearly, the restrict-

ion that the total cross-sectional area should be less than one-fifth

of the area enclosed by the median line of the section is very difficult

to satisfy for sections with those dimensions typically found in practice.

practice.

However, fig. 2.25 is somewhat distorted by the fact that

only support sections were considered. In cases of variable cross-

section this generally included considerable local thickening of the

webs. It should also be noted that any underestimation of maximum

shear stress is matched by a corresponding over-estimation on the

opposite face of the wall and that the concept of average shear stress

is usually sufficient for design purposes.

Perhaps a fairer estimate of the suitability of thin-walled

beam theory to the analysis of concrete box girder bridges is provided

by an assessment of the error in assumed torsional capacity brought

about by the variation in shear stress. For this evaluation the

error function is defined by the following algorithm:

$$E_T = \frac{\int_s \frac{\delta^3}{3} \cdot ds}{\frac{\Omega^2}{\oint \frac{ds}{\delta}} + \int_s \frac{\delta^3}{3} \cdot ds} \times 100\% \qquad 2.87$$

Here, the denominator is the total torsional second moment of area for

closed sections, given by eqn. 2.43, and the numerator is that component

of the second moment of area neglected in the theory.

The results of the error analysis, presented in fig. 2.26, show that approximately 40% of the bridges considered had less than a 10% error in their respective torsional second moments of area. Furthermore, these structures have been constructed over a 25 year period and do not necessarily reflect the continuing trend to more slender sections. Indeed, the average value of the dimensionless parameter $k\ell_{min}$ was approximately 15, and for only one bridge was it less than 10, the value usually selected as the limiting criterion below which thin-walled behaviour should be assumed. It would therefore appear from this limited study that for single cell box girders in which warping effects are significant the error introduced by the assumption of constant shear stress across the wall thickness is entirely satisfactory.

Symbol	Single Cell Box			I-Section			Channel	
	t_s/b	t_t/b	t_b/b	t_s/b	t_t/b	t_b/b	t_s/b	t_t/b
□	0.01	0.01	0.05	0.05	0.05	0.025	0.01	0.01
o	0.01	0.033	0.05	0.05	0.05	0.075	0.01	0.05
Δ	0.01	0.067	0.05	0.05	0.10	0.025	0.01	0.10
+	0.01	0.10	0.05	0.05	0.10	0.075	0.05	0.01
×	0.10	0.01	0.05	0.10	0.05	0.025	0.05	0.05
♦	0.10	0.033	0.05	0.10	0.05	0.075	0.05	0.10
✦	0.10	0.067	0.05	0.10	0.10	0.025	0.10	0.01
x̄	0.10	0.10	0.05	0.10	0.10	0.075	0.10	0.05
z	-	-	-	-	-	-	0.10	0.10

Table 2.2 Key of Wall Thickness/Breadth Ratios for Figures 2.15-2.24
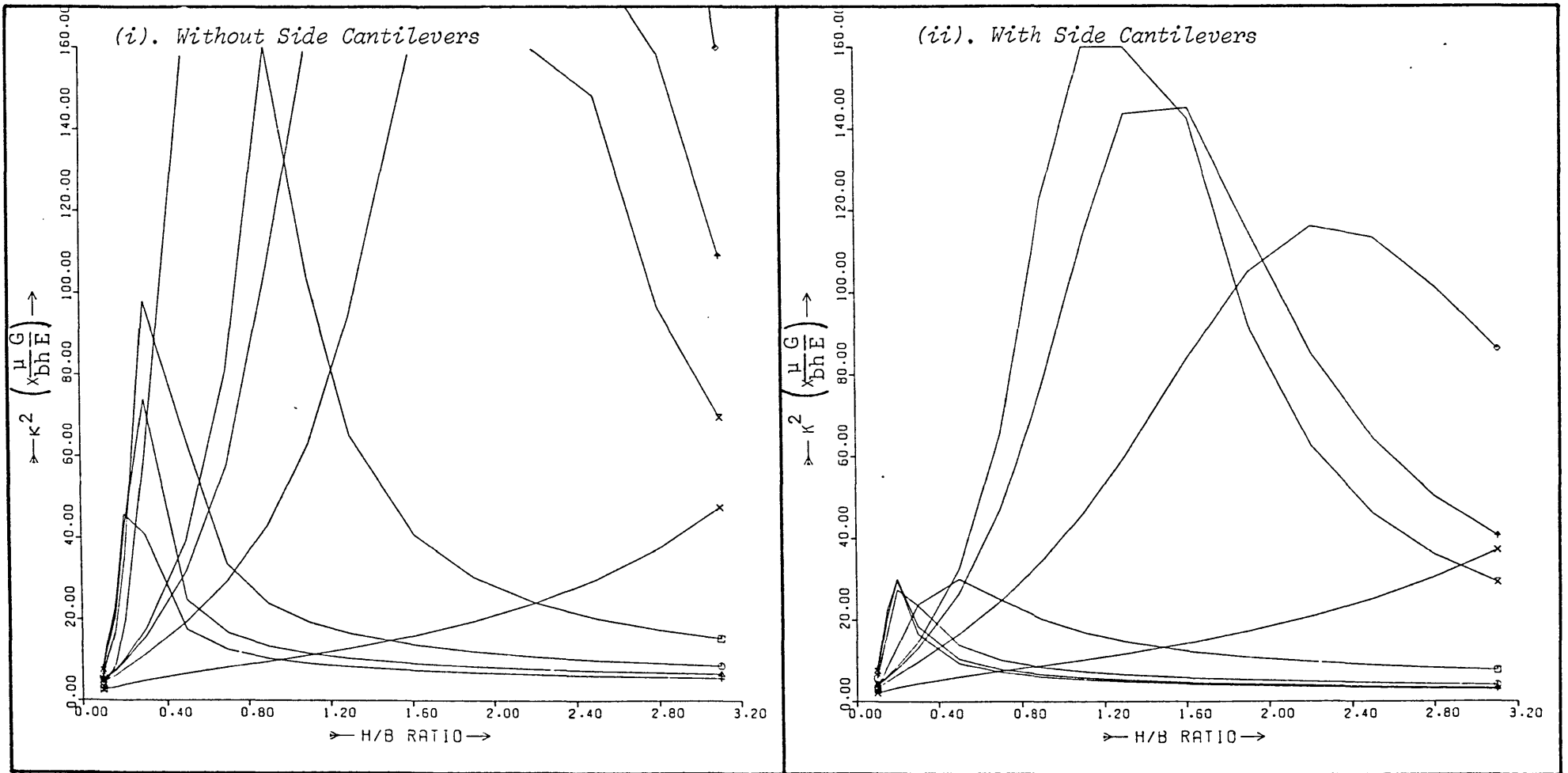
Figure 2.15 Decay Function, k^2, for Single Cell Boxes
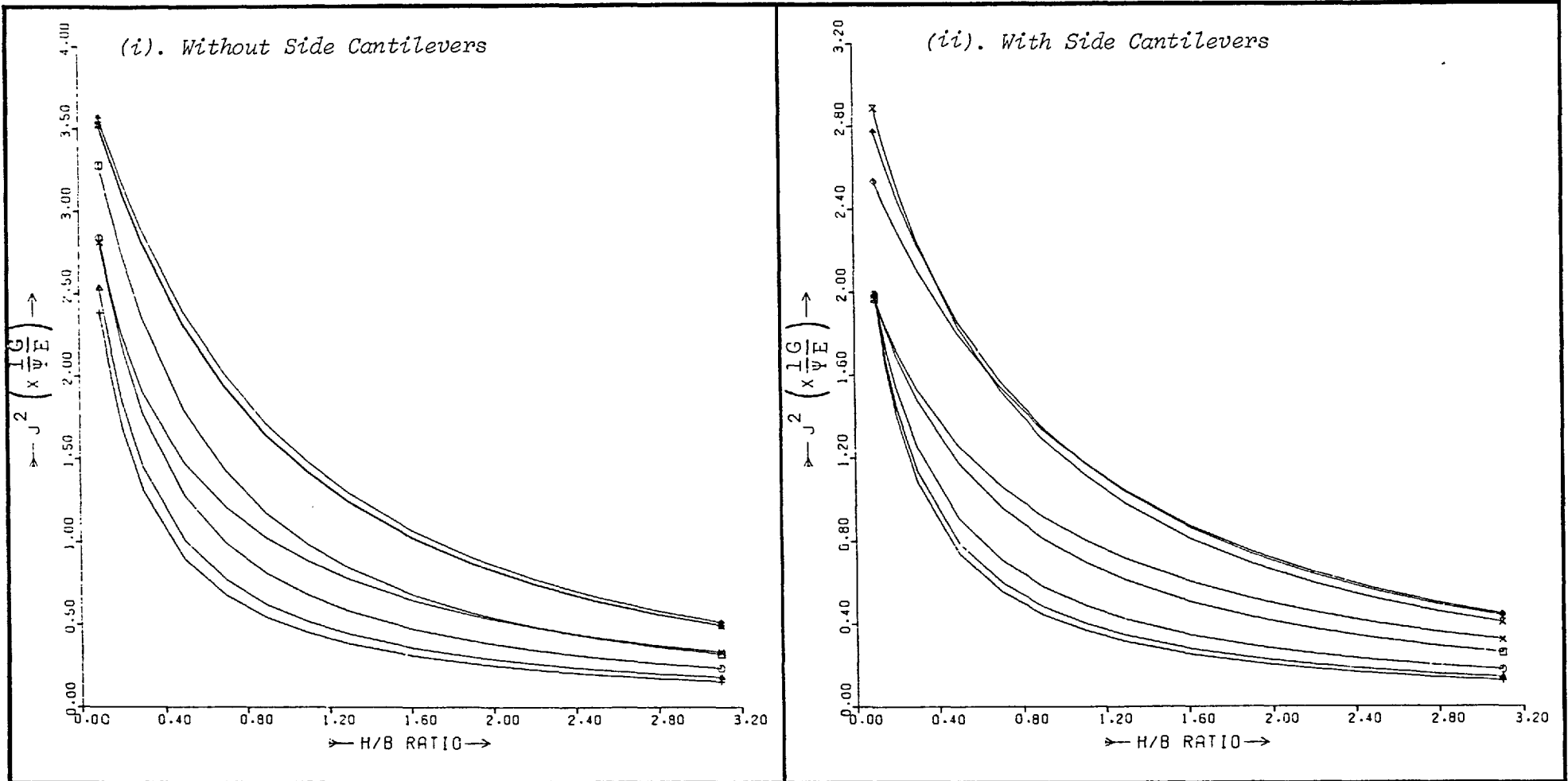
Figure 2.16   Torsion/Bending Stiffness Ratio, j^2, for Single Cell Boxes
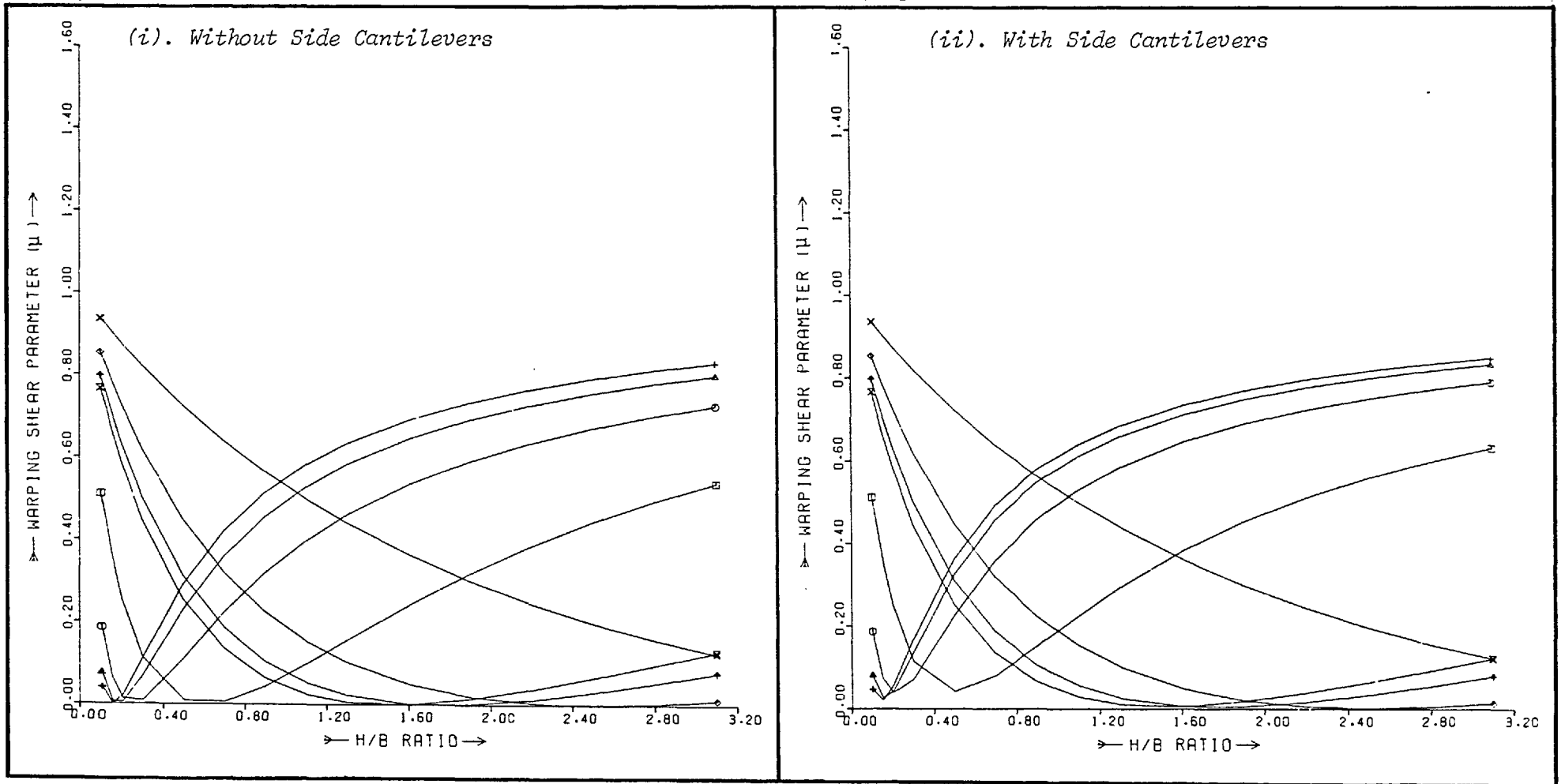
Figure 2.17   Warping Shear Parameter, μ, for Single Cell Boxes
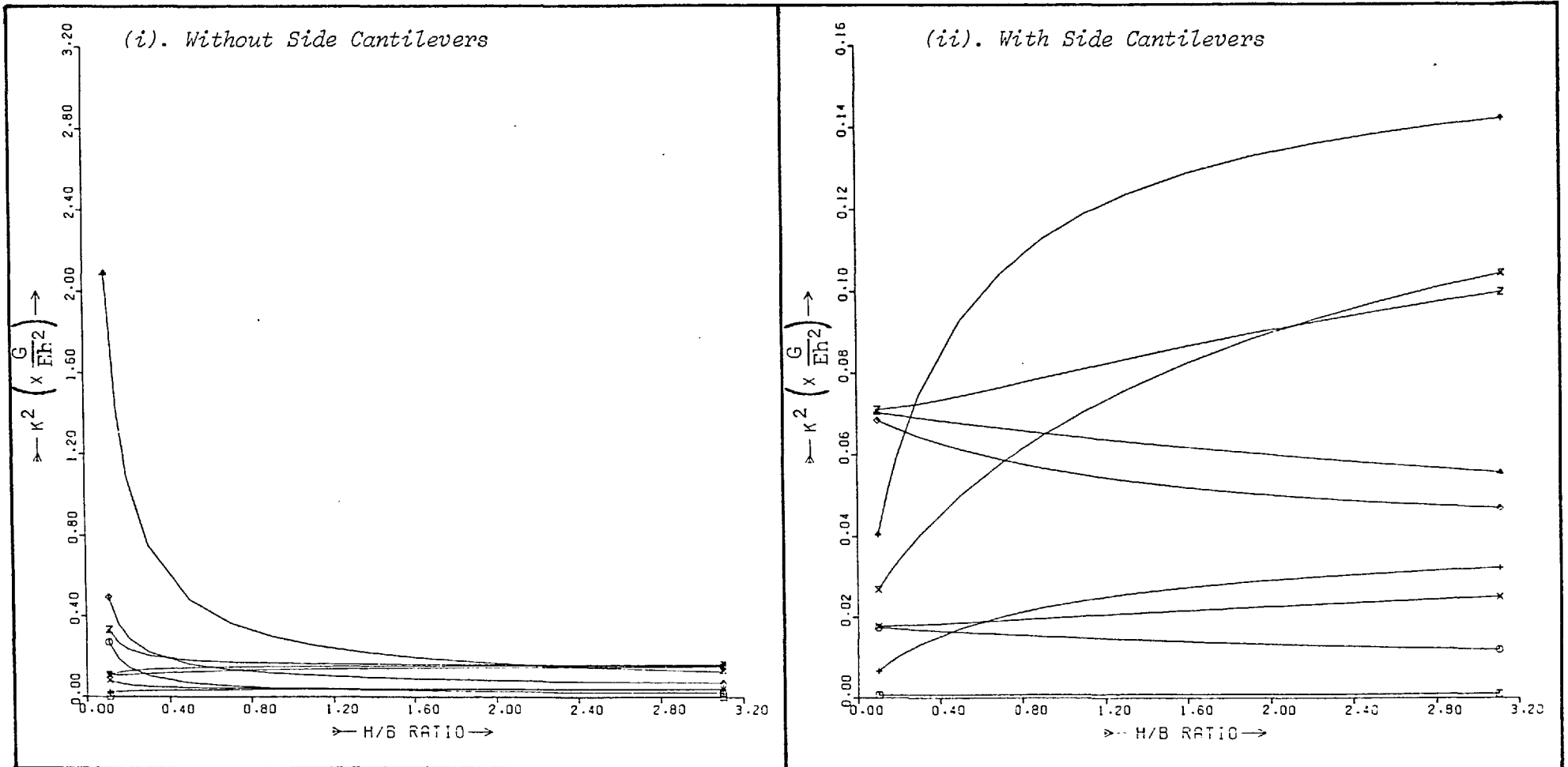
Figure 2.18 Decay Function, k^2, for Channel Sections
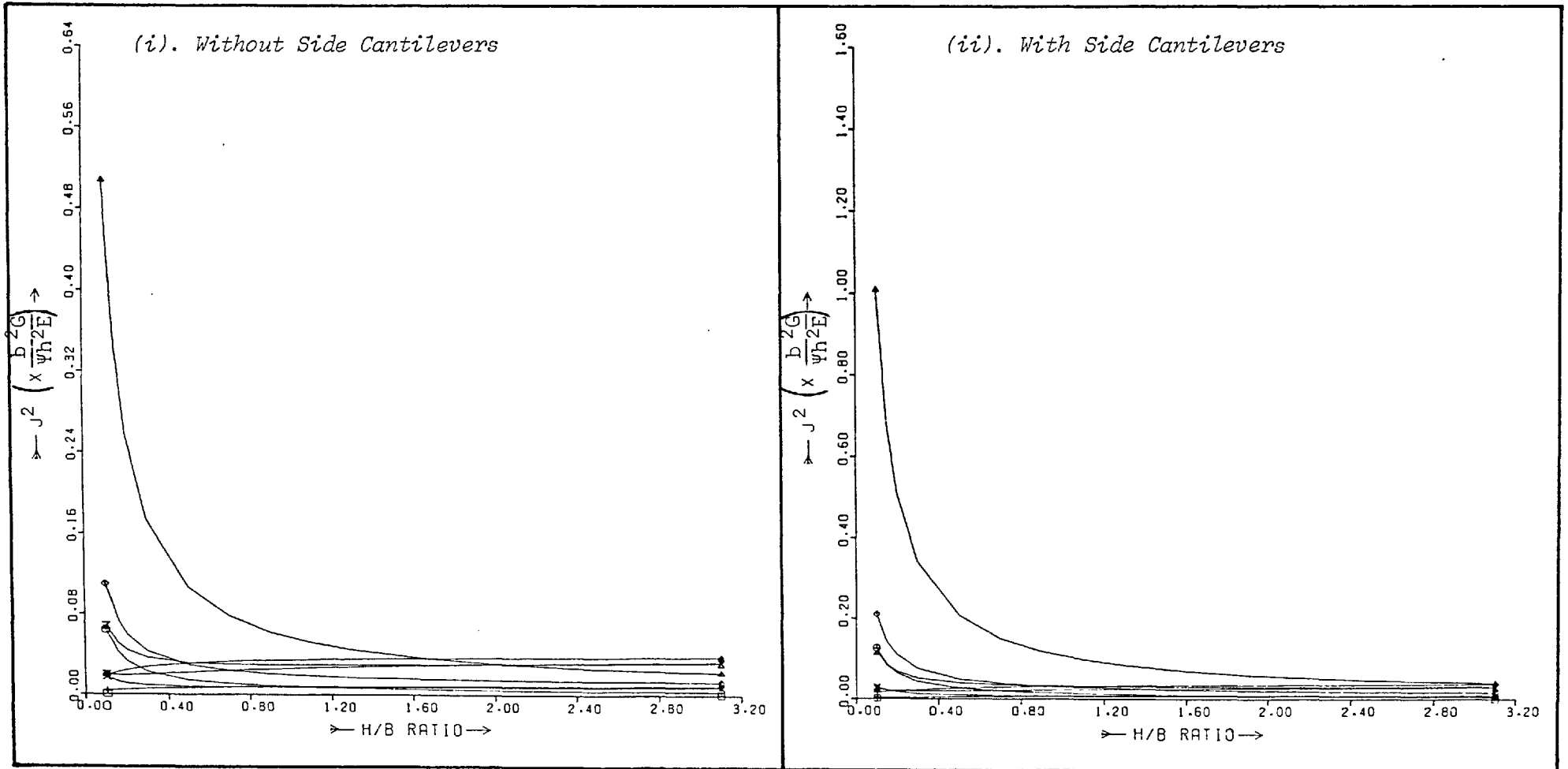
Figure 2.19 Torsion/Bending Stiffness Ratio, j^2, for Channel Sections
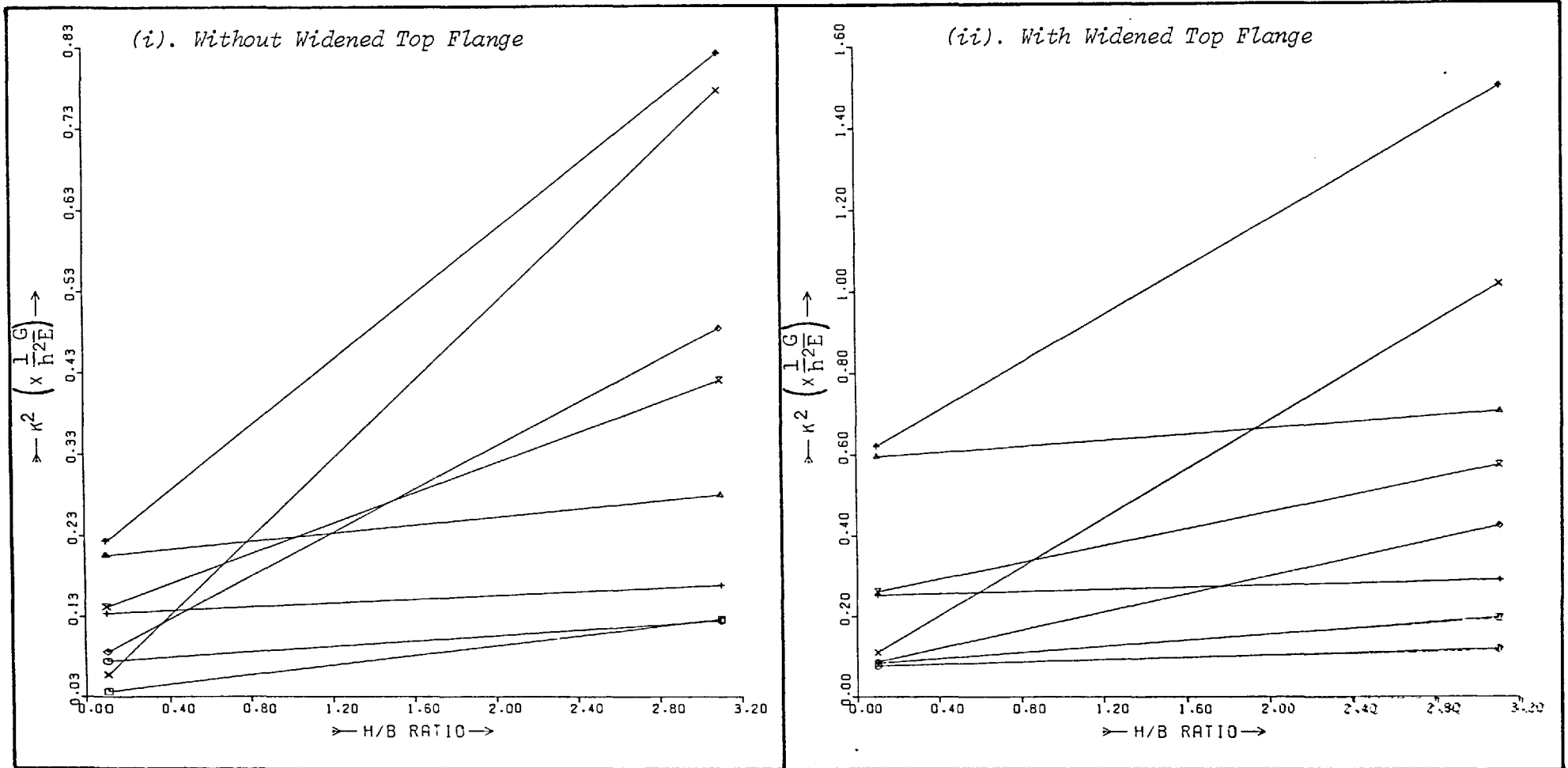
Figure 2.20   Decay Functio, k^2, for I-Sections
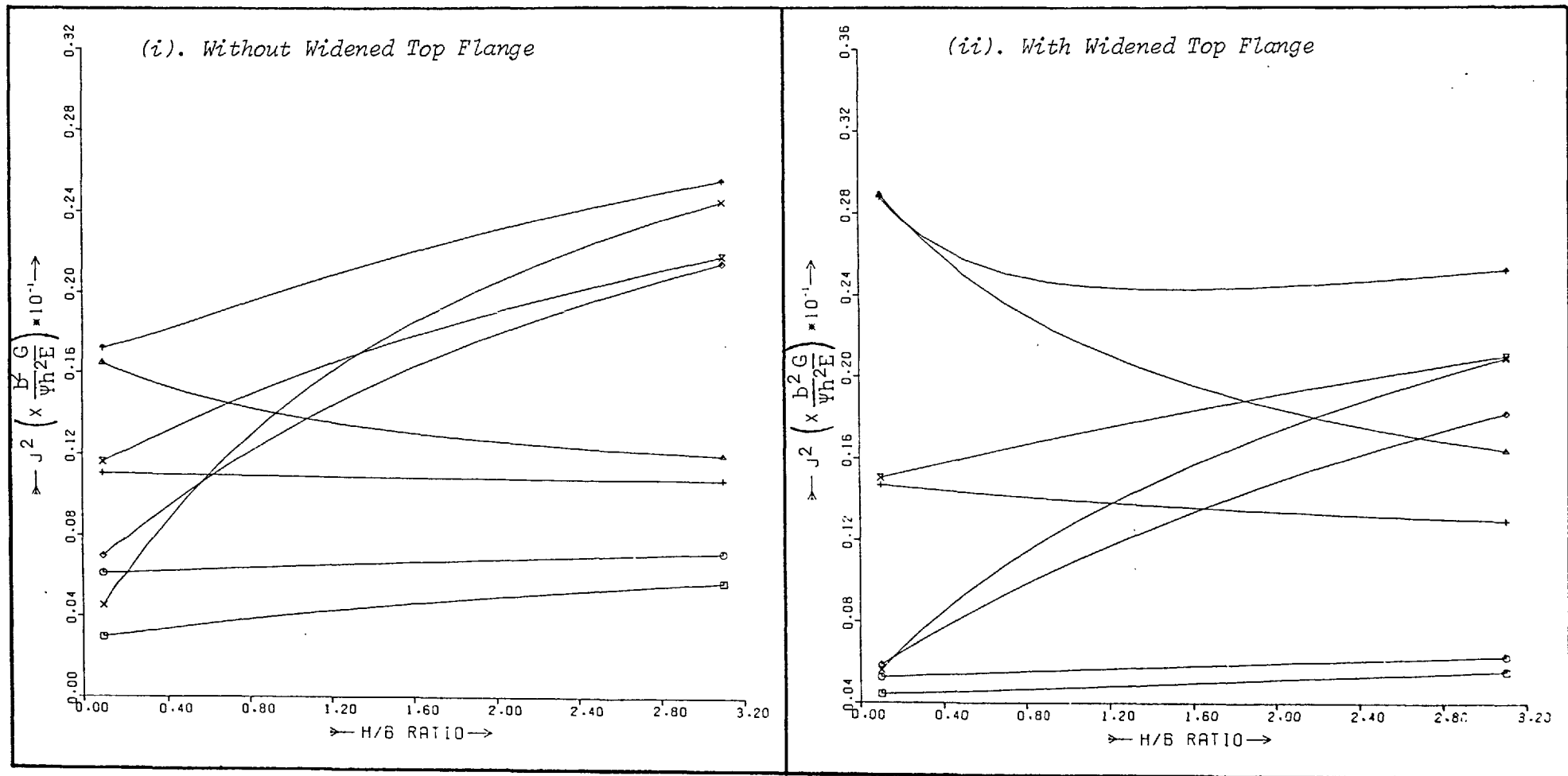
Figure 2.21 Torsion/Bending Stiffness Ratio, j^2, for I-Sections
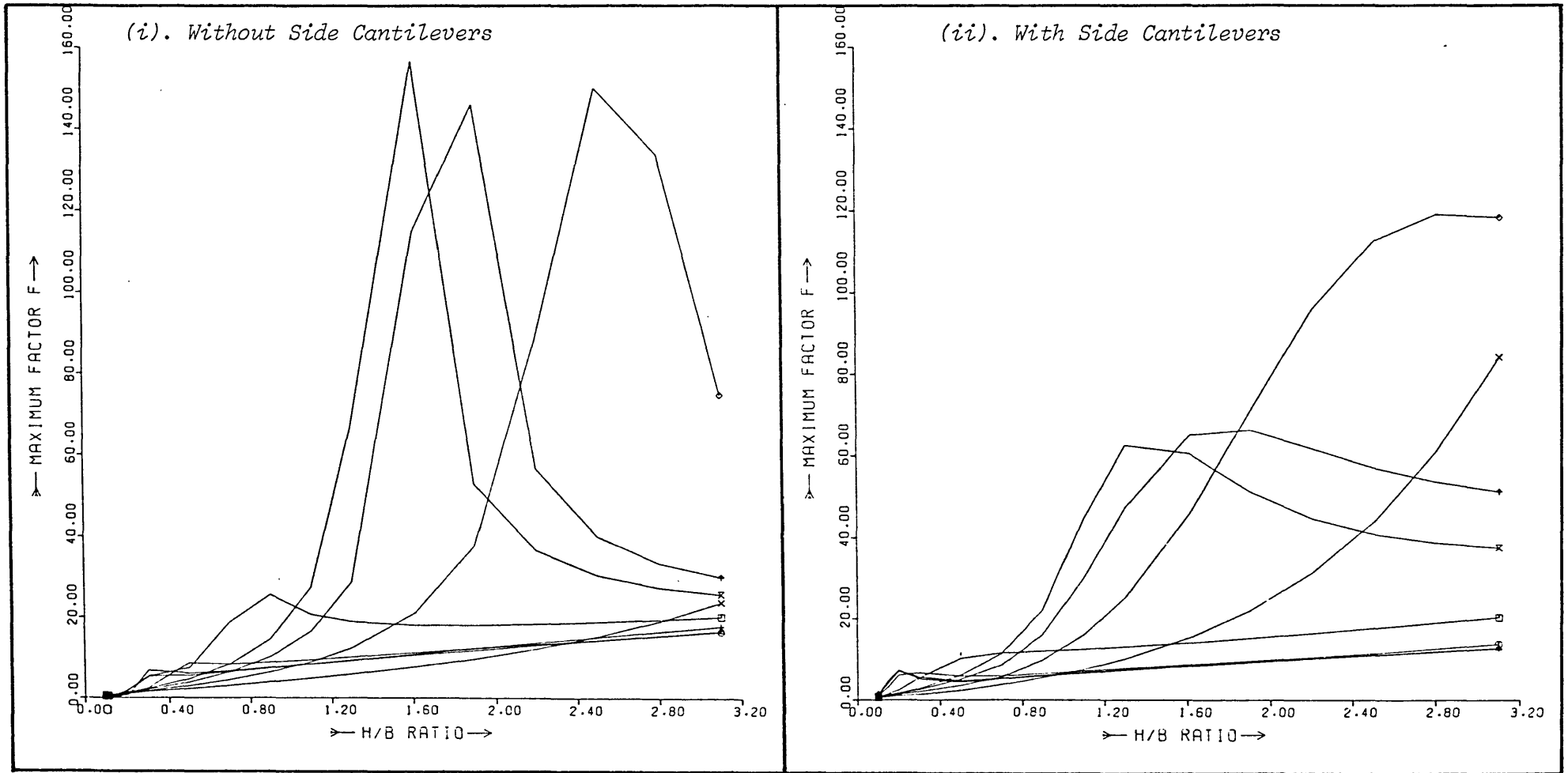
Figure 2.22   The Error Function F_{max} for Single Cell Boxes
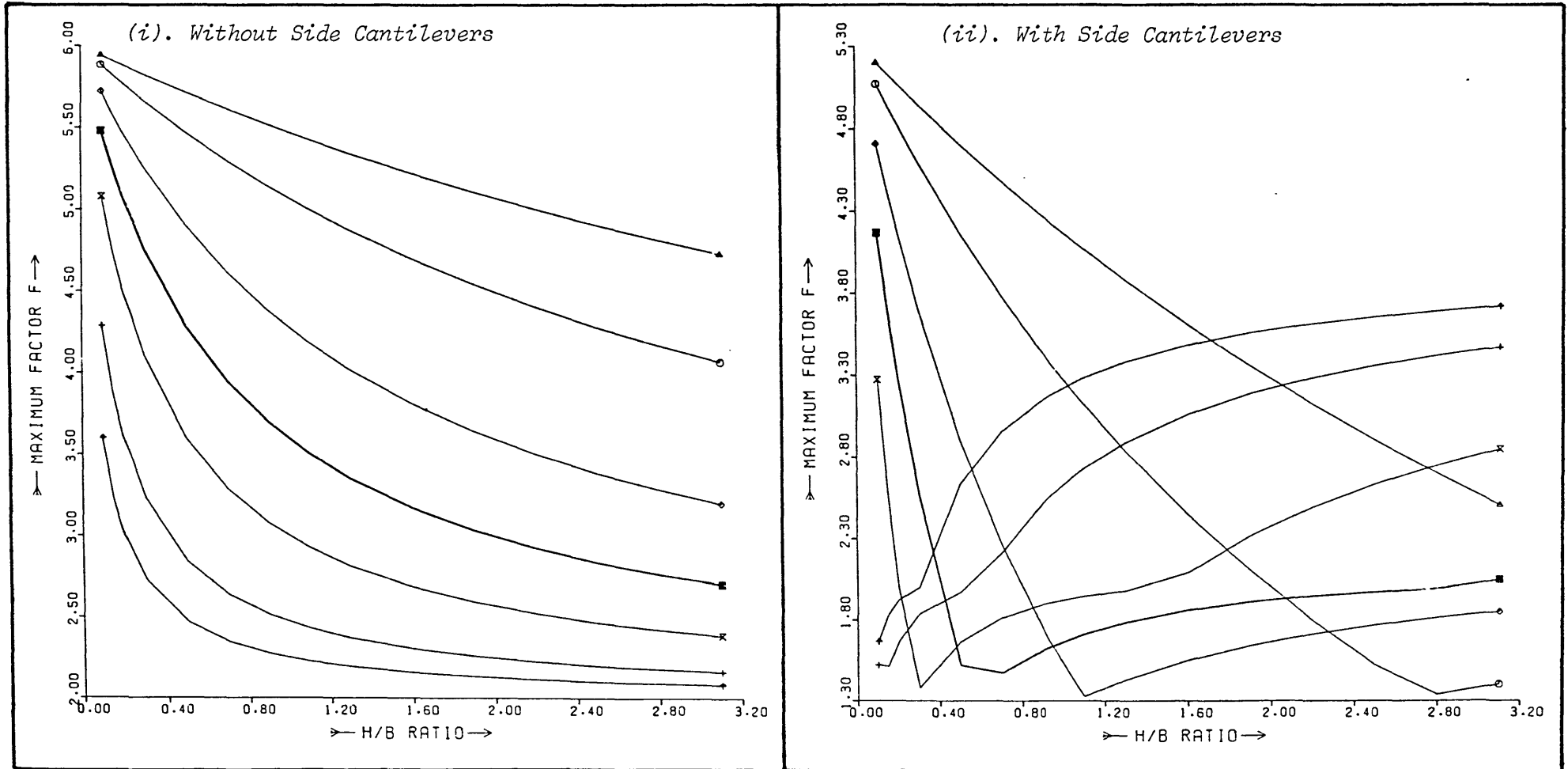
Figure 2.23 The Error Function F_{max} for Channel Sections
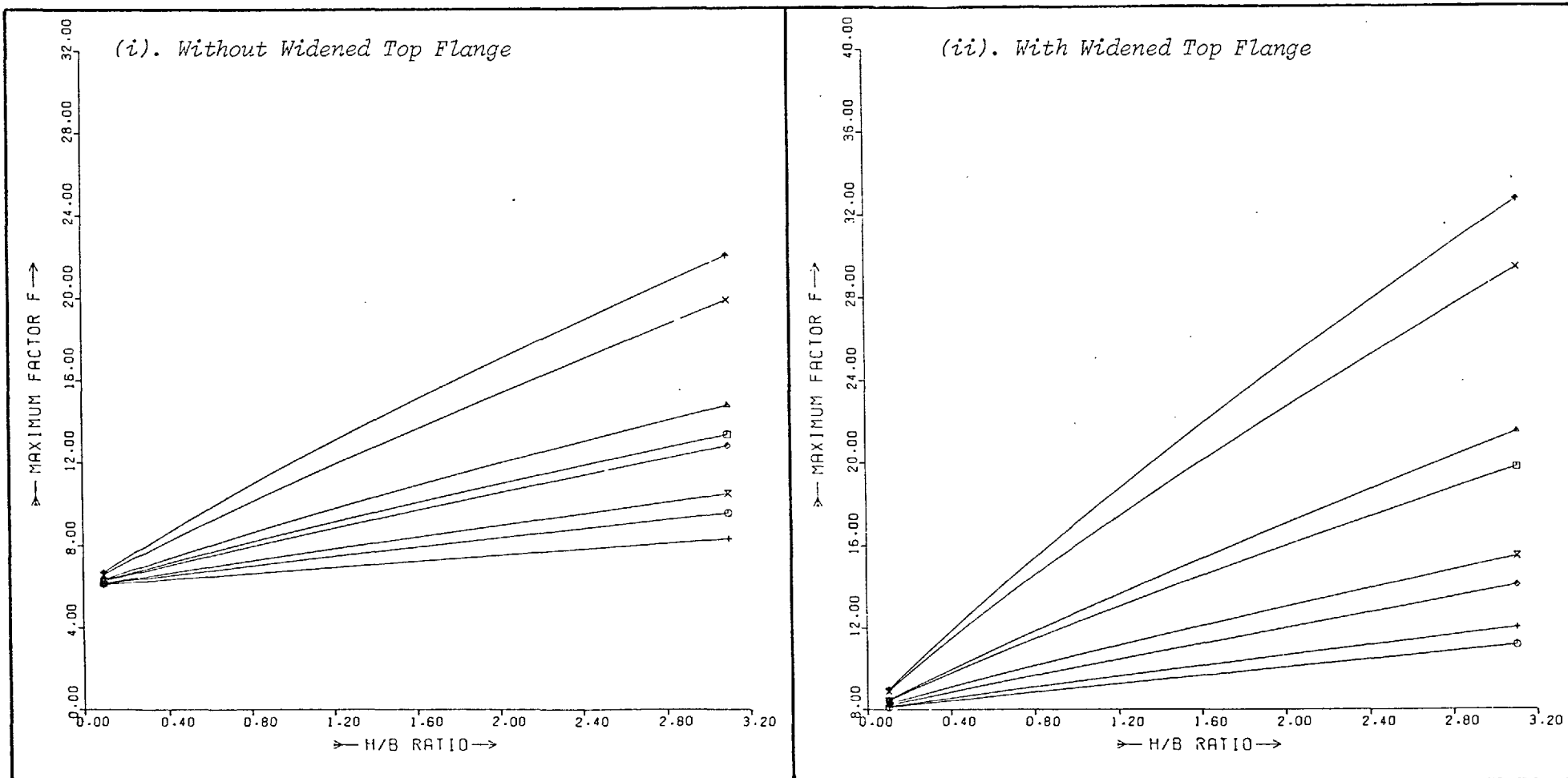
Figure 2.24   The Error Function F_{max} for I-Sections
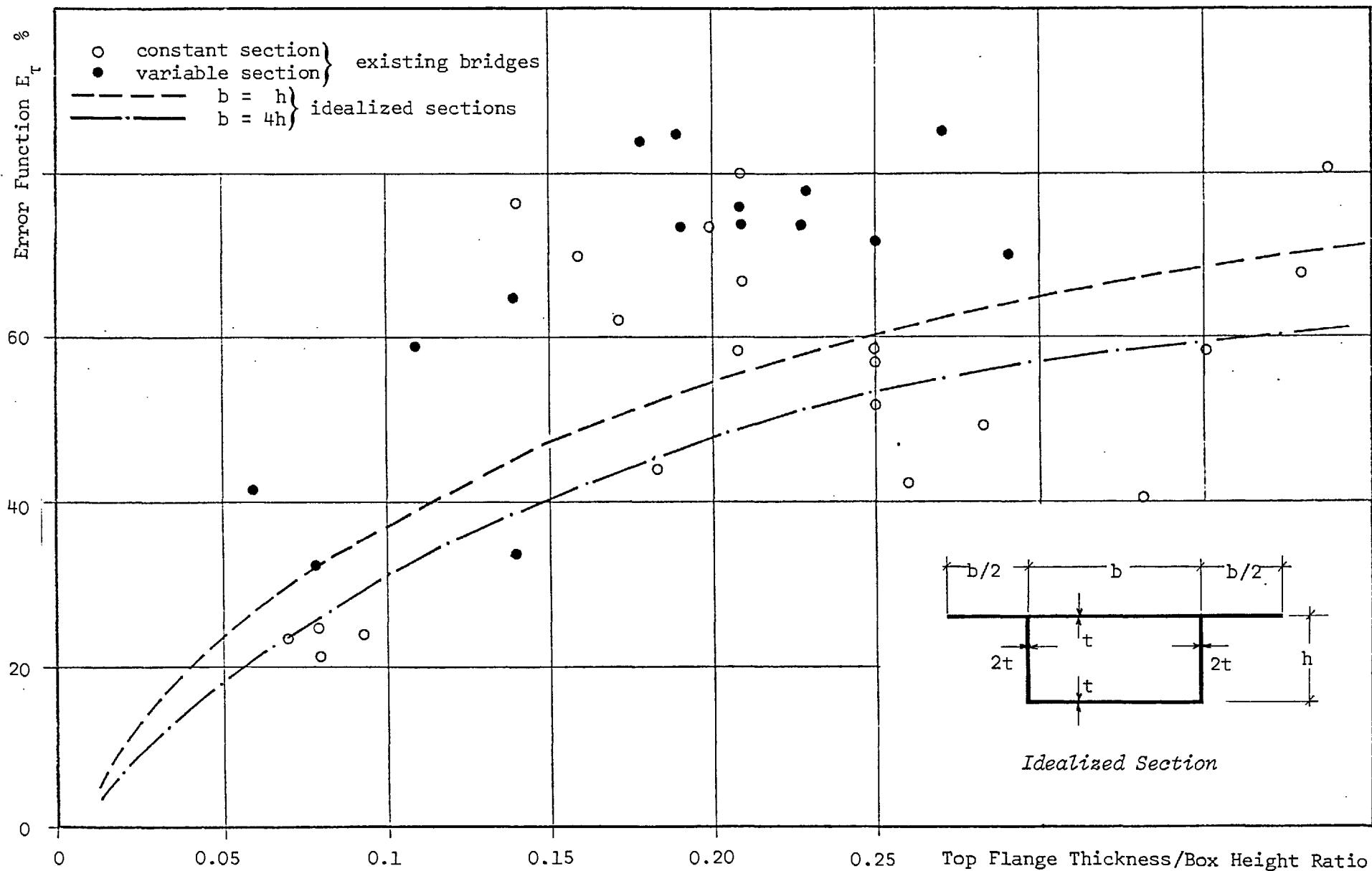
Figure 2.25   The Error in Maximum Shear Stress due to neglecting Variations in Shear Stress across the Wall Thickness
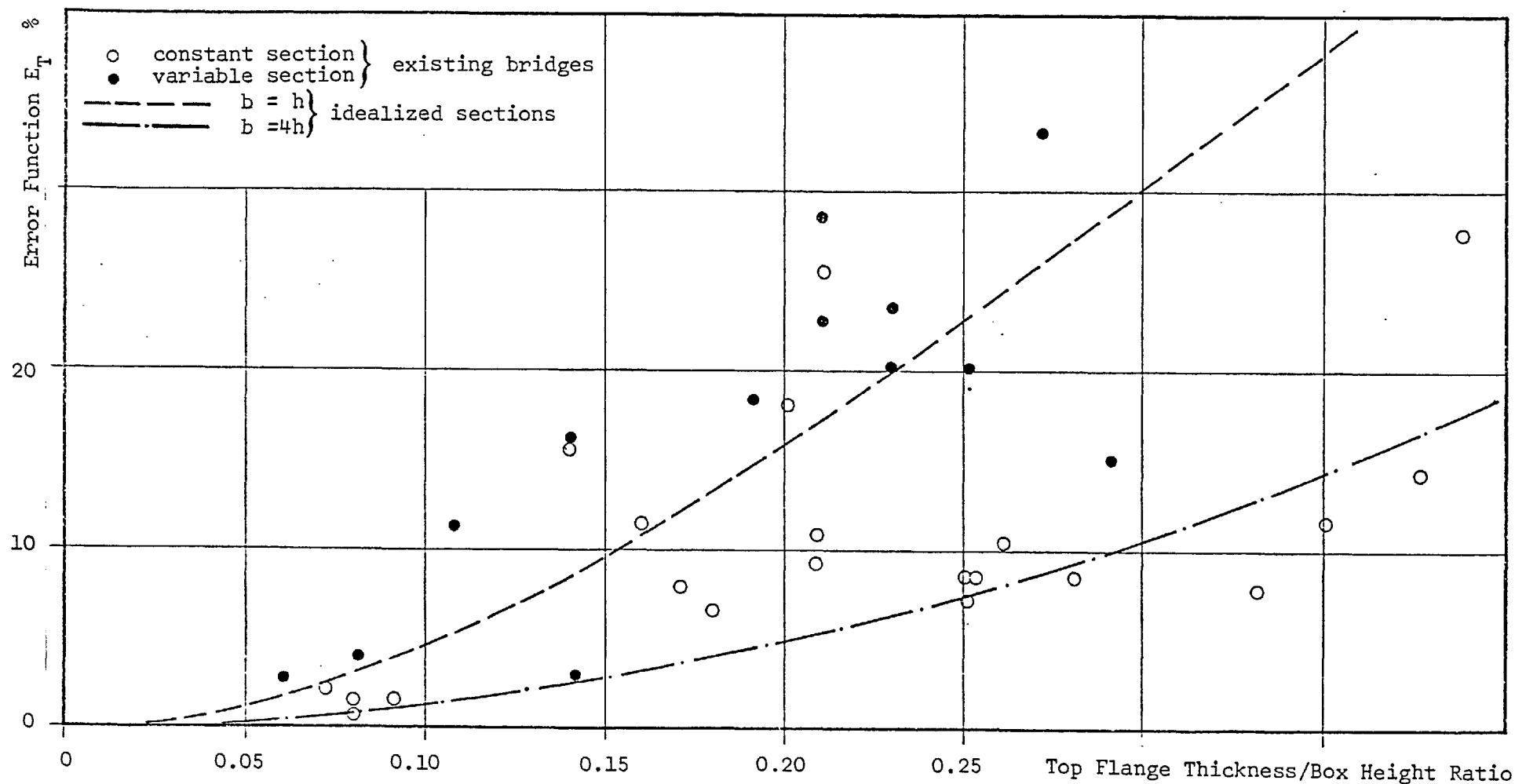
Figure 2.26   The Error in Torsional Capacity due to neglecting Variations in Shear Stress across the Wall Thickness

CHAPTER THREE

THE ELASTIC ANALYSIS OF CURVED, THIN-WALLED MEMBERS

3.1   INTRODUCTION

Although numerous methods of elastic analysis are already available, the most suitable approach for a particular application largely depends on the structural actions to be considered, the computational facilities available and the accuracy of solution required. In this chapter, limitations of the existing methods are first discussed with particular reference to two of the most important uses of thin-walled concrete sections, namely, the box girder bridge and the shear core.   A general stiffness method is then developed which is suitable for the analysis of complex structures of variable cross-section comprising both straight and curved thin-walled members.

3.1.1   Box Girder Bridges

With the present tendency to use more slender sections in this form of construction, simple beam theory is rarely adequate and warping torsion and distortional effects must frequently be taken into consideration.   A number of analytical methods have been developed for this purpose in recent years and these are summarized in Table 3.1. Based on studies[69,70] of over 500 publications on the subject of thin-walled beams, this table was originally presented by Maisel *et al*[71] in a paper on concrete box girder bridges.

Methods suitable for Hand Calculation

In a subsequent report on the analysis of straight, rectangular, single cell bridges of uniform cross-section, Maisel and Roll[70] have discussed the use and relative merits of methods (1) to (8) in some detail.   While individually these methods are somewhat limited

ANALYTICAL METHOD	TYPE OF STRUCTURAL ACTION CONSIDERED						
	Longitudinal Bending	St. Venant Torsion	Transverse Bending Distortion	Torsional Warping	Distortional Warping	Shear Lag	Local Effects
1. Simple Beam Theory	●	●					
2. Knittel[49]			●				
3. Equivalent Beam (Richmond)[92]			●		●		
4. Kupfer[56]			●		●		
5. Kollbrunner and Hajdin[51], Heilig[38]				●			
6. Beam-on-elastic-foundation Analogy[99]			●		●		
7. Reissner[91]						●	
8. Influence surfaces for plates[87] and frame analysis[15] for local transverse bending							●
9. Grillage Theory[113,114]	●	●	●				
10. Folded Plate Theory	●	●	●	●	●	●	●
11. Finite Strip Theory[17,65]	●	●	●	●	●	●	●
12. Finite Element Theory	●	●	●	●	●	●	●
13. Shell Theory	●	●	●	●	●	●	●

Table 3.1 Methods of Elastic Analysis for Concrete Box Girder Bridges[71]

in application, their combined use enables the effects of all the important structural actions to be realistically assessed with nothing· more powerful than a programmable calculator.

In structures where a significant proportion of the design load is provided by self weight alone, longitudinal bending is likely to be the dominant structural action. In such cases, simple beam theory (1) will generally give a sufficiently accurate estimate of web depth and thickness for initial design purposes. On the other hand, the thickness of the top flange is usually governed by local effects due to wheel loading and this can most easily be assessed using influence surfaces (8).

With the approximate dimensions thus determined, the remaining hand methods may then be used to check the adequacy of the section against warping and distortional effects induced by eccentric live loading. Maisel and Roll favour the beam-on-elastic-foundation analogy (6) for the analysis of distortional behaviour since it does not require significantly more computational effort than methods (2) to (4) and is applicable to a wider range of cross-sectional dimensions. Method (5) is recommended for evaluating the effects of warping restraint and, while this is essentially the analysis due to Vlasov[109], it has been extended to include both open and closed sections subject to a variety of torsional loads and conditions of end restraint.

Finally, although shear lag is rarely a problem in concrete bridges of typical proportion, it too is considered in (7), but for rectangular, single cell box girders only.

Computer-Based Methods

The last five methods outlined in Table 3.1 are more general in application than those already described but, as a result, usually

require the use of a large digital computer for solution. With the
exception of the grillage theory (9), these methods derive their
generality from the use of basic shell theory in their respective
analytical developments. However, the costs associated with computer-
based methods can often be prohibitive and, in practice, their use is
usually restricted to the analysis of complex structural
configurations.

When used directly, general shell theory (13) requires a
solution of the governing differential equations; for complex boundary
conditions or arrangements of load this can often only be achieved
numerically. However, by idealizing the structure into discrete
plate and shell elements, only connected at common nodal points, the
problems of setting up and solving complicated differential equations
are largely avoided. This is the technique employed in the finite
element method (12) in which stress/deformation relationships are
first established at each member node. Through the use of com-
patibility and equilibrium conditions, these stress/deformation
expressions are then assembled into a series of simultaneous equations
in which the nodal deformations are the only unknown quantities. The
problem has thus been reduced to one of solving a series of simultaneous
equations although the number of elements required to adequately model
a complex box girder bridge can often necessitate the use of a very
large computer and can incur substantial costs.

In the analysis of structures which are essentially cellular
beams, these disadvantages may be overcome to a large extent by the
use of the folded plate and finite strip methods, (10) and (11). In
the folded plate approach, each of the structural components (*e.g.* the

webs, flanges, diaphragms, etc.) is represented by a single plate or shell element hinged together along their common edges. The direct solution of the governing differential equations is then avoided by approximating the components of deformation and loading as a series of sinewave functions for which a solution is readily obtainable.

The finite strip method incorporates important features of both the previously described approaches. First, the cross-section is idealized into an assemblage of finite elements taking the form of strips running the full length of the member. Then, a solution for the longitudinal distribution of the various components of deformation and stress is obtained by employing a harmonic analysis in the same way as in the folded plate method.

The grillage analysis (9) is similar to the finite element method, in many respects, in that the structure is first idealized into an assemblage of representative elements and then a stiffness approach is employed for solution. However, since only beam elements are used in this theory, the various structural actions considered by the other computer-based methods cannot all be taken into account. Indeed, only longitudinal bending and St. Venant torsion effects are usually incorporated into the individual member stiffness matrices, although a good approximation of the transverse bending behaviour may also be obtained by representing the transverse slab action with idealized cross-beams of appropriate stiffness.

3.1.2   The Shear Core

The most recent state of the art report on the design of shear wall structures is provided by Pearce and Matthews[84], in which four major analytical methods are identified. These vary in

sophistication and are suitable for a wide variety of structural con-
figurations, ranging from single shear walls to the complex core
structures shown in fig. 1.5.

Simple Beam Theory

In this form of analysis the shear walls are assumed to act
independently of each other as simple cantilever beams (but made to
deflect together by the restraining action of the floors).   Since
only bending stressess are evaluated, the method is eminently suitable
for solution by hand calculation.   Although this approach is adequate
where the structure consists of solid, independent walls, it will
usually underestimate the total bending stiffness where any composite
action between the walls is provided by the building frame.

Frame Analogy

This analogy covers a variety of different methods in which
the shear walls and interconnecting beams are assumed to act as an
equivalent frame structure.   In its simplest form, the analysis may
be applied to a single pierced shear wall represented by two wide
columns of appropriate stiffness with the frame action provided by a
cross-beam at each level.   Normal hand methods of calculation may be
adequate in this case, although a computer-based stiffness or
flexibility approach will undoubtedly be necessary if axial and shear
deformations are to be taken into consideration.

The Continuous Shear Connection Method

By replacing all the cross-beams by a continuous shear medium
over the full height of the structure, the shear wall or core need no
longer be idealized into discrete storey height elements, and may once
more be considered as a simple cantilever beam.   A single governing
equation (expressed as a second order differential) is then sufficient

to describe the structural action and a solution may be obtained by hand calculation using a programmable calculator or small desk-top computer. Standard programs are readily available for this purpose although design charts could easily be prepared as an alternative.

Finite Element Method

While this method provides a powerful analytical tool, it will generally give insufficient information at the critical points (*e.g.* beam/wall connections) unless a very fine mesh is employed. Such an approach is therefore difficult to justify for the analysis of standard shear wall or shear core systems unless special problems exist. Nevertheless, this method can fulfil a useful function as a research technique, providing detailed solutions for determining the effectiveness of alternative simplified methods or for checking the results of model tests.

3.1.3   Limitations of the Existing Methods

Box Girder Bridges

Some of the first eight methods summarized in Table 3.1 have been derived for the analysis of straight, rectangular, single cell box girders only and may not be immediately suitable for other applications. This is particularly the case for the distortional and shear lag analyses but, since these structural actions (together with local effects) are beyond the scope of this thesis, the limitations of these methods will not be discussed here further.

On the other hand, simple beam theory (1) and torsional warping analysis (5) are, in their present form, equally applicable to most other cross-sectional and structural configurations. Continuity is readily accommodated by the methods of moment and bimoment distribution, the latter method recently developed by Khan and Tottenham[48] Curvature effects are also fully considered by, for example, Pippard

and Baker[86] in the case of solid and thick-walled beams, and by Dabrowski[25] and Konishi and Komatsu[53] for thin-walled sections. Nevertheless, if these two approaches are to remain suitable for hand calculation, they are still effectively restricted to the analysis of constant sections subject to simple systems of loading and restraint.

For structures incorporating features such as variations in cross-section, complex loading arrangements, irregular systems of support, curvature, continuity, skew, etc., recourse to one of the computer-based methods is usually necessary. In this connection, the generality of methods (9) to (12) is particularly attractive, whereas general shell theory (13) is rarely used due to difficulties encountered in deriving and solving the governing differential equations.

The harmonic form of solution, employed by the folded plate and finite strip methods, enables bridges with most general arrangements and systems of loading and restraint to be accommodated provided that the cross-section is constant between supports. However, only 29% of the 173 structures investigated by Swann[102] in his recent international survey of concrete box girder bridges actually complied with this last condition and these methods would seem to be severely restricted in their general application. Furthermore, the same survey indicated that no bridges above 70 m and only approximately half of those between 30 - 40 m spans, for example, displayed a constant cross-section, thus further limiting these methods to short span bridges where simplified analytical approaches are often favoured.

For complex structures with variable cross-sections, the grillage and finite element methods are undoubtedly the most suitable.

Their stiffness formulation also enables further complexities to be readily accommodated, such as irregular general arrangements caused by road junctions or alignment problems.

In the finite element method, the original configuration is closely represented by an assemblage of plate or shell elements.   By selecting suitable types of elements for each of the basic structural components, *i.e.* the webs, flanges, diaphragms, etc., the effects of all the primary and secondary actions associated with thin-walled beams may be readily included in the analysis.   However, even with the development of large elements especially for box girder applications[116], a complex general arrangement will usually necessitate the use of numerous elements for an accurate assessment of these effects.   As a result, significant costs can be incurred in the preparation of input data and in the computer time necessary for solution.   The correspondingly large volume of output generated by such an analysis is also difficult to assimilate and, in the form of local stress components, is not always directly suitable for design purposes.

In the alternative grillage approach, the structure is first idealized by a series of inter-connected beam elements.   These are usually positioned along the centreline of each web and assigned a proportion of the total flexural and torsional stiffness of the member. Recommendations are available elsewhere[113,114] for the correct apportionment of structural stiffness and also for the best methods of accommodating the effects of skew, etc..   On the other hand, curvature is usually approximated by a number of equivalent straight beams, although Sawko[95] and Tezcan and Ovunc[105] have recently developed a circular curved element which should permit significant savings to be made in both data preparation and computer running time.

The excellent load distribution properties, which are a characteristic feature of box girder bridges, may also be taken into consideration by representing the transverse actions of the flanges and diaphragms with closely spaced cross-beams of suitable shear stiffness. However, since the structural idealization is essentially two-dimensional, Maisel *et al*[71] consider this form of analysis to be most appropriate for pseudo-slab or multi-cellular sections with more than four cells. This is disputed by Hambly and Pennels[36] who have demonstrated that twin cell boxes can also be adequately modelled by the shear-flexible grillage although Maisel (in the discussion to his joint paper[71]) points out that localized distortional warping response due to a HB vehicle would not be well represented in this case. Furthermore, a fairly large amount of additional hand calculation is required if the method is to be applied to boxes with four cells and this reduces the justification for using a highly computerized analytical technique.

Finally, since only simple beam actions are considered in the formulation of the basic beam elements, this method cannot be expected to evaluate the effects of the additional structural actions outlined in Table 3.1. However, Reilly[90] and Takaba and Naruoka[103] have recently developed a straight beam element with a fourth degree of freedom in which the effects of warping restraint are considered. Unfortunately, this derivation is only immediately applicable to open sections since the effects of warping shear deformation associated with closed boxes has not been included.

The Shear Core

The cantilever beam approach outlined in §3.1.2 is too simplistic for the analysis of shear core structures and is more

appropriate for systems of independent shear walls.   On the other hand, the application of a three-dimensional finite element idealization to what is essentially a one-dimensional structure, necessitates the use of a large number of elements for a satisfactory solution.   It also incurs a penalty in terms of both time and cost.   Not surprisingly, therefore, the major analytical developments in recent years have taken place within the two remaining classifications, namely, the frame analogy and the continuous shear connection methods.

For simple open sections a solution in closed form due to Vlasov[109] is readily available.   However, since structures with this formation are torsionally very weak and subject to significant warping, cross-beams are invariably provided at each level.   In this case, the analyst may either consider the structure as an open section, representing the action of the beams at each level by externally applied bimoments, or, alternatively, as a pseudo-closed section in which the beams are replaced by a continuous membrane of equivalent shear stiffness.

In the former approach, the structure must first be idealized into storey height elements; the stiffness method has then been successfully employed by several researchers to obtain a solution.   The correct member stiffness matrix for the open section, in which the effects of warping restraint are fully taken into account, has been derived by Heiderbrecht and Swift[37], Mallick and Dungar[72] and Stafford Smith and Taranath[98].   Since the magnitude of the external bimoment applied at each level is a function of the state of deformation of the core, its effect may simply be incorporated into the analysis as a modification to the stiffness matrix of each storey height element.

The same structural idealization is also used by Liauw[63] who has adopted the transfer matrix method for solution, and by Irwin and Bolton[40] who use an energy approach based on the Rayleigh-Ritz method. Unlike the stiffness approach, where a digital computer is invariably required, these two methods are suitable for hand calculation with a programmable calculator. However, there is an inherent disadvantage in using this approach, not in the method of solution but in the initial structural idealization. By considering the structure as an open section and representing the action of the cross-beams as externally applied loads, no account can be taken of the change in the shear centre position which occurs due to the partial closure of the section.

In the alternative approach an attempt is made to represent the connectivity effect of the cross-beams by replacing them with a continuous shear membrane. The equivalent thickness of this membrane depends on the shear stiffness of the beams and is discussed more fully elsewhere[47,84]. The sectorial properties of the section may then be calculated in accordance with §2.3, and Khan and Stafford Smith[47], Michael[75] and Rosman[93] have all used this method to obtain a solution in closed form. The change in shear centre position is fully considered in this approach although, in the absence of a suitable stiffness formulation for closed sections, only simple structures of constant section can be analysed.

A comparative study of the two basic approaches has been undertaken by Khan and Stafford Smith[47] on simple core structures of identical square cross-section but with cross-beams of different depths. When the beam depth was only one-eighth of the floor height, the maximum bimoment and torsional deformations predicted by the two

- 115 -

methods compared very favourably. However, the frame analogy
underestimated the rotation and overestimated the bimoment by
approximately 10% when the beam depth was increased to a quarter of
the floor height, and by a factor of two as the beam depth/floor
height ratio approached half. Thus, while the stiffness approach
adopted by the frame analogy is attractive, the method has limited
application in the analysis of structures with substantial inter-
connecting beams.

Developments Considered in this Thesis

It has been demonstrated that in the case of box girder
bridges with complex general arrangements and cross-sectional configur-
ations, the most appropriate methods of analysis are those in which the
structure is considered as an assemblage of discrete elements. Of the
numerous techniques available only the finite element and grillage
analyses readily comply with this requirement. However, bridges,
even those incorporating junctions or other irregularities, are
essentially one-dimensional structures, and the three- and two-
dimensional idealizations respectively adopted by the finite element
and grillage methods are not entirely suitable.

While a stiffness approach is maintained, the remainder of
this chapter is devoted to developing a beam element which fully
considers the effects of warping and is applicable to all cross-
sectional configurations. In this way, all the important structural
actions identified in §1.3.1 can be taken into account while, at the
same time, considerably reducing the volume of input/output data and
the computer time necessary for solution.

In the case of members displaying a high degree of curvature,
further economies are possible by eliminating the need for a large

number of end-connected straight beam elements. For this purpose a circular curved beam element has also been developed. The data storage requirements, even for complex structures, is now within the capacity of most small desk-top computers and, therefore, this method should find immediate application in the design office.

The proposed analysis also further extends the usefulness of the continuous shear connection method in the design of shear cores since it provides a degree of generality that is not possible with a solution in closed form. Structures incorporating changes of cross-section, variable wall thicknesses and cross-beams of differing depth can now be analysed by this method without neglecting the effects of the changing shear centre position.

3.2   GENERAL SOLUTION FOR THIN-WALLED MEMBERS

For most beam configurations the values of the resultant bending moment, torsion, etc., at any point, may be simply obtained by considerations of equilibrium. However, this is not possible in the case of bimoment and warping torsion, and the longitudinal distributions of these terms must be determined from the governing fundamental equations. These have been derived previously in eqns. 2.35 and 2.69 for open and closed sections respectively.

3.2.1   Circular Curved Beams

The general solution presented here for circular curved members is based on the simply-supported girder system, shown in fig. 3.1, in which the bending moment and direct force are determinate quantities at any section, $z = r.\alpha$, along the beam. Furthermore, since the horizontal separation between the shear and centroidal axes is generally very small for all practical cases, the distance r now refers to the radius of curvature of either axis.
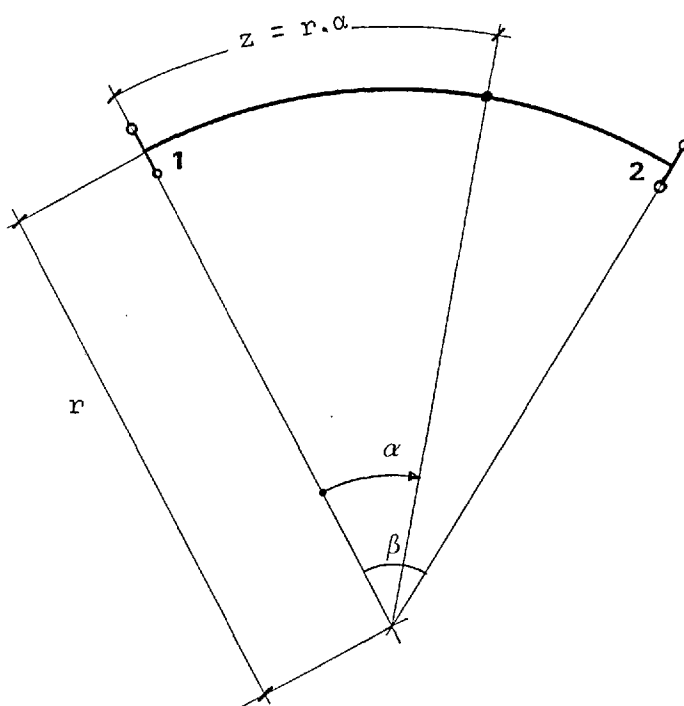
Figure 3.1 The Basic System for Circular Curved Members

Open Sections

The fundamental equation, derived in eqn. 2.35 for open sections, is solved by first considering the homogeneous differential equation

$$\phi^{iv} - k^2 . \phi'' = 0 \qquad\qquad 3.1$$

for which the general solution is

$$\phi = k_1 \sinh kz + k_2 \cosh kz + k_3 z + k_4 \qquad\qquad 3.2$$

The constants k_{1-4} are determined by substituting ϕ from this expression into eqns. 2.35 and 2.34, and by successively applying the following boundary conditions:

$$\phi = \phi_1; \quad \phi' = \phi_1'; \quad T = T_1; \quad B = B_1 \qquad\qquad 3.3$$

at $z = 0$ (*i.e.* at end 1 of the curved beam illustrated in fig. 3.1). In this way the reduced angle of twist, ϕ, is established in terms of the initial parameters at end 1 only, and is given by

$$\phi = \phi_1 + \phi_1' . \frac{\sinh kz}{k} + B_1 \frac{(1 - \cosh kz)}{GI_d} + T_1 \frac{(kz - \sinh kz)}{k.GI_d} \qquad 3.4$$

However, this solution is only strictly valid for beams subject to constant torsion ($T' = 0$), as depicted in fig. 2.1.

Now consider the circular curved member, shown in fig. 3.2, additionally loaded with concentrated torques, T_i (i=1, m), and uniformly distributed torques t_j (j=1, n), at various positions along the beam. The end forces $M_{1,2}$, $N_{1,2}$, and $V_{1,2}$, together with additional loads (not shown in fig. 3.2) applied throughout the span, also induce general distributions of bending moment, M, and direct force, N.

By taking moments about the tangent to the curved longitudinal axis at $z = r.\alpha$, we have

$$T = T_1 - \sum_{i=1}^{m} T_i - \sum_{j=1}^{n} t_j (z_{j1} - z_{j2}) - \int_0^z \frac{(M - N.y_o)}{r} . dz \qquad 3.5$$

$$\ell = \hat{r}.\beta$$
$$z = r.\alpha$$
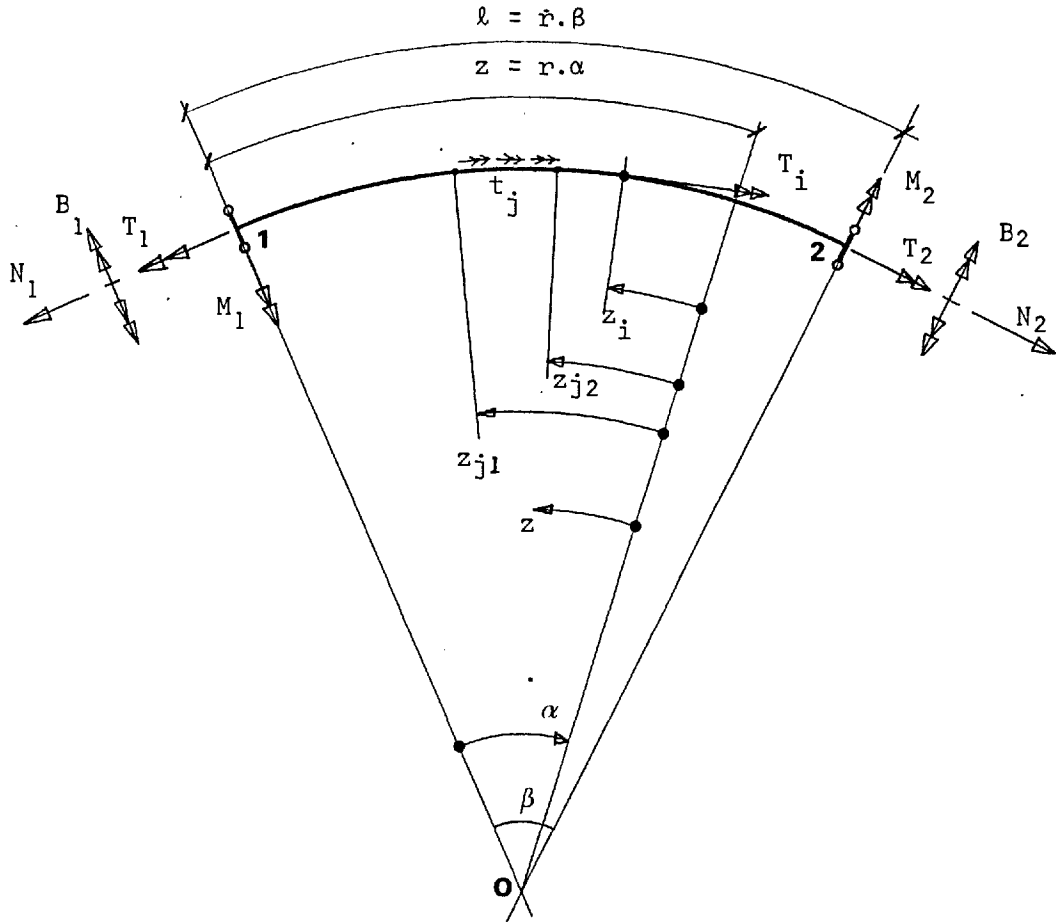
Figure 3.2   The Circular Curved Member subject to General Loading

After differentiation with respect to z, this takes a similar form

to eqn. 2.33 previously derived for the simple case.   If the distrib-

ution of bending moment and direct force along the beam are known,

which they are in the basic system, then the effects of the additional

torsional loading from eqn. 3.5 may be included in the original

solution[25] (eqn. 3.4), to give

$$\phi = \left\{ \text{Eqn. } 3.4 \right\} - \sum_{i=1}^{m} T_i \left[\frac{(kz_i - \sinh kz_i)}{kGI_d} \right] - \sum_{j=1}^{m} \frac{t_j}{GI_d} \left[\frac{(z_{j1}^2 - z_{j2}^2)}{2} \right] -$$

$$\left. \frac{(\cosh kz_{j1} - \cosh kz_{j2})}{k^2} \right] - \int_{o}^{z} \frac{(M - N.y_o)}{krGI_d} \cdot (k\bar{z} - \sinh k\bar{z}) d\bar{z} \qquad 3.6$$

Furthermore, by differentiating this expression twice with respect to z, and introducing eqns. 2.25 and 2.36 where appropriate, solutions for the unit twist, ϕ', and the bimoment, B, may also be obtained, in the following way:

$$\phi' = \phi_1' \cosh kz - B_1 k \frac{\sinh kz}{GI_d} + T_1 \frac{(1-\cosh kz)}{GI_d} - \sum_{i=1}^{m} T_i \cdot \frac{(1-\cosh kz_i)}{GI_d}$$

$$- \sum_{j=1}^{n} \frac{t_j}{kGI_d}\left[(kz_{j1} - kz_{j2}) - (\sinh kz_{j1} - \sinh kz_{j2}) \right] - \int_{o}^{z} \frac{(M-N \cdot y_o)}{rGI_d} \cdot (1-\cosh k\bar{z}) \cdot d\bar{z} \qquad 3.7$$

and

$$B = -\phi_1' GI_d \frac{\sinh kz}{k} + B_1 \cosh kz + T_1 \frac{\sinh kz}{k} - \sum_{i=1}^{m} T_i \cdot \frac{\sinh kz_i}{k}$$

$$- \sum_{j=1}^{n} \frac{t_j}{k^2} (\cosh kz_{j1} - \cosh kz_{j2}) - \int_{o}^{z} \frac{(M-Ny_o)}{kr} \cdot \sinh k\bar{z} \cdot d\bar{z} \qquad 3.8$$

Closed Sections

The homogeneous differential equation

$$f^{iv} - k^2 \cdot f'' = 0 \qquad 3.9$$

is derived from eqn. 2.69 and is applicable to all sections with closed, open/closed or multi-cellular configurations. The solution of this equation has the same general form as eqn. 3.2, although the constants are now determined by applying the following boundary conditions, at z = 0:

$$f = f_1 \; ; \quad f' = f_1' \; ; \quad T = T_1 \; ; \quad B = B_1 \qquad 3.10$$

Accordingly, for applications of constant torque, the dimensionless warping function, f, may be expressed as

$$f = f_1 + f_1' \cdot \frac{\sinh kz}{k} + B_1 \frac{(1-\cosh kz)}{\mu GI_d} + T_1 \cdot \frac{(kz-\sinh kz)}{\mu kGI_d} \qquad 3.11$$

in which the parameters μ, k are now those defined in eqns. 2.67 and 2.70, respectively. Furthermore, since the equilibrium condition (eqn. 3.5) is equally valid for sections with closed parts, eqn. 3.11 may be modified for the general case, to give

$$f = \left\{\text{Eqn. 3.11}\right\} - \sum_{i=1}^{m} T_i \cdot \frac{(kz_i - \sinh kz_i)}{kGI_d} - \sum_{j=1}^{n} \frac{t_j}{GI_d} \cdot \left[\frac{(z_{j1}^2 - z_{j2}^2)}{2} - \right.$$

$$\left. \frac{(\cosh kz_{j1} - \cosh kz_{j2})}{k^2} \right] - \int_{o}^{z} \frac{(M - N \cdot y_o)}{krGI_d} \cdot (k\bar{z} - \sinh k\bar{z}) . d\bar{z} \qquad 3.12$$

However, this solution for the warping function, f, is not particularly useful since the boundary conditions at a built-in-end are not $f_1 = f_1' = 0$ (in analogy with $\phi_1 = \phi_1' = 0$, for open sections), but $\phi_1 = f_1' = 0$. Nevertheless, by integrating eqn. 2.65 the following relationship is obtained:

$$f = \frac{1}{\mu} \cdot \left[\phi - \frac{T \cdot z}{GI_c} \right] + k_5 \qquad 3.13$$

from which, with z = 0 at end 1, we have

$$f_1 = \frac{\phi_1}{\mu} + k_5 \qquad 3.14$$

Now, by substituting f, f_1 from eqns. 3.13 and 3.14 into eqn. 3.12, the unknown constant of integration, k_5, is eliminated and an expression for the reduced angle of rotation, ϕ, is obtained, thus:

$$\phi = \phi_1 + f_1' \frac{\mu}{k} \sinh kz + B_1 \frac{(1 - \cosh kz)}{GI_d} + T_1 \frac{(kz - \mu \sinh kz)}{kGI_d}$$

$$- \sum_{i=1}^{m} T_i \cdot \frac{(kz_i - \mu \sinh kz_i)}{kGI_d} - \sum_{j=1}^{n} \frac{t_j}{GI_d} \cdot \left[\frac{(z_{j1}^2 - z_{j2}^2)}{2} - \frac{\mu}{k^2} (\cosh kz_{j1} - \cosh kz_{j2}) \right]$$

$$- \int_{o}^{z} \frac{(M - N \cdot y_o)}{krGI_d} \cdot (k\bar{z} - \mu \sinh k\bar{z}) . d\bar{z} \qquad 3.15$$

The other necessary terms f',B, are obtained directly by differentiating eqn. 3.15 twice with respect to z and introducing eqns. 2.48 and 2.70. For clarity, these expressions have been summarized in Table 3.2 together with eqns 3.15 and 3.5 for the functions ϕ and T, respectively. Furthermore, by putting $\mu = 1$ (and noting in this case that $f' = \phi'$), the equations in Table 3.2 reduce to those previously derived for open sections (eqns. 3.5-3.8), demonstrating once more the usefulness of the approximation introducted by Benscoter[11].

3.2.2   Straight Beams

The basic system used for the general solution of straight beams is shown in fig. 3.3, together with additional torsional loads T_i, t_j, applied throughout the span. Bending moments and direct forces of known distribution may also be present but have no torsional component and need not be considered further at this stage.
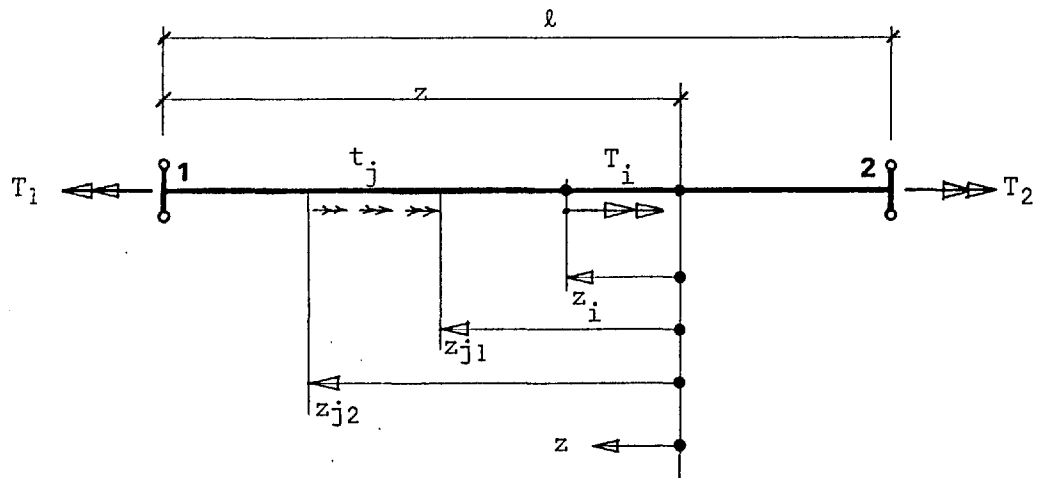
Figure 3.3   The Basic System for Straight Members

Taking moments at a point distance z from end 1, the resultant torque is given by

$$T = T_1 - \sum_{i=1}^{m} T_i - \sum_{j=1}^{n} t_j \ (z_{j1} - z_{j2}) \qquad 3.18$$

which is similar to eqn. 3.5 for curved beams except that the final term is no longer applicable. Accordingly, the stress resultants T, B, and the corresponding deformations ϕ, f', for straight members are derived directly from Table 3.2 where the final column due to member curvature has been omitted.

	ϕ_1	f'_1	B_1	T_1	T_i	t_j from z_{j1} to z_{j2}	Contribution due to curvature	
ϕ	1	$\dfrac{\mu \sinh kz}{k}$	$\dfrac{1-\cosh kz}{GI_d}$	$\dfrac{kz-\mu \sinh kz}{k \cdot GI_d}$	$-\sum\limits_{i=1}^{m} \dfrac{(kz-\mu \sinh kz_i)}{k \cdot GI_d}$	$-\dfrac{1}{GI_d} \cdot \sum\limits_{j=1}^{n} \left[\dfrac{z_{j1}^2-z_{j2}^2}{2} - \dfrac{\cosh kz_{j1}-\cosh kz_{j2}}{k^2} \right]$	$-\int\limits_0^z \dfrac{(M-N\cdot y_o)}{kr\, GI_d} \cdot (kz-\mu \sinh kz).dz$	3.15
f'	–	$\cosh kz$	$-\dfrac{k \sinh kz}{\mu\, GI_d}$	$\dfrac{1-\cosh kz}{GI_d}$	$-\sum\limits_{i=1}^{m} \dfrac{(1-\cosh kz_i)}{GI_d}$	$\dfrac{1}{kGI_d} \cdot \sum\limits_{j=1}^{n}\{[kz_{j1}-kz_{j2}] - [\sinh kz_{j1}-\sinh kz_{j2}]\}$	$-\int\limits_0^z \dfrac{(M-N\cdot y_o)}{r\, GI_d} \cdot (1-\cosh kz).dz$	3.16
B	$-\dfrac{\mu\, GI_d}{k} \cdot \sinh kz$		$\cosh kz$	$\dfrac{\mu \sinh kz}{k}$	$-\sum\limits_{i=1}^{m} \dfrac{\mu \sinh kz_i}{k}$	$-\dfrac{\mu}{k^2} \cdot \sum\limits_{j=1}^{n} [\cosh kz_{j1}-\cosh kz_{j2}]$	$-\int\limits_0^z \dfrac{(M-N\cdot y_o)}{kr} \cdot \mu \sinh kz . dz$	3.17
T	–	–	–	1	-1	$-\sum\limits_{j=1}^{n} [z_{j1}-z_{j2}]$	$-\int\limits_0^z \dfrac{(M-N\cdot y_o)}{r} . dz$	(3.5)

Table 3.2   Stress Resultants and Components of Deformation for Closed Sections

3.3   FLEXIBILITY ANALYSIS

Statically indeterminate frame or grillage type structures, which are capable of being idealised as a system of end-connected beam elements, may be analysed by two alternative methods. These are widely referred to as the flexibility and stiffness approaches although both methods use exactly the same conditions of equilibrium and compatibility to arrive at a solution. However, whereas the flexibility method first uses conditions of equilibrium, which then give rise to equations of joint compatibility, the reverse is true for the stiffness method.

The first step in the analysis of hyperstatic structures, by the flexibility method, is the introduction of sufficient imaginary releases to transform the system into determinate form. In general, the efficiency of the solution is not affected by the positioning of the releases, although, where the idealised system consists of members forming closed cells, they should be applied so as to establish a single-path structure.

In the determinate system, so formed, there are now sufficient equations of joint equilibrium to enable the redundant forces and applied loads to be defined in terms of the remaining member end-forces only. Furthermore, if a relationship between the member end-forces and the corresponding end-displacements can be established, then joint compatibility conditions may be introduced to provide a unique solution for the redundant forces. Subsequently, these may be substituted back into the equilibrium and compatibility equations for the evaluation of the remaining member end-forces and all the joint displacements.

Thus, the major requirement of this method is the determination of the general relationship between member end-loads and the corresponding

end-displacements in explicit form. For the member fully fixed at

end 1, this relationship may be expressed as

$$e_2 = F p_2$$

<div align="right">3.19</div>

where e_2, p_2 are the vectors containing the displacement and load

terms corresponding to the n degrees of freedom being considered at

end 2, and F is the nxn matrix to be determined. The matrix F is

generally referred to as the *flexibility* matrix and is evaluated in

§ 3.3.3 for curved and straight members where the effects of warping

restraint have been included.

3.3.1 Total Strain Energy

The concept of total strain energy (or more correctly

complementary energy) is frequently used for the evaluation of flexibility

matrices due to the ease with which the displacement terms may be

derived. For the loaded beam, the total strain energy, U, is given by

$$U = \frac{1}{2} \int_\ell \int_A \left(\frac{\sigma^2}{E} + \frac{\tau^2}{G} \right) . dA.dz$$

<div align="right">3.20</div>

where the integrals are effective over the entire cross-sectional area

and length of the member.

If the direct and shear stress components in eqn. 3.20 are

restated in terms of the applied load system at end 2 only, it follows

directly that the ith term in the displacement vector e_2 is given by

$$e_{2i} = \frac{\partial U}{\partial p_{2i}}$$

<div align="right">3.21</div>

where p_{2i} is the corresponding i^{th} load term.

Open Sections

For the case where only bending about the x-axis and torsion

(including the effects of warping restraint) are being considered, the

cross-sectional distributions of direct and shear stress (from eqn. 2.1)
are given by

$$\sigma = \frac{M}{\Psi I_x} \left[y - x. \frac{I_{xy}}{I_y} \right] + \frac{B.\omega}{I_w}$$

and

$$\tau = \frac{2T_{sv}.n}{I_d} - \frac{T_w.S_w}{\delta.I_w}$$

3.22

Here, the bimoment and warping torsion terms are based on the principle
sectorial co-ordinate system, whereas the x-axis corresponds to the
horizontal direction in order to account for vertical (gravitational)
loads more easily. Accordingly, the contribution due to bending moment
in the first of eqns. 3.22 is the more general term associated with a
non-principle co-ordinate system. In this the dimensionless parameter,
Ψ, is defined as

$$\Psi = 1 - \frac{I_{xy}^2}{I_x.I_y}$$

3.23

Clearly, for sections singly symmetric about either the x-axis or the
y-axis, $I_{xy} = 0$, $\Psi = 1$ and the direct stress contribution due to bending
moment reduces to that found in eqn. 2.1.

By introducing the stress components from eqn. 3.22 into
eqn. 3.20 and integrating over the cross-sectional area only, the total
strain energy is given by

$$U = \int_{o}^{\ell} \left\{ \frac{M^2}{2\Psi EI_x} + \frac{B^2}{2EI_w} + \frac{T_{sv}^2}{2GI_d} \right\} . dz$$

3.24

in which use has been made of the definitions of the various cross-
sectional and sectorial functions, together with the following
relationships determined by partial integration:

$$\int_A S_w . dA = 0 \quad ; \quad \int_A S_w^2 . dA = 0$$

The more useful expression, in terms of the total torque, T, is now obtained simply by putting $T_{sv} = T - T_w$ into eqn. 2.24, thus:

$$U = \int_o^\ell \left\{ \frac{M^2}{2\Psi EI_x} + \frac{B^2}{2EI_w} + \frac{T^2}{2GI_d} + \frac{T_w^2}{2GI_d} - \frac{T.T_w}{GI_d} \right\} . dz \qquad 3.25$$

Closed Sections

In the same way, the components of direct and shear stress for sections with closed parts are derived from eqn. 2.2 and take the more general form:

$$\sigma = \frac{M}{\Psi I_x} \left[y - x . \frac{I_{xy}}{I_y} \right] + \frac{B.\hat{\omega}}{I_{\hat{w}}}$$

$$\text{and} \quad \tau = \frac{T}{G.\delta} - \frac{B'.S_{\hat{w}}}{\delta.I_{\hat{w}}} \qquad \left. \right\} \qquad 3.26$$

Substituting the first of these expressions into eqn. 3.20 and using the alternative definition for shear stress given by eqn. 2.59, the total strain energy may be expressed as

$$U = \int_o^\ell \left\{ \frac{M^2}{2\Psi EI_x} + \frac{B^2}{2EI_{\hat{w}}} + \frac{G}{2} . \int_A \left[\frac{\partial w}{\partial s} + r_s . \phi' \right]^2 . dA \right\} . dz \qquad 3.27$$

With the warping displacement given by eqn. 2.46, for the case of mixed torsion, eqn. 3.27 may be rewritten in the following form:

$$U = \int_o^\ell \left\{ \frac{M^2}{2\Psi EI_x} + \frac{B^2}{2EI_{\hat{w}}} + \frac{G}{2} . \left[(\phi'-f')^2 I_c + I_d f'(2\phi'-f') \right] \right\} . dz \qquad 3.28$$

from which, on substitution for ϕ' and f' from eqns. 2.17 and 2.65, and noting that $T = GI_d \phi' + B'$, we obtain

$$U = \int_{0}^{\ell} \left\{ \frac{M^2}{2\Psi EI_x} + \frac{B^2}{2EI_w} + \frac{T^2}{2GI_d} + \frac{B'^2}{2\mu GI_d} - \frac{T.B'}{GI_d} \right\} . dz \qquad 3.29$$

Once more, by putting $\mu = 1$ and noting that $B' = T_w$, this expression takes exactly the same form as eqn. 3.25, previously derived for the case of open sections. Indeed, despite the very different methods of derivation often necessary for open and closed sections, this is always shown to be the case. Therefore, in subsequent work only closed sections have been considered and the appropriate substitutions must be introduced to make the theory applicable to open sections.

3.3.2   Evaluation of Stress Resultants

Consider the circular curved girder shown in fig. 3.4, built-in at end 1 and subjected to a system of end loads at point 2 only. From conditions of equilibrium, the stress resultants M, T and V may be expressed directly in terms of the applied loads, in the following way:

$$M = M_2 \cos\bar{\alpha} \pm (T_2 \pm V_2 r) \sin\bar{\alpha}$$

$$T = \mp M_2 \sin\bar{\alpha} + (T_2 \pm V_2 r) \cos\bar{\alpha} \qquad 3.30$$

$$V = V_2$$

On the other hand, the equation governing the distribution of bimoment along the beam has been derived previously in eqn. 3.17 in terms of the unknown support reactions at end 1 only. For a solution in the same general form as eqn. 3.30, these initial parameters must first be determined. By putting $z = 0$, we have

$$M_1 = M_2\cos\beta \pm (T_2 \pm V_2 r)\sin\beta$$

$$T_1 = \mp M_2\sin\beta + (T_2 \pm V_2 r)\cos\beta \mp V_2 r \qquad 3.31$$

$$V_1 = V_2$$
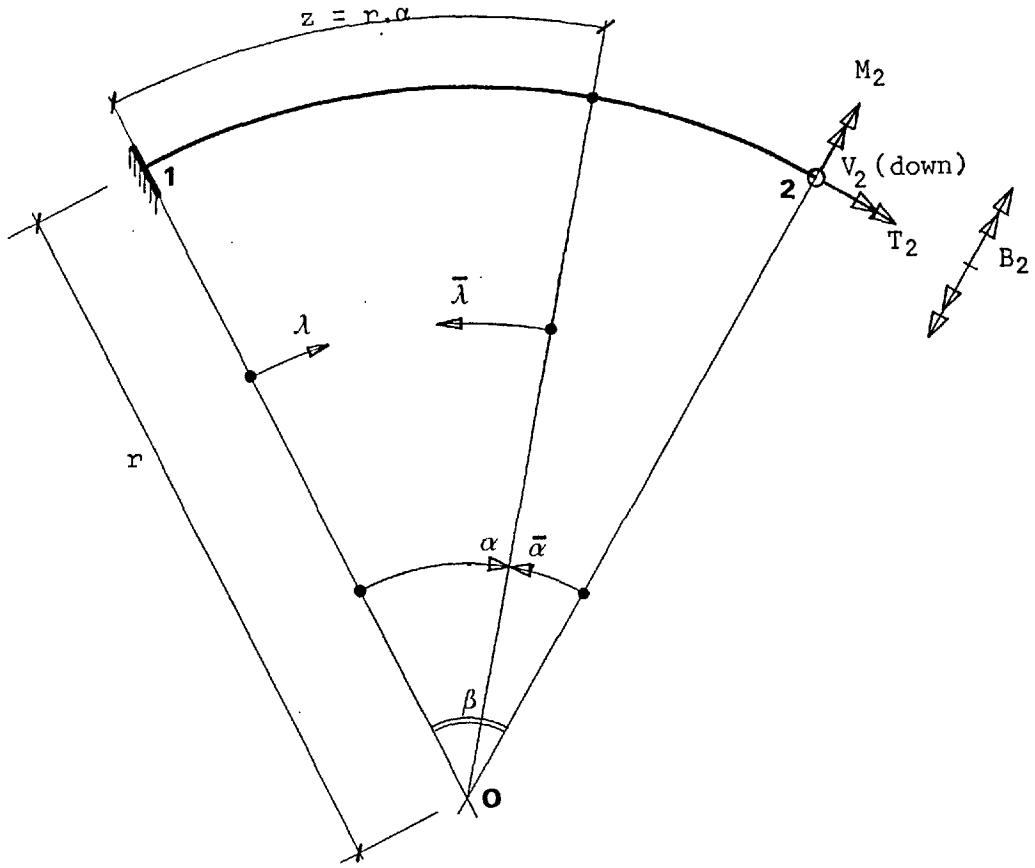
Figure 3.4   The Circular Curved Girder Built-in at End 1

and

$$B_1 = \frac{B_2}{\cosh k\ell} - T_1 \frac{\mu}{k} \tanh k\ell \mp \frac{\mu}{k.\cosh k\ell} \int_0^\beta M \sinh kr\bar{\alpha}.d\bar{\alpha} \qquad 3.32$$

Now by substituting for M and T_1 in this expression from eqns. 3.30 and 3.31, respectively, and evaluating the integral over the entire length of the beam, the following relationship for the fixed-end bimoment is obtained:

$$B_1 = \frac{B_2}{CH} - \mu(T_2 \pm V_2 r)\left(\frac{(1-\eta)}{k} \, C. \, \frac{SH}{CH} + \eta rS\right) \pm \mu V_2 \frac{rSH}{kCH}$$

$$\pm \mu M_2 \left(\frac{(1-\eta)}{k} \, S. \, \frac{SH}{CH} - \eta rC + \frac{\eta r}{CH}\right) \qquad\qquad 3.33$$

In addition to the dimensionless parameter, η, defined here by

$$\eta = \frac{1}{1+k^2 r^2} \qquad\qquad 3.34$$

the following trigonometrical abbreviations have also been introduced

in eqn. 3.33, and for clarity these will be used throughout:

$$C = \cos\beta$$
$$S = \sin\beta$$
$$CH = \cosh kr\beta$$
$$SH = \sinh kr\beta$$

$\left.\right\}$ 3.35

By introducing the appropriate terms from eqns. 3.30, 3.31

and 3.33 into eqn. 3.17 and remembering that $f_1' = 0$ at the built-in

end, the expression for bimoment may be written in terms of the end

2 load system only as

$$B = B_2 \frac{\cosh kr\alpha}{CH} + \frac{\mu}{k}\left[\mp M_2 S + (T_2 \pm V_2 r)C \mp V_2 r\right]\sinh kr\alpha \pm \frac{\mu}{k} V_2 r.\frac{SH}{CH}\cosh kr\alpha$$

$$-\mu(T_2 \pm V_2 r)\left(\frac{(1-\eta)}{k} \, C. \, \frac{SH}{CH} + \eta rS\right)\cosh kr\alpha \pm \mu M_2\left(\frac{(1-\eta)}{k} \, S. \, \frac{SH}{CH} - \right.$$

$$\left. \eta rC + \frac{\eta r}{CH}\right)\cosh kr\alpha \mp \frac{\mu}{kr}\int_{o}^{\alpha}\left[M_2\cos(\beta-\lambda)\pm(T_2\pm V_2 r)\sin(\beta-\lambda)\right]\sinh kr(\alpha-\lambda).d\lambda$$

$$3.36$$

On evaluating the integral and introducing the following

additional abbreviations:

$$c = \cos\bar{\alpha}$$

$$s = \sin\bar{\alpha}$$

$$ch = \cosh kr\bar{\alpha}$$

$$sh = \sinh kr\bar{\alpha}$$

$$\left.\right\} \quad 3.37$$

eqn. 3.36 may be considerably simplified and takes the form:

$$B = B_2(ch - \frac{SH}{CH}.sh) - \mu.\frac{(1-\eta)}{k.CH}\left[\mp M_2 S + (T_2 \pm V_2 r)C\right]sh \pm \mu r V_2 \frac{sh}{k.CH}$$

$$- \mu\eta r(T_2 \pm V_2 r)s \mp \mu\eta r M_2 \left[c - ch + \frac{SH}{CH}.sh\right] \qquad 3.38$$

Furthermore, by differentiating eqn. 3.38 with respect to z, and remembering that $dz = r.d\alpha = -r.d\bar{\alpha}$, an expression for B' is also obtained, such that

$$B' = -\frac{1}{r}.\frac{dB}{d\alpha} = B_2 k\left[\frac{SH}{CH}.ch - sh\right] + \mu\frac{(1-\eta)}{CH}\left[\mp M_2 S + (T_2 \pm V_2 r)C\right]ch$$

$$\mp \mu r V_2 \frac{ch}{CH} \mp \mu\eta kr M_2 \left[\frac{s}{kr} + sh - \frac{SH}{CH}.ch\right] + \mu\eta(T_2 \pm V_2 r)c \qquad 3.39$$

In the derivation of eqns. 3.33 and 3.38, the solutions of various complex integrals involving products of circular and hyperbolic functions have been required. Evaluation of these and other trigonometrical terms used throughout this analysis are given in Appendix 4.

Straight Beams

With reference to fig. 3.5 and Table 3.2, the various stress resultants for the end-loaded member at distance z are given by

$$M = M_2 + V_2.\bar{z}$$

$$T = T_2$$

$$V = V_2$$

$$\left.\right\} \quad 3.40a$$

and $\qquad$ $B = B_1 \cosh kz + \frac{\mu}{k} \cdot T_1 \sinh kz$ $\qquad$ 3.40b
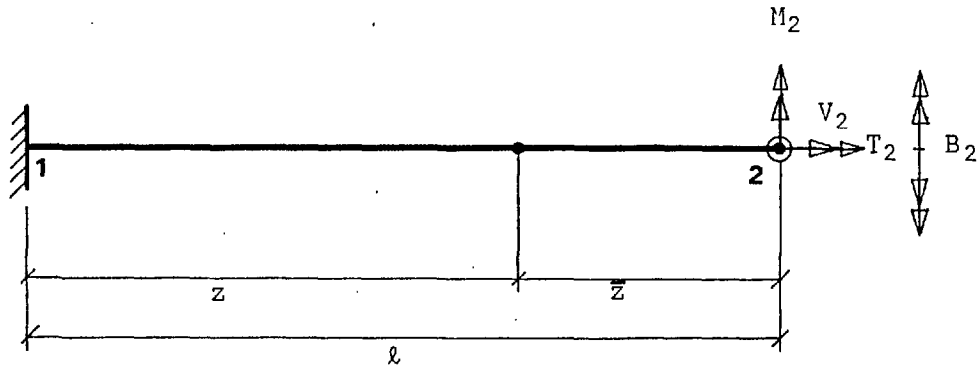
Figure 3.5   The Straight Girder Built-in at End 1

With B_1 obtained from eqn.3.40b (for z=ℓ), the distribution of bimoment may be expressed in terms of the end 2 forces only, as

$$B = B_2 \frac{\cosh kz}{\cosh k\ell} - \frac{\mu}{k} \cdot T_2 \frac{\sinh k(\ell-z)}{\cosh k\ell}$$ 3.41a

from which, after differentiating with respect to z, we have

$$B' = k \cdot B_2 \frac{\sinh kz}{\cosh k\ell} - \mu T_2 \frac{\cosh k(\ell-z)}{\cosh k\ell}$$ 3.41b

3.3.3   Formulation of the Flexibility Matrix

All the stress resultants considered in the total strain energy formula (eqn. 3.29) have now been expressed in terms of the applied load system at end 2 only and may be summarized in the following way:

$$
\begin{bmatrix} M \\ T \\ B \\ B' \end{bmatrix} =
\begin{bmatrix}
c_{11} & c_{12} & c_{13} & c_{14} \\
c_{21} & c_{22} & c_{23} & c_{24} \\
c_{31} & c_{32} & c_{33} & c_{34} \\
c_{41} & c_{42} & c_{43} & c_{44}
\end{bmatrix}
\begin{bmatrix} M_2 \\ T_2 \\ V_2 \\ B_2 \end{bmatrix}
$$

or in matrix notation by

$$\bar{p} = C\dot{p}_2 \qquad\qquad 3.42$$

In accordance with eqns. 3.30, 3.38 and 3.39 the connection

matrix **C** for curved beams is given by

$$
\begin{bmatrix}
c & \pm s & rs & 0 \\[2ex]
\mp s & c & \pm r(c-1) & 0 \\[2ex]
\mp C_1(c-ch)\pm C_2 sh & -C_1 s + C_3 sh & \mp r(C_1 s + C_4 sh) & ch + C_5 sh \\[2ex]
\mp\dfrac{C_1}{r}(S+krsh)\mp kC_2 ch & C_1\dfrac{c}{r} - kC_3 ch & \pm(C_1 c+C_4 krch) & -k(sh+C_5 ch)
\end{bmatrix}
\qquad 3.42a
$$

in which the constants C_{1-5} have been introduced for clarity and

are defined as

$$
\left.
\begin{aligned}
C_1 &= \mu nr \\[2ex]
C_2 &= \mu\left\{\frac{(1-n)}{k}\cdot\frac{S}{CH} - n^r\,\frac{SH}{CH}\right\} \\[2ex]
C_3 &= -\mu\cdot\frac{(1-n)}{k}\cdot\frac{C}{CH} \\[2ex]
C_4 &= \frac{\mu}{k.CH}\left\{(1-n)C - 1\right\} \\[2ex]
C_5 &= -\frac{SH}{CH}
\end{aligned}
\right\} \qquad 3.43
$$

With the total strain energy (eqn. 3.29) now expressible

in terms of the end 2 load system $\mathbf{p_2}$ only, the general flexibility

relationship from eqn. 3.19 may be written as

$$
\begin{bmatrix} v_2 \\ \phi_2 \\ v_2 \\ \phi_2' \end{bmatrix} = \begin{bmatrix} \dfrac{\partial U}{\partial M_2} \\[6pt] \dfrac{\partial U}{\partial T_2} \\[6pt] \dfrac{\partial U}{\partial V_2} \\[6pt] \dfrac{\partial U}{\partial B_2} \end{bmatrix} = \begin{bmatrix} f_{11} & f_{12} & f_{13} & f_{14} \\ f_{21} & f_{22} & f_{23} & f_{24} \\ f_{31} & f_{32} & f_{33} & f_{34} \\ f_{41} & f_{42} & f_{43} & f_{44} \end{bmatrix} \begin{bmatrix} M_2 \\ T_2 \\ V_2 \\ B_2 \end{bmatrix} \qquad 3.44
$$

where f_{mn} (m=1,4; n=1,4) are typical flexibility influence coefficients for the system (with four degrees of freedom) under consideration.

In accordance with eqn. 3.21, the ith component of deformation at end 2, e_{2i}, is also equivalent to

$$
e_{2i} = \frac{\partial U}{\partial \mathbf{P_{2i}}} = \int_{0}^{\ell} \left\{ \frac{M.M^*}{\Psi EI_x} + \frac{T.T^*}{GI_d} + \frac{B.B^*}{EI_{\hat{w}}} + \frac{B'.B'^*}{\mu GI_d} - \frac{B'.T^*}{GI_d} - \frac{T.B'^*}{GI_d} \right\}.dz \qquad 3.45
$$

in which, for example, the unit bending moment M^* is given by

$$
M^* = \frac{\partial M}{\partial \mathbf{P_{2i}}} \quad etc. \qquad 3.46
$$

i.e. by the numerical value of the end-force $\mathbf{P_{2i}}$ in the general definition of the term M (eqn. 3.30).

Furthermore, by expressing the stress resultants in eqn. 3.45 in terms of the end-loads $\mathbf{P_2}$ and connection matrix $\mathbf{C}$, a general equation for the derivation of individual influence coefficients is obtained, thus:

$$
3.47
$$
$$
f_{mn} = \int_{0}^{\ell} \left\{ \frac{c_{1m}c_{1n}}{\Psi EI_x} + \frac{c_{2m}c_{2n}}{GI_d} + \frac{c_{3m}c_{3n}}{EI_{\hat{w}}} + \frac{c_{4m}c_{4n}}{\mu GI_d} - \frac{c_{2m}c_{4n}}{GI_d} - \frac{c_{2n}c_{2m}}{GI_d} \right\}. dz
$$

By putting $k^2 = \dfrac{\mu GI_d}{EI_{\hat{w}}}$ \qquad (2.70)

and $j^2 = \dfrac{GI_d}{\Psi EI_x}$ \qquad (2.74)

and noting that $\displaystyle\int_0^{\ell} dz = -r \cdot \int_0^{\beta} d\bar{\alpha}$, eqn. 3.47 may be re-written

in a more convenient form, as

$$f_{mn} = \frac{-r}{GI_d} \int_0^{\ell} \left\{ j^2 c_{1m}c_{1n} + c_{2m}c_{2n} + \frac{k^2}{\mu} c_{3m}c_{3n} + \frac{1}{\mu} c_{4m}c_{4n} - c_{2m}c_{4n} - c_{2n}c_{4m} \right\} \cdot d\bar{\alpha}$$

$$3.48$$

The complex terms, resulting from the substitution of the

individual connection matrix coefficients from eqn. 3.45 into this

expression, have been integrated with the aid of Appendix 1 over the

entire span length. After considerable simplification the symmetrical

flexibility matrix **F** for the circular curved girder with four degrees

of freedom has been obtained and is presented in explicit form in

Appendix 2.1 in terms of the individual influence coefficients, f_{mn}.

Straight Beams

The relationship between the general stress resultants and

the applied forces at end 2, as expressed in eqn. 3.42, is equally

valid for straight members although the connection matrix **C** now takes

the following form:

$$\mathbf{C} = \begin{bmatrix} 1 & 0 & \bar{z} & 0 \\ 0 & 1 & 0 & 0 \\ 0 & -\dfrac{\mu}{k} \cdot \dfrac{\sinh k(\ell-z)}{\cosh k\ell} & 0 & \dfrac{\cosh kz}{\cosh k\ell} \\ 0 & \mu\dfrac{\cosh k(\ell-z)}{\cosh k\ell} & 0 & k\dfrac{\sinh kz}{\cosh k\ell} \end{bmatrix} \qquad 3.49$$

Substitution of the individual terms from this matrix into eqn. 3.47

enables the various flexibility influence coefficients to be determined

directly. For the straight member with four degrees of freedom, these

have been denoted g_{mn} (m=1,4; n = 1,4) and are presented in Appendix 2.3.

3.4   STIFFNESS ANALYSIS

The main requirement of this method, in common with the flexibility analysis, is the determination of a relationship between the end-forces and the corresponding end-displacements for each individual member. However, in this case, it is the end-displacements which are considered to be the unknown quantities and the relationship is required in the following general form:

$$\mathbf{p} = \mathbf{K}.\mathbf{d} \qquad\qquad 3.50$$

Here $\mathbf{p},\mathbf{d}$ are vectors containing the various force and displacement terms at both ends of the member, and $\mathbf{K}$ is the so-called stiffness matrix, symmetrical about the leading diagonal.

Before conditions of compatibility can be introduced, the end-forces and end-displacements for all members must first be described in terms of the same general co-ordinate system. This is achieved by a simple geometrical transformation and enables the member end-displacements to be replaced by the common joint displacements, which are always fewer in number. The individual member end-forces, defined in terms of the joint displacements, may now be combined in such a way as to satisfy the conditions of equilibrium at each joint. Thus the load vector now consists of all the joint load terms, the displacement vector contains the corresponding components of joint displacement, and the structure stiffness matrix is composed of the appropriate individual member stiffness matrices.

System restraints may now be imposed on the structure by modifying the various matrices and a unique solution for the joint displacements is obtained directly. It follows that back substitution of these displacements into eqn. 3.50 results in all the unknown member end-forces and end-displacements being established.

Choice of Analytical Method

The main theoretical difference between the stiffness
and the flexibility approaches is essentially the order in which the
conditions of joint compatibility and equilibrium are applied. However,
there are also some practical considerations which are probably more
important in determining the best method of analysis for a particular
structure. Basically, these are the degree of automation possible
and the amount of computing effort required for solution.

In the flexibility analysis it is the redundant forces
which are the unknown quantities and the number of equations to be
solved is evidently equal to the degree of indeterminacy of the
structure. However, the initial choice of the imaginary releases must
satisfy certain conditions and this can involve time consuming check
procedures if attempted automatically by computer or, alternatively,
additional input by the analyst. On the other hand, in the stiffness
method, a solution is required for all the components of joint
displacement and the number of equations is therefore directly
equivalent to the number of independent degrees of freedom present in
the system. However, once the geometry of the structural idealisation
has been input, together with the dimensions and elastic properties of
the elements, the method is entirely automatic.

In terms of the number of equations to be solved the
flexibility method would appear to have a real advantage in most
applications, except perhaps in the analysis of highly redundant spatial
systems. However, this is not always found to be the case. Indeed,
with the capacity and speed of modern computers, the solution of large
sets of linear equations is rarely a problem and the entirely automatic
procedure followed by the stiffness method usually proves overwhelmingly
attractive.

3.4.1   Formulation of the Member Stiffness Matrix

The individual coefficients which make up the member stiffness matrix, K (from eqn. 3.50), are usually determined directly by integrating the appropriate differential equations. For the circular curved girder in which warping restraint effects are being considered, these are given by

$$f^{iv} - k^2 . f'' = \frac{\mu}{r.EI_{\hat{w}}} \left\{ tr + M - N.y_o \right\} \tag{2.69}$$

$$\text{and} \quad v'' + \frac{v}{r^2} = \frac{-M}{\Psi EI_x} + \frac{\phi}{r} \tag{3.51}$$

Here, eqn 3.51 is the differential equation governing bending about the horizontal axis, first derived by Dabrowski[25], in which the dimensionless geometric function Ψ has been previously defined in eqn. 3.23 for the case of non-principle x, y axes. However, these expressions are not independent of each other, as is the case for straight members, and the solution of simultaneous differential equations in explicit form is generally considered to be a difficult problem.

A different approach has therefore been adopted, whereby the stiffness matrix is obtained numerically from the flexibility matrix, F , previously derived in accordance with eqn. 3.19. In order to obtain a direct relationship between the two matrices, eqn. 3.50 must first be restated in the following form:

$$\begin{bmatrix} P_1 \\ P_2 \end{bmatrix} = \begin{bmatrix} K_{11} & K_{12} \\ K_{21} & K_{22} \end{bmatrix} \begin{bmatrix} d_1 \\ d_2 \end{bmatrix} \tag{3.52}$$

in which p_1, d_1 and p_2, d_2 represent the force and displacement

submatrices corresponding to the four degrees of freedom at ends

1 and 2, respectively. Furthermore, it is also possible to connect

p_1 and p_2 by an equilibrium matrix E such that

$$p_1 + Ep_2 = 0 \qquad\qquad 3.53$$

in which, from eqns. 3.31 and 3.33, we know that E is equal to

$$
\left[
\begin{array}{c|c|c|c}
C & \pm S & rS & 0 \\
\hline
\pm S & C & \pm r(1-C) & 0 \\
\hline
0 & 0 & 1 & 0 \\
\hline
\pm\mu\eta\left[krS\cdot\dfrac{SH}{CH} -C + \dfrac{1}{CH}\right] & -\mu\eta r\left[krC\cdot\dfrac{SH}{CH} + S\right] & \mp\mu\eta r^2\left[krC\cdot\dfrac{SH}{CH} + S-\dfrac{SH}{\eta rCH}\right] & \dfrac{1}{CH}
\end{array}
\right]
\qquad 3.54
$$

Now consider the circular curved girder, shown in fig. 3.6a,

built-in at end 1 and subject to end-forces p_1 and p_2. The system

undergoes end-displacements equivalent to $d_1 = 0$ and $d_2 = e_2$

where the displacement vector e_2 has been previously defined in

eqn. 3.19 for the cantilever girder. If a system of rigid-body

displacements d_{1*} , d_{2*} , is now superimposed on the member, as indicated

in fig. 3.6b, the equilibrium of the system is unchanged. Since zero

total work is done, it follows that

$$p_1^t d_{1*} + p_2^t d_{2*} = 0 \qquad\qquad 3.55$$

Furthermore, by substituting for p_1 in this expression from eqn. 3.54,

a simple relationship between the rigid-body end-displacements is

obtained, thus:

$$\qquad\qquad\qquad\qquad\qquad\qquad\qquad\qquad\qquad 3.56$$

$$d_{2*} = E^t d_{1*}$$
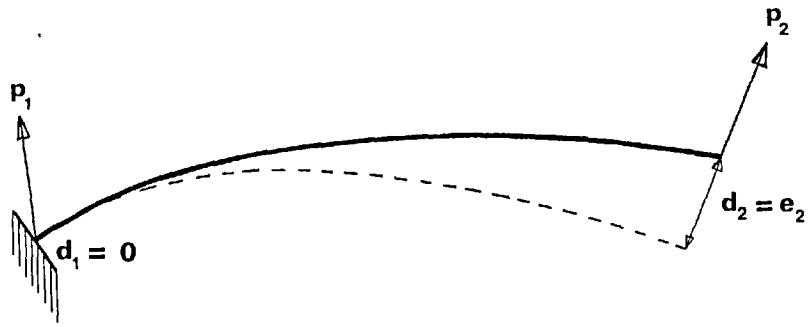
Figure 3.6a   Displacement System for the Cantilever Beam
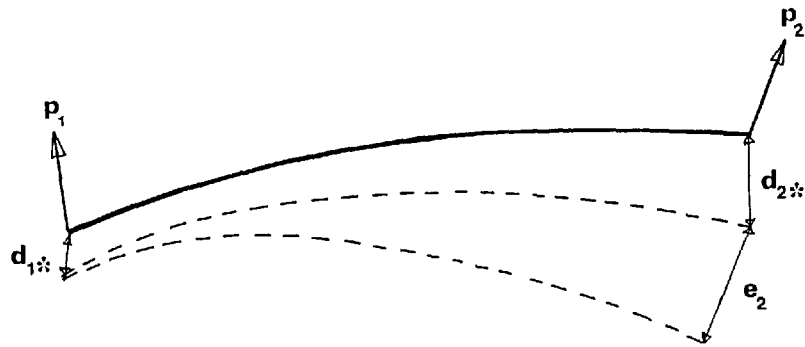
Figure 3.6b   Rigid-Body Displacement System

Clearly, the general displacement vectors d_1 , d_2 , in eqn. 3.52 must include the end-displacements due to both elastic deformations and rigid-body movements, whereby

$$\left. \begin{array}{rcl} d_1 & = & d_{1*} \\[2mm] d_2 & = & d_{2*} \; + \; e_2 \end{array} \right\} \quad 3.57$$

If the rigid-body displacement terms in this expression are eliminated by introducing eqn. 3.56, the displacement vector e_2 is given by

$$e_2 \quad = \quad d_2 \quad - \quad E^t d_1 \qquad 3.58$$

which on substitution into eqns. 3.19 and 3.53, yields

$$\left. \begin{array}{rcl} p_1 & = & (E\,\bar{F}^1 E^t).d_1 \quad - \quad (E\bar{F}^1).d_2 \\[2mm] p_2 & = & (-\bar{F}^1 E^t).d_1 \quad + \quad \bar{F}^1.d_2 \end{array} \right\} \quad 3.59$$

By comparing eqns. 3.52 and 3.59 the following definitions

for the member stiffness sub-matrices are obtained:

$$
\begin{aligned}
\mathbf{K_{11}} &= \mathbf{E}\bar{\mathbf{F}}^{-1}\mathbf{E}^t \\
\mathbf{K_{12}} &= -\mathbf{E}\bar{\mathbf{F}}^{-1} \\
\mathbf{K_{21}} &= -\bar{\mathbf{F}}^{-1}\mathbf{E}^t \\
\mathbf{K_{22}} &= \bar{\mathbf{F}}^{-1}
\end{aligned}
\right\} \qquad 3.60
$$

and these enable the complete member stiffness matrix to be determined

from the previously defined flexibility and equilibrium matrices only.

Although the expressions derived in eqn. 3.60 are equally

correct for straight and curved beams subject to all forms of loading,

additional care should be exercised when considering the effects of

warping restraint. For example, the relationship between bimoments at

ends 1 and 2, used in establishing the equilibrium matrix $\mathbf{E}$ in eqn. 3.54,

is that previously derived in eqn. 3.33 for the case of the cantilever

girder in the development of the flexibility analysis. However, this

is not strictly correct since in the equilibrium approach it can no

longer be assumed that the initial parameter f_1' equates to zero. The

general expression given by eqn. 3.17 should therefore be used instead,

with $z = \ell$. This can most easily be accommodated by modifying the end

force vector to include the warping function term, thus;

$$
\mathbf{P_1} = \begin{bmatrix} M_1 \\ T_1 \\ V_1 \\ B_1 - \frac{\mu}{k}\cdot GI_d \cdot \frac{SH}{CH} \cdot f_1' \end{bmatrix} \qquad 3.61
$$

in which case the equilibrium matrix $\mathbf{E}$ remains unchanged.

Therefore, after establishing the complete member stiffness

matrix in the form of eqn. 3.53, it is necessary to alter the fourth

element on the leading diagonal in the submatrix $\mathbf{K_{11}}$ (corresponding

to the end deformation f_1') by the addition of the coefficient

$\left\{\dfrac{\mu}{k} \cdot GI_d \cdot \dfrac{SH}{CH}\right\}$, in order to reduce $\mathbf{p_1}$ to its desired form.

Straight Beams

The definition of the stiffness sub-matrices in eqn. 3.60 is

equally applicable to straight members. However, in this case, the

member flexibility matrix $\mathbf{G}$ is that detailed in Appendix 2.3 and the

equilibrium matrix is derived from eqns. 3.40 and 3.41 and takes the

following form:

$$\mathbf{E} \;=\; \begin{bmatrix} 1 & 0 & \ell & 0 \\ 0 & 1 & 0 & 0 \\ 0 & 0 & 1 & 0 \\ 0 & -\dfrac{\mu \sinh k\ell}{k \cosh k\ell} & 0 & \dfrac{1}{\cosh k\ell} \end{bmatrix} \qquad 3.62$$

Alternatively, a direct derivation of the stiffness matrix

is now possible by solving the appropriate fundamental equations.

On passing to the limit $r \to \infty$, eqns. 2.69 and 3.51 are effectively

uncoupled and may be restated as

$$f^{iv} - k^2 . f'' = \dfrac{\mu t}{EI_{\hat{w}}} = 0$$

$$\text{and} \qquad v'' = \dfrac{-M}{\Psi EI_x} \qquad\qquad\Bigg\}\qquad 3.63$$

Clearly, the first of these independent equations has the same general

solution as eqn. 3.2 and enables the individual components of end-

deformation f_1, f_1', f_2, f_2', to be evaluated in terms of the end-loads

-

T_1, B_1, T_2, B_2, only. Equating one of these components of
deformation to unity (while putting the others to zero) results in
four simultaneous equations, the solution of which provides the
stiffness coefficients in the column associated with the non-zero
deformation. By separately equating the remaining components to unity,
three more sets of simultaneous equations are formed from which the
remaining coefficients in the stiffness matrix are determined
(Appendix 3.1).

However, in §3.2.1 the appropriate boundary conditions for
closed sections were shown to be ϕ_1, f_1, ϕ_2', f_2', and ideally a
solution is required in these terms. This has been achieved by
introducing the relationship between ϕ and f (from eqn. 2.65) and
modifying the member stiffness matrix accordingly. The result is
presented in A.3.2 and may be combined with the familiar bending/shear
matrix in A.3.3 to form the full 8 x 8 member stiffness matrix for the
straight beam with four degrees of freedom at each end.

3.4.2 Transformation into System Co-ordinates

The member stiffness matrix and the corresponding force and
displacement vectors have so far been established with reference to
local co-ordinate systems (x_1, z_1 and x_2, z_2), defined by the orientation
of the member ends. However, before individual stiffness matrices may be
assembled into a single stiffness matrix for the structure, these must
first be restated in terms of common system axes, here denoted x^*, z^*.

In the case of straight members, the angle subtended between
local and system axes is the same everywhere along the beam and trans-
formation is relatively simple. However, for curved girders, not only
does the subtended angle differ at each end but the 'direction' of
curvature is once again a necessary consideration. The system axes
and the direction of positive rotation are defined in fig. 3.7 for both
types of curvature.

$a.$ *Positive Curvature*

$b.$ *Negative Curvature*
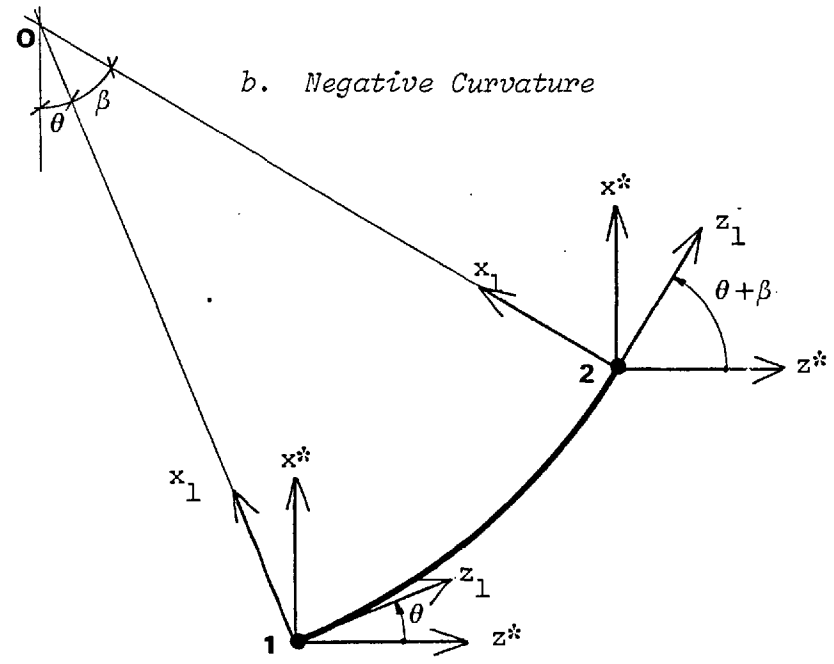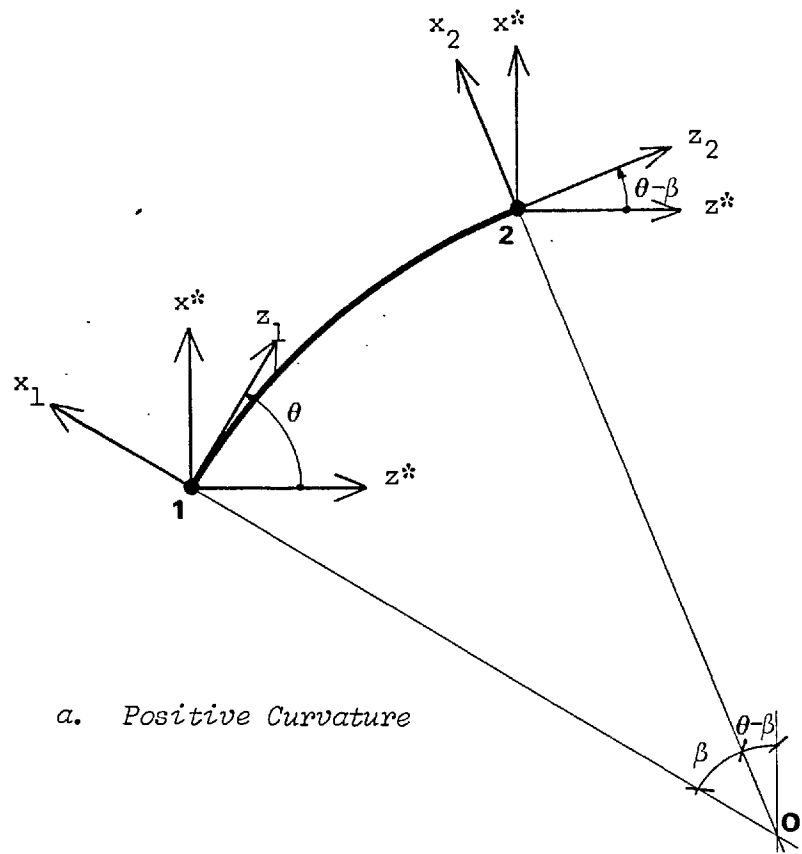
Figure 3.7   Definition of Positive and Negative Curvature in System Axes

Load and displacement vectors may now be expressed in system co-ordinates in the following way:

$$p_1' = T_1 p_1$$

$$p_2' = T_2 p_2$$

$$\left.\right\} \quad 3.64$$

and

$$d_1' = T_1 d_1$$

$$d_2' = T_2 d_2$$

$$\left.\right\} \quad 3.65$$

in which the transformation matrices T_1, T_2, corresponding to ends 1 and 2 respectively, are given by

$$
T_1 = \begin{bmatrix}
\cos\theta & -\sin\theta & 0 & 0 \\
\sin\theta & \cos\theta & 0 & 0 \\
0 & 0 & 1 & 0 \\
0 & 0 & 0 & 1
\end{bmatrix}
$$

and   3.66

$$
T_2 = \begin{bmatrix}
\cos(\theta \pm \beta) & -\sin(\theta \pm \beta) & 0 & 0 \\
\sin(\theta \pm \beta) & \cos(\theta \pm \beta) & 0 & 0 \\
0 & 0 & 1 & 0 \\
0 & 0 & 0 & 1
\end{bmatrix}
$$

By substituting for p_1, p_2, d_1, d_2, from eqns. 3.64 and 3.65 into eqn. 3.53 and pre-multiplying by the appropriate transformation matrix from eqn. 3.66, we obtain

$$
\begin{bmatrix} p_1 \\ p_2 \end{bmatrix}
=
\begin{bmatrix}
T_1 K_{11} T_1^{-1} & T_1 K_{12} T_2^{-1} \\
T_2 K_{21} T_1^{-1} & T_2 K_{22} T_2^{-1}
\end{bmatrix}
\begin{bmatrix} d_1 \\ d_2 \end{bmatrix}
\qquad 3.67
$$

in which, due to the orthogonal nature of both transformation matrices, it is permissible to put

$$T_1^{-1} = T_1^t$$
$$T_2^{-1} = T_2^t$$

3.68

Therefore, eqn. 3.67 may be written more simply as

$$p' = T K T^t . d' = K'd'$$

3.69

in which

$$T = \begin{bmatrix} T_1 & 0 \\ 0 & T_2 \end{bmatrix}$$

3.70

Assembly of the complete stiffness matrix for the structure now proceeds in the usual way. First, the components of displacement at the ends of the m members are expressed solely in terms of the n nodal displacement vectors. In this way conditions of compatibility are satisfied and the total number of unknown displacement terms is reduced from 8m to 4m for the four degrees of freedom system being considered here. Joint equilibrium is then ensured by equating all the member end-forces meeting at a joint with the corresponding components of applied load. This results in 4n load/displacement equations, which may be expressed in the following general form:

$$p^* = K^* . d^*$$

3.71

in which K^* is a 4n x 4n symmetrical matrix, often sparsely filled for the type of structures being considered, and consisting mostly of elements grouped about the leading diagonal.

3.4.3   Support Conditions

As yet no account has been taken of the support restraints and an infinite number of rigid-body displacements are possible.

Accordingly, the structure stiffness matrix is still singular in its present form and must first be modified before a unique solution for the joint displacements can be obtained.

It is apparent from eqn. 3.66 that both the shear and bimoment terms are only effective about the vertical y-axis and therefore remain unaltered by the transformation into system co-ordinates. It follows that restraint of either vertical displacement or warping deformation at a joint is simulated by removal of the appropriate row and column from eqn. 3.71, in the usual way.

Complete rotational restraint about two orthogonal axes in the horizontal plane or about one of the system axes may also be accommodated in the analysis by a similar modification. However, in assemblages of circular curved girders, rotation is commonly restricted about a local member axis (e.g. for torsional restraint only). In general this does not coincide with a system axis and a more complex modification of eqn. 3.71 is therefore required. Now consider the local member axes x, z, shown in fig. 3.8, separated from the system axes x^*, z^* by the angle θ. The corresponding positive rotations ϕ_x, ϕ_z and ϕ_x^*, ϕ_z^* are related in the following way:

$$\begin{bmatrix} \phi_x^* \\ \\ \phi_z^* \end{bmatrix} = \begin{bmatrix} \cos\theta & -\sin\theta \\ \\ \sin\theta & \cos\theta \end{bmatrix} \begin{bmatrix} \phi_x \\ \\ \phi_z \end{bmatrix} \qquad 3.72$$

from which, for restraint about the local z-axis ($\phi_z = 0$), for example, we have

$$\phi_x^* = \phi_z^* \cdot \cot\theta \qquad 3.73$$
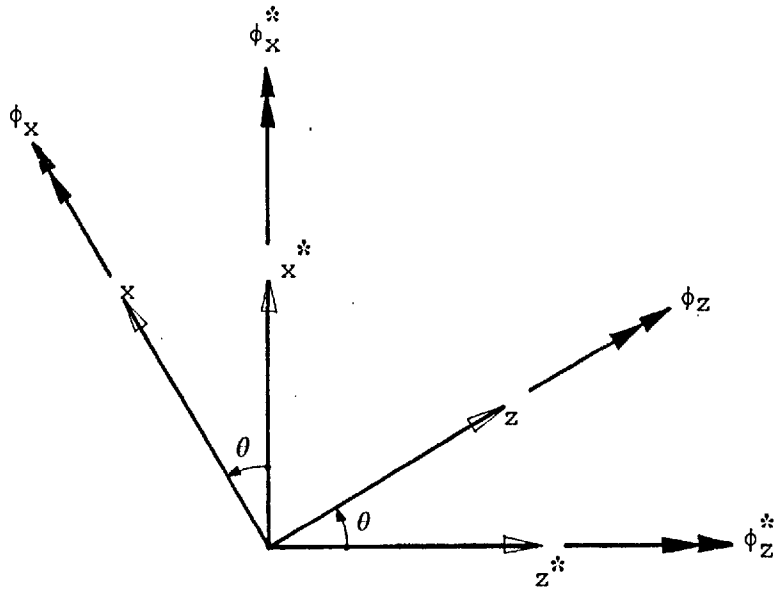
Figure 3.8   Rotations in Local and System Co-ordinates

By multiplying the column of the structure stiffness matrix, corresponding to ϕ_x^* , by cot θ throughout, and adding it to that associated with the displacement ϕ_z^*, it is possible to completely remove the original column from the K^* matrix together with the term ϕ_x^* from the displacement vector d^*. However, in order to restore the rank and symmetrical nature of the stiffness matrix, the corresponding row of K^* and p^* must now be similarly modified.

A solution for the rotation ϕ_z^* , together with the remaining terms in the reduced displacement vector d^* is then obtained by inverting K^* in the usual way. The only other unknown, ϕ_x^*, may now be determined from eqn. 3.73 and, subsequently, this enables all the member end-forces to be evaluated in accordance with eqn. 3.69 (in system co-ordinates).

However, it should be noted that the multiplier cot θ tends to infinity for certain values of the subtended angle θ and this can lead to ill-conditioning of the structure stiffness matrix. This should therefore only be used in the range:

$$\frac{n\pi}{4} < \theta < 3\,\frac{n\pi}{4}$$

and in other cases the same result is achieved by using the inverse

of eqn. 3.73 and by alternatively removing the column and row associated

with the displacement term $\overset{*}{\phi}_z$.

3.4.4   Fixed-End Forces due to Uniformly Distributed Loads

Consider half of the circular curved girder, of total arc

length $2\ell = 2r\beta$, built-in at both ends and subjected to uniformly

distributed shear and torsional loads of intensity p and t per unit

length, respectively (fig. 3.9). At midspan ($\alpha = \beta$) we know from

conditions of symmetry that $V_2 = T_2 = 0$, although the quantities

B_2, $M_2 \neq 0$ are as yet unknown.
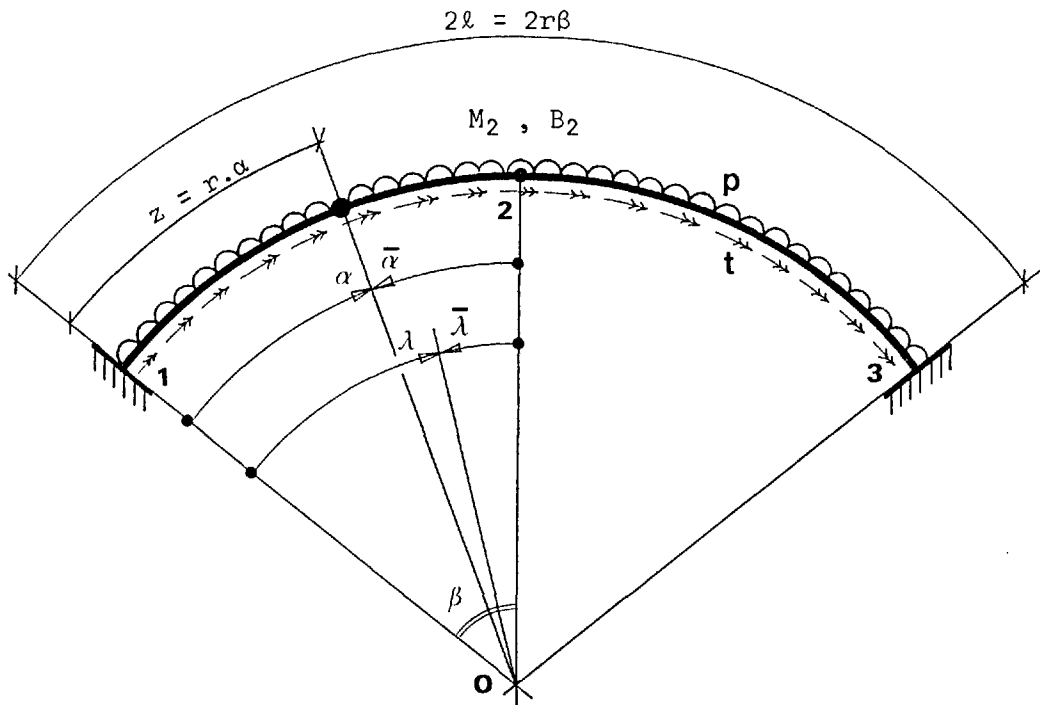
Figure 3.9   The Circular Curved Member subject to Uniformly
Distributed Loads p,t

By considering equilibrium at $z = r.\alpha$, the stress resultants M, T and V are determined from the following equations:

$$M = M_2 \cos\bar{\alpha} + (pr^2 \pm tr) . \int_0^{\bar{\alpha}} \sin\bar{\lambda}.d\bar{\lambda}$$

$$T = \mp M_2\sin\bar{\alpha} \mp pr^2 \int_0^{\bar{\alpha}} (1 - \cos\bar{\lambda}).d\bar{\lambda} + tr \int_0^{\bar{\alpha}} \cos\bar{\lambda}.d\bar{\lambda}$$

$$V = pr \int_0^{\bar{\alpha}} d\bar{\lambda}$$

$$\left. \right\} \quad 3.74$$

After integration these simplify to

$$M = (M_2 - pr^2 \mp tr) \cos\bar{\alpha} + (pr^2 \pm tr)$$

$$T = \mp(M_2 - pr^2 \mp tr) \sin\bar{\alpha} \mp pr^2\bar{\alpha}$$

$$V = pr\bar{\alpha}$$

$$\left. \right\} \quad 3.75$$

from which, by putting $\alpha = \beta$, the reactions at the built-in end are obtained, thus:

$$M_1 = (M_2 - pr^2 \mp tr)C + (pr^2 \pm tr)$$

$$T_1 = \mp(M_2 - pr^2 \mp tr)S \mp pr^2 \beta$$

$$V_1 = pr\beta$$

$$\left. \right\} \quad 3.76$$

The fixed-end bimoment is once again determined from eqn. 3.17. By substituting for M, T_1, from eqns. 3.75 and 3.76, respectively, and integrating over the length of the half-girder, we have

$$B_1 = \frac{B_2}{CH} \pm \mu(M_2 - pr^2 \mp tr) \left[\frac{(1-\eta)}{k} S \frac{SH}{CH} - \frac{nr}{CH} (C.CH-1) \right]$$

$$3.77$$

$$\mp \frac{\mu pr}{k^2} . \frac{SH}{CH} \left[\frac{SH}{CH} - kr\beta \right]$$

A general expression for B at z = r.α is now obtained by introducing the various quantities from eqns. 3.75-3.77 into eqn. 3.17. After integrating and simplifying this may be written in terms of the variable angle $\bar{\alpha}$, in the following way:

$$B = B_2\left\{ch - \frac{SH}{CH}\,sh\right\} \pm \mu(M_2 - pr^2 \mp tr)\left\{\left[\frac{(1-\eta)}{k}\cdot\frac{S}{CH} - \eta r\,\frac{SH}{CH}\right]sh - \eta r(c-ch)\right\}$$

$$\pm \frac{\mu pr}{k^2 CH}\left\{\beta krsh + ch - \frac{SH}{CH}\,sh - CH\right\}$$

<div align="right">3.78</div>

in which the trigonometrical abbreviations are those previously defined in eqns. 3.35 and 3.37. Finally, by differentiating this expression with respect to z, the longitudinal distribution of warping torsion, B', is given by

$$B' = B_2 k\left\{\frac{SH}{CH}\,ch - sh\right\} \mp \mu(M_2 - pr^2 \mp tr)\left\{\left[(1-\eta)\,\frac{S}{CH} - \eta kr\,\frac{SH}{CH}\right]ch\right.$$

$$\left. + \eta(s + krsh)\right\} \mp \frac{\mu pr}{k\cdot CH}\left\{\beta krch + sh - \frac{SH}{CH}\,ch\right\}$$

<div align="right">3.79</div>

All the stress resultants have thus been expressed in terms of the uniformly distributed applied loads, p, t, and the redundant central forces B_2, M_2, only. In accordance with eqn. 3.44, these are more easily written in matrix formation as

$$\begin{bmatrix} M \\ T \\ B \\ B' \end{bmatrix} = \begin{bmatrix} c_{11} & c_{12} & c_{13} & c_{14} \\ c_{21} & c_{22} & c_{23} & c_{24} \\ c_{31} & c_{32} & c_{33} & c_{34} \\ c_{41} & c_{42} & c_{43} & c_{44} \end{bmatrix} \begin{bmatrix} (M_2 - pr^2 \mp tr) \\ B_2 \\ pr^2 \\ tr \end{bmatrix}$$

<div align="right">3.80</div>

where the connection matrix is given by

$$
\mathbf{C} = \left[
\begin{array}{c|c|c|c}
c & 0 & 1 & \pm 1 \\
\hline
\mp s & 0 & \mp\bar{\alpha} & 0 \\
\hline
\mp C_1(c-ch)\pm C_2 sh & ch+C_5 \cdot sh & \pm C_6\{(\beta kr+C_5)sh+ch-CH\} & 0 \\
\hline
\mp \dfrac{C_1}{r}(s+krsh)\mp kchC_2 & -k(sh+C_5 ch) & \mp C_6 k\{sh+(\beta kr+C_5)ch\} & 0
\end{array}
\right]
\qquad 3.81
$$

Here, the constant C_6 is defined, in addition to those in eqn. 3.43, as

$$
C_6 = \frac{\mu}{k^2 r \cdot CH} \qquad\qquad 3.82
$$

From conditions of symmetry we know that both the warping displacement and rotation due to bending are zero at midspan. This yields two simultaneous equations of the form:

$$
\left.
\begin{array}{l}
v_2' = \dfrac{\partial U}{\partial M_2} = 0 \\[4mm]
\text{and} \qquad f_2' = \dfrac{\partial U}{\partial B_2} = 0
\end{array}
\right\} \qquad 3.83
$$

from which the unknown quantities B_2, M_2 may be established.

By expressing the total strain energy in eqn. 3.29 in terms of the connection matrix coefficients, eqn. 3.83 may be alternatively written as

$$
\int_0^\beta \left\{ (M_2 - pr^2 \mp tr)\left[j^2 c_{11}^2 + c_{21}^2 + \frac{k^2}{\mu}\cdot c_{31}^2 + \frac{1}{\mu}\cdot c_{41}^2 - 2c_{21}c_{41} \right] + pr^2\left[j^2 c_{11}c_{13} + c_{21}c_{23} \right. \right.
$$

$$
\left. + \frac{k^2}{\mu}\cdot c_{31}c_{33} + \frac{1}{\mu}\cdot c_{41}c_{43} - c_{41}c_{23} - c_{21}c_{43} \right] + B_2\left[\frac{k^2}{\mu}c_{32}c_{31} + \frac{1}{\mu}c_{41}c_{41} - c_{41}c_{21} \right]
$$

$$
\left. + tr\left[j^2 c_{14}c_{11} \right] \right\} \cdot d\bar{\alpha} = 0
$$

and

$$3.84$$

$$\int_0^\beta \left\{ (M_2 - pr^2 \mp tr) \left[\frac{k^2}{\mu} c_{32} c_{31} + \frac{1}{\mu} c_{42} c_{41} - c_{21} c_{42} \right] + pr^2 \left[\frac{k^2}{\mu} c_{32} c_{33} + \frac{1}{\mu} c_{42} c_{43} - c_{23} c_{42} \right] \right.$$

$$\left. + B_2 \left[\frac{k^2}{\mu} \cdot c_{32}^2 + \frac{1}{\mu} \cdot c_{42}^2 \right] \right\} . d\bar{\alpha} \ = \ 0$$

which after integration and considerable simplification reduce to

$$\mp (M_2 - pr^2 \mp tr) \left\{ \frac{\beta}{2}(j^2 + 1 + \mu\eta) + \frac{SC}{2} \left[j^2 - 1 + \mu\eta(3 - 2\eta) \right] + \mu\eta(1 - \eta) \left[\frac{SH}{krCH} \left(1 - \frac{2krS}{SH} \right) - krS^2 \frac{SH}{CH} \right] \right\}$$

$$+ k\eta \frac{SH}{CH} \left\{ 1 - \frac{krS}{SH} \right\} . B_2 \mp pr^2 \left\{ \beta C - S_j^2 - S + \mu\eta \left[\frac{\beta}{CH} - \beta C - \frac{SH}{krCH^2} + \beta krS \frac{SH}{CH} + \frac{S}{CH^2} \right] \right\} \mp trSj^2 = 0$$

and

$$3.85$$

$$\pm (M_2 - pr^2 \mp tr) \left\{ k\eta \frac{SH}{CH} \left[1 - kr \frac{S}{SH} \right] \right\} + B_2 \left\{ \frac{kSH}{\mu rCH} \right\} \mp pr^2 \cdot \frac{1}{rCH} \left\{ \beta - \frac{SH}{krCH} \right\} \ = \ 0$$

Eliminating the term B_2 from eqn. 3.85 enables the central bending

moment, M_2, to be evaluated in explicit form, thus:

$$(M_2 - pr^2 \mp tr) \ = \ \frac{trSj^2 - pr^2 \left[S(j^2 + 1 - \mu\eta\beta kr \cdot \frac{CH}{SH}) + C\beta(\mu\eta - 1) \right]}{\frac{\beta}{2}(j^2 + 1 - \mu\eta) + \frac{SC}{2} \left[j^2 - 1 - \mu\eta(2\eta - 3) \right] - \mu\eta(1 - \eta)krS^2 \cdot \frac{CH}{SH}} \qquad 3.86$$

Substitution of this result into either of eqns. 3.85 provides

a solution for the only other unknown B_2, which, due to the complexity of

the statement, is best derived numerically. In this way, the various

stress resultants (from eqns. 3.75, 3.78 and 3.79) and the fixed-end

forces (from eqns. 3.76 and 3.77) may now be fully expressed in terms of

the uniformly distributed applied loads only.

At this point it is of some interest to consider the force system for a 'warpless' beam (Neuber Tube[74]) for which $I_w = 0$, $\eta = 0$ and $\mu = 0$. On passing to the limit $kr \to \infty$, we have

$$\lim_{kr \to \infty} (M_2 - pr^2 \mp tr) = \frac{trSj^2 - pr^2 \left[S(j^2+1) - C\beta \right]}{\frac{\beta}{2}(j^2+1) + \frac{SC}{2}(j^2-1)} \qquad 3.87$$

a result which was first established by Pippard and Baker[86] for circular bow girders of solid section.

Graphical Presentation

A double format has been used throughout the subsequent graphical presentation in which the left- and right-hand frames of each figure represent the effects due to uniformly distributed torsional and shear loads, respectively. Each graph shows the variations in a particular stress resultant with respect to either the included angle of the member or the distance along the member; each of the plotted lines represents a different pair of values for the dimensionless functions j^2 and $k\ell$. For clarity, the lines are only identified by a symbol at their ends and the key provided in Table 3.3 is valid for all figures (page 183).

The unknown central moment, M_2, derived in eqn. 3.86, and the unknown central bimoment, B_2, obtained by substituting the numerical value of M_2 into eqn. 3.85, are shown in figs. 3.10 and 3.11 respectively. With M_2, B_2 thus determined, the fixed end stress resultants M_1, B_1, T_1 are easily derived from eqns. 3.76 and 3.77 and are shown in figs. 3.12-3.14. These are the nodal quantities required to represent uniformly distributed loads in the stiffness analysis developed in this chapter. The various graphs so far described cover a wide range

of circular girders with included angles of up to 80° but are also applicable to straight beams where $2\beta = 0^{\circ}$.

In Figs. 3.10-3.14 the warping shear parameter μ has been equated to unity and the graphs therefore apply to open sections only. Furthermore, the effects of changing μ are difficult to predict since the parameter not only appears explicitly in the various formulae but is also included in the derivation of the decay function k (eqn. 2.70). Thus, in order to demonstrate the different response of sections with closed parts, the various stress resultants M_2, B_2, M_1, B_1, T_1 are shown in figs. 3.15-3.19, respectively, for the typical value of $\mu = 0.5$. While the bending and torsional moments are in no way independent of the warping shear parameter, the magnitude of these stress resultants does not greatly differ with changing μ. On the other hand, the bimoment terms are influenced considerably, although it would appear that a good approximation is given by the product of μ and the corresponding open section value of bimoment.

As the parameter $k\ell$ tends to infinity, the significance of any bimoment terms is reduced and the behaviour of the beam more closely resembles that of a solid section. By assigning $k\ell$ the numerical value of 200, the magnitude of the various bimoments is negligible (as can be seen in figs. 3.11, 3.13, 3.16 and 3.18) and the various components of bending and torsional moments thus obtained are essentially those for solid sections (as defined by eqns. 3.75 and 3.87).

The distribution of bending moment, bimoment, torsion and warping torsion along the half-beam are shown in figs. 3.20-3.23, for $\mu = 1$, and in figs. 3.24-3.27, for $\mu = 0.5$. Due to the extra parameter involved, it is no longer possible to present the results for a wide

range of included angles and only the results for $2\beta = 10^{\circ}$ are given here. The distributions of bending moment due to shear loading, shown in figs. 3.20 and 3.24, are largely unaffected by variations in any of the dimensionless parameters j^2, $k\ell$ or μ. However, this is not the case for the bending moments created by torsional loads which are clearly influenced by changes in all three. The distributions of bimoment, shown in figs. 3.21 and 3.25 are relatively independent of variations in j^2 for both shear and torsional loading and, once more, a good approximation of the effects of the warping shear parameter is apparently given by the product of μ and the open section value of bimoment.

The distribution given in fig. 3.22 is the total torque along the beam and in the case of open sections ($\mu = 1$) this comprises both warping torsion (fig. 3.23) and St. Venant torsion. For all values of j^2 and $k\ell$ the component of warping torsion is equal to the total torsion at both the centre and support sections, while the difference between figs. 3.22 and 3.23 represents the distribution of St. Venant torsion along the beam. On the other hand, the distribution of torsion shown in fig. 3.26 (for $\mu = 0.5$) is due entirely to the resistive effects of the constant St. Venant shear flows created around the closed parts of the section. That distribution shown in fig. 3.27 is given by the first derivative of the bimoment and has no torsional component, although it is numerically equivalent to the product of μ and the resultant torque at both the centre and support sections of the beam. In figs. 3.23 and 3.27, for $k\ell = 200$, the magnitude of the warping torsion is very nearly zero everywhere and has therefore been omitted from the graphs for clarity.

$M_2 = F(2r\beta)t$

$M_2 = F.(2r\beta)^2 p$
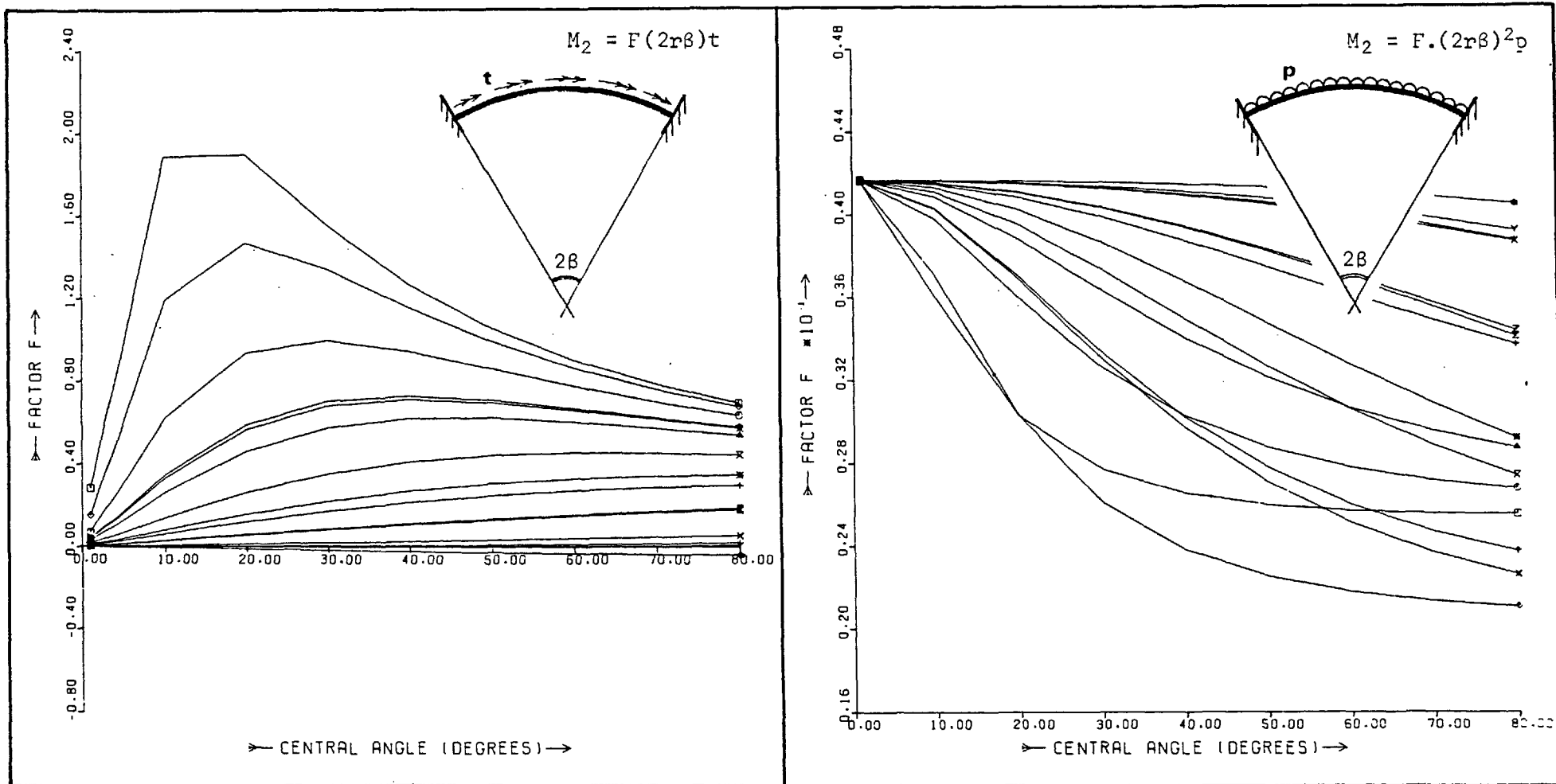
Fig. 3.10 Central Bending Moment due to Uniformly Distributed Shear and Torsional Loads ($\mu = 1$)
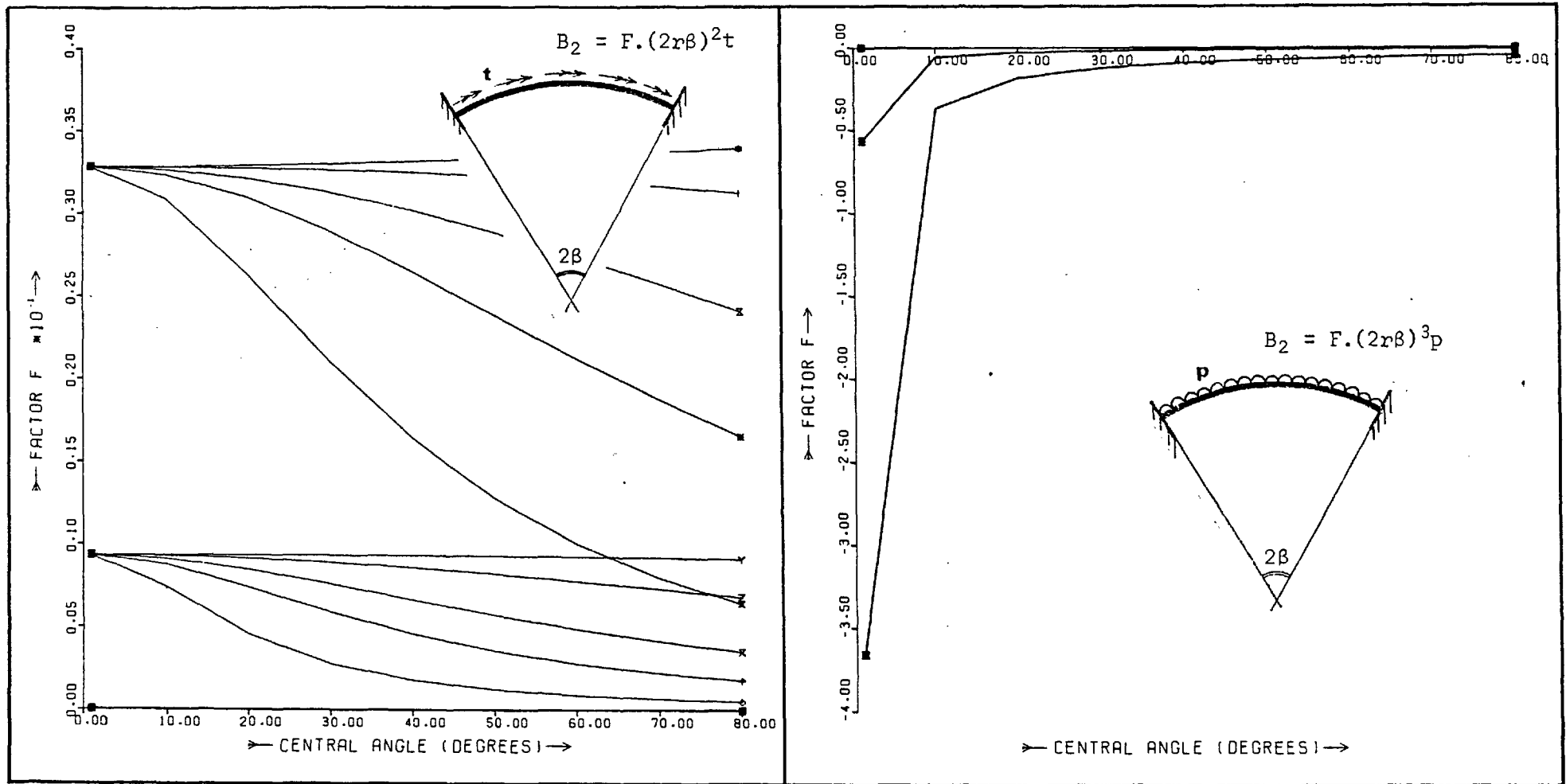
Fig. 3.11   Central Bimoment due to Uniformly Distributed Shear and Torsional Loads ($\mu = 1$)
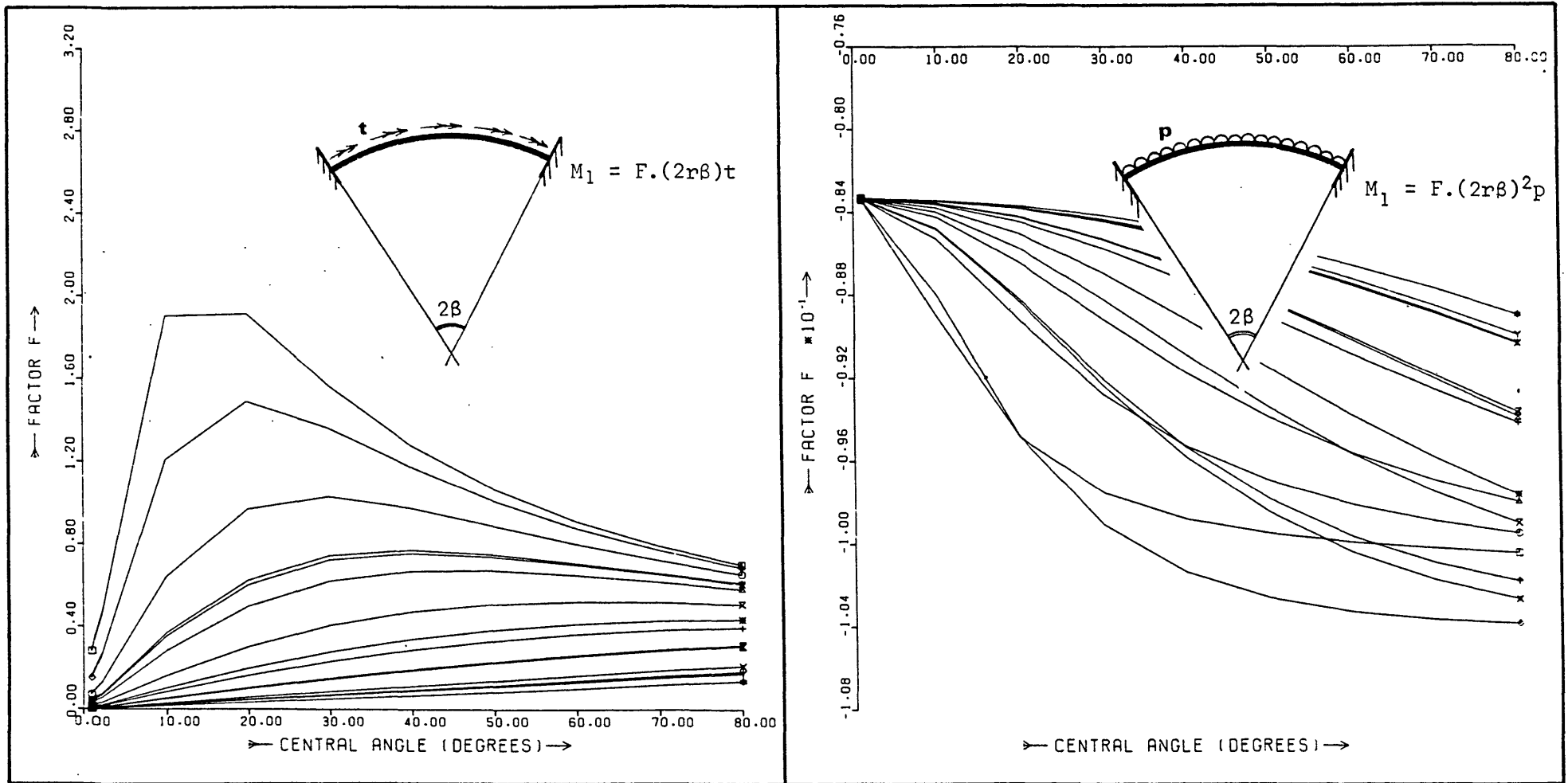
Fig. 3.12 Fixed End Bending Moment due to Uniformly Distributed Shear and Torsional Loads ($\mu = 1$)
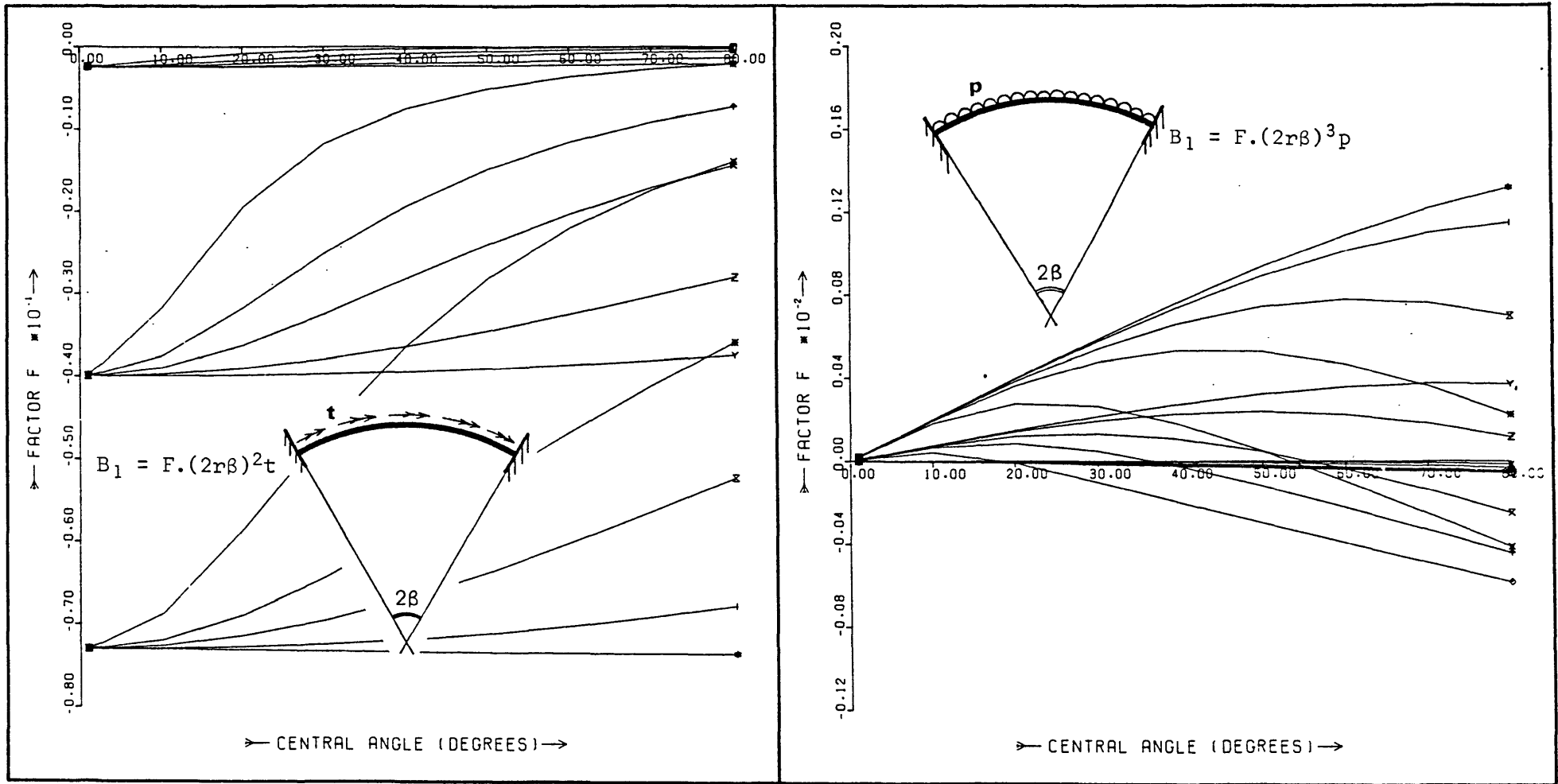
Fig. 3.13 Fixed End Bimoment due to Uniformly Distributed Shear and Torsional Loads ($\mu = 1$)
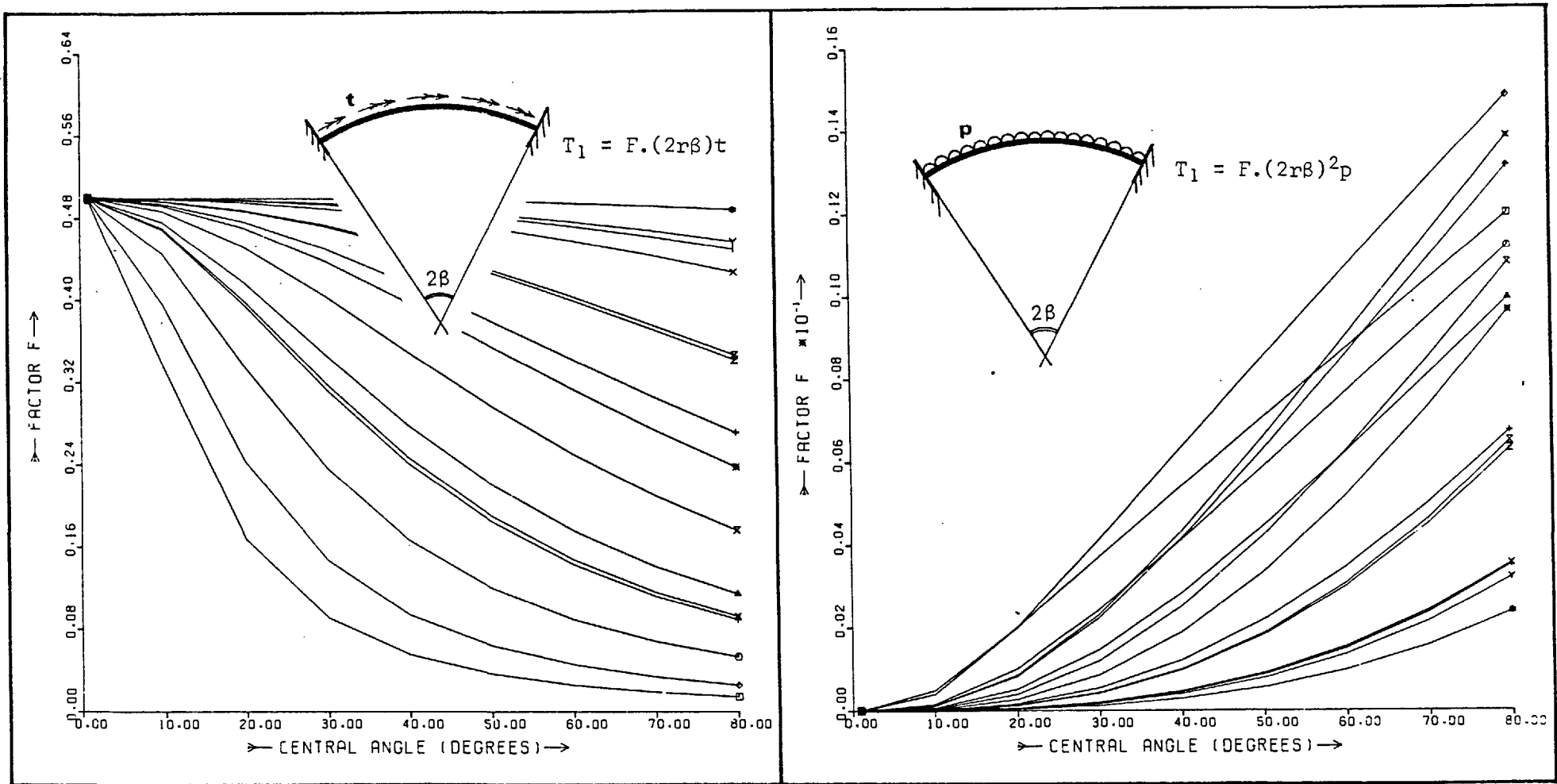
Fig. 3.14 Fixed End Torsional Moment due to Uniformly Distributed Shear and Torsional Loads ($\mu = 1$)
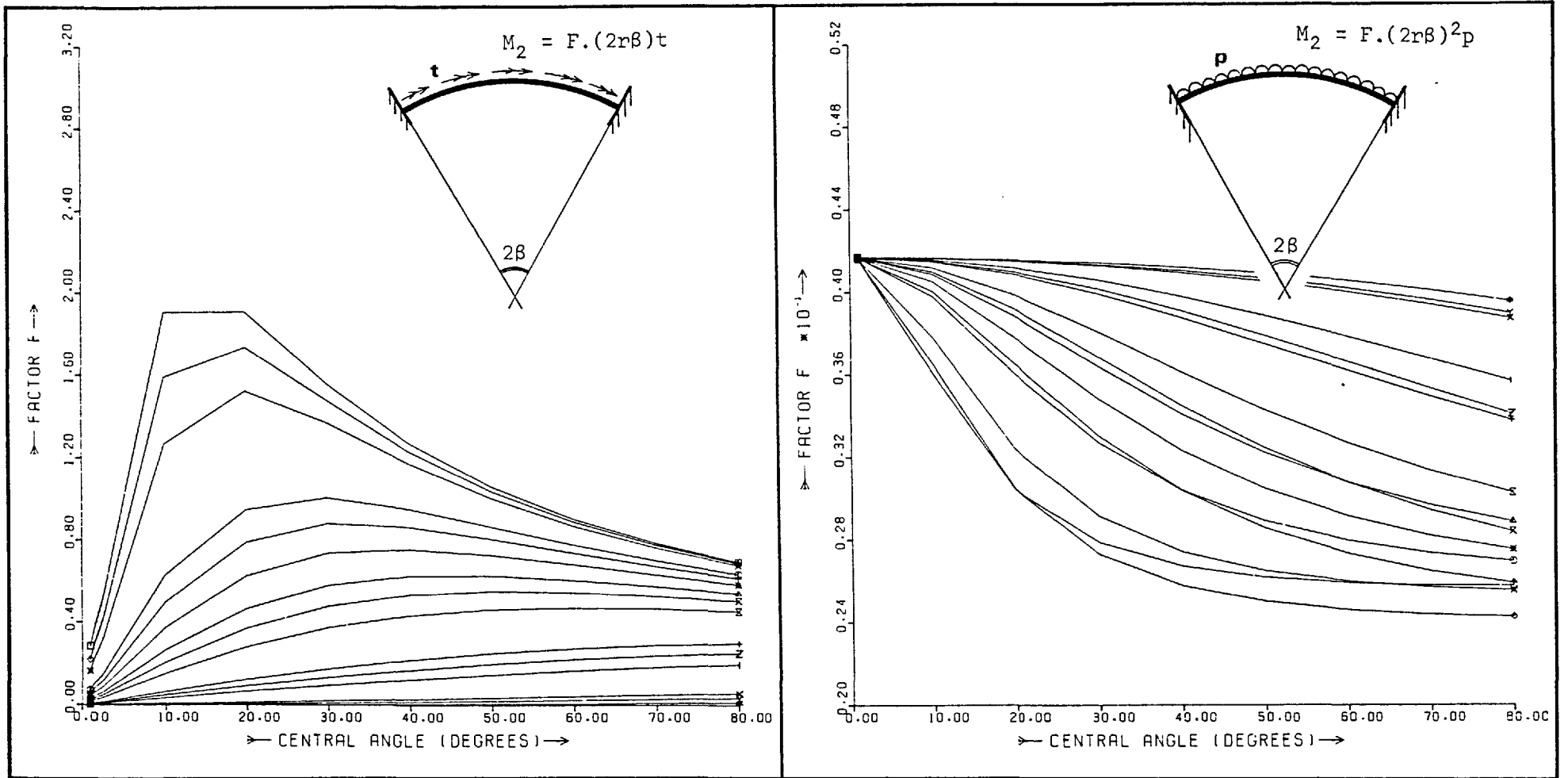
Figure 3.15   Central Bending Moment due to Uniformly Distributed Shear and Torsional Loads ($\mu = 0.5$)
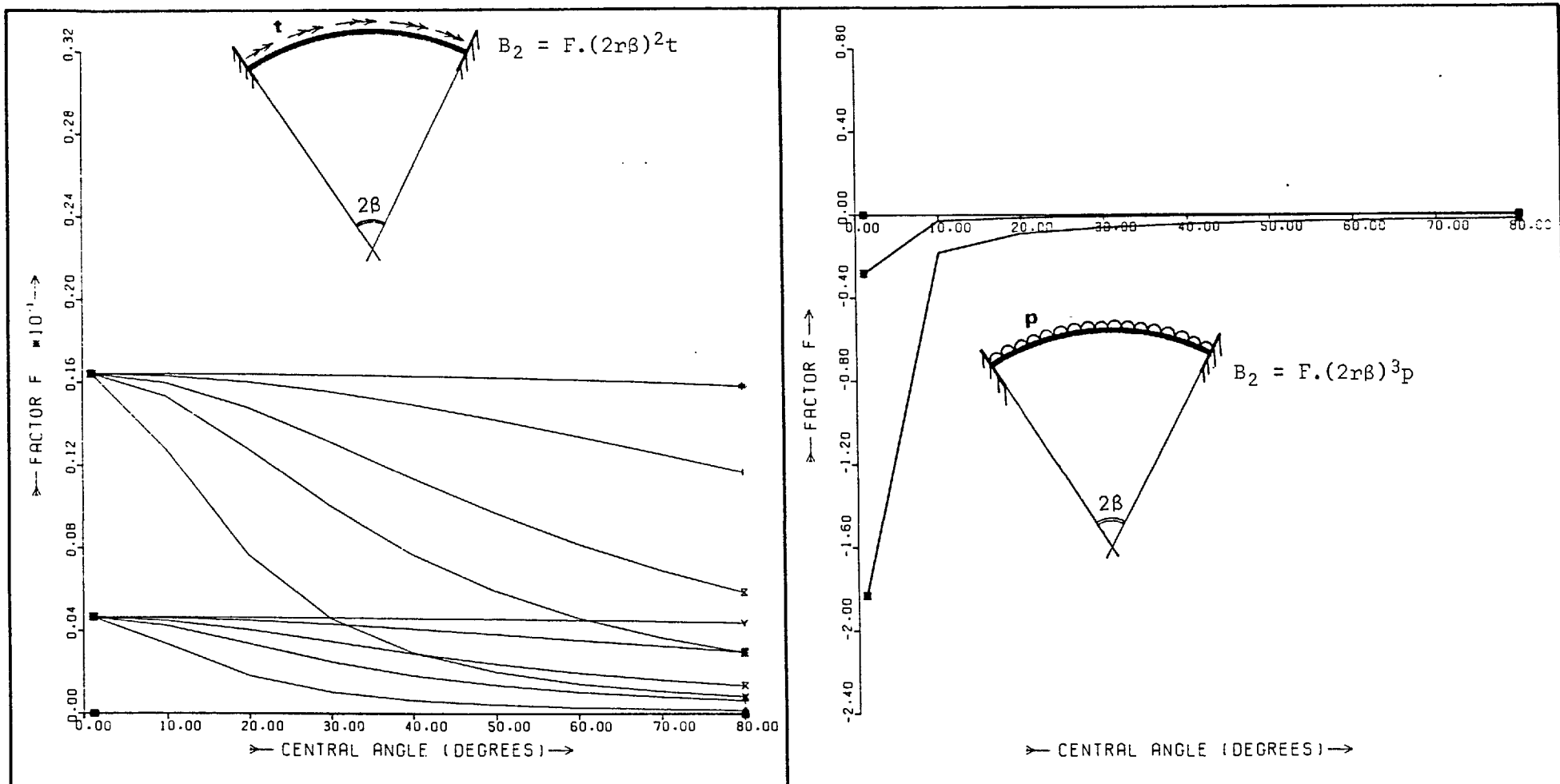
Fig. 3.16 Central Bimoment due to Uniformly Distributed Shear and Torsional Loads (μ = 0.5)
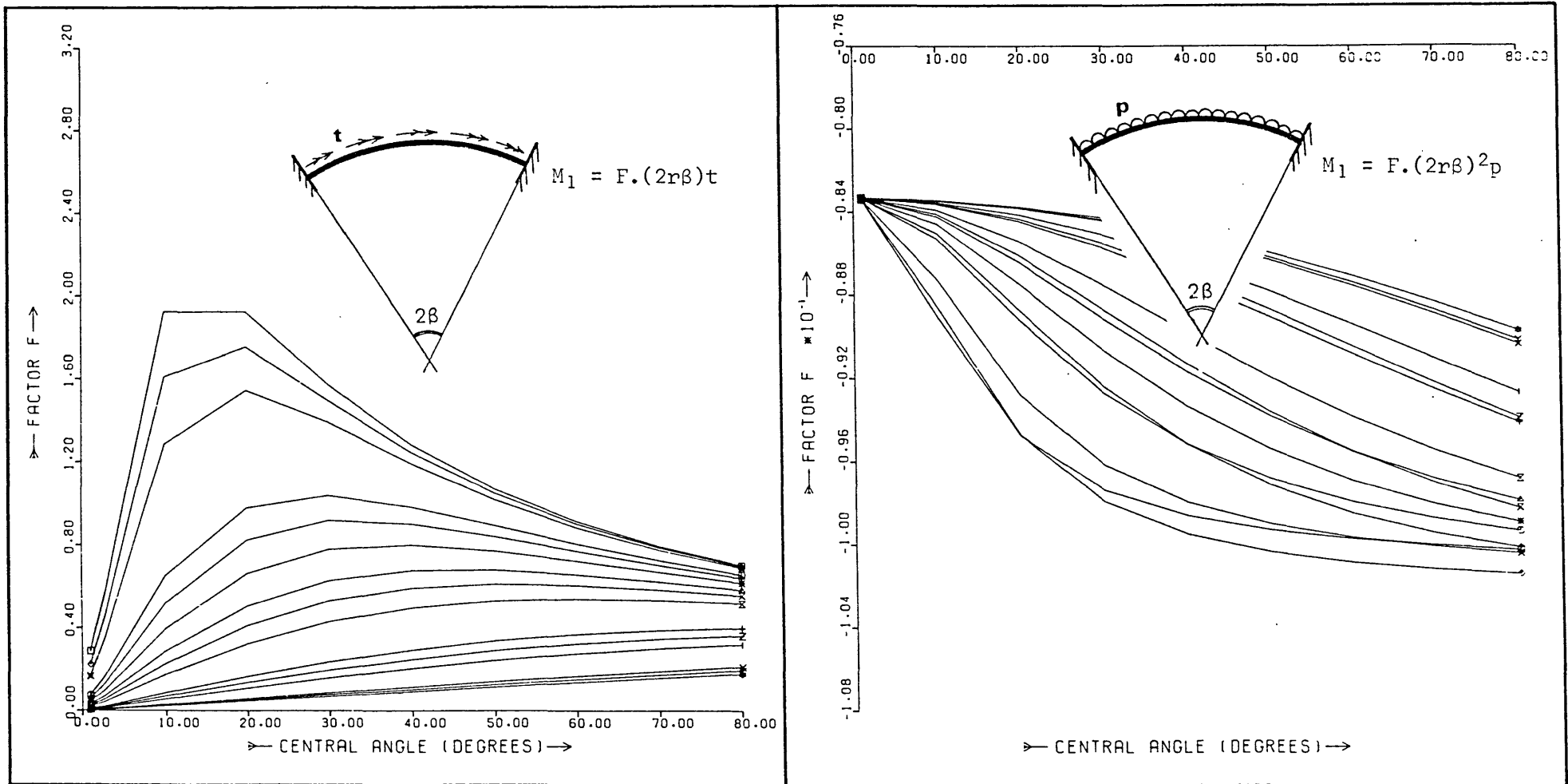
Fig. 3.17 Fixed End Bending Moment due to Uniformly Distributed Shear and Torsional Loads (μ = 0.5)
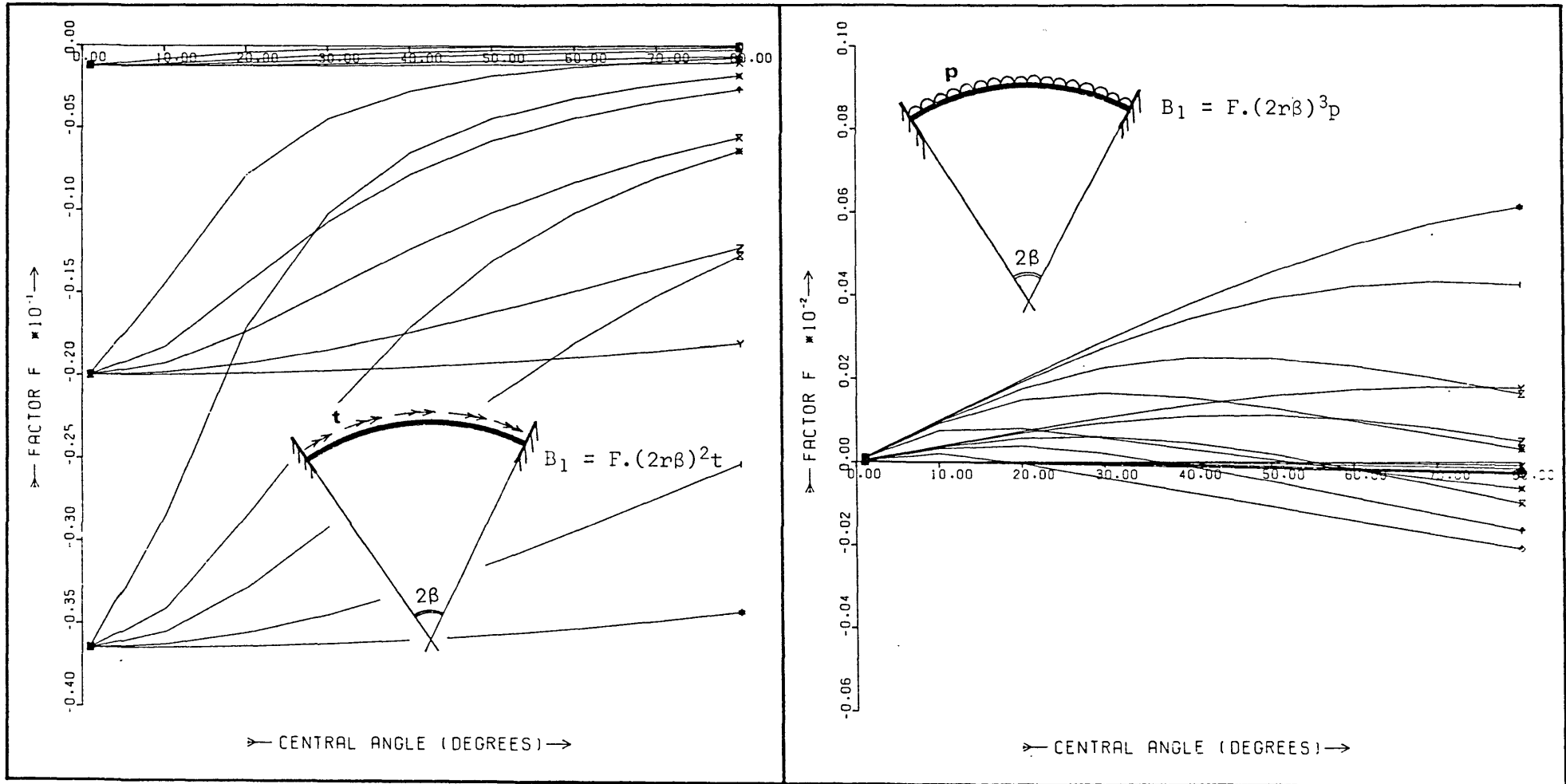
Fig. 3.18 Fixed End Bimoment due to Uniformly Distributed Shear and Torsional Loads (μ = 0.5)
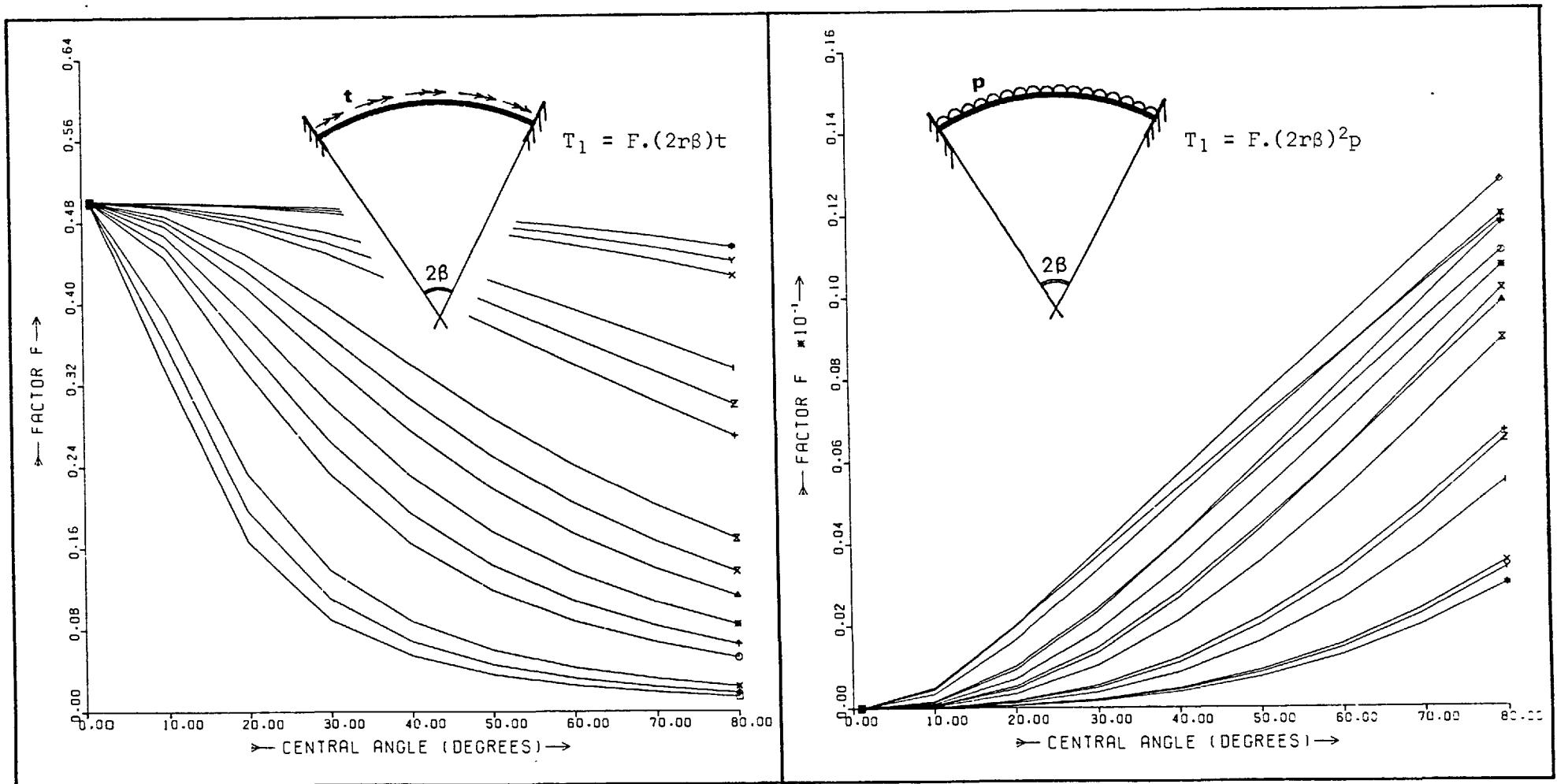
Fig. 3.19 Fixed End Torsional Moment due to Uniformly Distributed Shear and Torsional Loads (μ = 0.5)
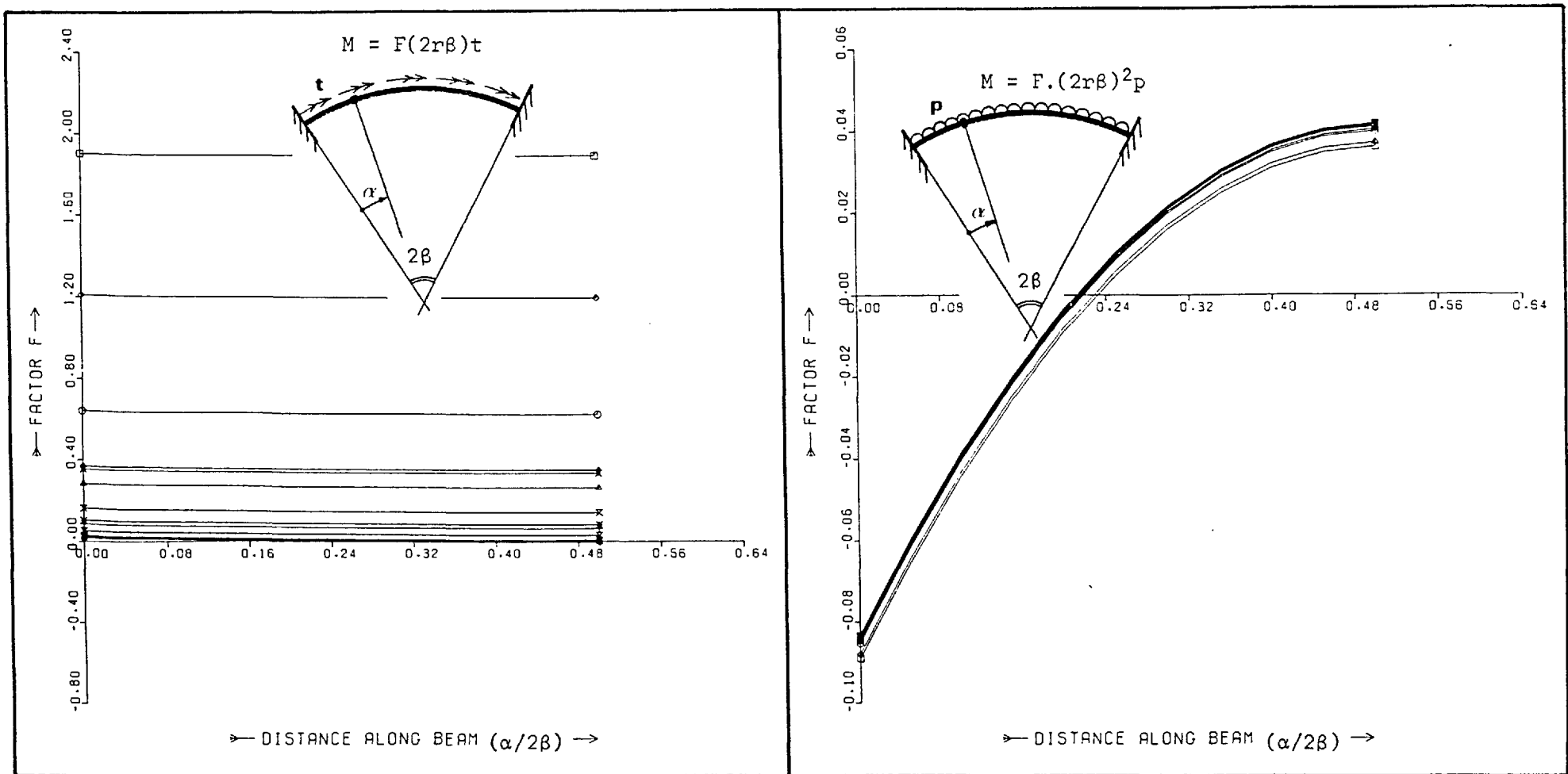
Fig. 3.20   Distribution of Bending Moment due to Uniformly Distributed Shear and Torsional Loads (2β=10°; μ=1)
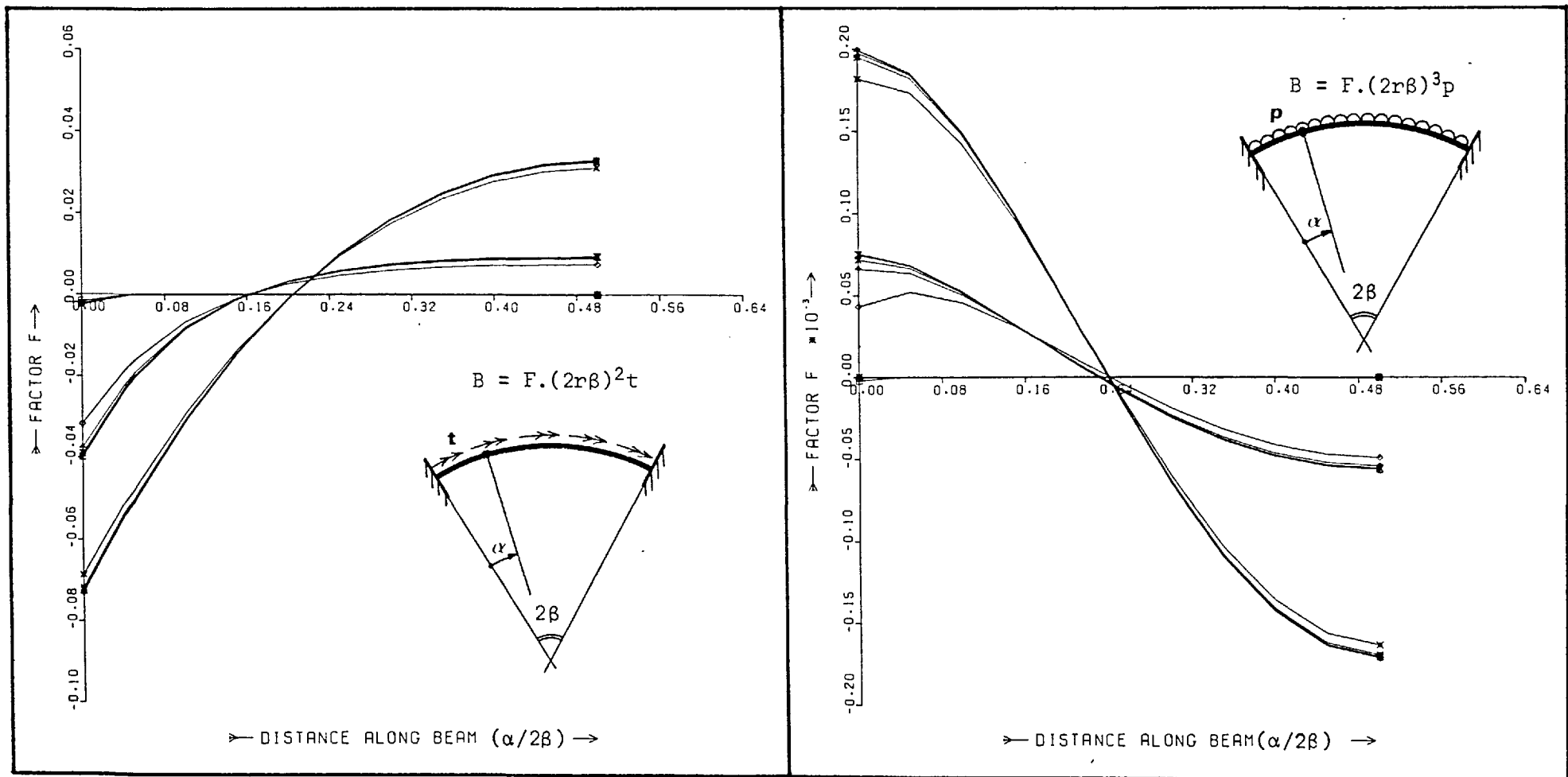
Fig. 3.21 *Distribution of Bimoment due to Uniformly Distributed Shear and Torsional Loads* (2β = 10°; μ = 1)
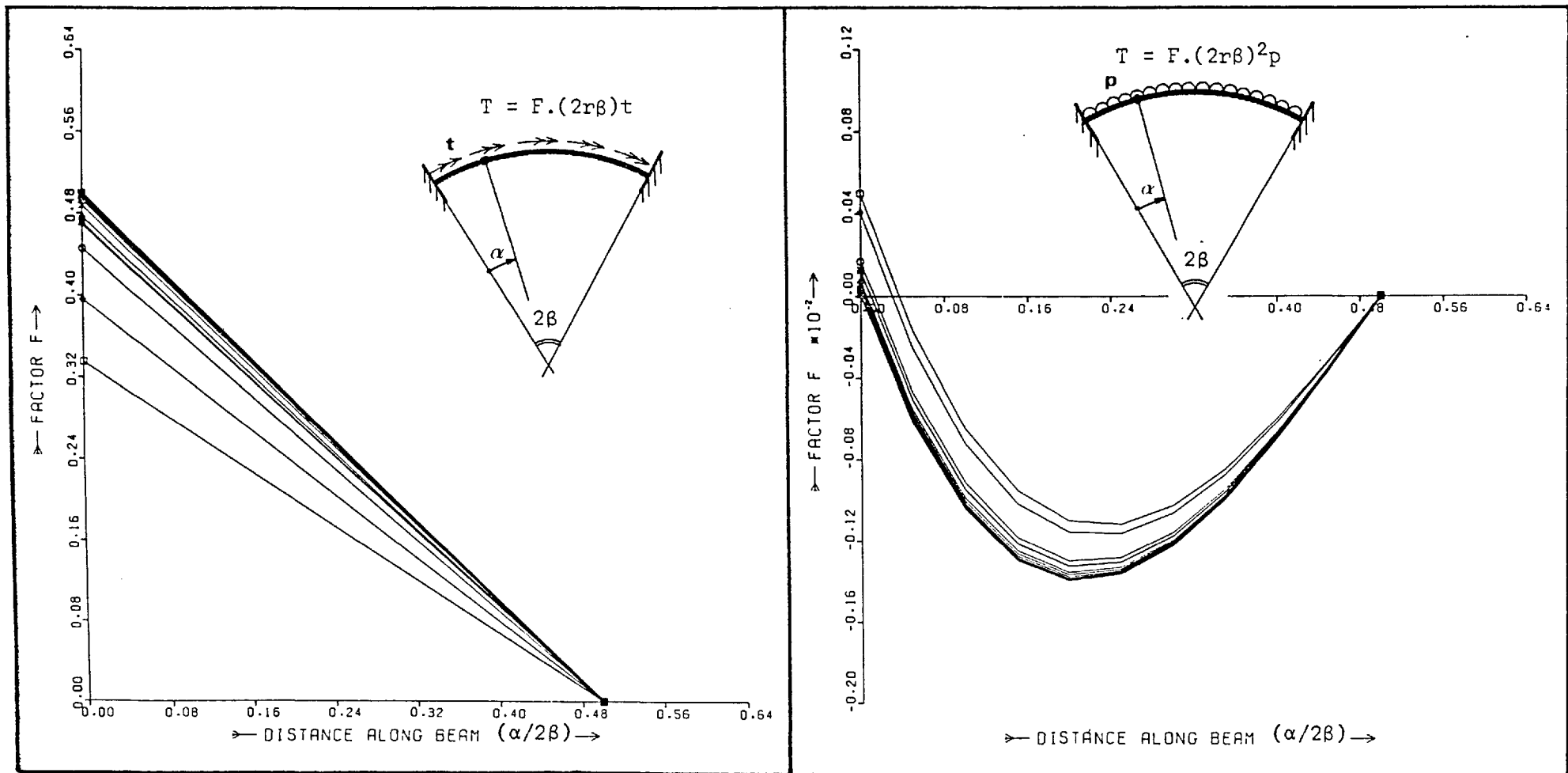
Fig. 3.22   Distribution of Torsion due to Uniformly Distributed Shear and Torsional Loads (2β = 10°; μ = 1)
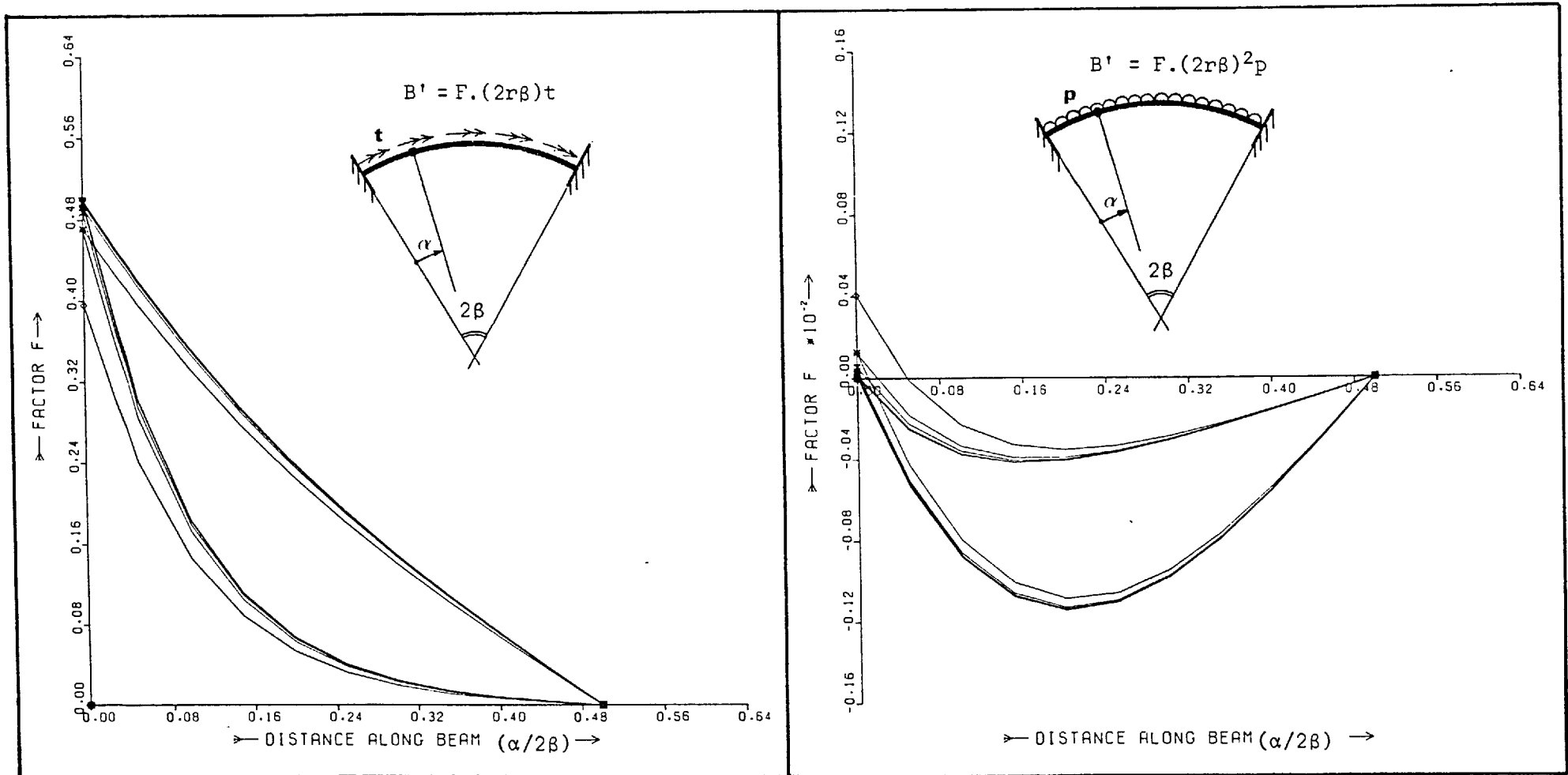
Fig. 3.23 Distribution of Warping Torsion due to Uniformly Distributed Shear and Torsional Loads $(2\beta = 10^{\circ}; \mu = 1)$
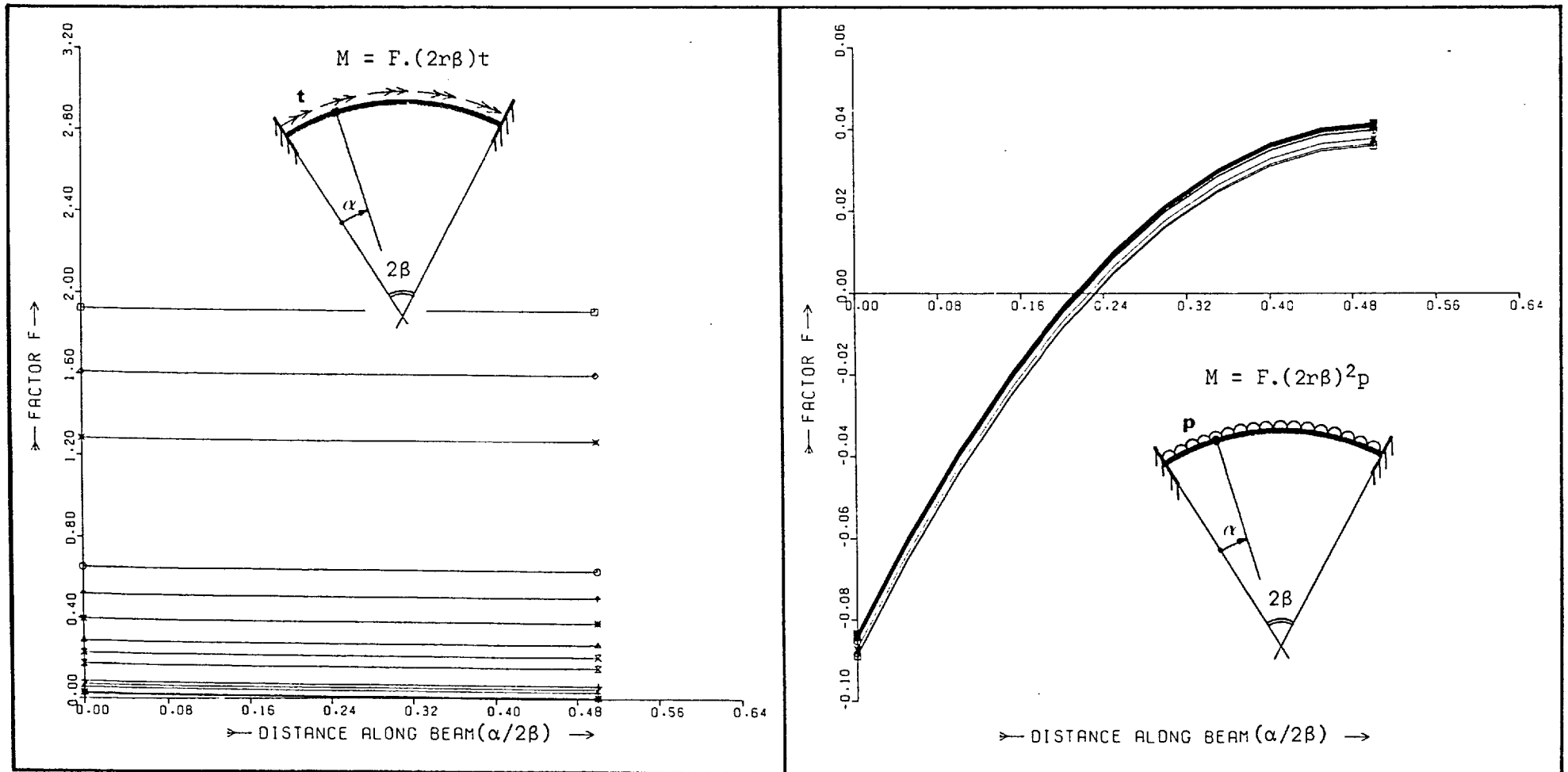
Fig. 3.24 Distribution of Bending Moment due to Uniformly Distributed Shear and Torsional Loads (2β = 10°; μ = 0.5)
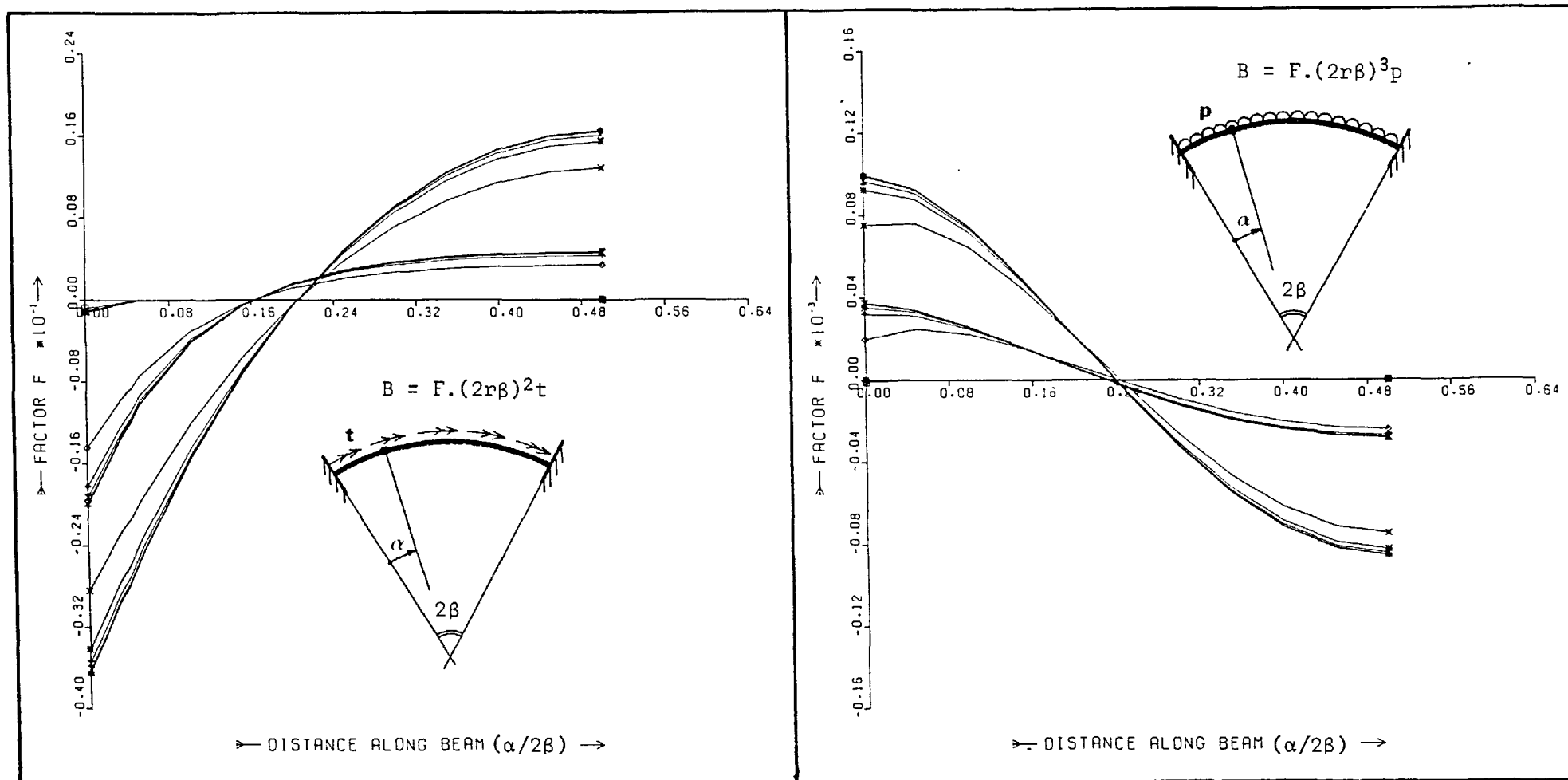
Fig. 3.25 Distribution of Bimoment due to Uniformly Distributed Shear and Torsional Loads $(2\beta = 10^{o}; \mu = 0.5)$
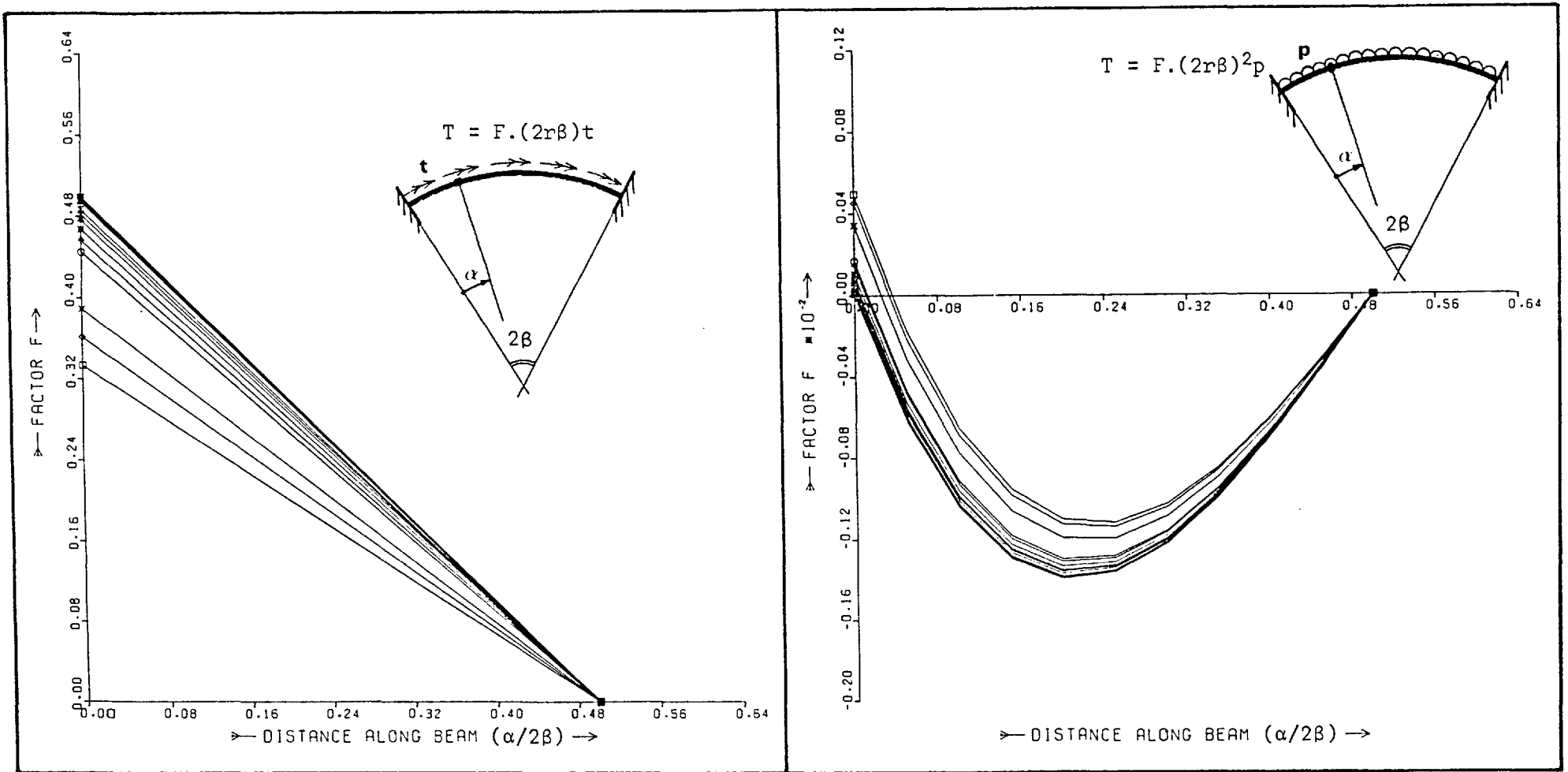
Fig. 3.26 Distribution of Torsion due to Uniformly Distributed Shear and Torsional Loads (2β = 10°; μ = 0.5)
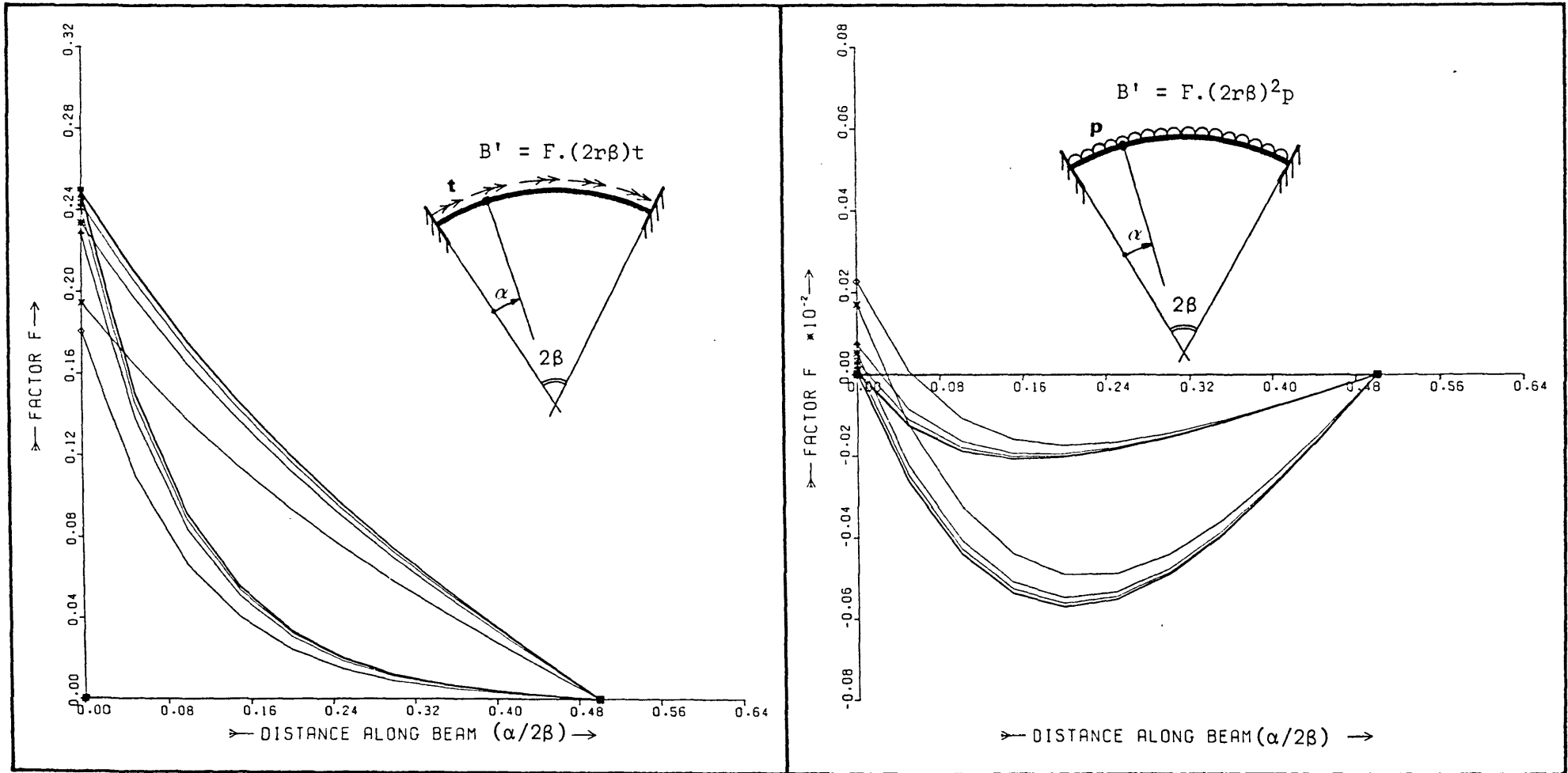
Fig. 3.27 Distribution of Warping Torsion due to Uniformly Distributed Shear and Torsional Loads (2β = 10°; μ = 0.5)

3.4.5   Fixed-End Forces Due to Concentrated Point Loads

Once again, consider the left-hand half of the circular

curved girder of total arc length $2\ell = 2r\beta$, shown in fig. 3.28. The

member is built-in at both ends and subjected to concentrated shear

and torsional loads denoted P_o and T_o, respectively. The point of

application of these loads subtends an angle ξ from the centreline of

the beam and the central forces M_2, T_2, V_2 and B_2 are as yet unknown.
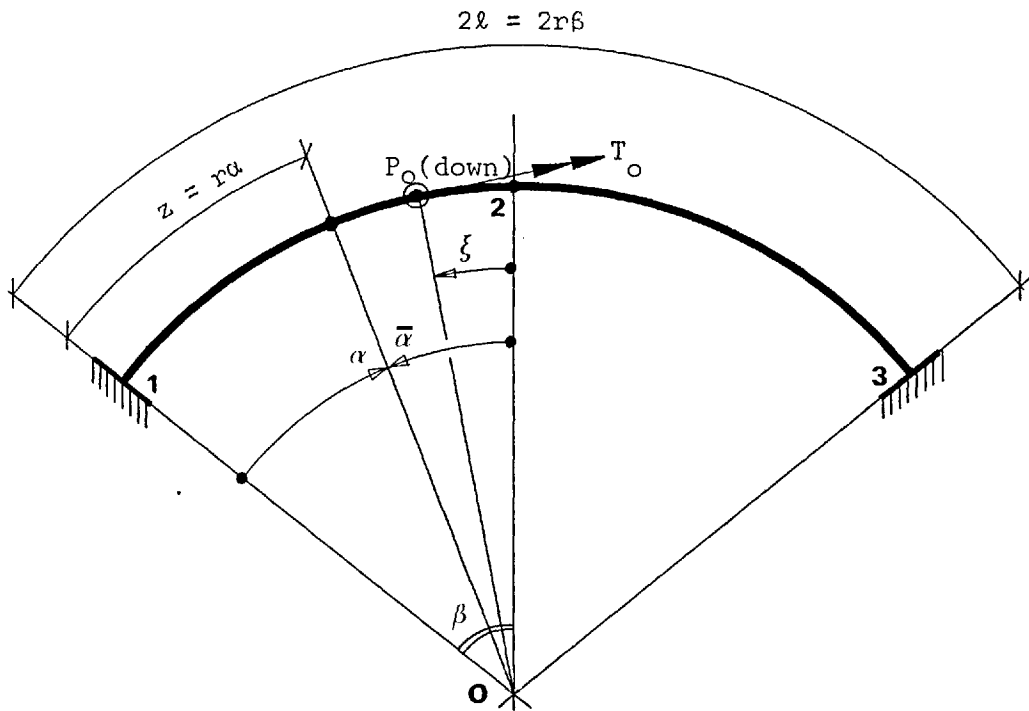
Figure 3.28   The Circular Curved Girder subject to Concentrated

Loads P_o, T_o

From conditions of equilibrium at a distance $z = r.\alpha$ along the beam, we have

$$M = M_2\cos\bar{\alpha} \pm (T_2 \pm P_2 r)\sin\bar{\alpha} \pm \left[(T_o \pm P_o r)\sin(\bar{\alpha}-\xi) \right]$$

$$T = \mp M_2\sin\bar{\alpha} + (T_2 \pm P_2)\cos\bar{\alpha} \mp P_2 r + \left[(T_o \pm P_o r)\cos(\bar{\alpha}-\xi) \mp P_o r \right]$$

$$V = \mp P_2 + \left[P_o \right] \qquad\qquad 3.92$$

where the final terms in brackets are only to be included where $\bar{\alpha} > \xi$. The fixed-end bimoment is derived as before (eqn. 3.33) but with the followed additional terms due to the modified distribution of bending moment and torsion from eqn. 3.92.

$$B_1 = \left\{ \text{Eqn. 3.33} \right\} - \frac{\mu SH}{kCH}\left[(T_o \pm P_o r)\cos(\beta-\xi) \mp P_o r \right] + \frac{\mu T_o}{kCH}\sinh kr\xi$$

$$- \frac{\mu}{kCH}(T_o \pm P_o r)\int_o^{(\beta-\xi)} \sin(\beta-\xi-\lambda).\sinh kr(\beta-\lambda).d\lambda \qquad 3.93$$

where the first and second additional terms are due to the modified fixed-end torsion, T_1, and applied torque T_o, respectively. The final expression represents the torsional effects of the modified bending moment distribution, M, and should therefore only be integrated over the range $0 < \lambda < (\beta-\xi)$. After integration and rearrangement, eqn. 3.93 simplifies to:

$$B = \left\{ \text{Eqn. 3.33} \right\} - \mu(T_o \pm P_o r)\left[\frac{(1-\eta)}{k}\frac{SH}{CH}\cos(\beta-\xi) + \eta r\sin(\beta-\xi) \right]$$

$$+ \frac{\mu T_o}{CH}\frac{(1-\eta)}{k}\sinh kr\xi \mp \frac{\mu P_o r}{k\ CH}(\eta\sinh kr\xi - SH) \qquad 3.94$$

The general bimoment expression can now be obtained directly by substitution of the various quantities from eqns. 3.92 and 3.94 into eqn. 3.17, and is found to be similar to eqn. 3.38 but with the following additions:

$$B = \left\{Eqn.3.38\right\} + \left\{\begin{matrix}\text{Additional terms}\\ \text{in } B_1\\ \text{from Eqn. 3.94}\end{matrix}\right\}\cosh kr\alpha + \frac{\mu}{k}(T_o \pm P_o r \cos(\beta-\xi) \mp P_o r)\sinh kr\alpha$$

$$- \underline{\frac{T_o \mu}{k}\cdot\sinh kr(\alpha-\beta+\xi)} + \frac{\mu}{k}(T_o \pm P_o r)\left|\sin(\beta-\xi-\lambda)\cdot\sinh kr(\alpha-\lambda)\cdot d\lambda\right. \qquad 3.95$$

Here, the contribution of the applied torque is shown underlined and is only to be included when α is in the range $0 < \alpha < (\beta-\xi)$. Furthermore, although the terms in the integral are not influenced by the position of the section under consideration, the limits are different and should be taken as

$$\lambda = 0 \rightarrow \alpha \qquad \text{for } 0 < \alpha < (\beta-\xi)$$

$$\text{and} \quad \lambda = 0 \rightarrow (\beta-\xi) \qquad \text{for } (\beta-\xi) < \alpha < \beta$$

Eqn. 3.95 may be solved and rearranged to give, for $0 < \alpha < (\beta-\xi)$

$$B = \left\{Eqn.\ 3.38\right\} - \mu(T_o \pm P_o r)\left[\frac{(1-n)}{k}\frac{sh}{CH}\cdot\cos(\beta-\xi) + nr\sin(\alpha-\xi)\right]$$

$$+ \frac{\mu T_o}{CH}\frac{(1-n)}{k}\sinh kr\xi\cdot\cosh kr\alpha \mp \frac{\mu P_o r}{kCH}\left[n\sinh kr\xi\cdot\cosh kr\alpha - sh\right] \qquad 3.96$$

and for $(\beta-\xi) < \alpha < \beta$

$$B = \left\{Eqn.3.38\right\} - \mu(T_o \pm P_o r)\left\{\frac{(1-n)}{k}\frac{sh}{CH}\cdot\cos(\beta-\xi) - nr\left[(\cosh kr(\beta-\xi) - \cosh kr\alpha)\sin(\beta-\xi)\right.\right.$$

$$\left.\left. - \frac{1}{kr}(\sinh kr(\beta-\xi) - \sinh kr\alpha)\cos(\beta-\xi) - \frac{\sinh kr\xi\cdot\cosh kr\alpha}{kr\cdot CH}\right]\right\} \pm \frac{\mu P_o r sh}{kCH}$$

$$+ \frac{\mu T_o}{kCH}sh\cdot\cosh kr(\beta-\xi) \qquad 3.97$$

The general distribution of forces along the beam are thus defined in terms of the two applied loads P_o, T_o and the four as yet unknown central forces M_2, T_2, V_2 and B_2, only. At this stage it is

convenient to split the loading into two separate systems consisting of either a pair of equal or a pair of equal but opposite half-loads as shown in fig. 3.29. Each pair of loads is equally spaced about the beam centreline and when superimposed these are equivalent to the original load system.
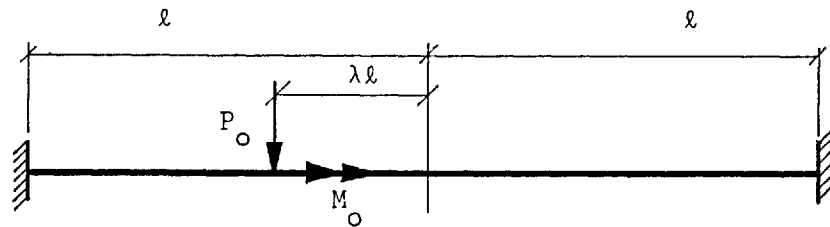
a. *General Loading System*
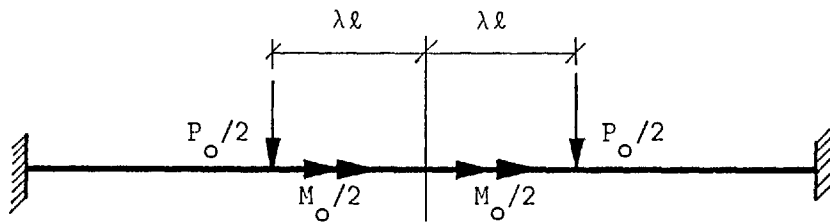
b. *Symmetrical Components of Load*
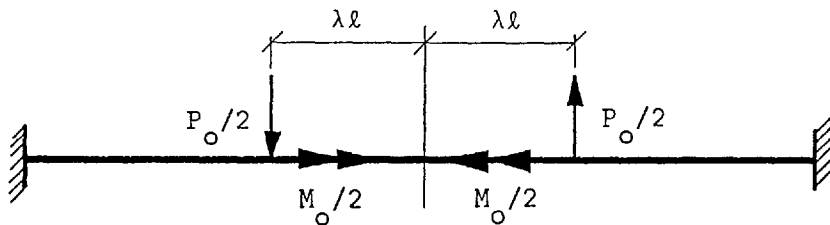
c. *Antisymmetrical Components of Load*

Fig. 3.29   Symmetrical and Antisymmetrical Components of Load

Considering the first component of load (fig. 3.29b), we know from symmetry that the following boundary conditions exist at the beam centreline:

$$T_2, \ V_2 = 0 \quad \text{and} \quad v_2', \ f_2' = 0$$

Therefore, for this arrangement, the total strain energy from eqn. 3.29

may be expressed in terms of M_2, B_2 and the applied loads only

(since T_2, $V_2 = 0$). Furthermore, the two remaining boundary conditions

enable a pair of simultaneous equations to be established from which

M_2, B_2 may be determined, thus:

$$v_2' = \frac{\partial U}{\partial M_2} = 0$$

and
$$f_2' = \frac{\partial U}{\partial B_2} = 0$$

$$\left.\begin{array}{c}\\ \\ \\ \\ \\ \\ \end{array}\right\} \quad 3.98$$

For the case of asymmetric loading, shown in fig. 3.29c, the

appropriate boundary conditions at the beam centreline, are

$$M_2, \; B_2 \;=\; 0 \quad \text{and} \quad \phi_2, \; v_2 \;=\; 0$$

and the remaining unknown beam forces T_2, V_2 may now be obtained from

the following equations:

$$\phi_2 = \frac{\partial U}{\partial T_2} = 0$$

and
$$v_2 = \frac{\partial U}{\partial V_2} = 0$$

$$\left.\begin{array}{c}\\ \\ \\ \\ \\ \\ \end{array}\right\} \quad 3.99$$

The four unknown central beam forces have therefore been

established and the stress resultants may now be determined from

eqns. 3.92, 3.96 and 3.97 at any section along the beam. However, due

to the extreme complexity of the resulting equations the exact solution

has not been presented here in explicit form and is best obtained

numerically. Furthermore, the number of unknown parameters makes a

graphical presentation impracticable for the general case and such a

presentation will therefore be restricted to the most useful application

of centreline loading ($\xi = 0$).

Central Point Loading

It is immediately apparent that the left-hand half of the centrally loaded beam is identical to the fixed-end girder previously considered in the derivation of the general flexibility matrix, fig. 3.4. From conditions of symmetry we also know that the following boundary conditions are valid on the centreline:

$$v_2' = 0; \quad f_2' = 0$$

$$\text{and} \quad T_2 = \frac{T_o}{2}; \quad V_2 = \frac{P_o}{2}$$

$$\text{3.100}$$

In accordance with eqn. 3.44 these conditions may be incorporated into a pair of simultaneous equations in the following way:

$$\frac{\partial U}{\partial M_2} = v_2' = f_{11} \cdot M_2 + f_{12} \cdot \frac{T_o}{2} + f_{13} \cdot \frac{P_o}{2} + f_{14} \cdot B_2 = 0$$

$$\frac{\partial U}{\partial B_2} = f_2' = f_{41} \cdot M_2 + f_{42} \cdot \frac{T_o}{2} + f_{43} \cdot \frac{P_o}{2} + f_{44} \cdot B_2 = 0$$

$$\text{3.101}$$

where f_{11} etc. are the flexibility influence coefficients detailed in Appendix 2.1.

By eliminating the term B_2 from eqn. 3.101, a solution for the unknown central bending moment is obtained, thus:

$$M_2 = \left\{ \left[\frac{P_o r}{2} \mp \frac{T_o}{2} \right] \left[\frac{S^2}{2} \left[j^2 - 1 + \mu n(3 - 2n) \right] + \mu n(1-n) \frac{krS}{SH} (C.CH-1) \right] \right.$$

$$\left. + \frac{P_o r}{2} \left[(c-1)(1-\mu n) + \mu n \ kr \ \frac{S}{SH} (CH-1) \right] \right\} \Big/ \{DENOM\} \qquad \text{3.102}$$

where $\{DENOM\}$ represents the denominator from eqn. 3.86, derived previously for the case of uniformly distributed loads.

A solution for the unknown central bimoment, B_2, may also be obtained by either eliminating M_2 from eqns. 3.101, or by substituting M_2 from eqn. 3.102 into one of eqns. 3.101. Due to the complexity of the expressions this is best achieved numerically.

Subsequently eqn. 3.102 may be reduced to a form suitable for solid sections in the same way as that for the uniformly distributed loads (eqn. 3.87). This is achieved by passing to the limit $kr \rightarrow \infty$, thus:

$$\lim_{kr \rightarrow \infty} M_2 = \frac{\pm T_o \frac{S^2}{2}(1 - j^2) + P_o r \left\{ \frac{S^2}{2}(1 - j^2) + (C - 1) \right\}}{\beta(j^2 + 1) + SC(j^2 - 1)} \qquad 3.103$$

In its reduced form this expression for the unknown central bending moment corresponds to that derived by Pippard and Baker[86] for circular bow girders.

Graphical Presentation

The unknown central stress resultants M_2, B_2, evaluated from eqns. 3.101 and 3.102 with $\mu = 1$, are shown in figs. 3.30 and 3.31 respectively. By substituting these quantities into eqns. 3.31 and 3.32 the fixed end forces M_1, B_1, T_1 for open sections may be determined numerically and are expressed in figs. 3.32 - 3.34. The lines represent the same values of j^2, $k\ell$ as used in figs. 3.10 - 3.27 for uniformly distributed loads and are those given in Table 3.3. The various central and fixed end forces M_2, B_2, M_1, B_1, and T_1 are also shown in figs. 3.35 - 3.39 for sections with closed parts ($\mu = 0.5$) although the effects of intermediate values of μ can usually be interpolated with sufficient accuracy.

The longitudinal distribution of bending moment, bimoment, torsion and warping torsion can now be evaluated from eqns. 3.30, 3.38 and 3.39 and are shown in figs. 3.40 - 3.43 for open sections ($\mu = 1$),

and in figs. 3.44 - 3.47 for closed sections (μ = 0.5). The comments made during the graphical presentation of uniformly distributed loads in §3.4.4 are equally valid here and once again it has only been possible to present the results for a single included angle of $2\beta = 10^{\circ}$.

j^2 \ $k\ell$	200	10	3
0.005	⊡	◇	⊠
0.020	⊙	⟰	✳
0.050	△	✕	⋈
0.200	+	Z	⎮
1.000	✕	Y	✡

Table 3.3   Key for Figs. 3.10-3.27 and Figs. 3.30-3.47
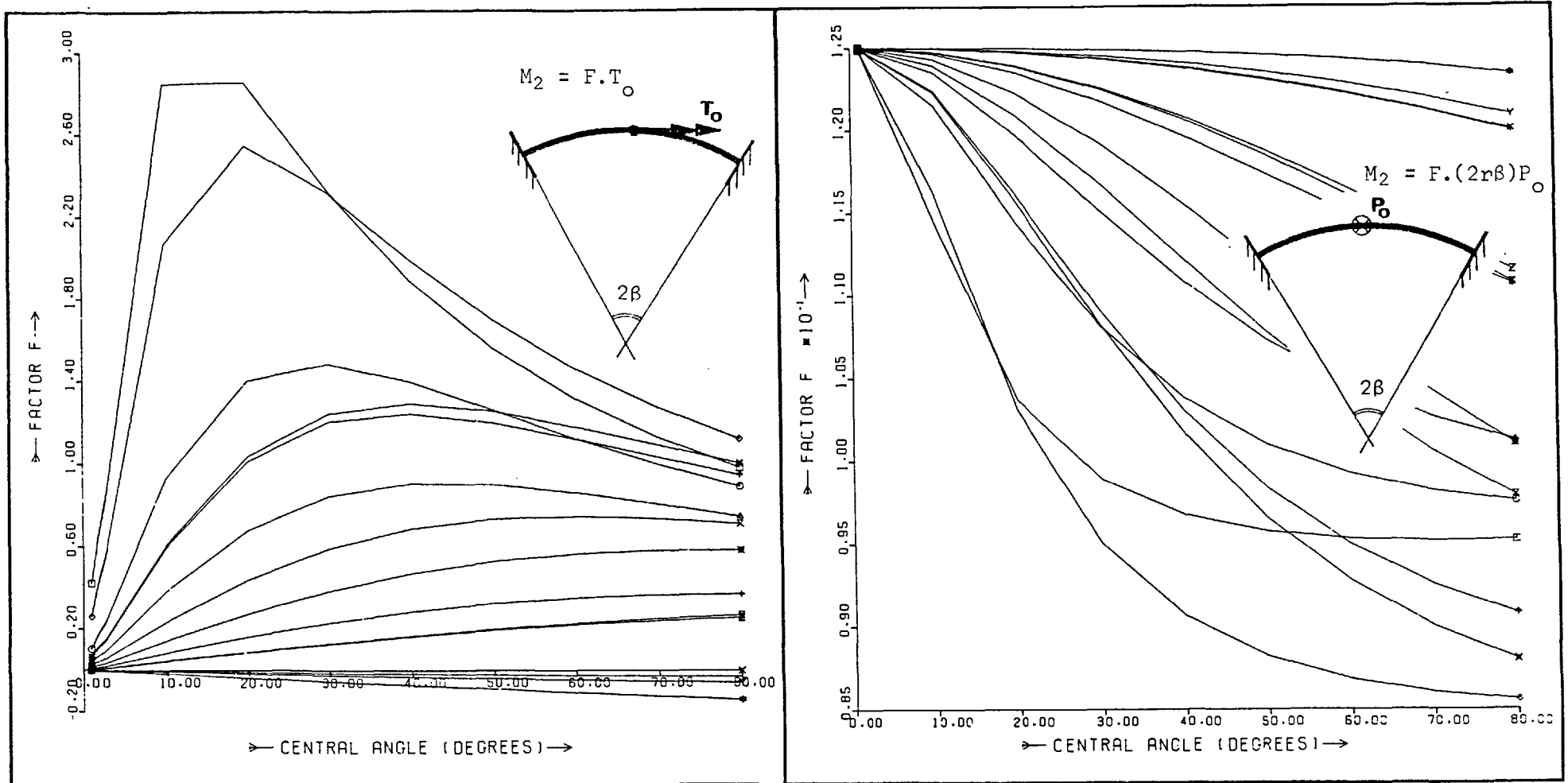
Fig.3.30 Central Bending Moment due to Concentrated Shear and Torsional Loads ($\mu = 1$)
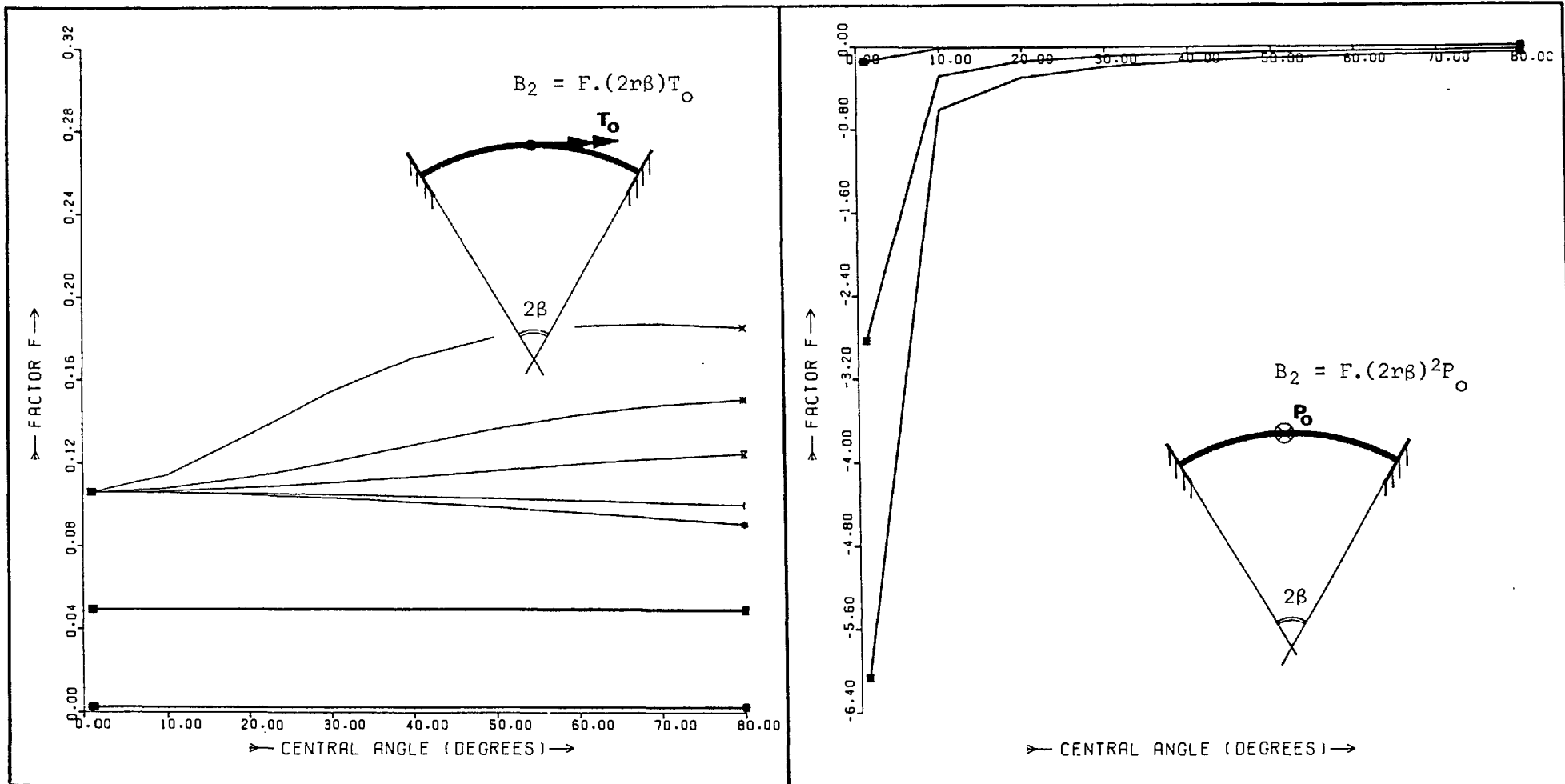
Fig. 3.31 Central Bimoment due to Concentrated Shear and Torsional Loads (μ = 1)
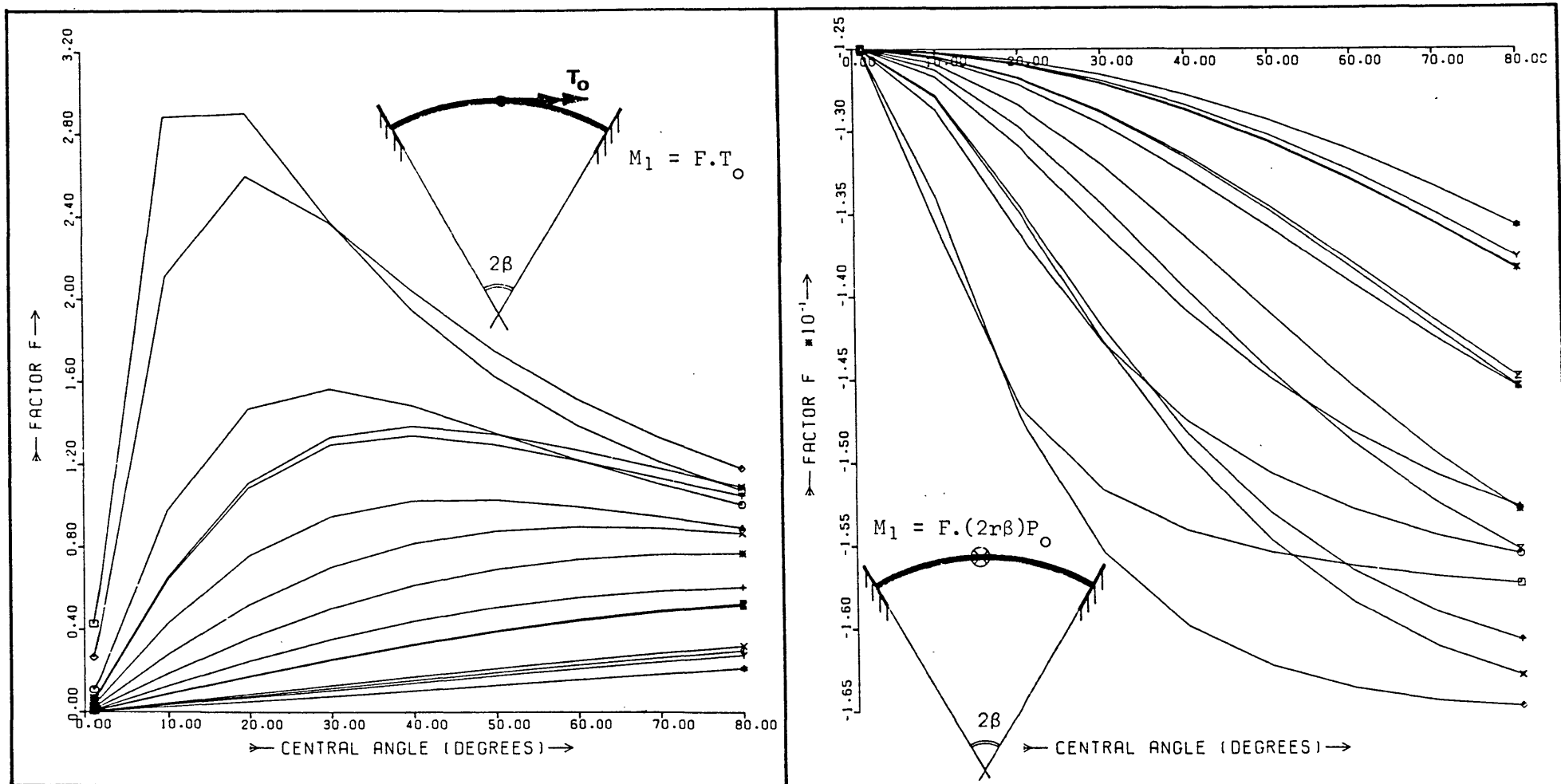
Fig. 3.32 *Fixed End Bending Moment due to Concentrated Shear and Torsional Loads* ($\mu = 1$)
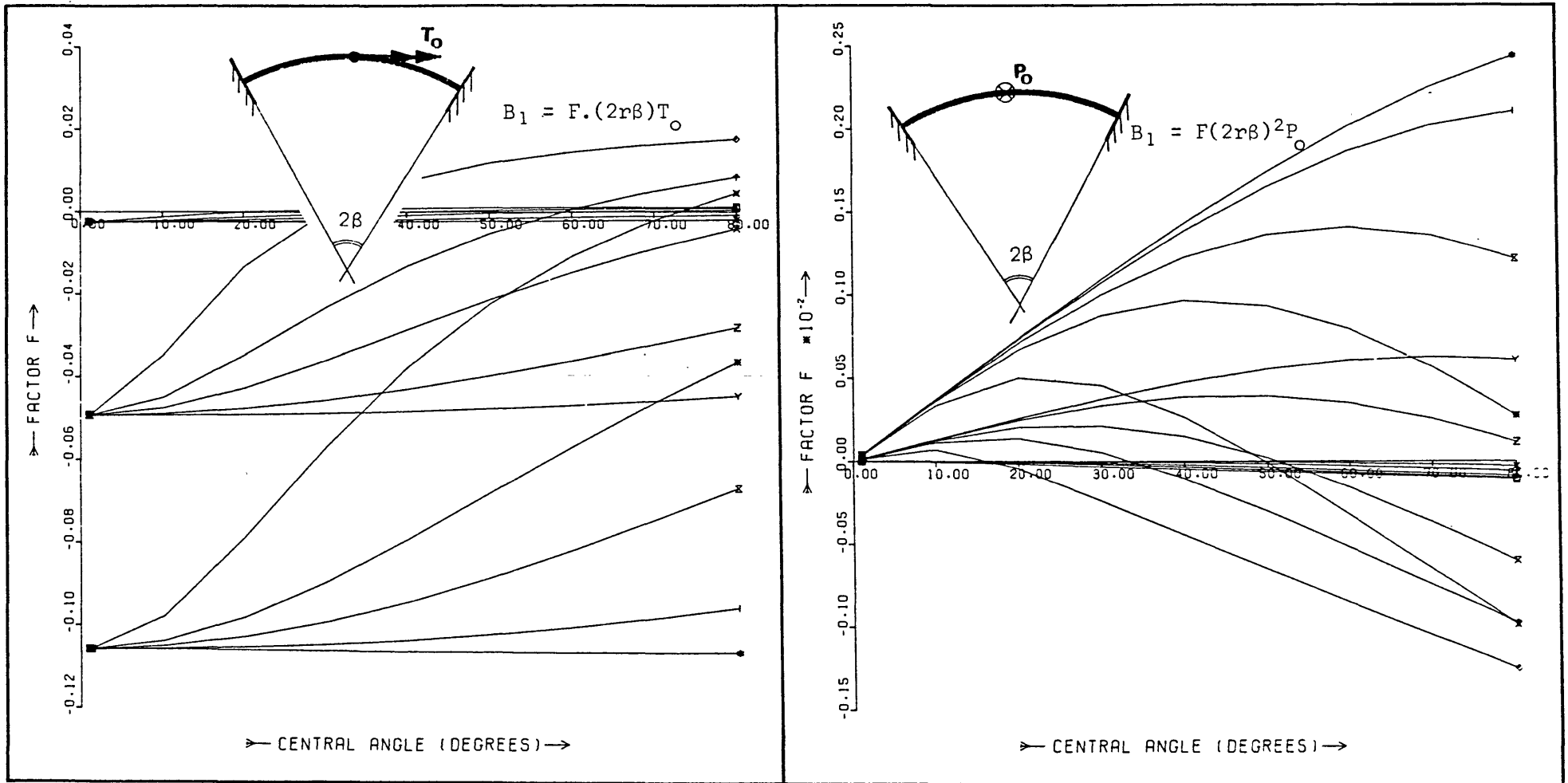
Fig. 3.33 Fixed End Bimoment due to Concentrated Shear and Torsional Loads ($\mu = 1$)
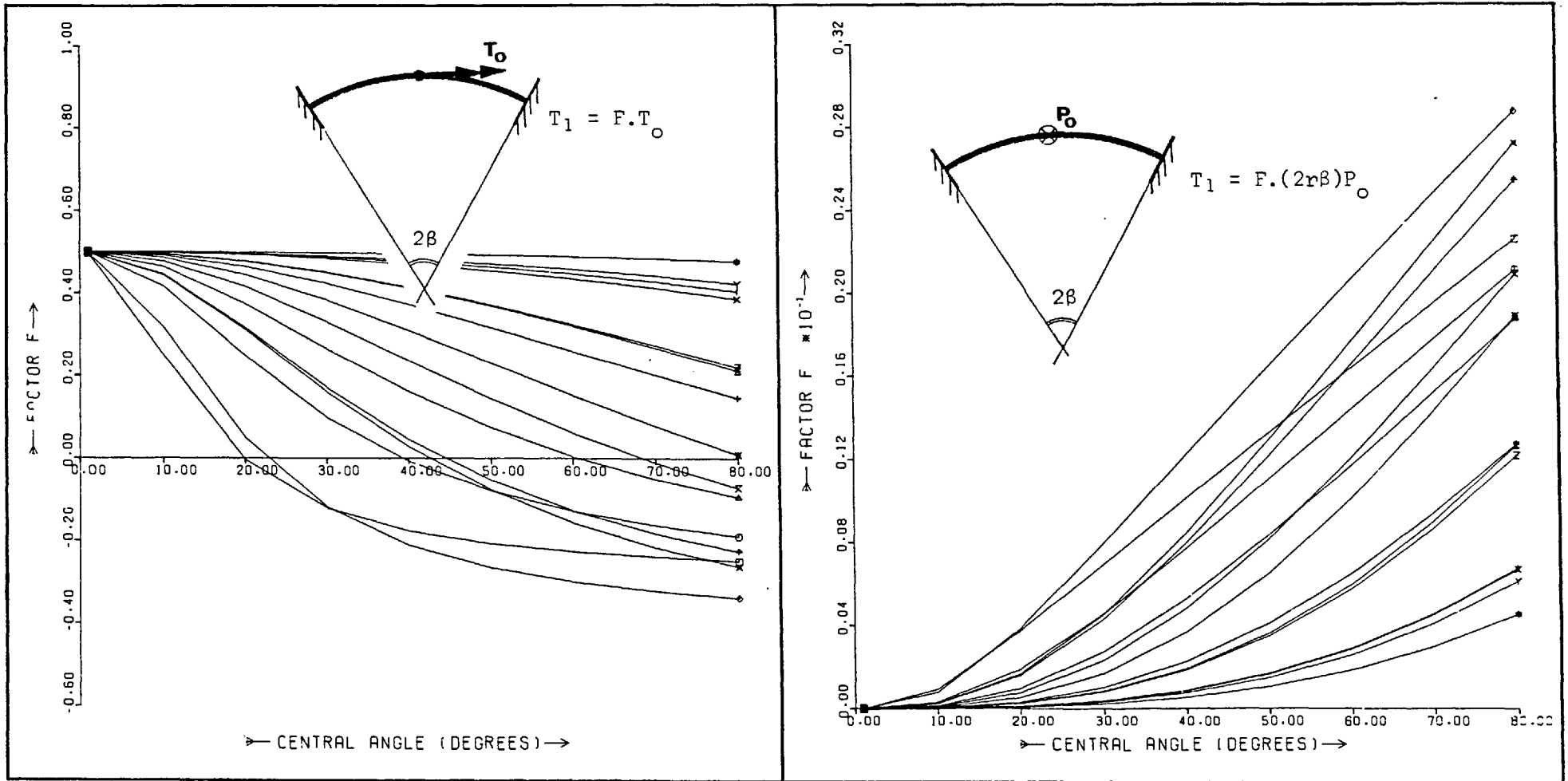
Fig. 3.34 Fixed End Torsional Moment due to Concentrated Shear and Torsional Loads (μ = 1)
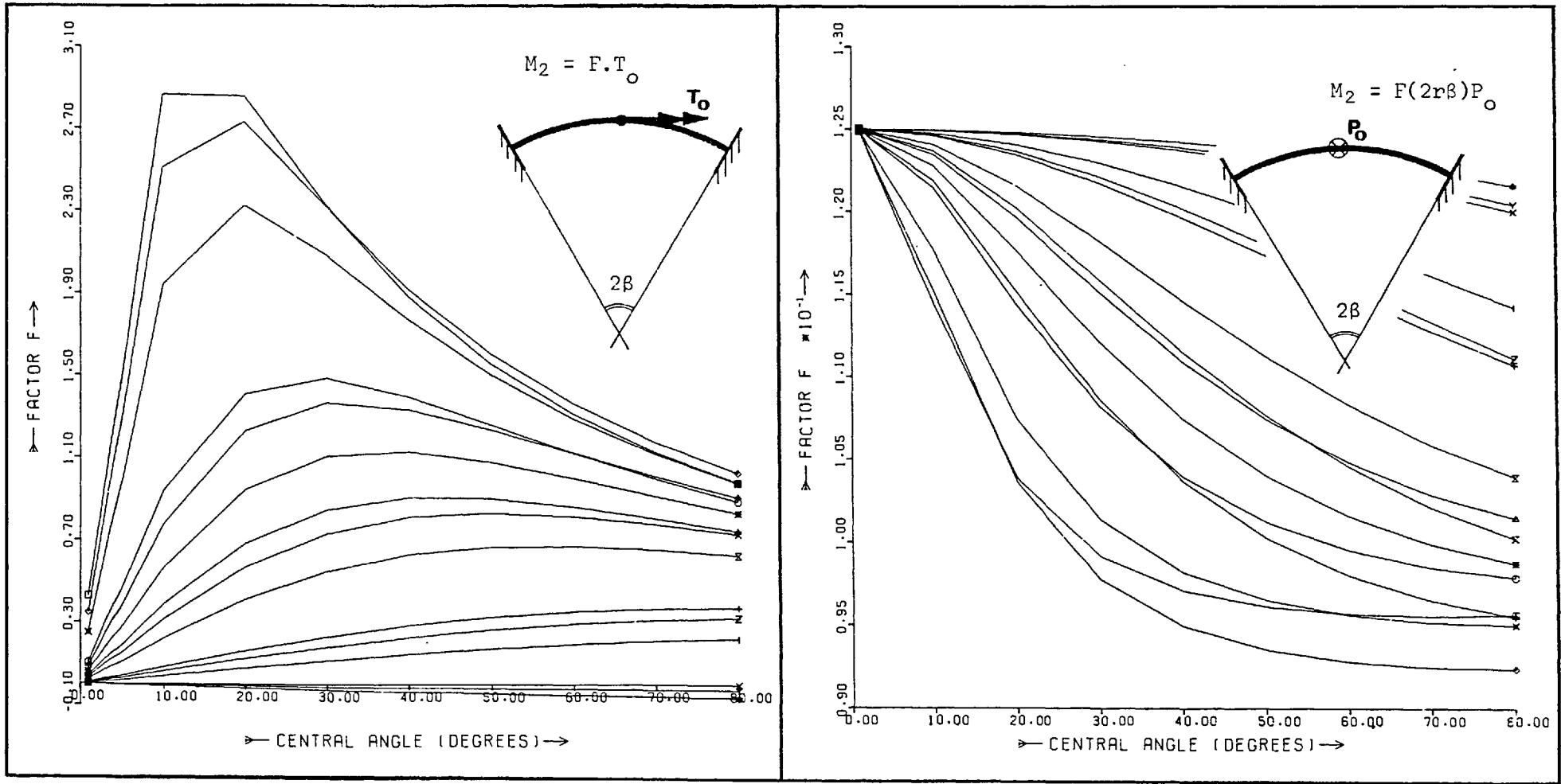
Fig. 3.35 Central Bending Moment due to Concentrated Shear and Torsional Loads (μ = 0.5)
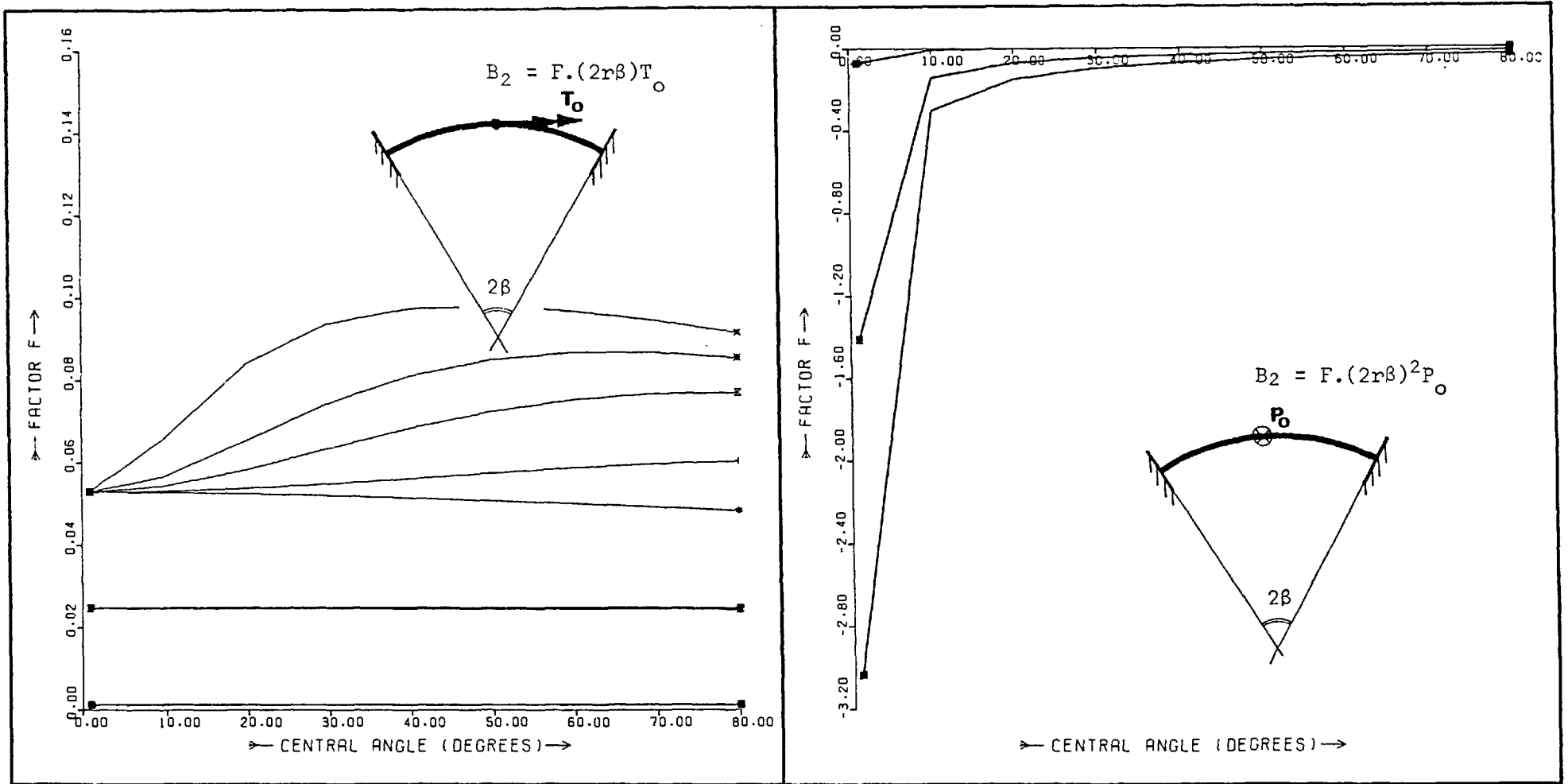
Fig. 3.36   Central Bimoment due to Concentrated Shear and Torsional Loads (μ = 0.5)
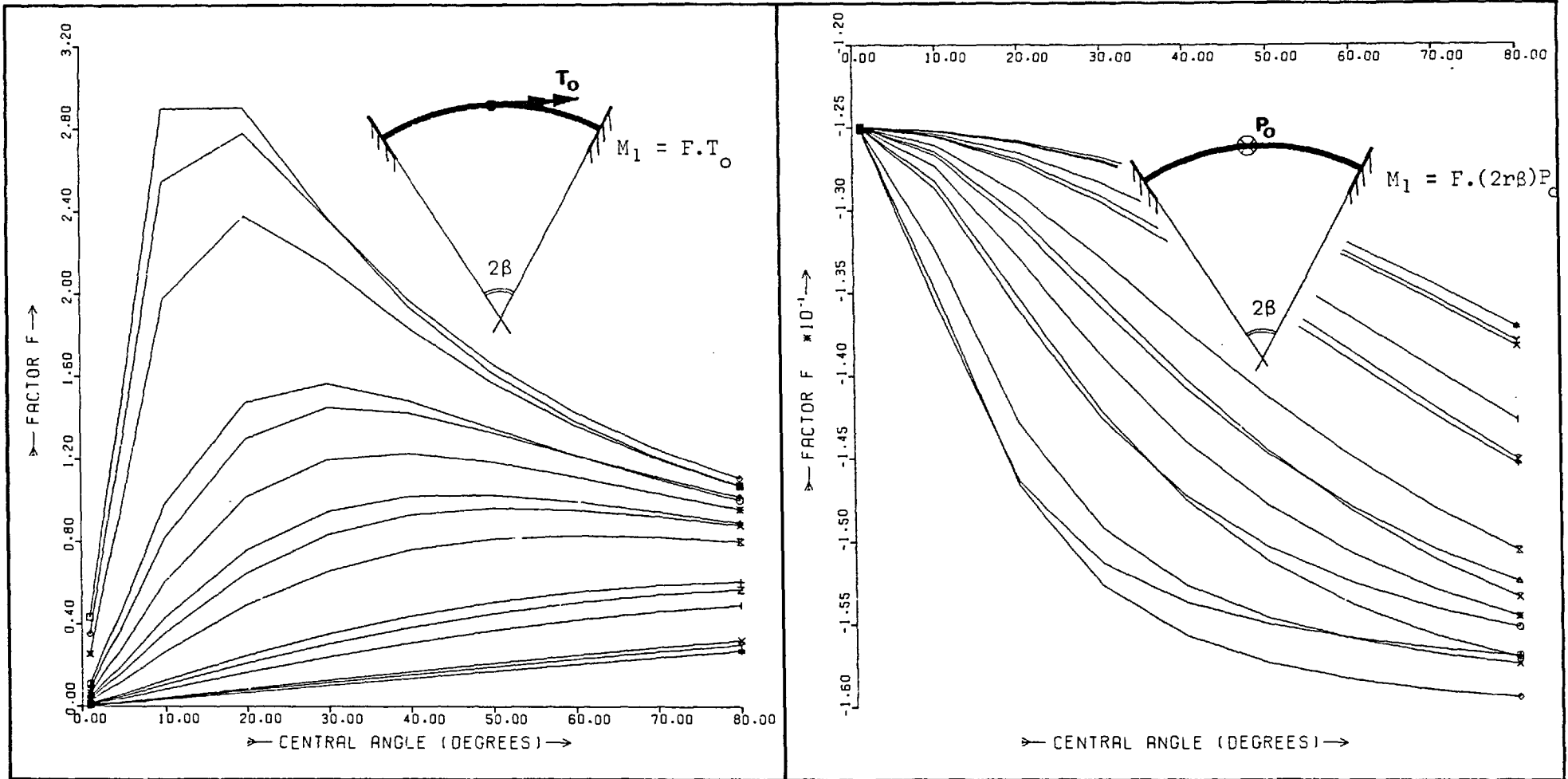
Fig. 3.37 Fixed End Bending Moment due to Concentrated Shear and Torsional Loads (μ = 0.5)
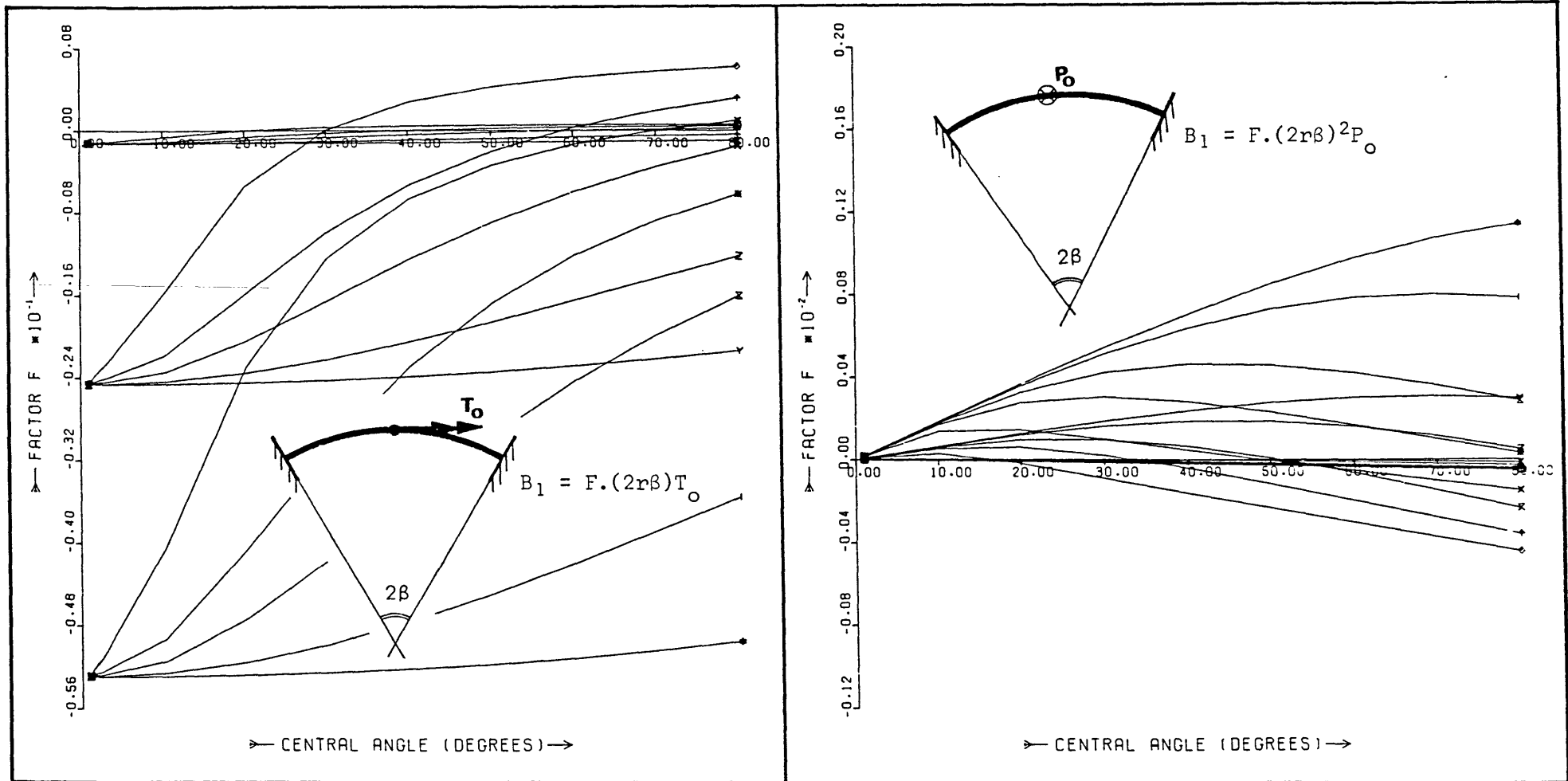
Fig. 3.38 Fixed End Bimoment due to Concentrated Shear and Torsional Loads ($\mu = 0.5$)
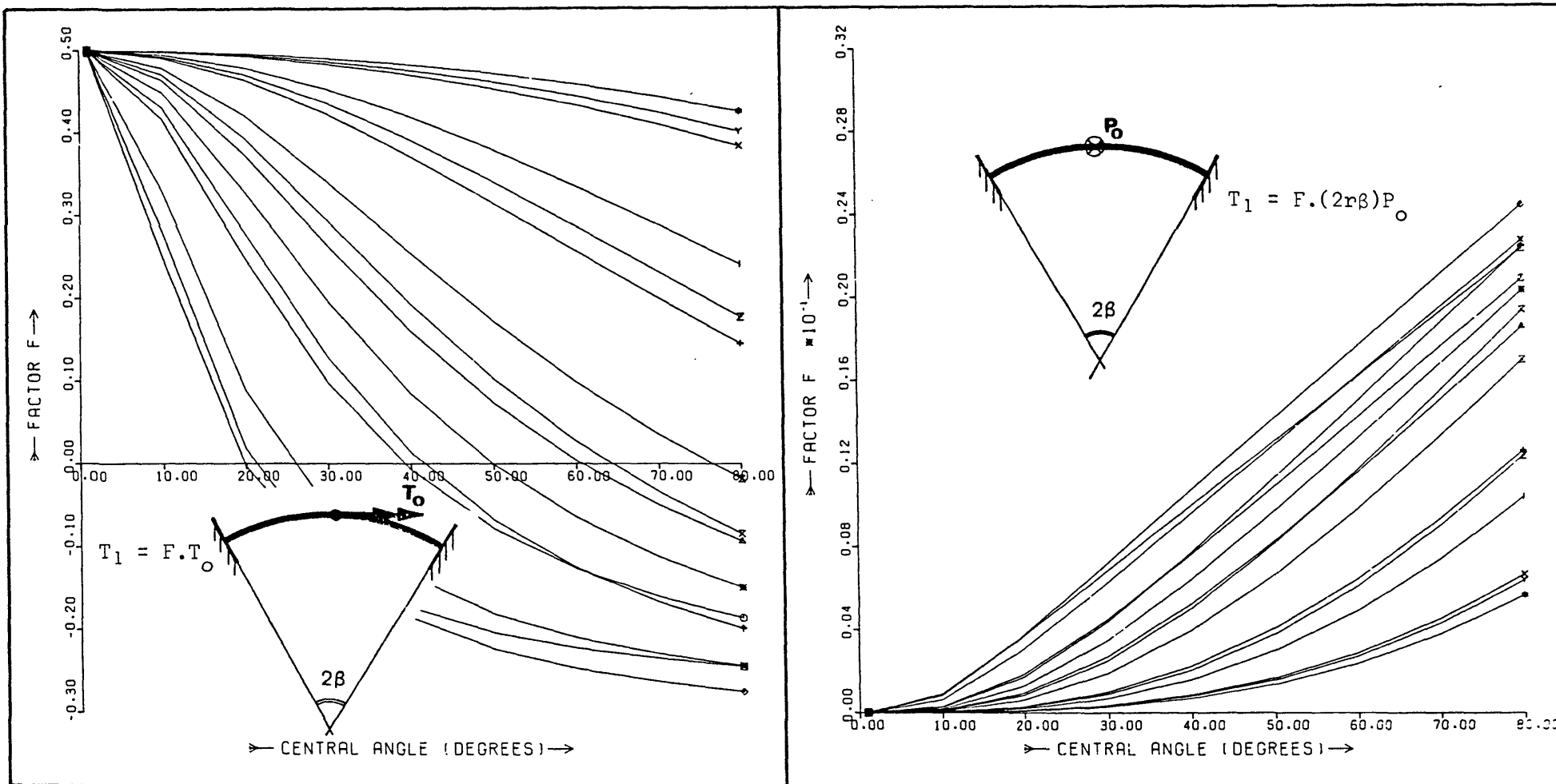
Fig. 3.39   Fixed End Torsional Moment due to Concentrated Shear and Torsional Loads (μ = 0.5)
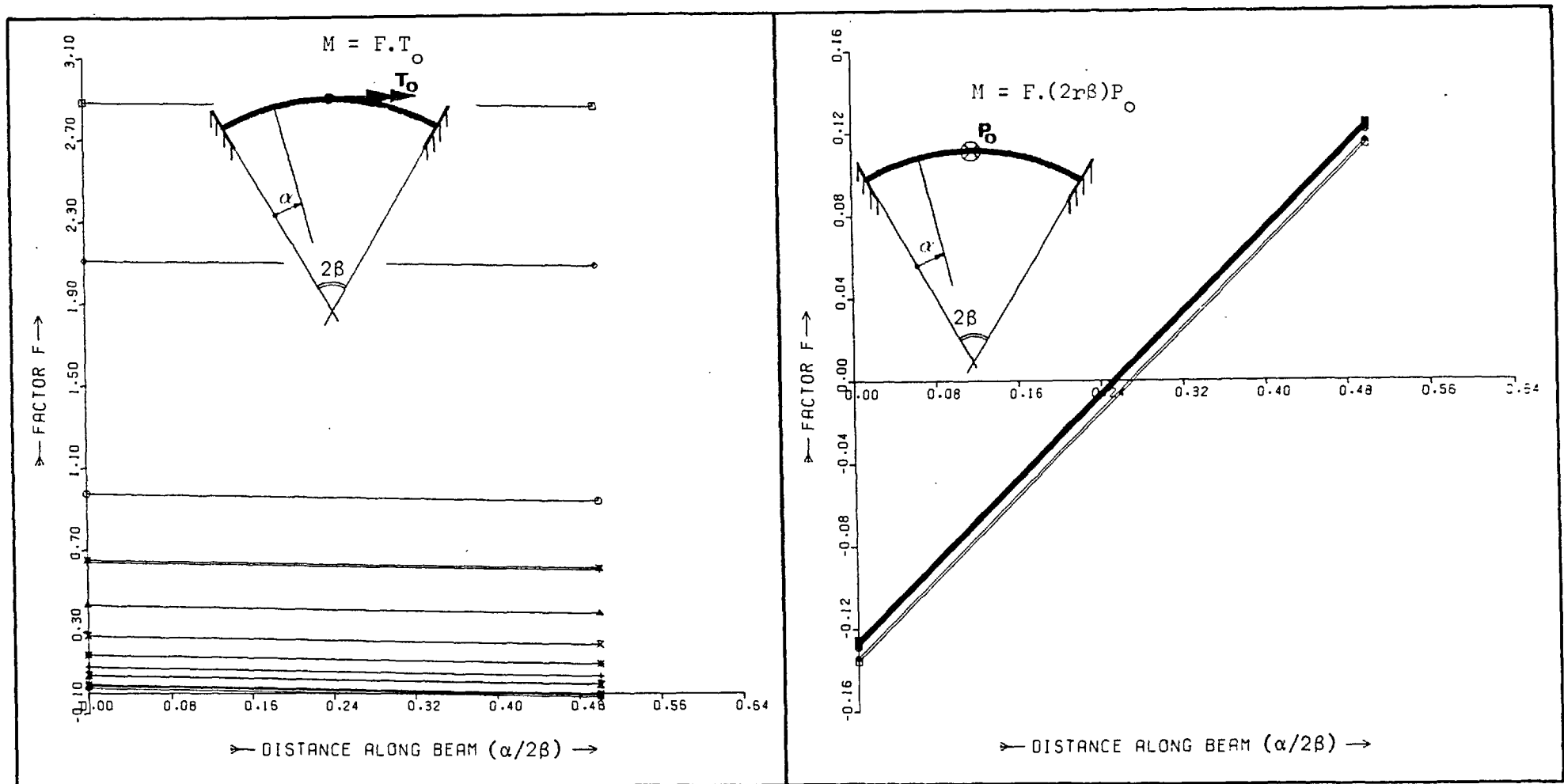
Fig. 3.40 Distribution of Bending Moment due to Concentrated Shear and Torsional Loads ($2\beta = 10^{\circ}$; $\mu = 1$)
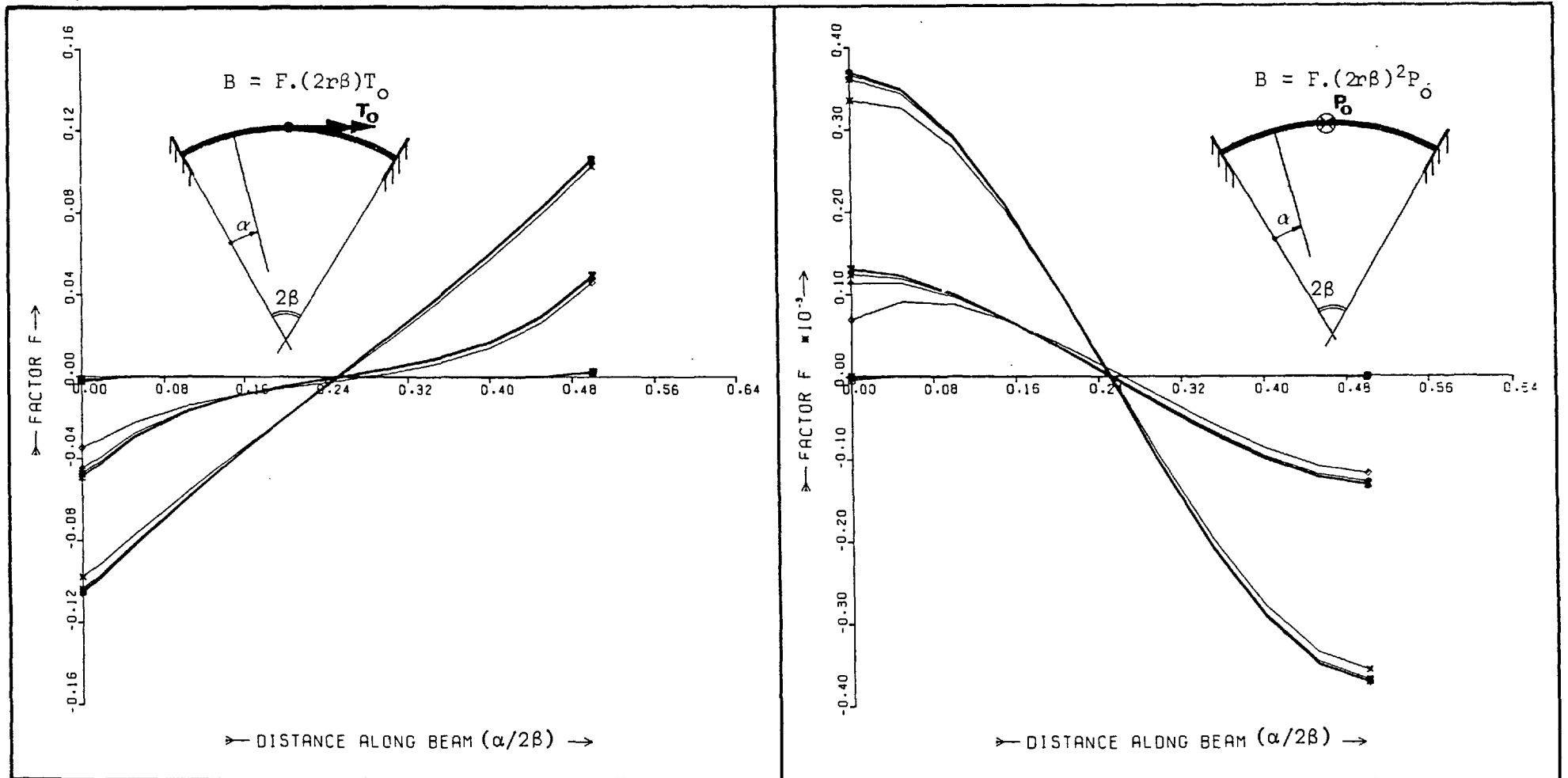
Fig. 3.41 Distribution of Bimoment due to Concentrated Shear and Torsional Loads (2β = 10°; μ = 1)
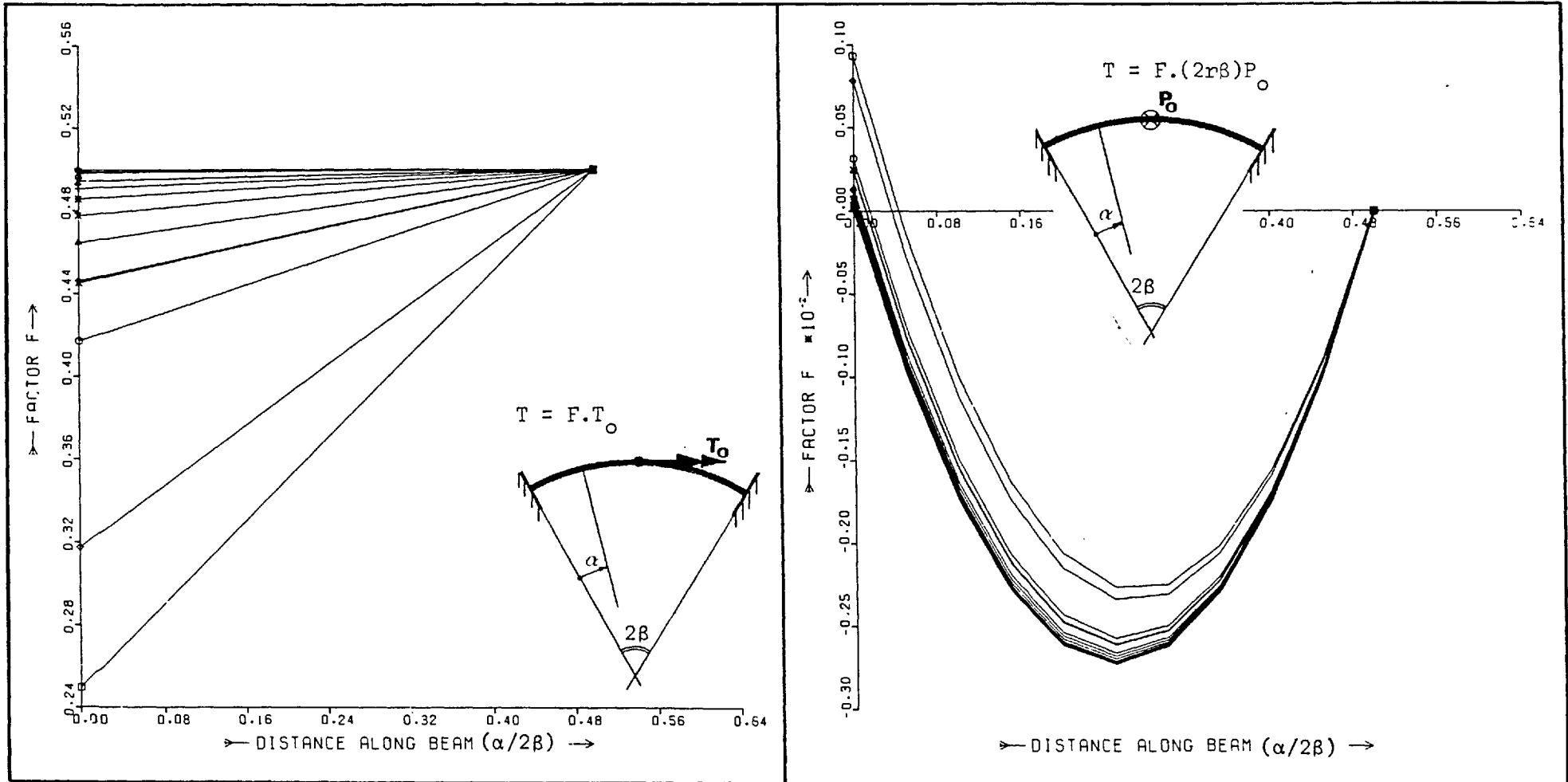
Fig. 3.42 Distribution of Torsion due to Concentrated Shear and Torsional Loads ($2\beta = 10^{o}$; $\mu = 1$)
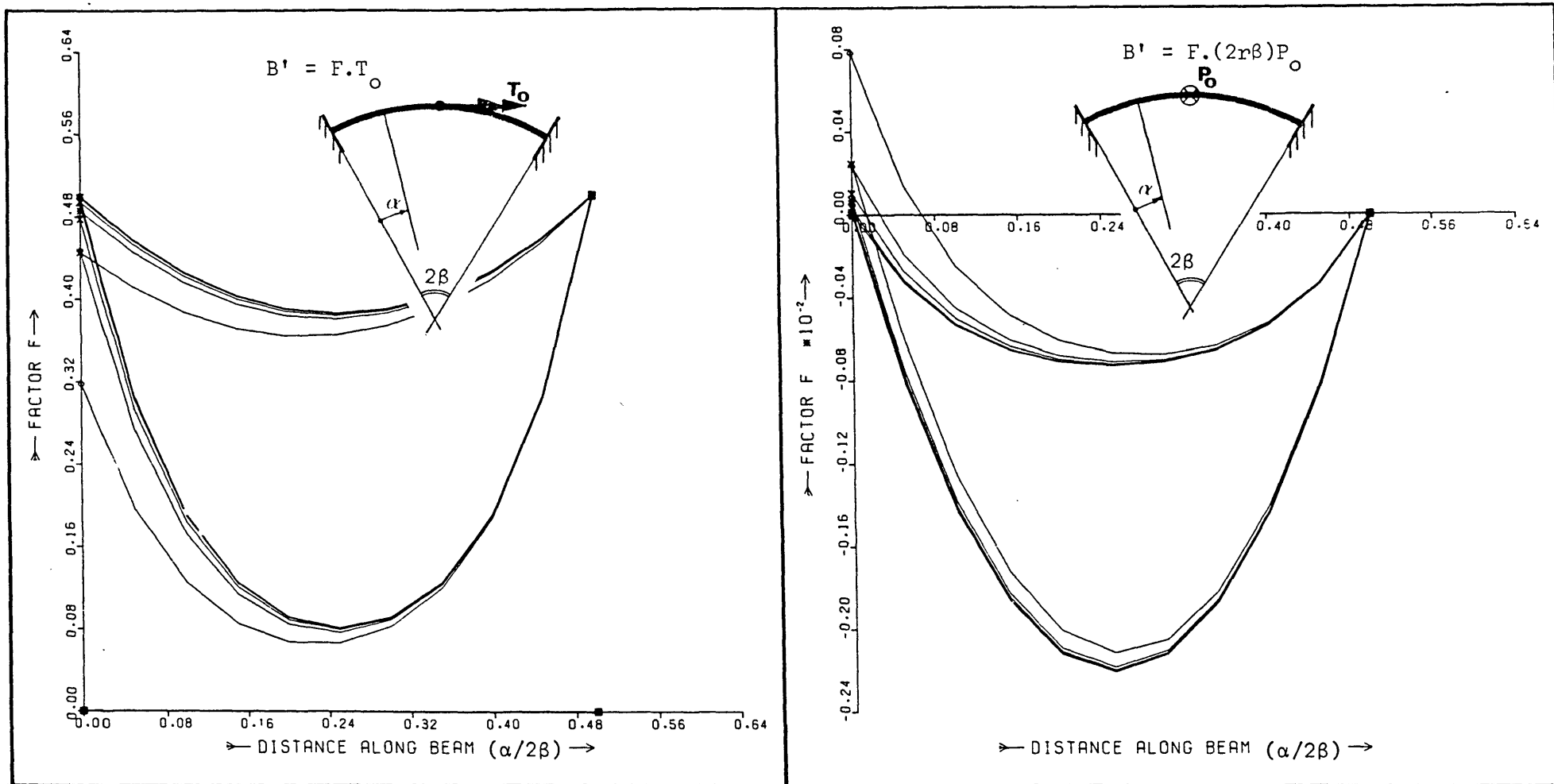
Fig. 3.43 *Distribution of Warping Torsion due to Concentrated Shear and Torsional Loads* $(2\beta = 10^{O}; \mu = 1.0)$
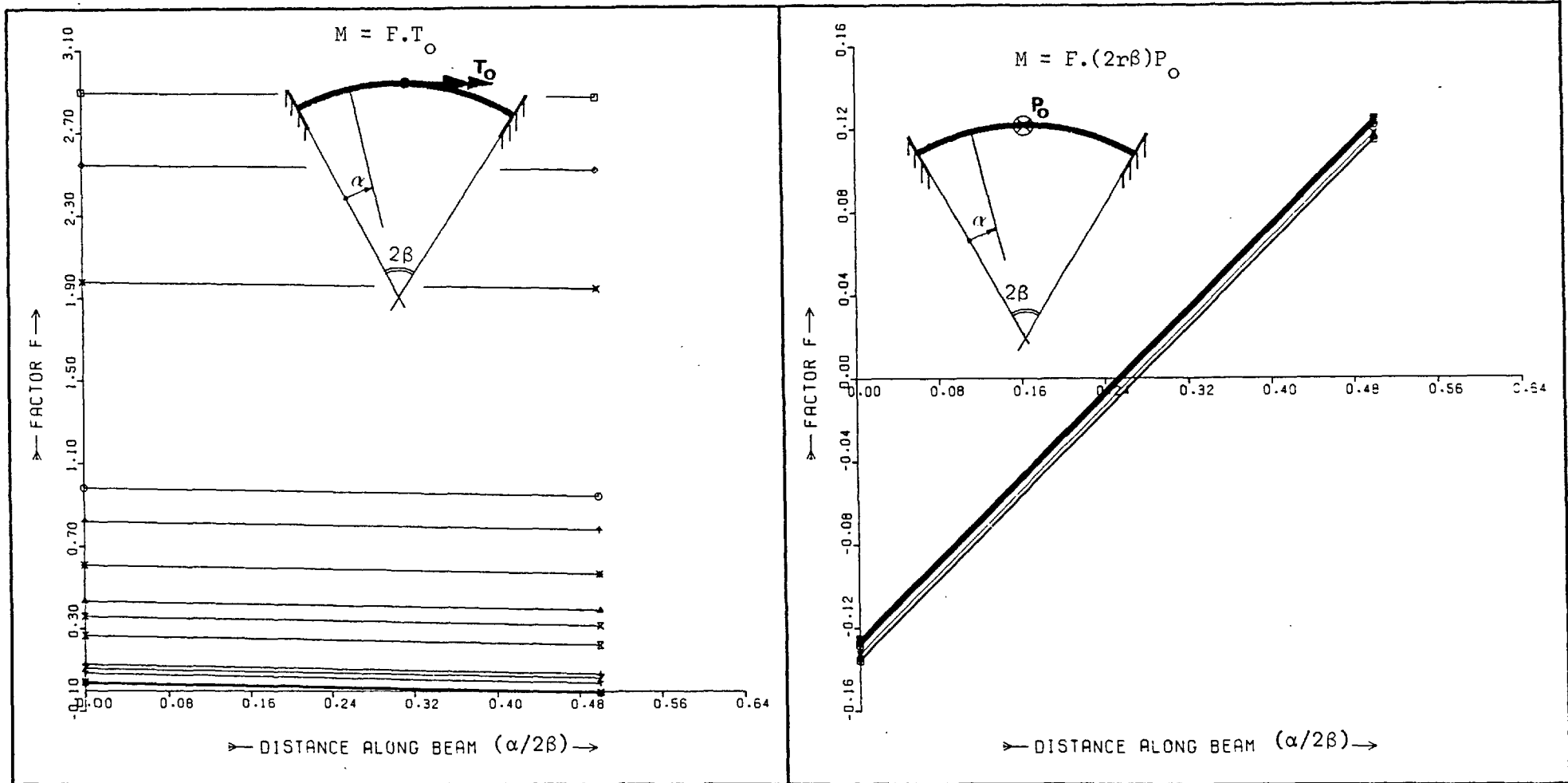
Fig. 3.44 Distribution of Bending Moment due to Concentrated Shear and Torsional Loads $(2\beta = 10^{o}; \mu = 0.5)$
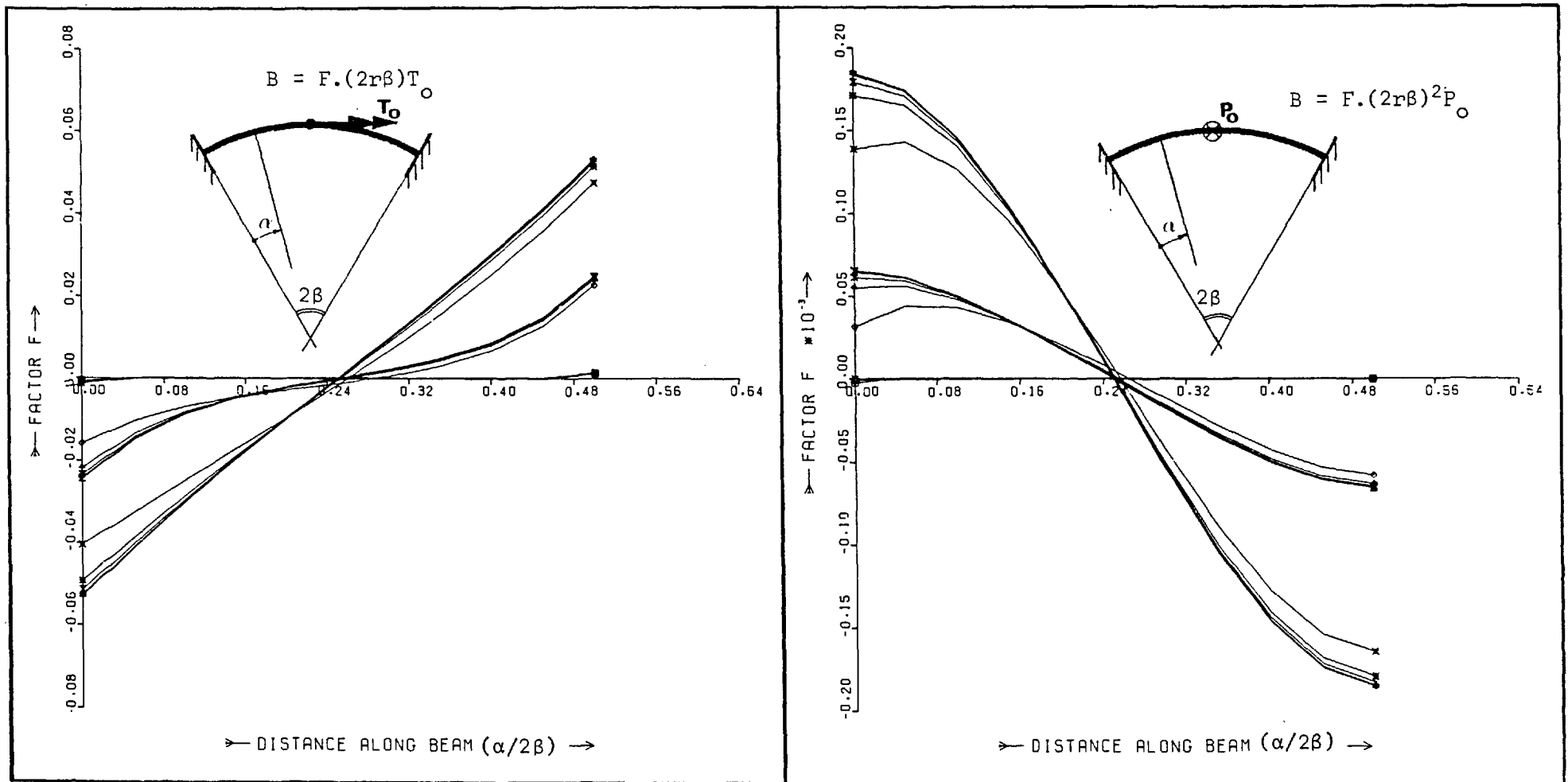
Fig. 3.45 Distribution of Bimoment due to Concentrated Shear and Torsional Loads (2β = 10°; μ = 0.5)
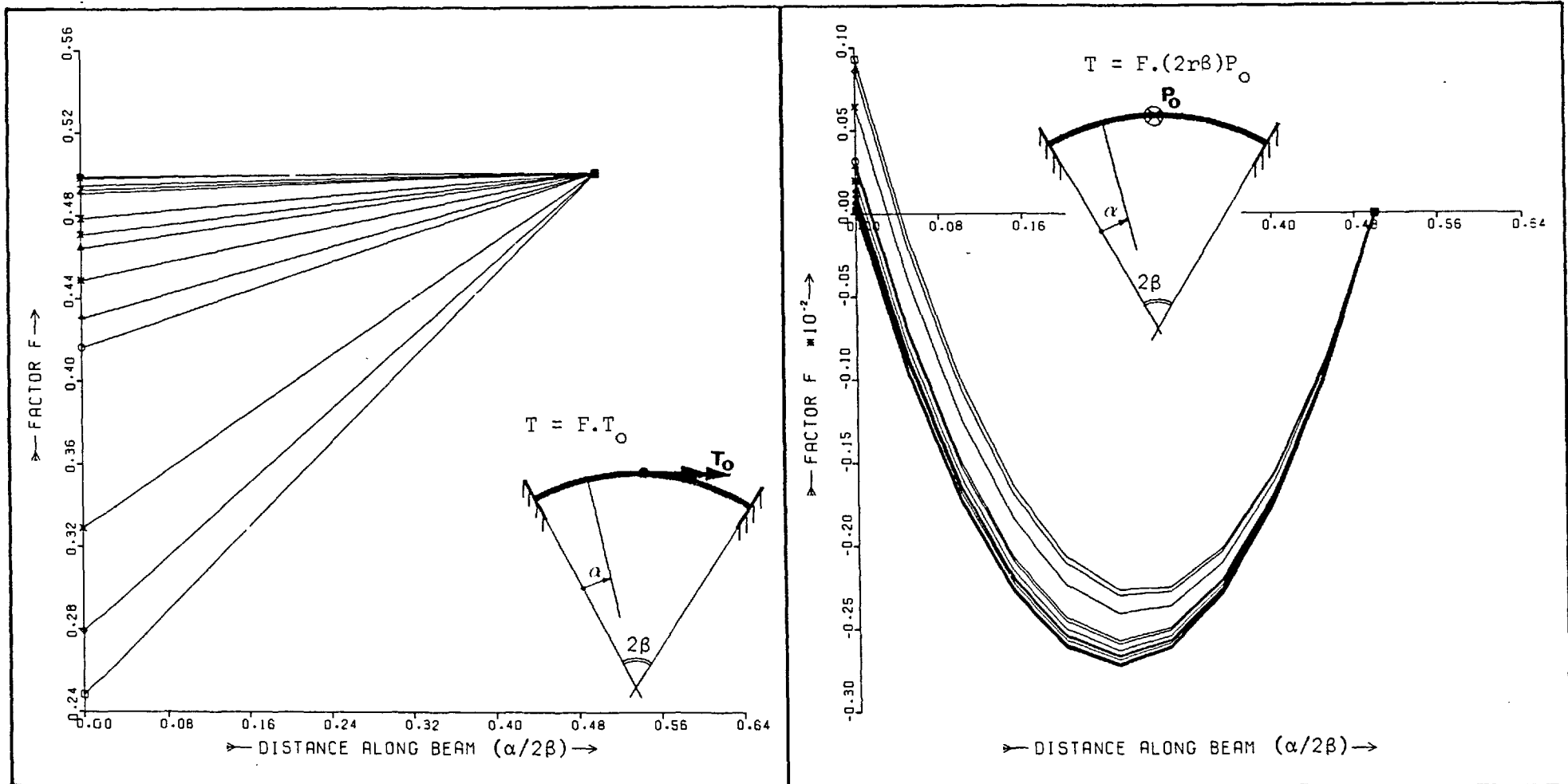
Fig. 3.46   Distribution of Torsion due to Concentrated Shear and Torsional Loads (2β = 10°;   μ = 0.5)
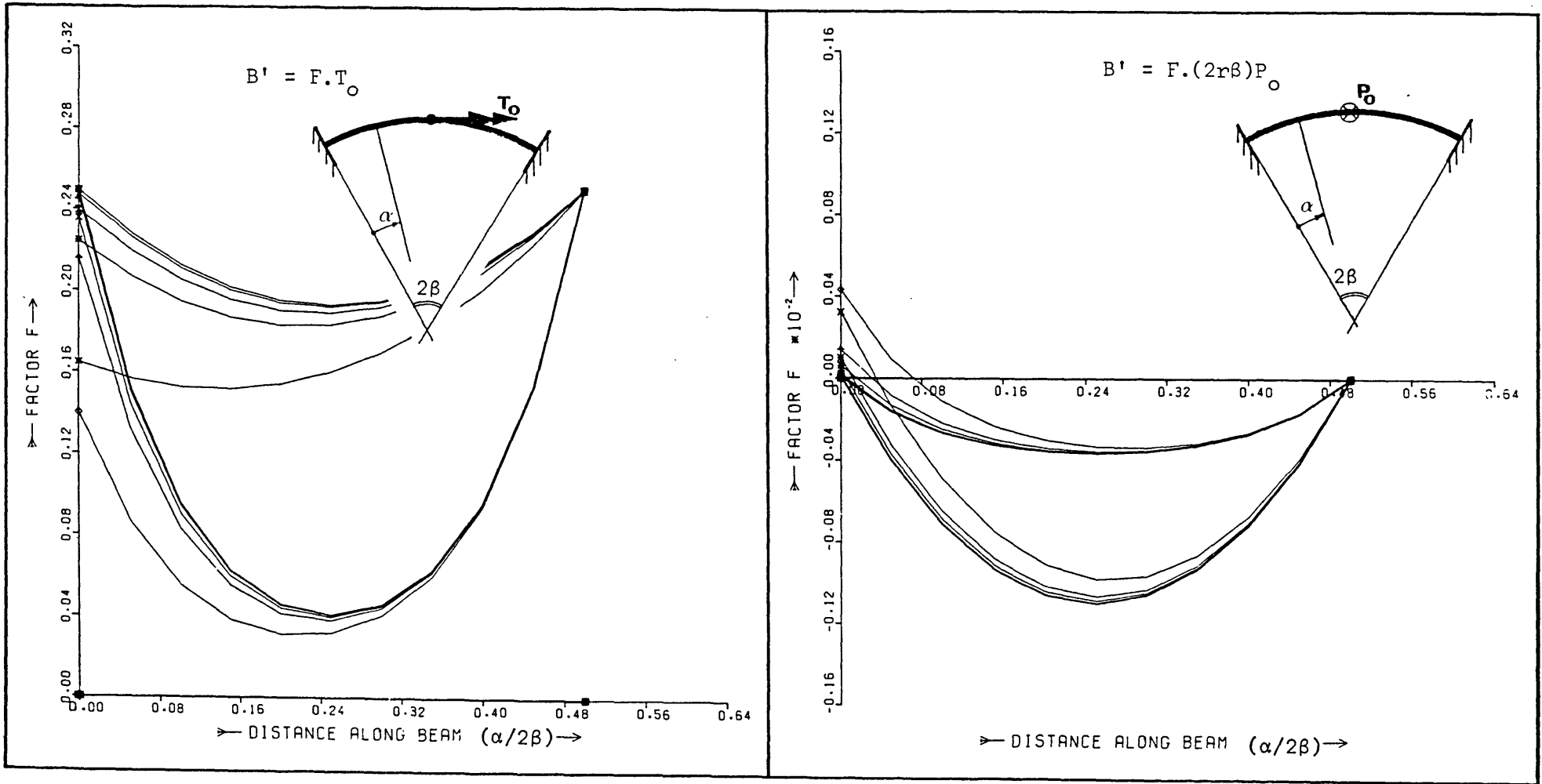
Fig. 3.47 Distribution of Warping Torsion due to Concentrated Shear and Torsional Loads ($2\beta = 10^O$; $\mu = 0.5$)

CHAPTER 4

COMPUTER ANALYSIS OF THIN-WALLED STRUCTURES
INCLUDING THE EFFECTS OF WARPING

The generality provided by the stiffness method of solution

is an important characteristic especially in the analysis of structures

incorporating features such as changes of section, complex systems of

loading and support, curvature, skew and other irregularities.   For

structures comprising thin-walled sections this has often necessitated

the use of finite element techniques since the familiar grillage method,

in its original form, only considers simple beam actions.   However,

grillage theory has recently been applied to the analysis of open

section bridges by Reilly[90] who has extended the stiffness formulation

to include the effects of warping restraint in straight members.   A

similar approach has also been employed by Heiderbrecht and Swift[37],

Mallick and Dungar[72] and Stafford Smith and Taranath[98] in the analysis

of shear core structures which may be conveniently idealized as open

section tubes.

The development of the straight beam element in Chapter 3

permits the grillage method to be further extended to the analysis of

structures comprising closed members.   This includes box girder bridges

and shear cores with large interconnecting beams.   The parallel

development of a suitable curved beam element also provides the

opportunity for significant economies to be made in the analysis of

structures displaying curvature since considerably fewer elements are

generally required.

In the remainder of this chapter a computer program incor-

porating the stiffness formulation for these new elements is first

described and then demonstrated in the analysis of two complex structures. Subsequently, the errors introduced by either neglecting warping effects or by idealizing curved members as one or more equivalent straight beams are both investigated for the wide range of sections typically found in practice.

4.1   THE COMPUTER PROGRAM

The stiffness approach adopted in the previous chapter is essentially a computer-based analytical technique and is unsuitable for hand calculation for even the simplest of structural configurations. However, no existing grillage program was readily available that could accommodate the extra degree of freedom necessary for the analysis of thin-walled members without considerable modification.   Furthermore, most existing programs concentrate on the efficient solution of the system stiffness matrix by taking bandwidth, symmetry, etc. into consideration, although for the one-dimensional idealization proposed here, in which full use is made of the more efficient curved beam element, this procedure is no longer of primary importance.   It was, therefore, decided to write a more suitable computer program capable of analysing complex structures of medium size in which curvature and warping effects are fully considered.

4.1.1   Program Structure

A flow chart describing the structure of the computer program is presented in fig. 4.1.   In this chart the matrix terminology is that previously used in Chapter 3 and defined at the beginning of the thesis. The program consists of four major subroutines each containing several of the computational steps identified in fig. 4.1.   This is convenient for repetitive calculations such as formulation of the individual member stiffness matrices, transformation from local to
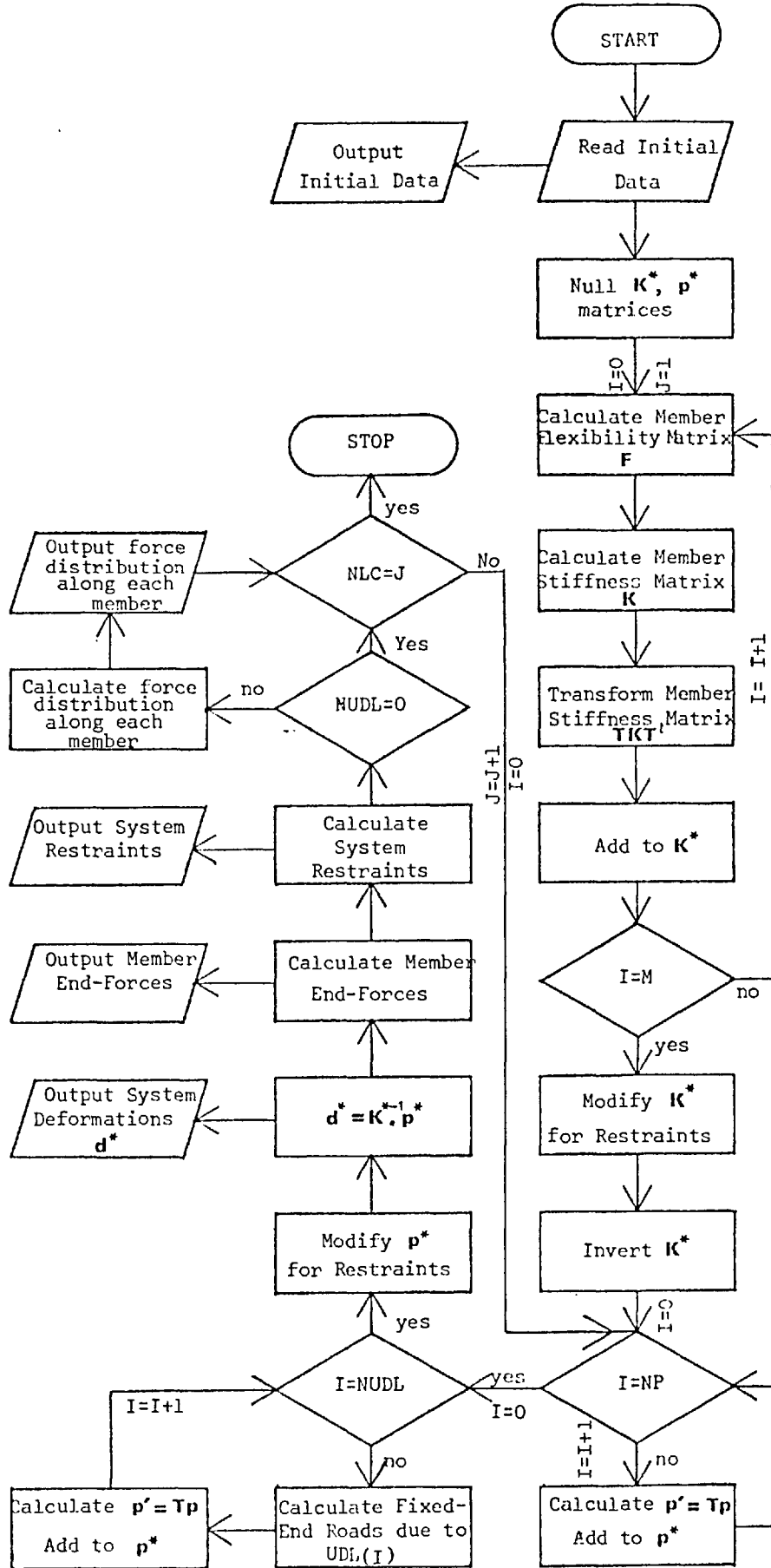
Figure 4.1   Flow Chart for Grillage Analysis including the Effects of Warping

system co-ordinates, assembly of the system stiffness matrix, etc., and enables each subroutine to be developed separately and checked thoroughly before use.

The program language is Fortran IV and thus the first step is to assign limiting dimensions to the various arrays. Input data describing the structural configuration and the geometrical and material properties of the constituent members is then read into store, and also immediately output as a checking procedure. The format of all the input/output data together with the various options available are described in more detail in §4.1.2.

Before proceeding further, the system stiffness matrix, $\mathbf{K}^*$, and the load vector, $\mathbf{p}^*$, are set to zero. This is in preparation for the addition of the individual member coefficients which are calculated in accordance with §3.4.1 in one of the subroutines. A different subroutine is used depending on whether the member is straight or displays either positive or negative curvature, although the resulting member stiffness matrix must be transformed into system co-ordinates (§3.4.2) before assembly.

When the system stiffness matrix is complete, appropriate rows and columns are removed or modified in order to take account of the various system restraints. This procedure is detailed in §3.4.3 and is necessary to make $\mathbf{K}^*$ non-singular before solution is possible. The NAG subroutine F01ABF has been used for inversion and this is readily available in most computer systems. It provides an accurate solution for any set of real, symmetric, positive definite linear equations expressible in the form $\mathbf{Ax} = \mathbf{b}$. The routine uses Cholesky's method to decompose $\mathbf{A}$ into triangular matrices, such that $\mathbf{A} = \mathbf{LL}^t$, where $\mathbf{L}$ is the lower triangular matrix. An approximation to $\mathbf{x}$ is found by

forward and backward substitution. This enables a residual matrix $r = b - Ax$ to be evaluated and a correction matrix to be determined from the solution of $LL^t . d = r$. The original solution of x is then replaced by $(x + d)$ and the process repeated until full machine accuracy is achieved. Whereas the problem is specified in terms of single precision variables, double precision inner-products are used throughout the calculation. Furthermore, only one additional vector of the same size as x is required for working space although no account is taken of band width in order to reduce the total storage requirement.

The program, in its existing form, can accommodate two different types of loading. Firstly, bending moment, torsion, vertical shear and bimoment may all be applied as concentrated loads at the nodes in the usual way. This is only satisfactory for the application of uniformly distributed loads if a large number of elements is used, in which case, the loading may be idealized into a series of equivalent point loads. However, one of the main justifications for using curved beam elements is that fewer are generally required, and for this reason a second method of specifying loading has also been made available. This facility is provided by a special subroutine which calculates the fixed-end stress resultants, in accordance with §3.4.4, for both shear and torsional uniformly distributed loads. It then transforms them into system co-ordinates and applies them as nodal forces.

When assembly of the system load vector p^* is complete, removal or modification of particular coefficients can take place to account for the various system restraints. By pre-multiplying the resultant vector by the previously inverted stiffness matrix, K^{*-1}, a unique solution is obtained for the vector of system deformations. The individual terms from this vector may then be substituted back into the

transformed member load/displacement equations to provide all the un-known member end forces.

So as not to discourage the use of long beam elements in the initial structural idealization, a further output subroutine has been included in the program. By taking the values of the fixed-end forces for each member, the magnitude of the various stress resultants can be calculated at any number of intermediate positions by using eqns. 3.75 and 3.78. This is a useful routine and provides as much information on the longitudinal distribution of forces as is required.

Finally, with the major part of the computational effort going into setting up and solving the system stiffness matrix, $\mathbf{K}^{*-1}$, this may be stored and subsequently used for the solution of any additional load cases. This is an important feature of all stiffness methods and is particularly useful in bridge analysis when many different com-binations of lane load must be taken into consideration.

4.1.2   Input/Output Data

Due to the complex configurations of structures for which this program is most suited, and to the relatively coarse idealization facilitated by the development of the circular curved beam element in Chapter 3, automatic data generation is inappropriate and has not been included in the program. The necessary input data are punched on standard 80-column cards with the fixed format described in Table 4.1. All the integer parameters are set on the first card, thus defining the size of the various arrays and the storage necessary for solution. There then follow N/4, M, NCR, NL and NUDL cards specifying the node angles, member designation and properties, restraints, point loads and uniformly distributed loads, respectively.

The exact format of the generated output is not important but comes under the following subheadings:

	Parameter	Description	Format
Integer Parameters	M	Number of members	6I10
	N	Number of nodes	
	NCR	Number of system restraints	
	NL	Number of concentrated loads	
	NUDL	Number of uniformly distributed loads	
	NS	Number of sections between nodes at which generalized forces are to be calculated (only if NUDL ≠ 0)	
Angles (I=1,N)	GAMMA (I)	Tangential angle (in radians) of structure at each node point. If two straight members meet at a node this value is not used	4F20.15
Member Designation and Properties (I = 1, M)	NODE1 (I)	Node number at end 1 of member (I)	2I10
	NODE2 (I)	Node number at end 2 of member (I)	
	ANGLE (I)	Angle subtended by straight member (I) in system co-ordinates at end 1. This value is not used if member (I) is curved.	F12.9
	RADIUS (I)	Radius of curvature (or length if member (I) is straight)	F9.3
	EIX (I)	Bending stiffness of member (I)	3E15.4
	GID (I)	Pure torsional stiffness of member (I)	
	EIW (I)	Warping stiffness of member (I)	
	UM (I)	Warping shear parameter of member (I)	F10.8
Restraints (I = 1, NCR)	NODENO (I)	Node number of restraint (I)	3I10
	NOTYPE (I)	Type of restraint (I) i.e. 1 = Bending rotation 2 = Torsional rotation 3 = Vertical deflection 4 = Warping deformation	
	NTYPE (I)	Only required when NOTYPE(I) = 1 or 2. If NTYPE (I)=0 then restraint is in system co-ordinates; if NTYPE (I) = 1 then restraint is in member co-ordinates (and the value of GAMMA (NODENO (I) is used).	
Point Loads (I = 1, NL)	LOADNO (I)	Incorporates node position and load type, i.e. LOADNO(I) = (4 x node number + load type) of load (I), where load type 1, 2, 3 or 4 is equivalent to moment, torsion, shear or bimoment, respectively.	I10
	PLOAD (I)	Numerical value of concentrated load	F20.10
U.D. Loads (I = 1,NUDL)	MEMNO (I)	Member reference number subject to loading	I10
	TLOAD (I)	Uniformly distributed torsional load	2F20.10
	PLOAD (I)	Uniformly distributed vertical shear load	

Table 4.1 Description of Input Parameters

(i)   Member designation and properties

(ii)   Concentrated loads

(iii)   Uniformly distributed loads

(iv)   Deflections in system co-ordinates

(v)   Deflections in local co-ordinates

(vi)   Fixed-end forces in local co-ordinates

(vii)   System restraints

(viii)   Distribution of stress resultants between nodes

An option exists for suppressing either (iv) or (v) while subheadings

(ii), (iii) and (viii) are only printed out when the integer parameters

NL, NUDL and NS, respectively, are not equal to zero.

The NAG subroutine described in §4.1.1 for inverting the

system stiffness matrix also incorporates a checking procedure which

outputs a failure message in case of error.   A Type 1 error is caused

by the matrix not being positive definite (possibly due to rounding

errors), while a Type 2 error indicates that the refinement process

fails to converge in which case the stiffness matrix is ill-conditioned.

The second type of failure has frequently occurred during the

development of this program when one or more of the idealized members

possesses a relatively low warping stiffness.   In such cases, the

dimensionless parameter $k\ell$ is usually large, and this results in a very

small coefficient on the leading diagonal of the system stiffness matrix

corresponding to the bimoment term of the affected member.   When

this occurs either the beam element length must be reduced or the

offending row and column must be removed entirely from the stiffness

matrix.   In the latter case this is equivalent to only considering

the original three degrees of freedom for the particular member although

it has the additional effect of providing full warping restraint

to the adjacent members.

4.2   BIFURCATED BRIDGES

Elevated highway structures in urban areas are invariably complicated by the presence of bifurcated junctions, decks of high curvature, irregular systems of support and wide side cantilevers. However, it is by no means obvious which analytical methods provide the most efficient structural solution in terms of accuracy, computer time and overall cost, and there is little experimental evidence available to form the basis of a meaningful comparison.

In 1968, a joint Ministry of Transport Engineering Section/ Road Research Laboratory committee was established to investigate the special structural problems associated with elevated highways. With the eventual aim of providing a comprehensive suite of computer programs, the committee recommended the testing and verification of analytical techniques as and when they became available. This work was further divided into four separate classifications[12], namely

(a)   Comparison of analytical techniques with results of model tests on quadrilateral decks. Three types of deck were to be considered:

         (i)   solid reinforced concrete slabs,

         (ii)   voided reinforced concrete slabs, and

         (iii)   stiffened composite steel and concrete decks.

(b)   Comparison of analytical techniques with results of tests on four idealized, small scale, bifurcated bridge models in the linear elastic range. The four alternative forms of construction were as follows:

         (i)   prestressed concrete spine beam construction,

         (ii)   prestressed concrete multi-cellular construction,

(iii)   composite steel and plate girder construction, and

(iv)   composite steel and concrete box girder construction.

(c)   Comparison of analytical techniques with results of tests on

four large scale microconcrete and steel bifurcated bridge

models.   The forms of construction were those previously

investigated in phase (b), and each model was to be tested

up to and beyond working load and eventually to failure.

(d)   Assessment of the results from the first three phases and

user testing of selected programs.

The elevated road junctions modelled in phases (b) and (c)

did not correspond to existing structures but were defined by the general

arrangement shown in fig. 4.2.   In order to avoid unnecessary duplication

of loading equipment, the same planform was used for all the models in

each phase, although only the prestressed concrete spine beam option is

discussed here in detail.

4.2.1   Description of the Spine Beam Models

The elastic response of the idealized bifurcated bridge was

adequately represented for the purposes of phase (b) by a 1/50th scale

indirect model.   This was manufactured from an araldite/sand mixture

and the construction and testing are described in detail by Billington

and Dowling[12,13,14].   However, in order to represent more closely the

inelastic behaviour of the structure in phase (c) a larger direct model

was necessary, plate 4.1.   This alternative form of construction is

described by Waldron, Pinkney and Perry[111,112].   The constituent

materials of the full scale structure were accurately modelled using

microconcrete, welded steel mesh reinforcement and small diameter pre-

stressing strand, and size effects were largely avoided by selecting

a 1/12th scale [110].
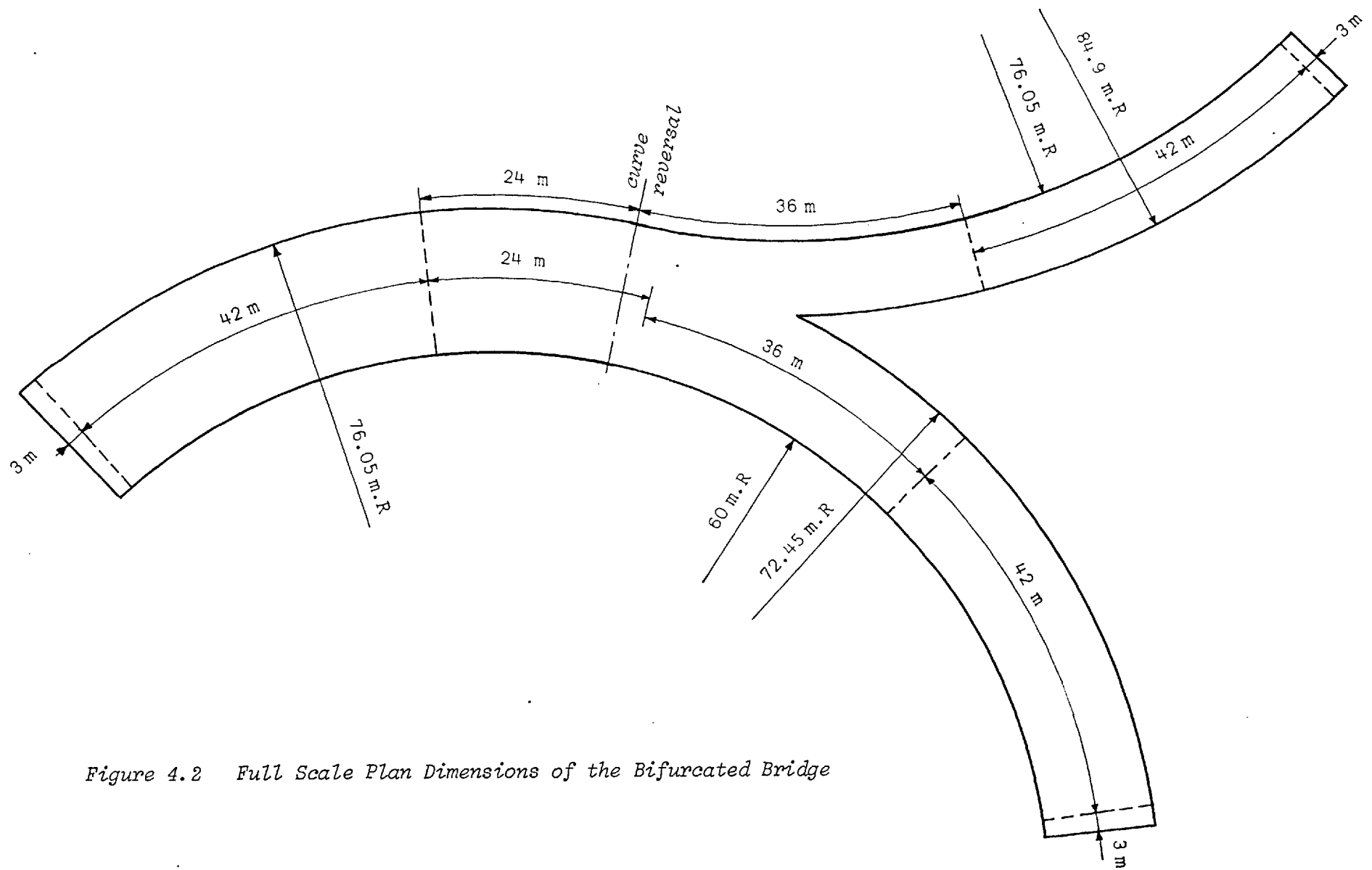
Figure 4.2   Full Scale Plan Dimensions of the Bifurcated Bridge

Plate 4.1   The Microconcrete Bifurcated Bridge Model

Since the general arrangements of the two spine beam models are essentially the same, only the dimensions for the larger model are presented in fig. 4.3; those for the indirect model may be obtained by simple geometric scaling. The layout is typical of many urban motorway bridges and basically represents part of an elevated roundabout with an associated slip road. It incorporates many common features such as high member curvature and wide side cantilevers, and consists of a twin cell box girder bifurcating into two separate boxes of single cell configuration. The structure is continuous over three central supports while only torsional restraint and simple support are provided at the three ends. Distortion is adequately prevented by diaphragms positioned at each support and, with the exception of the larger of the two outer single cell girders, at intermediate points along each span. Frequent changes of cross-section also occur within the spans, particularly due to local thickening of the bottom flange at internal supports. The dimensions of various typical cross-sections are shown in figs. 4.4 - 4.7.

Loading Arrangements

The following forms of loading were considered:

(i)   self weight

(ii)   uniformly distributed load

(iii)   settlement of supports

(iv)   HB vehicle loading

(v)   knife-edge loading

(vi)   point loads.

Provision was made in the design of the loading rig for the first three conditions while the remainder were more conveniently simulated by externally applied loads. Only conditions (i), (ii) and (vi) are
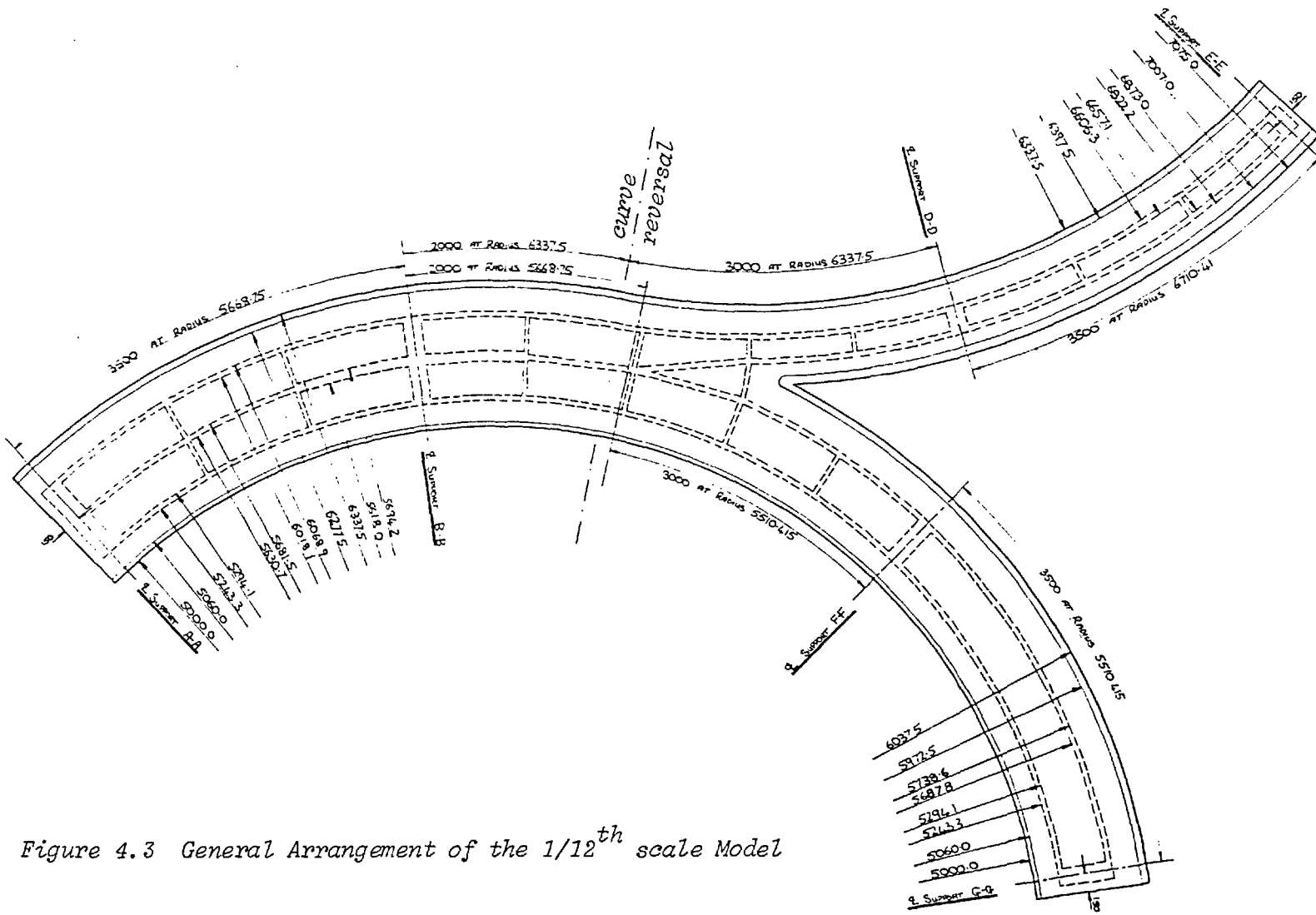
Figure 4.3   General Arrangement of the 1/12th scale Model
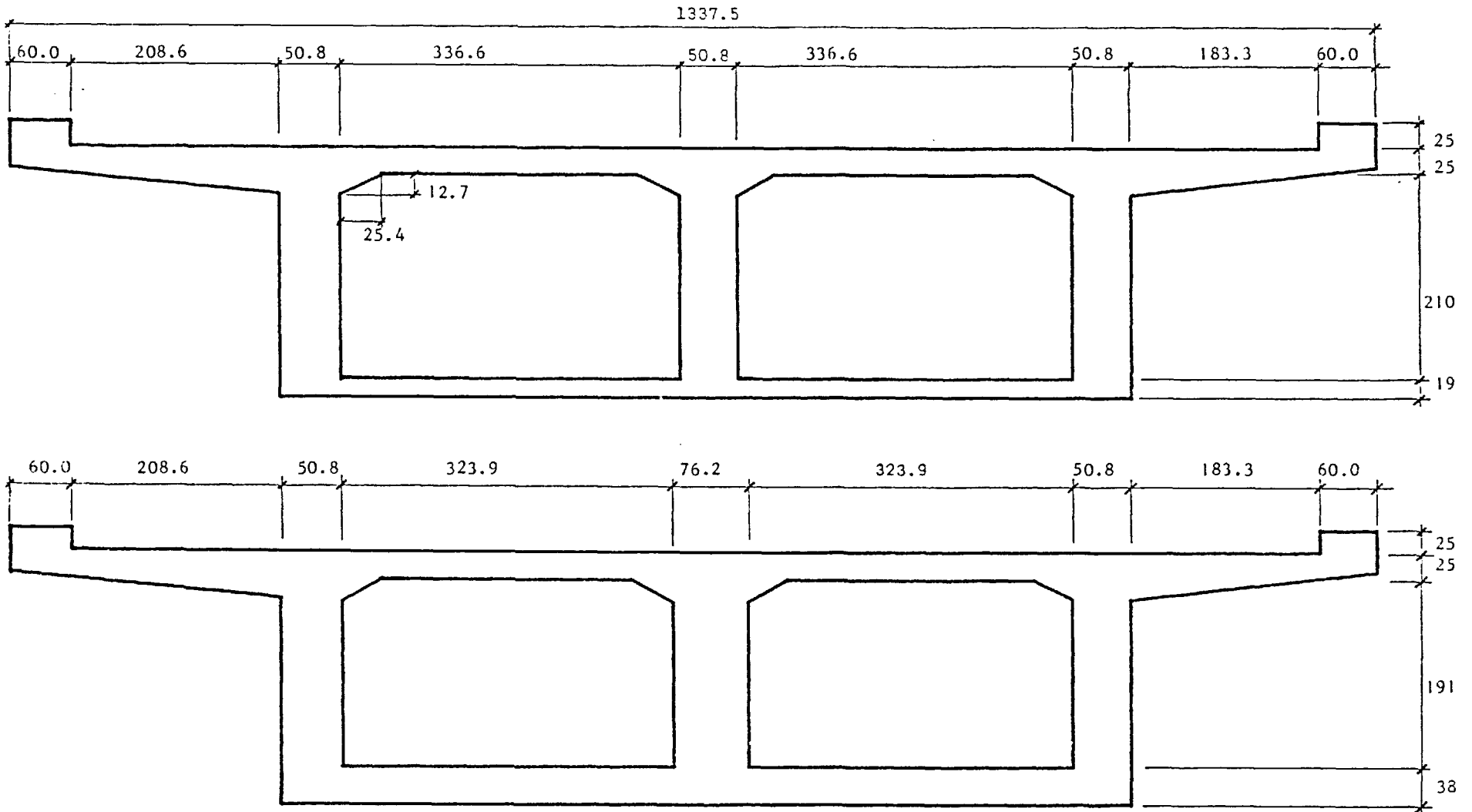
Figure 4.4   Sections A-A and B-B of the 1/12th scale Model
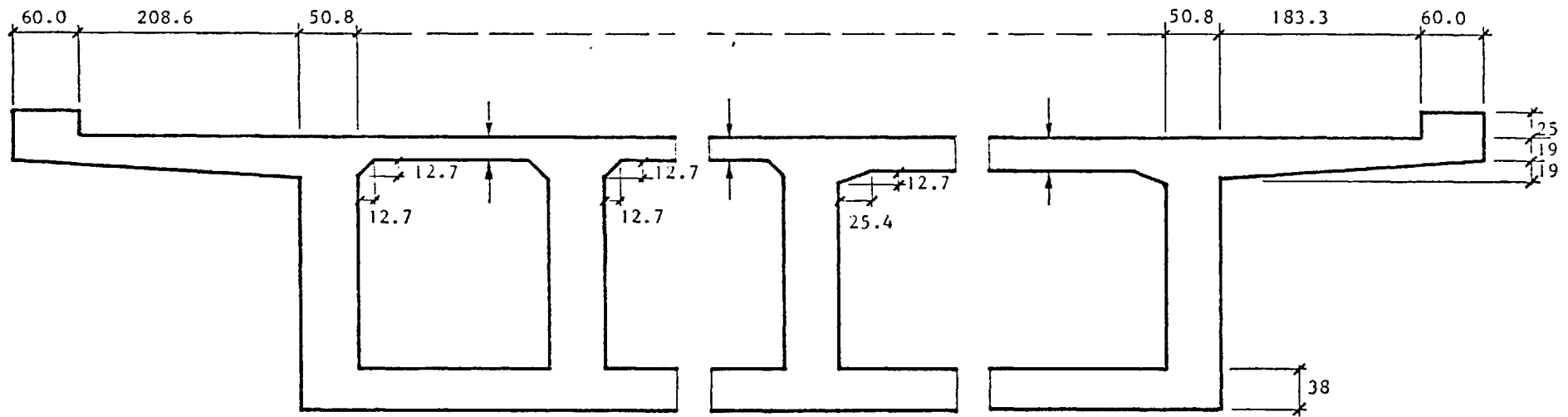
Figure 4.5   Section C-C of the 1/12th scale Model
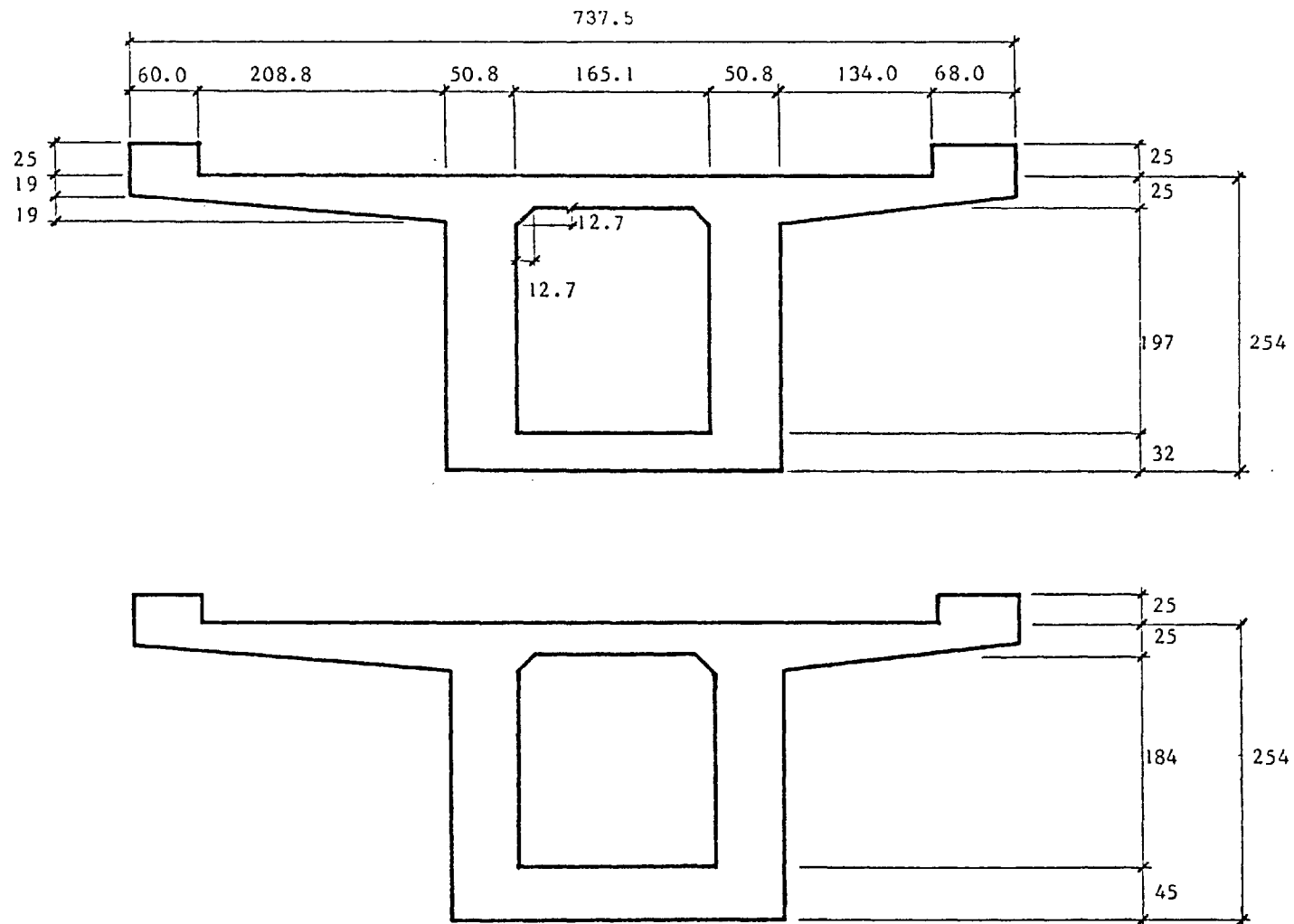
Figure 4.6   Sections D-D and E-E of the 1/12th scale Model
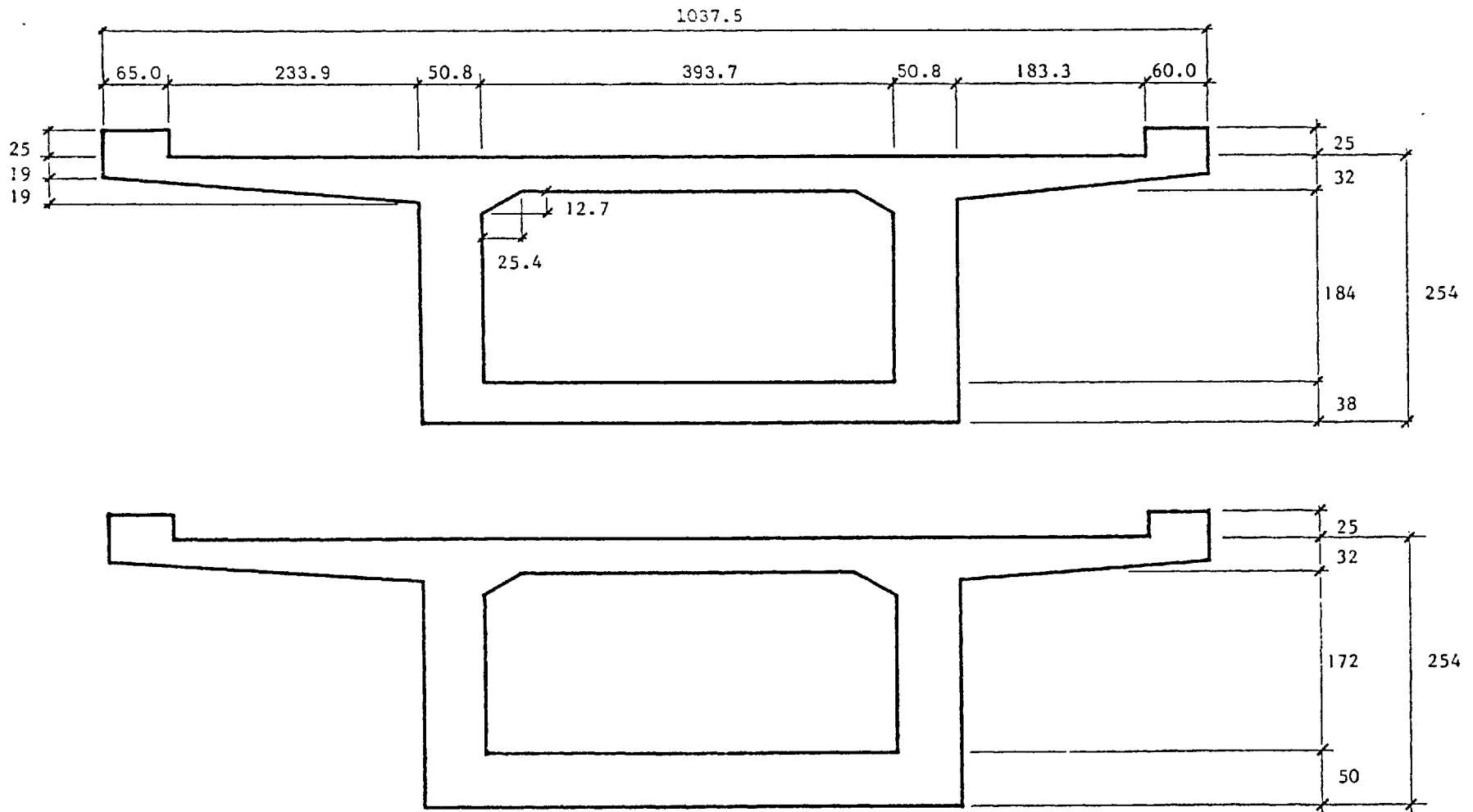
Figure 4.7 Sections F-F and G-G of the 1/12th scale Model

considered in the subsequent analysis and, therefore, discussion regarding the possible positions and methods of application will be limited to these forms of loading.

Similitude requirements, which are discussed more fully elsewhere[112], show that the primary effect of structural modelling is to reduce the self weight stresses by a factor corresponding to the reduction in scale. The density of the material used for model construction must therefore be increased accordingly although, in practice, this is more easily achieved by applying additional dead weight in the form of permanent applied load. Furthermore, by idealizing the additional weight as a uniformly distributed load, it has been possible in this case to use the same loading facilities for applying both dead and live load.

For this purpose the plan area of the model was divided into the fourteen sectors shown in fig. 4.8. These are each one carriageway wide and generally one span in length. Each sector was loaded by a separate hydraulic jack reacting against the laboratory floor, the load being transmitted uniformly to the slab by a complex system of spreader beams. The additional self weight was also applied through the spreader beam assembly but was provided by concrete blocks permanently connected at convenient points throughout the loading system.

4.2.2   Structural Idealization

The results from the load tests on the 1/50th scale model are readily available and will be used to verify the application of the proposed analytical method to complex bridge structures. Apart from the reduction in scale, this model only differs from the microconcrete
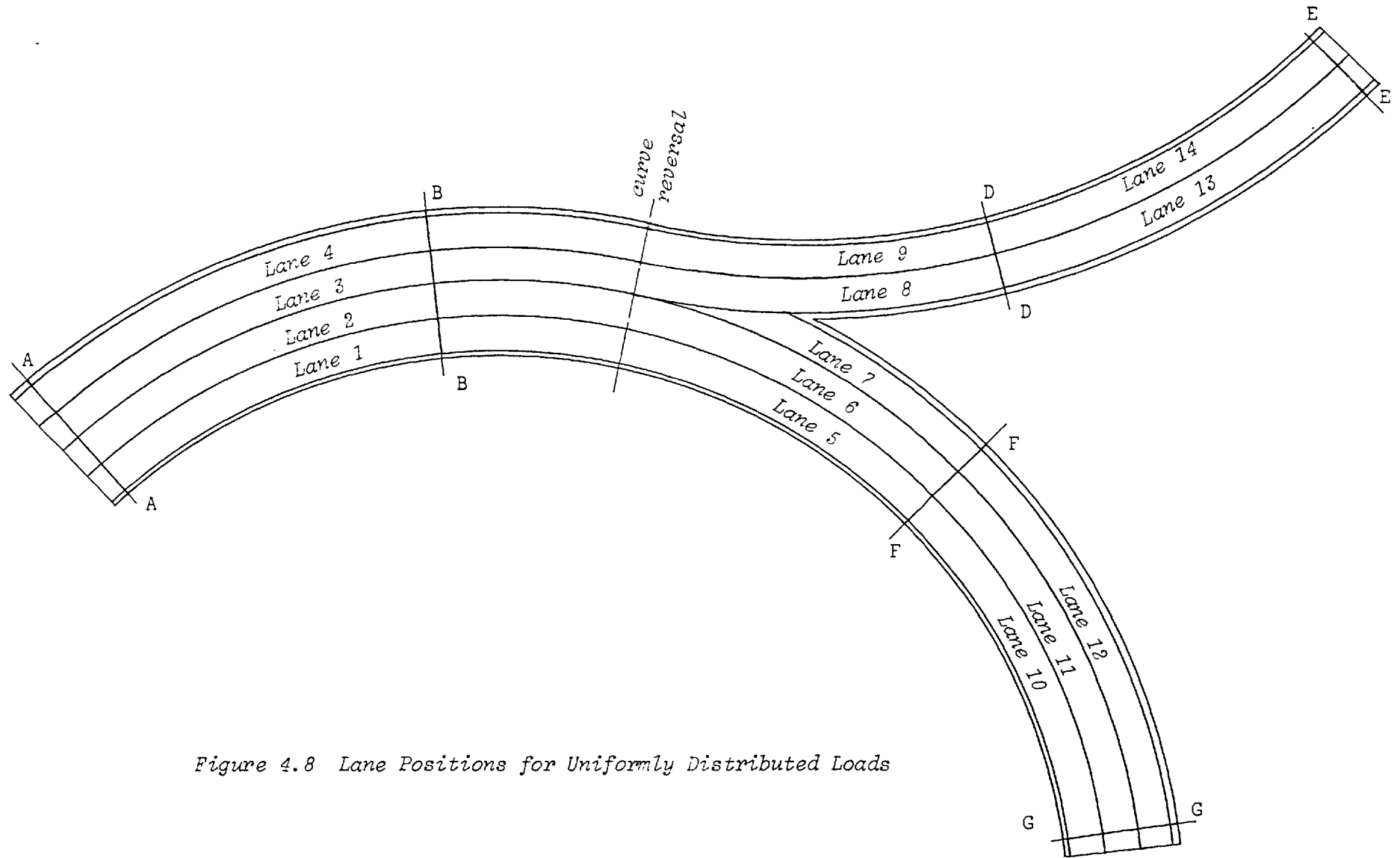
Figure 4.8 Lane Positions for Uniformly Distributed Loads

model described in §4.2.1 in some minor respects. These include the following:

(i)   bottom fillets are provided in each cell in addition to those shown in figs. 4.4 - 4.7;

(ii)   the cantilevers have no edge beams;

(iii)   the bottom flanges are not locally thickened at the internal supports;

(iv)   intermediate diaphragms are not provided in the three outer spans; and

(v)   the layout of webs at the bifurcation differs as is shown in fig. 4.9.

The geometrical properties of the three main cross-sections have been calculated in accordance with §2.3 and §2.4, and then re-calculated to include the effects of curvature as detailed in §2.4.4 and Appendix 1. The computer program[85] previously described in §2.5.2 has been used for this purpose and the results are tabulated in Table 4.2. In this table the co-ordinates of the centroid x_G, y_G, have been measured from the intersection of the top flange and the web nearest to the centre of curvature. This centroid position is then taken as the origin in the determination of the co-ordinates x_s, y_s, defining the shear centre. In the subsequent computation of the parameters j^2 and k^2, the values assumed for Young's modulus of elasticity and Poisson's ratio are those determined by Billington and Dowling[12] and given by

$$E = 1.72 \times 10^4 \text{ N/mm}^2$$

and $\nu = 0.26$

The structure has been idealized for the purposes of analysis into two straight beam elements and sixteen circular curved beam elements, as shown in fig. 4.10. The designation and radius of
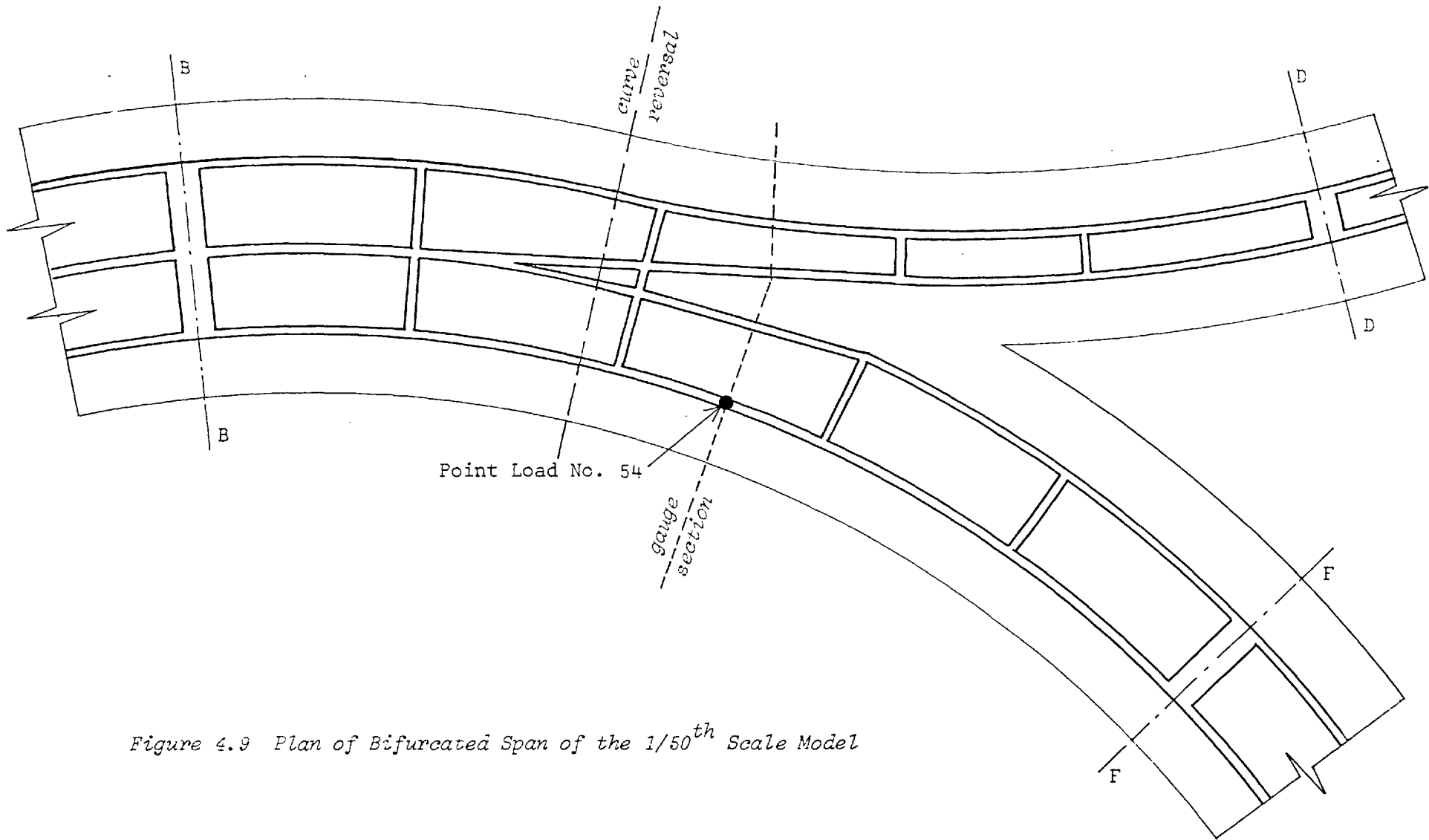
Figure 4.9   Plan of Bifurcated Span of the 1/50th Scale Model

Point Load No. 54

curve reversal

gauge section

B

B

D

D

F

F

Quantity	Units	Twin Cell		Small Single Cell		Large Single Cell	
		Straight	Curved	Straight	Curved	Straight	Curved
x_G	mm	91.43	86.72	22.68	21.82	53.70	51.31
y_G	mm	-19.63	-19.63	-18.18	-18.02	-20.53	-20.54
x_S	mm	- 1.54	- 4.03	1.70	2.81	- 1.56	- 2.06
y_S	mm	- 5.86	- 5.77	1.51	1.58	- 5.97	- 5.93
I_x	mm^4	0.224×10^7	0.224×10^7	0.113×10^7	0.112×10^7	0.198×10^7	0.197×10^7
I_y	mm^4	0.275×10^8	0.275×10^8	0.339×10^7	0.339×10^7	0.124×10^8	0.124×10^8
I_{xy}	mm^4	-0.121×10^6	0.275×10^5	0.599×10^5	0.860×10^5	-0.969×10^5	-0.544×10^4
I_d	mm^4	0.473×10^7	0.478×10^7	0.100×10^7	0.989×10^6	0.344×10^7	0.345×10^7
I_c	mm^4	0.100×10^8	0.999×10^7	0.137×10^7	0.135×10^7	0.526×10^7	0.526×10^7
$I_{\hat{w}}$	mm^6	0.354×10^{10}	0.347×10^{10}	0.215×10^9	0.213×10^9	0.770×10^9	0.775×10^9
ψ	-	0.9998	0.9999	0.9991	0.9981	0.9996	1.0000
μ	-	0.5270	0.5215	0.2701	0.2674	0.3460	0.3441
j^2	-	0.8379	0.8468	0.3512	0.3543	0.6894	0.6949
k^2	mm^{-2}	2.794×10^{-4}	2.851×10^{-4}	4.985×10^{-4}	4.982×10^{-4}	6.134×10^{-4}	6.079×10^{-4}

Table 4.2   Geometrical Properties calculated for the $1/50^{th}$ scale Bifurcated Bridge Model
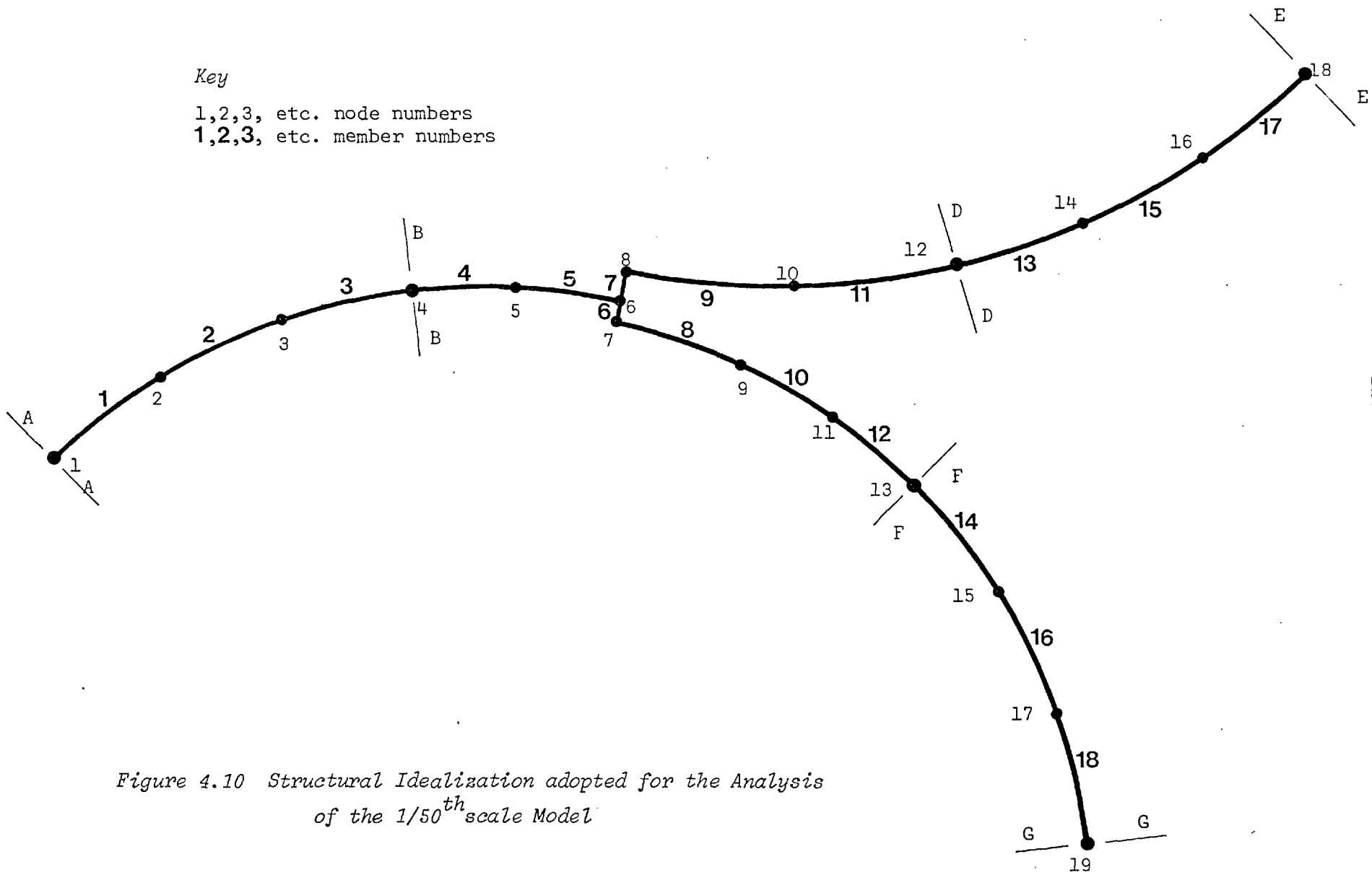
Figure 4.10   Structural Idealization adopted for the Analysis of the 1/50th scale Model

curvature of the various members, together with the tangential angle

at each node point, are given in Table 4.3.   Details of the different

components of structural stiffness assigned to each member have been

determined from Table 4.2 and are presented in Table 4.4.

The bifurcation has been modelled by connecting the circular

curved members 5, 8 and 9 to a cross-beam represented by the two straight

members 6 and 7.   In order to make this simple idealization more

effective, the straight members have been assigned the relatively large

bending and torsional stiffnesses detailed in Table 4.4.   This effect-

ively prevents deformation of the cross-beam (but not rigid-body dis-

placements), thus ensuring that the full bending and torsional moments

are transmitted between the ends of the circular curved members.   At the

same time, it is important that the cross-beam should not provide sign-

ificant warping restraint.   For this reason, only a very small value

of the warping shear parameter, μ, has been specified for these members.

However, this has the effect of reducing the numerical value of the

dimensionless decay function $k\ell$ and can lead to ill-conditioning of the

members 6 and 7 is also reduced by a similar degree.   The final values

of $k\ell$ for all the idealized members are given in Table 4.5.

4.2.3   Loading Idealization

The facilities provided in the computer program for applying

load are detailed in §4.1.1.   These are basically the application of

concentrated loads at nodal points, or uniformly distributed shear and

torsional loads over the length of an idealized beam element.

In the subsequent investigation, analytical and experimental

results will be compared for fourteen cases of uniformly distributed

load.   These represent all the lane positions shown in fig. 4.8.   In

addition, one point load will also be considered; this is positioned as

Member Ref.No.	End 1	End 2	Tangential Angle (radians)		Radius (mm) (or length)
			End 1	End 2	
1	1	2	0.9330019202	0.7271952314	1351.57
2	2	3	0.7271952314	0.5213885427	1351.57
3	3	4	0.5213885427	0.3155818540	1351.57
4	4	5	0.3155818540	0.1577909270	1351.57
5	5	6	0.1577909270	0	1351.57
6	6	7	-1.5707963270	-1.5707963270	(37.27)
7	6	8	1.5707963270	1.5707963270	(83.75)
8	7	9	0	-0.1452077429	1314.30
9	8	10	0	0.2366863905	1606.68
10	9	11	-0.1452077429	-0.3630193571	1314.30
11	10	12	0.2366863905	0.4733727811	1606.68
12	11	13	-0.3630193571	-0.5808309714	1314.30
13	12	14	0.4733727811	0.6473398681	1606.68
14	13	15	-0.5808309714	-0.7955648332	1314.30
15	14	16	0.6473398681	0.8213069551	1606.68
16	15	17	-0.7955648332	-1.0102986950	1314.30
17	16	18	0.8213069551	0.9952740422	1606.68
18	17	19	-1.0102986950	-1.2150325569	1314.30

Table 4.3   Member Designation, Orientation and Radius of Curvature

Ref. Nos.	EI_x $(N.mm^2)$	GI_d $(N.mm^2)$	$EI_{\hat{w}}$ $(N.mm^4)$	μ
1 - 5	3.853×10^{10}	3.228×10^{10}	6.089×10^{13}	0.527
9-17 (odd)	1.944×10^{10}	6.825×10^9	3.800×10^{12}	0.270
8-18 (even)	3.406×10^{10}	2.348×10^{10}	1.324×10^{13}	0.346
6, 7	1.000×10^{12}	0.750×10^{12}	1.000×10^{15}	0.010

Table 4.4   Structural Properties assigned to each Member

Member Ref. No.	Arc Length (mm)	Decay Function $k\ell$
1, 2, 3	278.2	4.65
4, 5	213.3	3.57
6	37.3	0.10
7	83.8	0.23
8	190.8	4.73
10, 12	286.26	7.09
14, 16, 18	277.8	6.88
9, 11	380.3	8.49
13, 15, 17	279.5	6.25

Table 4.5   The Decay Function, $k\ell$, for each Idealized Member

indicated in fig. 4.9.   This corresponds to load case number 54 in the model test for which results are readily available[14].   However, since there is no provision for applying either a point load within the length of a beam element or a uniformly distributed load over part of a beam element, an additional node (point 9) has had to be located in the bifurcated span.   This is positioned at the point of application of load case number 54 in order that the eccentric point load can be replaced directly by a vertical shear load and a concentrated torque. Node point 9 also coincides with the end of the half lane (lane number 7 in fig. 4.8) and enables this lane load to be represented by a uniformly distributed load applied to members 10 and 12 only.

For each of the fourteen cases of lane load it is also necessary to determine the effective eccentricity in order to reduce the uniformly distributed load into its shear and torsional components.
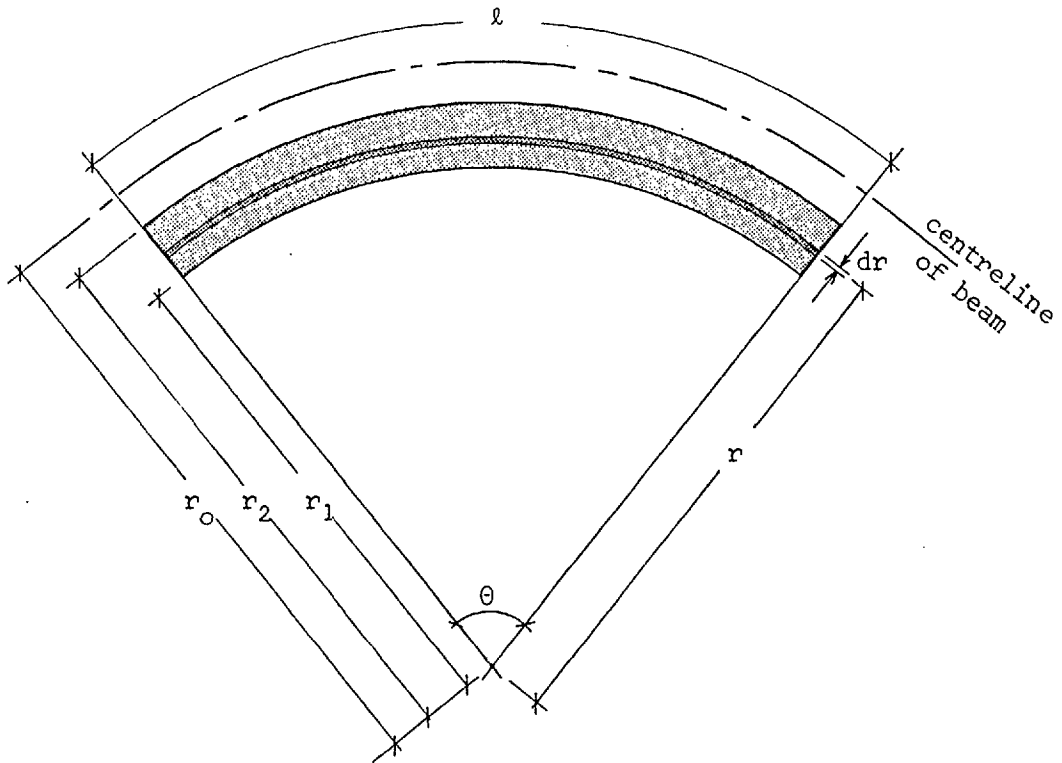
Figure 4.11   Element of Circular Curved Lane Loading

Consider the element of lane loading shown in fig 4.11, subtended by the central angle Θ.   The radius of curvature of the incremental sector dr is denoted by r, and the inner and outer radii bounding the element are defined as r_1 and r_2, respectively.   The plan area of the entire sector is then given by

$$A = \frac{\Theta}{2} (r_2^2 - r_1^2) \qquad\qquad 4.1$$

while the arc length of the idealized beam element of radius r_o is evaluated from

$$\ell = r_o \cdot \Theta \qquad\qquad 4.2$$

By dividing the total lane load by the combined arc length of the idealized beam elements over which the load is applied, the component of uniformly distributed shear load is obtained directly.   Alternatively, this may be expressed in terms of eqns. 4.1, 4.2 and the applied pressure, q, thus:

$$p = \frac{A}{\ell} \quad . \quad q = \frac{(r_2^2 - r_1^2)}{2r_o} \quad . \quad q \qquad 4.3$$

However, before the torsional load can be determined, the radius of the effective centre of action, R, must be established for the uniformly loaded beam. This is calculated from the following expression:

$$R.A = \int_{r_1}^{r_2} r^2 \, \theta. \, dr \qquad 4.4$$

which after evaluation of the integral and substitution for A from eqn. 4.1, gives

$$R = \frac{2}{3} \left[\frac{(r_2^3 - r_1^3)}{(r_2^2 - r_1^2)} \right] \qquad 4.5$$

This then enables the torsional component of uniformly distributed load, t, to be expressed in terms of the shear component, p, in the following way:

$$t = p \quad . \quad (r_o - R) \qquad 4.6$$

The loading required to represent each of the fourteen lane load cases is detailed in Table 4.6. This has been evaluated for each lane by introducing into eqns. 4.1 - 4.6 the total load applied in the model test (given in column 2 of Table 4.6), together with the appropriate inside and outside radii of the loaded area, etc.. The remaining load case consists of a point load of 225.5 N applied at an eccentricity of 52.5 mm on the centreline of the inside web at the section identified in fig. 4.9. This is equivalent to applying a point load of 225.5 N and a concentrated torque of 11838.75 N.mm at node 9 of the idealized structure.

4.2.4   Structural Analysis

The longitudinal distributions of the various stress resultants are shown in figs. 4.12 - 4.17 for the fifteen load cases previously

Lane Load No.	Total Lane Load (N)	Lane Area (mm^2)	Pressure (N/mm^2 x 10^{-3})	Beams Loaded	Radius of Action (mm)	Effective Eccentricity (mm)	p (N/mm)	t (N)
1	411.2	55 879	7.359	1, 2, 3	1257.34	94.23	0.4928	46.44
2	423.6	59 080	7.170	1, 2, 3	1329.33	22.24	0.5076	11.29
3	436.1	62 280	7.002	1, 2, 3	1401.31	-49.74	0.5226	-25.99
4	447.2	65 481	6.829	1, 2, 3	1473.29	-121.72	0.5359	-65.23
5	486.8	81 129	6.000	4, 5 8, 10, 12	1257.34 1257.34	94.23 56.96	0.4018 0.4132	37.86 23.53
6	500.6	85 776	5.836	4, 5 8, 10, 12	1329.33 1329.33	22.24 -15.03	0.4132 0.4249	9.19 -6.39
7	255.9	43 966	5.800	10, 12	1401.31	-87.01	0.4451	-38.73
8	505.1	87 763	5.755	4, 5 9, 11	1401.31 1641.26	-49.74 -34.58	0.5031 0.4232	-25.02 14.63
9	503.4	86 945	5.790	4, 5 9, 11	1473.29 1569.28	-121.72 37.40	0.4839 0.4071	-58.91 -15.23
10	417.0	57 398	7.265	14, 16, 18	1257.34	56.96	0.5003	28.50
11	430.8	60 685	7.099	14, 16, 18	1329.33	-15.03	0.5168	-7.77
12	441.4	63 973	6.900	14, 16, 18	1401.31	-87.01	0.5296	-46.08
13	435.2	61 664	7.058	13, 15, 17	1641.26	-34.58	0.5190	17.95
14	424.1	58 958	7.193	13, 15, 17	1569.28	37.40	0.5058	-18.92

Table 4.6   Idealization of Lane Loading into Components of Shear and Torsional Uniformly Distributed Load

described in § 4.2.3. To facilitate the plotting of results, the structure has been idealized as three straight members connected at the bifurcation.

In general, the effects of lane loading on the three outer spans disappeared rapidly at points distant from the loaded span. Accordingly, the results due to loading lanes 1-4 and 10-14 have only been plotted as far as the bifurcation, and the resultant distributions of bending moment, torsion and bimoment for these load cases are shown in figs. 4.12, 4.14 and 4.16 respectively. However, since the single point load and the remaining lane loads 5-9 were all applied within the central span, the longitudinal distributions of the various stress resultants have been plotted over the entire structure and are presented in figs. 4.13, 4.15 and 4.17.

Comparison with Model Results

Extensive instrumentation was a feature of all the bifurcated bridge models and primarily consisted of surface gauging with electrical resistance strain gauges. In general, these were closely spaced around a number of important cross-sections throughout the models, on both the inside and outside faces. This enabled the recorded strain to be separated into its component parts and also provided the transverse distribution of the various components around each of the selected sections.

Since the gauges were all monitored by an automatic data logging system, results were readily accessible for later processing by computer and have, in the case of the $1/50^{th}$ scale models, been output in a more useful form as components of stress. Consequently, before the results of the analytical study could form the basis of a meaningful comparison, they also had to be presented in this way. This was
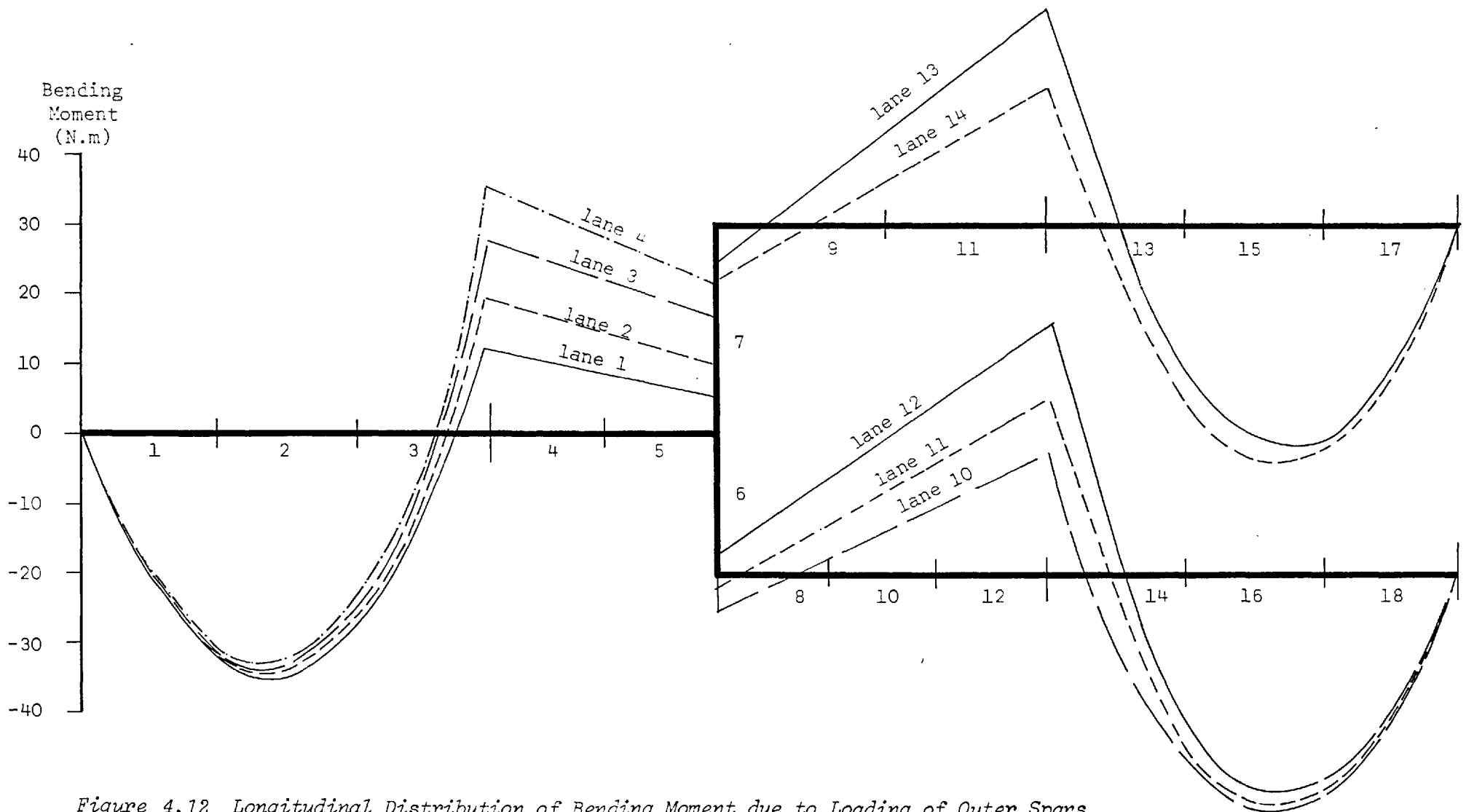
Figure 4.12   Longitudinal Distribution of Bending Moment due to Loading of Outer Spans
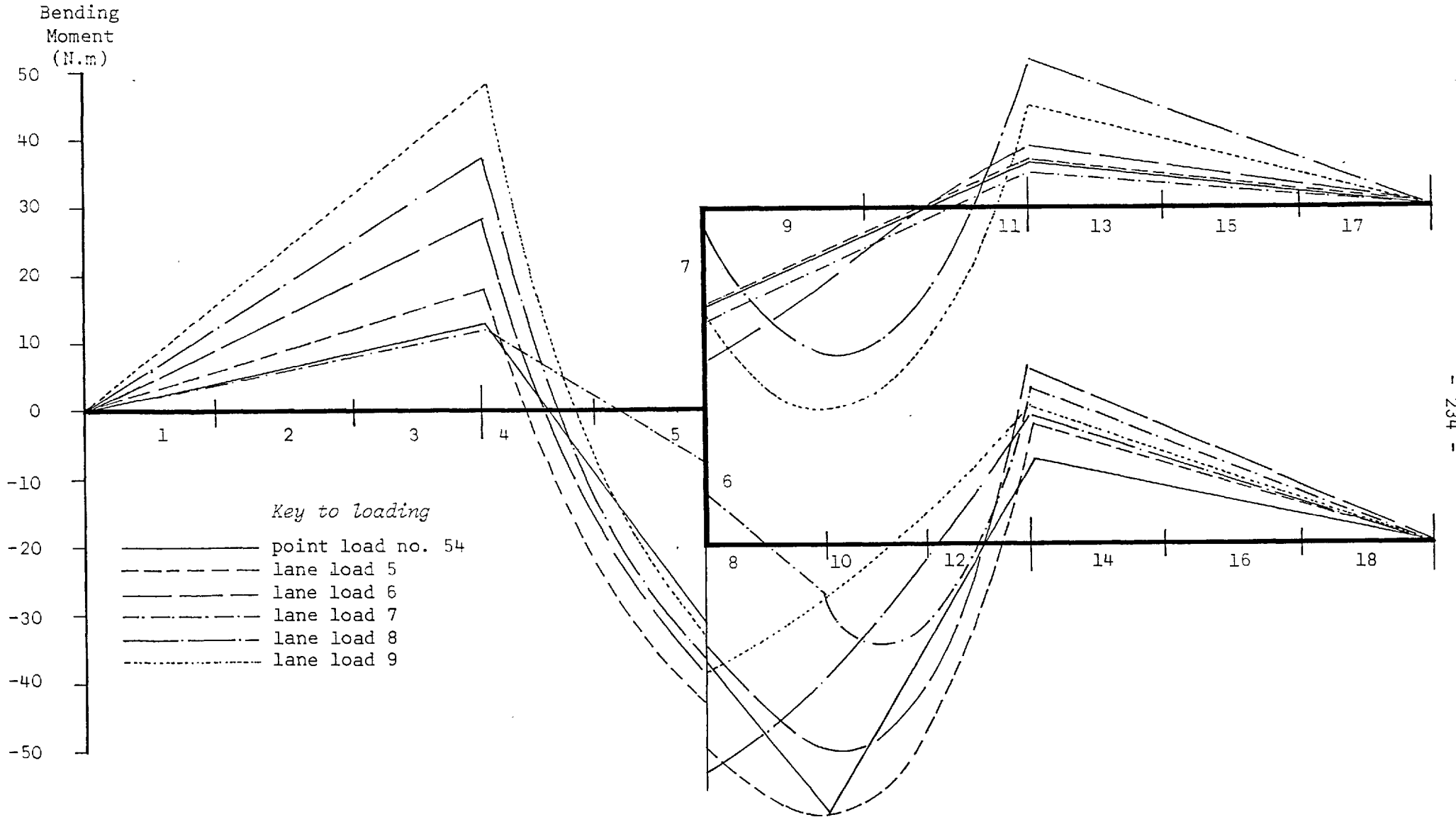
Figure 4.13   Longitudinal Distribution of Bending Moment due to loading of Bifurcated Span
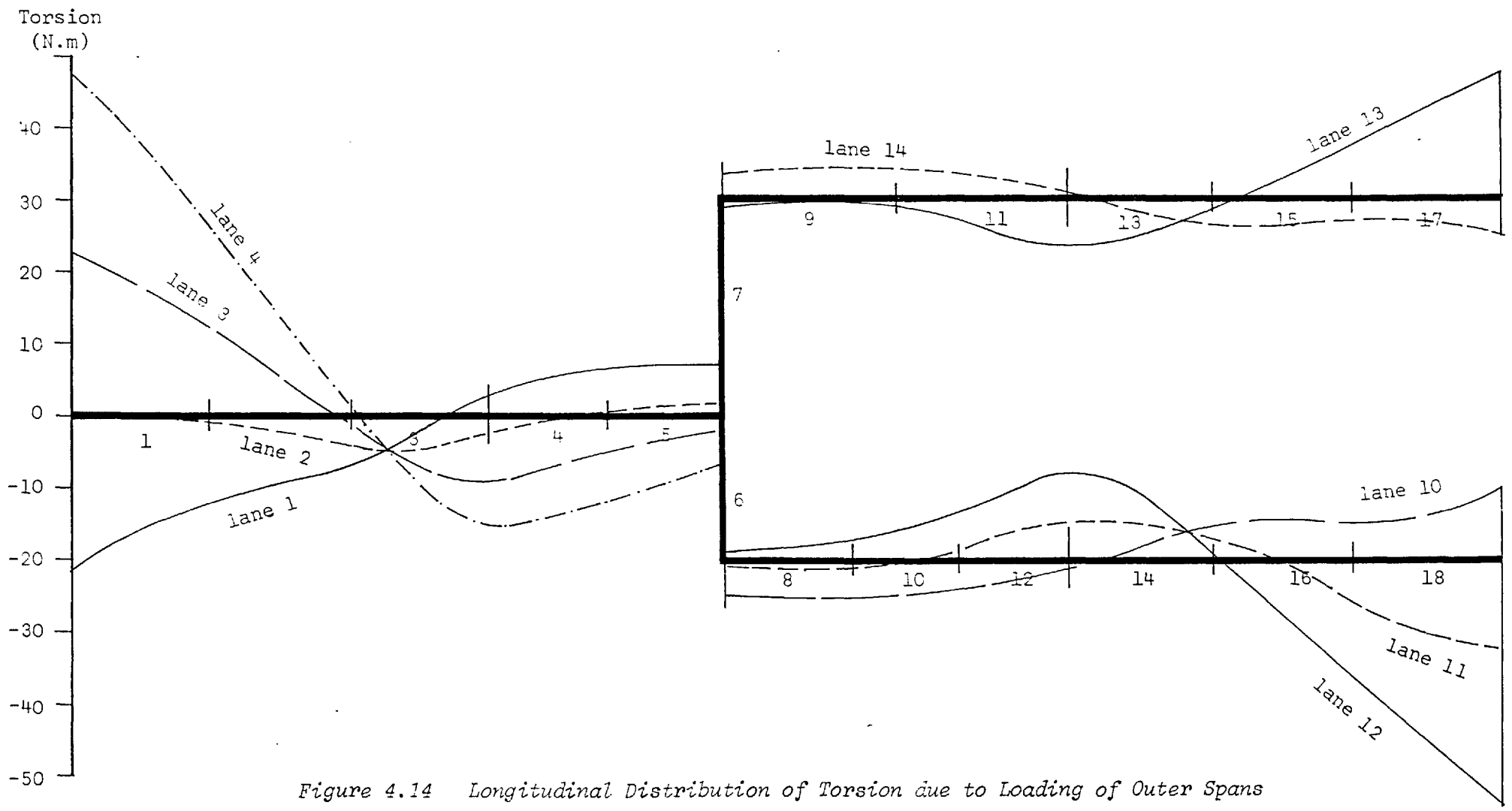
Figure 4.14   Longitudinal Distribution of Torsion due to Loading of Outer Spans

Torsion
(N.m)

Key to loading

——————— point loading no. 54
— — — — — lane load 5
— — — — lane load 6
— · — · — lane load 7
— ·· — ·· — lane load 8
············· lane load 9

40
30
20
10
0
-10
-20
-30
-40

15 17
9   11   13
7
6
1   2   3   4   5
8   10   12   14   16   18
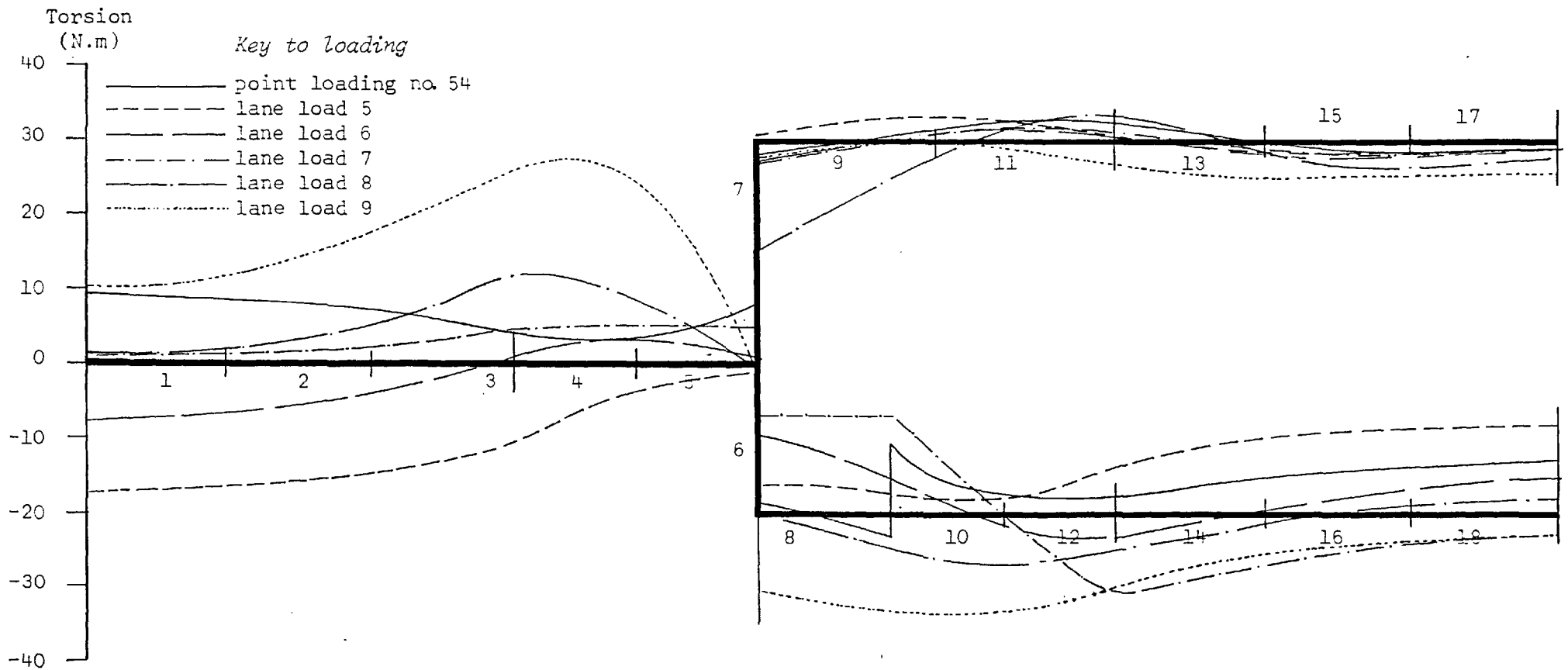
Figure 4.15   Longitudinal Distribution of Torsion due to Loading Bifurcated Span
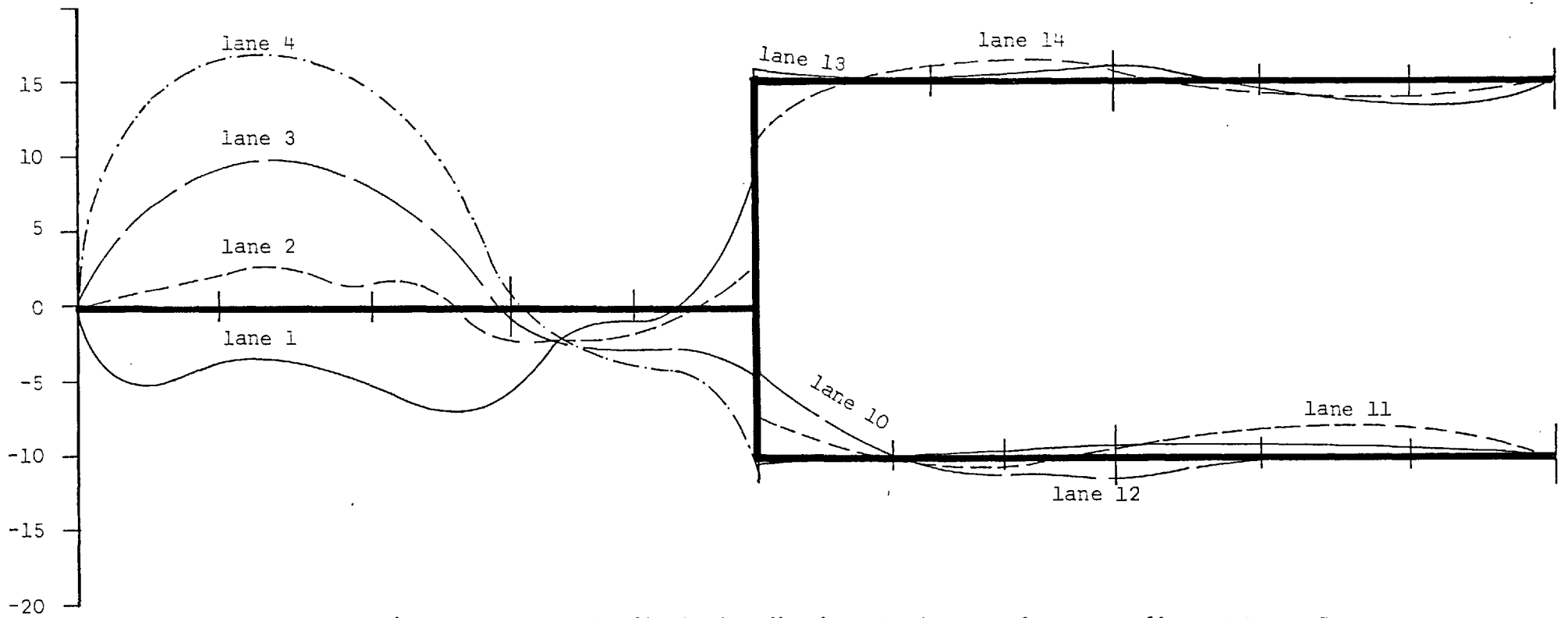
Figure 4.16   Longitudinal Distribution of Bimoment due to Loading of Outer Spans
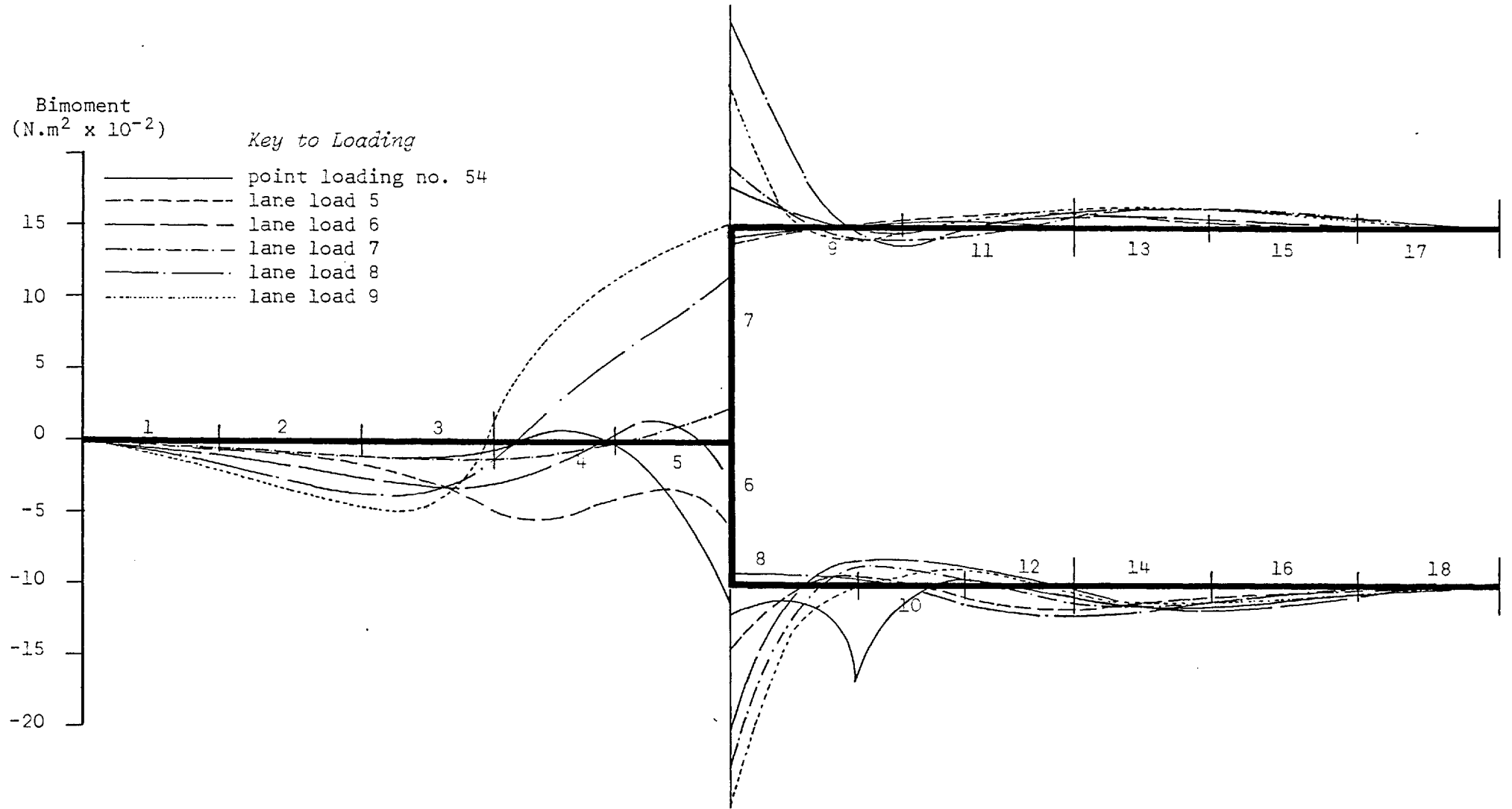
Figure 4.17   Longitudinal Distribution of Bimoment due to Loading of Bifurcated Span

achieved by introducing into eqn. 2.82 the appropriate values of the geometrical properties, obtained from Table 4.2, and the stress resultants, determined in the computer analysis.

Only one cross-section is presented here for each load case and this has invariably been selected to coincide with a fully gauged section.   For lanes located in the outer spans, the centre of the loaded span has been used, while for the point load and for the remaining lane loads in the bifurcated span, the selected section is the gauge section identified in fig. 4.9.

The transverse distributions of direct stress due to loading lanes 1 - 14 are presented in numerically ascending order in figs. 4.18 - 4.31.   In addition, the results due to the eccentric point load at node 9 are shown in fig. 4.32.   In all these figures, hatching represents the distribution of direct stress determined from the computer solution whereas the circles are point estimates recorded during the model test[13,14].

There is, in general, very good agreement between the analytical and experimental results, but with certain noticeable exceptions.   In particular, the direct stresses predicted by the computer program for lane load 4 are approximately 50% higher than those obtained from the model test.   The two distributions shown in fig. 4.21 are, however, very similar in shape and both apparently take account of the eccentric positioning of the load.   Table 4.7 has been prepared in an attempt to try and establish the reasons for this and other less significant discrepancies.   In this table the computed bending moment for each load case is compared with that determined from the test results at the appropriate cross-section.   While the magnitude of the bending moment
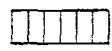
Distribution of Direct Stress
from the Computer Analysis

o   Results from the Model Test[13]

-0.275   -0.289   -0.309   -0.331   -0.349

0.518   0.552   0.592

- 240 -
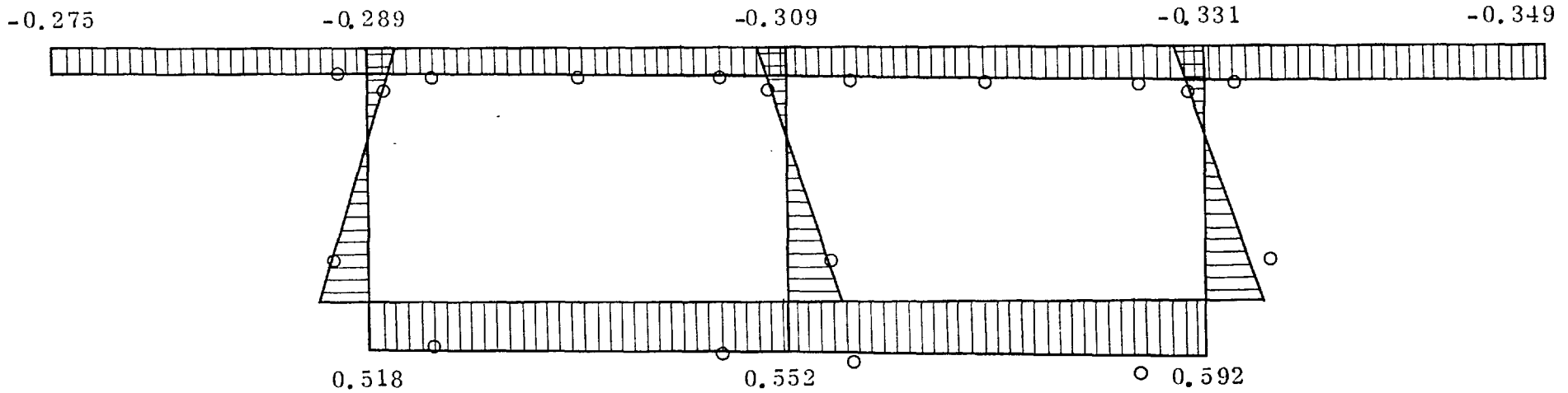
Figure 4.18   Distribution of Direct Stress at the Centre of the Loaded Span due to Loading Lane 1

Distribution of Direct Stress
from the Computer Analysis

o   Results from the Model Test[13]

-0.272   -0.297   -0.308   -0.318   -0.353

0.528   0.551   0.572

- 241 -
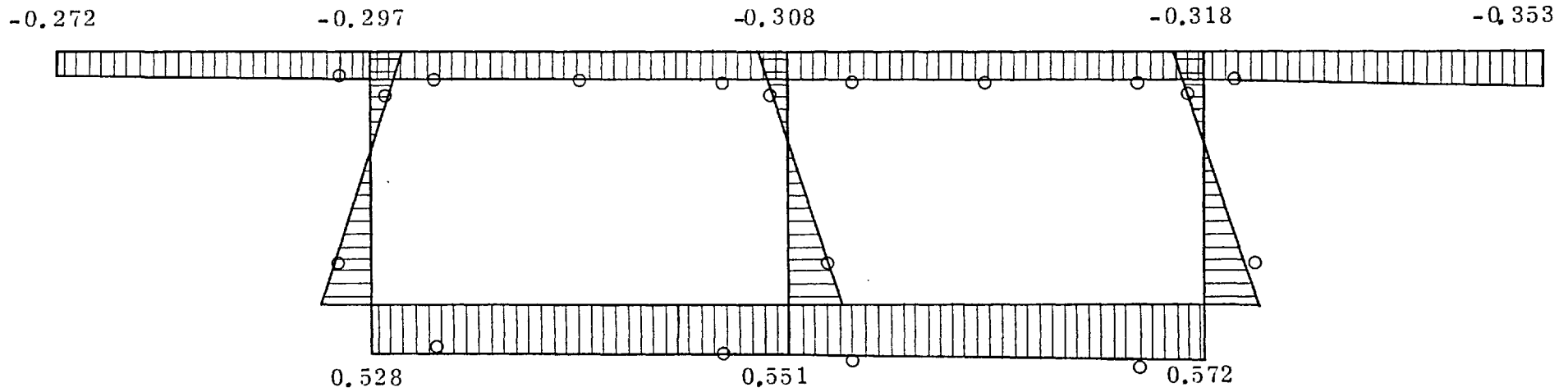
Figure 4.19   Distribution of Direct ·Stress at the Centre of the Loaded Span due to Loading Lane 2

Key
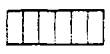
Distribution of Direct Stress
from the Computer Analysis

o   Results from the Model Test[13]

-0.265   -0.317   -0.307   -0.287   -0.366

0.564   0.550   0.522
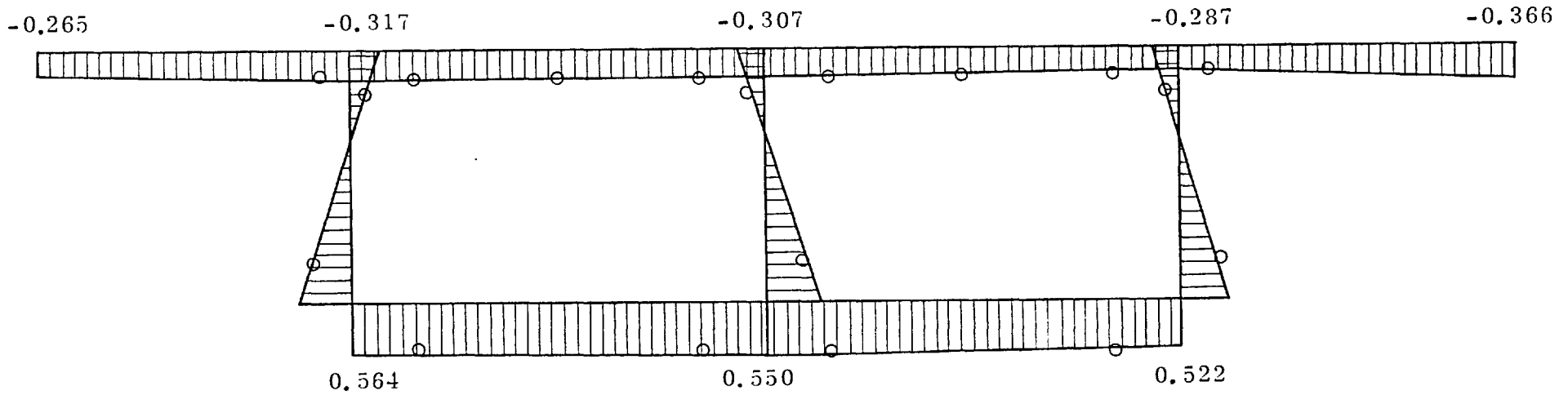
Figure 4.20   Distribution of Direct Stress at the Centre of the Loaded Span due to Loading Lane 3

Key
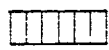
Distribution of Direct Stress
from the Computer Analysis

o   Results from the Model Test[13]

-0.256   -0.338   -0.305   -0.253   -0.380

0.599   0.547   0.469
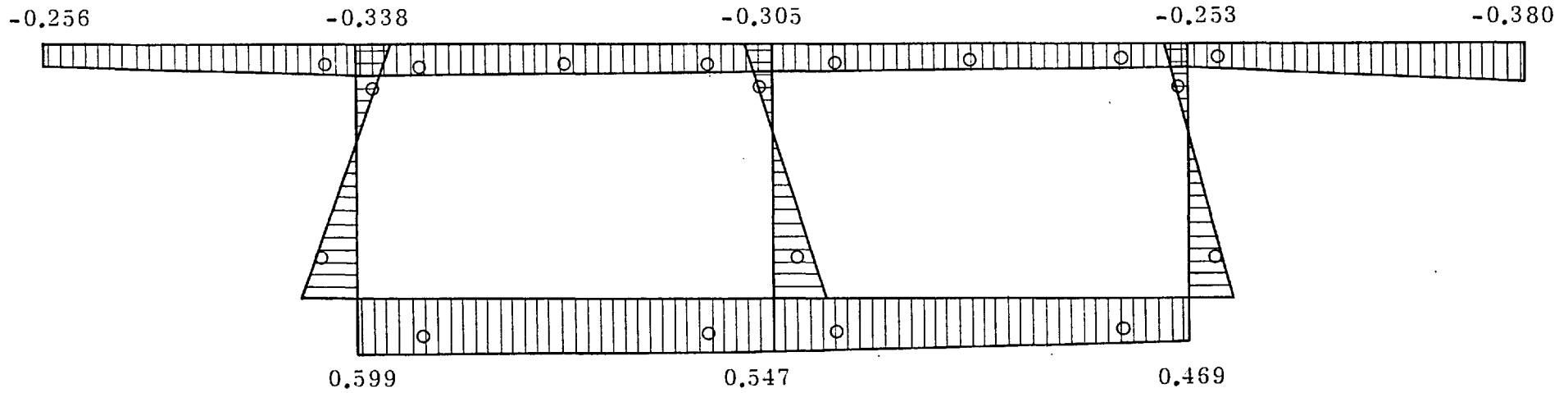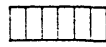
Figure 4.21   Distribution of Direct Stress at the Centre of the Loaded Span due to Loading Lane 4

Distribution of Direct Stress
from the Computer Analysis

o   Results from the Model Test[13]

-0.180   -0.169   -0.190   -0.402   -0.429   -0.462

0.348   0.349   0.608   0.655
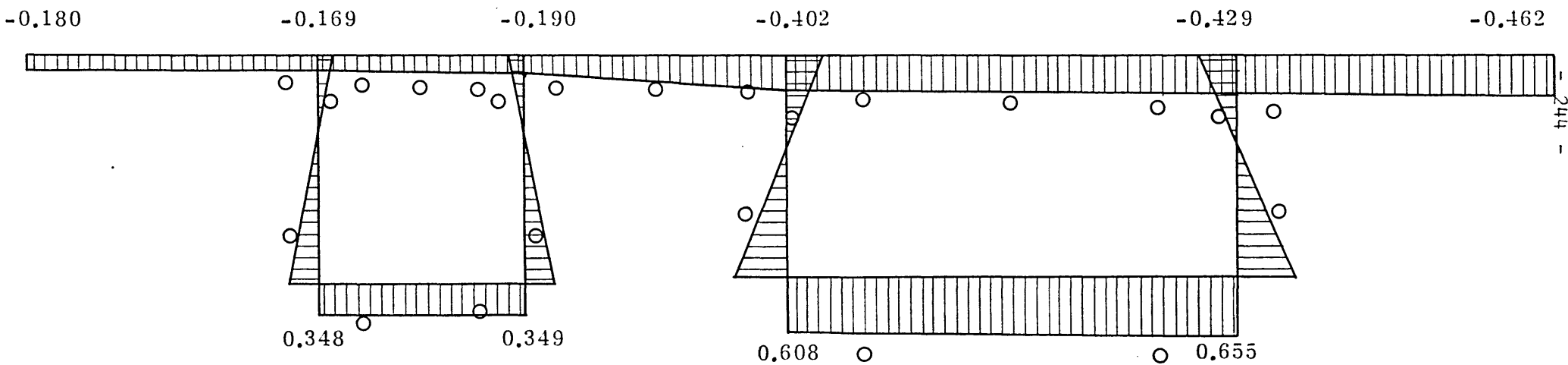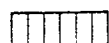
Figure 4.22   Distribution of Direct Stress at the Centre of the Loaded Span due to Loading Lane 5

Distribution of Direct Stress
from the Computer Analysis

o   Results from the Model Test[13]

-0.289   -0.283   -0.306   -0.297   -0.291   -0.347

245 -

0.571   0.579   0.439   0.457
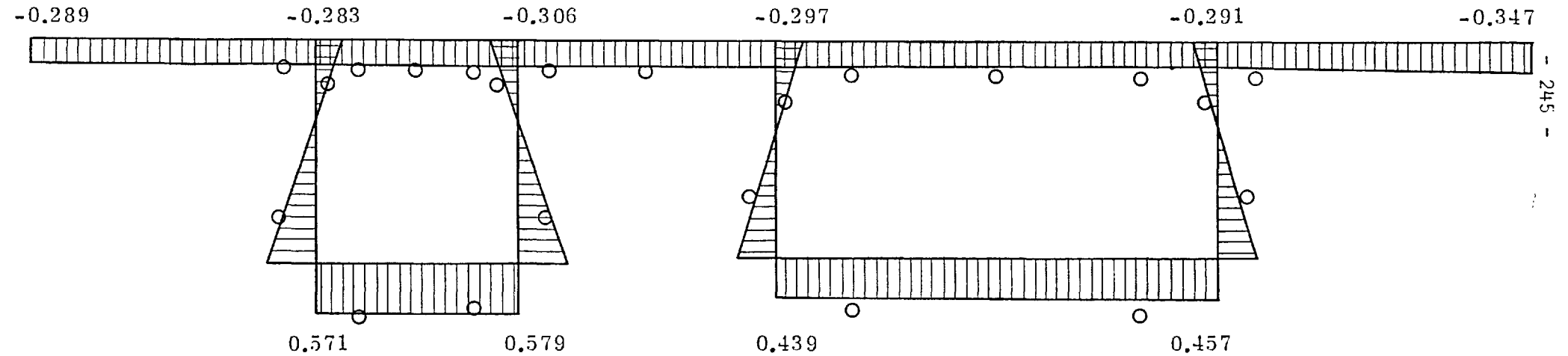
Figure 4.23 Distribution of Direct Stress at the Centre of the Loaded Span due to Loading Lane 6
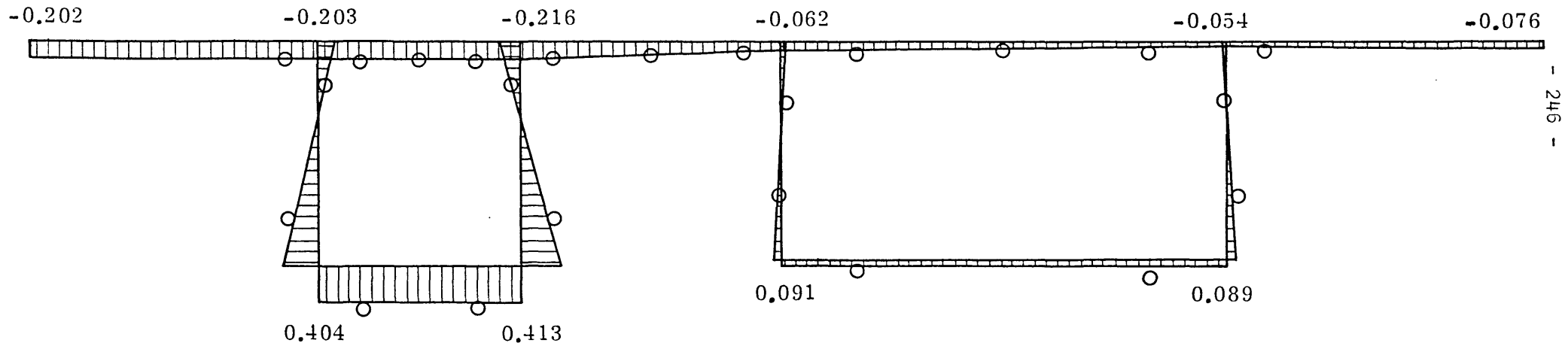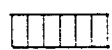
Figure 4.24 Distribution of Direct Stress at the Centre of the Loaded Span due to Loading Lane 7

Key

Distribution of Direct Stress
from the Computer Analysis

o   Results from the Model Test[13]

-0.260   -0.251   -0.275   -0.236   -0.234   -0.275

0.509   0.515   0.350   0.365
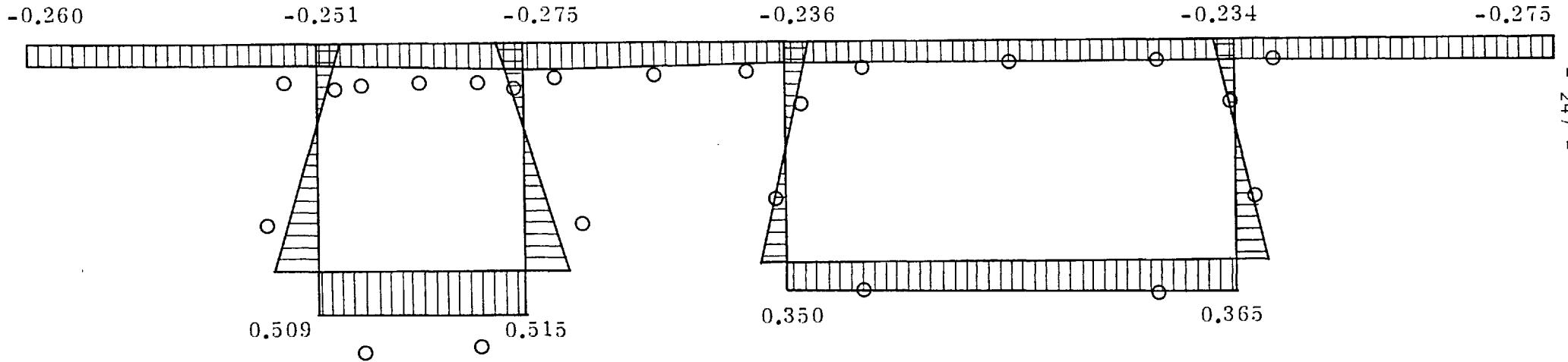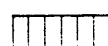
Figure 4.25 Distribution of Direct Stress at the Centre of the Loaded Span due to Loading Lane 8

Distribution of Direct Stress
from the Computer Analysis

o   Results from the Model Test[13]

-0.395 -0.410 -0.422 -0.107 -0.102 -0.127

0.801 0.826

0.157 0.161
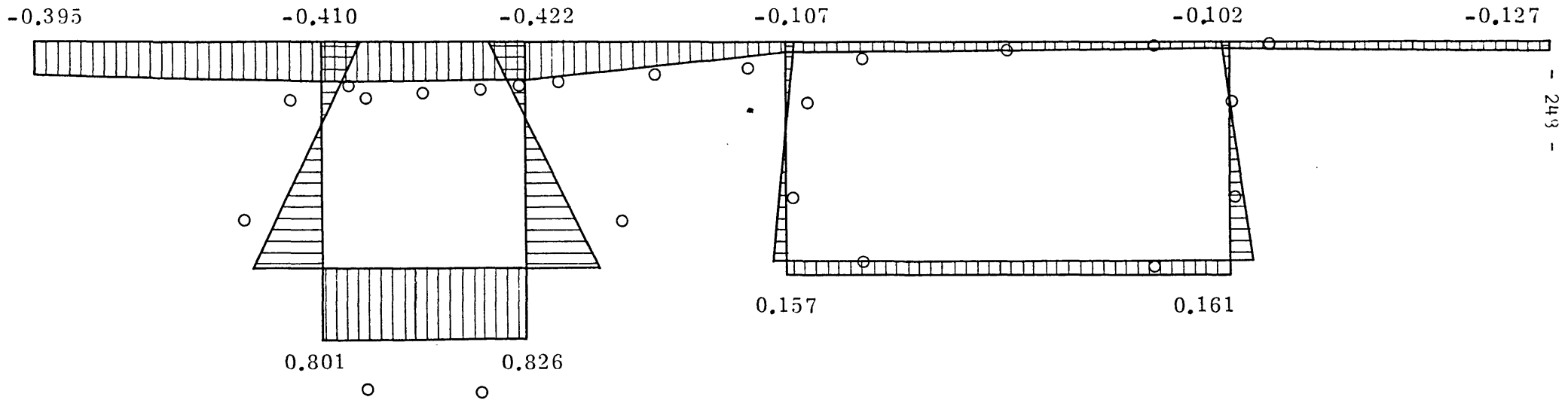
Figure 4.26 Distribution of Direct Stress at the Centre of the Loaded Span due to Loading Lane 9

Key

Distribution of Direct Stress
from the Computer Analysis

o   Results from the Model Test[13]

-0.328   -0.341   -0.374   -0.390

0.521   0.566
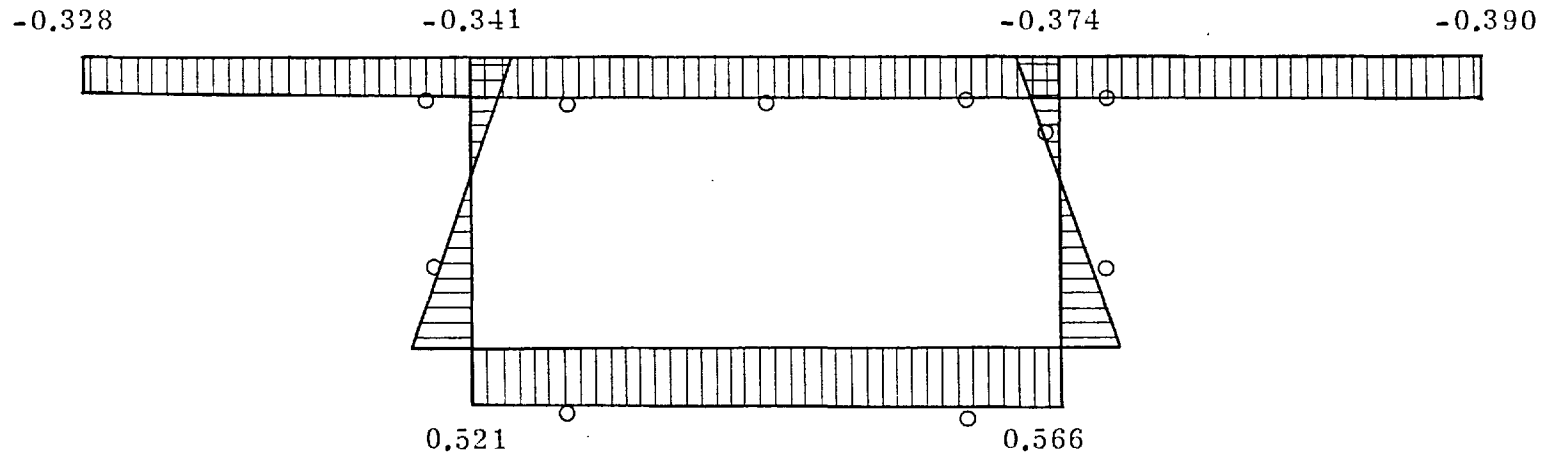
Figure 4.27   Distribution of Direct Stress at the Centre of the Loaded Span due to Loading Lane 10

Key

Distribution of Direct Stress
from the Computer Analysis

o   Results from the Model Test[13]

-0.302   -0.360   -0.349   -0.424

0.531   0.549
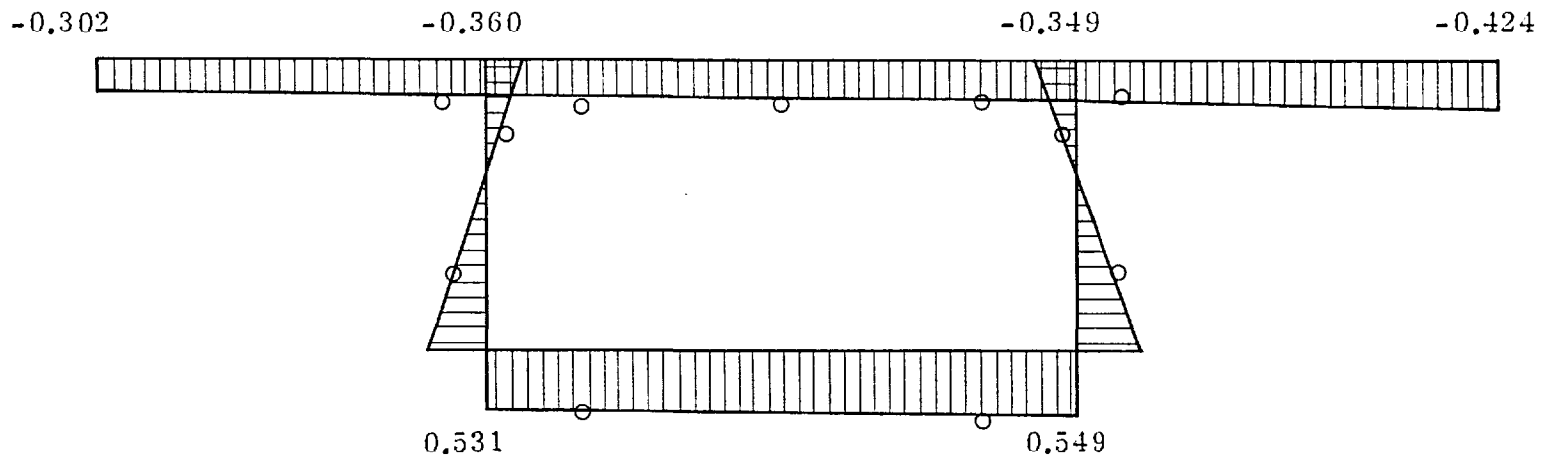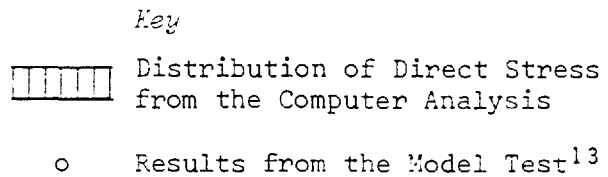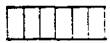
Figure 4.28 Distribution of Direct Stress at the Centre of the Loaded Span due to Loading Lane 11

Key

Distribution of Direct Stress
from the Computer Analysis

o   Results from the Model Test[13]

-0.275   -0.376   -0.319   -0.416

0.537   0.527
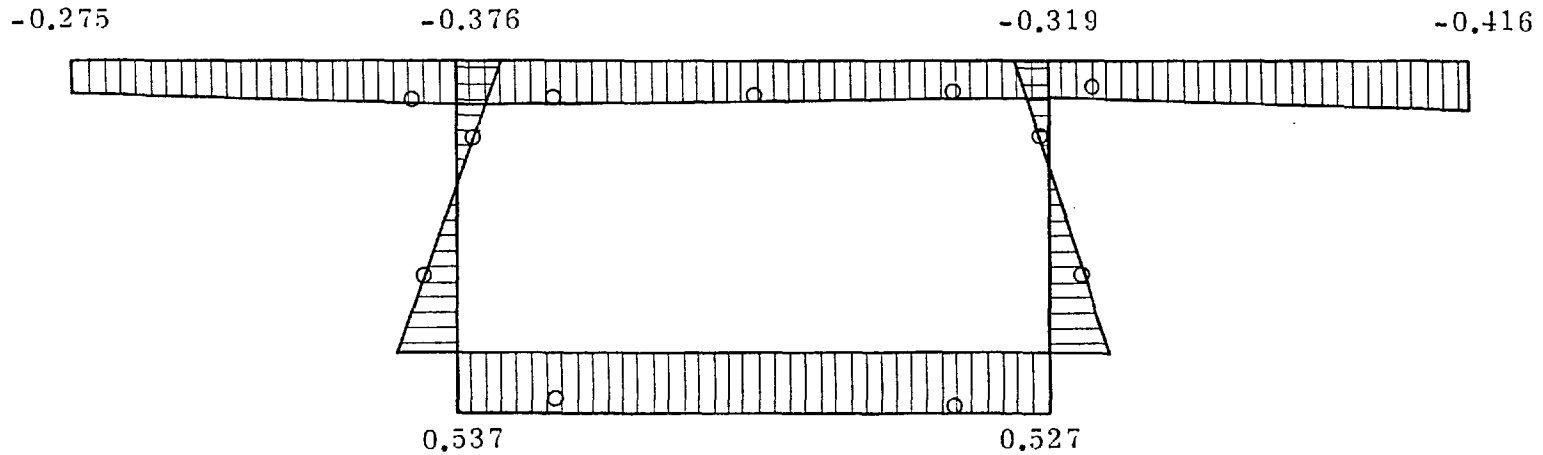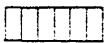
Figure 4.29   Distribution of Direct Stress at the Centre of the Loaded Span due to Loading Lane 12

Key

▭ Distribution of Direct Stress
from the Computer Analysis

o   Results from the Model Test[13]

-0.537   -0.468   -0.558   -0.462

1.006   0.986
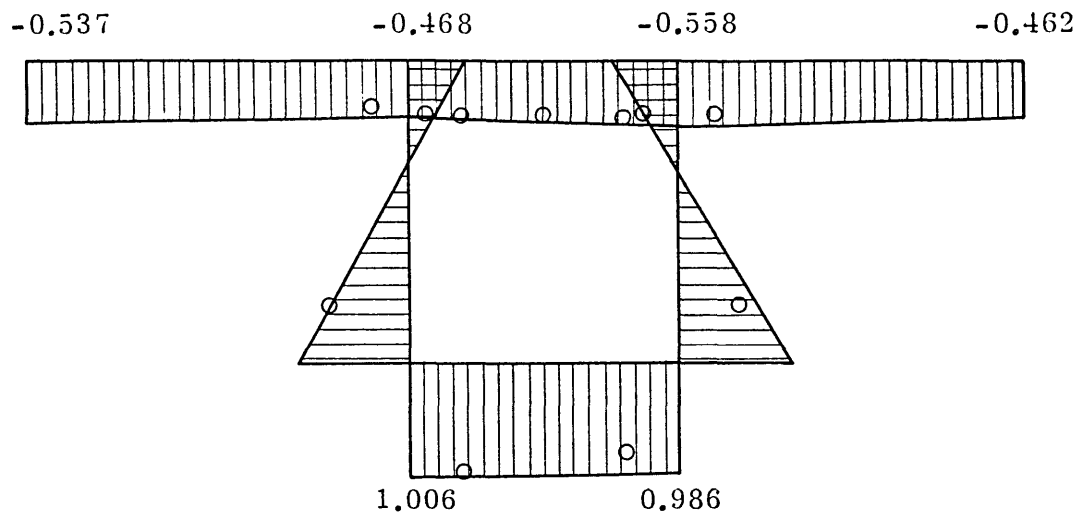
Figure 4.30 Distribution of Direct Stress at the Centre of the Loaded Span due to Loading Lane 13

Key

Distribution of Direct Stress
from the Computer Analysis

o   Results from the Model Test[13]

-0.532   -0.549   -0.567   -0.587

1.074   o   1.104
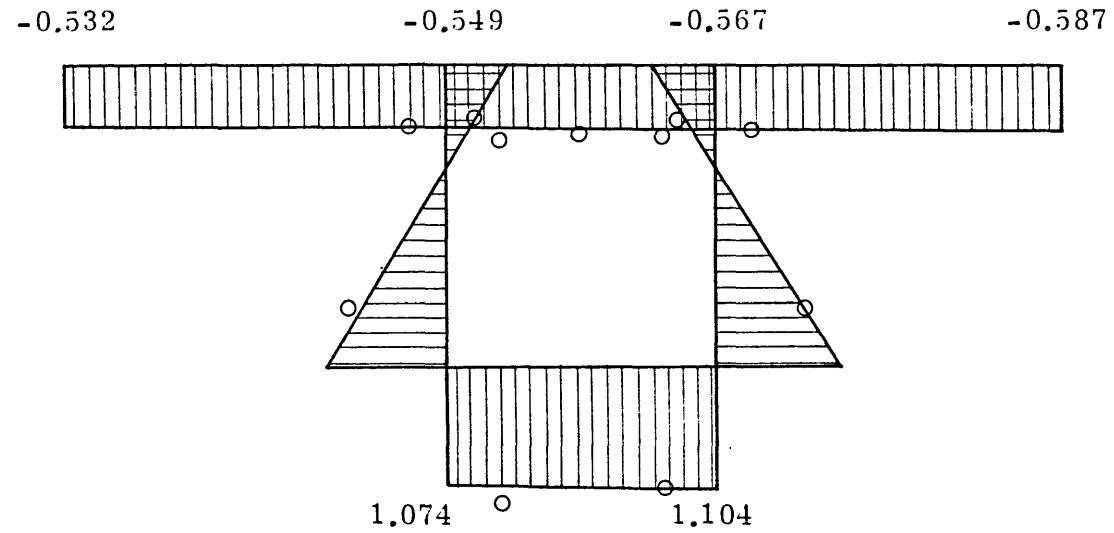
Figure 4.31 Distribution of Direct Stress at the Centre of the Loaded Span due to Loading Lane 14
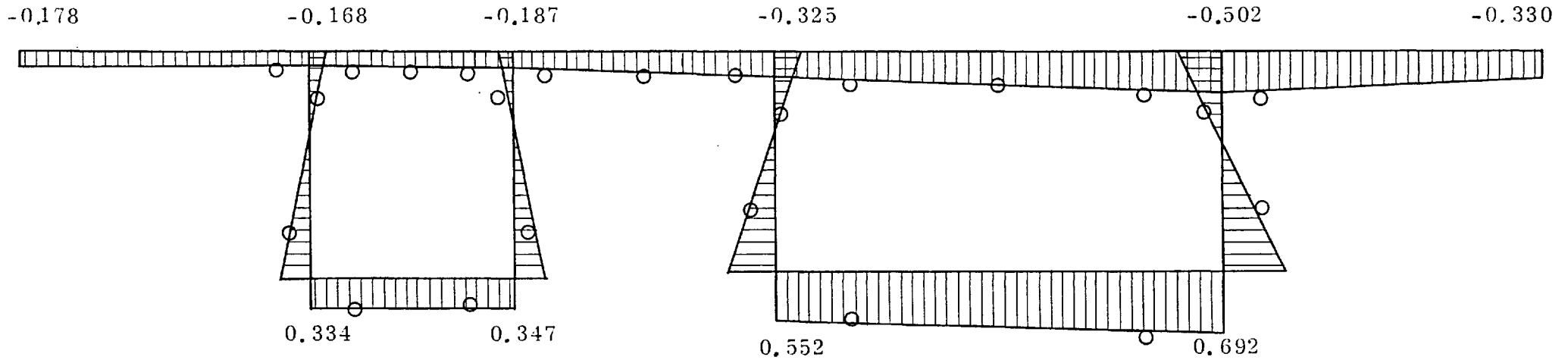
Figure 4.32   Distribution of Direct Stress at the Centre of the Loaded Span due to Point Loading No. 54

- 256 -

Load Case	Bending Moment (N.mm x 10^3)	
	Model Test	Computer Analysis
1	39.20	35.19
2	34.99	34.98
3	32.69	34.71
4	22.80	34.25
5	62.94	50.58
6	52.80	46.16
7	24.20	19.78
8	46.26	39.26
9	43.90	36.50
10	37.27	34.62
11	35.66	34.05
12	27.17	33.14
13	26.75	31.67
14	34.58	34.60
Point Load	46.04	49.45

*Table 4.7   Comparison of Bending Moments
determined from the Computer Analysis
with those from the Model Test*

is readily available from the computer analysis, this quantity can only

be approximated in the case of the model test results.   For this purpose,

the direct stresses recorded in each of the flanges were averaged,

multiplied by the appropriate lever arm and flange area, and then summed

together.   The bending resistance provided by the web elements was also

estimated, the neutral axis being well defined by the points of zero
strain.

Despite the simplifying assumptions in these calculations, the
bending moments associated with the first three load cases compare very
favourably with those from the computer analysis.   However, the total
bending moment induced in the model by loading lane 4 is significantly
lower and, in view of the similarity of loading intensity with load
cases 1 - 3, this would suggest that either the loading arrangement
or the instrumentation in the model was at fault.

A similar, but less severe, discrepancy in the calculation of
bending moment is also evident at the centre section of the other two
outer spans, DE and FG.   These are represented by lanes 12 and 13 in
Table 4.7 and are similar to lane 4 in that they are also positioned on
the outside curve of their respective spans.   Once again, no convincing
explanation can be offered for this behaviour although the hogging
moment over the adjacent internal supports appears to show a corres-
ponding increase for these particular load cases.

For the five cases of uniformly distributed load in the central
span, the results from the computer analysis were consistently 15% less
than those calculated for the model.   Nevertheless, the moments obtained
for the point load compare favourably with each other and would seem to
discount the possibility of incorrect member stiffness or material
properties being used.

Despite these variations in the absolute values of the stress
resultants, the similarity in shape of the stress distributions from
the computer and model results is encouraging.   Although this structural
configuration is not highly susceptible to the creation of warping
restraint stresses, the profile of direct stress due to bimoment effects

is well established and is particularly noticeable in the wide side cantilevers. ' Unfortunately, without gauge elements on the cantilever tips this distribution cannot be verified, although this will be possible when the results from the $1/12^{th}$ scale microconcrete model become available.

4.3 A CONTINUOUS ROAD BRIDGE OF COMPOSITE CONSTRUCTION

The effectiveness of the computer program developed in §4.1 is further demonstrated in the analysis of a composite road bridge. While this is not an existing structure, nor one for which model test results are readily available, it has already been used by several authors to verify methods of analysis relating to curved, thin-walled sections[52,53,103]. In addition to providing a useful check and means of comparison with existing analytical approaches, this structure is also used extensively in §4.4 during the evaluation of errors introduced by neglecting the effects of curvature, warping, etc..

4.3.1 Description

Konishi and Komatsu[52] originally proposed the layout and cross-sectional configuration of this structure which represents a three-span bridge carrying two traffic carriageways. Continuity is maintained over two central supports and torsional restraint is additionally provided at the free ends. An angle of 64° is subtended by the circularly curved central span and the arc length along the centreline of this member is equal to the length of the two straight outer spans. A constant cross-section is assumed throughout which, together with a plan of the structure, is shown in fig. 4.33. Distortion of the twin spine single cell section is prevented by adequate vertical cross bracing between the individual spines and the concrete top flange is assumed to act compositely with the rest of the section.
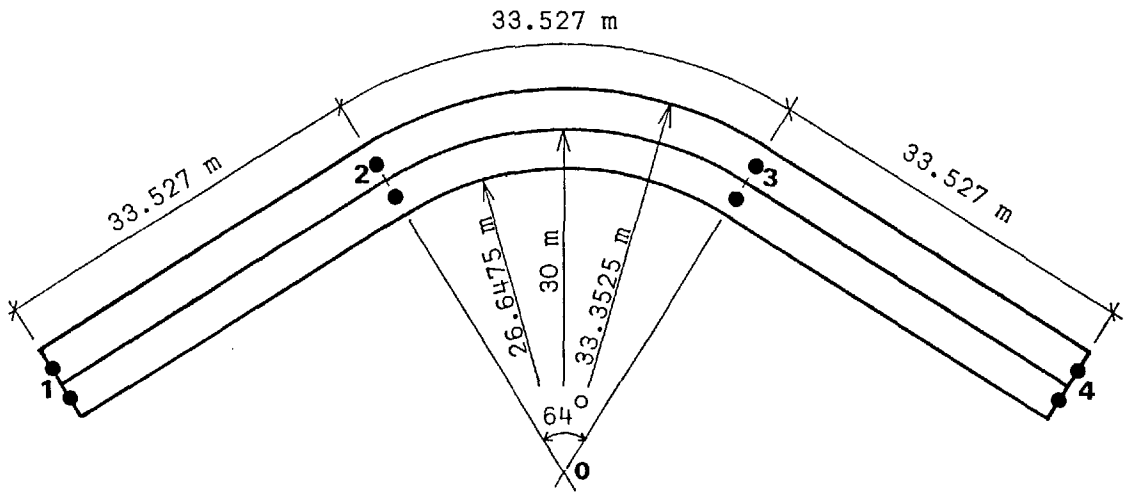
a. Plan
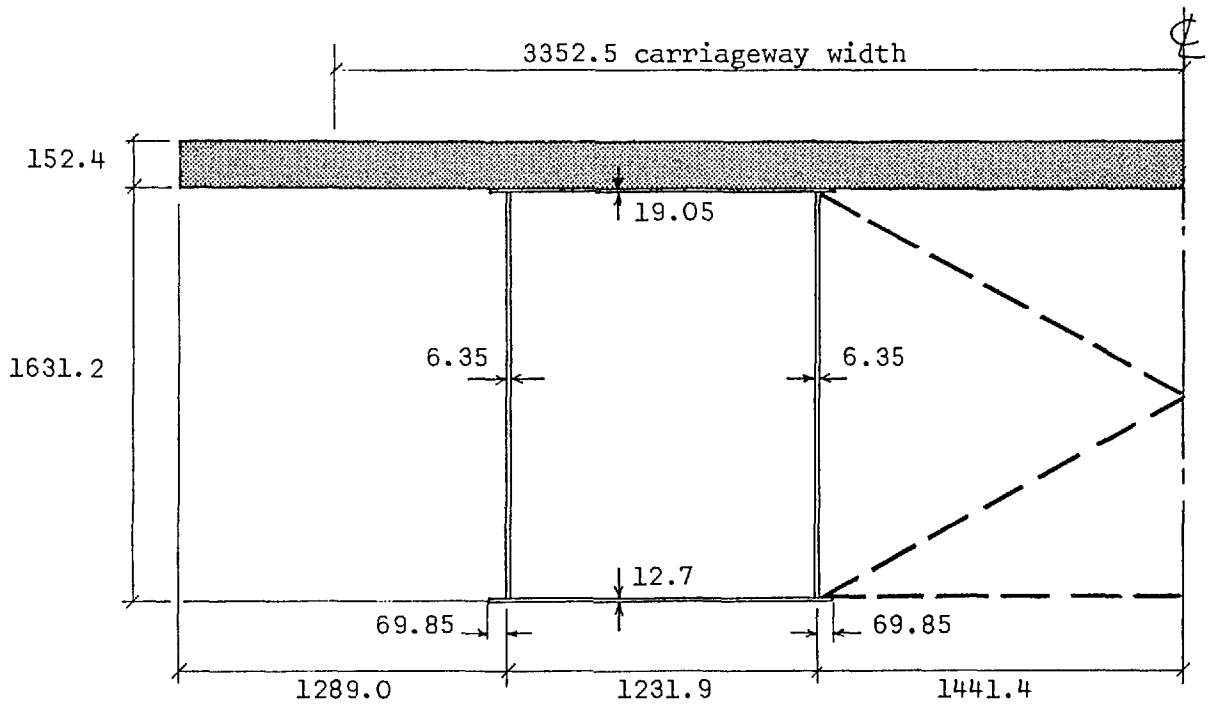
b. Typical cross-section

Figure 4.33 Continuous Road Bridge of Composite Construction

Cross-sectional Properties

The geometrical properties of the section are listed in the

original papers by Konishi and Komatsu[52,53] and evidently take account of

the effects of curvature in the central span.   These properties have

been used directly by Takaba and Naruoka[103] and are presented here in

Table 4.8.   However, insufficient information has been made available

to check these quantities exactly, particularly with respect to the

effective modulus of elasticity assumed for the concrete.   There is

also an apparent inconsistancy between the value of the shear modulus

of steel adopted by Konishi and Komatsu (8.00 kg/cm^2) and that adopted

by Takaba and Naruoka (7.88 kg/cm^2).

Nevertheless, by assuming an elastic modular ratio of 7 and

by neglecting the additional shear capacity provided by any horizontal

cross-bracing between the spines[25], the geometrical properties have been

re-calculated for both the straight and curved sections.   These results

are also presented in Table 4.8.   The computer program developed by

Pinkney[85] has been used for this purpose and while all the important

properties compare very favourably for the straight section, the values

of I_d and $I_{\hat{w}}$ are underestimated by approximately 5% and 12%, respectively,

when curvature is taken into consideration.   Furthermore, Konishi and

Komatsu have not adopted the concept of the warping shear parameter, μ,

and have therefore neglected the interactive effect of the shear forces

due to the connectivity condition of the closed cell.

Loading Conditions

In the original investigations[52,53,103],a point load of 1 tonne

was successively applied at the centre of each span on the centreline and

on the extreme inside and outside edges of the carriageway (at an

Quantity	Units	Konishi & Komatsu[52]		Waldron	
		Straight	Curved	Straight	Curved
x_G	mm	0	0	0	-163.63
y_G	mm	-	-	1327.94	1327.90
x_s	mm	0	0	0	-240.11
y_s	mm	-	-	499.76	496.56
I_x	mm^4	0.102×10^{12}	0.103×10^{12}	0.102×10^{12}	0.102×10^{12}
I_y	mm^4	-	-	0.147×10^{13}	0.147×10^{13}
I_{xy}	mm^4	-	-	0	0.136×10^{10}
I_d	mm^4	0.498×10^{10}	0.502×10^{10}	0.497×10^{11}	0.529×10^{11}
I_c	mm^4	-	-	0.315×10^{12}	0.312×10^{12}
I_w	mm^6	0.488×10^{18}	0.481×10^{18}	0.468×10^{18}	0.425×10^{18}
ψ	-	1.0000	-	1.0000	1.0000
μ	-	1.0000	1.0000	0.8422	0.8305
j^2	-	0.1857	0.1857	0.1856	0.1976
k	mm^{-1}	1.972×10^{-4}	1.979×10^{-4}	1.846×10^{-4}	1.984×10^{-4}

Table 4.8   Geometrical Properties of the Continuous Road Bridge of Composite Construction

eccentricity of ± 3.3525 m).   Since the structure is symmetrical about the centre of the curved span, this amounted to six different load cases. The same loading conditions have also been used throughout the present investigation and, in the first instance, this enables results obtained from the stiffness approach to be compared with those from an existing analytical method.

Structural Idealization

Since there is no facility in the computer analysis for applying

loads within the length of a beam element, additional node points have

been positioned in the centre of each span. The basic structural

idealization therefore comprises two straight beams in each of the outer

spans and two circular curved beams in the central span. This layout

is shown in fig. 4.34 together with the values of structural stiffness

assigned to each beam element. These are the quantities used by

Konishi and Kamatsu in their original investigations in which the

following elastic moduli for steel were assumed:

$$E_s = 2.1 \times 10^6 \text{ kg/cm}^2$$

$$G_s = 0.8 \times 10^6 \text{ kg/cm}^2$$

Furthermore, a value of unity has been specified for the warping shear

parameter, μ, in order to comply exactly with the assumptions made in

the previous analysis[52,53].
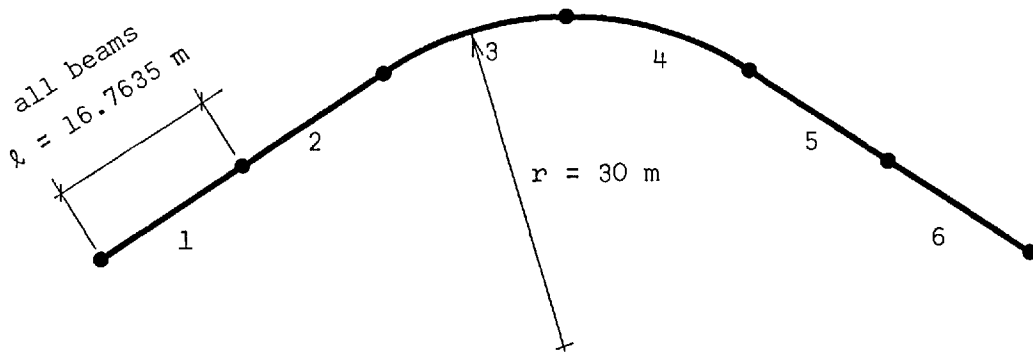
Member Ref. No.	EI_x (kg.cm^2)	GI_d (kg.cm^2)	EI_w (kg.cm^4)
1-2, 5-6	2.1485×10^{13}	3.9855×10^{12}	1.0249×10^{18}
3-4	2.1546×10^{13}	4.0220×10^{12}	1.0108×10^{18}

Figure 4.34 Structural Idealization of the Composite
Road Bridge

4.3.2   Structural Analysis

The idealized structure with the general arrangement and
properties given in fig. 4.34 has been analysed for the six load cases
previously identified in this section.   The resultant longitudinal
distributions of bending moment and bimoment are respectively shown in
figs. 4.35 and 4.36.   To facilitate the presentation of results, these
distributions have only been plotted over one half of the structure for
each of the loading conditions.   While clearly this is sufficient for
loads applied at the centre of the structure, it also covers the most
highly stressed region in the case of loads applied to the outer spans.

In their original paper, Konishi and Komatsu produced a solution
for this bridge by first expressing the distribution of the various stress
resultants in terms of the applied loads and the unknown bending moments
and bimoments at the internal supports.   They then derived an expression
for the total strain energy in the system and employed the principle of
least work to evaluate the indeterminant quantities.   This is similar
to the method adopted in §3.4.4 and §3.4.5 for establishing the fixed
end forces in circular curved members with built-in ends, and is entirely
satisfactory for simple continuous structures.   Furthermore, since it is
an 'exact' method and only differs from the stiffness approach in the
formulation adopted for solution, an identical result would be expected.
From the limited information available this is apparently the case.
Indeed, for the six loading conditions considered, the stress resultants
calculated at the centre of the loaded span (presented in Table 4.9 in
italics), all agree to ± 1% with the published results[103].   This is
well within the expected tolerance due to rounding errors and further
verifies the effectiveness of the computer program developed in this
chapter.
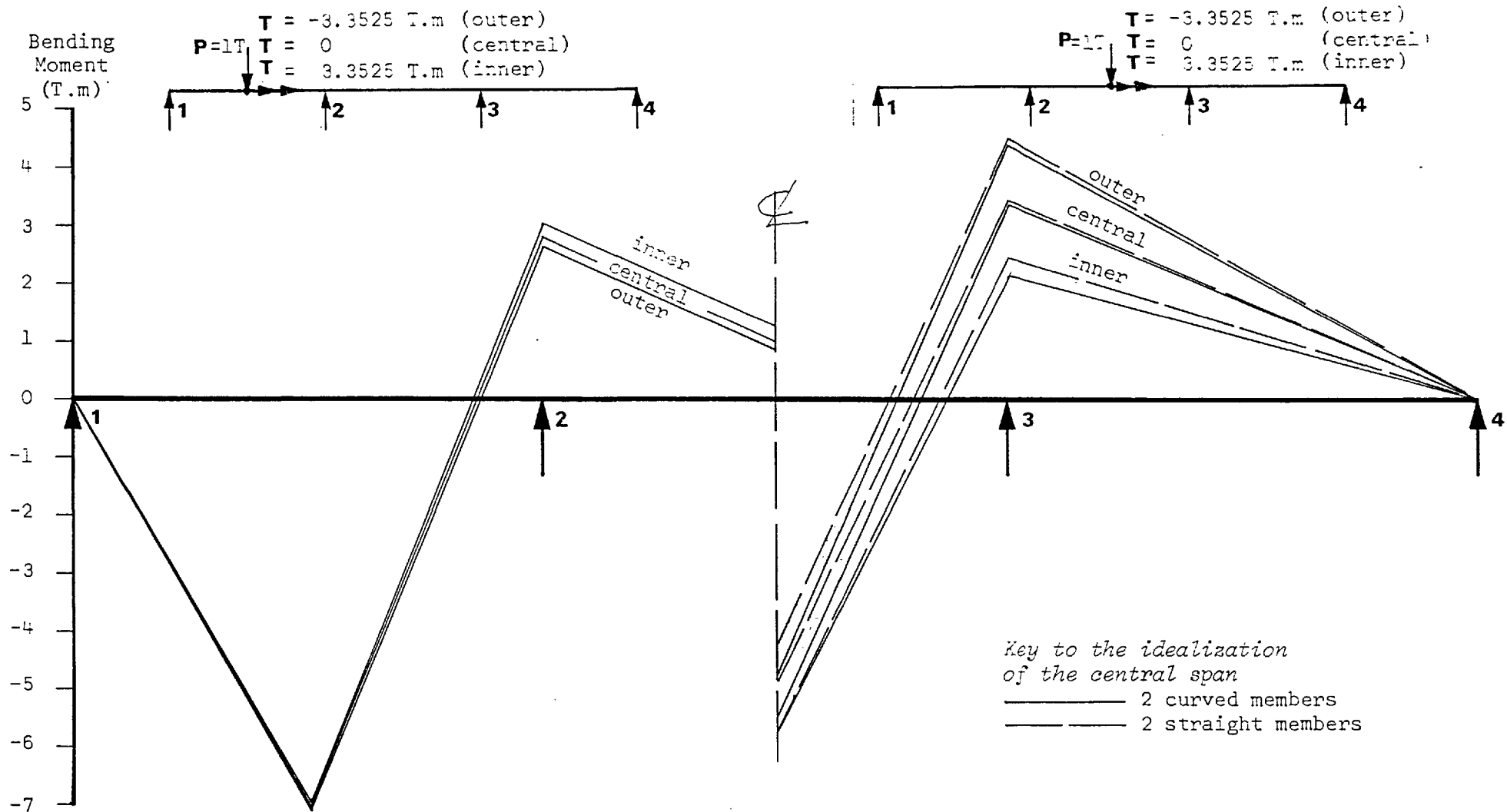
Figure 4.35   Longitudinal Distribution of Bending Moment in the Composite Road Bridge
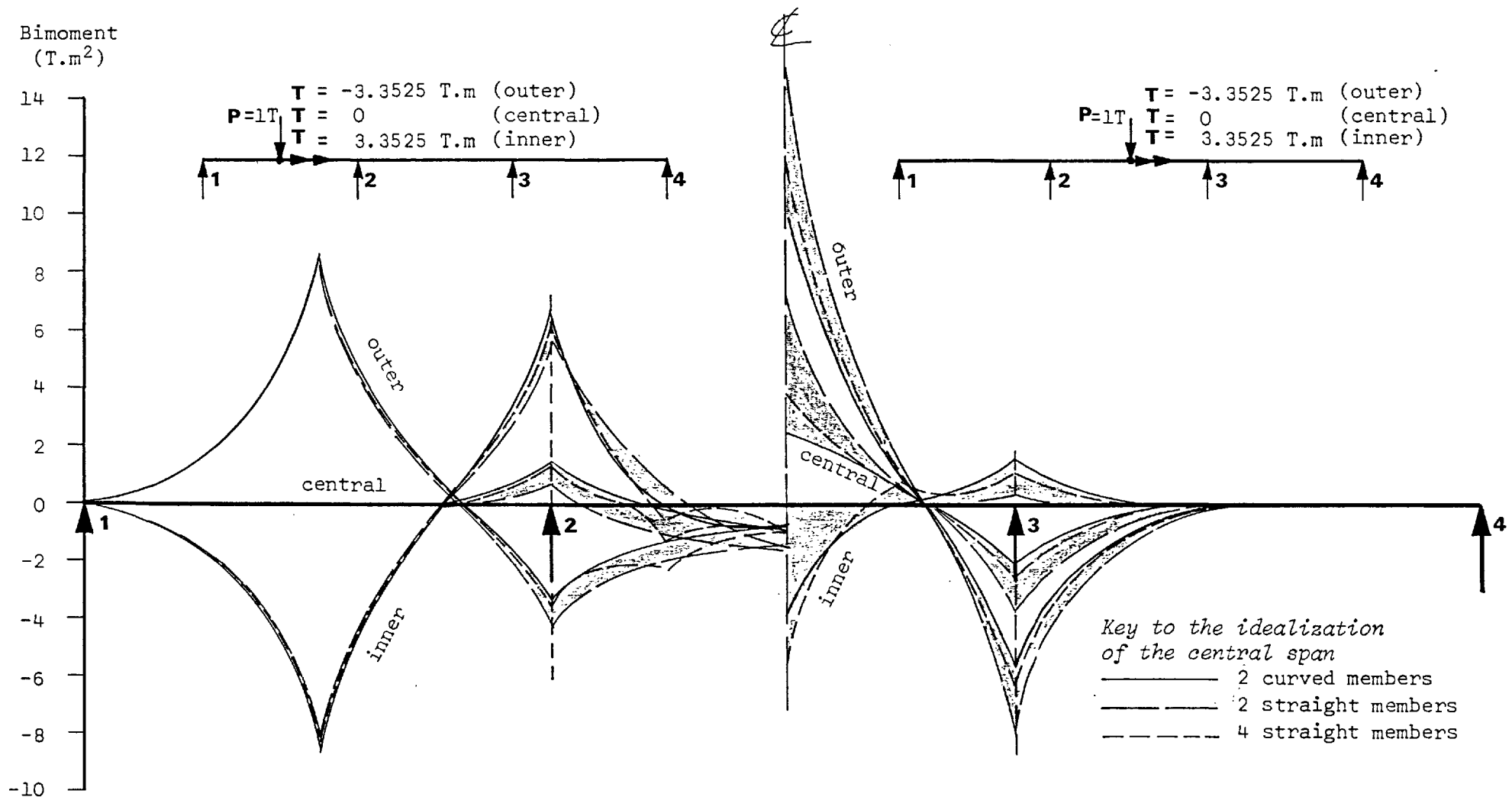
Figure 4.36   Longitudinal Distribution of Bimoment in the Composite Road Bridge

	No. of beams in central span	Outer Spans			Central Span		
		Outside Lane Loaded	Middle Lane Loaded	Inside Load Loaded	Outside Lane Loaded	Middle Lane Loaded	Inside Load Loaded
Bending Moment	2 (curved)	-705.80	-696.92	-688.00	-515.47	-544.91	-574.36
	2	-693.26	-689.04	-684.82	-498.68	-521.36	-544.03
	4	-698.55	-690.82	-683.09	-512.46	-539.86	-567.22
	8	-700.29	-691.42	-682.55	-514.50	-543.49	-572.46
	16	-700.76	-691.58	-682.40	-514.92	-544.32	-573.74
Torsional Moment	2 (curved)	157.66	4.45	-148.80	167.62	0	-167.63
	2	155.55	2.11	-151.33	167.63	0	-167.63
	4	157.13	3.87	-149.39	167.63	0	-167.62
	8	157.63	4.44	-148.75	167.62	0	-167.62
	16	157.78	4.59	-148.58	167.62	0	-167.63
Shear	2 (curved)	-0.4291	-0.4157	-0.4104	-0.5	-0.5	-0.5
	2	-0.4136	-0.4110	-0.4085	-0.5	-0.5	-0.5
	4	-o.4167	-0.4121	-0.4075	-0.5	-0.5	-0.5
	8	-0.4177	-0.4125	-0.4072	-0.5	-0.5	-0.5
	16	-0.4180	-0.4126	-0.4071	-0.5	-0.5	-0.5
Bimoment	2 (curved)	83 552	546	-82 460	101 813	24 504	-52 804
	2	83 292	259	-82 773	145 208	69 906	- 5 396
	4	83 485	475	-82 536	116 266	38 872	-38 522
	8	83 547	545	-82 457	106 451	28 568	-49 315
	16	83 564	564	-82 436	103 789	25 786	-52 217

Table 4.9   Comparison of Stress Resultants obtained from different Structural Idealizations

4.4   ASSESSMENT OF ANALYTICAL ERRORS

A method of analysis is now available for structures comprising

both straight and curved thin-walled members, and in a form suitable for

solution by desk-top computer.   Nevertheless, it must be accepted that

designers will still often prefer to use hand methods of calculation or

computer-based methods with which they already have some experience.

Almost invariably these other methods of analysis will require the

introduction of initial simplifying assumptions, such as disregarding

warping restraint or member curvature effects.   The validity of some

of the more important assumptions is therefore investigated here and,

wherever possible, the associated errors have been quantified for a

range of sections with those dimensions typically found in practice.

4.4.1   Errors due to neglecting Curvature Effects

Curvature introduces a further complexity into the analysis of

structures since bending and torsional moments are no longer independent

quantities but interact along the length of the member.   These problems

can be largely avoided by representing the curved girder as an

equivalent straight girder, for the purposes of analysis, a simpli-

fication which also considerably reduces the computational effort

required for solution.   However, since this approximation is usually

only acceptable when the degree of curvature is small, an alternative

method is also available whereby the geometry of the original member

is closely represented by a series of end-connected straight beam

elements.   In general, this method involves significantly more calcu-

lation, due to the additional degrees of freedom introduced into the

system, and is therefore only an attractive alternative when computer

facilities are available.

Before the validity of such an idealization can be established

for a particular application, errors introduced into the calculation of

the various stress resultants must first be estimated.   Little factual

information·is available for this purpose although Hambly[35], for example,

suggests that it is generally permissible to represent a circular curved

member subtending a central angle of less than $20°$ as an equivalent

straight member.   In such cases, it is usual to adopt an identical

cross-sectional configuration for the idealized beam and to represent

the span by the arc length of the original curved member.

Sawko[95] has made a more detailed investigation of the errors

associated with an equivalent straight beam idealization.   This has

taken the form of a computer-based study covering a wide range of

included angles and torsional/bending stiffness ratios.   The straight

beam configuration on which this investigation is based consists of the

member shown in fig. 4.37, built-in at both ends.   The supports are

skewed at an angle of $\pm \Theta/2$ and separated by the original chord length,

$\ell = 2r.\sin(\Theta/2)$.
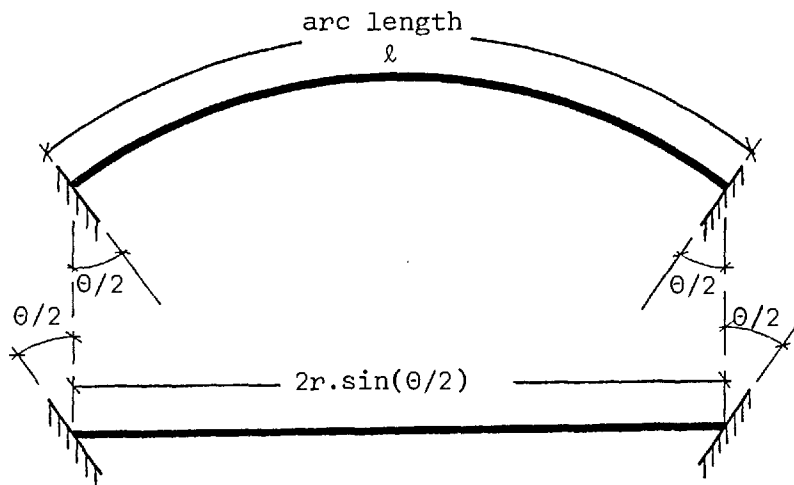
*Figure 4.37   Equivalent Straight Beam Idealization of the
Circular Curved Member*

The general error function selected by Sawko as being representative of the inaccuracies introduced by such an idealization is given by

$$E_i = \frac{k_{ii} - k_{ii}^*}{k_{ii}} = 100\%$$ \hfill 4.7

Here, E_i is the error function associated with the ith stress resultant, and k_{ii}, k_{ii}^* are the ith diagonal elements in the stiffness matrices of the curved and straight beams respectively. This is equivalent to determining the percentage error between the ith stress resultant at the end of each beam due to the application of a unit value of the corresponding component of deformation at the same point.

Only solid beams were considered in the original investigation and the functions reproduced in figs. 4.38 - 4.40 represent the errors associated with the actions of bending moment, torsion and shear, respectively. These graphs indicate the possibility of significant errors, even for members displaying typical cross-sectional proportions and subtending relatively small central angles. Unfortunately, several mistakes have subsequently been discovered in the initial formulation of the stiffness matrix for the equivalent straight member, thus invalidating these error functions.

The correct stiffness matrix may however be obtained by first inverting the straight beam flexibility matrix **G'**, given in Appendix 2.4, and then transforming the resultant matrix in accordance with eqn. 3.67 to take account of the skewed supports. Alternatively, a direct solution is possible by inverting the transformed straight beam flexibility matrix **H'**, given in Appendix 2.6. The stiffness matrix for the circular curved member was correctly derived by Sawko and is obtained in this thesis by inverting the flexibility matrix **F'** (Appendix 2.2). By incorporating the appropriate diagonal elements

from the newly derived member stiffness matrices into eqn. 4.7, the
error functions have been recalculated and are shown in figs. 4.41 -
4.43, respectively.

These functions have subsequently been used to investigate
the possible inaccuracies due to the idealization of the bifurcated
bridge structure, described in §4.2. The three outer spans AB, DE and
FG have been selected for this study and these correspond to the twin
cell, small single cell and large single cell, respectively. Estimates
of percentage error have been abstracted directly from figs. 4.38 - 4.43
for the appropriate values of stiffness ratio, j^2 (obtained from Table
4.2), and are presented in fig. 4.44 for each of the three spans. From
this figure it is clear that the functions originally proposed by Sawko
grossly overestimate the likely error in calculating the bending and
shear stiffnesses. They do however correspond closely in the case of
torsion for angles in excess of approximately 8°.

Two different idealizations have been considered whereby each
curved outer span is replaced by (i) a single equivalent straight
member, and (ii) a series of nine straight beam elements of equal
length. Percentage errors determined from fig. 4.44 are given in
Table 4.10 for each span. Evidently the nine beam idealization
adopted in the original grillage analysis of this structure (fig. 6.1)
introduces errors of less than 0.5% into the calculation of the three
primary components of stiffness in all instances. Furthermore, even
for the single equivalent straight beam, the maximum error in bending
or shear stiffness is estimated to be less than 4.5%, although signifi-
cant inaccuracies are predicted in the case of torsion. For purposes
of comparison, the incorrect error functions have also been tabulated in
Table 4.10. Errors of up to 20% are indicated in the computed values
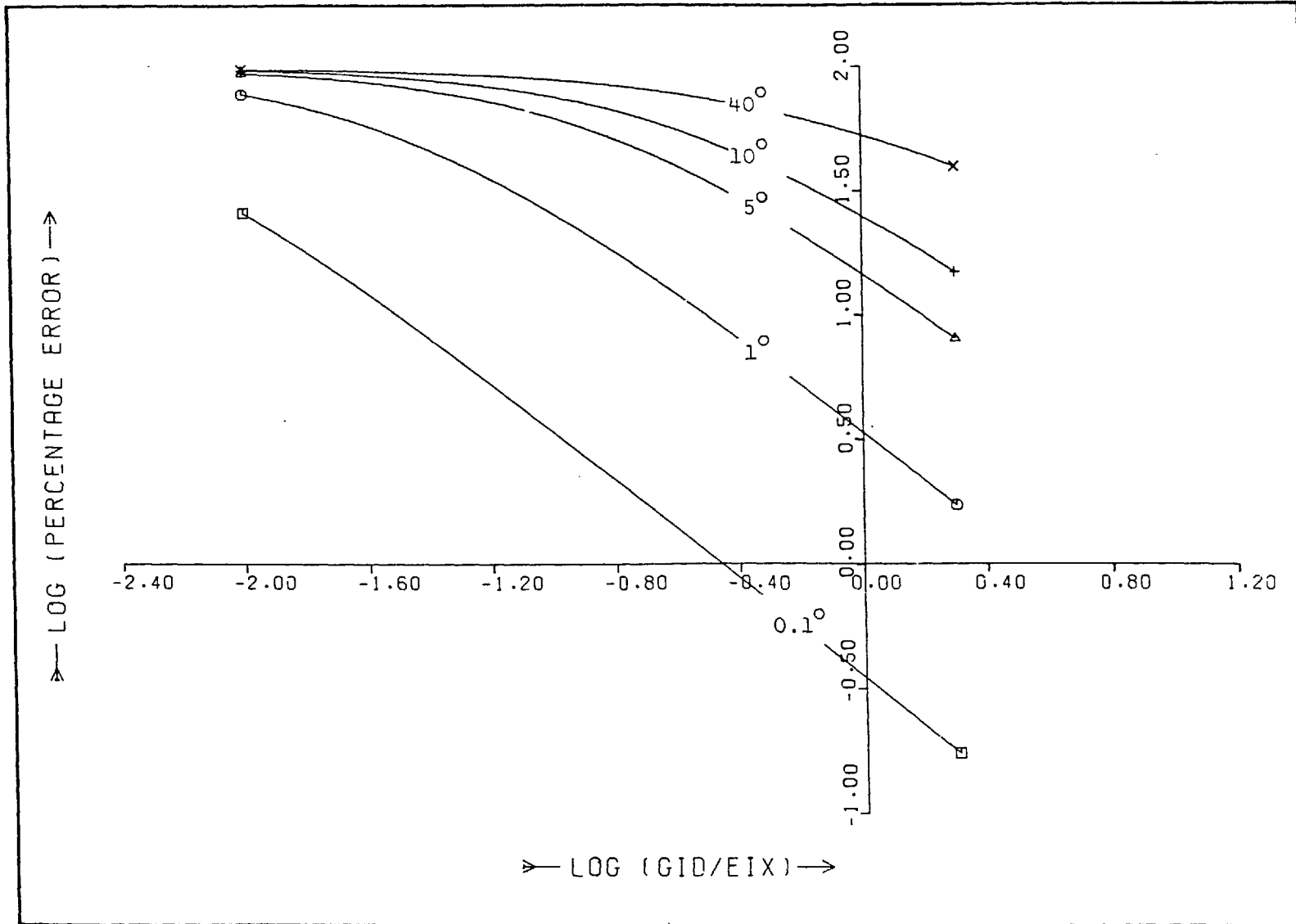
Figure 4.38   Percentage Error in Bending Moment due to neglecting Member Curvature (INCORRECT)
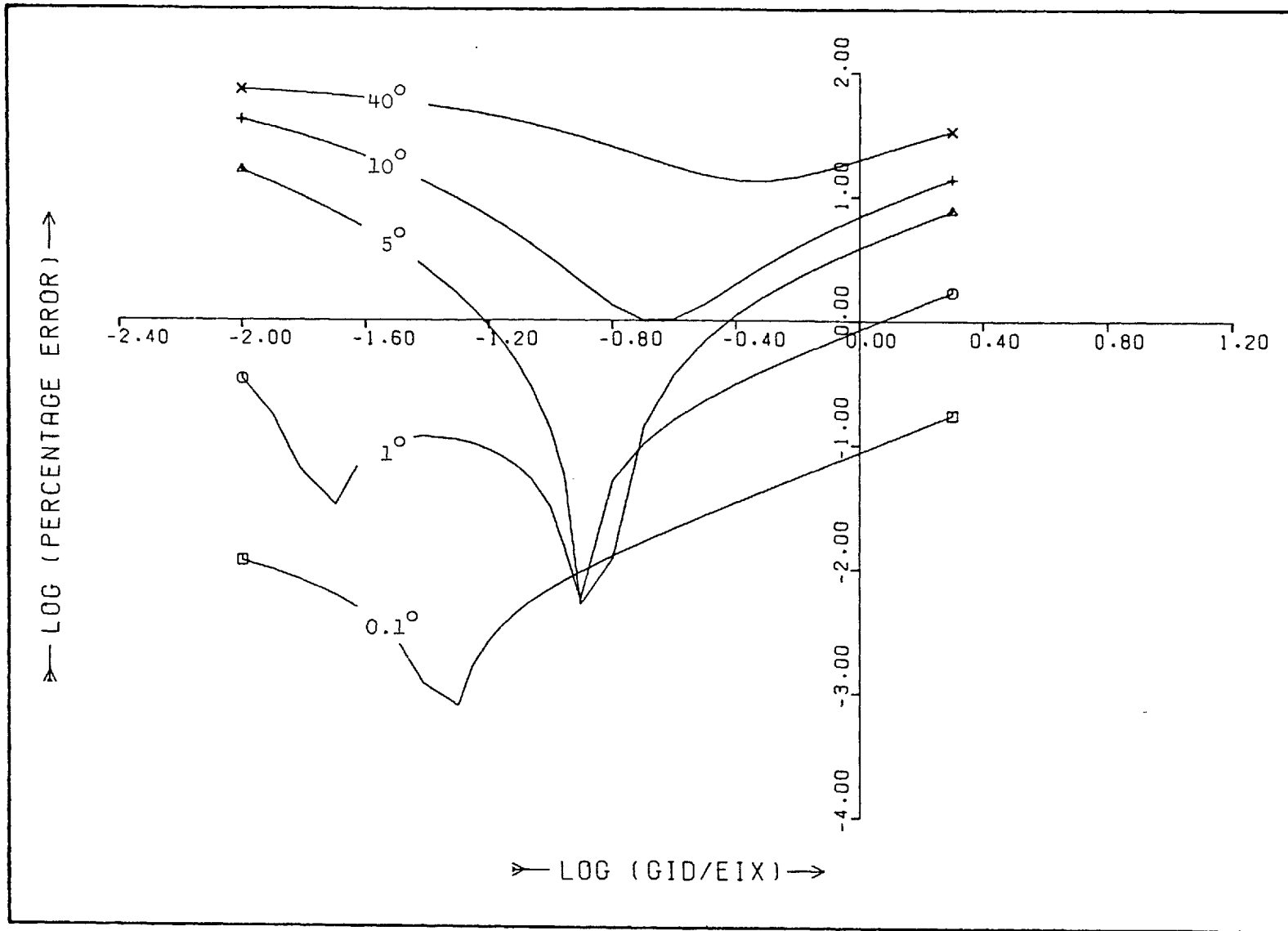
Figure 4.39 Percentage Error in Torsion due to neglecting Member Curvature (INCORRECT)
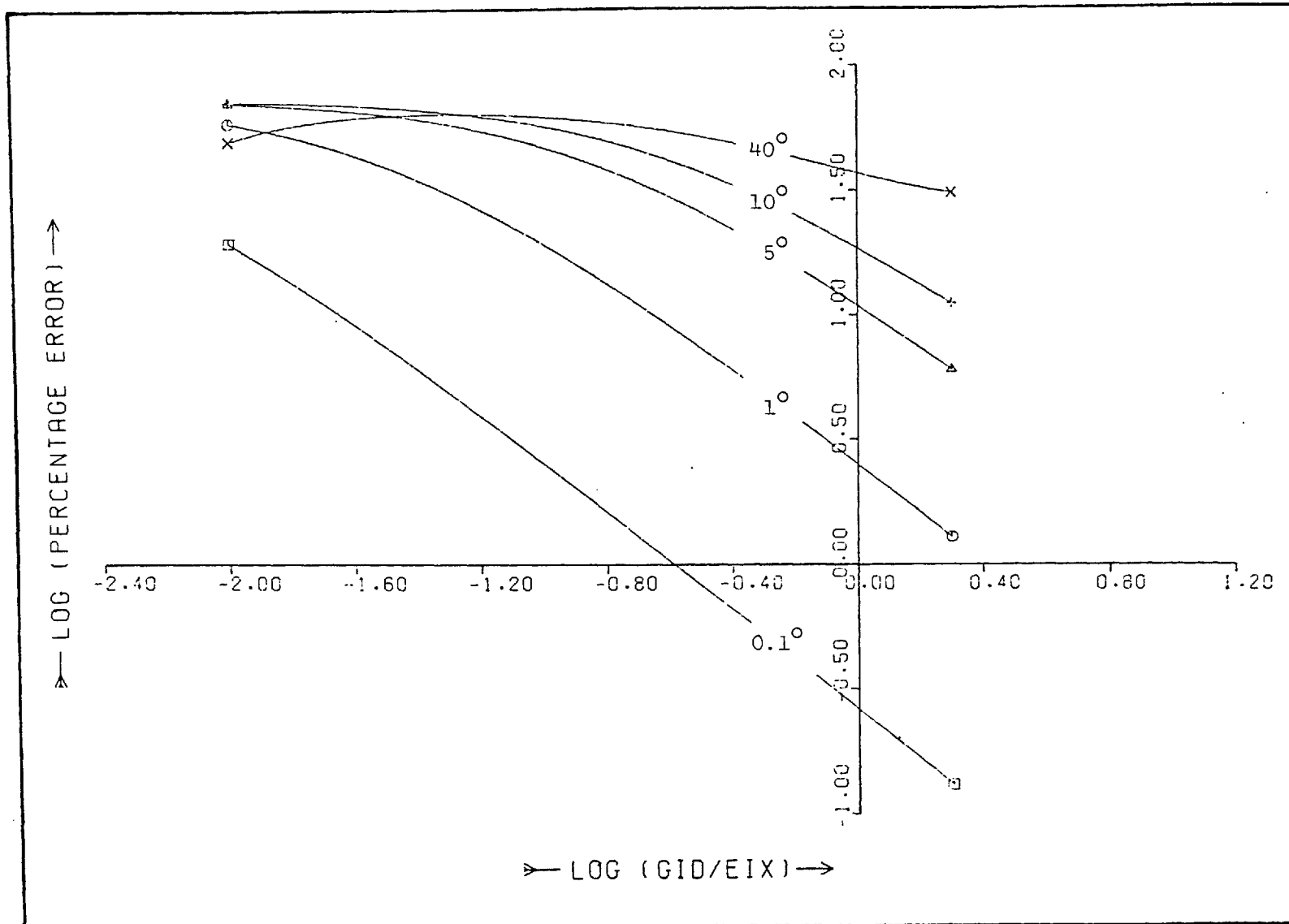
Figure 4.40 Percentage Error in Shear due to neglecting Member Curvature (INCORRECT)
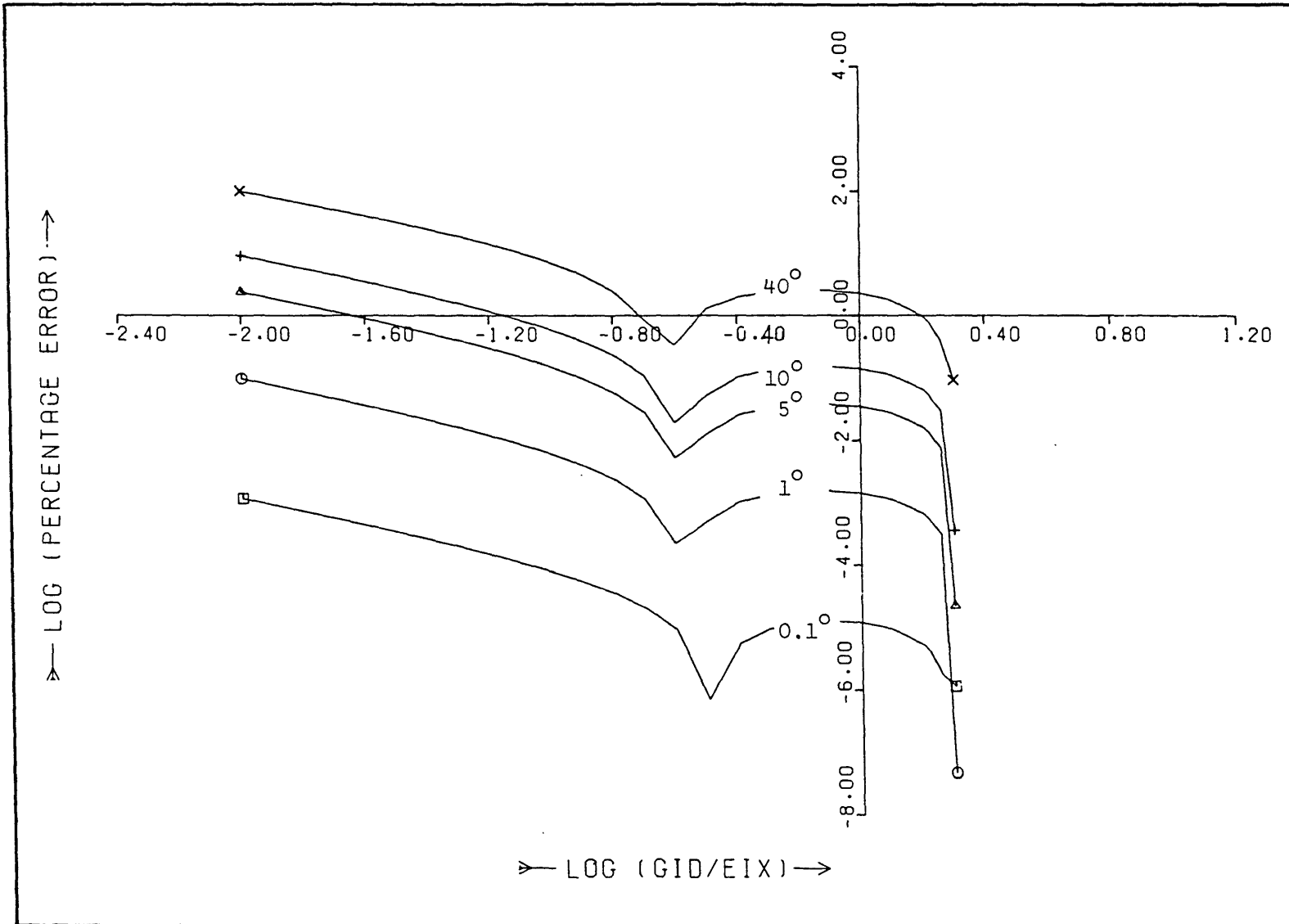
Figure 4.41   Percentage Error in Bending Moment due to neglecting Member Curvature
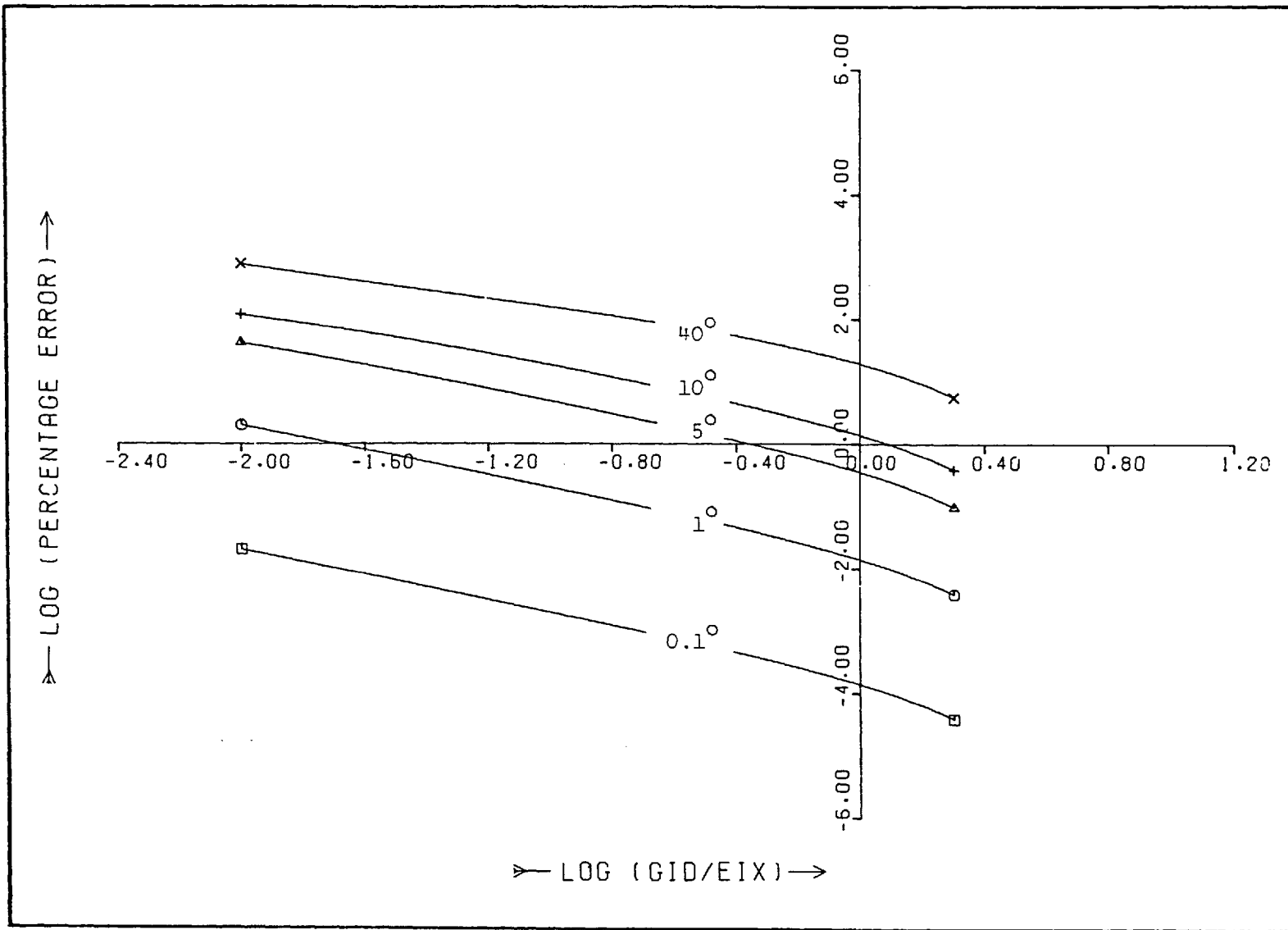
Figure 4.42   Percentage Error in Torsion due to neglecting Member Curvature
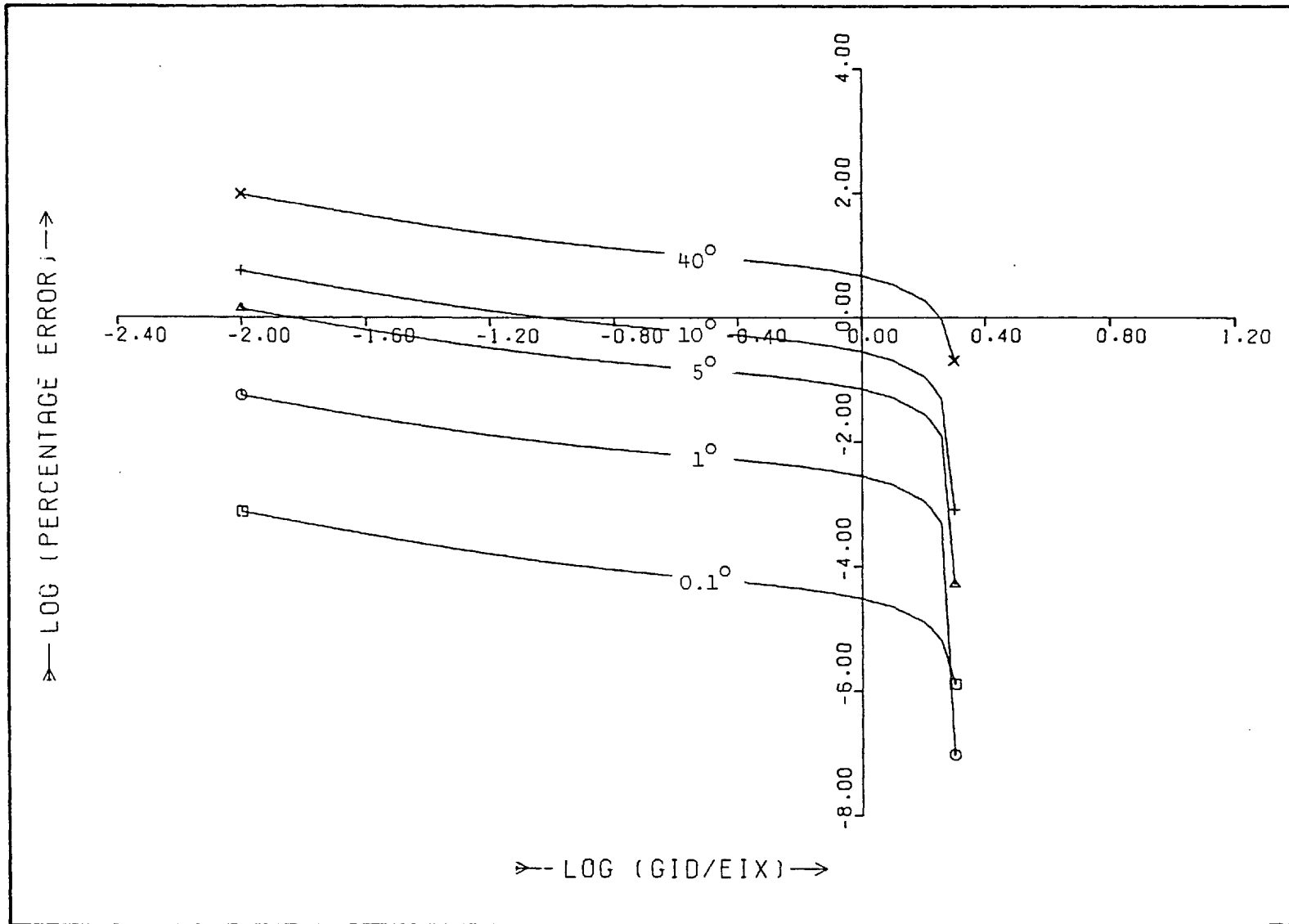
Figure 4.43   Percentage Error in Shear due to neglecting Member Curvature
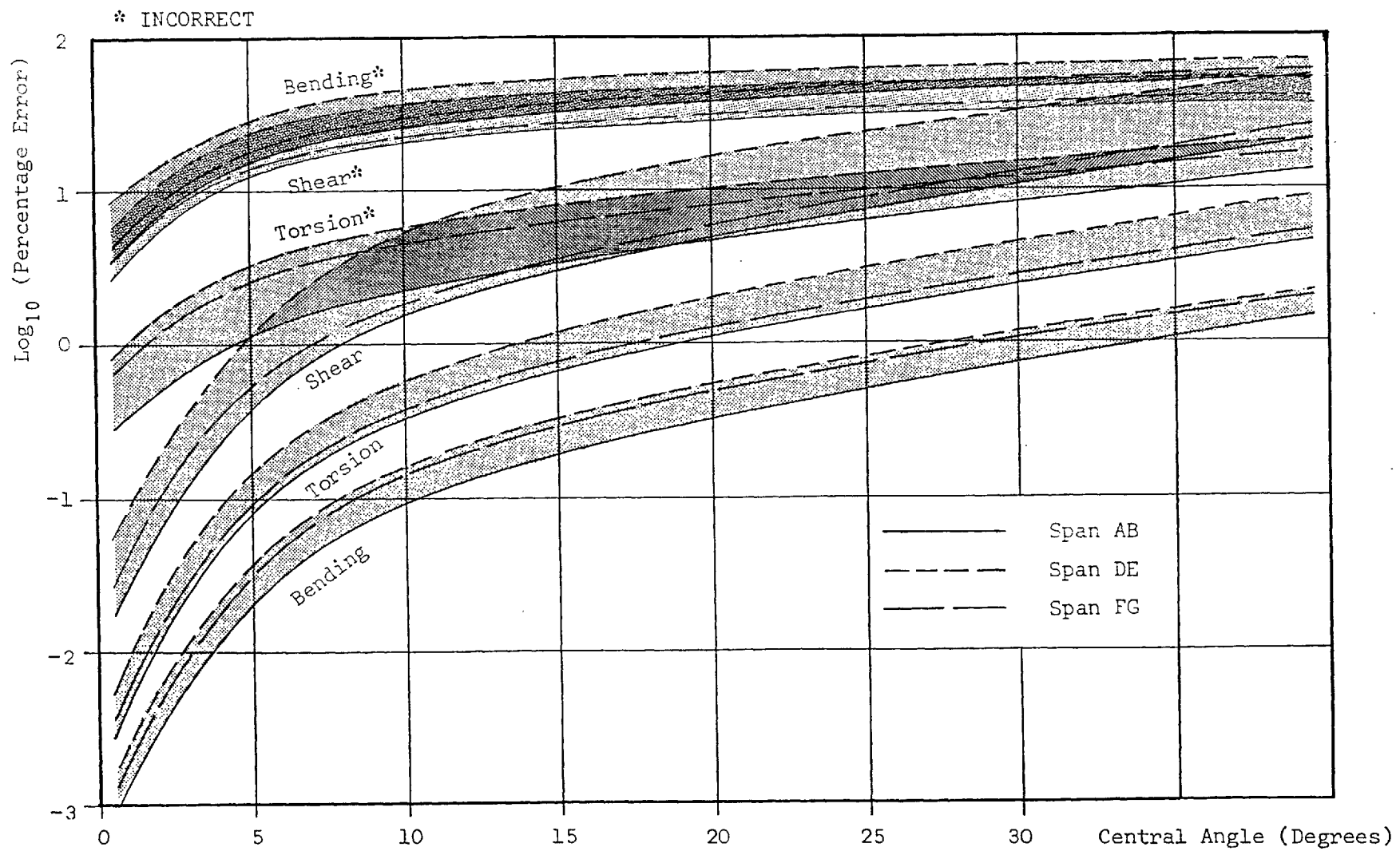
Figure 4.44 Percentage Error in Bending Moment, Torsion and Shear due to the Idealization of the Bifurcated Bridge

	Span AB $(j^2 = 0.838)$		Span DE $(j^2 = 0.351)$		Span FG $(j^2 = 0.689)$	
	1 Beam $(\theta=35.38^{\circ})$	9 Beams $(\theta=3.94^{\circ})$	1 Beam $(\theta=29.90^{\circ})$	9 Beams $(\theta=3.32^{\circ})$	1 Beam $(\theta=36.34^{\circ})$	9 Beams $(\theta=4.04^{\circ})$
Moment	1.12	0.01	1.17	0.02	1.58	0.02
Torsion	15.89	0.20	31.62	0.45	19.95	0.32
Shear	3.16	0.04	4.47	0.06	3.98	0.06
Moment†	50.12	12.59	63.10	19.95	56.23	15.14
Torsion†	11.22	0.89	14.79	2.24	15.14	2.00
Shear†	33.88	10.00	42.66	15.14	39.81	12.02

† incorrect

Table 4.10   Percentage Error in the Computation of Member Stiffness in the Outer Spans of the Bifurcated Bridge

of bending and shear stiffness for the nine beam idealization while those for the case of torsion are not greatly different from the correct values.

Straight Beam Idealization including the Effects of Warping

This useful form of error analysis has been extended to include the effects of warping in thin-walled sections. The basic idealization detailed in fig. 4.37 is retained, although the stiffness matrices for the circular curved and equivalent straight beams are now derived by inverting the flexibility matrices **F** and **H** (from Appendices 2.1 and 2.5), respectively. By introducing the appropriate diagonal elements into eqn. 4.7, error functions are obtained for each of the four degrees of freedom associated with thin-walled sections. These correspond to the three stress resultants previously considered in the error analysis of solid beams together with a fourth function defining the error in the bimoment term.

These functions are difficult to present in graphical form due

to the extra variables included in the analysis, $i.e.$ the decay and warping shear parameters. Nevertheless, results are plotted in figs. 4.45 - 4.60 for a representative range of these variables covering central angles of 40°, 10°, 5° and 1°, and warping shear parameters with the numerical value of either 1.0 or 0.5. Seven or eight lines appear on every graph, each line representing a different value of the dimensionless decay function kr of between 0.5 and 50. An additional line is also plotted on all of the graphs (with the exception of those relating to bimoment) and this corresponds to the properties of the solid beam ($i.e.$ kr → ∞; μ = 0). Despite the limited number of functions presented, figs. 4.45 - 4.60 provide sufficient information for most practical applications since intermediate values can usually be interpolated to the required degree of accuracy.

In order to fully evaluate the use of these graphs, an error analysis has been undertaken for the continuous road bridge of composite construction detailed in §4.3. For this purpose, the central curved span was idealized by several alternative assemblages of straight beams, comprising either 16, 8, 4 or 2 elements. A full structural analysis was then performed on each of these configurations using the computer program previously described in this chapter. Six load cases were considered for each structural idealization, corresponding to the applications of point load identified in §4.3.1. This permitted the results to be compared directly with those from the original 'exact' solution for which the central span was represented by two curved beam elements. Values of the various stress resultants determined from the analyses are presented in Table 4.9 (p.266); the percentage error in each computed quantity with respect to the original solution is also given in Table 4.11.
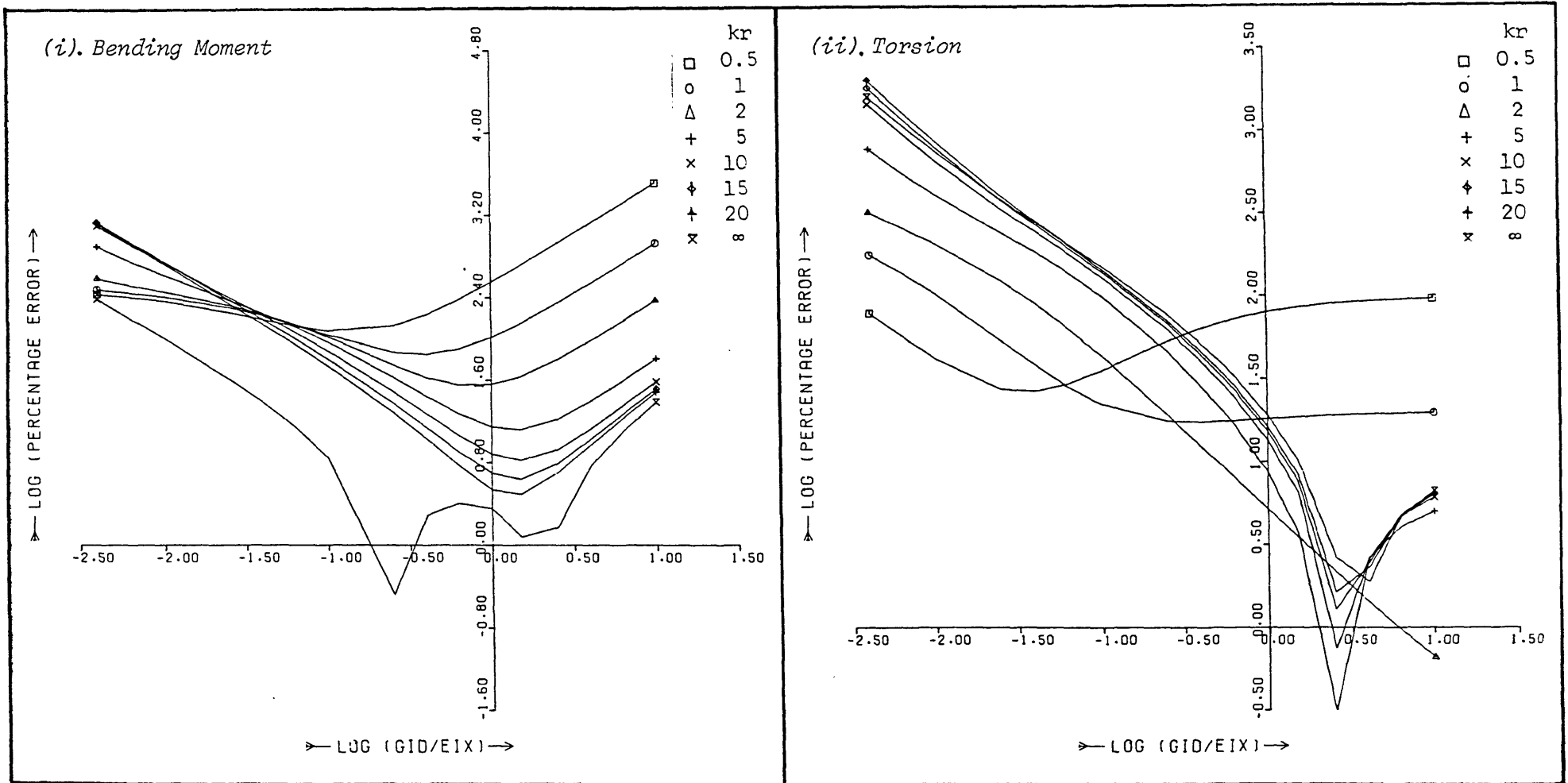
Figure 4.45   Percentage Error in (i). Bending Moment and (ii). Torsion due to neglecting Member Curvature ($\theta = 40^{\circ}; \mu = 1$)

(i). Shear

kr
□ 0.5
○ 1
△ 2
+ 5
× 10
✦ 15
✚ 20
✕ ∞

← LOG (PERCENTAGE ERROR) →

4.80

4.00

3.20

2.40

1.60

0.80

0.00

-0.80

-1.60

-2.50 -2.00 -1.50 -1.00 -0.50 0.00 0.50 1.00 1.50

►— LOG (GID/EIX) →

(ii) Bimoment

kr
□ 0.5
○ 1
△ 2
+ 5
× 10
✦ 15
✚ 20

← LOG (PERCENTAGE ERROR) →

2.00

1.50

1.00

0.50

0.00

-0.50

-1.00

-1.50

-2.00

-2.50 -2.00 -1.50 -1.00 -0.50 0.00 0.50 1.00 1.50

►— LOG (GID/EIX) →
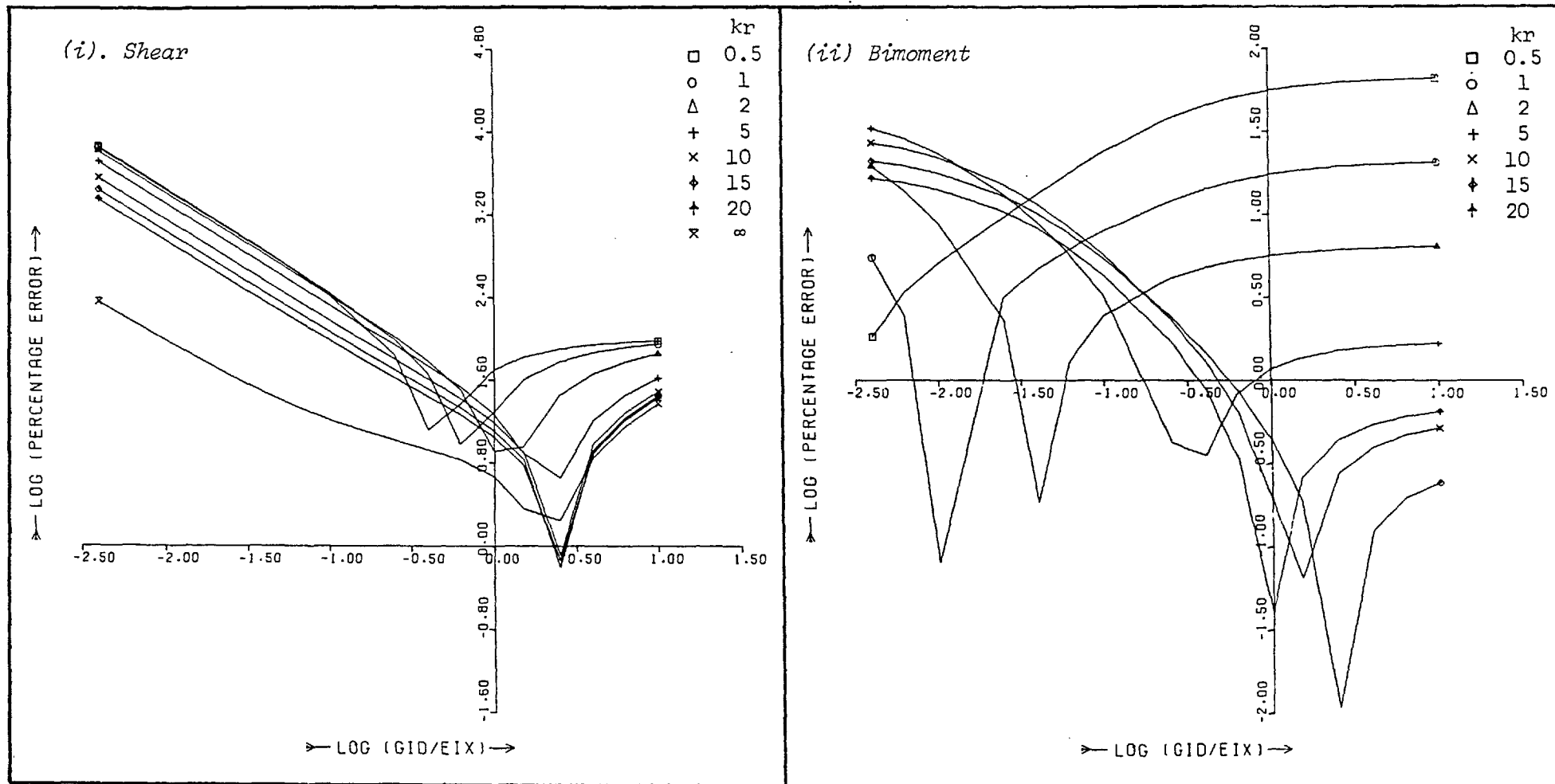
Figure 4.46   Percentage Error in (i). Shear and (ii). Bimoment due to neglecting Member Curvature ($\theta = 40°$; $\mu = 1$)
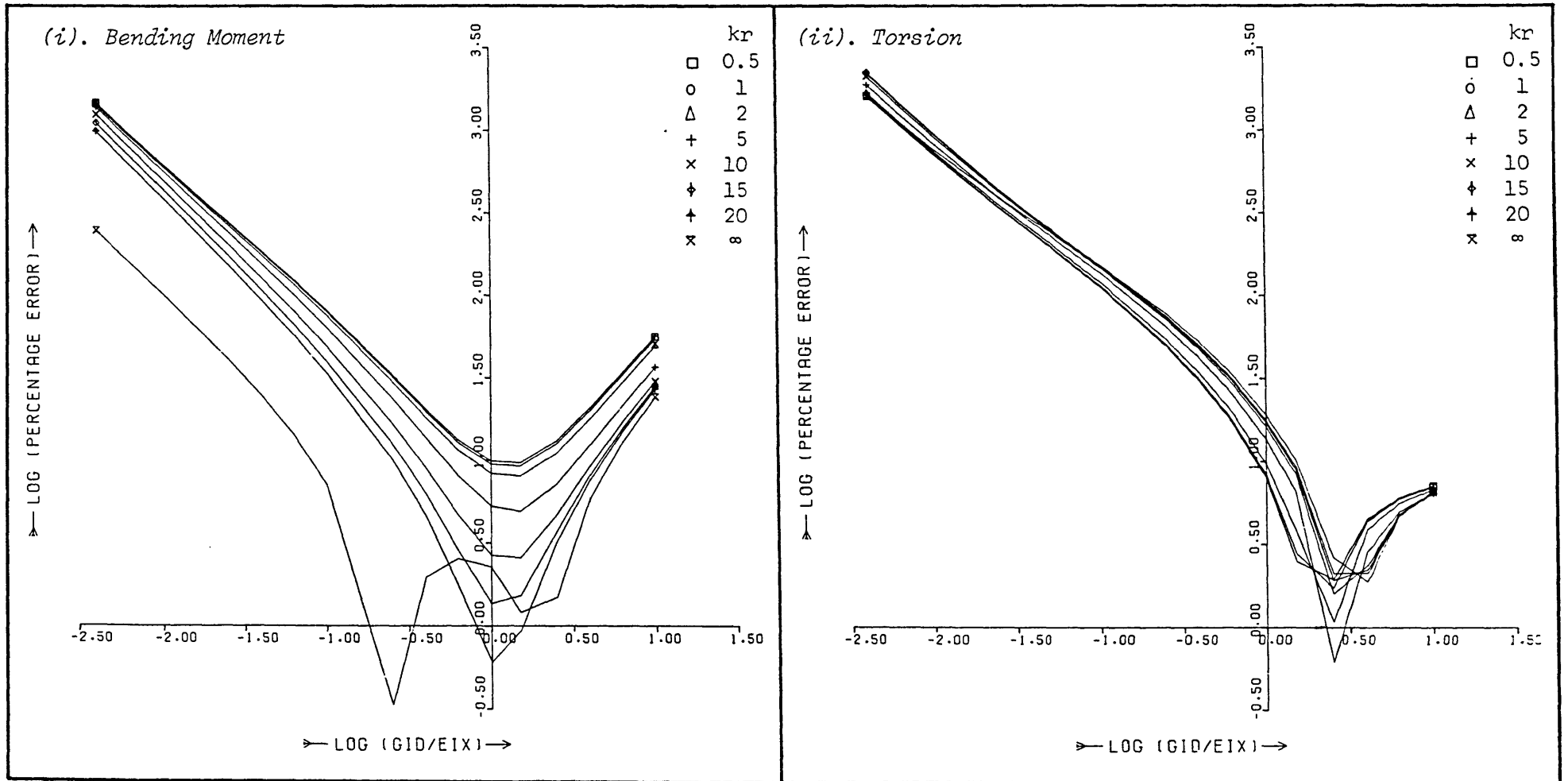
Figure 4.47   Percentage Error in (i). Bending Moment and (ii). Torsion due to neglecting Member Curvature (θ = 40°; μ = 0.5)

Figure 4.48   Percentage Error in (i). Shear and (ii). Bimoment due to neglecting Member Curvature ($\theta = 40°$; $\mu = 0.5$)
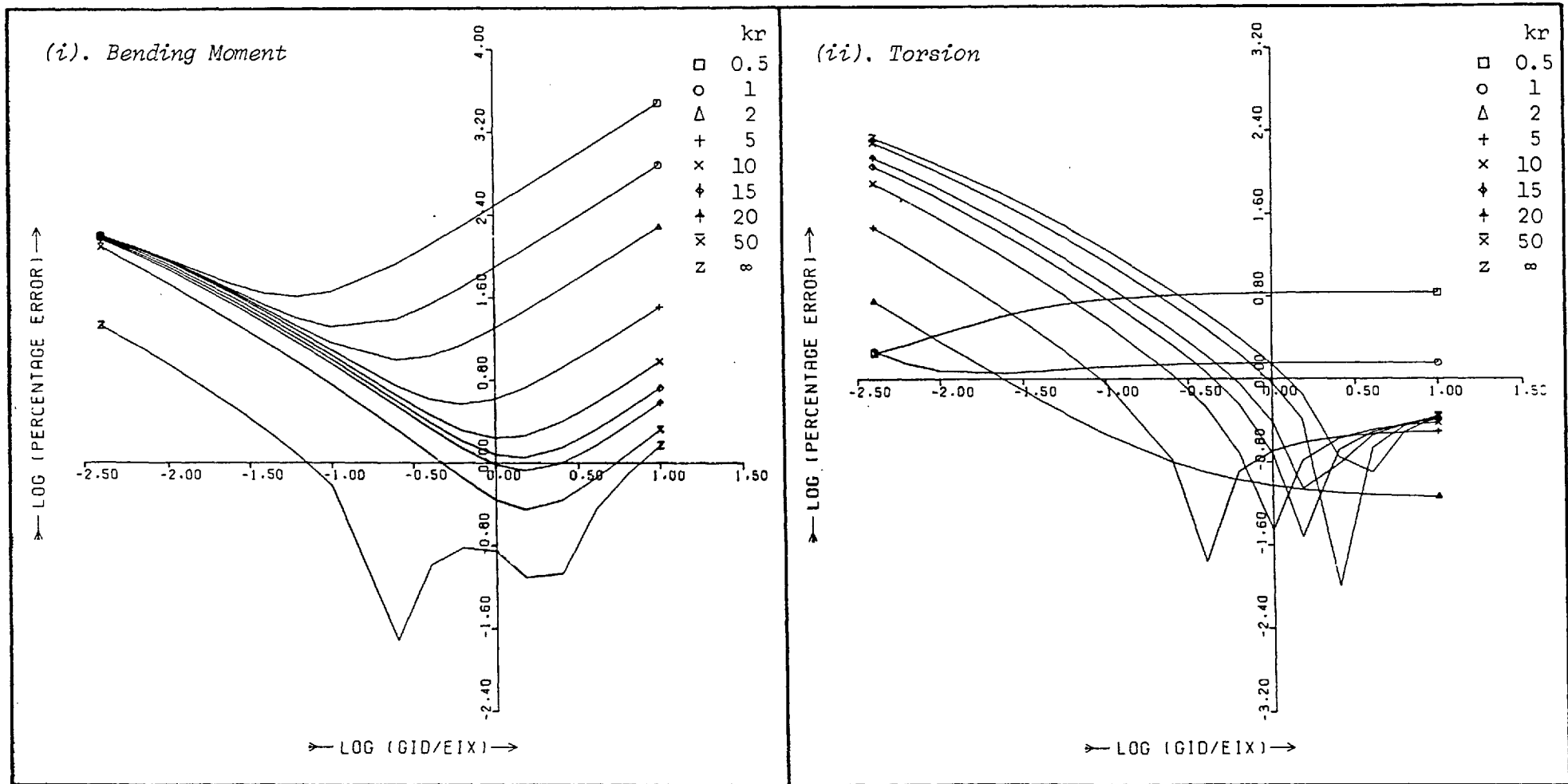
Figure 4.49 Percentage Error in (i). Bending Moment and (ii). Torsion due to neglecting Member Curvature ($\theta = 10^{o}$; $\mu = 1$)

Figure 4.50   Percentage Error in (i) Shear and (ii). Bimoment due to neglecting Member Curvature ($\theta = 10°$; $\mu = 1$)
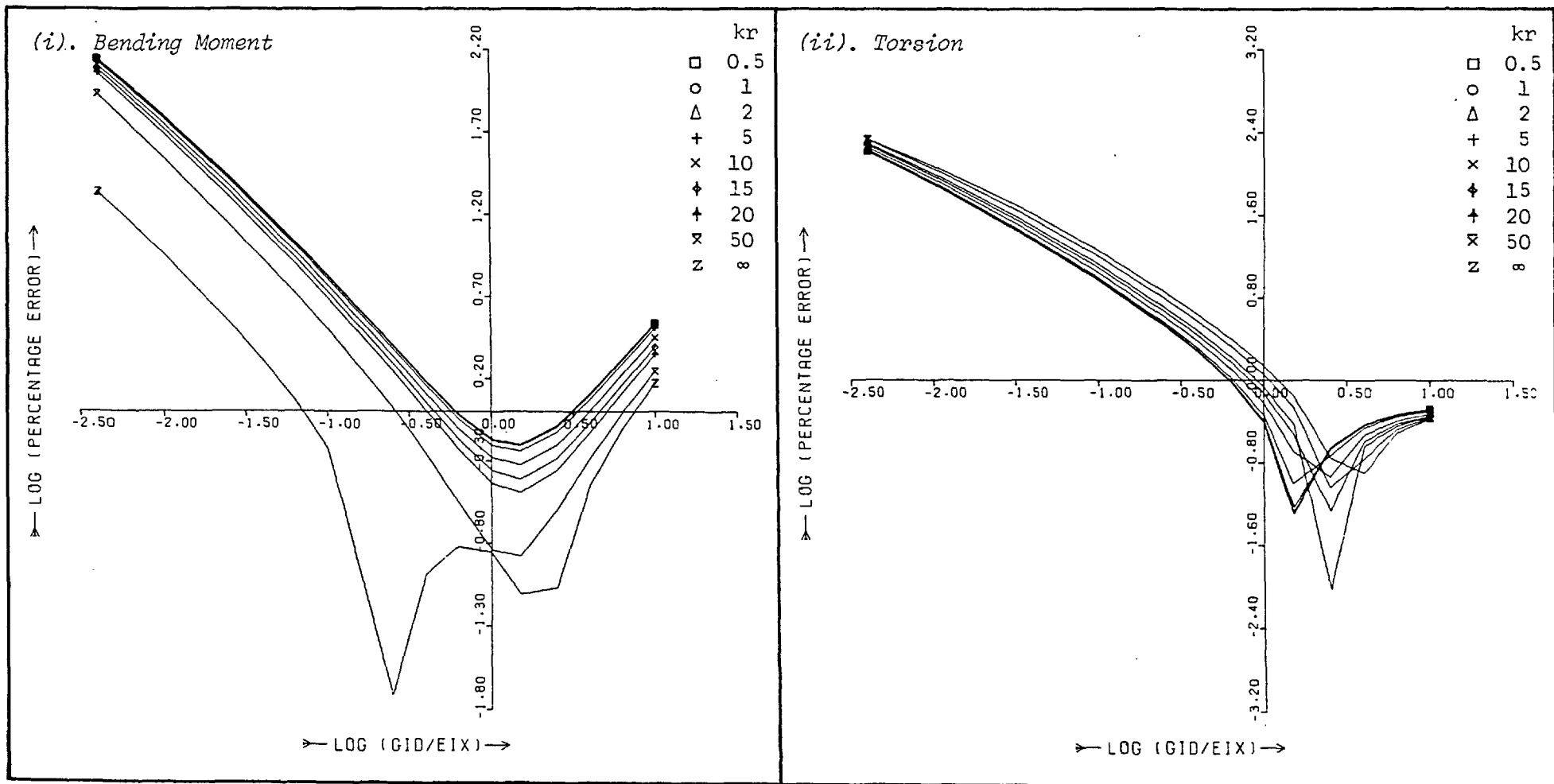
Figure 4.51   Percentage Error in (i). Bending Moment and (ii). Torsion due to neglecting Member Curvature ($\theta = 10°$; $\mu = 0.5$)
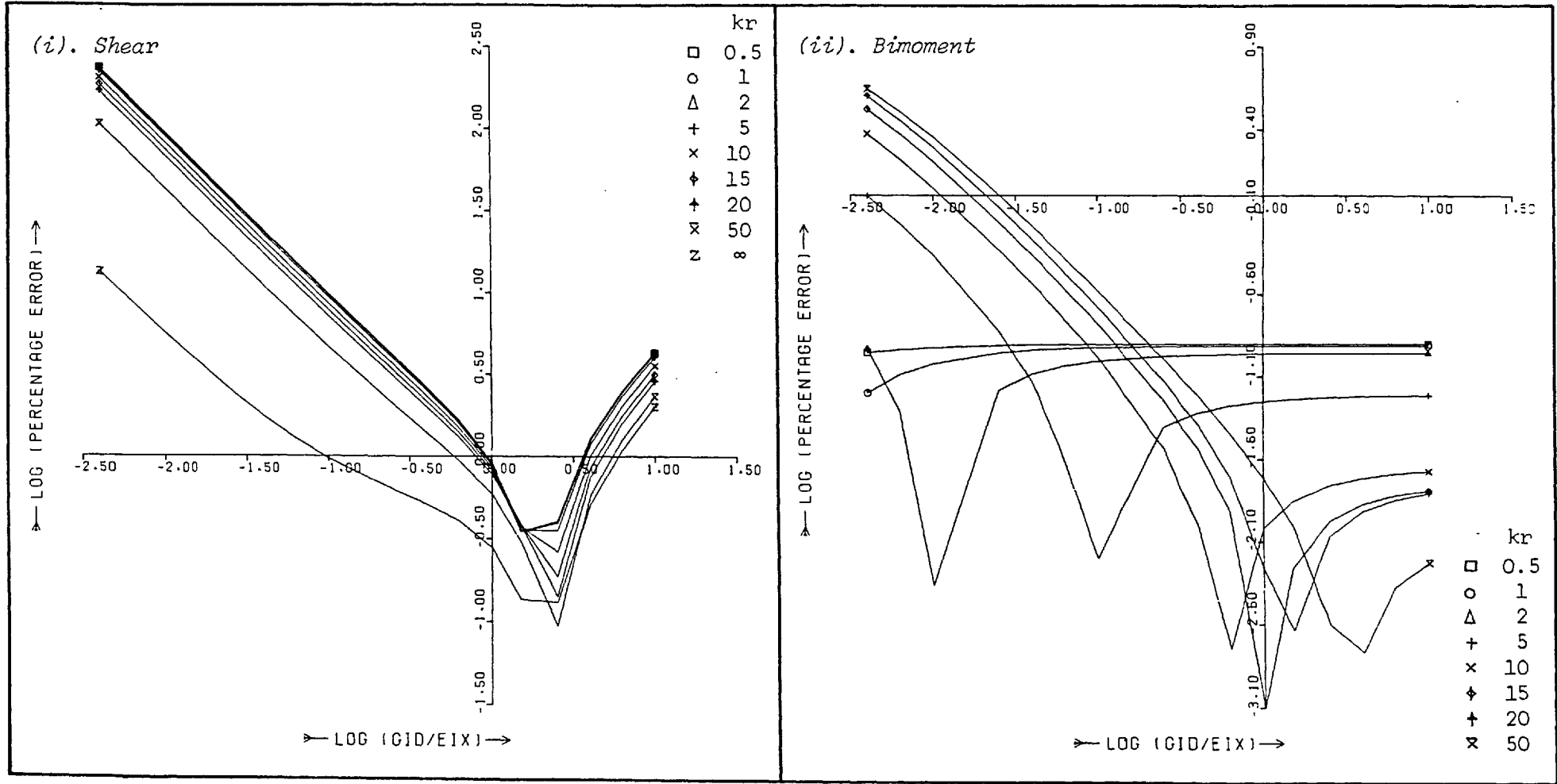
Figure 4.52   Percentage Error in (i). Shear and (ii). Bimoment due to neglecting Member Curvature ($\theta = 10^{\circ}$; $\mu = 0.5$)

(i). Bending Moment

	kr
□	0.5
○	1
Δ	2
+	5
×	10
✦	15
✚	20
x̄	50
z	∞

← LOG (PERCENTAGE ERROR) →

4.00
3.20
2.40
1.60
0.80
0.00
-0.80
-1.60
-2.40

-2.50 -2.00 -1.50 -1.00 -0.50 0.00 0.50 1.00 1.50

►— LOG (GID/EIX) →

(ii). Torsion

	kr
□	0.5
○	1
Δ	2
+	5
×	10
✦	15
✚	20
x̄	50
z	∞

← LOG (PERCENTAGE ERROR) →

3.20
2.40
1.60
0.80
0.00
-0.80
-1.60
-2.40
-3.20

-2.50 -2.00 -1.50 -1.00 -0.50 0.00 0.50 1.00

►— LOG (GID/EIX) →
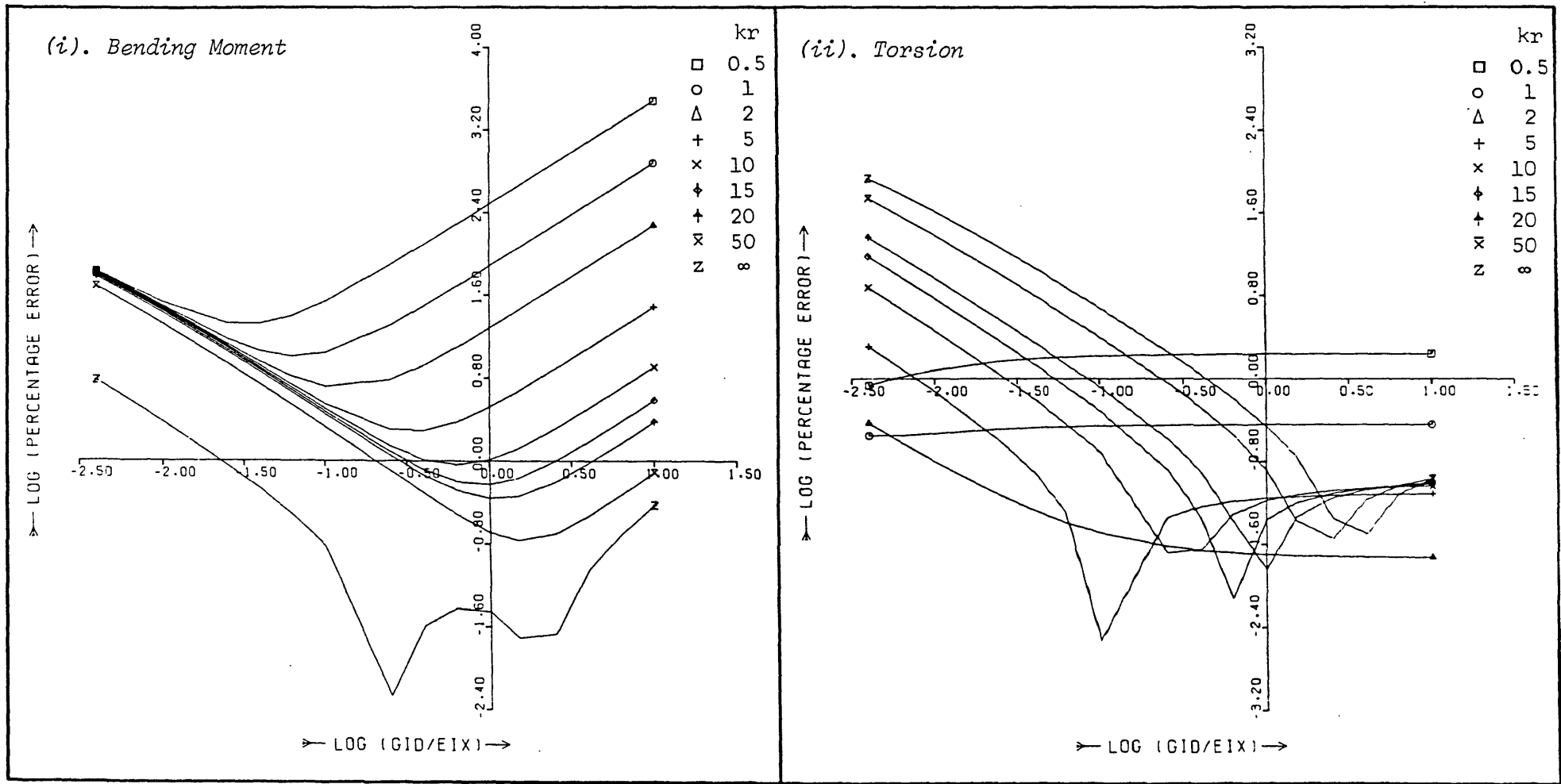
Figure 4.53 Percentage Error in (i). Bending Moment and (ii). Torsion due to neglecting Member Curvature $(\theta = 5°; \mu = 1)$
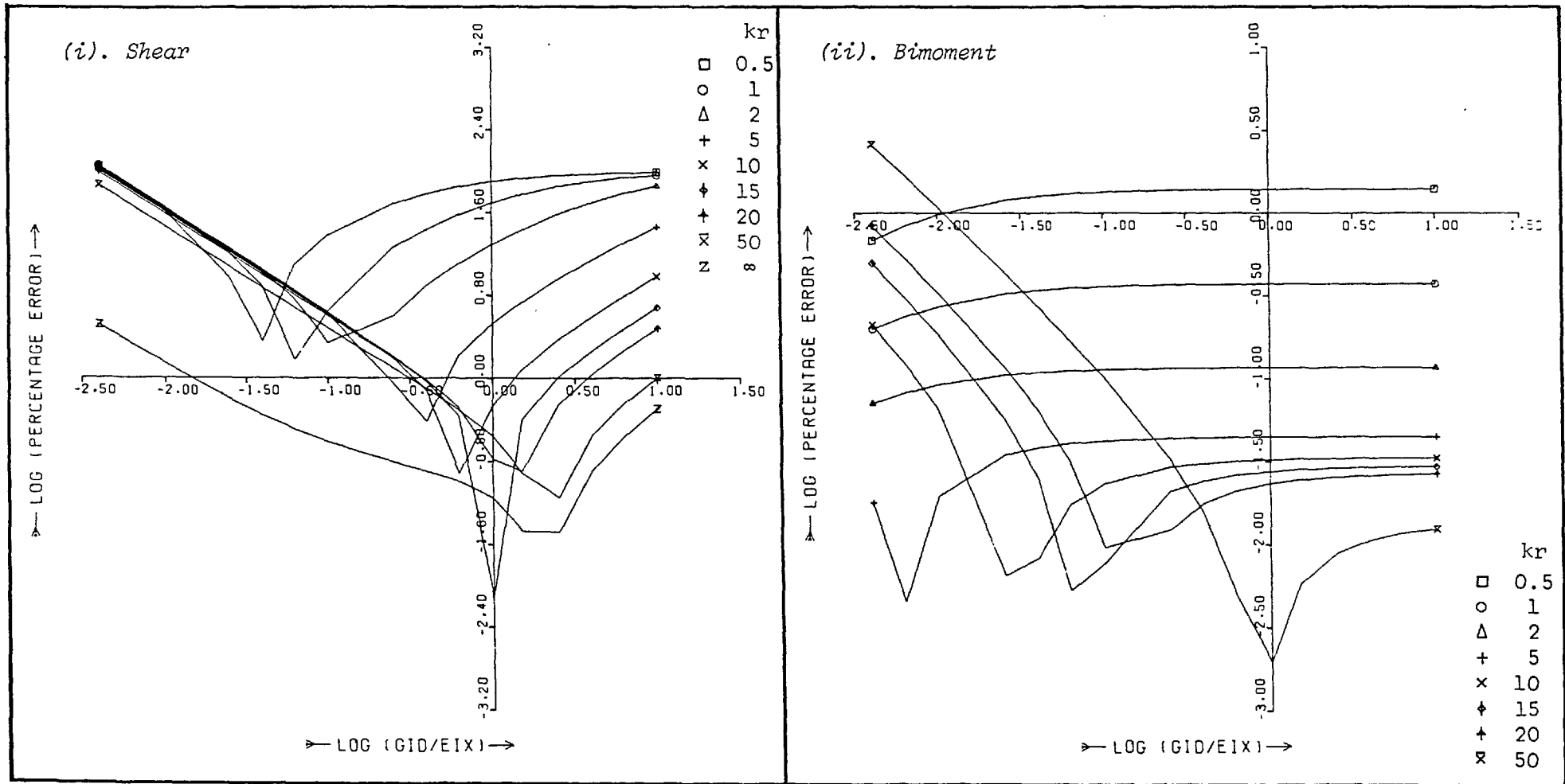
Figure 4.54   Percentage Error in (i). Shear and (ii). Bimoment due to neglecting Member Curvature (θ = 5°; μ = 1)
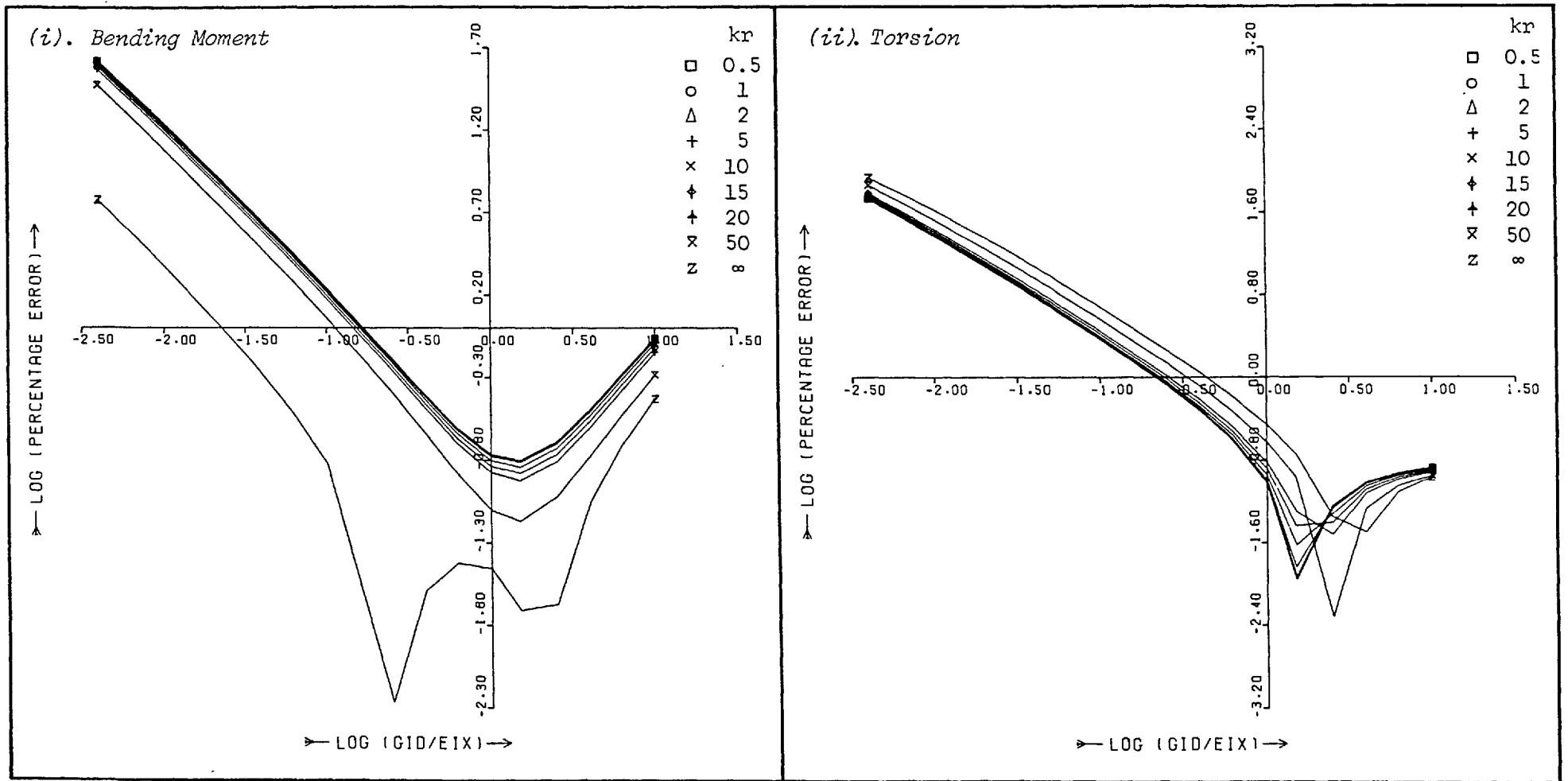
Figure 4.55 Percentage Error in (i). Bending Moment and (ii). Torsion due to neglecting Member Curvature ($\theta = 5^{\circ}$; $\mu = 0.5$)
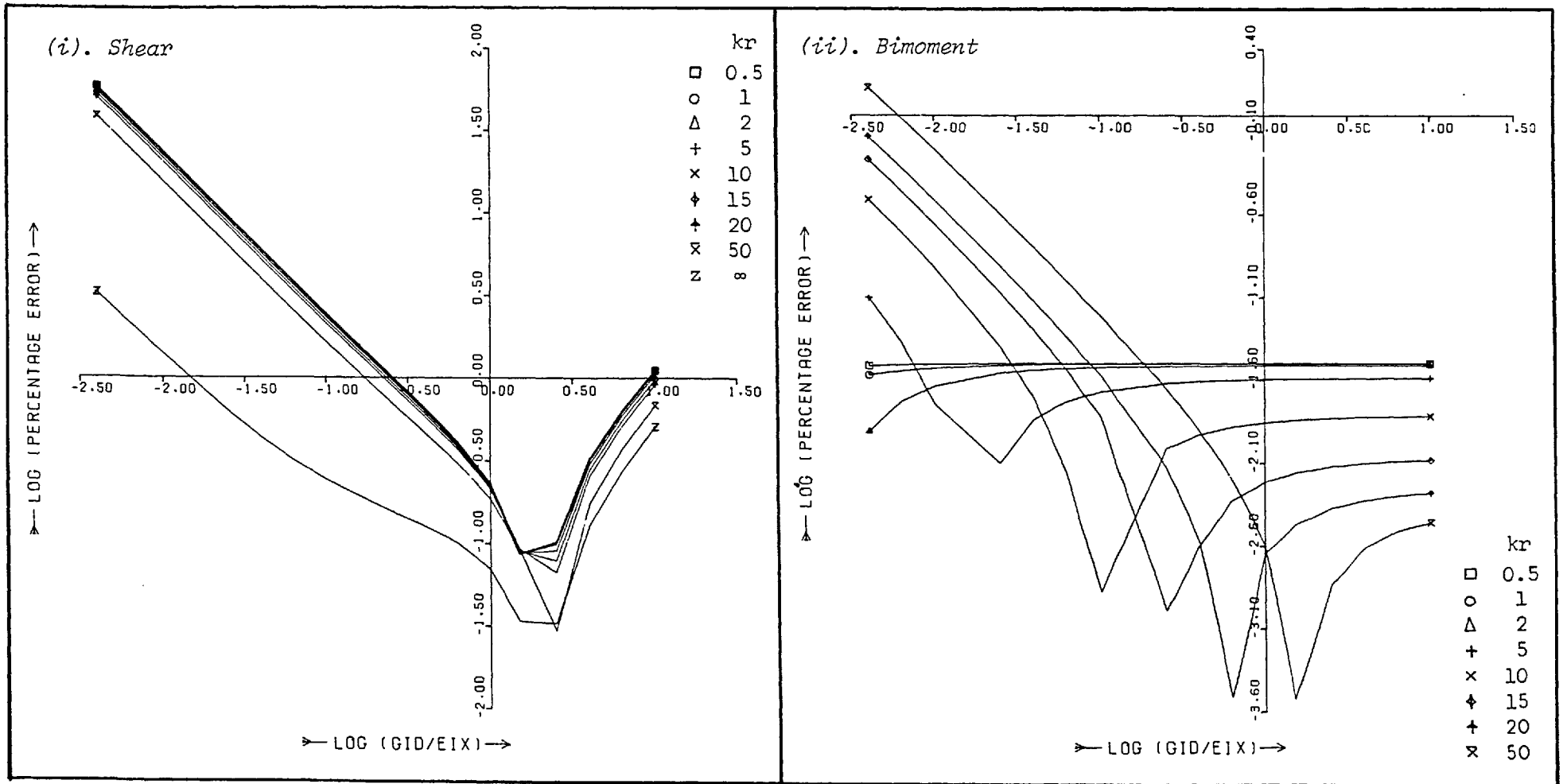
Figure 4.56   Percentage Error in (i). Shear and (ii). Bimoment due to neglecting Member Curvature (θ = 5°; μ = 0.5)
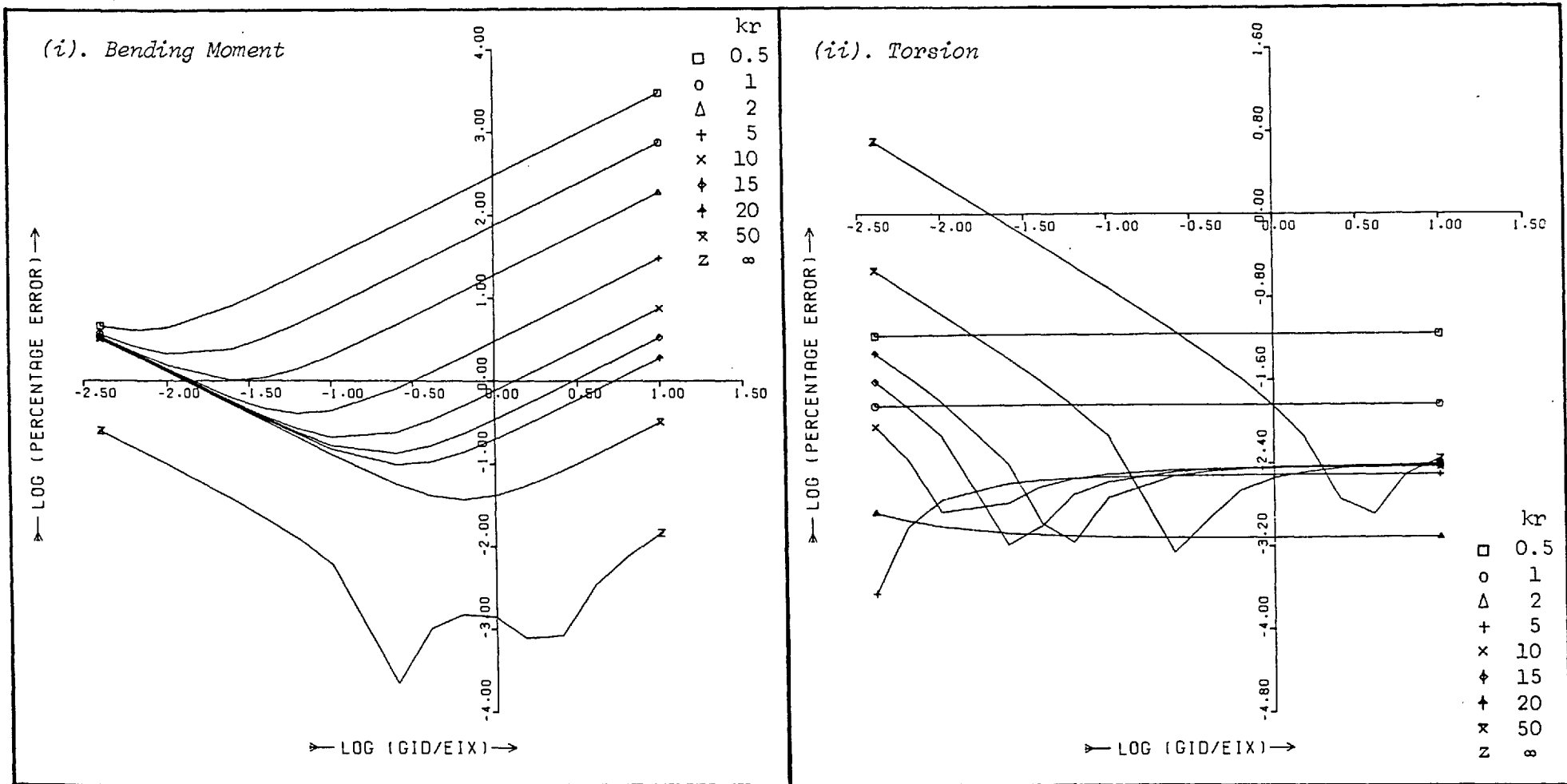
Figure 4.57   Percentage Error in (i). Bending Moment and (ii). Torsion due to neglecting Member Curvature (θ = 1°; μ = 1)

(i). Shear

(ii). Bimoment

← LOG (PERCENTAGE ERROR) →

➤— LOG (GID/EIX) →

	kr
□	0.5
○	1
△	2
+	5
×	10
⧈	15
✚	20
⊠	50
z	∞

	kr
□	0.5
○	1
△	2
+	5
×	10
⧈	15
✚	20
⊠	50
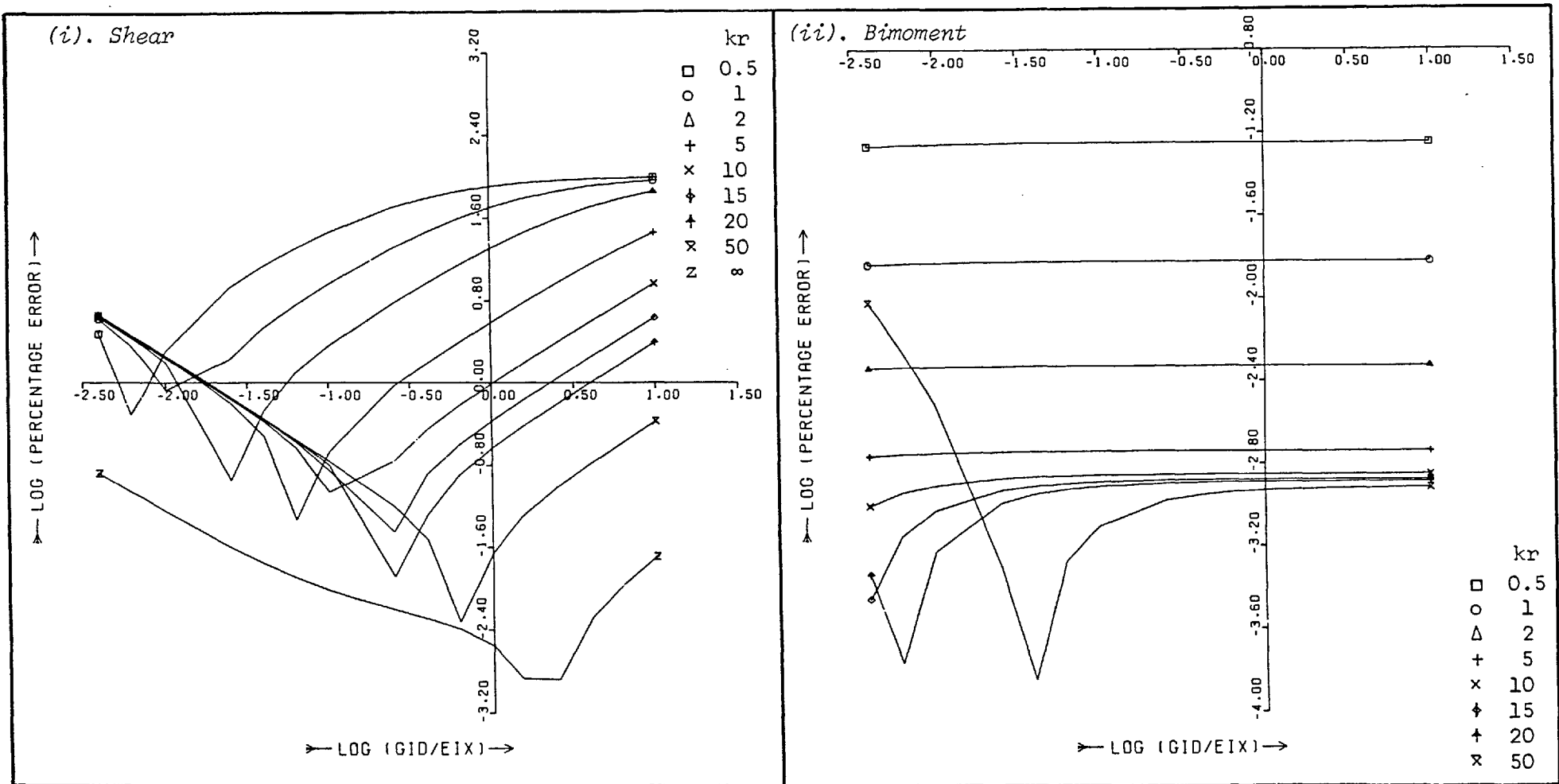
Figure 4.58   Percentage Error in (i). Shear and (ii). Bimoment due to neglecting Member Curvature ($\theta = 1°$; $\mu = 1$)

(i). Bending Moment
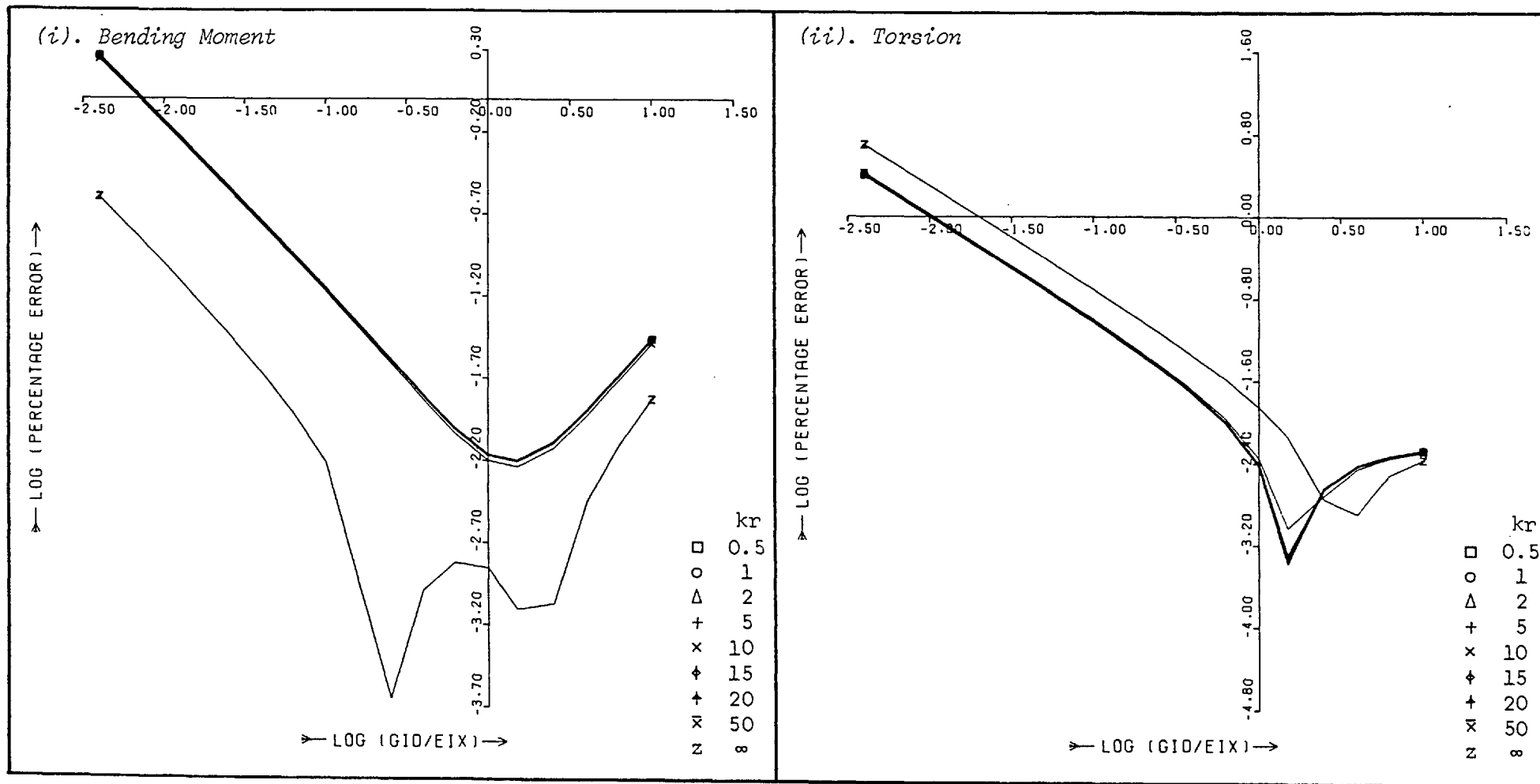
(ii). Torsion

Figure 4.59 Percentage Error in (i). Bending Moment and (ii). Torsion due to neglecting Member Curvature ($\theta = 1^\circ$; $\mu = 0.5$)
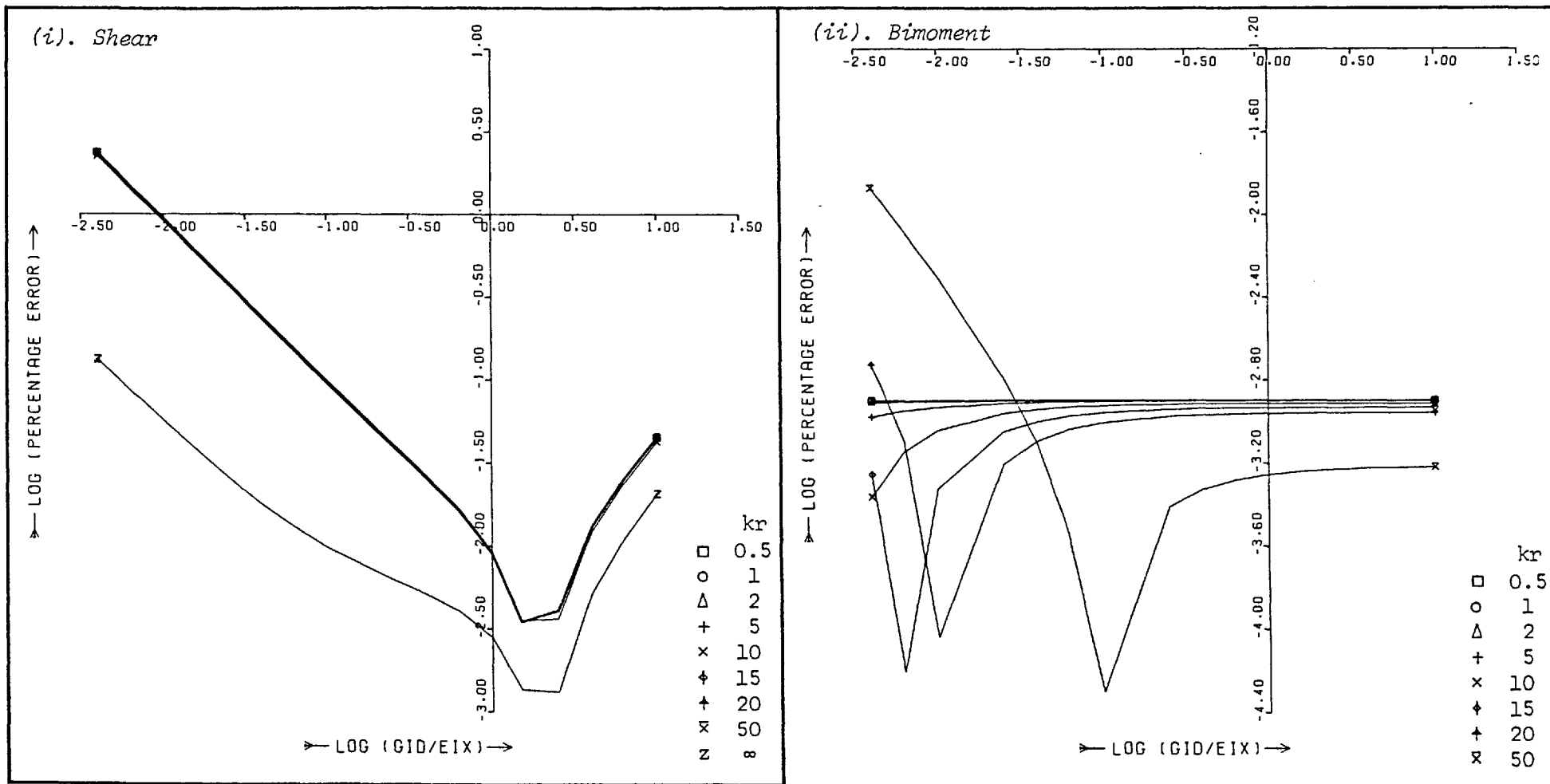
Figure 4.60   Percentage Error in (i). Shear and (ii). Bimoment due to neglecting Member Curvature (θ = 1°; μ = 0.5)

	No. of beams in central span	Outer Spans			Central Span		
		Outside Lane Loaded	Central Lane Loaded	Inside Lane Loaded	Outside Lane Loaded	Central Lane Loaded	Inside Lane Loaded
Moment	2	1.77	1.13	0.47	3.26	4.32	5.28
	4	1.02	0.88	0.71	0.58	0.93	1.24
	8	0.78	0.79	0.78	0.19	0.26	0.33
	16	0.71	0.76	0.81	0.11	0.11	0.11
Torsion	2	1.36	52.58	1.68	0	0	0
	4	0.36	13.03	0.40	0	0	0
	8	0.06	0.22	0.01	0	0	0
	16	0.06	3.15	0.13	0	0	0
Shear	2	1.55	1.13	0.46	0	0	0
	4	0.81	0.87	0.71	0	0	0
	8	0.60	0.77	0.78	0	0	0
	16	0.50	0.75	0.80	0	0	0
Bimoment	2	0.31	52.51	0.38	42.62	185.30	89.79
	4	0.08	13.04	0.09	14.20	58.64	27.05
	8	0.01	0.17	0.01	4.56	16.59	6.61
	16	0.01	3.29	0.03	1.94	5.23	1.11

Table 4.11   Percentage Errors in Stress Resultants obtained

from different Structural Idealizations

Since the numerical value of j^2 is known for this particular structure, the general error functions described in figs. 4.45 - 4.60 may be presented in a more convenient form.   These are shown in figs. 4.61 - 4.64 for the actions of bending moment, torsion, shear and bi-moment, respectively, where the horizontal axis now represents the

variable central angle ($\theta = 1^{o} - 40^{o}$). Estimates of the percentage error

in each component of member stiffness have subsequently been determined

for the various structural idealizations comprising either 16, 8, 4 or 2

straight beam elements in the central span (*i.e.* for $\theta = 4^{o}$, 8°, 16° or

32°). These results are tabulated in Table 4.12 for two different

values of the dimensionless decay function kr in each case. The first

value, kr = 6, has been determined from the actual cross-sectional

properties given in Table 4.8, while the second, kr = ∞, assumes solid

beam properties.

Wide discrepancies between the results presented in Tables 4.11

and 4.12 are apparent but must be expected. In the first of these

tables the recorded errors relate to differences in the computed values

of the various stress resultants, whereas in the second, the tabulated

quantities represent the errors in each component of member stiffness.

In determining the stress resultants, the structure is considered as an

assemblage of end-connected members which, due to the support conditions

and general arrangement, is subject to a complex system of combined

loads. On the other hand, the components of member stiffness are

calculated independently of each other for the fully fixed member shown

in fig. 4.37.

The largest errors in the computed values of bending moment and

bimoment occurred for the three load cases applied to the central span,

Table 4.11. Although the maximum error in bending moment was only

approximately 5% (between the idealizations alternatively comprising

two curved and two straight members), the percentage error in bimoment

was significantly larger. Variations in results due to the different

structural idealizations are more clearly visible over the length of the

structure in figs. 4.35 and 4.36. As expected, there was no discrepancy
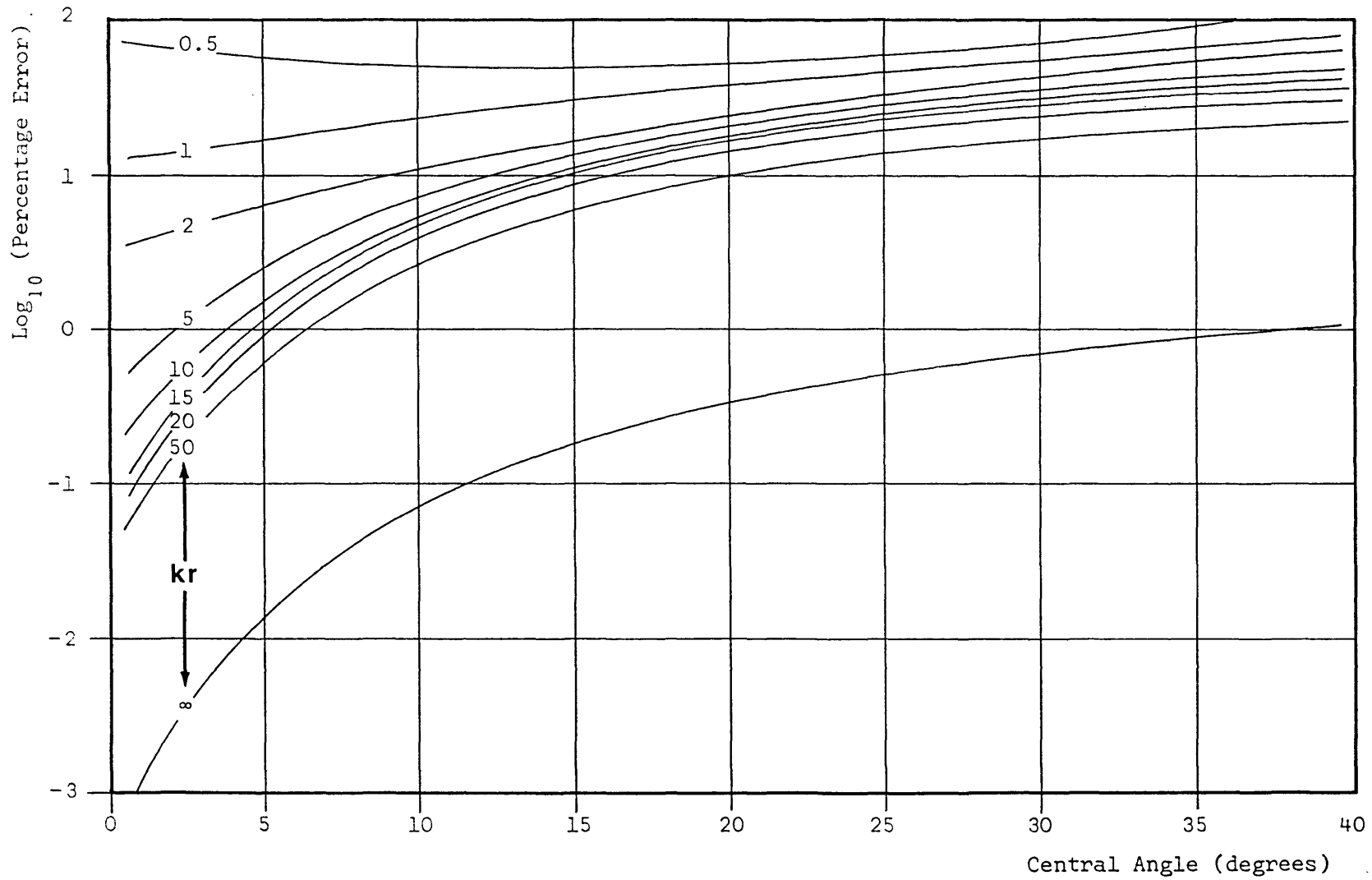
Figure 4.61   Percentage Error in Bending Stiffness in the Composite Road Bridge
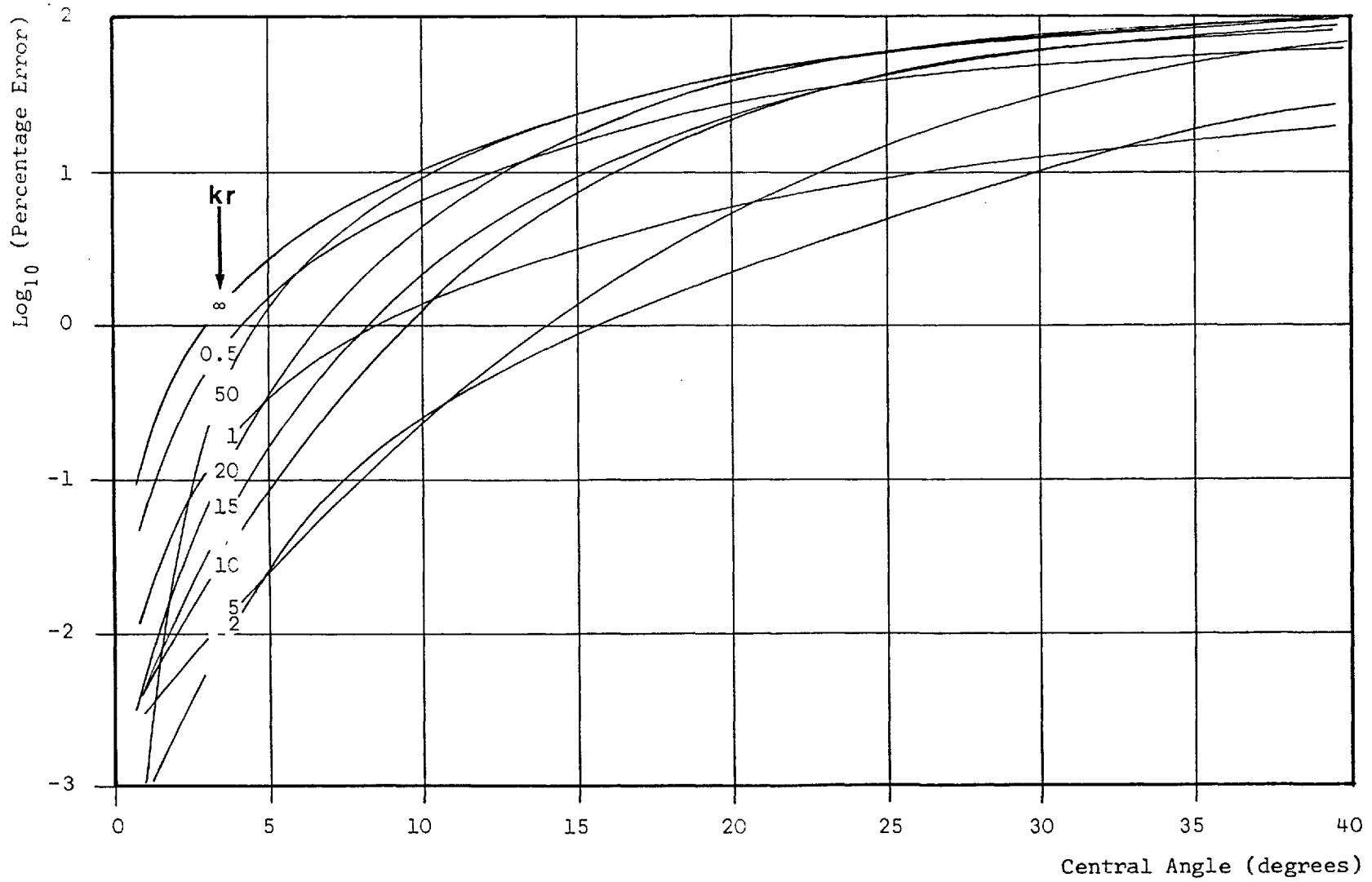
Figure 4.62   Percentage Error in Torsional Stiffness in the Composite Road Bridge
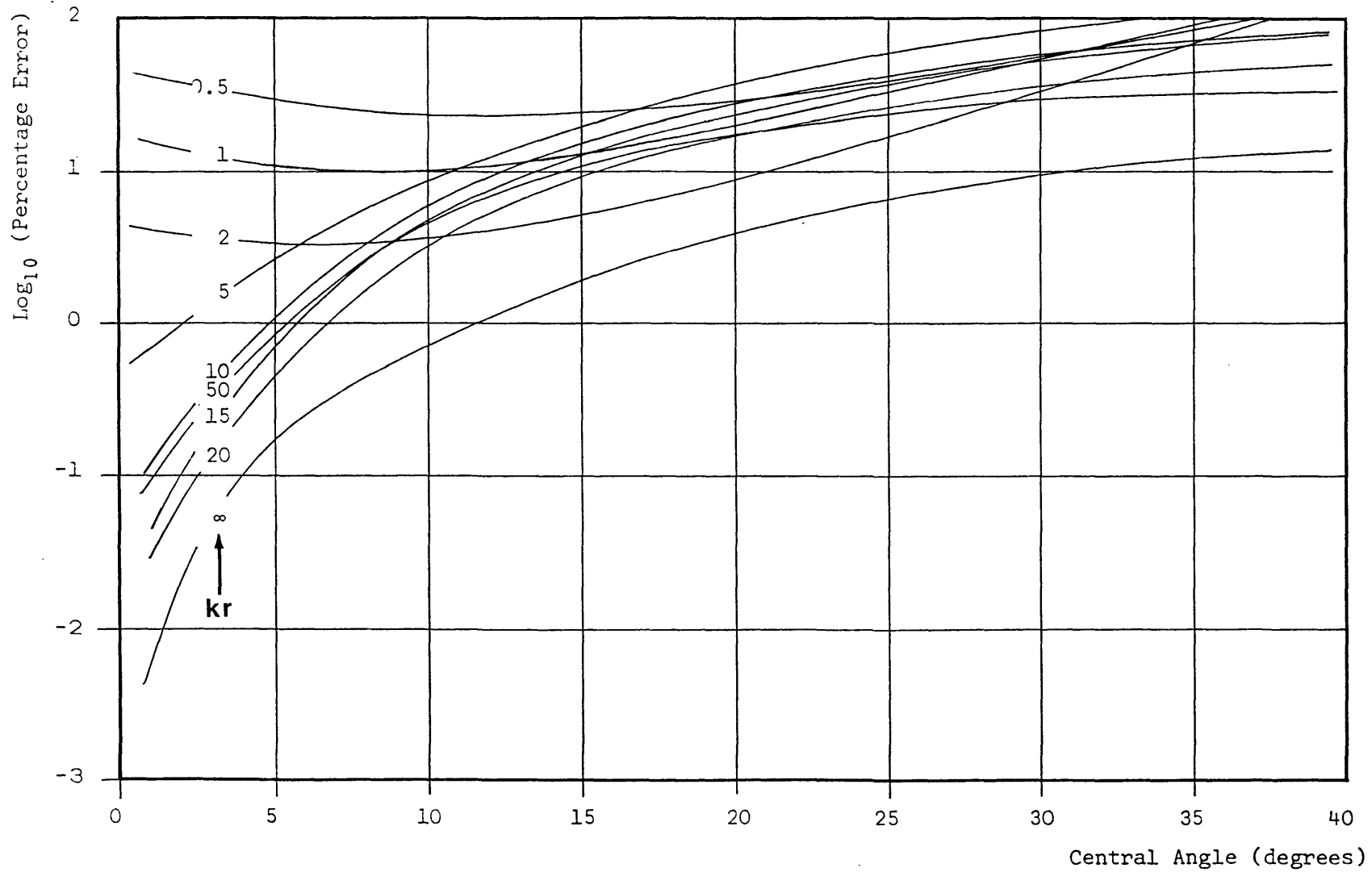
Figure 4.63 Percentage Error in Shear Stiffness in the Composite Road Bridge
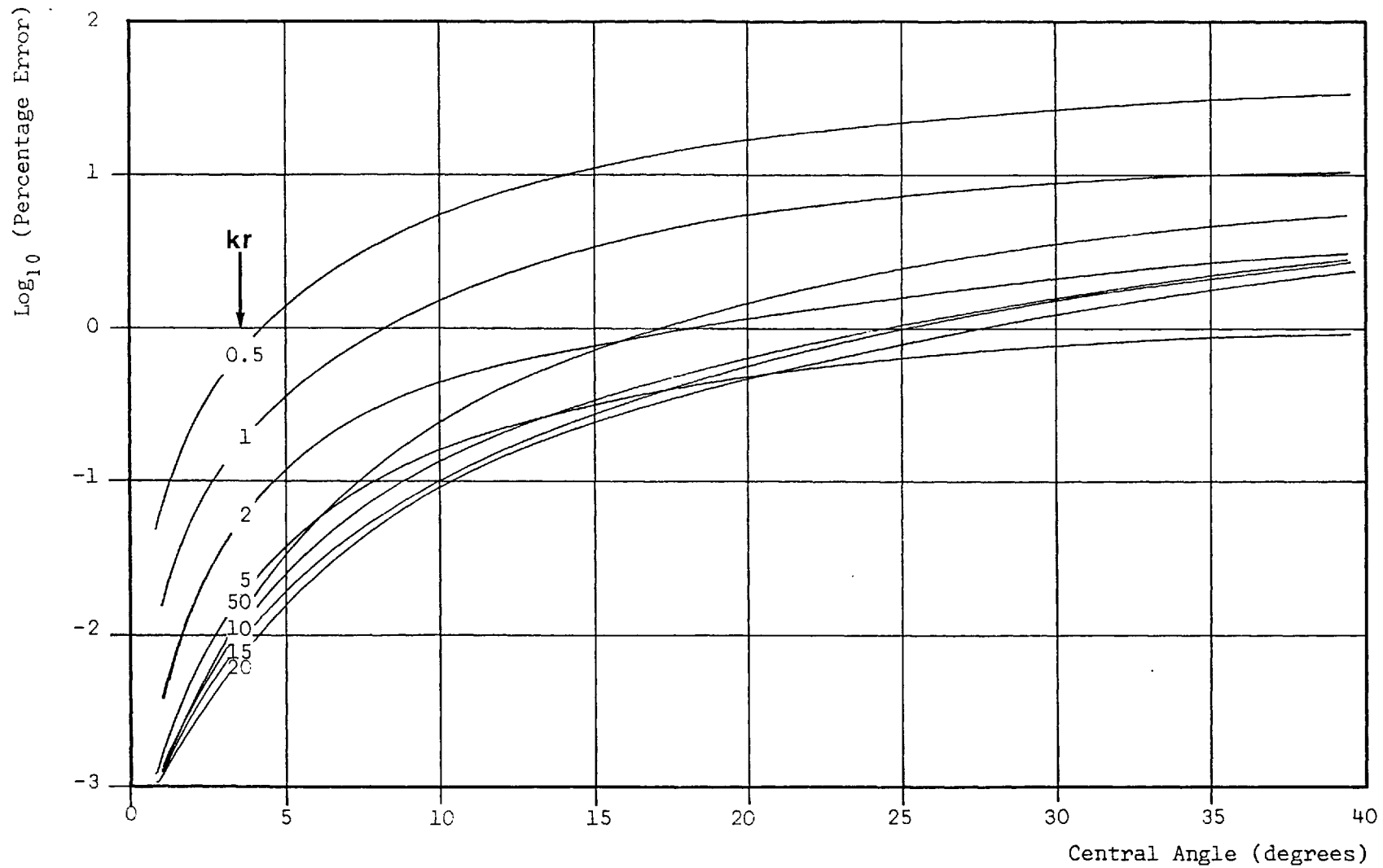
Figure 4.64   Percentage Error in Warping Stiffness in the Composite Road Bridge

No. of beams in central span	Estimated Error (%)	
	kr = 6	kr = ∞
Moment 2	39.81	0.79
4	14.13	0.20
8	4.47	0.04
16	1.78	0.01
Torsion 2	44.67	79.43
4	2.51	28.18
8	0.16	6.31
16	0.02	1.78
Shear 2	79.43	11.22
4	17.78	2.24
8	5.01	0.45
16	1.58	0.10
Bimoment 2	1.00	—
4	0.35	—
8	0.09	—
16	0.02	—

Table 4.12 Estimated Error in the Computation of Member Stiffness for different Structural Idealizations

in the computed values of shear and torsion for the symmetrical point loads. However, this was not the case for loads applied to the outer span, although the percentage errors were generally very much smaller than the corresponding differences in member stiffness.

In conclusion, the percentage errors in the computed values of bimoment and bending moment were respectively under- and over-estimated by the error functions calculated in accordance with eqn. 4.7.

In general, these functions provided a better estimate of the errors in bending moment and shear when solid beam properties were assumed; the opposite was true for torsional effects. Differences between results recorded in Tables 4.11 and 4.12 are primarily due to the impracticability of taking the non-diagonal coefficients from the member stiffness matrix into consideration during the formulation of the stiffness error function. Thus, the large apparent changes in member stiffness brought about by adopting a straight beam idealization are often due almost entirely to the different mechanics of load transference. Accordingly these changes will not necessarily be reflected in the computed values of the various stress resultants in any practical application.

4.4.2   Errors due to neglecting Warping Effects

By neglecting thin-walled behaviour, computational effort necessary for solution can be significantly reduced. Further economies are possible in the analysis of curved members if these can be alternatively represented by one or more straight beam elements in which warping effects are also neglected. Therefore, as a first step in this investigation, the differences in stiffness between the curved, thin-walled member and the straight, solid member have been calculated. The term k_{ii}^* in the error function (defined in eqn. 4.7) now represents the ith diagonal coefficient in the stiffness matrix for the equivalent straight member with solid beam properties. However, since warping effects have been disregarded, only the components of bending, shear and torsional stiffness can be included in the study. Moreover, the error functions corresponding to shear force are identical to those previously determined in §4.4.1 and thus only bending and torsional stiffness need be considered.

- 304 -

The necessary error functions are presented in figs. 4.65 - 4.72 with the various identifying parameters covering the same numerical range as before. Subsequently, this has enabled the variations in stiffness to be determined due to the idealization of the composite road bridge previously detailed in §4.3. The appropriate values of the dimensionless terms j^2, kr for this structure are given in Table 4.8, and the results from this investigation are tabulated in Table 4.13 for kr = 6 and kr = ∞, as before.

In comparison with the results from Table 4.12, in which the effects of warping have been fully considered, there is little apparent change in bending stiffness in the case of the actual decay function (kr = 6). However, in all other instances, large variations are evident between results from the two tables. This is particularly noticeable in the case of the torsional component which further demonstrates the very different mechanics of torque resistance when thin-walled effects are considered.

No. of beams in central span	Estimated Error (%)	
	kr = 6	kr = ∞
Moment	2	35.48	11.22
	4	14.13	5.62
	8	3.98	2.00
	16	1.00	0.56
Torsion	2	31.62	35.48
	4	70.79	9.55
	8	79.43	19.95
	16	89.13	47.86

Table 4.13 Estimated Errors in the Computation of Bending and Torsional Stiffness (neglecting Warping Effects)
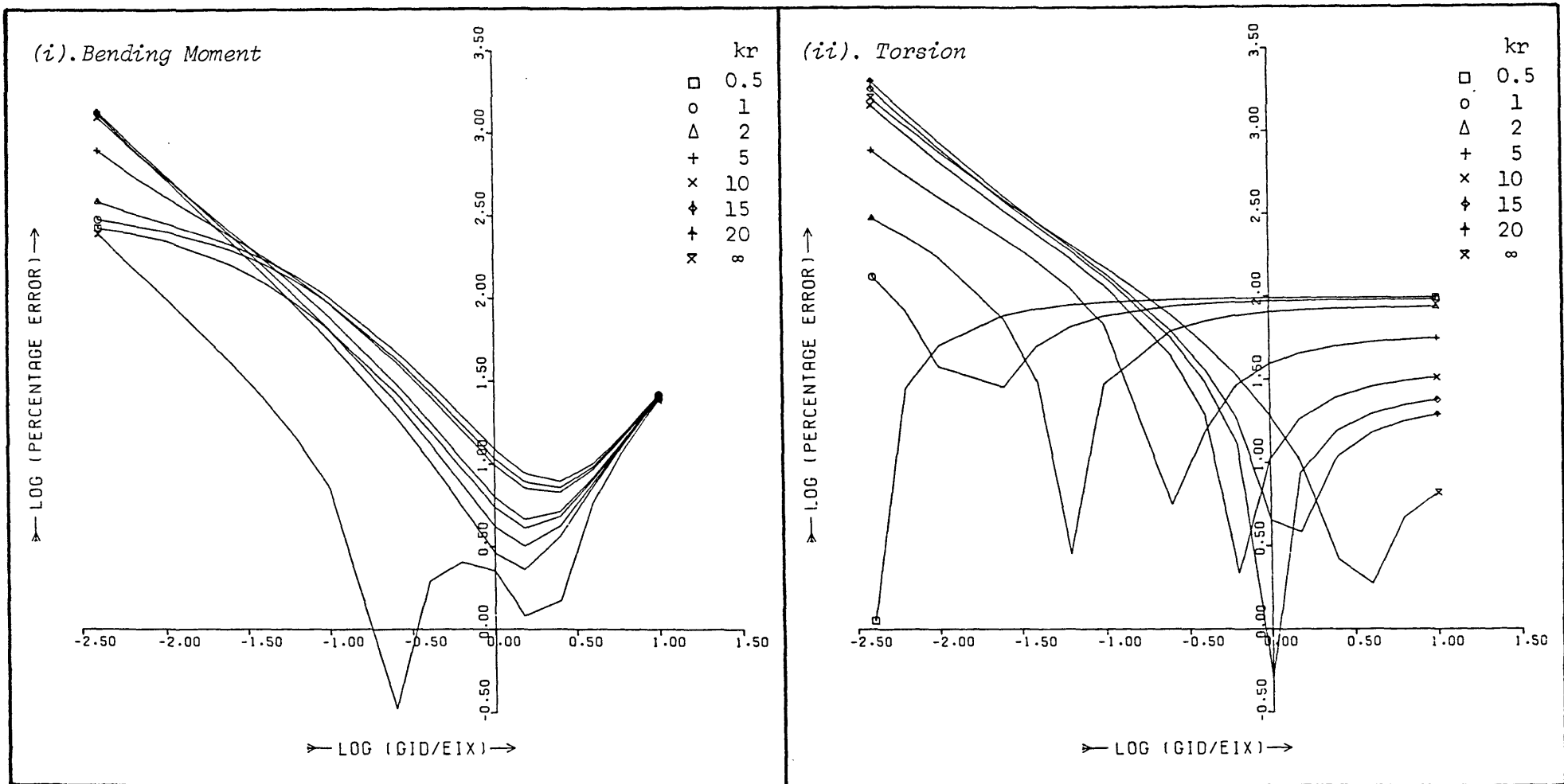
Figure 4.65 Percentage Error in (i). Bending Moment and (ii). Torsion due to neglecting Member Curvature and Warping Effects ($\theta = 40^{\circ}$; $\mu = 1$)
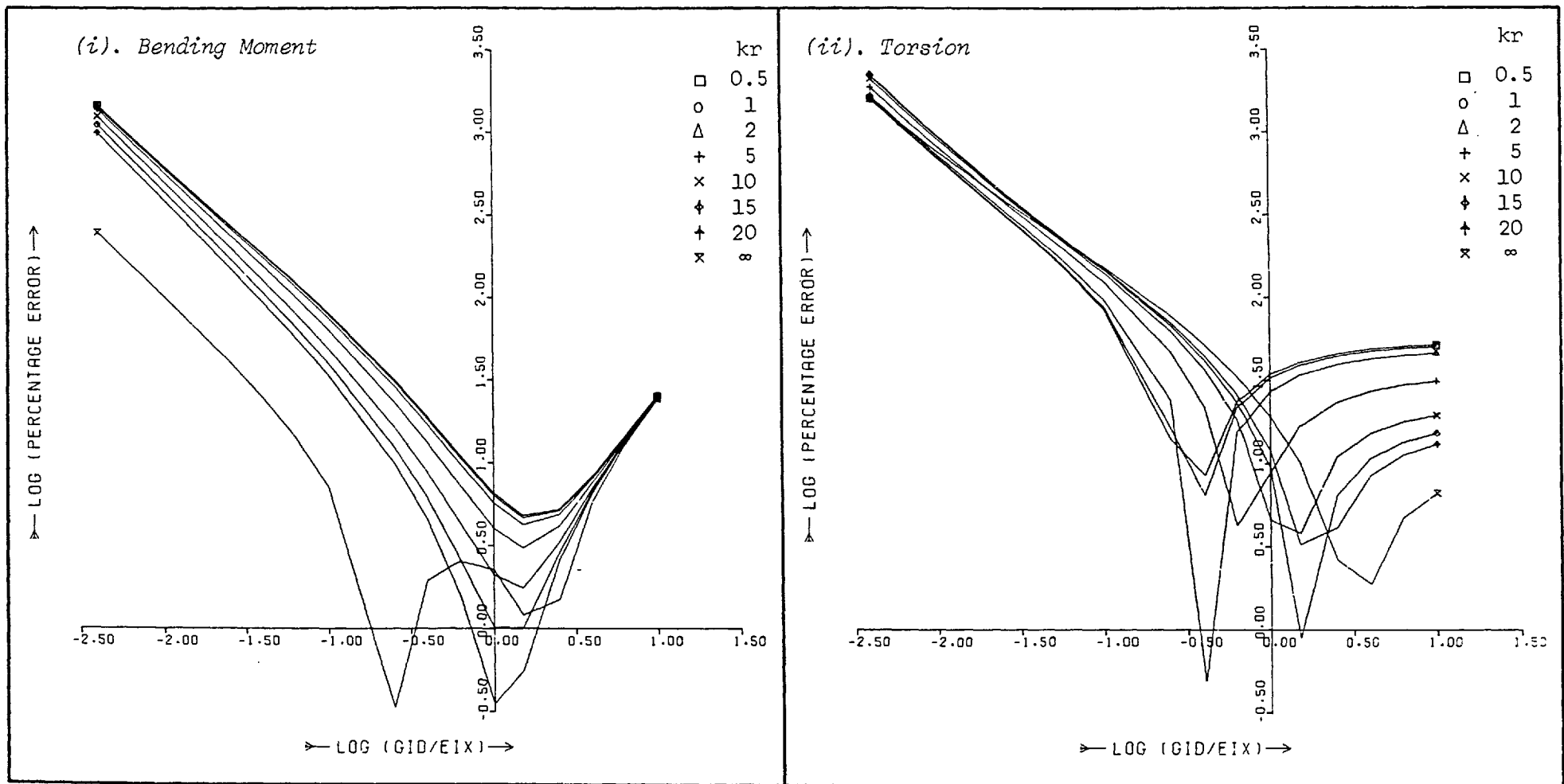
Figure 4.66   Percentage Error in (i). Bending Moment and (ii). Torsion due to neglecting Member Curvature and Warping Effects (θ = 40°; μ = 0.5)
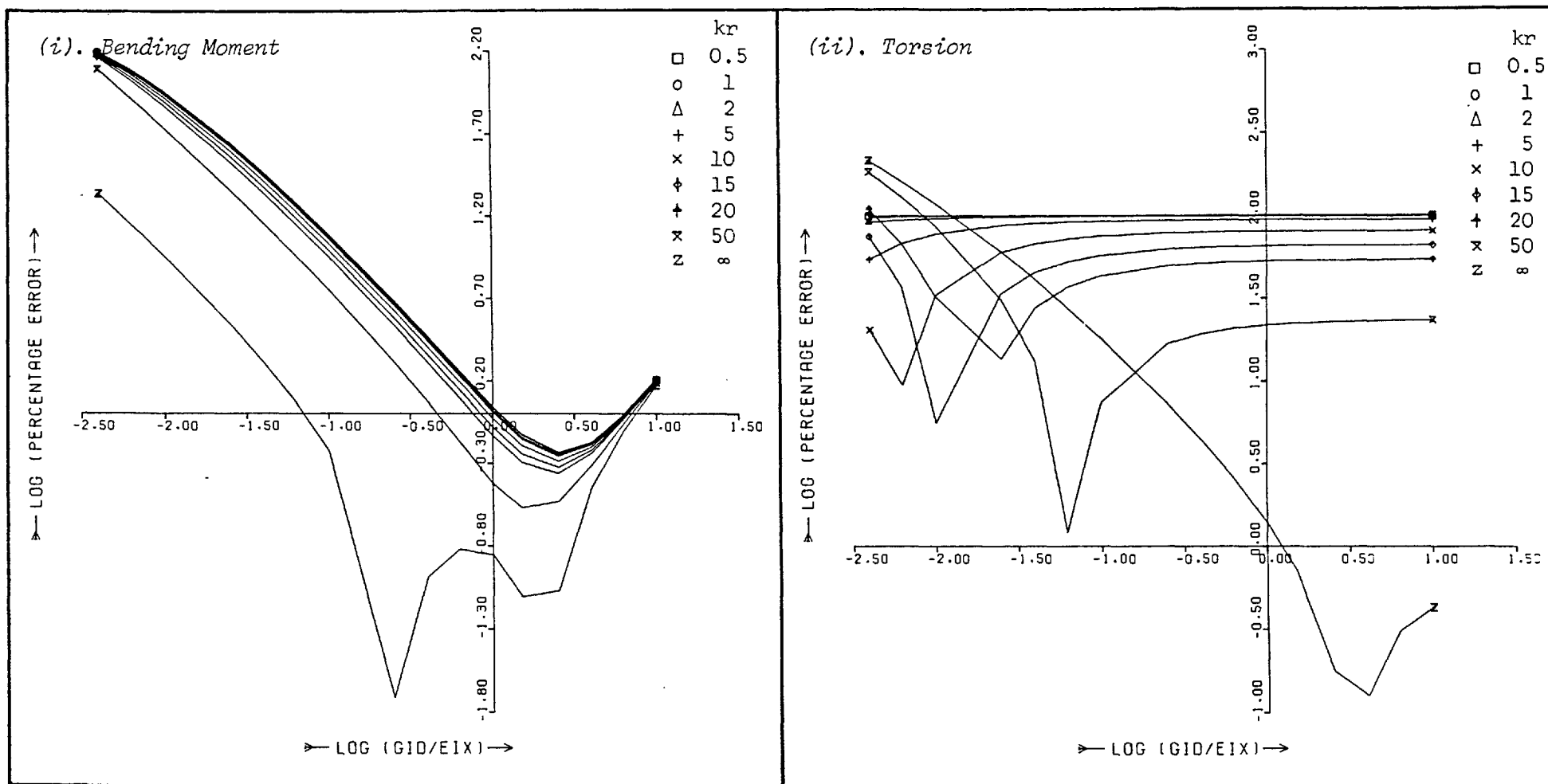
Figure 4.67   Percentage Error in (i). Bending Moment and (ii). Torsion due to neglecting Member Curvature and Warping Effects $(\theta = 10^{\circ}; \mu = 1)$
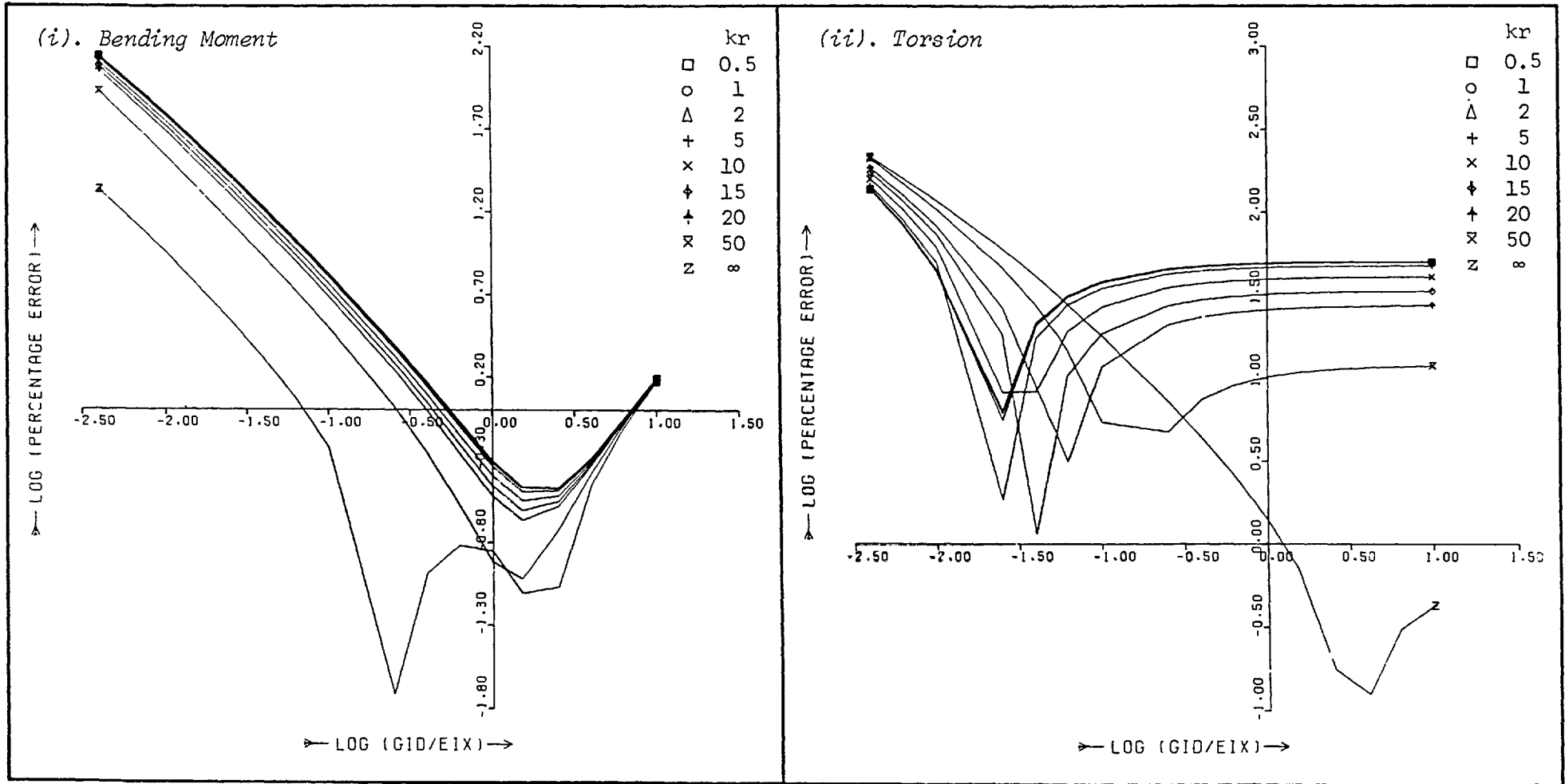
Figure 4.68   Percentage Error in (i). Bending Moment and (ii). Torsion due to neglecting Member Curvature and Warping Effects ($\theta = 10°$; $\mu = 0.5$)
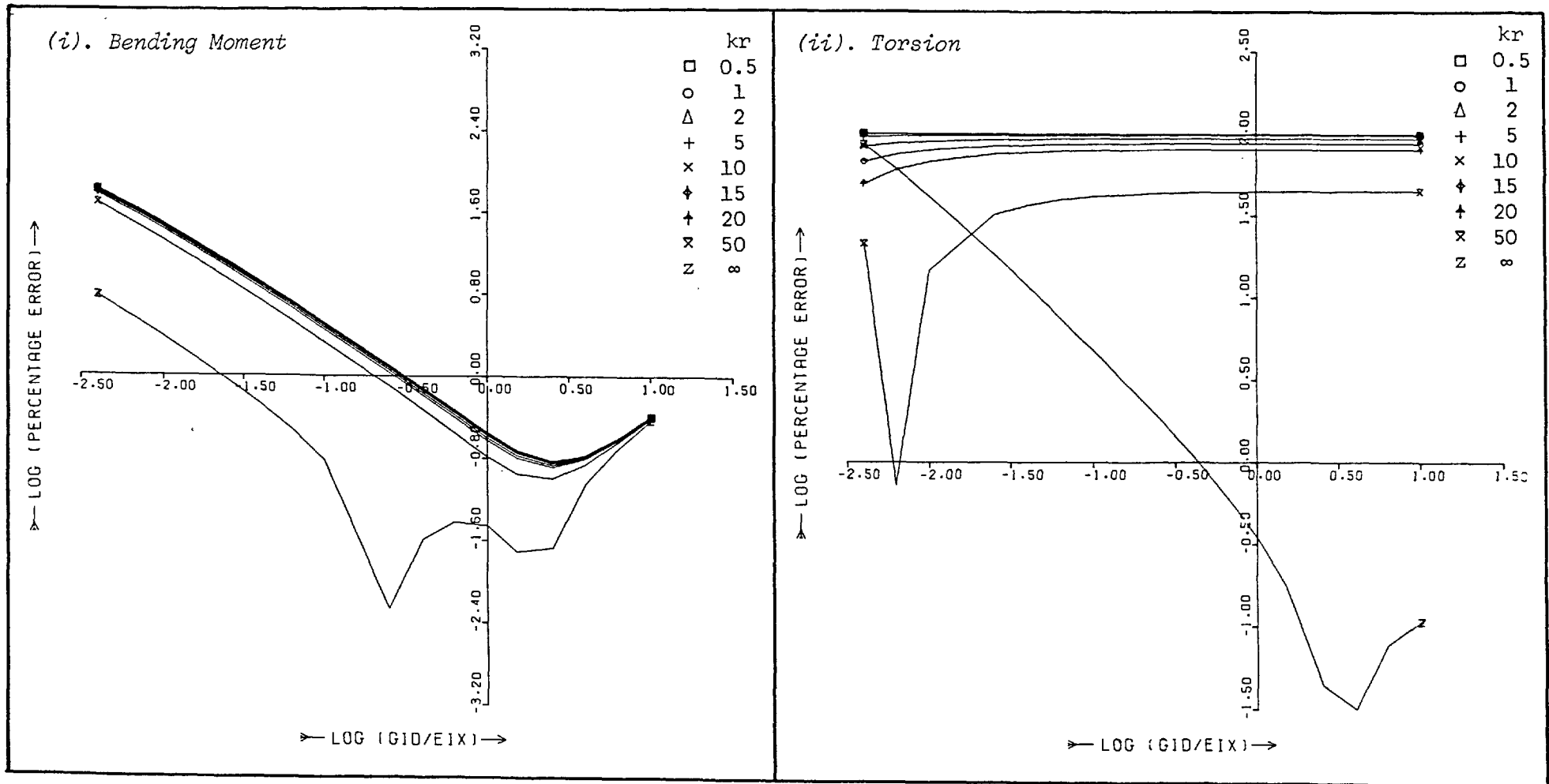
Figure 4.69   Percentage Error in (i). Bending Moment and (ii). Torsion due to neglecting Member Curvature and Warping Effects ($\theta = 5^{\circ}$; $\mu = 1$)
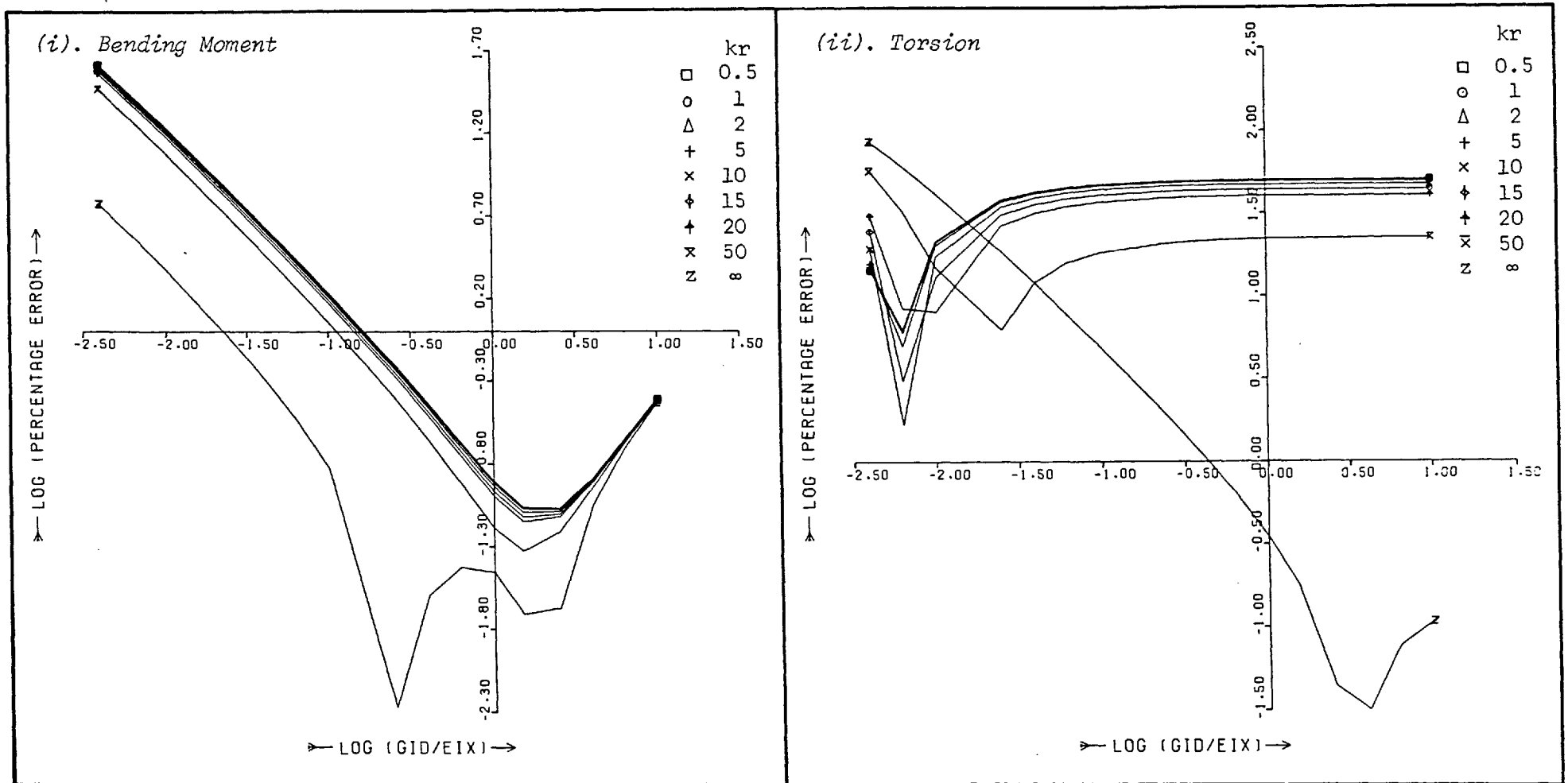
Figure 4.70   Percentage Error in (i). Bending Moment and (ii). Torsion due to neglecting Member Curvature and Warping Effects ($\theta = 5^{\circ}$; $\mu = 0.5$)
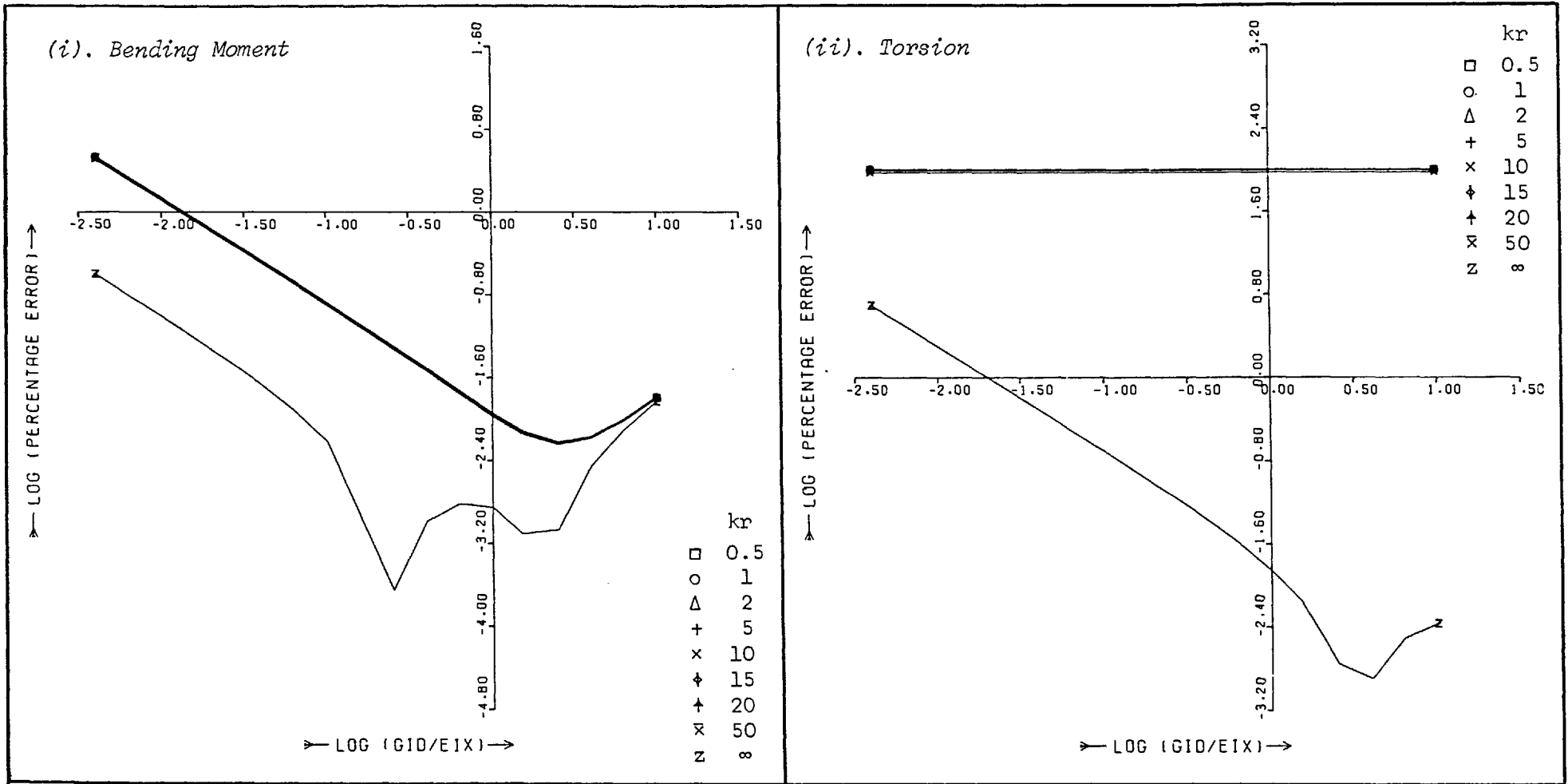
Figure 4.71   Percentage Error in (i). Bending Moment and (ii). Torsion due to neglecting Member Curvature and Warping Effects (θ = 1°; μ = 1)
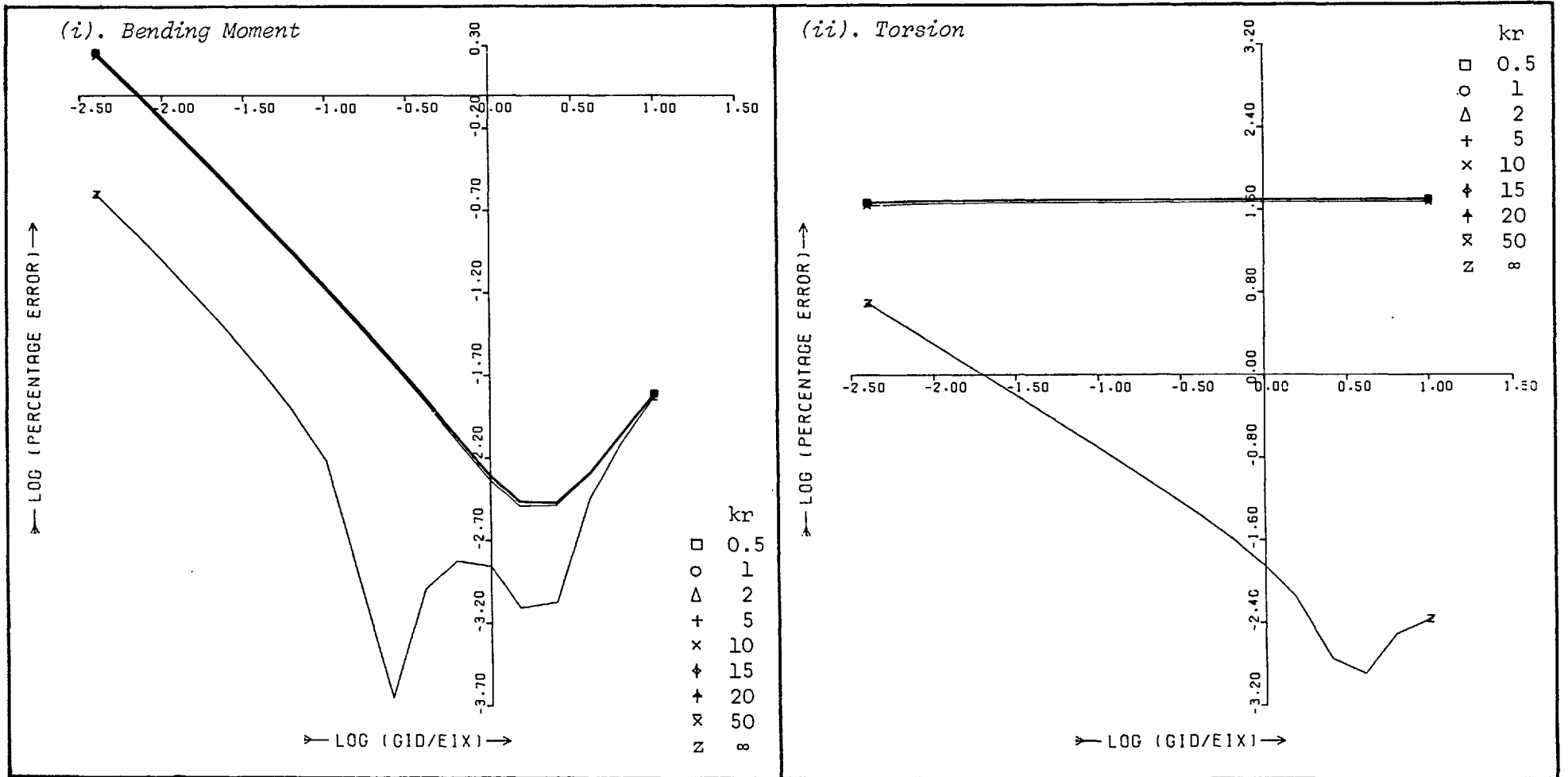
Figure 4.72 Percentage Error in (i). Bending Moment and (ii). Torsion due to neglecting Member Curvature and Warping Effects (θ = 1°; μ =0.5)

The stiffness formulation presented here and in §4.4.1 provides useful information with regard to the variation in individual components of member stiffness. However, since the relative proportions of the various stress resultants are not known for the general case, this method is unable to take account of the non-diagonal terms in the stiffness matrices and thus cannot provide an accurate estimate of the probable errors due to the various structural idealizations. An alternative approach has therefore been adopted whereby the errors introduced by neglecting warping effects can be fully evaluated.

In the analysis of bridge structures, the distribution of direct stress is primarily influenced by only two stress resultants, namely, bending moment about the horizontal axis and bimoment. A realistic appraisal of the effects of bimoment in any particular application may therefore be obtained by formulating an error function from the general direct stress equation (eqn. 2.2), thus:

$$E_\sigma = \left\{ \frac{B.\omega}{I_{\hat{w}}} \middle/ \frac{M.y}{I_x} \right\} \times 100\% \qquad\qquad 4.8$$

This expression represents the magnitude of the direct stress due to the bimoment term as a percentage of that due to the resultant bending moment at the same point.

Although this function can be evaluted everywhere on the cross-section, errors due to neglecting bimoment are usually only important at positions where the section is already highly stressed in bending. Accordingly, only the top and bottom flanges need be considered for which the distances from the neutral axis, y_t, y_b, are usually very nearly constant in each case. Therefore, by determining the maximum value of the sectorial co-ordinate in both the top and bottom flanges, $\hat{\omega}_{t(max)}$, $\hat{\omega}_{b(max)}$, eqn. 4.8 may be redefined in the following way:

$$E_{\sigma t} = \frac{B}{M} \cdot \frac{I_x}{I_{\hat{\omega}}} \cdot \frac{\hat{\omega}_{t(max)}}{y_t} = \frac{B}{M} \cdot F_t \times 100\%$$

$$E_{\sigma b} = \frac{B}{M} \cdot \frac{I_x}{I_{\hat{\omega}}} \cdot \frac{\hat{\omega}_{b(max)}}{y_b} = \frac{B}{M} \cdot F_b \times 100\%$$

$$\left.\begin{array}{c}\\ \\ \\ \\\end{array}\right\} \quad 4.9$$

By utilizing these equations, an estimate of the percentage error due to neglecting warping effects is now obtainable for any value of bimoment and bending moment at a particular section. Furthermore, since the maximum sectorial co-ordinate in each flange is almost invariably matched by a sectorial co-ordinate of approximately equal but opposite magnitude, the resultant error function may be considered as either an increase or reduction in the maximum direct stress due to bending in each flange.

The application of this error analysis is first demonstrated in the case of the bifurcated bridge structure detailed in §4.2. Each of the fourteen lane loads (fig. 4.8) and the single point load previously used in the structural analysis have been considered. For loads applied to the outside spans, the appropriate central cross-section has been selected for investigation. On the other hand, the twin-cell section adjacent to the bifurcation (the right-hand end of member 5 in fig. 4.10) has been used for the five lane loads and the point load applied within the bifurcated span. Maximum percentage errors at each of these sections are given in Table 4.14 for two alternative sets of cross-sectional properties. In the first, the necessary geometrical functions have been calculated assuming straight beam properties whereas, in the second, the curved beam analysis according to Konishi and Komatsu[53] has been used. All the necessary geometrical properties are tabulated in Table 4.2, while the sectorial co-ordinates for both the straight and curved beam representations are shown in fig. 4.73. However, in the error analysis of curved members it is necessary to multiply the error function given in eqn. 4.9 by the term ρ/R. This takes account of the more general

Load Case	Moment (Nm)	Bimoment $(Nm^2 \times 10^{-3})$	Straight Properties		Curved Properties	
			$E_{\sigma t}(\%)$	$E_{\sigma b}(\%)$	$E_{\sigma t}(\%)$	$E_{\sigma b}(\%)$
1	35.19	40.73	4.9	4.5	5.0	4.5
2	34.98	24.99	3.0	2.8	3.1	2.8
3	34.71	94.62	11.5	10.6	11.9	10.7
4	34.25	167.68	20.7	19.1	21.3	19.2
5	44.66	64.65	6.1	5.7	6.3	5.7
6	38.87	31.15	3.4	3.1	3.5	3.1
7	8.14	20.21	10.5	9.7	10.8	9.7
8	36.54	116.93	13.5	12.5	13.9	12.5
9	33.08	149.72	19.1	17.7	19.7	17.7
10	34.62	1.56	0.7	0.2	0.7	0.2
11	34.05	18.62	7.8	2.4	8.6	2.5
12	33.14	39.81	17.2	5.2	18.8	5.5
13	31.67	20.58	13.6	2.6	14.5	2.6
14	34.60	1.10	0.7	0.1	0.7	0.1
point load	30.57	112.52	15.5	14.4	16.0	14.4

Table 4.14   Maximum Percentage Error in Direct Stress due to neglecting the Effects of Warping in the Bifurcated Bridge

expression for direct stress given in eqn. 2.82.   In this case, the position of the maximum value of the factor F may no longer be obvious from inspection and will frequently have to be obtained by computing its value at several critical points on each flange.

The straight and curved beam properties are very similar and this is reflected in the results given in Table 4.14.   For loads applied to the outer spans, the resultant bimoments are most significant for the lanes on the outside curve in each case (lanes 4, 12 and 13).   The percentage errors due to neglecting these warping restraint stresses are typically of the order of 15-20%.   While the top and bottom flanges

of the twin cell box are almost equally affected, stress variations are far more sizable in the top flange of both the single cell sections.

A similar error analysis has also been undertaken for the composite road bridge described in §4.3. The six load cases previously identified have been considered and the resultant bending moments and bimoments are those obtained from the 'exact' solution employing two curved beams in the central span. The variable multiplier ρ/R has once again been included in the computation of the error functions for members displaying curvature, and the results are presented in Table 4.15. Straight and curved beam properties have been used for the determination of stress at the centre sections of the outer and central spans, respectively. For support sections, results for both straight and curved beam properties have been presented.

		Load Position	Moment (Tm)	Bimoment (Tm^2)	Straight Properties		Curved Properties	
					$E_{\sigma t}$ (%)	$E_{\sigma b}$ (%)	$E_{\sigma t}$ (%)	$E_{\sigma b}$ (%)
Outside Span Loaded	Centre	Inner	-6.88	-8.25	83.5	74.5	-	-
		Central	-6.97	0.05	0.5	0.5	-	-
		Outer	-7.06	8.36	82.5	73.6	-	-
	Support	Inner	3.00	6.32	146.7	131.0	151.9	137.2
		Central	2.83	1.49	36.8	32.8	38.1	34.4
		Outer	2.65	-3.34	87.9	78.5	91.1	82.3
Central Span Loaded	Centre	Inner	-5.74	-5.28	-	-	66.4	59.9
		Central	-5.45	2.45	-	-	32.5	29.3
		Outer	-5.15	10.18	-	-	142.5	128.8
	Support	Inner	2.19	1.49	47.3	42.2	49.0	44.3
		Central	3.33	-2.05	42.8	38.2	44.3	40.0
		Outer	4.47	-5.58	87.0	77.6	90.1	81.4

Table 4.15   Maximum Percentage Error in Direct Stress due to neglecting the Effects of Warping in the Composite Road Bridge

The percentage error in the maximum value of direct stress due to neglecting warping effects in this structure is considerably larger than for the prestressed concrete bridge previously investigated. This is reflected in the value of the dimensionless decay function, $k\ell$, which is approximately equal to 6 for the composite bridge but typically 15-20 for the bifurcated bridge. For eccentrically applied loads in both the outer and central spans, the direct stress due to bimoment comprises between 20-60% of the total maximum direct stress at the centre and support sections. Thus, in some instances, the bimoment imposes larger direct stresses than the bending moment. At the support sections, the results obtained by using curved and straight beam properties were not greatly different and in all cases the stresses due to bimoment were of equal significance to both the top and bottom flanges.

For this method to be useful in determining whether warping effects should be considered in the analysis of a particular structure, the values of bending moment and bimoment must first be calculated at several critical sections. Since a full analysis (including the effects of warping) would defeat the object of this preliminary investigation, the values of the two stress resultants have been tabulated in Table 4.16 in explicit form for several important configurations and types of applied load. This table enables bending moment and bimoment to be determined at the centre of a simply supported beam and at the root of a cantilever. Both straight and circular curved arrangements have been considered subject to shear and torsional loads (either uniformly distributed or concentrated). For the curved girder built-in at both ends and subject to the same general loading, the values of bending moment and bimoment at the centre and end sections may be obtained directly from figs. 3.10 - 3.19 & 3.30 - 3.39.

(i).   Simply Supported Beam

	Load Type	Stress Resultant for Curved Member	Stress Resultant for Straight Member
Bending Moment	T	$\mp\frac{1}{2}\tan(\theta/2)$	0
	t	$\mp r\left\{1 - 1/\cos(\theta/2)\right\}$	0
	P	$-\frac{r}{2}\tan(\theta/2)$	$-\ell/4$
	p	$-r^2\left\{1/\cos(\theta/2) - 1\right\}$	$-\ell^2/8$
Bimoment	T	$\frac{\mu\eta r}{2}\left\{kr.\tanh(kr\theta/2) + \tan(\theta/2)\right\}$	$\frac{\mu}{2k}\tanh(k\ell/2)$
	t	$\mu\eta r\left\{1/\cos(\theta/2) - 1/\cosh(kr\theta/2)\right\}$	$\frac{\mu}{k^2}\left\{1 - 1/\cosh(k\ell/2)\right\}$
	P	$\frac{\mu\eta r^2}{2}\left\{\tanh(kr\theta/2)/kr - \tan(\theta/2)\right\}$	0
	p	$-\mu\eta r^3\left\{1/k^2r^2\cosh(kr\theta/2) + 1/\cos(\theta/2)\right\} + \mu r/k^2$	0

(ii).   Cantilever Beam

	Load Type	Stress Resultant for Curved Member	Stress Resultant for Straight Member
Bending Moment	T	$\pm\sin\theta$	0
	t	$\pm r(1 - \cos\theta)$	0
	P	$r.\sin\theta$	ℓ
	p	$r^2(1 - \cos\theta)$	$\ell^2/2$
Bimoment	T	$-\mu\eta r \sin\theta + kr.\cos\theta.\tanh kr\theta)$	$-\frac{\mu}{k}\tanh k\ell$
	t	$-\frac{\mu(1-\eta)}{k^2}\left\{\begin{matrix}kr.\sin\theta.\tanh kr\theta - \\ \cos\theta + 1/\cosh kr\theta\end{matrix}\right\}$	$\frac{\mu}{k^2}\{1-k\ell\tanh k\ell -1/\cosh k\ell\}$
	P	$\mp\mu\{\eta r^2\sin\theta + \tanh kr\theta.(\eta kr^2\cos\theta - 1/k)\}$	0
	p	$\mp\mu r^3\{\eta kr.\sin\theta.\tanh kr\theta - \eta(\cos\theta - 1/\cosh kr\theta) + \tanh kr\theta(\tanh kr\theta - kr\beta)/k^2r^2\}$	0

Table 4.16   Values of Bending Moment and Bimoment at (i). the Centre of a Simply Supported Beam, and (ii). the Root of a Cantilever

Although the information presented here covers the large

majority of simple structural configurations, the error analysis may be

usefully extended to include continuous members by adopting the method

of bimoment distribution recently proposed by Khan and Tottenham[48].

However, in order to determine the error function, E_σ, the sectorial

co-ordinates and warping moment of inertia must also be evaluated for

each section.   Some limited help has already been made available for

this purpose in Chapter 2 for a range of typical cross-sections, namely,

the rectangular box, the channel and I-sections (fig. 2.14).   The

resultant functions F (given by the greater of F_t and F_b) corresponding

to these cross-sections are shown in figs. 2.22 - 2.24.   While the range

of wall thickness/height ratios is limited, it is possible to interpolate

these graphs to a sufficient degree of accuracy for preliminary design

purposes.

4.4.3   Other Sources of Error

Representing curved members by one or more equivalent straight

beam elements and neglecting thin-walled effects are, undoubtedly, the

two primary sources of potential analytical error.   However, other

inaccuracies are also possible and these will be discussed here with

reference to the two bridges previously described in this chapter.

The Warping Shear Parameter

In their original analysis of the continuous road bridge,

Konishi and Komatsu[53] took no account of the interactive effect of the

shear stresses (due to the connectivity condition of the closed cells)

on the response of the section to warping restraint.   This is equivalent

to setting the warping shear parameter to unity, which is only strictly

the case for open sections.   However, the actual values of μ have

already been calculated and are presented in Table 4.8 for both the

	Method of Structural Idealization	Outer Spans			Central Span		
		Outside Lane Loaded	Central Lane Loaded	Inside Lane Loaded	Outside Lane Loaded	Central Lane Loaded	Inside Load Loaded
Moment	Original Solution	*-705.80*	*-696.92*	*-688.00*	*-515.47*	*-544.91*	*-574.36*
	μ from Table 4.8	-704.47 (0.19)	-697.10 (0.03)	-689.73 (0.25)	-509.11 (1.23)	-542.56 (0.43)	-576.01 (0.29)
	Different Shear Centre	-	-	-	-511.92 (0.69)	-543.48 (0.26)	-570.81 (0.62)
Torsion	Original Solution	*157.66*	*4.45*	*-148.80*	*167.62*	*0*	*-167.63*
	μ from Table 4.8	158.87 (0.77)	3.79 (14.83)	-151.29 (1.67)	167.63 (0.01)	0 (0)	-167.62 (0.01)
	Different Shear Centre	-	-	-	187.81 (12.05)	8.18 (-)	-147.44 (12.04)
Shear	Original Solution	*-0.4201*	*-0.4157*	*-0.4104*	*-0.5*	*-0.5*	*-0.5*
	μ from Table 4.8	-0.4202 (0.02)	-0.4158 (0.02)	-0.4114 (0.24)	-0.5 (0)	-0.5 (0)	-0.5 (0)
	Different Shear Centre	-	-	-	-0.5 (0)	-0.5 (0)	-0.5 (0)
Bimoment	Original Solution	*83 552*	*546*	*-82 460*	*101 813*	*24 504*	*-52 804*
	μ from Table 4.8	75 653 (9.45)	623 (14.10)	-74 406 (9.77)	92 401 (9.24)	22 796 (6.97)	-46 809 (11.35)
	Different Shear Centre	-	-	-	111 122 (9.14)	28 277 (15.40)	-43 495 (17.63)

Table 4.17 Percentage Error in Stress Resultants due to variations in (i). the Warping Shear Parameter, μ, and (ii). the Shear Centre Position

curved and straight members. Subsequently, the structure has been re-analysed with the new values of the warping shear parameter but with the remaining geometrical properties unaltered. The resultant forces at the centre of each span are presented in Table 4.17 for each of the six load cases previously considered. Values printed in italics represent the original solution, whereas the figures in parentheses are equivalent

to the percentage error due to neglecting the term μ.

The effect of the warping shear parameter is difficult to assess for the general case. Not only does it appear explicitly in most of the member flexibility coefficients, but it is also an integral part of the decay function, k (eqn. 2.67), thus directly influencing the numerous hyperbolic functions incorporating this term. It is clear from Table 4.17 that the three primary stress resultants are not greatly affected by variations in the value of μ. Nevertheless, errors of 7-14% are apparent in the bimoment term, somewhat less than the approximately 16% reduction in the warping shear parameters. Obviously this also has an effect on the error functions determined in §4.4.2 which must be reduced proportionately.

The Shear Centre Position

One of the effects of including curvature in the determination of cross-sectional properties is to alter the shear centre position. In the case of the composite road bridge, the location of the shear centre is given in Table 4.8 for both the straight and curved sections. The difference is only equivalent to a horizontal change in position of approximately 5% of the total section breadth, but has apparently been ignored by Konishi and Komatsu[53] and Takaba and Naruoka[103] in their respective analyses.

In order to take account of these effects, the structure has been re-analysed for the three point loads within the central span which are affected. The results are given in Table 4.1 where the figures in parentheses denote the percentage error with respect to the results from the original analysis for which $\mu = 1$. As expected, in the case of the two eccentric loads, this modification has resulted in errors of approximately ±12% in the computed value of the torsional moment. Significant errors in the calculation of bimoment are also apparent (upto 17%).

Curvature Effects

The idealization of a curved member by a number of equivalent straight beam elements introduces errors which have been fully discussed in §4.4.1. These are essentially errors in the longitudinal distribution of the various stress resultants brought about by the different structural configuration. However, certain other aspects of member curvature can, if neglected, introduce further inaccuracies into the analysis. In particular, the derivation of the various geometrical section properties is influenced by curvature, a fact that has already been demonstrated in Tables 4.2 and 4.8 for the two bridges previously described. Variations in each of the section properties have subsequently been detailed in Table 4.18 for the composite road bridge section and for the three primary sections in the bifurcated bridge. These are expressed as percentage differences with respect to the values calculated for the curved sections.

Clearly, with the exception of the torsional and warping moments of inertia in the case of the composite bridge, differences in the important sectional properties are negligible. Furthermore, despite the different formulation of the stress equations in which curvature effects are included (eqn. 2.82), the total strain energy equations (eqn. 3.29), derived in terms of the various stress resultants, is unaltered. Thus, the use of the very similar geometrical properties calculated for the curved section will have a negligible effect on the longitudinal distribution of the various stress resultants as computed using straight beam properties.

However, the use of the theory proposed by Konishi & Komatsu[53], in preference to the conventional theory for straight beams, results in two more important discrepancies. The first is a change in the centroidal and shear centre positions. This can significantly alter the torsional

Geometrical Section Property	Bifurcated Bridge			Composite Road Bridge
	Span AB	Span DE	Span FG	
I_x	0	-0.89	-0.51	0
I_d	1.05	-1.11	0.29	6.05
I_c	-1.01	-1.48	0	-0.96
I_ω	-2.02	-0.94	0.65	-10.12
μ	-1.05	-1.01	-0.67	-1.41

Table 4.18   Percentage Error in the Various Geometrical
Section Properties due to Member Curvature

moment in the loaded span and has been briefly discussed previously in
this section.   The second concerns the different transverse distribution
of stress which results from fully considering the effects of curvature.
In the case of bending and direct forces, the resultant distribution
of direct stress is modified by the variable R/ρ (eqn. 2.82).   For the
twin cell box in the bifurcated bridge this is equivalent to an increase
in direct stress of approximately 13% at the tip of the cantilever on
the inside curve with a corresponding reduction of the opposite side
of the section.   With regard to the warping restraint stresses, these
are not multiplied by the same function in the stress equation although
the effects of curvature are included in the derivation of the various
sectorial properties.   The sectorial co-ordinates for the bifurcated
and composite road bridges are shown in figs. 4.73 and 4.74 respectively.
Differences of up to ± 10% are evident at the top and bottom of each web
although more significant variations occur at the ends of some of the
side cantilevers.   Thus, while it is generally permissible to use
straight beam section properties for the analysis of curved, thin-walled
beams, curvature effects must be fully considered in the determination
of the transverse distribution of stress.
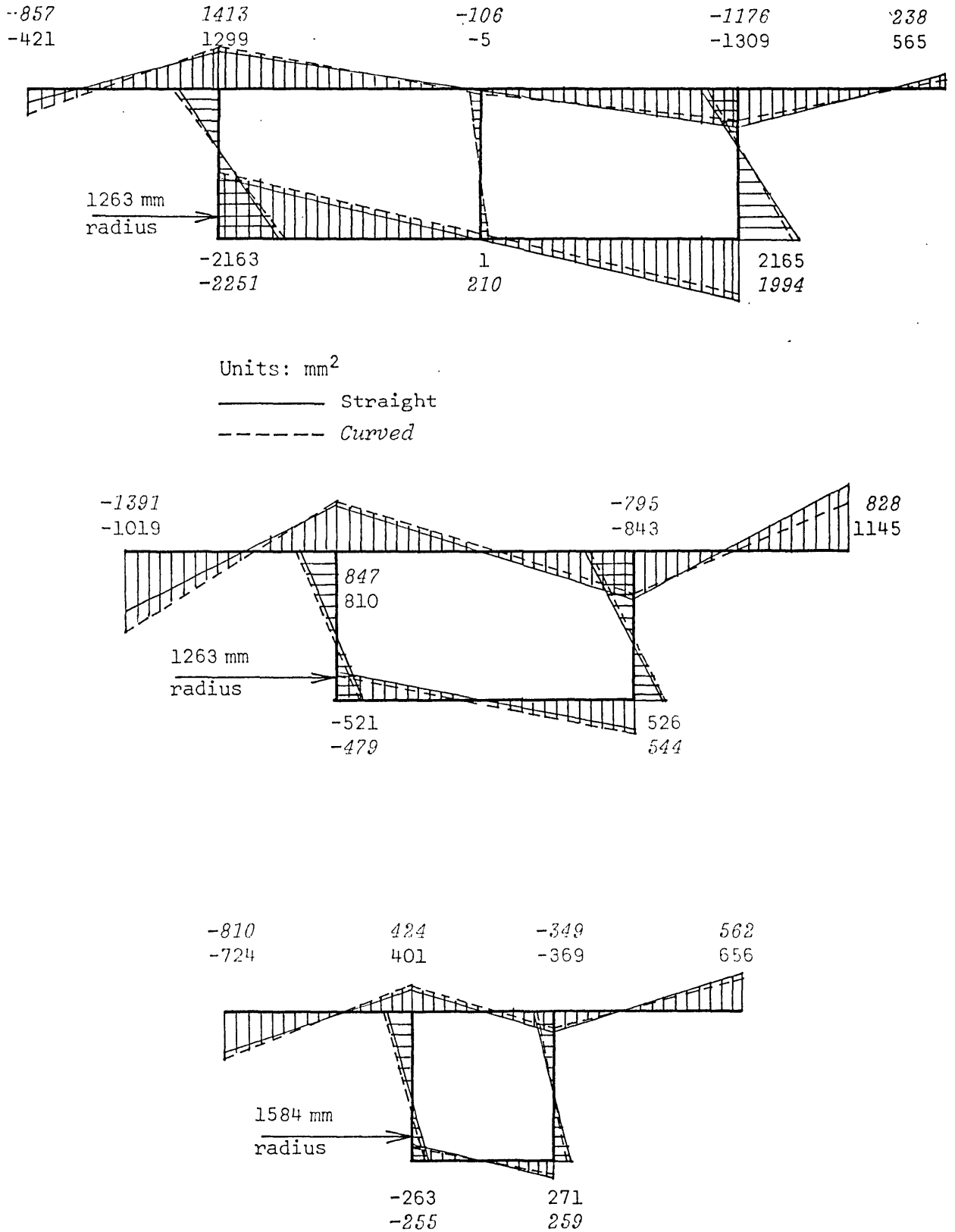
Figure 4.73   Sectorial Co-ordinates of the Three Primary Sections in the 1/50th scale Bifurcated Bridge Model
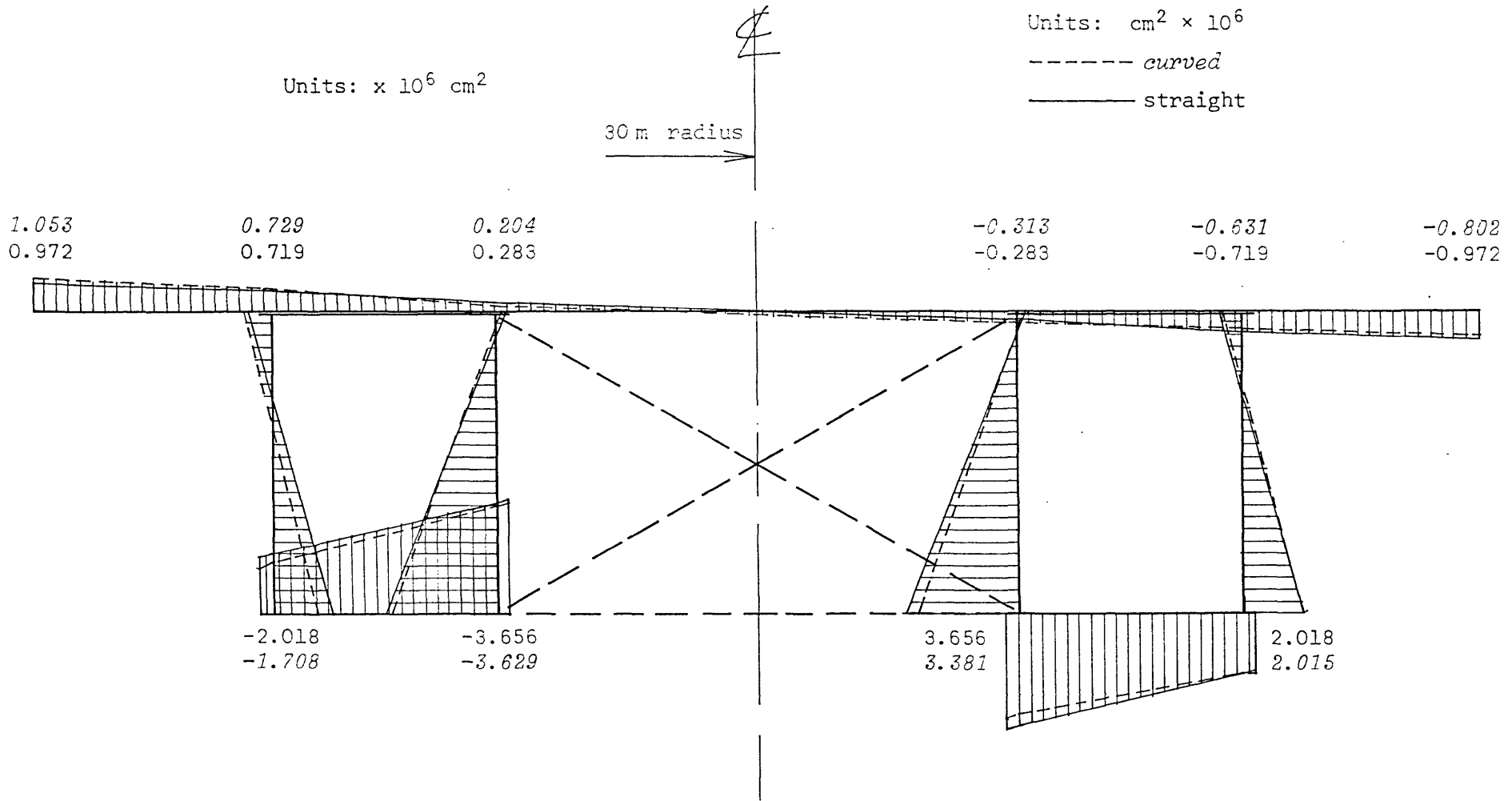
Figure 4.74   Sectorial Co-ordinates of the Composite Section used in the Continuous Road Bridge

CHAPTER FIVE

ULTIMATE LOAD ANALYSIS OF REINFORCED AND PRESTRESSED CONCRETE MEMBERS SUBJECT TO COMBINED LOADS

5.1   INTRODUCTION

During the recent revision of many international Codes
of Practice   to include the principles of limit state design, it
became apparent that there was a shortage of reliable information on
the post-cracking behaviour of reinforced and prestressed concrete
beams in torsion. This form of loading, often combined with other
actions, is becoming increasingly common with the use of highly curved
road bridges and other modern structural configurations. However,
over the past decade, the situation has noticeably improved and
results from numerous experimental and theoretical investigations into
all aspects of the subject have been published.

The results of research in the U.S.A.[2,4] have been incor-
porated into the American building code in the form of complicated
empirical relationships, whereas in Europe a more rational approach has
been adopted.[20] First, a distinction is made between the two possible
types of torsion, one arising from equilibrium requirements and the
other from a need to satisfy conditions of compatibility. Lampert[59]
defines these two torques in the following way:

i.   Equilibrium torsion - a torsion is required to maintain
       equilibrium in the structure.

ii. Compatibility torsion - a twist is required to maintain
       compatibility in the structure.

Clearly, in statically determinate structures, only equilibrium torsion
exists, while in indeterminate structures both types are possible.

In general, if the torsion in an indeterminate structure

can be eliminated by simply releasing redundant restraints, then it is compatibility torsion. This may then be disregarded at the ultimate limit state, where only equilibrium torsion need be considered, provided the designer is satisfied that the resulting crack widths, deflections, etc., will not impair the performance of the structure. The theoretical approach for the analysis of equilibrium torsion, adopted in the CEB code[20], is based on simple failure models developed from the post-cracking behaviour.

5.1.1 Observed Inelastic Behaviour

Reinforced concrete beams respond to increases in bending moment by progressive cracking and a gradual deterioration of section stiffness. On the other hand, under pure torsional loads, behaviour before and after cracking is distinctly different and the transition between the two stages is usually rapid, fig. 5.1. In the uncracked state the torsional moment is resisted solely by St. Venant shear stresses, determined for the homogeneous, isotropic cross-section by elastic analysis. After cracking, tensile stresses in the concrete are transferred to the steel, resulting in a completely different mechanism of torque resistance in which the density and location of the reinforcement are of prime importance. Since the transition between the two states occurs when the principle tensile stresses in the concrete exceed the cracking strength, prestressing is often effectively employed where the full uncracked stiffness is required to satisfy serviceability requirements under working load conditions.

In simple rectangular beams, subject to pure torsion, cracks appear initially at the centre of the longer sides and at an angle corresponding to the direction of principle tensile stress (approximately 45°). Under additional small increases in load, these rapidly propagate around the entire perimeter of the beam until the familiar pattern of
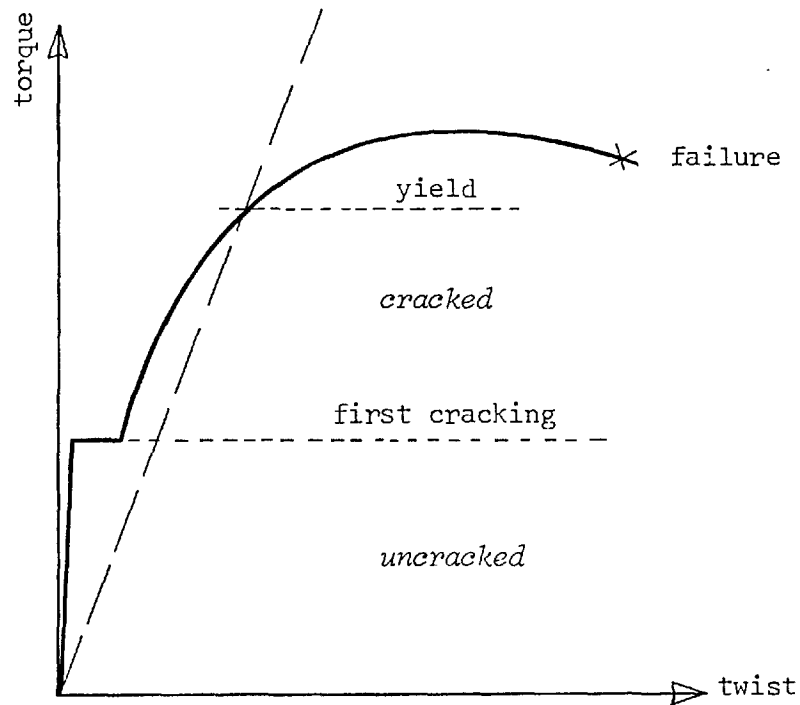
Figure 5.1   Load /Displacement Curve for Pure Torsion

spiralling cracks is fully developed. Redistribution of internal

forces takes place during this transitional period until, in the

fully-cracked state, all tensile forces are taken by the reinforcement,

leaving only the concrete diagonals formed between shear cracks to

resist compression. At this stage the concrete core of a solid beam

is ineffective and the member may be regarded as thin-walled for the

purposes of analysis.

After more extensive cracking and redistribution, the

inclination of the concrete diagonals is likely to change, notably

after yield of either the longitudinal or stirrup steel. In this state

the member can sustain further increases of load until the other

component of steel also develops its full yield force. The spiralling

cracks on three sides of the beam then open up and the collapse

mechanism is completed by the formation of a skewed compression

zone on the remaining face.

5.1.2   Methods of Analysis

The various methods which are available for the strength

analysis of reinforced and prestressed concrete members, subject to

torsion combined with other loads, are summarized in Table 5.1. The

first nine methods are studies of the structural mechanics at the

ultimate limit state and, as such, provide general failure criteria for

all combinations of applied load, usually in the form of non-dimensional

interaction equations. However, the ratio of the various load types must

be known everywhere in the structure and these methods are therefore

restricted to the analysis of determinate systems. While the remaining

methods in Table 5.1 are more general in application and have been

used for the analysis of simple redundant structures, their scope is

limited.

Failure Criteria

The stress methods (1) include the maximum tensile stress

theory and the internal friction theory, due to Cowan[23]. These take

no account of the continual readjustments of stresses brought about by

progressive cracking and are, therefore, not entirely suitable for

making a rational strength evaluation. Furthermore, it has been shown[94]

that when applied to a series of beams tested over a wide range of

torque/bending moment ratios, these methods can result in gross over-

and under-estimations of the actual strength.

Methods (2) to (4) are all variations of the well known space

truss analogy and are based on the observed behaviour of concrete

members in the fully cracked state. In its original form, the theory

assumed a constant 45° crack angle of failure, and was developed for
the analysis of reinforced concrete beams subject to pure torsion.
Recently, the method has been much improved by the introduction of a
modified failure model with variable crack inclination, and further
developments have also enabled the effects of shear force to be
included.

The ultimate equilibrium method (5) is formulated from
conditions of equilibrium at an assumed failure surface, in which a
skewed compression zone is joined by spiralling cracks on the remaining
sides of the beam. As with the truss analogy, strain compatibility is
neglected, and the method has also been modified to account for the
application of shear force (6). Furthermore, Lampert[59] has shown that
methods (2) to (6) are equally valid for the analysis of prestressed
beams provided that the yield stress of the stressed and unstressed
reinforcement is attained at approximately the same level of additional
strain. This has been further demonstrated by comprehensive experimental
and theoretical investigations.[30,39,44,118]

For over-reinforced sections, or where insufficient rotational
capacity is available to develop the full yield strain in all elements
of reinforcement, compatibility conditions have been introduced in
addition to the requirements of equilibrium. These equilibrium/
compatibility methods (7) are complex and time consuming to apply and
as a result have not gained favour with design engineers. Furthermore,
due to the increased number of unknown quantities, it has usually
been necessary to assume a fixed crack angle, thereby ignoring the
effects of redistribution due to progressive cracking. However, as
computer based methods with iterative forms of solution, these studies
are more promising and can provide information at all stages up to failure.

ANALYTICAL METHOD	TYPE OF STRUCTURAL ACTION CONSIDERED				
	Longitudinal Bending	St. Venant Torsion	Shear Force	Torsional Warping	Distortion
1. Stress Methods[23]	●	●			
2. Fixed Angle Space Truss Analogy[89]	●	●			
3. Variable Angle Space Truss Analogy[60]	●	●			
4. Modified Space Truss Analogy[28]	●	●	●		
5. Ultimate Equilibrium Method[62]	●	●			
6. Modified Ultimate Equilibrium Method[29]	●	●	●		
7. Equilibrium/Compatibility Methods[10,76,88,94]	●	●	●		
8. General Theory of Plasticity[43,60,78]	●	●	●		
9. Empirical and Semi-empirical Methods[2,4]	●	●	●		
10. Plastic Analysis of Grillages[73]	●	●			
11. Plastic Analysis of Curved Members[45,120]	●	●			
12. Inelastic Finite Element Analysis[16]	●	●	●	●	
13. Distortional Analysis of Straight Box Girders[97]	●				●

Table 5.1   Methods of Ultimate Load Analysis for Structures subject to Combined Loads

The analyses covered by (8) do not establish new
interaction equations but show that the space truss and ultimate
equilibrium methods are essentially special cases of the lower bound
theory of plasticity. Suitable upper bound techniques are also
introduced, thus enabling the general theory of plasticity to be
rigorously applied to the analysis of reinforced and prestressed
concrete members.

Extensive experimental investigations have accompanied most
of the analytical methods presented here and a large volume of data is
now available covering all aspects of torsional behaviour up to
failure. Subsequently, these results have been used as a basis for
many empirical or semi-empirical studies (9). While the resulting
interaction curves and surfaces tend to be conservative they do provide
sufficient accuracy for initial design purposes.

Analysis of Indeterminate Systems

The methods considered so far are only truly applicable
to the analysis of statically determinate systems where the loading
regime is known uniquely at every position along the beam. The ultimate
load is then determined when the selected failure criterion is first
reached at any point. However, in practice, equilibrium torsion is also
commonly found in indeterminate structures such as grillages and
curved beams. In this case, the prevailing system of stress resultants
can no longer be evaluated without knowing the variations in structural
stiffness due to cracking.

The usual plastic theories, employed for the analysis of
torque-free systems, are based on the introduction of plastic hinges
at points in the structure where the full moment capacity has been
developed. Sufficient hinges are provided to reduce the structure to a

determinate form, thereby enabling the ultimate load to be established. Thus, the main problem in analysing highly indeterminate systems is the correct positioning of the plastic hinges, and various analytical methods are now available for obtaining an optimal solution.

For members subject to combined loads it may also be assumed that a plastic hinge forms when the selected criterion governing failure has been reached. However, this can now occur under an infinite number of applied load ratios and it is difficult to formulate the problem for the general case. Furthermore, when a hinge has been established, problems arise with the introduction of additional hinges since redistribution can invalidate the assumed load ratio at the first hinge. As a result of this complexity only very simple structural configurations have been analysed to date (10).

Additional problems exist in the analysis of curved beams (11) since the optimum hinge positions are no longer obvious from inspection and finite difference or similar techniques must be employed. For these reasons, it is not yet feasible to determine the true dual solution for complex systems and a simple upper bound approach is all that is available.

The generality of the finite element method makes its use for inelasticity and plasticity applications very attractive. The non-linear analysis of non-homogeneous anisotropic bodies is well advanced (12) and is immediately applicable to shear wall and box girder problems. However, since a direct solution of the problem is generally not possible, an incremental analysis using numerical techniques is necessary and this can seriously restrict the usefulness of the method. Furthermore, as with all computer based techniques, the preparation of data for complex structures and the assimilation of output are still real disadvantages.

Finally, with regards to distortion, no comprehensive method of analysis is yet available. However, for simple configurations recourse to the upper bound method of the general theory of plasticity is possible (13) although a meaningful lower bound solution is unlikely to be readily obtainable.

Future Developments

The need for comprehensive ultimate load analyses of indeterminate structures is clear. However, the greatest potential for improvement appears to be with the continuing development of inelastic finite element techniques and these are beyond the scope of this work.

With regard to establishing reliable failure criteria for beams subject to combined loads, methods (2) to (6) have found wide acceptance, although certain shortcomings are evident in their development to date. Accordingly, the derivations of these methods are now briefly presented and the existing limitations discussed. Improvements are then suggested to account for the application of shear force in a more rigorous fashion and to extend the theory to include the effects of warping restraint in open sections.

5.2　　　　SIMPLIFIED FAILURE MODELS

5.2.1　　　Assumptions

The ultimate load theories presented here are based on the behaviour of two quite different failure models. Each of these methods of analysis has been verified by extensive experimental research and the following common assumptions have been made in their respective derivations.

1.　The beam is fully under-reinforced so that both longitudinal and stirrup steel yield at failure. Implicit in this assumption is the fact that the reinforcement has sufficient strain capacity to enable the full failure mechanism to develop.

2.　Adequate steel is provided in both directions to prevent failure at first cracking.

3.　The reinforcement is properly detailed to avoid secondary failures. In this respect, the spacing and anchorage of stirrup steel requires special attention.

4.　All longitudinal steel not actually in the compression zone yields at failure thereby justifying the idealisation of the reinforcement to corner bars.

5.　All the reinforcement displays a perfect elasto-plastic stress/strain relationship. Increases in strength after yield due to work hardening, etc., have been neglected.

6.　The compression zone may form about a line joining any two adjacent corner bars (with certain exceptions[59]).

7.　No shear forces are carried by the concrete compression zone or transmitted by aggregate interlock, dowel action, etc.

8.　The concrete is assumed to have no tensile strength.

9.　Concrete behaviour does not initiate or influence collapse. The main causes of premature concrete failure have been studied

in detail by Lampert & Thürlimann[60] and include

a.   failure of the concrete compression zone

          (*i.e.* over-reinforced sections),

b.   excessive shearing strains, where the angle of crack

          formation deviates significantly from 45°, and

c.   compression failure of the concrete diagonals which

          develop between cracks.

10.   Where warping of the cross-section occurs it is unrestrained longitudinally, thereby ensuring that the torsional moment is resisted entirely by St. Venant shear stresses.

11.   The elastic and plastic deformations do not produce significant changes of geometry. This enables the original configuration to be used for formulating the equations of equilibrium.

5.2.2   Space Truss Method

The analogy between a truss and a fully cracked reinforced concrete beam was first considered by Rausch[89] (1929) for the case of pure torsion. The concrete compression diagonals were assumed to develop at a fixed angle of 45° and failure occurred with yield of either the longitudinal or transverse steel. More recently (1971), Lampert & Thurlimann[59,60] have revived interest in the space truss by introducing an improved model in which the inclination of the concrete diagonals is variable and dependent upon the relative amounts of longitudinal and stirrup reinforcement.

Consider the simple rectangular beam, shown in fig. 5.2 which is assumed to be symmetrical about the y-axis with the yield force of the bottom steel greater than or equal to that of the top ($Z_{by} \geqslant Z_{ty}$). The reinforcement has been apportioned to the corners in the following way:
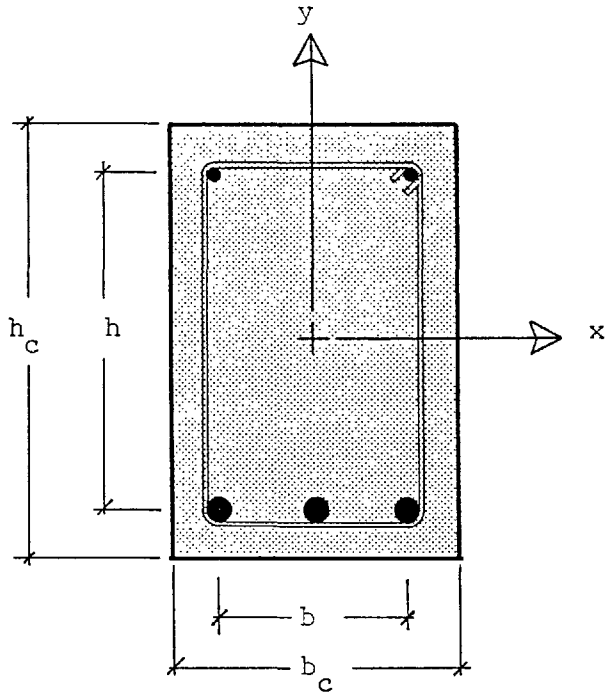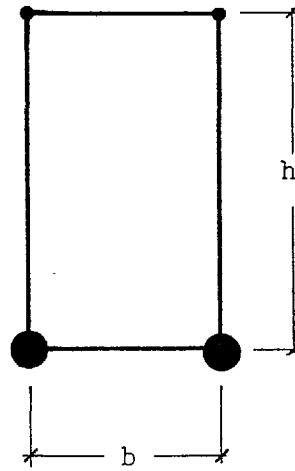
a. Reinforced Concrete Beam   b. Space Truss Analogy   c. Ultimate Equilibrium Method
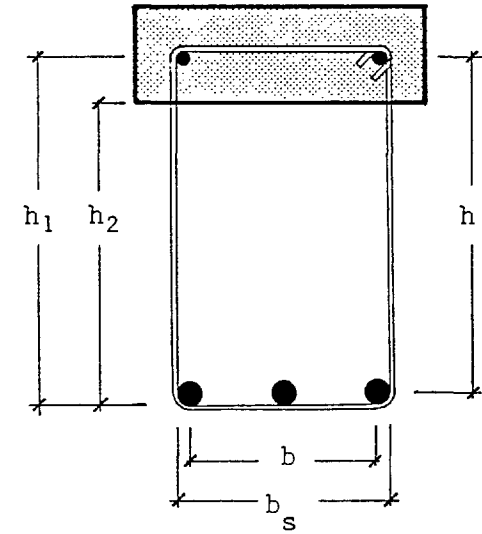
Figure 5.2   Idealization of a Rectangular Reinforced Concrete Beam for the Simplified Failure Models

$$\left[\frac{1}{2} + \frac{y_i}{h}\right] \text{ to the top;} \qquad \left[\frac{1}{2} - \frac{y_i}{h}\right] \text{ to the bottom}$$

and then

$$\left[\frac{1}{2} + \frac{x_i}{b}\right] \text{ to the RH side;} \qquad \left[\frac{1}{2} - \frac{x_i}{b}\right] \text{ to the LH side}$$

where x_i, y_i are the co-ordinates of the ith bar with respect to the beam centre. Thus, for the simplified model considered here, the idealised section (fig. 5.2b) remains statically equivalent to the original system.

Under the combined actions of torsion, bending moment and direct force, cracks develop in the shear walls at a constant angle α to the longitudinal axis. The diagonal concrete elements, so formed, act as compression struts and the longitudinal and transverse components of reinforcement complete the truss geometry (fig. 5.3). By considering equilibrium of forces in the shear walls, in both in-plane directions, the stress in the concrete struts, σ_c, and the tensile force in the stirrups, D, are given by

$$\sigma_c = \frac{F_{sv}}{\delta.\cos\alpha.\sin\alpha} \qquad 5.1$$

and

$$D = \sigma_c.\delta.s.\sin^2\alpha = F_{sv}.s.\tan\alpha \qquad 5.2$$

where F_{sv} is the constant shear flow given by the Bredt-Batho formula (2.44)

Furthermore, from three of the remaining conditions of equilibrium, we have

$$N = 2(Z_t + Z_b) - 2F_{sv}(b + h)\cot\alpha \qquad 5.3$$

$$M_x = (Z_t - Z_b)h \qquad 5.4$$

$$T_{sv} = \Omega.F_{sv} \qquad (2.44)$$

in which Z_t, Z_b represent the force in each of the idealised top

and bottom corner bars, respectively. Under increasing load, either

the top or bottom component of longitudinal steel will eventually

yield and, by eliminating the unknown component of steel force

(corresponding to the reinforcement in the compression zone) from

eqns 5.3 and 5.4, the final crack angle α_y may be determined. Thus,

for yield of the bottom steel

$$\tan \alpha_y = \frac{F_{sv} \cdot P}{(4Z_{by} + \frac{2}{h} M_x - N)} \qquad 5.5a$$

and for yield of the top steel

$$\tan \alpha_y = \frac{F_{sv} \cdot P}{(4Z_{ty} - \frac{2}{h} M_x - N)} \qquad 5.5b$$

Moreover, for fully under-reinforced sections, it is assumed that

the stirrups and the longitudinal steel both reach their respective

yield stresses at failure. Thus the final crack angle, defined above,

must also simultaneously satisfy eqn. 5.2. Accordingly, by

combining eqns. 5.2 and 5.5 to eliminate the shear flow, F_{sv},

we have, for yield of the bottom steel

$$\tan^2\alpha_y = \frac{D_y \cdot P}{s(4Z_{by} + \frac{2}{h} M_x - N)} \qquad 5.6a$$

and for yield of the top steel

$$\tan^2\alpha_y = \frac{D_y \cdot P}{s(4Z_{ty} - \frac{2}{h} M_x - N)} \qquad 5.6b$$

Alternatively, by eliminating the final crack angle from eqns. 5.2

and 5.5 and introducing the Bredt-Batho definition of shear flow

(eqn. 2.44), an expression is obtained for the ultimate capacity of the beam under the action of combined loads. For yield of the bottom and top steel, respectively, this is

$$N - \frac{2}{h} M_x + \frac{T^2 sp}{\Omega^2 D_y} = 4Z_{by} \qquad 5.7a$$

$$N + \frac{2}{h} M_x + \frac{T^2 sp}{\Omega^2 D_y} = 4Z_{ty} \qquad 5.7b$$

The ultimate value of each component of load may be evaluated by equating the remaining loads to zero in eqns. 5.7a and 5.7b. Clearly, the actual ultimate capacity of the beam for each load type must be the smaller of the two values thus calculated and accordingly, we have

$$N_u = 4Z_{ty}$$

$$M_{xu} = -2hZ_{by} \qquad \qquad 5.8$$

and $$T_{svu} = \Omega.\sqrt{\frac{4D_y.Z_{ty}}{s.p.}}$$

Finally, by rearranging eqn. 5.7 and introducing the appropriate ultimate loads from eqn. 5.8, the following general interaction equations are established.

$$\lambda . \frac{N}{N_u} + \frac{M_x}{M_{xu}} + \lambda . \frac{T^2_{sv}}{T^2_{svu}} = 1 \quad \text{(for yield of the bottom steel)} \qquad 5.9a$$

and

$$\frac{N}{N_u} - \frac{1}{\lambda} . \frac{M_x}{M_{xu}} + \frac{T^2_{sv}}{T^2_{svu}} = 1 \quad \text{(for yield of the top steel)} \qquad 5.9b$$

where λ represents the ratio of yield forces in the top and bottom reinforcement given by

$$\lambda = \frac{Z_{ty}}{Z_{by}} \quad (< 1) \qquad 5.10$$
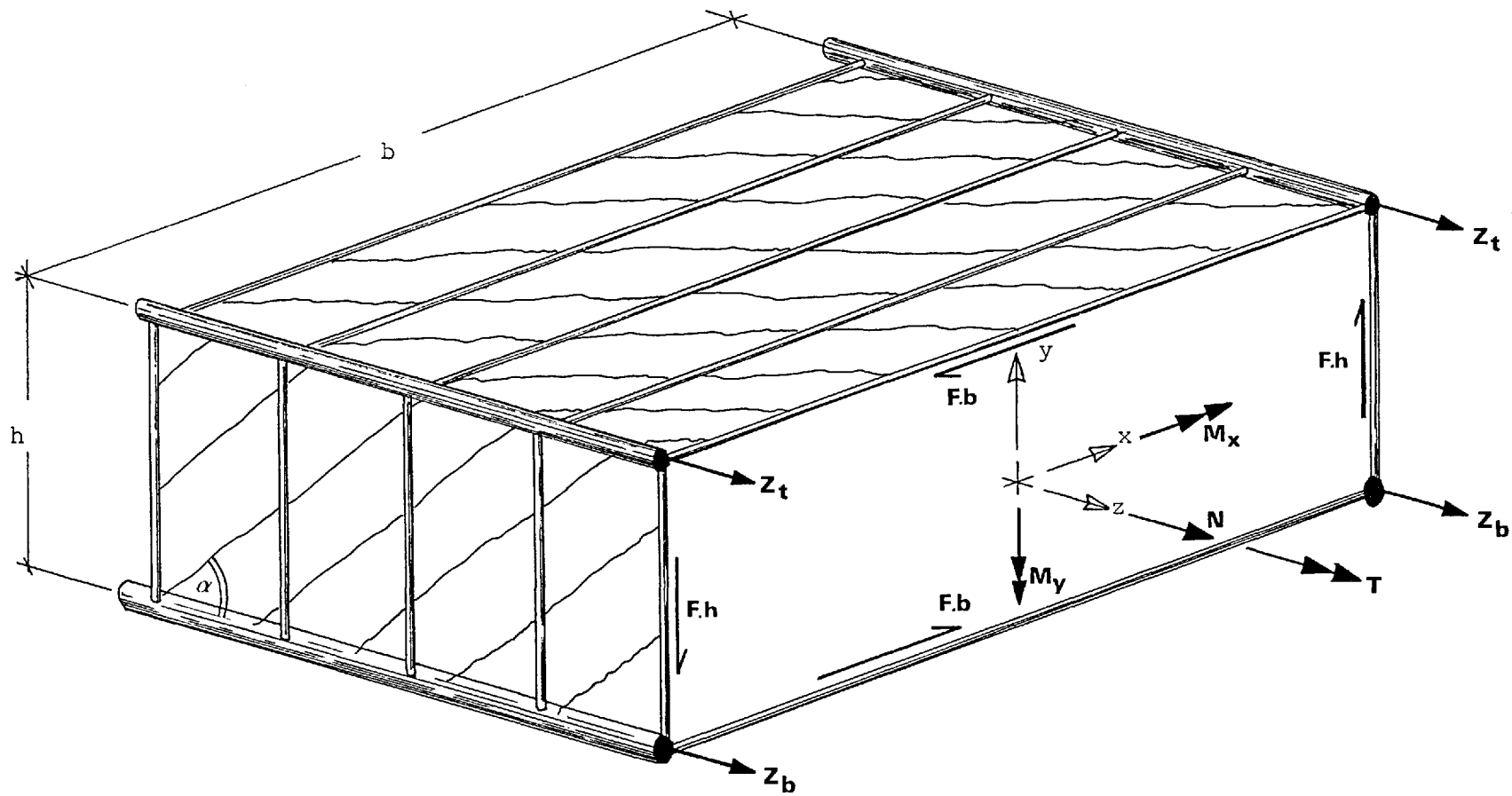
Figure 5.3   The Idealized Space Truss

These interaction equations are expressed graphically in fig. 5.4 for combined bending moment and torsion only (N = 0). Several typical values of the reinforcement ratio are used and it is apparent that for $\lambda \neq 1$ the torsional capacity of a beam is actually enhanced, under certain levels of bending moment, with a maximum value of

$$\left. \begin{aligned} \frac{T_{sv}}{T_{svu}} &= \sqrt{\frac{\lambda+1}{2\lambda}} \\[2em] \text{when} \qquad \frac{M}{M_u} &= \frac{(1-\lambda)}{2} \quad . \end{aligned} \right\} \qquad 5.11$$

Optimum Design for Torsion

It is evident from eqn. 5.6 that the angle at which the spiralling cracks form at failure is primarily governed by the relative quantities of transverse and longitudinal reinforcement. For the case of identical top and bottom steel ($\lambda=1$), the total quantity of reinforcement per unit beam length, Q, may be conveniently expressed in terms of the appropriate yield forces as

$$Q = 4Z_y + D_y \cdot \frac{p}{s} \qquad 5.12$$

and for design purposes it is sensible to require this value to be a minimum. For the application of pure torsion we have, from eqns. 5.2 and 5.5, at yield

$$\left. \begin{aligned} D_y &= F_{sv} \cdot s \cdot \tan\alpha_y \\[2em] \text{and} \qquad Z_y &= \frac{F_{sv} \cdot p}{4\tan\alpha_y} \end{aligned} \right\} \qquad 5.13$$

which on substitution into eqn. 5.12 gives

$$Q = F_{sv} \cdot p(\cot\alpha_y + \tan\alpha_y) \qquad 5.14$$

$$-\frac{1}{\lambda} \cdot \frac{M}{M_u} + \frac{T^2}{T_u^2} = 1$$ (Top Steel Yields)

$$\frac{M}{M_u} + \lambda \cdot \frac{T^2}{T_u^2} = 1$$ (Bottom Steel Yields)
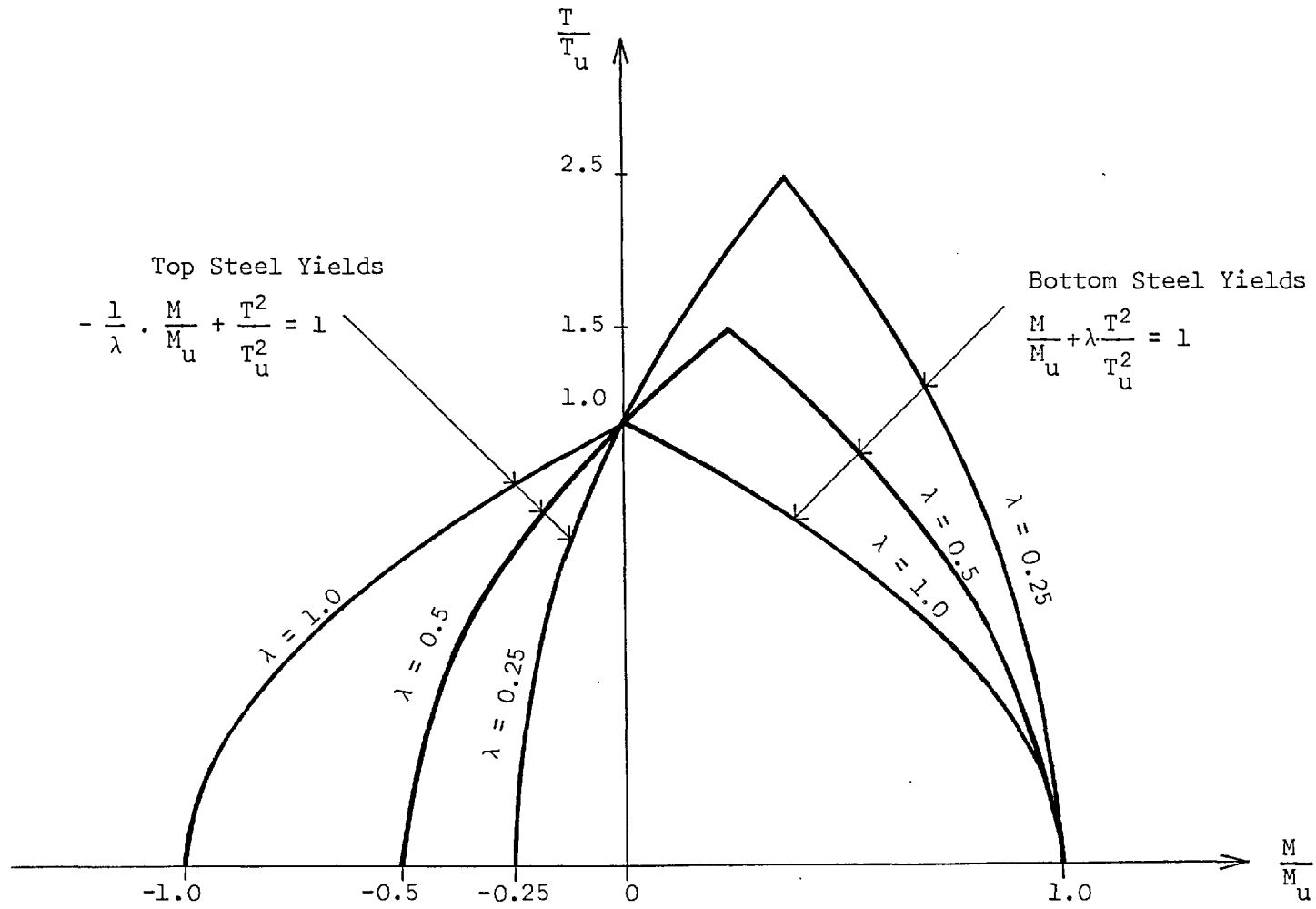
Figure 5.4   Moment/Torsion Interaction Curve

After differentiating this expression with respect to the

crack angle α_y, we have

$$\frac{dQ}{d\alpha_y} = F_{sv} \cdot p(\sec^2\alpha_y - \mathrm{cosec}^2\alpha_y) \qquad 5.15$$

which must equate to zero for minimum steel.

The non-trivial solution of eqn. 5.15 gives $\alpha_y = 45^\circ$

which on substitution into eqn. 5.13 provides the following

relationship:

$$4Z_y = \frac{p}{s} \cdot D_y \qquad 5.16$$

This is the solution of 'equal' longitudinal and transverse

reinforcement first derived by Rausch[89] half a century ago, and is

incorporated into many modern codes of practice $^{e.g.}$ [20] for simple

design against torsional loading.

5.2.3   Ultimate Equilibrium Method

In this method internal steel and concrete forces at an

assumed failure surface are equated with externally applied loads.

The failure surface, characterized by spiralling cracks on three

sides of the beam and joined by a skewed compression zone on the fourth,

is based on the tests conducted in Moscow in the late 1950's.

Accordingly, this form of analysis is also frequently referred to in

technical literature as the skew-bending method or Russian approach.

The first theoretical and experimental observations were published by

Lessig[62] and the method was soon adopted as a basis for further

modification and improvement by Lyalin[66], Grozdev et al[34], Goode and

Helmy[33] and Collins et al[19].

Consider the assumed failure surface of the simple
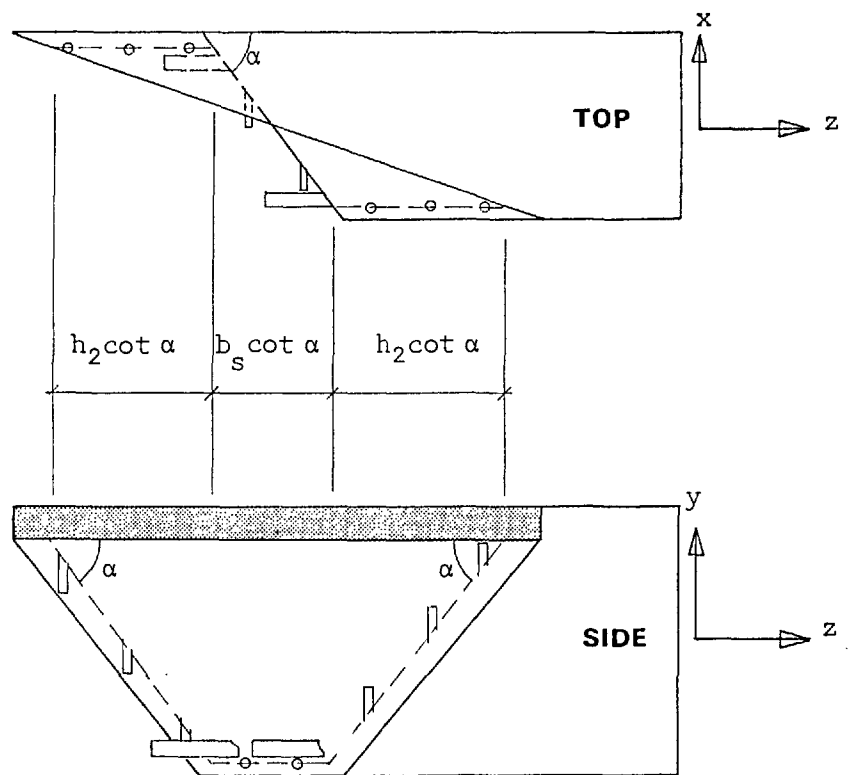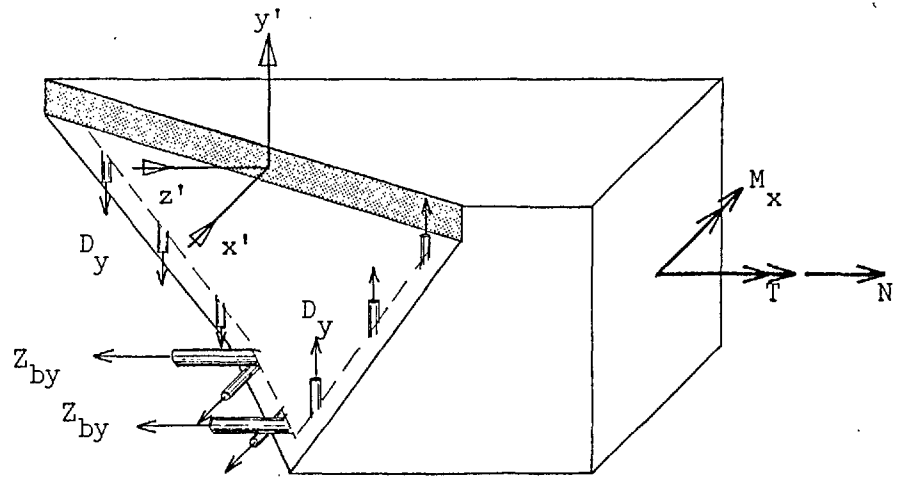
Figure 5.5   Assumed Failure Mechanism for the Ultimate
Equilibrium Method

rectangular beam, shown in fig. 5.5. All the required information is obtained from two moment equations, taken about the centre of the skewed compression zone, which for this simplified model coincides with the centroid of the top steel. For moments about the x'-axis and z'-axis, we have

$$N \cdot \frac{h}{2} - M_x = 2Z_{by} \cdot h - \frac{D_y h_2}{s} (h_2 + b_s) \cot\alpha_y^2$$

and

$$T_{sv} = \frac{D_y b_s}{s} (h_1 + h_2) \cot\alpha_y$$

$$\left. \right\} \quad 5.17$$

which may be combined to eliminate $\cot\alpha_y$, thus:

$$N \cdot \frac{h}{2} - M_x = \frac{h_2(h_2 + b_s)}{b_s^2(h_1 + h_2)2} \cdot \frac{sT_{sv}^2}{D_y} = 2Z_{by} \cdot h \qquad 5.18$$

Here, the various lever-arms are those defined in fig. 5.7c and if the following approximations are introduced

$$h_1 = h_2 = h \qquad \text{and } b_s = b \qquad\qquad 5.19$$

then eqn. 5.18 is clearly identical to eqn 5.7a, previously derived by the space truss method.

Alternatively, by selecting a failure model in which the skewed compression zone forms at the bottom of the section, and on introducing the simplifying approximations from eqn. 5.19, eqn. 5.7b is also obtained. The capacity of the reinforced beam is therefore governed by the same general interaction equations derived in eqns. 5.9a and 5.9b in which the individual ultimate loads are those expressed in eqn. 5.8.

5.2.4   Provision for Shear Loading

The ultimate equilibrium method has been further extended[29,68,77] to cover the analysis of beams which are subject to vertical shear in addition to bending moment and torsion. Although such a loading arrangement is more realistic and likely to find practical application, a modified failure model is required resulting in equilibrium equations of greater complexity.

Figure 5.6 shows a reinforced concrete beam, subject to constant values of shear force and torsion along its length. As a result, the bending moment is no longer constant over the finite length of the assumed failure surface but has a linearly varying longitudinal distribution.

Furthermore, the application of vertical shear (fig. 5.7) has the effect of modifying the constant shear flow, F_{sv}, due to pure torsion, by the quantity $\pm F_v$ in the webs, thus:

$$
\begin{aligned}
F_b &= F_{sv} \\
F_l &= F_{sv} - F_v \\
F_r &= F_{sv} + F_v
\end{aligned}
\right\} \quad 5.20
$$

where

$$F_{sv} = T_{sv}/\Omega \qquad (2.44)$$

$$F_v = V/2h \qquad 5.21$$

By restating eqn. 5.2 at yield, for the general case, as

$$\cot\alpha_{iy} = F_i \cdot \frac{s_i}{D_{iy}} \qquad 5.22$$

it is apparent that the final crack angle is no longer constant but a function of the shear flow F_i, in the ith shear wall.
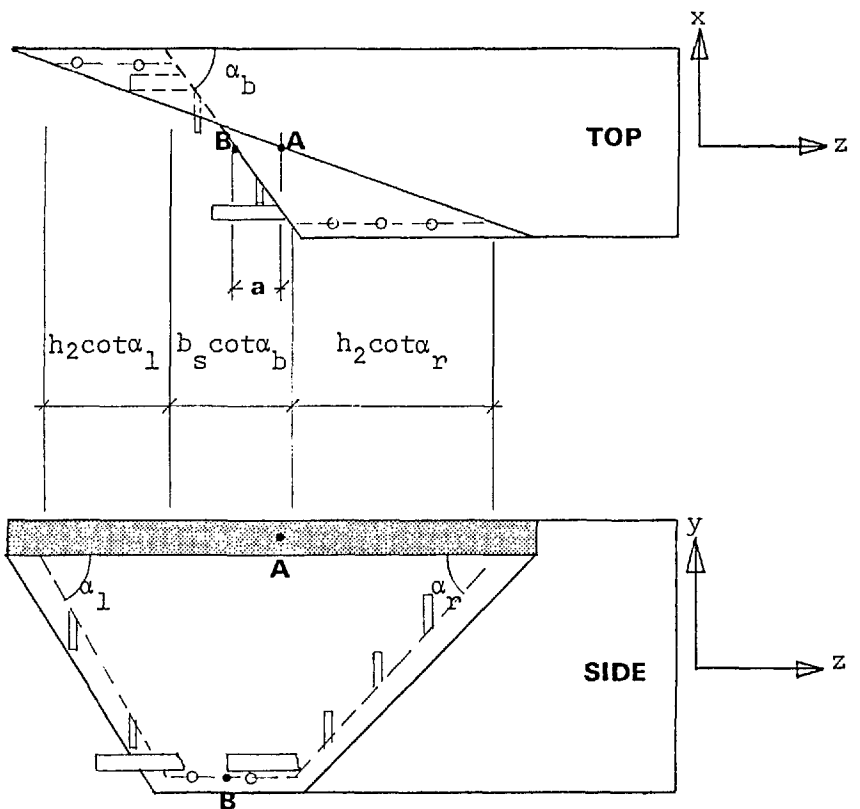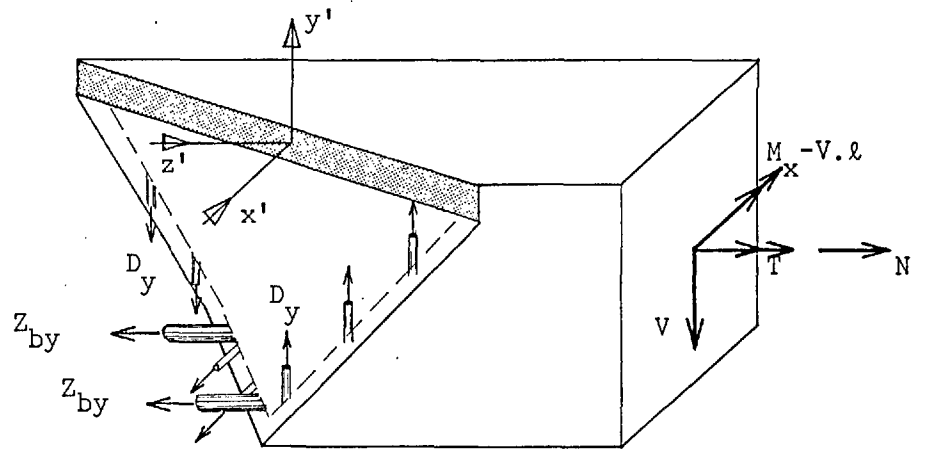
Figure 5.6   Assumed Failure Mechanism for the Ultimate
Equilibrium Method including the Effects of Shear
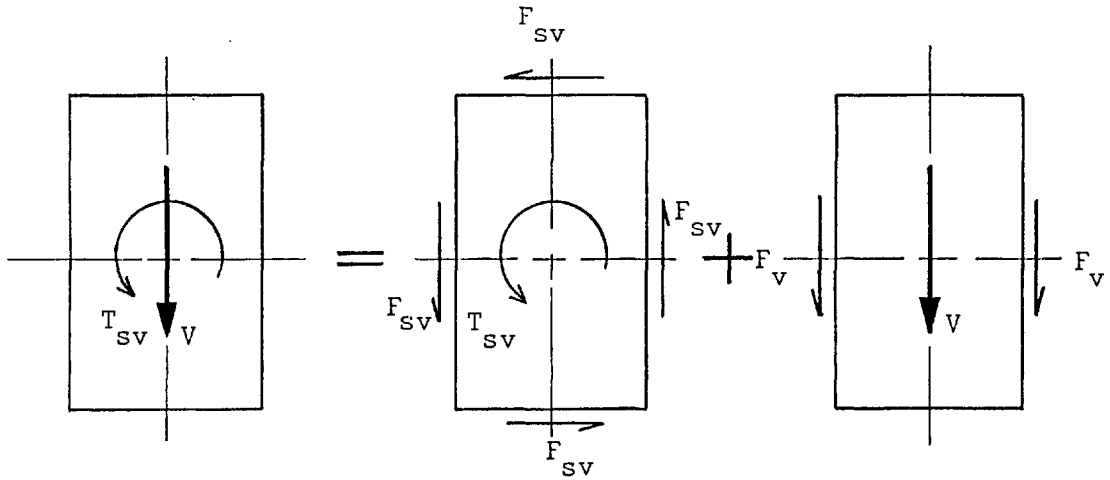
Figure 5.7   Distribution of Shear Flow due to Combined Torsion and Vertical Shear Force

Accordingly, the crack inclinations are now denoted α_{ly}, α_{ry} and α_{by} corresponding to the left-hand, right-hand and bottom faces, respectively, and by introducing eqn. 5.20 into 5.22, are given by

$$\cot\alpha_{ly} = (F_{sv} - F_v)\frac{s}{D_y}$$

$$\cot\alpha_{ry} = (F_{sv} + F_v)\frac{s}{D_y}$$

$$\cot\alpha_{by} = F_{sv}\cdot\frac{s}{D_y}$$

$$\left.\begin{array}{c} \\ \\ \\ \end{array}\right\} \quad 5.23$$

Once again, moments are taken about two perpendicular axes at the centre of the assumed compression zone and a vertical equilibrium equation is used to eliminate the additional unknown. Therefore, for moments taken about the x'-axis

$$V.a - M_x = 2Z_{by}.h - \frac{D_y}{s}\cdot h_2\cot\alpha_{ry}\left[\frac{b_s}{2}\cot\alpha_{by} + \frac{h}{2}\cot\alpha_{ly}\right]$$

$$- \frac{D_y}{s}\cdot h_2\cot\alpha_{ly}\left[\frac{b_s}{2}\cot\alpha_{by} + \frac{h}{2}\cot\alpha_{ry}\right]$$

$$5.24$$

for moments about the z'-axis

$$T_{sv} = \frac{D_y}{s} \left[b_s h_1 \cot\alpha_{by} + \frac{h_2 b_s}{2} (\cot\alpha_{ry} + \cot\alpha_{ly}) \right]$$ 5.25

and from equilibrium of the vertical forces, we have

$$V = \frac{D_y}{s} \cdot h_2 (\cot\alpha_{ry} - \cot\alpha_{ly})$$ 5.26

In eqn. 5.24 the resultant bending moment has been given the reference value M_x at the centre of the bottom reinforcement (denoted point B in fig. 5.6). The bending moment at the centre of the compression zone (point A) is therefore $M_x - V.a$, where the distance a represents the longitudinal separation of the two points and is given by

$$a = (h_2 \cot\alpha_{ly} + b_s \cot\alpha_{by} + h_2 \cot\alpha_{ry})/2 - (h_2 \cot\alpha_{ly} + \frac{b_s}{2} \cot\alpha_{by})$$

$$= \frac{h_2}{2} (\cot\alpha_{ry} - \cot\alpha_{ly})$$ 5.27

By using this expression and the appropriate terms from eqn. 5.23, eqns. 5.24-5.26 may be combined in the following way:

$$-M_x + V^2 \cdot \frac{s}{4D_y} + T^2 \frac{sp}{8D_y b^2 h} = 2Z_{by} \cdot h$$ 5.28

Alternatively, this may be rearranged in the form of the following general interaction equation:

$$\frac{M_x}{M_{xu}} + \lambda \cdot \frac{T_{sv}^2}{T_{svu}^2} + \lambda \cdot \frac{V^2}{V_u^2} = 1$$ 5.29

where, in addition to the ultimate loads derived in eqn. 5.8, the ultimate shear force has the value

$$V_u = \sqrt{\frac{8D_y Z_{ty} h}{s}}$$ 5.30

A similar derivation is possible for a failure model in which the compression zone forms about the bottom reinforcement, in which case the interaction equation describing collapse is given by

$$- \frac{1}{\lambda} \cdot \frac{M_x}{M_{xu}} + \frac{T_{sv}^2}{T_{svu}^2} + \frac{V^2}{V_u^2} = 1 \qquad 5.31$$

However, for beams subject to high torsional and vertical shear stresses but relatively small levels of applied bending moment, a third failure surface is also possible. Under such a system of loads, cracking is likely to originate in the more heavily stressed side in which the shear flows, due to both the applied torque and shear force, are additive. With increasing load the cracks propagate across the top and bottom faces until a collapse mechanism is established with the compression zone forming on the opposite side wall at failure, fig. 5.8.
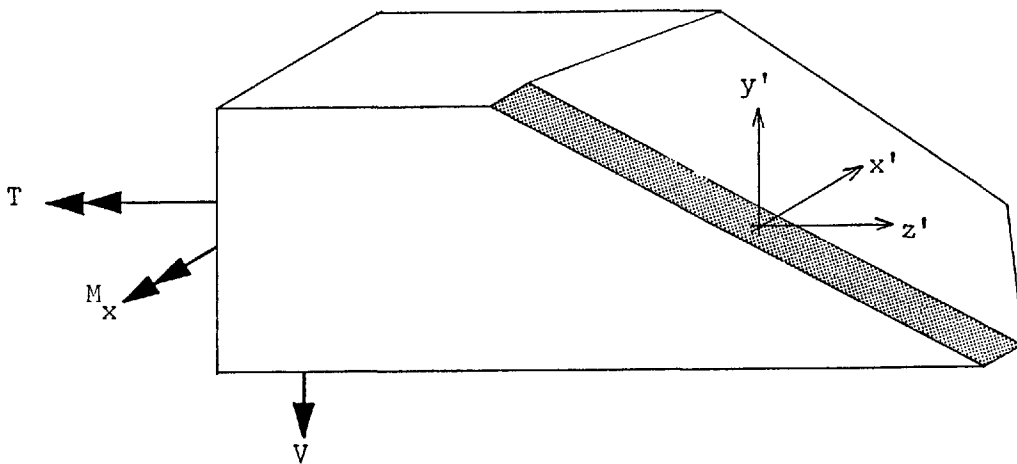
Figure 5.8   Failure Mechanism with Side Compression Zone

Moments taken about the y' and z' axes, together with
equilibrium of the vertical forces, yield sufficient information
for the following interaction equation to be derived

$$\frac{T_{sv}^2}{T_{svu}^2} + \frac{V^2}{V_u^2} + \sqrt{\frac{8h}{p}} \cdot \frac{T_{sv}V}{T_{svu}V_u} = \frac{(1+\lambda)}{2\lambda} \qquad 5.32$$

Here the same approximations have been introduced as before and the
steel ratio λ and the ultimate loads are those previously defined in
eqns. 5.8, 5.10 and 5.30.

The interaction equations 5.29 and 5.31, corresponding
to bottom and top steel failures respectively, are presented graphically
in fig. 5.9. The surface of revolution, derived in eqn. 5.32 for a
side failure, has been superimposed and the hatched area represents
the loading régime where this type of failure is likely to predominate.
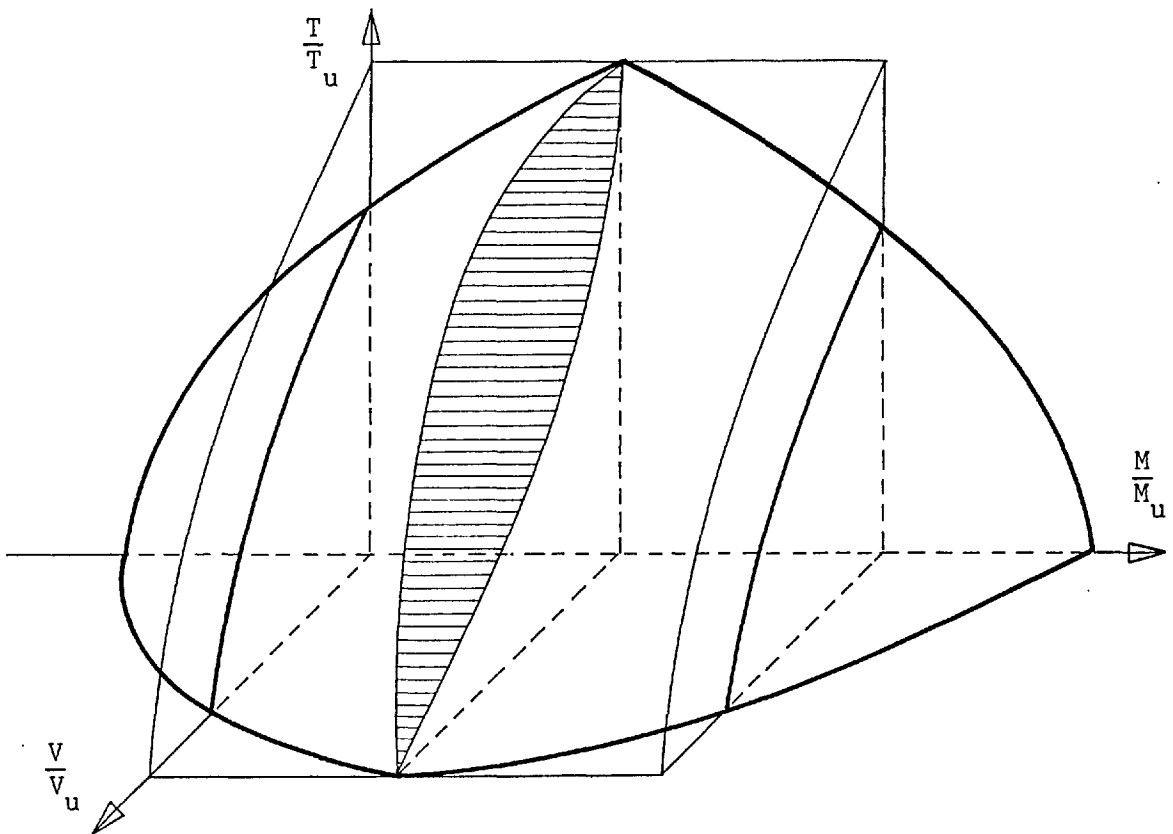
Figure 5.9   Moment/Torsion/Shear Interaction Surface

5.2.5   Limitations of the Simplified Failure Models

Both failure models form a sound basis for the strength analysis of reinforced and prestressed concrete members, subject to combined loads, and have been widely accepted in practice. In general, the assumptions summarized in §5.2.1 are not unduly restrictive and apply equally to most other forms of ultimate load analysis. In particular, assumptions (7), (8) and (11) are common analytical simplifications, and (1), (2), (3) and (9) merely ensure that the beam is fully under-reinforced and that collapse is not initiated by premature concrete failure. Only assumptions (4), (5), (6) and (10) relate specifically to the simplified analyses considered here and discussion will therefore be restricted to these points. Basically, (4), (5) and (6) all have a bearing on the actual position of the compression zone at failure while (10) essentially restricts the analysis to closed sections, since warping torsion is usually more significant in beams of open profile.

Position of the Compression Zone

For a particular mode of failure, the exact depth of the concrete compression zone is easily calculated from a knowledge of the ultimate strength and position of the various elements of longitudinal reinforcement. Several investigators have proposed adjustments to the theory to account for this variation in lever-arm, although the gain in accuracy is generally small for most practical applications. Furthermore, these modifications still assume that the compression zone forms parallel to one of the faces and it is, perhaps, this assumption that requires further investigation.

For idealised, singly-symmetric sections subject to torsion and bending moment only, the assumption that the compression zone forms at either the top or bottom of the beam is entirely satisfactory.

However, when shear is also included in the loading, certain anomalies are apparent which further restrict the applicability of the simple failure models. For example, by taking moments about the y'-axis for the top and bottom failure modes (fig. 5.6), we have

$$a \left(\frac{b}{s} \cdot D_y \cot\alpha_{by} \right) = 0 \qquad\qquad 5.33$$

from which, on introduction of eqns. 5.23 and 5.27, it may be concluded that either $V = 0$ or $T_{sv} = 0$. Therefore, eqns. 5.29 and 5.31 are only truly applicable where bending moment is present with either torsion or shear and are not suitable for studying the full interaction of combined loads. Furthermore, for the side mode of failure shown in fig. 5.8, moments taken about the x'-axis give

$$M_x = (Z_{ty} - Z_{by}) \cdot \frac{h}{2} \qquad\qquad 5.34$$

which, on introduction of eqns. 5.8 and 5.10, may be restated as

$$\frac{M_x}{M_{xu}} = \frac{(1-\lambda)}{4} \qquad\qquad 5.35$$

Therefore, although the applied bending moment does not appear in eqn. 5.32, the interaction equation governing a side mode of failure is only strictly correct when the condition derived in eqn. 5.35 is satisfied.

In practice, less restrictive conditions have been imposed on the use of the general interaction equations. It has been suggested, for example, that a top or bottom failure is probable in instances of either low shear or low torsion, and that a side mode of failure is more likely with high shear and torsion and low bending moment[29] However, it is clear that for more complex loading the simple failure models have reached the limit of their usefulness and an improved model is required.

Warping Torsion

Assumption (10) highlights a further limitation in that the theory is only truly applicable to St. Venant's torsion. In thin-walled

beams the torsional moment applied is rarely resisted by St. Venant shear stresses alone and, wherever warping is longitudinally restrained, these are supplemented by bimoment and warping torsional stresses. For closed box girders of practical cross-sectional dimensions, the inaccuracies due to neglecting these effects are usually small. However, this is certainly not the case when considering thin-walled open sections, especially after cracking, when the pure torsion capacity is often negligible in comparison to that of warping torsion[20].

These shortcomings do not detract from the undoubted usefulness of the simplified failure models for the analysis of simply systems but rather emphasise the limitations of their application. For beams subject to combined bending and torsional moments the simplicity of the approach is indeed attractive. This is particularly true when used for design purposes since complex formulae are often subject to error . or misinterpretation. However, when shear and warping restraint stresses are additionally considered, the assumption that the compression zone forms parallel to one side of the beam is unsatisfactory and a more general failure model is required.

5.3 AN ADVANCED FAILURE MODEL - CLOSED SECTIONS

It is clear that the apparent anomalies in the simplified methods are due to the inherent inflexibility of the selected model. Furthermore, during experimental investigations into the behaviour of reinforced concrete beams subject to combined load, this author has observed several instances in which the compression zone has formed about one of the corners at failure. Johnston and Zia[44] and Goode[32] have also made similar observations during tests on prestressed and reinforced concrete beams, respectively. A refined model is therefore proposed which enables the effects of additional shear loads to be accommodated in a more rigorous fashion and at the same time eliminates the need for assumptions (4), (5) and (6) in §5.2.1.

In the previous section the ultimate equilibrium method has been used as a basis for including shear in an approximate manner, although similar results have also been achieved by using the space truss analogy[28,58]. Thus, the two methods, while conceptually very different, have so far provided identical failure criteria for all applications of combined load. The theoretical differences between the two methods have been investigated by Kuyt[57] who concludes that identical results will always be obtained provided that the approximations outlined in eqn. 5.19 are introduced. These only relate to the lever-arms of the various components of transverse reinforcement since the lever-arm of the main steel is the same in both theories. Furthermore, Lampert[59] argues that the centrelines of the longitudinal steel are the most appropriate points for defining the dimensions of the idealised section since the corner bars are essential in the transfer of the transverse steel forces between adjacent shear walls. For members of practical dimensions, where reinforcement diameters are very much smaller than the breadth of the individual shear walls, the

difference is almost certainly neglegible. However, for beams

typically used in laboratory investigations, the difference can be

appreciable and the space truss analogy is likely to be conservative.

In reality, the actual distinction between the two approaches

only relates to the technique whereby the unknown crack angle is

determined. Indeed, both are essentially lower bound methods in the

general theory of plasticity in which equations of equilibrium are used

to arrive at a solution. An upper bound approach, based on kinematic

theory, has also been derived[60] for combined bending and torsion and

provides the dual solution. Therefore, any difference between the space

truss analogy and the ultimate equilibrium method are due entirely to the

approximations introduced during the initial idealization of the section

and not to the method of analysis.

Thus, since there are no obvious theoretical advantages

associated with either method, the final choice for the advanced approach

must be made on practical considerations alone. On this basis the space

truss analogy has several overriding attractions despite the more

widespread use of the ultimate equilibrium method by other researchers.

For example, the formulation of the space truss analogy is often more

straightforward since the equations of equilibrium are derived at a

single point along the member; for the alternative method, a failure

surface of finite length must first be assumed. Although there is no

apparent advantage in the analysis of simple rectangular sections, this

is not the case when the effects of shear are included. Under these

circumstances, the ultimate equilibrium method requires a more complex

failure surface to account for variations in bending moment which occur

over the length of the failure surface. This has already been demon-

strated in §5.2.4. However, when warping restraint effects are con-

sidered, in addition to bending moment and shear in both directions, additional complexities are introduced.   Furthermore, the ultimate equilibrium method only produces the correct solution if the true failure surface has been selected initially.   For asymmetrical sections with irregular arrangements of reinforcement this is difficult to ensure and once again the direct formulation of the space truss method is preferable.

5.3.1 Location of the Compression Zone

In the simplified method of analysis, failure was assumed to occur with the neutral axis parallel to any one face of the section. This is no longer a necessary requirement for the advanced failure model in which the compression zone can form at any position around the perimeter.   However, since a corner failure is now conceptually possible, the assumption that the centre of action of the compression zone coincides with the centroid of the unyielded steel is unrealistic.

Therefore, one of the first requirements of the advanced method is to establish the location of the centre of action of the compression zone for any orientation of the neutral axis.   A computer program has been written for this purpose which enables the characteristics of the compression zone to be determined for a finite number of different neutral axis orientations.   The procedure adopted for solution incorporates an iterative technique which first requires the section to be represented as an assemblage of discrete elements.   These are based on a rectangular grid, as shown in fig. 5.10b for the typical box section, and should be more finely spaced at the corners in order to provide an accurate evaluation of compressive forces for corner modes of failure. In its existing form the program has provision for a maximum of 512 elements; this enables the rectangular section to be represented as
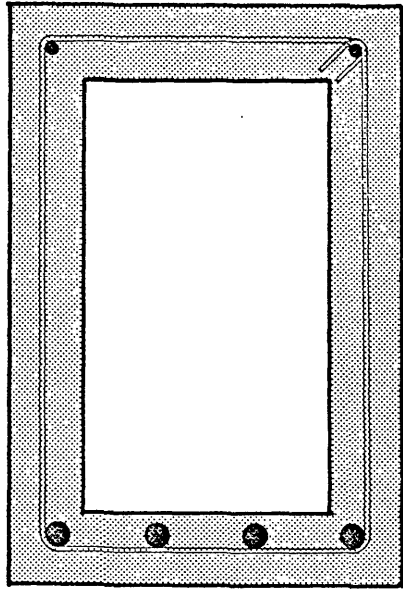
a. Typical Reinforced Concrete
Box Section
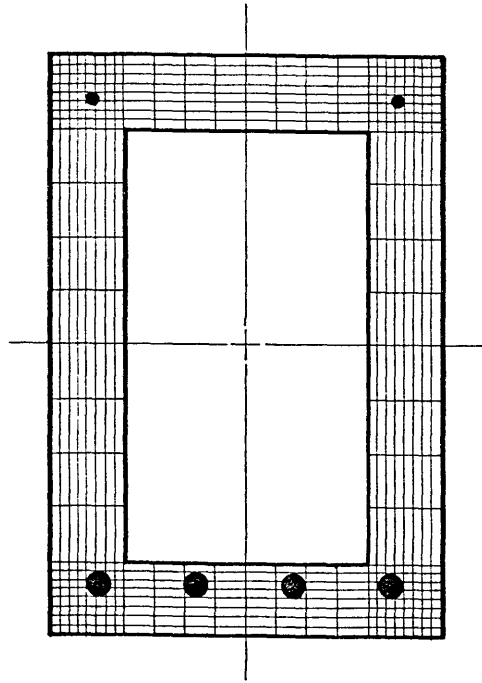
b. Rectangular Grid defining
Concrete Elements
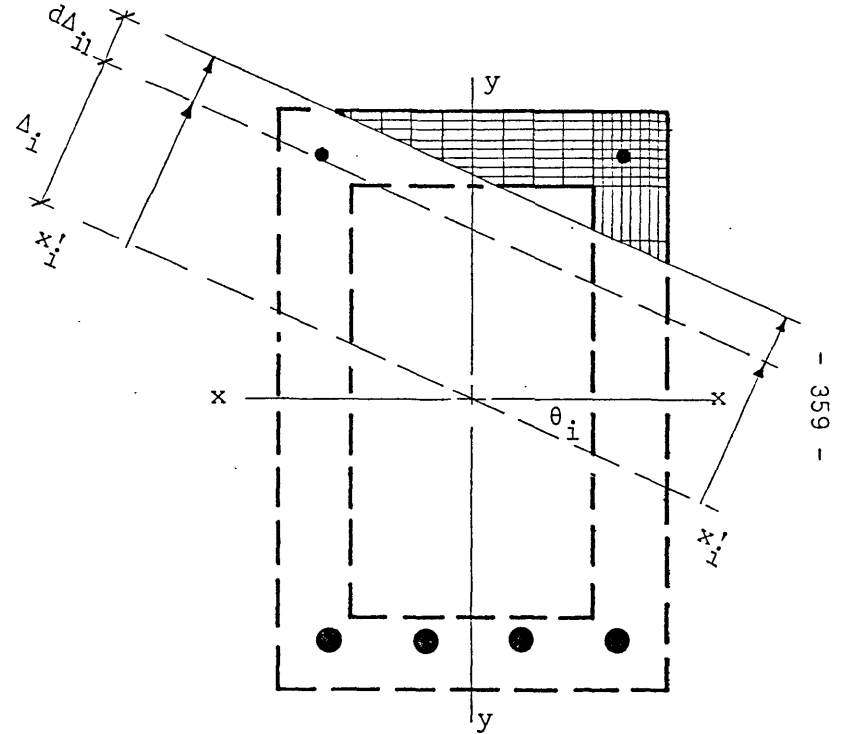
c. Neutral Axis and Compression
Zone at Failure

Figure 5.10   Representation of a Typical Box Section as an Assemblage of Rectangular Elements

eight solid rectangular components (two flanges, two webs and four corners), each comprising 8 x 8 elements. However, the program is also suitable for solid beams (utilizing a similar idealization) or for irregular sections including those with an open configuration.

A flow chart describing the action of the computer program is shown in fig. 5.11. In the first instance, the netural axis $x_i' - x_i'$ is orientated at an angle θ_i and is assumed to pass initially through the section centre (fig. 5.10c). Then, by locating the extreme concrete fibre in compression and assigning to it the input value of the maximum permissible strain, the distribution of longitudinal strain is defined over the entire cross-section. The Bernoulli hypothesis of plane sections applies in this analysis, and concrete is assumed to have no tensile capacity.

With the strain thus determined, the effective stress at the centre of each concrete and steel element is calculated from the appropriate stress/strain curve. These curves form part of the initial input data and are discussed later. The total compressive force in the steel and concrete above the neutral axis is then computed and compared with the tensile steel force from below the axis. If the total compressive force exceeds that in tension, the neutral axis must be moved in the direction of the compression zone while maintaining its initial orientation. The first displacement, Δ, is predetermined in the program and is a function of the section geometry. The procedure is repeated and the discrepancy in compressive and tensile forces is calculated once again. Since two such values are now available, the program makes use of a specially developed algorithm to predict the most likely change in the neutral axis position, $d\Delta_{i1}$, for a balanced failure to occur (fig. 5.10c). This iterative technique is continued

START → Read and Output Initial Data

Set
I=1; J=1; Δ=0;

I=I+1; J=1

Set Orientation of Neutral Axis to θ_j

Set eccentricity of Neutral Axis to Δ

Calc. eccentricity of extreme concrete fibre from N. Axis

Calculate strain at the centre of each steel & conc. element

Calc. force in each steel element (Z_t = tension; Z_c = comp.)

Calc. force in each concrete element in compression (F_c)

Set
$\Delta = \Delta_{init.}$

J=20
I=1 & J=1
Forces Balance

no no no

yes yes yes

I=N

no

Calculate $\Sigma Z_t xy$; $\Sigma Z_t x$; $\Sigma Z_t y$

yes

STOP

Output Computed Data

Figure 5.11   Flow Chart for Computing the Position of the Compression Zone at Failure

until the compressive and tensile forces agree to within a specified
tolerance.   An upper limit of 20 iterations has been set in the program,
in case of convergence problems, although 3-6 iterations are usually
sufficient for an imbalance of less than 0.1%.   When this condition
is satisfied, the centre of action of the compressive forces is com-
puted together with the total force in the concrete and in both com-
ponents of steel.

A different orientation of the neutral axis, θ_{i+1}, is then
selected automatically and the procedure is repeated for solution.
However, since the depth of the neutral axis does not alter signifi-
cantly with a small change in orientation, the final displacement of
the previous neutral axis (given by $\Delta_i + d\Delta_{i1} + d\Delta_{i2} \ldots$) is now used
as an estimate of the new initial displacement, Δ_{i+1}.

A description of all the necessary input data and the selected
format (standard 80 column cards) is given in Table 5.2.   The stress/
strain curve adopted for the concrete elements is the rectangular-
parabolic relationship defined in CP110[123].   Values of concrete cube
strength and limiting concrete strain form part of the input data;
the partial safety factor, γ_m, is taken to be unity.   In the case of
steel, the short term design curve from CP110 has also been used, and
has the form shown in fig. 5.12a.   This relationship is defined in
terms of the $\sigma - \varepsilon$ co-ordinates at the four changes of slope where γ_m
is once again of unit value.   These identifying co-ordinates are input
for each bar separately (Table 5.2) thus enabling sections comprising
different types of longitudinal steel to be analysed.   Any element of
prestressing steel can then be accommodated by simply reducing the
capacity of the steel by the appropriate value of prestrain, as shown
in fig. 5.12b.   However, in this situation, a preload equivalent to

	Parameter	Description	Format
Problem Size	M	Number of main concrete segments	2I5
	N	Number of steel elements	
Integer Parameters defining the Section	AMIN	Initial Orientation of neutral axis, θ_1	7F10.2
	AMAX	Final orientation of the neutral axis, θ_n	
	DA	Increment of orientation, $d\theta$ $i.e.\ \theta_2 = \theta_1 + d\theta$, etc.	
	ACCP	Acceptable error (%) between tensile and compressive forces	
	FCU	Concrete cube strength (N/mm^2)	
	ECU	Limiting concrete strain $(\mu\varepsilon)$	
	P	Prestressing force (N)	
Designation of Concrete Segments (I = 1, M)	W(1,I)	Length of segment (I) in x-direction	5F10.2
	W(2,I)	Length of segment (I) in y-direction	
	W(3,I)	Orientation (degrees, positive clockwise)	
	W(4,I)	Offset in x-direction	
	W(5,I)	Offset in y-direction	
	W(6,I)	Number of elements in x-direction	2I10
	W(7,I)	Number of elements in y-direction	
Designation and Properties of each Steel Element (J = 1, N)	Z(1,J)	Area of steel element (J), (mm^2)	11F7.1
	Z(2,J)	Location in x-direction	
	Z(3,J)	Location in y-direction	
	Z(4,J)	Strain $(\mu\varepsilon)$	
	Z(5,J)	Stress (N/mm^2)	
	Z(6,J)	Strain $(\mu\varepsilon)$	
	Z(7,J)	Stress (N/mm^2)	
	Z(8,J)	Strain $(\mu\varepsilon)$	
	Z(9,J)	Stress (N/mm^2)	
	Z(10,J)	Strain $(\mu\varepsilon)$	
	Z(11,J)	Stress (N/mm^2)	

(Z(4,J) through Z(11,J): See fig. 5.12)

Table 5.2 Format of Input Data for the Computation of the Centre of Action of the Compression Zone

a. Unstressed Reinforcement

b. Prestressed Reinforcement
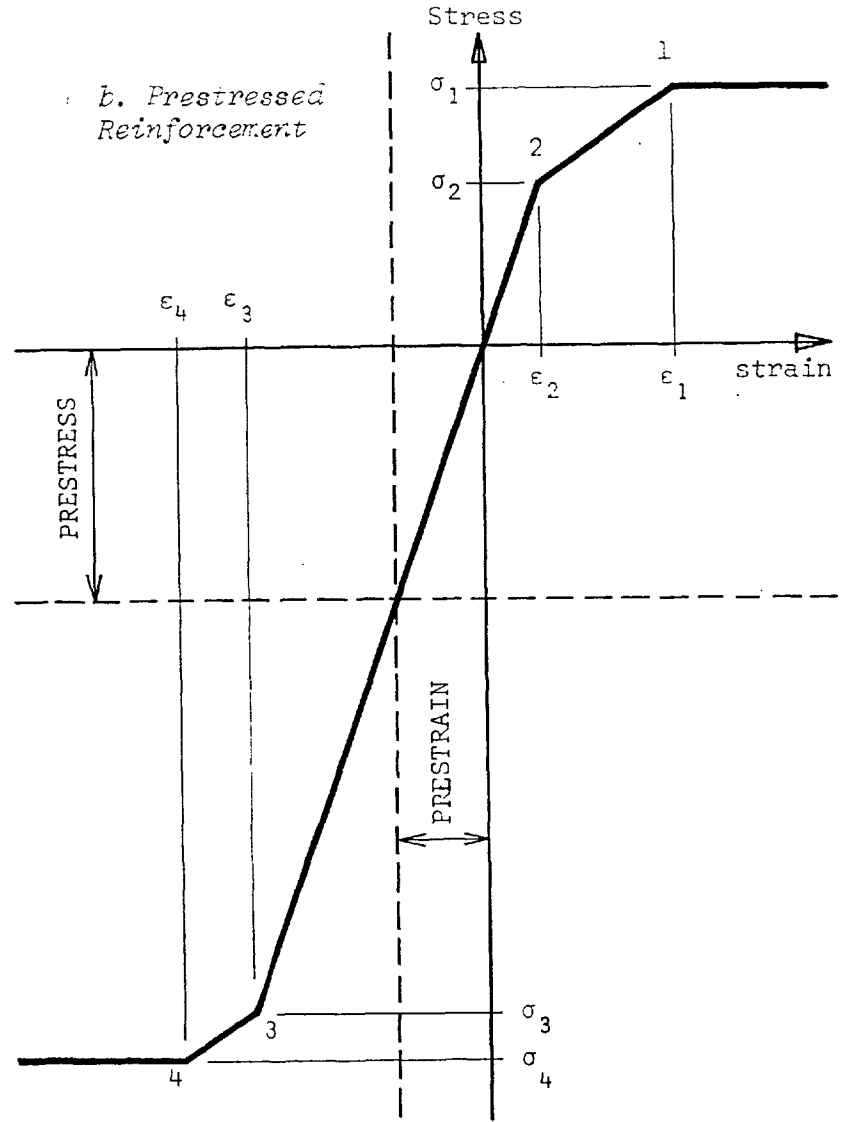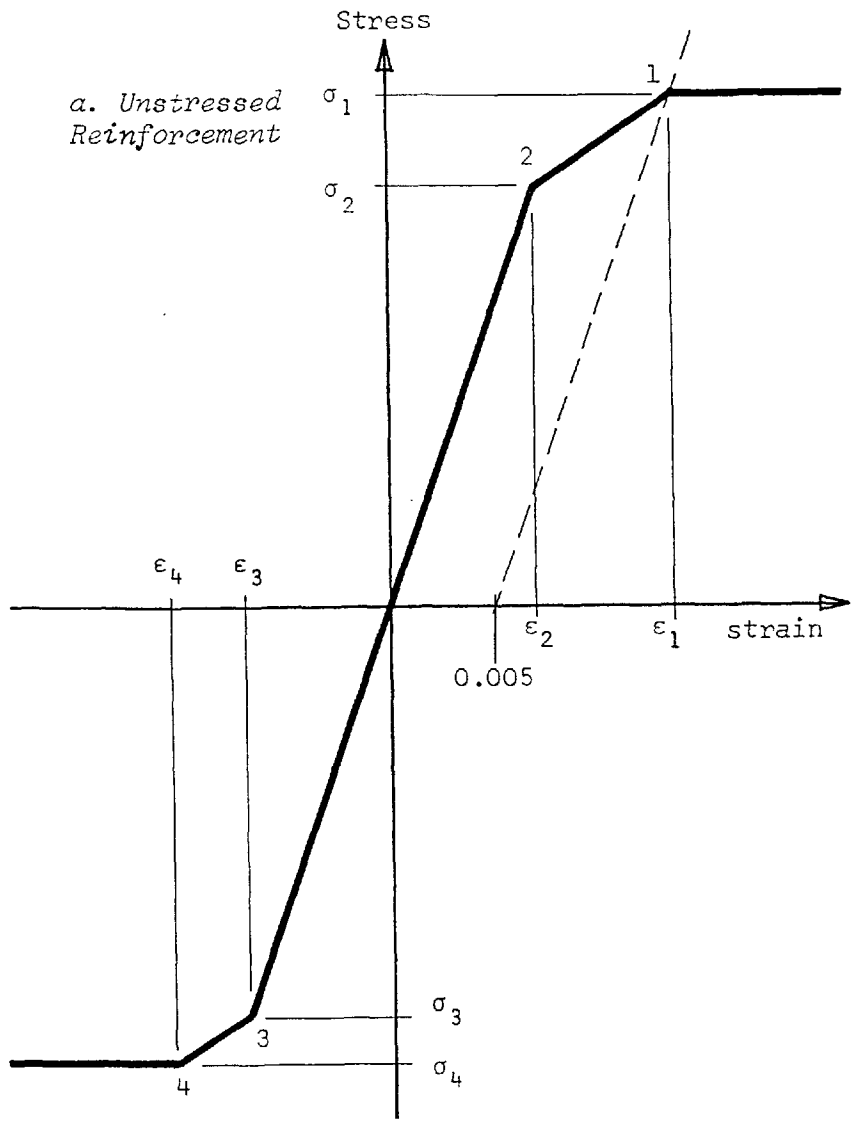
Figure 5.12   Idealized Stress/Strain Curve for Steel Reinforcement

the total prestressing force in all the elements of steel must also be specified in the input data and is then included in the subsequent calculation of the total compressive force.

An idealized single cell box girder is presented here as an example of the performance of the computer program. The selected section is singly-symmetric about the vertical axis, has a constant wall thickness of 50 mm and is 450 mm square overall. Reinforcement consists of high yield steel bars (425 N/mm^2) with an area of 200 mm^2 in each of the top corners and of 400 mm^2 in each of the bottom corners.

The section has subsequently been analysed for a variety of different neutral axis orientations. Results of the study are shown in fig. 5.13 for an initially horizontal orientation which was then increased in increments of 10°. The various lines on this figure relate to different values of axial load between 0 - 60 kN. Since the same stress/strain curve has been used for the steel in each case, these are not prestressing forces but represent a series of externally applied end loads.

Clearly, the axial loads have little effect on the final position of the compression zone when the neutral axis is parallel to any of the concrete faces. Furthermore, the computed centre of action in each of these cases is just outside the wall centreline. This fully justifies the simplification adopted in §5.2 in which the centre of action was assumed to be coincident with the centroid of the unyielded steel. However, for failures about the corners, the effective centre of the compression zone is often well within the centreline dimensions, particularly when the section is subjected to high end loads.

5.3.2 Formulation of the General Interaction Equation

The advanced failure model is similar to the simplified version
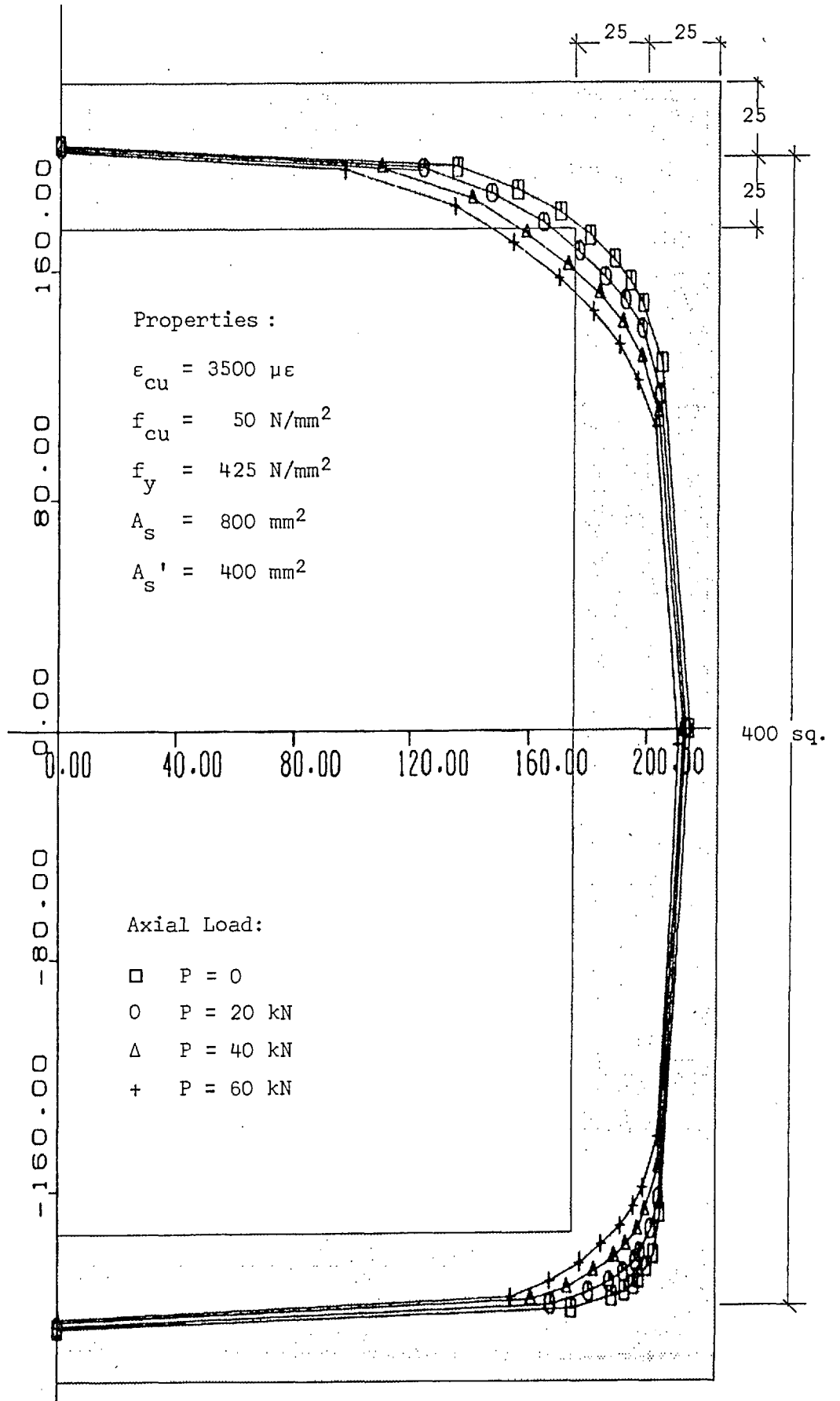
*Figure 5.13 Position of the Centre of Action of the Compressive
Forces in an Idealized Box Section subject to Axial Load*

adopted in §5.2.2 in as far as the shear flow in each wall (between reinforcement bars) is taken to be constant. The total compressive force is also assumed to act at a single point at failure, although there is no longer any requirement for this to be coincident with the centroid of the unyielded steel.

The two equilibrium conditions (eqns. 5.3 and 5.4) may now be restated, together with two further equations of equilibrium, in the following general form:

$$\sum_{i=1}^{m} Z_i - Z = N + \sum_{j=1}^{n} F_j.b_j.\cot \alpha_j$$

$$\sum_{i=1}^{m} Z_i.y_i - Z.y = M_x + \sum_{j=1}^{n} F_j.b_j.y_j.\cot \alpha_j$$

$$\sum_{i=1}^{m} Z_i.x_i - Z.x = M_y + \sum_{j=1}^{n} F_j.b_j.x_j.\cot \alpha_j$$

$$\sum_{i=1}^{m} Z_i.x_i.y_i - Z.xy = W + \sum_{j=1}^{n} F_j.b_j.x_j.y_j.\cot \alpha_j$$

5.36

where Z is the total compressive force (steel and concrete)

Z_i is the tensile force in the ith component of reinforcement

x,y are the co-ordinates of the total compressive force, Z

x_i, y_i are the co-ordinates of the ith component of reinforcement

x_j, y_j are the co-ordinates of the centre of the jth shear wall

F_j, b_j, α_j respectively represent the shear flow, breadth and

angle with respect to the jth shear wall.   In addition, the term W in the fourth of eqns. 5.36 is equivalent to a system of longitudinal warping forces which have zero resultant direct force or bending moment. This is not strictly a bimoment due to warping restraint, in the sense defined in Chapter 2, but may be conveniently thought of as an externally applied bimoment.

By multiplying the first three expressions in eqn. 5.36 by $x.y$, x and y, respectively, they may subsequently be combined with the fourth expression in such a way as to eliminate the total compressive force term, Z. Then, on introducing the general definition of $\cot \alpha_j$ (from eqn. 5.22) for the jth wall element, we have

$$x.y.N - x.M_x - y.M_y + W + x.y. \sum_{j=1}^{n} F_j^2 b_j \frac{s_j}{D_j}$$

$$- x. \sum_{j=1}^{n} F_j^2 b_j \frac{s_j}{D_j} y_j - y. \sum_{j=1}^{n} F_j^2 b_j \frac{s_j}{D_j} x_j + \sum_{j=1}^{n} F_j^2 b_j \frac{s_j}{D_j} x_j y_j$$

$$= x.y. \sum_{i=1}^{m} Z_i - x. \sum_{i=1}^{m} Z_i y_i - y. \sum_{i=1}^{m} Z_i x_i + \sum_{i=1}^{m} Z_i x_i y_i$$

$$5.37$$

By expanding the right-hand side of this equation and rearranging, this may be written more simply as

$$RHS = \sum_{i=1}^{m} Z_i x_{ci} y_{ci} \qquad 5.38$$

where x_{ci}, y_{ci} are the co-ordinates of the ith steel element in tension with reference to the centre of action of the compressive forces. Thus, it only remains to determine the shear flows $F_j (j = 1, n)$ explicitly in terms of the various stress resultants for eqn. 5.37 to be rewritten in the form of a general interaction equation.

The Rectangular Beam

Consider the idealized reinforced or prestressed concrete beam detailed in fig. 5.14 which is singly symmetric about the vertical axis. Direct thrust and torsion are applied about the section centre while components of bending moment and shear force are applied with

respect to both the vertical and horizontal axes. Accordingly, the shear flows in each wall (subscripted t, b, l or r for the top, bottom, left- and right-hand sides, respectively) may be alternatively expressed as

$$F_t = F_{sv} + F_{vx}$$

$$F_b = F_{sv} - F_{vx}$$

$$F_l = F_{sv} + F_{vy}$$

$$F_r = F_{sv} - F_{vy}$$

5.39
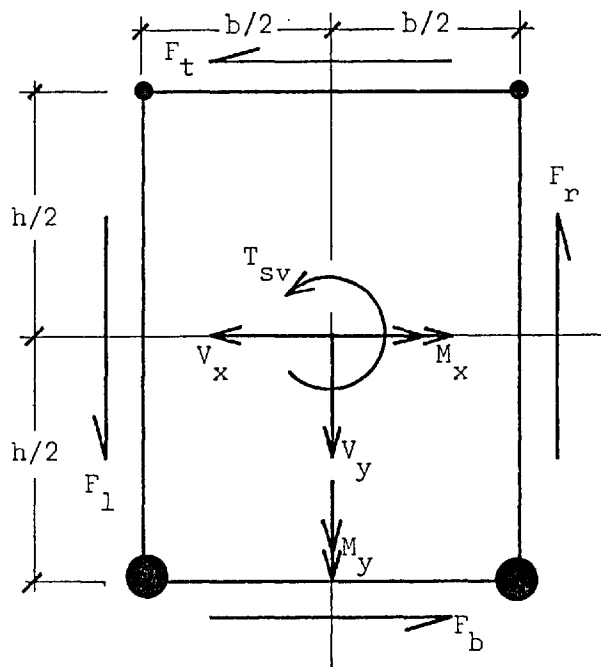
Figure 5.14   Idealized Rectangular Beam adopted for the Advanced Failure Model

In general, there is also a component of shear flow in each wall element due to the system of warping stresses, W. However, since forces created by warping restraint are rarely a problem in closed sections at ultimate load, these have been entirely neglected from the study at this stage.

On substitution of the appropriate terms from eqn. 5.39 into eqn. 5.37, and after considerable rearrangement, we have, at failure

$$xyN - xM_x - yM_y + \frac{s}{D_y}\left\{(F_{sv} + F_{vx})^2 (y - h/2)bx\right.$$

$$+ (F_{sv} - F_{vy})^2(x - b/2)hy + (F_{sv} + F_{vy})^2(x + b/2)hy\left.\right\} =$$

$$\sum_{i=1}^{m} Z_{iy} \cdot x_{ci} y_{ci} \qquad\qquad 5.40$$

where the spacing and yield force of the stirrups are assumed to be constant on all sides. Furthermore, the various components of shear flow may also be written in the following form:

$$F_{sv} = T_{sv}/\Omega \qquad\qquad (2.44)$$

$$F_{vy} = V_y/2h \qquad\qquad (5.21)$$

$$F_{vx} = V_x/2b \qquad\qquad 5.41$$

After substitution of these expressions into eqn. 5.40 and division throughout by the right-hand side, an interaction equation is finally derived, thus:

$$\frac{N}{N_u} + \frac{M_x}{M_{xu}} + \frac{M_y}{M_{yu}} + \frac{T_{sv}^2}{T_{svu}^2} + \frac{V_x^2}{V_{xu}^2} + \frac{V_y^2}{V_{yu}^2} - \frac{h}{y}\sqrt{\frac{2b}{p}} \cdot \frac{T_{sv}}{T_{svu}} \frac{V_x}{V_{xu}}$$

$$+ \frac{b}{x}\sqrt{\frac{2h}{p}} \cdot \frac{T_{sv}}{T_{svu}} \frac{V_y}{V_{yu}} \qquad = \qquad 1 \qquad\qquad 5.42$$

In the derivation of eqn. 5.42, various ultimate load terms have been introduced and are defined in the following way:

$$N_u = \frac{\Sigma Z_{iy} x_{ci} y_{ci}}{xy}$$

$$M_{xu} = - \frac{\Sigma Z_{iy} x_{ci} y_{ci}}{x}$$

$$M_{yu} = - \frac{\Sigma Z_{iy} x_{ci} y_{ci}}{y}$$

$$T_{svu} = \Omega\sqrt{\frac{D_y \cdot \Sigma Z_{iy} x_{ci} y_{ci}}{spxy}}$$

$$\left.\right\} \quad 5.43$$

$$V_{xu} = \sqrt{\frac{2bD_y \ \Sigma \ Z_{iy} x_{ci} y_{ci}}{sxy}}$$

$$V_{yu} = \sqrt{\frac{2hD_y \ \Sigma \ Z_{iy} x_{ci} y_{ci}}{sxy}}$$

The summations in all of these terms are carried out over the range

$i = 1, m$ and are only effective for elements of reinforcement in tension.

5.3.3 Theoretical Investigation of Observed Corner Failures

Well documented experimental results already exist for an exten-

sive series of ultimate load tests on prestressed concrete beams. The

series comprised thirty-seven beams with the hollow cross-section shown

in fig. 5.15, and were constructed and tested by Johnston and Zia[44] under

different combinations of bending moment, torsion and shear. Five of

the beams have been omitted from this study since they had no stirrup

reinforcement and thus did not comply with assumption (1) in §5.2.1

relating to fully under-reinforced sections. In addition, the ultimate

torsional capacity computed for one of the other beams was evidently

less than the torque necessary for the full development of cracks.

Failure was therefore delayed until first cracking and this result has

also been excluded from the subsequent theoretical investigation. Of

the remaining beams, approximately one-third were tested under bending

moment and torsion only and, as expected, failure invariably occurred

with the neutral axis parallel to one or other of the concrete faces.

However, the other two-thirds of the beams were subjected to various

combinations of bending moment, torsion and shear. In approximately

20% of these tests failure was observed about one of the corners.

Cross-sectional Idealization

The idealization of the concrete sections is detailed in fig.

5.15b. Each web and flange element has a thickness corresponding to

the minimum wall thickness in the original section while the dimensions
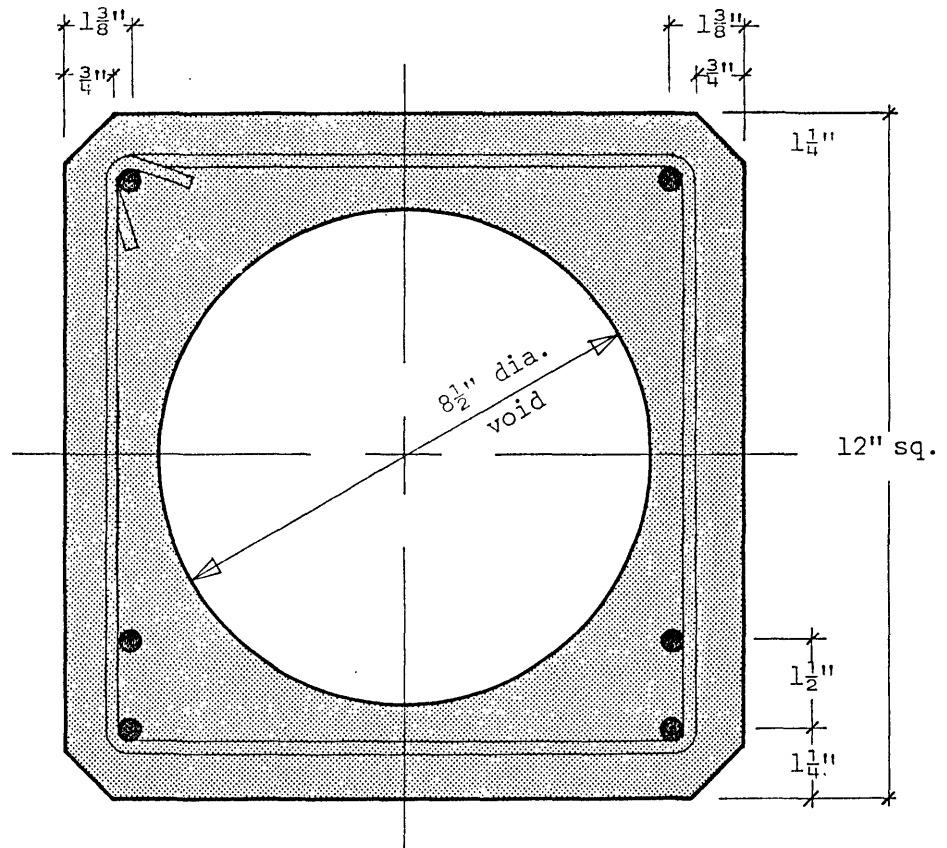
a. *Cross-section of Prestressed Concrete Beams*
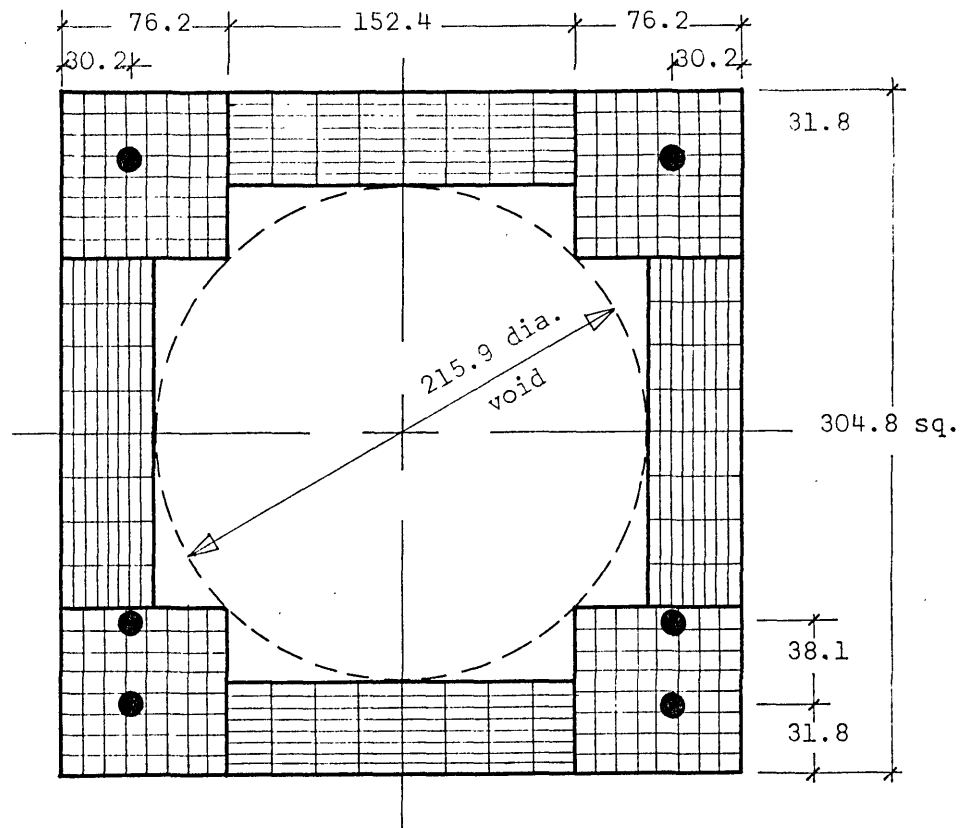
b. *Idealization adopted for the Computer Analysis*

Figure 5.15   Cross-section of Prestressed Concrete Beams tested in Combined Bending, Torsion and Shear[44]

of the square corner elements are defined by the diameter of the void.
Since the neutral axis is always well within the assumed concrete
section at failure, neglecting the small area of concrete adjacent to
the circular void has no effect. However, this is not the case in
the approximate idealization of the corner elements where the external
corner chamfer has not been taken into account. This results in an
over-estimation of the concrete area in the most highly stressed zone,
the result of which tends to increase the offset of the neutral axis
from the section centre. Nevertheless, this effect is nullified to a
large degree since the limiting concrete strain is also invariably
located at one of the corners. Thus, the most highly stressed region
always occurs in the non-existent corner chamfer which has a small total
area. The effective stress on the remaining (and relatively much
larger) concrete area in compression is therefore correspondingly
reduced and this requires the neutral axis to return towards the section
centre for a balanced failure.

Since the position of the netural axis is not greatly influenced
by the adopted idealization of the concrete section, the quantity of
of steel in the tensile zone and its eccentricity from the axis of zero
strain is also relatively unaffected. However, this is not necessarily
the case with respect to the position of the centre of action. The
stress distribution across the compression zone is clearly altered by
including the corner chamfers and has the general effect of increasing
the distance of the centre of action from the section centre. Never-
theless, in trial calculations in which the chamfer has been included,
the error was always less than 2% of the effective lever-arm to the
main tension steel and is thus well within anticipated experimental
error.

Location of the Compression Zone

Six 9.5mm diameter stress relieved prestressing strands were used in each section. These were symmetrically disposed about the vertical axis. Each of the bottom four strands were pretensioned to an initial value of 62 kN whereas the top pair were only nominally stressed to 9 kN. Total losses in each pair of strands were measured at the time of test and are detailed by Johnston and Zia[44] separately for each beam. However, since the level of prestress is a necessary input parameter in the computer program detailed in §5.3.1, a full analysis of each section has been avoided by determining the mean value of effective stress for each pair of cables. These levels of effective prestress did not vary greatly between beams (standard deviation < 20 N/mm^2 in all instances) and are presented in Table 5.3 together with the four pairs of values defining the stress/strain relationship for each cable position (fig. 5.12).

Quantity		Top Cables	Bottom Cables
Mean prestress (N/mm^2)		32	878
Mean prestrain ($\mu\epsilon$)		160	4392
σ_1	Stress (N/mm^2) (see fig. 5.12)	1818	971
σ_2		1448	601
σ_3		-1511	-2358
σ_4		-1881	-2728
ϵ_1	Strain ($\mu\epsilon$) (see fig. 5.12)	14090	9858
ϵ_2		7240	3008
ϵ_3		-7560	-11792
ϵ_4		-14410	-18642

Table 5.3   Mean Levels of Prestress and Stress/Strain Relationships adopted for the Computer Analysis

The entire series of test beams were constructed from three different batches of concrete. Two standard 12" x 6" diameter cylinders were also cast for each beam and the mean compressive strength, f_{cy} (p.s.i.), is given in Table 5.4. To convert these values to the equivalent cube strength, f_{cu}, adopted by CP110[123], the following empirical relationship stated by Neville[80] has been employed:

$$f_{cy} = \left[0.76 + 0.2 \log_{10} \frac{f_{cu}}{2850}\right].f_{cu} \qquad\qquad 5.44$$

Here, the cylinder and cube strengths are given in p.s.i. although the derived values of f_{cu} are also presented in Table 5.4 in SI units.

Casting Number	f_{cy}^{44} (p.s.i.)	f_{cu}^{80} (p.s.i.)	f_{cu} (N/mm^2)
1	4063	5020	34.62
2	5853	6985	48.17
3	5353	6440	44.41

Table 5.4 Mean Concrete Compressive Strengths at the Time of Test

The section was subsequently analysed using the computer program detailed in §5.3.1. This was repeated three times in order to take account of the varying cube strengths of the different concrete mixes. Limiting compressive strain at the extreme concrete fibre was specified as 3500 $\mu\varepsilon$ in all cases, while the total compressive force due to pre-stressing was calculated from the effective stresses in Table 5.3 to be 184.8 kN. Computed co-ordinates of the centre of action of the compressive forces are tabulated in Table 5.5 together with the term $\sum_i Z_i.x_{ci}y_{ci}$ derived previously in eqn. 5.38. Variations between the x, y co-ordinates, determined for the different concrete cube strengths, are more clearly visible in fig. 5.16.

Neutral Axis Orientation	Casting No.1(34.62 N/mm^2)			Casting No.2(48.17 N/mm^2)			Casting No.3(44.41 N/mm^2)		
	x(mm)	y(mm)	Π(MN.mm^2)	x(mm)	y(mm)	Π(MN.mm^2)	x(mm)	y(mm)	Π(MN.mm^2)
0°	0	126.67	-87.20*	0	132.82	-89.57*	0	131.39	-89.02*
10°	29.72	125.49	2698.33	40.25	129.57	3641.84	37.81	128.65	3448.11
20°	58.85	120.01	4773.01	71.73	122.82	6152.66	68.89	122.16	5828.05
30°	79.79	112.48	6015.48	89.22	116.05	7106.00	87.04	115.17	6822.28
40°	94.25	104.38	6743.85	100.62	108.97	7605.12	99.14	107.91	7385.33
50°	104.91	94.71	7049.60	109.37	100.89	7874.21	108.36	99.44	7669.90
60°	113.31	81.69	6959.14	116.52	89.94	7822.35	115.71	88.16	7611.41
70°	120.62	60.86	6236.29	123.04	72.31	7222.35	122.46	69.85	6988.13
80°	126.07	28.25	4370.37	130.05	41.39	5284.72	129.20	38.51	5082.02
90°	128.04	-3.82	1747.46	133.48	-2.35	1939.41	132.09	-2.69	1893.43
100°	126.53	-35.10	-228.12	130.04	-44.40	-1045.23	129.21	-42.30	-820.68
110°	120.96	-63.89	-2015.10	123.50	-75.08	-2904.20	122.87	-72.57	-2692.21
120°	114.05	-82.29	-2836.72	117.28	-90.76	-3649.40	116.46	-88.89	-3474.75
130°	106.40	-94.69	-3198.37	110.50	-100.80	-3993.72	109.47	-99.29	-3834.81
140°	97.31	-104.26	-3458.04	102.50	-108.56	-4156.10	101.19	-107.47	-4024.78
150°	84.66	-112.10	-3529.91	91.72	-115.41	-4109.15	90.16	-114.56	-3976.89
160°	64.39	-119.30	-3067.59	74.05	-122.07	-3621.62	71.84	-121.41	-3481.59
170°	32.58	-125.43	-1680.33	40.65	-129.61	-2335.61	38.87	-128.67	-2179.63
180°	0	-127.24	50.85*	0	-131.64	55.55*	0	-130.57	54.78*

* see eqn. 5.49

Table 5.5   Computed Co-ordinates of the Centre of Action of the Compressive Forces
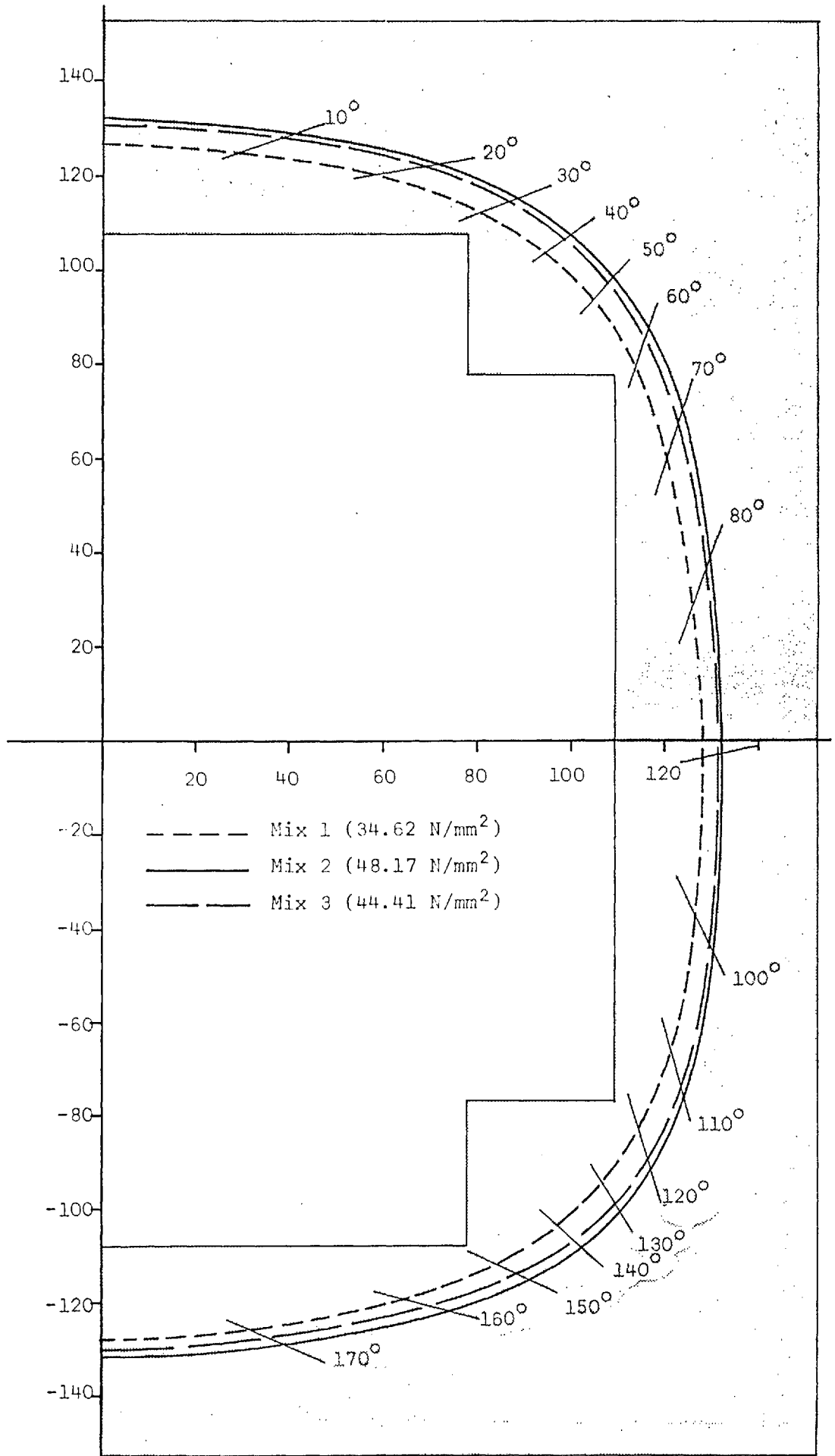
Figure 5.16 Loci of the Centres of Action of the Compressive
Forces corresponding to Casting Numbers 1-3

Theoretical Investigation

The concrete mix number and levels of applied load are listed in Table 5.6 for each of the thiry-one beams under consideration. This information has been abstracted from a table given by Johnston and Zia[44], and retains the original beam referencing system. Thus, the letter H refers to hollow sections while the numbers signify the shear span/ depth ratio, stirrup spacing (ins.) and the beam number, in that order.

For the stress resultants considered in this series of tests, eqn. 5.42 reduces to

$$\frac{N}{N_u} + \frac{M_x}{M_{xu}} + \frac{T_{sv}^2}{T_{svu}^2} + \frac{V_y^2}{V_{yu}^2} + \frac{b}{x}\sqrt{\frac{2h}{p}} \cdot \frac{T_{sv}}{T_{svu}} \frac{V_y}{V_{yu}} = 1 \qquad 5.45$$

However, since the stress/strain curves of the steel have been suitably modified to take account of the initial stress in the cables, pre- stressing effects must also be included in the interaction equation as external loads. Thus, the direct tension, N, is due entirely to the initial prestressing force (P = - 184.8 kN), while the term M_x repre- sents the sum of the bending moments due to both prestress and live loading. By introducing the various ultimate load expressions from eqn. 5.43 into eqn. 5.45 and rearranging, we therefore have

$$- x.M_x + \frac{spxy}{\Omega^2 D_y} \cdot T_{sv}^2 + \frac{sxy}{2hD_y} \cdot V_y^2 + \frac{sby}{\Omega.D_y} T_{sv}.V_y$$

$$= \sum_{i=1}^{n} Z_{iy} x_{ci} y_{ci} + Px(y + y_e) \qquad 5.46$$

where y_e is the vertical eccentricity of the initial prestressing force, P, measured from the section centre. The right-hand side of eqn. 5.46 has already been computed for a wide range of neutral axis positions and is denoted Π in Table 5.5.

Beam Ref. Number	Casting Ref. Number	Torsion/Shear Ratio($2T_{sv}/V_y b$) γ_1	Torsion/Bending Ratio($-T_{sv}/M$) γ_2
H-0-3-1	1	∞	∞
H-0-3-2	1	∞	4.83
H-0-3-3	1	∞	1.22
H-0-3-4	1	∞	2.20
H-0-3-5	1	∞	0.37
H-0-3-6	1	∞	0.61
H-0-6-1	1	∞	∞
H-0-6-2	1	∞	3.10
H-0-6-3	1	∞	0.22
H-0-6-5	2	∞	0.45
H-0-6-6	2	∞	0.11
H-4-3-1	1	9.88	4.52
H-4-3-2	1	4.96	1.85
H-4-3-3	3	1.25	0.34
H-4-3-4	3	0.62	0.29
H-4-3-5	2	2.50	0.51
H-4-6-1	2	10.00	3.10
H-4-6-2	2	0.62	0.19
H-4-6-3	2	1.25	0.24
H-4-6-4	3	0.63	0.11
H-4-6-5	3	2.47	1.23
H-6-3-1	2	10.07	1.36
H-6-3-2	2	4.91	1.12
H-6-3-3	2	2.50	0.33
H-6-3-4	2	1.89	0.17
H-6-3-5	2	1.26	0.12
H-6-6-1	3	9.42	4.31
H-6-6-2	3	4.82	2.05
H-6-6-3	3	2.48	0.37
H-6-6-4	3	0.63	0.06
H-6-6-5	3	1.26	0.12

Table 5.6   Casting and Loading Details for Prestressed Concrete Beam Tests[44]

The various geometrical parameters for this cross-section are determined from fig. 5.15 and are given by

$$b = 244.4 \text{ mm}$$

$$h = 241.4 \text{ mm}$$

$$p = 971.6 \text{ mm}$$

$$\Omega = 118.0 \times 10^3 \text{ mm}^2$$

Stirrup spacing for each beam is specified (in inches) by the second digit in the beam reference number. Thus, the figures 3 and 6 represent spacings of s = 76.2 mm and s = 152.4 mm, respectively. In addition, since the yield stress of the transverse reinforcement is recorded[44] as 270 N/mm^2, each leg of the 6.36 mm diameter stirrups has a yield force of D_y = 8551 N.

By introducing the numerical values of these various parameters into eqn. 5.46, a simple quadratic equation is derived in terms of the applied torque, T_{sv}, thus:

$$T_{sv}^2 \left\{ 8.1603 + \frac{16.221}{\gamma_1^2} + \frac{1982.1}{x.\gamma_1} \quad xys \right\} \times 10^{-12} + \frac{x.T_{sv}}{\gamma_2} = \Pi \qquad 5.47$$

In this expression, the loading ratios γ_1, γ_2, and the stirrup spacing, s, are uniquely defined for each beam. On the other hand, the co-ordinates of the centre of action of the compressive forces, x, y, together with the quantity Π, are variables dependent upon the orientation of the neutral axis. It therefore only remains to substitute the appropriate numerical values from Tables 5.5 and 5.6 into eqn. 5.47 for a solution of the applied torque necessary for failure in each case.

A programmable calculator was sufficient for determining the positive roots of each equation. These are presented in Tables 5.7 - 5.9 for the beams constructed from casting numbers 1-3, respectively. Clearly, when x = 0 (i.e. for θ = 0°, 180°), only the trivial solution

θ	BEAM REFERENCE NUMBER (Failure Torque in N.mm × 10⁷)										
	H-O-3-1	H-O-3-2	H-O-3-3	H-O-3-4	H-O-3-5	H-O-3-6	H-O-6-1	H-O-6-2	H-O-6-3	H-4-3-1	H-4-3-2
0°	3.387	3.198	2.847	3.051	2.028	2.446	2.353	2.253	1.317	–	–
10°	3.411	3.281	2.926	3.132	2.094	2.519	2.412	2.311	1.361	2.551	2.073
20°	3.297	3.161	2.793	3.006	1.951	2.377	2.331	2.226	1.262	2.732	2.313
30°	3.283	3.138	2.749	2.974	1.877	2.314	2.321	2.209	1.209	2.802	2.404
40°	3.320	3.164	2.748	2.988	1.837	2.289	2.348	2.227	1.178	2.867	2.471
50°	3.378	3.207	2.753	3.014	1.789	2.262	2.388	2.255	1.141	2.930	2.525
60°	3.477	3.279	2.763	3.058	1.718	2.220	2.459	2.305	1.087	3.013	2.584
70°	3.700	3.433	2.769	3.144	1.569	2.118	2.613	2.409	0.978	3.168	2.673
80°	4.442	3.892	2.685	3.333	1.191	1.776	3.141	2.715	0.722	3.604	2.840
90°	–	–	–	–	–	–	–	–	–	–	–
100°	0.909	1.500	3.963	2.423	12.448	7.618	0.643	1.111	10.451	1.379	2.106
110°	2.047	2.325	3.324	2.698	7.371	4.970	1.448	1.665	6.066	2.140	2.308
120°	2.205	2.416	3.146	2.693	6.081	4.327	1.554	1.724	4.934	2.215	2.282
130°	2.260	2.442	3.060	2.678	5.516	4.046	1.598	1.741	4.435	2.227	2.246
140°	2.341	2.506	3.057	2.718	5.219	3.925	1.655	1.784	4.163	2.268	2.248
150°	2.446	2.599	3.103	2.793	5.059	3.889	1.729	1.849	4.006	2.322	2.259
160°	2.534	2.677	3.145	2.859	4.942	3.869	1.792	1.904	3.889	2.322	2.197
170°	2.571	2.708	3.150	2.879	4.833	3.829	1.818	1.925	3.787	2.111	1.872
180°	2.535	2.670	3.105	2.838	4.764	3.774	1.792	1.897	3.732	–	–

Table 5.7   Predicted Failure Torques (θ = 0° – 180°) for Beams from Casting No. 1 (34.62N/mm²)

	BEAM REFERENCE NUMBER (Failure Torque in N.mm × 10^7)										
θ	H-0-6-5	H-0-6-6	H-4-3-5	H-4-6-1	H-4-6-2	H-4-6-3	H-6-3-1	H-6-3-2	H-6-3-3	H-6-3-4	H-6-3-5
0°	1.751	0.853	–	–	–	–	–	–	–	–	–
10°	1.778	0.863	1.543	1.871	0.559	0.792	2.454	2.091	1.385	1.001	0.766
20°	1.751	0.828	1.724	2.010	0.629	0.893	2.606	2.305	1.511	1.055	0.798
30°	1.702	0.780	1.742	2.028	0.638	0.904	2.610	2.333	1.506	1.028	0.773
40°	1.680	0.748	1.753	2.054	0.643	0.909	2.625	2.358	1.499	1.007	0.753
50°	1.668	0.720	1.764	2.090	0.648	0.913	2.652	2.389	1.492	0.986	0.734
60°	1.650	0.681	1.763	2.135	0.648	0.910	2.682	2.418	1.469	0.949	0.702
70°	1.602	0.609	1.731	2.213	0.638	0.886	2.714	2.442	1.401	0.871	0.637
80°	1.384	0.436	1.523	2.349	0.563	0.760	2.656	2.363	1.141	0.651	0.467
90°	–	–	–	–	–	–	–	–	–	–	–
100°	4.358	16.550	4.312	1.398	1.553	2.682	3.101	3.078	6.340	10.043	10.177
110°	3.173	9.987	3.157	1.622	1.142	1.883	2.855	2.733	4.191	6.122	6.109
120°	2.194	8.382	2.883	1.655	1.043	1.691	2.787	2.639	3.676	5.140	5.075
130°	2.802	7.629	2.740	1.669	0.991	1.591	2.752	2.587	3.416	4.640	4.545
140°	2.741	7.153	2.638	1.683	0.954	1.517	2.735	2.553	3.231	4.281	4.161
150°	2.703	6.793	2.531	1.690	0.914	1.441	2.716	2.511	3.052	3.941	3.797
160°	2.670	6.484	2.356	1.674	0.848	1.321	2.659	2.418	2.792	3.490	3.319
170°	2.699	6.213	1.951	1.614	0.696	1.055	2.516	2.167	2.229	2.584	2.378
180°	2.642	6.107	–	–	–	–	–	–	–	–	–

Table 5.8   Predicted Failure Torques ($\theta = 0^{\circ} - 180^{\circ}$) for Beams from Casting No. 2 (48.17N/mm^2)

θ	BEAM REFERENCE NUMBER (Failure Torque in N.mm × 10^7)								
	H-4-3-3	H-4-3-4	H-4-6-4	H-4-6-5	H-6-6-1	H-6-6-2	H-6-6-3	H-6-6-4	H-6-6-5
$0°$	–	–	–	–	–	–	–	–	–
$10°$	1.109	0.794	0.486	1.240	1.864	1.567	1.084	0.377	0.636
$20°$	1.245	0.893	0.527	1.428	2.001	1.747	1.207	0.388	0.677
$30°$	1.263	0.910	0.525	1.480	2.027	1.789	1.224	0.376	0.669
$40°$	1.275	0.922	0.523	1.520	2.061	1.828	1.237	0.367	0.659
$50°$	1.281	0.931	0.519	1.558	2.103	1.869	1.246	0.358	0.648
$60°$	1.276	0.933	0.509	1.596	2.155	1.915	1.246	0.342	0.627
$70°$	1.239	0.920	0.480	1.647	2.246	1.984	1.223	0.309	0.578
$80°$	1.060	0.823	0.439	1.709	2.446	2.106	1.080	0.226	0.439
$90°$	–	–	–	–	–	–	–	–	–
$100°$	3.902	2.110	2.681	1.343	1.219	1.338	3.048	4.829	5.353
$110°$	2.696	1.562	1.706	1.414	1.546	1.534	2.215	2.867	3.257
$120°$	2.399	1.427	1.464	1.407	1.595	1.554	2.012	2.354	2.723
$130°$	2.248	1.357	1.345	1.395	1.616	1.557	1.909	2.107	2.457
$140°$	2.139	1.307	1.260	1.386	1.635	1.561	1.836	1.926	2.265
$150°$	2.026	1.253	1.178	1.363	1.645	1.553	1.759	1.759	2.084
$160°$	1.848	1.161	1.051	1.302	1.630	1.512	1.632	1.540	1.836
$170°$	1.457	0.945	0.818	1.122	1.553	1.368	1.336	1.114	1.350
$180°$	–	–	–	–	–	–	–	–	–

Table 5.9   Predicted Failure Torques ($\theta = 0° - 180°$) for Beams from Casting No. 3 (44.41N/mm²)

of eqn. 5.47 is possible whereby either $T_{sv} = 0$ or $V_y = 0$.   This is

the anomaly previously identified during the development of the simpli-

fied theory in §5.2.5, which demonstrates that failure with the neutral

axis parallel to either the top or bottom faces is not possible when

shear force and torsion are both present.   Nevertheless, eleven beams

were tested in the absence of shear and for these eqn. 5.47 may be

reduced to the following form:

$$8.1603 \times 10^{-12}.ys.T_{sv}^2 + \frac{T_{sv}}{Y_2} = \Pi^* \qquad 5.48$$

the term Π^* is also calculated in the computer analysis of the cross-

section and replaces Π in Table 5.6 for $\theta = 0°$, $180°$.   The definition

of this quantity is given by

$$\Pi^* = \sum_{i=1}^{n} Z_{iy}y_{ci} + P(y + y_e) \qquad 5.49$$

where the summation is once again effective for the elements of rein-

forcement in tension.

Similar problems arise when the y co-ordinate is computed to

have zero value.   For beams with reinforcement symmetrically disposed

about the horizontal axis, this will occur where $\theta = 90°$, although this

is not generally the case.   In these circumstances, eqn. 5.47 reduces to:

$$M_x = - P.y_e \qquad 5.50$$

which is a necessary condition for failure with the neutral axis in this

position.   This is the other anomaly discussed in §5.2.5 and indicates

that a true side failure can only occur under specific conditions of

applied bending moment.

In the series of tests described here, the reinforcement is

asymmetrical about the x-axis and, accordingly, the y co-ordinate is

never zero at $\theta = 90°$.   Nevertheless, a small numerical value has

been obtained in all cases (Table 5.5) and this usually results in two positive roots being obtained from the solution of eqn. 5.47. Since one of these roots was invariably very large, the other very small, failure was never predicted to occur at this position and thus the solutions at $\theta = 90^{\circ}$ have been omitted from Tables 5.7 - 5.9, for clarity.

Clearly, failure is not possible under a particular system of applied loads at each of the neutral axis positions for which a solution has been obtained. Indeed, equilibrium of the system at the instant of collapse is only possible for failure mechanisms corresponding to stationary values (local maxima or minima) on the torque/orientation curve. This condition is more clearly demonstrated in fig. 5.17 where T/θ curves have been plotted for three typical beams which displayed entirely different modes of failure. In the case of H-0-3-5 and H-0-3-1, more than one local maximum/minimum exists and thus failure is governed by the smallest of these stationary values (*i.e.* at $\theta = 0^{\circ}$ and $\theta = 180^{\circ}$, respectively). On the other hand, beam number H-4-6-5 has only one stationary value at $\theta = 110^{\circ}$ although the predicted ultimate torque is almost constant over the range $\theta = 20^{\circ} - 160^{\circ}$. Top, bottom and side modes of failure are therefore to be expected for beams H-0-3-5, H-0-3-1 and H-4-6-5, respectively, and this corresponds exactly to the observed collapse behaviour.

Nevertheless, several discrepancies are apparent between the observed failure mechanisms and those predicted by Johnston and Zia[44]. In particular, beams H-4-3-4, H-4-6-2, H-4-6-3 and H-4-6-4 all failed with the neutral axis forming about one of the corners instead of parallel to the vertical side. Torsion/orientation curves for these beams are plotted in fig. 5.18 and, in each case, the predicted

ultimate torque is very nearly constant for $\theta = 20^{\circ} - 70^{\circ}$. While this is very similar to the T/θ curve for the typical side failure presented in fig. 5.17, the behaviour is distinctly different for orientations in excess of 90° where relatively large ultimate torques are predicted.

Four other beams were also observed to fail in modes not predicted by the original theory; the appropriate T/θ curves are plotted in fig. 5.19. Whereas side failures were expected for beams H-0-6-1, H-4-3-1 and H-6-6-1, minimum stationary values can be seen to occur at $\theta = 180^{\circ}$, 155° and 150°, respectively. These compare very favourably with the observed positions of the compression zone at failure which formed at the bottom of the section for H-0-6-1 and at the bottom and side simultaneously in the case of the other two beams. A simultaneous failure about the bottom and side faces was also observed for the fourth beam, H-0-3-3, the T/θ curve of which is also shown in fig. 5.19. In this case, stationary points exist at both $\theta = 40^{\circ}$ and $\theta = 140^{\circ}$ with absolute values which differ by only approximately 10%. This bears a close resemblance to the curve for beam H-4-6-5, shown in fig. 5.17, and therefore indicates the probability of a side failure.

By using the advanced ultimate load theory developed in §5.3.2, thirteen of the twenty beams tested in combined bending, tension and shear are predicted to fail with the compression zone forming about one of the corners. This is significantly more than the four beams for which this collapse mechanism was observed. However, this does not indicate a major disparity between test and theory and is largely due to the criteria selected here to define such a failure (*i.e.* the minimum stationary value should occur between $\theta = 20^{\circ}$ and $\theta = 160^{\circ}$, and computed values of ultimate torque in the top and bottom corners

should differ by more than 20%). Indeed, in two of the thirteen anticipated corner modes of collapse, a simultaneous side and bottom failure was observed. In the majority of the remainder, the computed orientation of the neutral axis at failure was within 20° of the horizontal and would therefore be difficult to distinguish from a failure about one of the section faces.

Because of the generally good agreement between observed and predicted modes of failure, torque/orientation curves have not been plotted here for all the beams. Nevertheless, minimum stationary values are directly obtainable from Tables 5.17-5.19, and are shown shaded for clarity. Subsequently, the collapse mechanisms determined from this advanced method of ultimate load analysis have been tabulated (Table 5.10) and compared with those predicted and observed by Johnston and Zia[44]. A measure of the accuracy of the theory is also presented in Table 5.10 in the form of the ratio of ultimate torques as determined by test and theory. While an excellent correlation is generally obtained, the theory is shown to be conservative in cases where the combined loading includes a high level of shear. However, this is a common feature of all ultimate load approaches and is due to neglecting dowel action and aggregate interlock effects.

Predicted Failure
Torque (N.mm × 10^7)
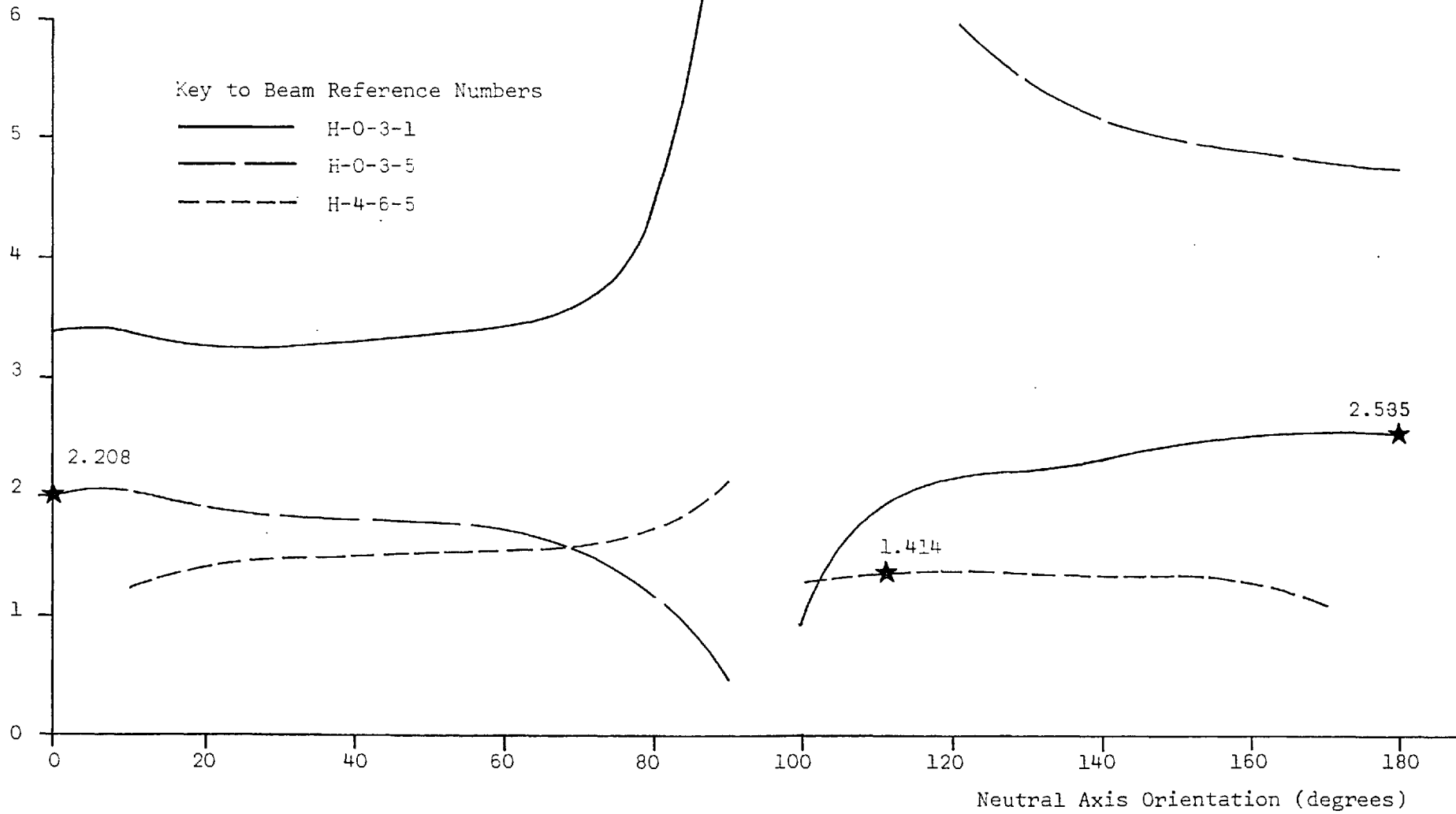
Figure 5.17   Torque/Orientation Curves for Beams displaying Typical Top, Bottom and Side Modes of Failure.

Predicted Failure
Torque (N.mm × 10^7)

Key to Beam Reference Numbers

H-4-3-4

H-4-6-2

H-4-6-3

H-4-6-4

0.913

0.933

0.648

0.527

Neutral Axis Orientation (degrees)

– 389 –
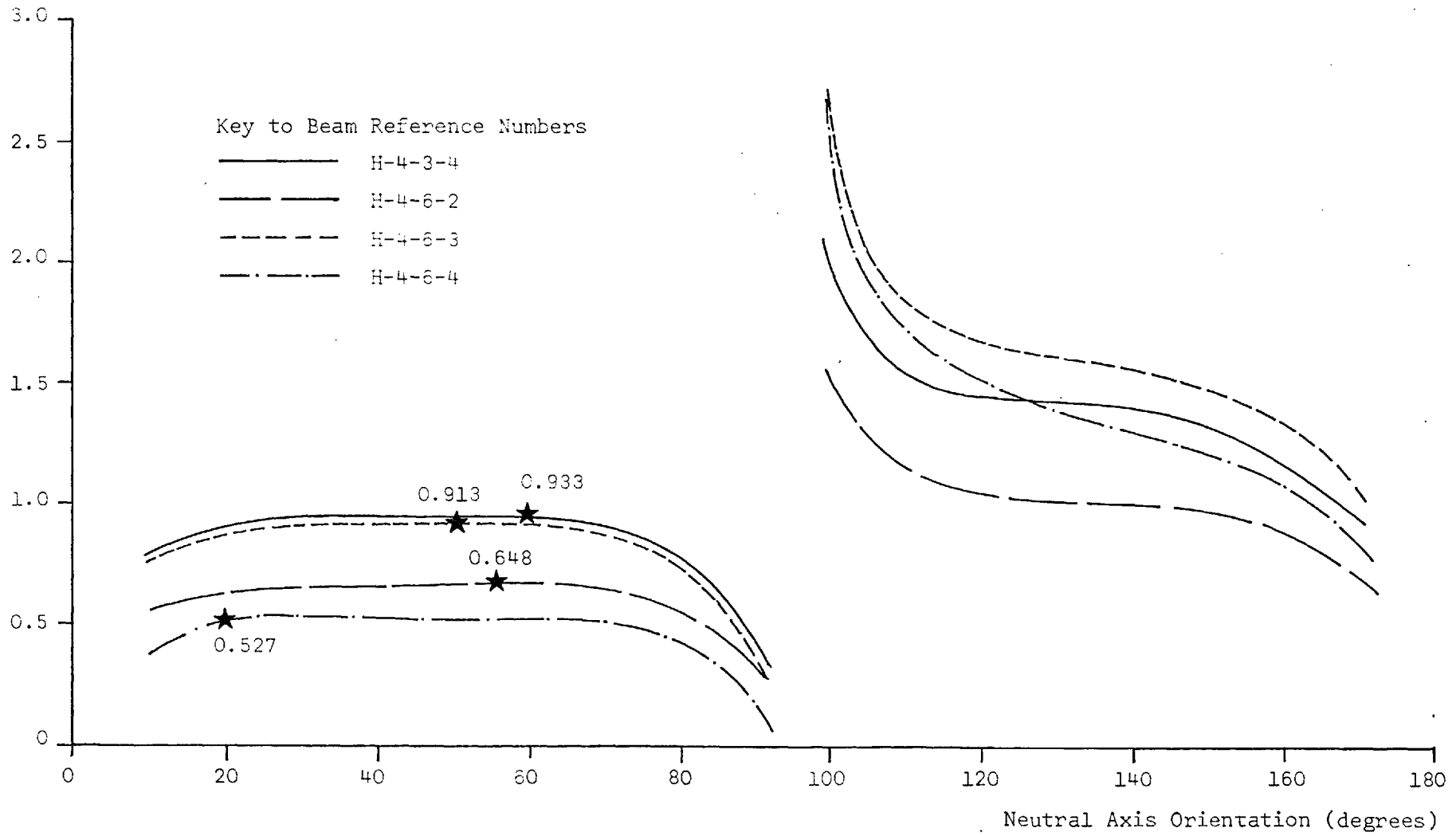
Figure 5.18   Torque/Orientation Curves for Beams displaying a Corner Mode of Failure

Predicted Failure
Torque (N.mm × 10^7)

Key to Beam Reference Numbers

————	H-0-3-3
— — —	H-0-6-1
- - - - -	H-4-3-1
-·-·-·-	H-8-6-1

2.748

2.322

1.792

1.645

Neutral Axis Orientation (degrees)
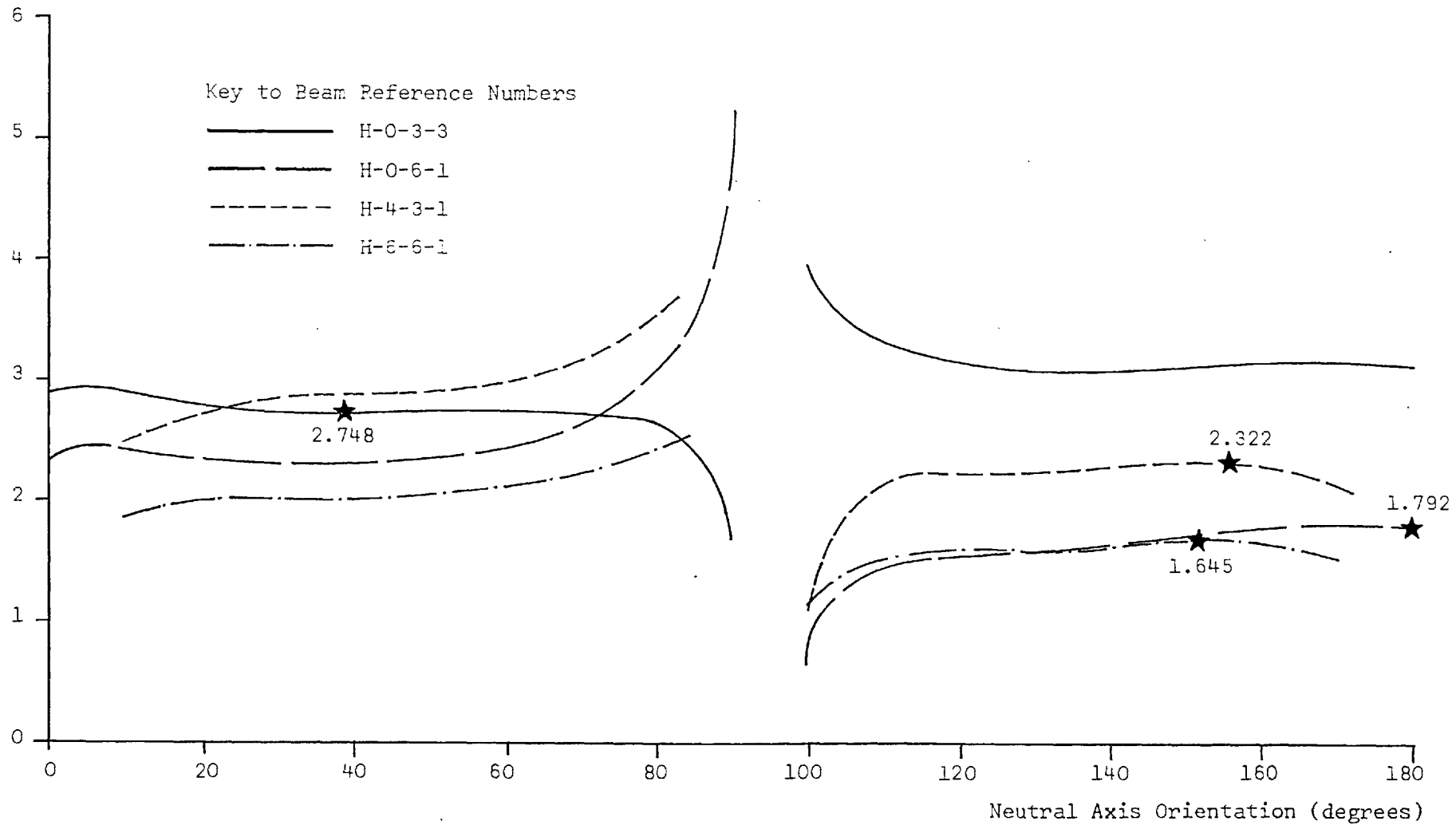
Figure 5.19   Torque/Orientation Curves for Beams displaying an unexpected Mode of Failure

Beam Ref. Number	Position of Compression Zone at Failure			Ultimate Torque (test/theory)	
	Johnston[44]	Waldron	Observed	Johnston[44]	Waldron
H-0-3-1	bottom	bottom	bottom	0.89	0.94
H-0-3-2	bottom	bottom	bottom	1.02	0.99
H-0-3-3	bottom	side	side/bottom	1.08	1.03
H-0-3-4	bottom	side	bottom	1.10	1.00
H-0-3-5	top	top	top	1.01	1.15
H-0-3-6	top	top	top	1.06	1.10
H-0-6-1	side	bottom	bottom	0.96	1.11
H-0-6-2	bottom	bottom	bottom	1.01	1.07
H-0-6-3	top	top	top	1.02	1.29
H-0-6-5	top	top	top	0.92	1.17
H-0-6-6	top	top	top	1.07	1.28
H-4-3-1	side	corner	side/bottom	0.98	1.07
H-4-3-2	side	side	side	1.02	1.03
H-4-3-3	side	corner	side	0.97	1.19
H-4-3-4	side	corner	corner	0.73	0.85
H-4-3-5	side	corner	side	1.10	1.28
H-4-6-1	bottom	corner	bottom	1.04	1.20
H-4-6-2	side	corner	corner	0.97	1.22
H-4-6-3	side	corner	corner	1.00	1.29
H-4-6-4	side	corner	corner	1.07	1.65
H-4-6-5	side	side	side	1.29	1.36
H-6-3-1	side	side	side	1.11	1.04
H-6-3-2	side	side	side	1.11	1.06
H-6-3-3	side	corner	side	1.04	1.38
H-6-3-4	top	corner	top	1.17	1.66
H-6-3-5	top	corner	top	1.09	1.49
H-6-6-1	side	corner	side/bottom	1.10	1.27
H-6-6-2	side	side	side	1.12	1.25
H-6-6-3	side	corner	side	1.12	1.36
H-6-6-4	top	top	top	1.12	1.57
H-6-6-5	top	top	top	1.08	1.72

Table 5.10   Comparison between Observed and Predicted Modes of Failure and Ultimate Torques

5.4   AN ADVANCED FAILURE MODEL - OPEN SECTIONS

The anomalies brought about by the introduction of the effects
of shear force into the simplified methods have been explained in the
previous section.   A more general failure model has been proposed
which also makes provision for corner failures.   Nevertheless, even
in this advanced form, the ultimate load analysis of under-reinforced
members is still effectively restricted to those displaying solid or
closed cross-sections.   This further limitation has already been dis-
cussed in §5.2.5 and is due to the inability of the methods to take
account of bimoment and warping torsion effects.   Thus, a general
method of ultimate load analysis does not exist for an important range
of concrete structures including shear cores and bridges of open section.

A method which takes warping effects into consideration is
therefore proposed which is based on a similar general failure model
to that presented in §5.3.   However, since the formulation of the
interaction equation is now dependent upon the sectorial co-ordinates
and the position of the shear centre after cracking, these must first
be determined.

5.4.1   Stress Analysis of Cracked Sections

Consider the thin-walled open section shown in fig. 5.20 for
which the centroid, before and after cracking, is denoted by the points
G and G_c, respectively.   The principal co-ordinate system X_c, Y_c, for
the cracked section subtends an angle ϕ with the original principal
axes X, Y.

The position and orientation of the principal neutral axes of
the cracked section are determined by satisfying the following
equations:

$$\int_c x_c \cdot dA_c = \int_c y_c \cdot dA_c = \int_c x_c y_c \cdot dA_c = 0 \qquad\qquad 5.51$$

in which the integrations are taken over the remaining effective area
of the cracked section. Concrete is assumed to have no tensile capacity
in these calculations, and the area of any steel must be multiplied by
the appropriate modular ratio throughout the analysis.

The position of any point on the cross-section may then be
defined in either principal co-ordinate system by using the following
geometrical relationships:

$$x = \Delta_x + x_c \cos\phi + y_c \sin\phi$$
$$y = \Delta_y - x_c \sin\phi + y_c \cos\phi$$

$$\left.\vphantom{\begin{matrix}a\\a\end{matrix}}\right\} 5.52$$

and

$$x_c = (x - \Delta_x)\cos\phi - (y - \Delta_y)\sin\phi$$
$$y_c = (x - \Delta_x)\sin\phi + (y - \Delta_y)\cos\phi$$

$$\left.\vphantom{\begin{matrix}a\\a\end{matrix}}\right\} 5.53$$

In these expressions x, y and x_c, y_c refer to the uncracked and cracked
co-ordinates respectively; Δ_x, Δ_y represent the change in position of
the centroid after cracking with reference to the uncracked co-ordinate
system.

Sectorial Co-ordinates

In fig. 5.20, the points S, S_c, refer respectively to the
position of the shear centre before and after cracking. From eqn.
2.14 the change in principal sectorial co-ordinates over the incre-
mental distance ds may be alternatively expressed, in either system, as

$$d\omega = r_s \cdot ds$$
$$d\omega_c = r_{sc} \cdot ds$$

$$\left.\vphantom{\begin{matrix}a\\a\end{matrix}}\right\} 5.54$$

Furthermore, the distance ℓ_s between shear centres is given by

$$\ell_s = \frac{e_{yc}}{\cos\beta} = \frac{e_{xc}}{\sin\beta} \qquad\qquad 5.55$$

where e_{xc}, e_{yc} represent the movement of the shear centre after cracking
with reference to the cracked co-ordinated system. With reference to
fig. 5.20 this may be alternatively expressed as
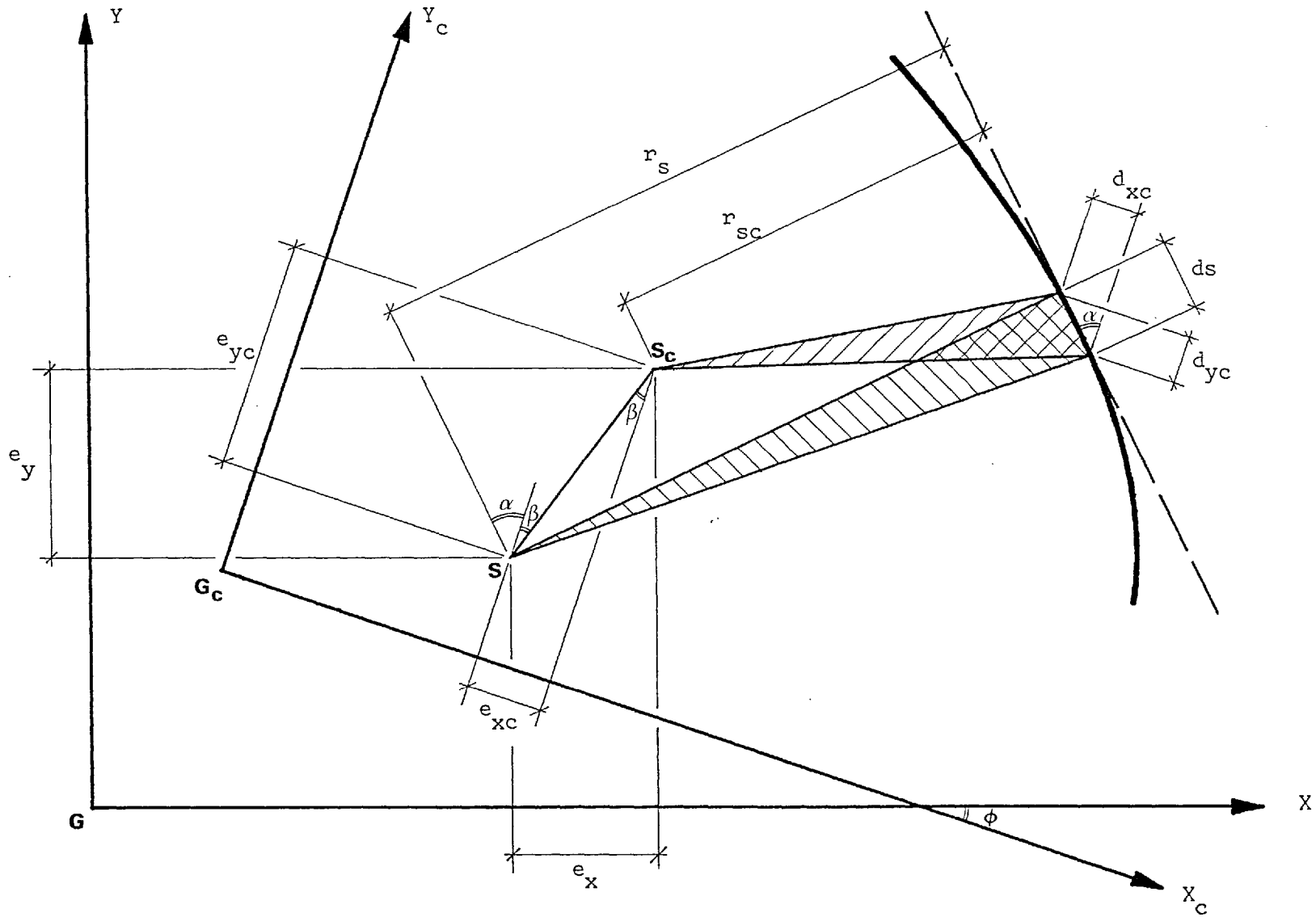
*Figure 5.20   Cracked and Uncracked Co-ordinate Systems
adopted in the Calculation of Sectorial Co-ordinates*

$$\ell_s = \frac{(r_s - r_{sc})}{\sin(\alpha + \beta)}$$ 5.56

By expanding the sine term in eqn. 5.56 and introducing the functions $\sin\beta$, $\cos\beta$ from eqn. 5.55, the following expression is obtained:

$$(r_s - r_{sc}) = e_{xc} \cos\alpha + e_{yc} \sin\alpha$$ 5.57

It is also apparent from fig. 5.20 that $\sin\alpha$, $\cos\alpha$, have the following definitions:

$$\sin\alpha = \frac{dx_c}{ds} ; \quad \cos\alpha = \frac{-dy_c}{ds}$$ 5.58

By combining eqns. 5.54, 5.57 and 5.58 in such a way as to eliminate the terms α and ds, the incremental change in sectorial co-ordinate after cracking, $d\omega_c$, may then be written as:

$$d\omega_c = d\omega + e_{xc} \cdot dy_c - e_{yc} \cdot dx_c$$ 5.59

After integration this takes the following form:

$$\omega_c = \omega + e_{xc} \cdot y_c - e_{yc} \cdot x_c + K$$ 5.60

Furthermore, by introducing x_c, y_c from eqn. 5.53 into eqn. 5.60, and noting that

$$\left. \begin{array}{l} e_{xc} = e_x \cos\phi - e_y \sin\phi \\[2mm] e_{yc} = e_x \sin\phi + e_y \cos\phi \end{array} \right\}$$ 5.61

the distribution of sectorial co-ordinates after cracking may be alternatively expressed in terms of the uncracked co-ordinate system as

$$\omega_c = \omega + e_x(y - \Delta_y) - e_y(x - \Delta_x) + K$$ 5.62

Position of the Shear Centre after Cracking

The constant of integration in eqns. 5.60 and 5.62 and the position of the shear centre after cracking are determined from the following conditions:

$$\int_c \omega_c \cdot dA_c = \int_c \omega_c x_c \cdot dA_c = \int_c \omega_c y_c \cdot dA_c = 0$$ 5.63

in addition to those already stated in eqn. 5.51. Then, by alternatively multiplying eqn. 5.60 by dA_c, $y_c \cdot dA_c$ and $x_c \cdot dA_c$, and integrating over the entire cracked area, we have

$$\left. \begin{aligned} K &= -\frac{1}{A_c} \int_c \omega \cdot dA_c \\[2ex] e_{xc} &= -\frac{1}{I_{xc}} \int_c \omega y_c \cdot dA_c \\[2ex] e_{yc} &= \frac{1}{I_{yc}} \int_c \omega x_c \cdot dA_c \end{aligned} \right\} \qquad 5.64$$

In this expression the second moments of area I_{xc}, I_{yc}, are defined in terms of the principal co-ordinate system for the cracked section, thus:

$$\left. \begin{aligned} I_{xc} &= \int_c y_c^2 \cdot dA_c \\[2ex] I_{yc} &= \int_c x_c^2 \cdot dA_c \end{aligned} \right\} \qquad 5.65$$

5.4.2   Formulation of the General Interaction Equation

Although the transverse distribution of direct stress at a section is modified by first cracking, the levels of the various stress resultants remain unaltered when referred to the original principal axes. Accordingly, we have

$$\left. \begin{aligned} N &= \int_u \sigma \cdot dA &= \int_c \sigma_c \cdot dA_c \\[2ex] M_x &= \int_u \sigma y \cdot dA &= \int_c \sigma_c y \cdot dA_c \\[2ex] M_y &= \int_u \sigma x \cdot dA &= \int_c \sigma_c x \cdot dA_c \\[2ex] B &= \int_u \sigma \omega \cdot dA &= \int_c \sigma_c \omega \cdot dA_c \end{aligned} \right\} \qquad 5.66$$

where σ, σ_c, describe the uncracked and cracked state of direct stress, and the integration limits u, c, represent the original and final effective areas, respectively. Alternatively, if the new (cracked) principal neutral axes are used, the following relationships hold:

$$\left.\begin{aligned}
N_c &= \int_u \sigma \cdot dA &&= \int_c \sigma_c \cdot dA_c \\
M_{xc} &= \int_u \sigma y_c \cdot dA &&= \int_c \sigma_c y_c \cdot dA_c \\
M_{yc} &= \int_u \sigma x_c \cdot dA &&= \int_c \sigma_c x_c \cdot dA_c \\
B_c &= \int_u \sigma \omega_c \cdot dA &&= \int_c \sigma_c \omega_c \cdot dA_c
\end{aligned}\right\} \quad 5.67$$

By substituting x_c, y_c, ω_c from eqns. 5.53 and 5.62 into eqn. 5.67, the stress resultants corresponding to the cracked and un-cracked co-ordinate systems may be expressed in terms of each other, thus:

$$\left.\begin{aligned}
N_c &= N \\
M_{xc} &= (M_x - N.\Delta_y)\cos\phi - (M_y - N.\Delta_x)\sin\phi \\
M_{yc} &= (M_x - N.\Delta_y)\sin\phi + (M_y - N.\Delta_x)\cos\phi \\
B_c &= B + e_x(M_x - N.\Delta_y) - e_y(M_y - N.\Delta_x) - \frac{N}{A_c}\int_c \omega \cdot dA_c
\end{aligned}\right\} \quad 5.68$$

Evidently, from the last of eqns. 5.68, it is possible for a bimoment to develop after cracking even though one was not applied in the original system. The significance of this result is demonstrated by Zbirohowski-Koscia[121] in a worked example in which the maximum direct stress at a section is approximately doubled at first cracking.

So far, in the analysis of cracked sections, the elements of steel in tension have been considered to be in the elastic state. Changes in the principal co-ordinate systems are therefore due solely

to the transfer of tensile stresses from the concrete to the reinforce-
ment at first cracking.   However, since eqns. 5.66 and 5.67 are simply
equilibrium relationships, eqn. 5.68 is equally applicable to the
inelastic state.   At failure, the bimoment term, B_c, may therefore be
defined in accordance with the final expression in eqn. 5.67 as

$$B_c + \sum_{j=1}^{n} F_j^2 \frac{s_j}{D_{jy}} \omega_{cj} = \sum_{i=1}^{m} Z_{iy} . \omega_{ci} - Z.\omega_c \qquad 5.69$$

where ω_{ci}, ω_{cj} represent the sectorial co-ordinates of the ith component
of reinforcement in tension, and the centre of the jth shear wall
element respectively.   Once again, the compressive forces, Z, at failure,
are assumed to act at a single point, the sectorial co-ordinate of
which is denoted ω_c.

On substitution of B_c from eqn. 5.69 into the last of eqns.
5.68, we have

$$B + e_x(M_x - N.\Lambda_y) - e_y(M_y - N.\Lambda_x) - \frac{N}{A_c} \int_c \omega.dA_c$$

$$+ \sum_{j=1}^{n} F_j^2 \frac{s_j}{D_{jy}} \left\{ \omega_j + e_x(y_j - \Lambda_y) - e_y(x_j - \Lambda_x) - \frac{1}{A_c} \int_c \omega.dA_c \right\}$$

$$= \sum_{i=1}^{m} Z_{iy} \omega_{ci} - Z.\omega_c \qquad 5.70$$

This forms the basis of a general interaction equation which, after
dividing through by the right-hand side, may be expressed in terms of
the various stress resultants and their corresponding ultimate values
only.

5.4.3   Experimental Investigation

The effect of warping restraint on the ultimate capacity of
thin-walled concrete members has also been investigated experimentally.

Tests were conducted on four straight beams of simple open section, comprising two singly-symmetric channel sections, and two I-beams, symmetric about both principal axes.

Construction Details

An overall length of 2.4 m and a common wall thickness of 25 mm were used throughout. This enabled construction and testing to be simplified and permitted the re-use of external formwork. Cross-sectional dimensions of each pair of I-beams and each pair of channel sections were identical; these are shown in fig. 5.21, together with the general arrangements of reinforcement.

Longitudinal steel was essentially the same in each pair of beams although the transverse reinforcement varied, comprising either a single or double stirrup leg in each wall. Round mild steel bars of either 10 or 12 mm diameter were used for the main reinforcement and these were located at the junctions of all web and flange elements. Stirrups were cut and bent on a special jig to ensure accuracy of assembly and were manufactured from 4 mm diameter steel of similar quality. Stress/strain relationships determined from several specimens of each bar size are presented in fig. 5.22. Although the stresses at failure are higher than expected, each type of steel displays a long strain plateau after yield. This is an essential characteristic for redistribution to occur after yield of either the transverse or longitudinal component of reinforcement, and is a necessary requirement of the theory developed in §5.4.2 in which fully under-reinforced behaviour was assumed.

Accuracy was an important consideration during fabrication since a nominal side cover of only 2.5 mm was provided to the stirrups. To facilitate this process, the main bars were threaded at each end and
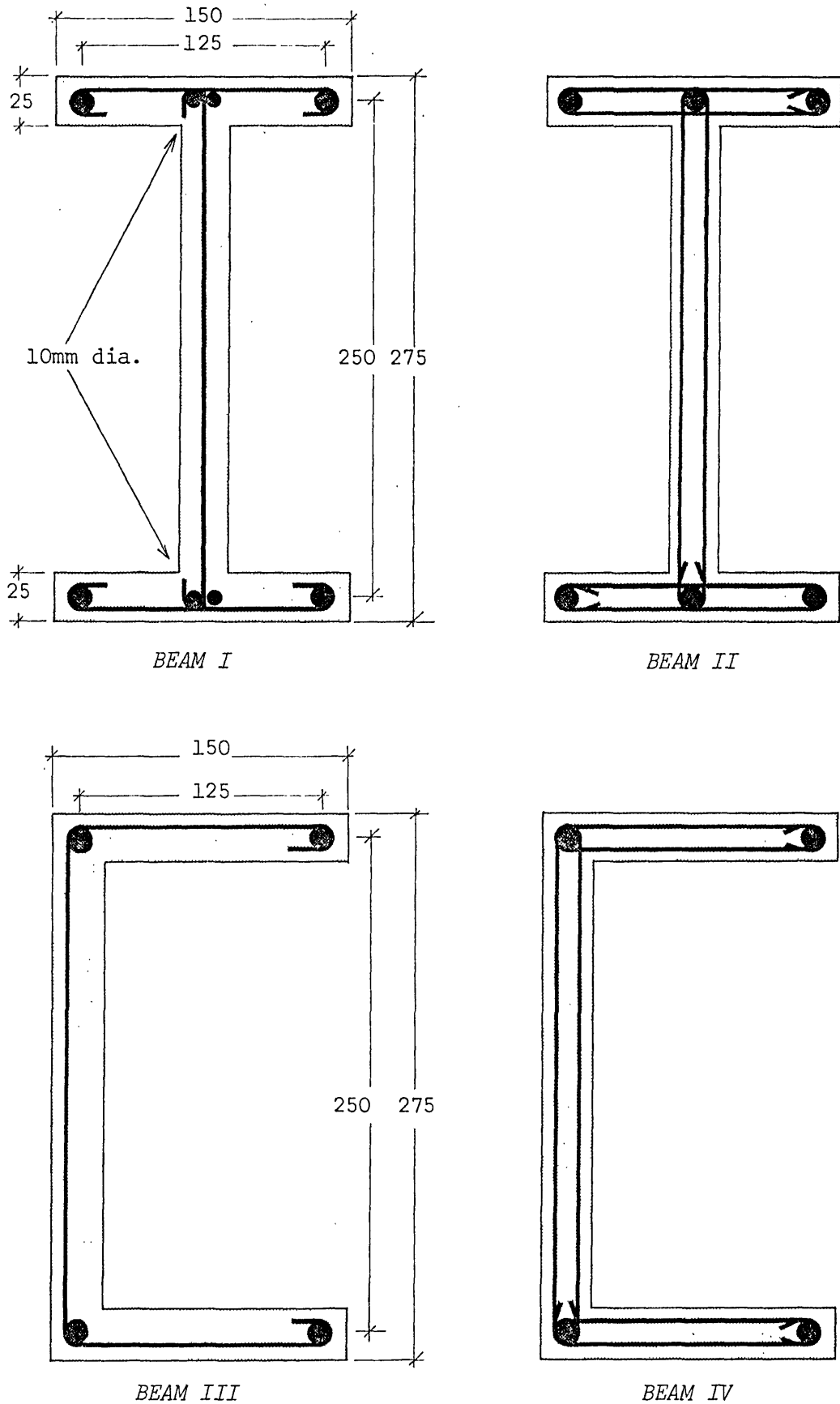
Figure 5.21 General Arrangement of Four Open Section Beams

Stress (N/mm^2)

Nominal Dia.(mm)	Mean Dia.(mm)	Yield Force (T)	Yield Stress(N/mm^2)	Ultimate Force(T)	Ultimate Stress(N/mm^2)	Ultimate Strain (%)
4	3.997	0.57	453	0.66	521	7.5
10	10.118	3.00	372	4.06	496	20.0
12	12.040	4.92	431	6.48	567	22.5
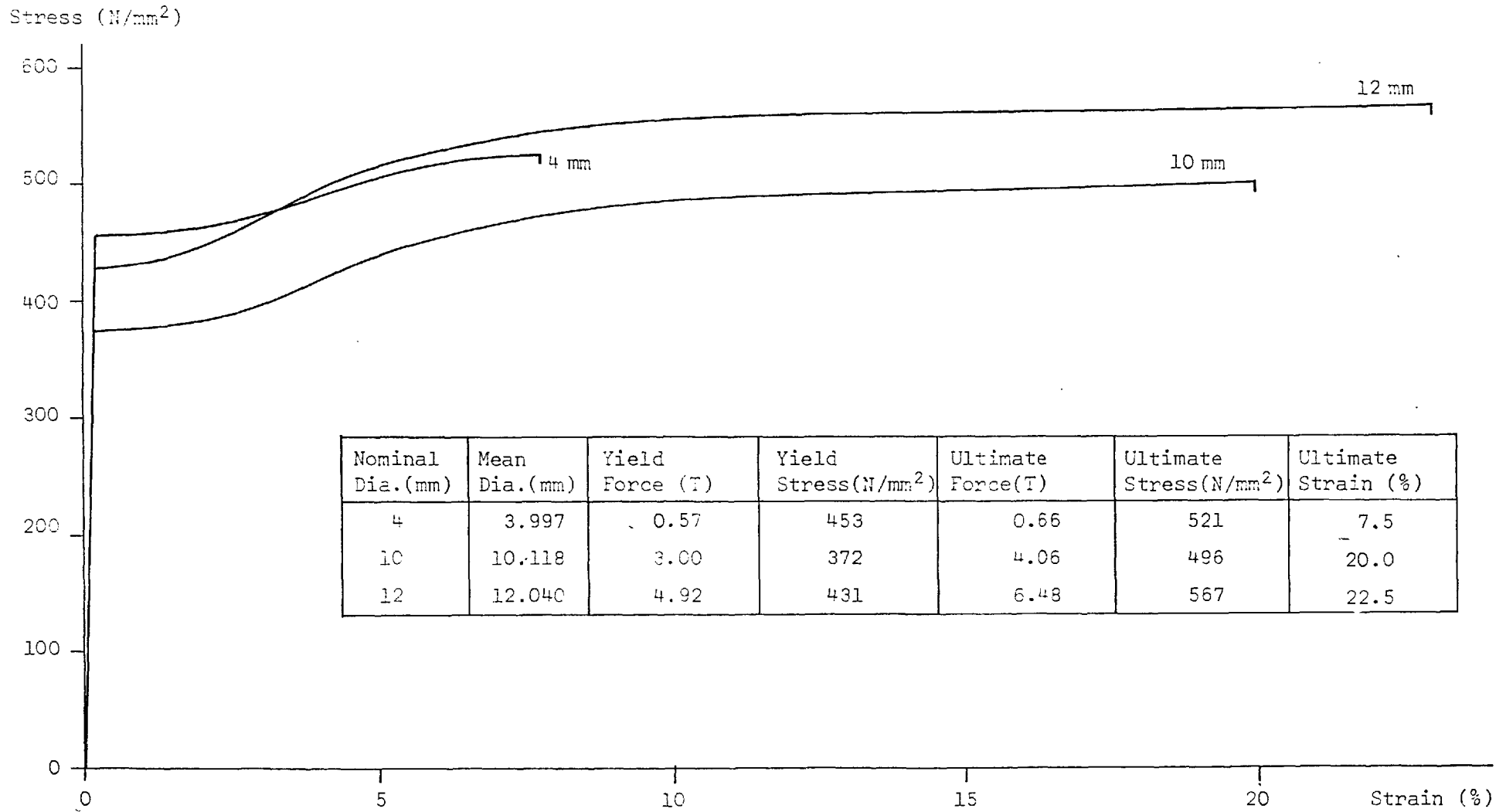
Strain (%)

Figure 5.22   Stress/Strain Relationship for 4, 10 and 12mm Diameter Reinforcement Bars

passed through accurately drilled holes in the steel end plates. The application of a slight prestress to each bar was then generally sufficient to ensure correct positioning throughout the span, although small microconcrete spacing blocks were also used near the centre to support the weight of the reinforcement cage. In view of the method of construction, it was possible for the main steel to slip at the beam ends due to the application of large torsional loads. Positive anchorage was therefore provided by casting in a nut screwed on to the threaded end of each main bar.

Although the same external formwork was used for all specimens, the open profile of each beam was formed with disposable inserts manufactured from high density polystyrene. These were accurately shaped before fixing to the external formwork and were subsequently cut out after casting and stripping. By adopting this method of construction it was also possible to provide cross-bracing at frequent intervals along the beam. Bracing was fabricated from a number of 4 mm diameter wires provided with a hook at one end. These were pushed into the polystyrene at an appropriate angle and then anchored around the main steel. Later, after casting and removal of the formwork, the individual wires at each of the selected cross-sections were welded together, thus forming an excellent diaphragm with negligible out-of-plane stiffness. Cross-bracing of this type was provided at approximately 300 mm centres throughout the span. However, at the centre of each beam, warping deformation was completely prevented by the symmetrical nature of the proposed method of testing. It was therefore possible to provide a 75 mm thick diaphragm at this position without inducing additional warping restraint stresses.

Instrumentation primarily consisted of surface strain gauges,

together with the measurement of displacements and rotations at a
number of sections along each beam. However, a limited number of
electrical resistance strain gauges were also used to monitor the state
of strain in the main steel at the centre section. For this purpose
two foil gauges of 40 mm gauge length were attached diametrically
opposite each other on each corner bar. These were checked, water-
proofed and calibrated before assembly of the reinforcement cage. The
central region containing the strain gauges is shown in plates 5.1 for
the channel section with single stirrup legs. This also provides a
detailed view of the formwork, diaphragm and general reinforcement
arrangement. The I-beam with double stirrup legs is similarly shown
in plate 5.2.

Because of the very thin walls and small cover, a micro-
concrete was selected with a maximum aggregate size of approximately
2.4 mm. This was the gap-graded mix previously used for the con-
struction of the 1/12th scale bifurcated bridge model described in
§4.2. Information regarding the workability, compressive strength,
etc. was readily available and the mix proportions (by weight) were as
follows:

Coarse Sand (B.S. sieve sizes 7-14)	1.375
Fine Sand (B.S. sieve sizes 52-100)	1.375
Ordinary Portland Cement	1.000
Water	0.515

A detailed investigation of the probable size effects in structural
models has already been undertaken and is reported elsewhere[110]. Since
these effects can be significant, a more accurate assessment of the
mechanical properties of the microconcrete was obtained by taking
$\frac{1}{4}$ scale contral specimens from each mix. However, compressive strength

Plate 5.1   Channel Section with Single Stirrup Reinforcement.
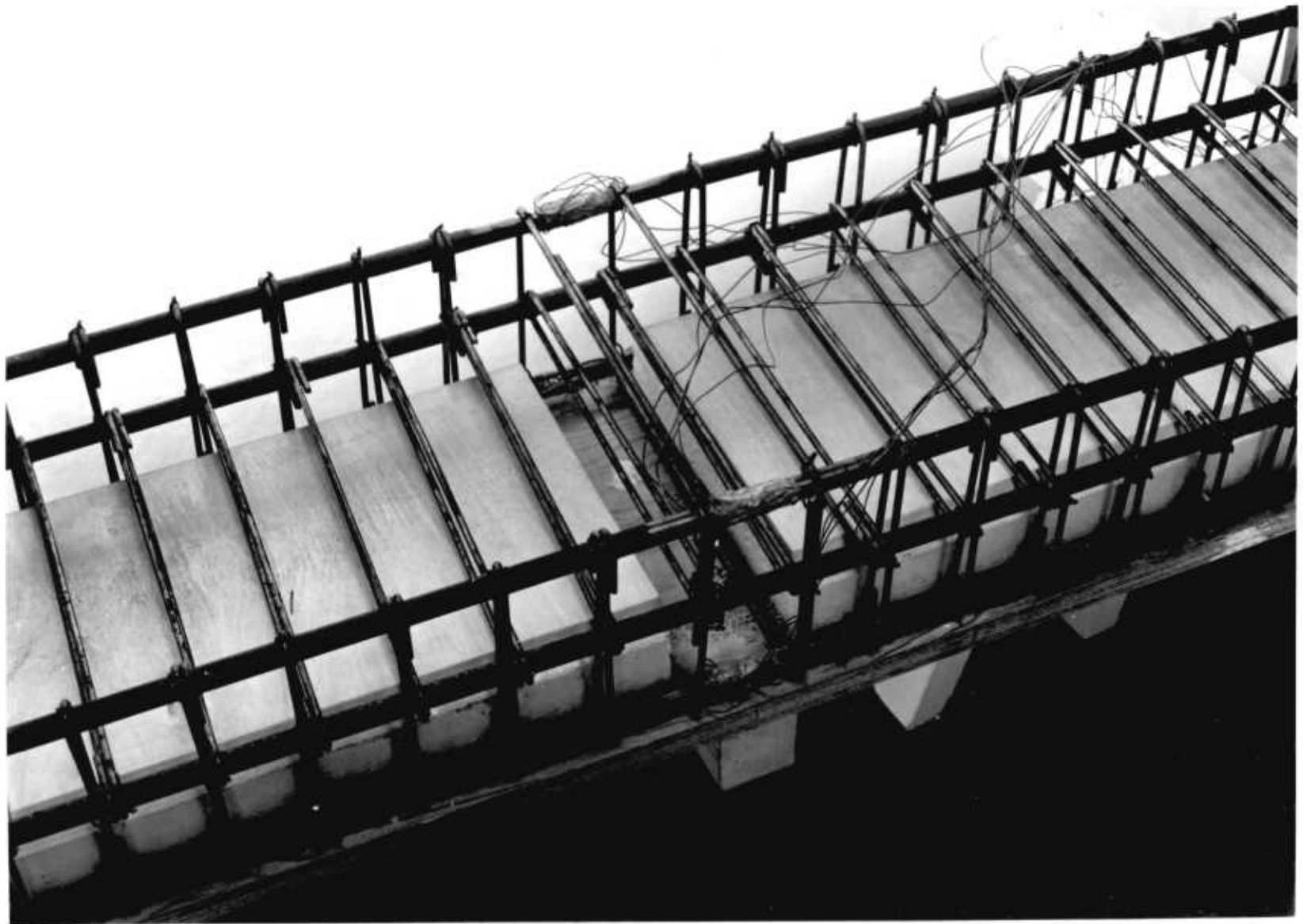
Plate 5.2   I-Section with Double Stirrup Reinforcement.

did not vary greatly between castings and the mean value at the time of test was calculated to be $f_{cu} = 51.22$ N/mm^2.

A vibrating table was used for compacting the microconcrete with generally good results.   External formwork was stripped at 24 hours; the disposable inserts were removed 48 hours later.   Cross-bracing wires were also welded together at this time in order to prevent cross-sectional distortion during the curing period.   This resulted in some longitudinal shrinkage cracks positioned in the haunches, although the behaviour during testing was not noticeably affected.   All the beams were cured for 14 days under damp hessian and polythene sheeting prior to storage in the temperature and humidity controlled environment of the laboratory.

Test Procedure

Each beam was tested under an identical arrangement of loading and support, designed so as to apply a significant level of bimoment at the centre section.   Knife-edge bearings provided simple support at both ends, resulting in an effective span length of 2.3 m in all cases. In addition, the ends were torsionally restrained by applying a reactive couple to the top and bottom flanges, and sufficient sliding bearings were also incorporated into the support system to ensure freedom of movement in the longitudinal direction.

A single point load was applied eccentrically to the centre section through a lever-arm clapmed to the solid concrete diaphragm. Load from a hydraulic jack fixed to the laboratory floor was trans-mitted through a flexible prestressing strand to the underside of the lever-arm.   The jack used for this purpose was free to rotate about its point of fixity and, thus, did not impose any unfavourable restraint on the system.

By selecting a different eccentricity for each test it was possible to cover a range of alternative load combinations. However, while the torque/bending moment ratio could easily be varied, the levels of bimoment and shear force were fixed proportionately by the constant span length.

Instrumentation consisted of over fifty surface strain gauges and inclinometers in addition to the electrical resistance strain gauges already described. However, the purpose of this extensive gauging was to monitor the cracked behaviour of the beam along its length, and is therefore not directly relevant to an assessment of the ultimate capacity of the critical central section. Loads were applied in increments of approximately 10% of the computed ultimate value. Screw adjusters, provided at each point of contact in the end reaction frames, were then used to reset the beam ends to their initial location and orientation (plate 5.3). Fifteen minutes were allowed for each loading increment for the system to stabilize before recording the various strains, deflections and rotations. During this period the position and extent of the cracks were marked on the beam surface.

Results

Only those results pertinent to the ultimate load condition will be presented here. These consist of main reinforcement strains and central beam rotations recorded throughout the tests, together with the ultimate loads and the computed values of the various stress resultants at failure.

In fig. 5.23, central rotations have been plotted against torque for each of the four beams. Three distinct phases of behaviour were apparent, the first of which was relatively short and represented the response of the uncracked sections. After first cracking, tensile
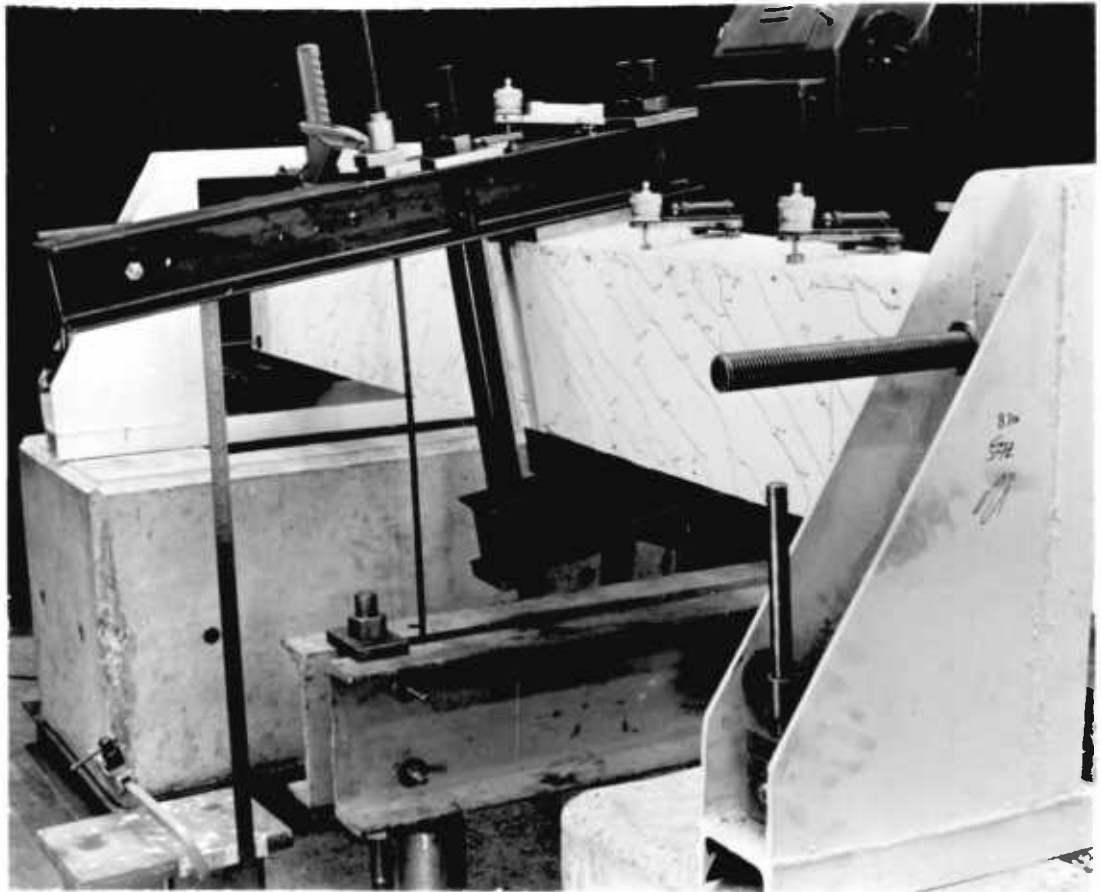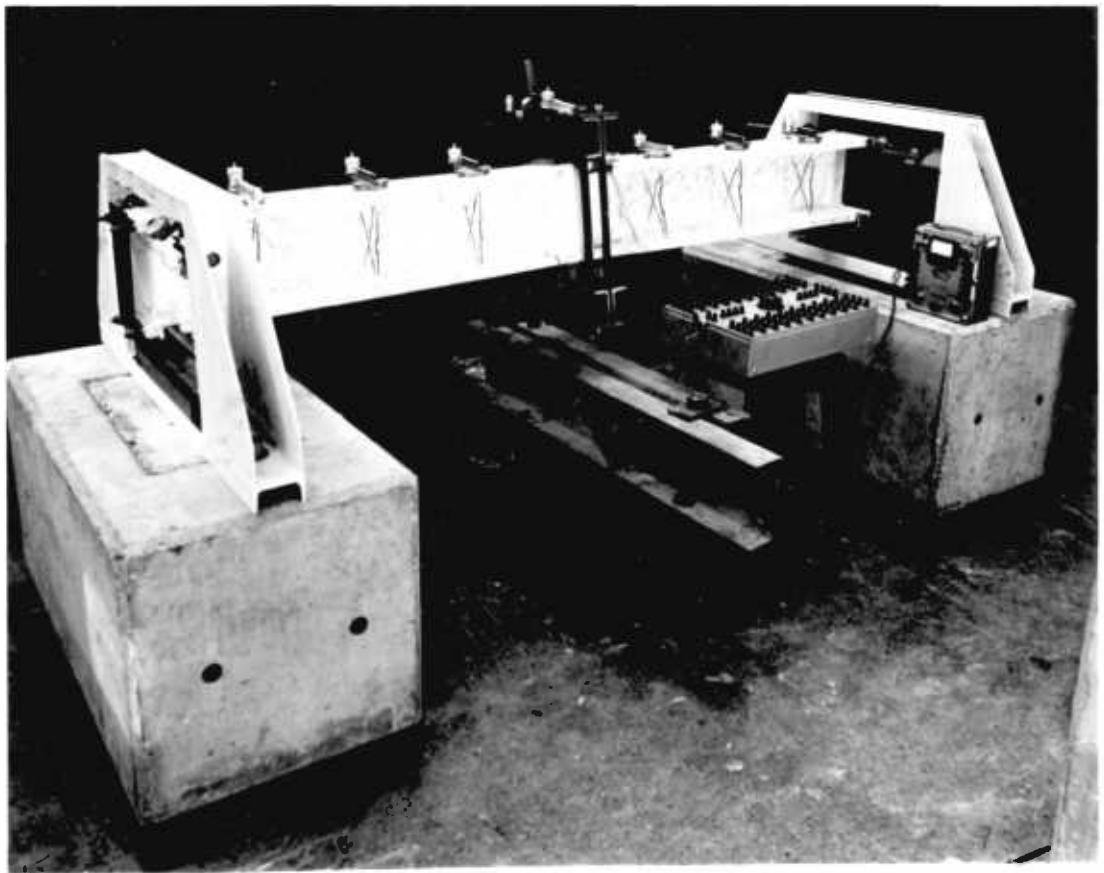
Plate 5.3   Test Arrangement for Channel Section.
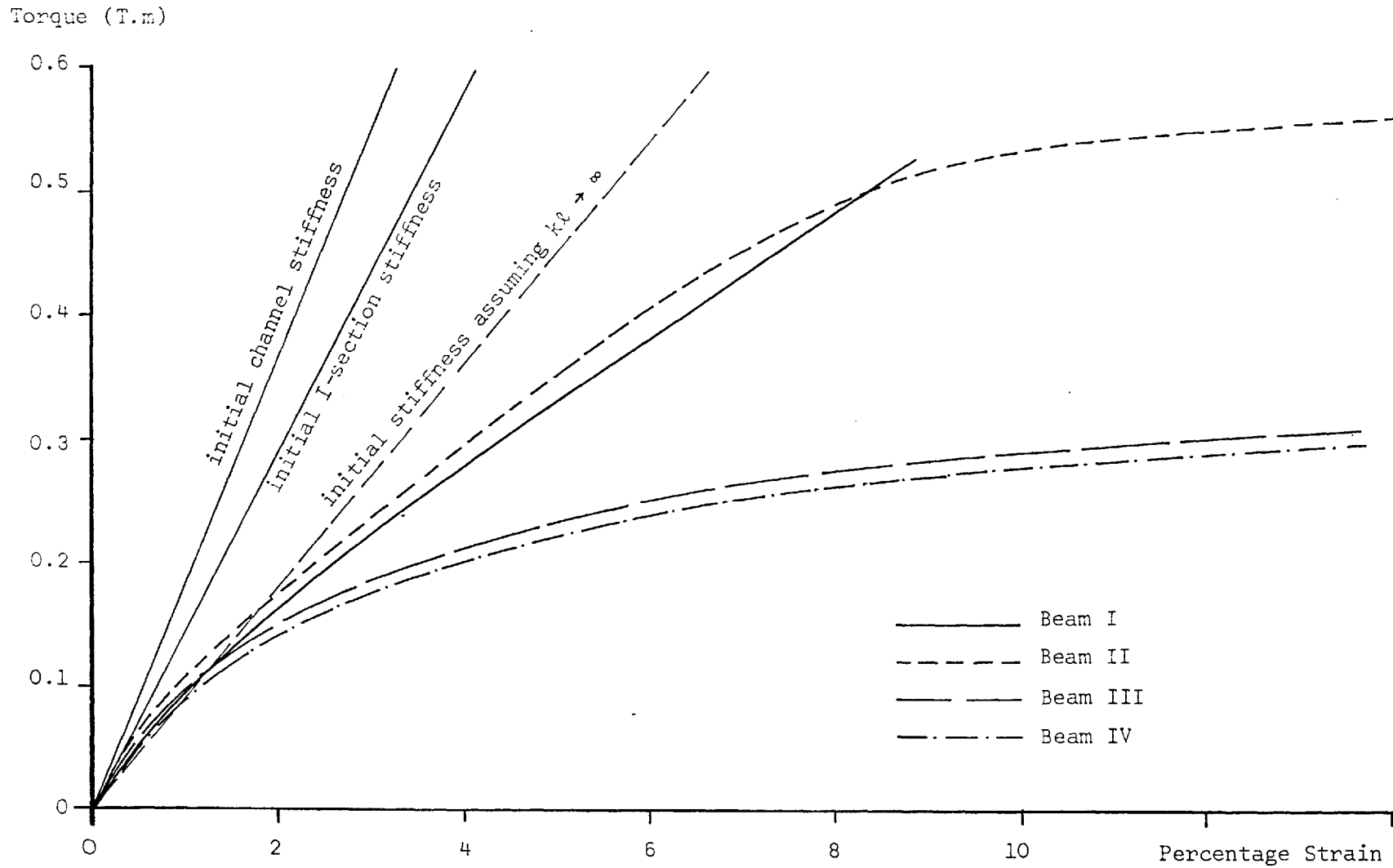
Figure 5.23   Torque/Rotation Curves at the Central Section of Four Open Section Beams

stresses in the concrete were gradually transferred to the steel until the familiar truss action was fully developed. In the case of the two I-beams, transition from the uncracked to the cracked state was rapid and the second phase was remarkably linear. Finally, after yield of both components of steel, the section stiffness was considerably reduced and further small increments of load could only be resisted by the strain hardening effects of the reinforcement (fig. 5.22). Large deformations were apparent at this stage and failure eventually occurred, in all cases, when the central angle of rotation was in excess of 14°. Unfortunately, the central inclinometer failed during testing of the I-section with single stirrup legs (beam I) and, thus, the final phase after yield of the main steel has not been recorded.

Several straight lines are also shown in fig. 5.23, the slopes of which represent the initial torsional stiffness of the two types of cross-section. If warping restraint effects are assumed to be negligible ($k\ell \rightarrow \infty$), the following relationship holds:

$$\phi = \frac{T\ell}{4GI_d} \qquad\qquad 5.71$$

In this expression, T is the total torque applied at the centre section and is equal to twice the torque in each of the two half-spans. The second moment of area for pure torsion, I_d, and the shear modulus, G, are determined from eqns. 2.18 and 2.83, respectively. Values of Young's modulus and Poisson's ratio for the microconcrete are required for this purpose and these have been previously determined from a large number of tests during the construction of the bifurcated bridge. Accordingly, by using the common cross-sectional dimensions given in fig. 5.21, and with

$$E = 24.7 \ kN/mm^2$$

$$\nu = 0.150$$

we have

$$GI_d = 2.94 \times 10^7 \text{ kN. mm}^2$$

From fig. 5.23 it is clear that the torsional stiffness determined in this way does not accurately represent the initial behaviour of either type of beam. However, if warping effects are included, the change in central angle is alternatively given by[25]

$$\phi = \frac{T\ell}{4GI_d} \left\{ 1 - \frac{\tanh (k\ell/2)}{k\ell} \right\}$$ 5.72

In this expression the effective length, ℓ, is equal to 2300 mm in all cases, whereas the decay function, k, must be determined from eqns. 2.14, 2.26 and 2.36 for each section and has the following values:

$k = 0.00166 \text{ mm}^{-1}$ (channel)

$k = 0.00222 \text{ mm}^{-1}$ (I-section)

Eqn. 5.72 may thus be expressed in the form of the two other straight lines in fig. 5.23 which are in good agreement with the observed behaviour.

Strains on opposite sides of each corner bar at the centre section were also recorded throughout the tests. Subsequently, these have been averaged and are plotted in figs. 5.24 - 5.27 with respect to the applied load. In the case of the two I-beams, bars A and C were both initially in compression thus reflecting the significance of the bimoment effects. However, as load was increased, bending about the horizontal axis assumed a greater significance. This effect was noticeable in all beams, particularly after yield of bar B, at which point any additional tensile forces due to bending had to be resisted by bar C alone. With the exception of beam I, this resulted in only one corner bar being in compression at failure.
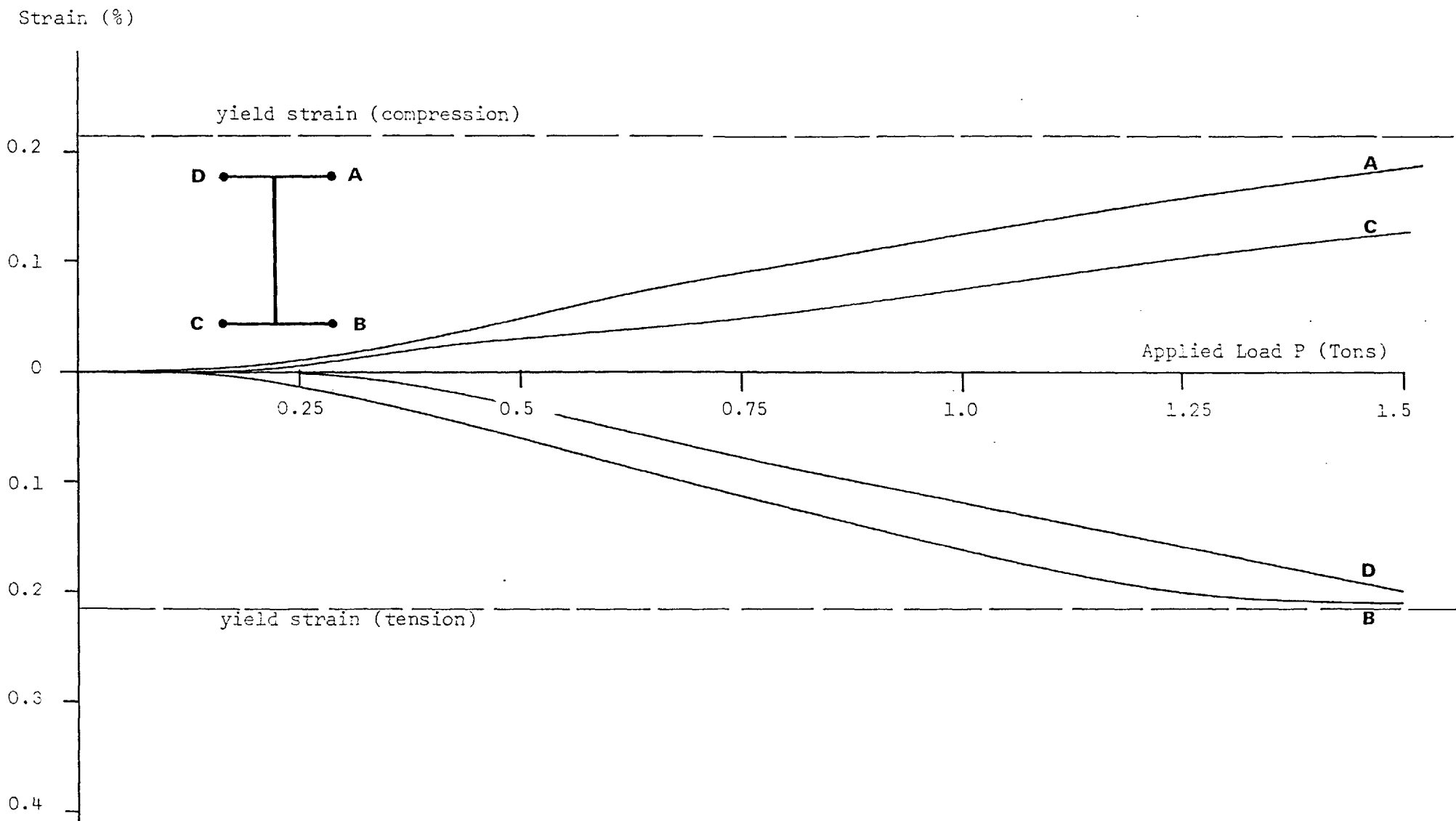
Figure 5.24 Average Longitudinal Strain in the Corner Bars of Beam I
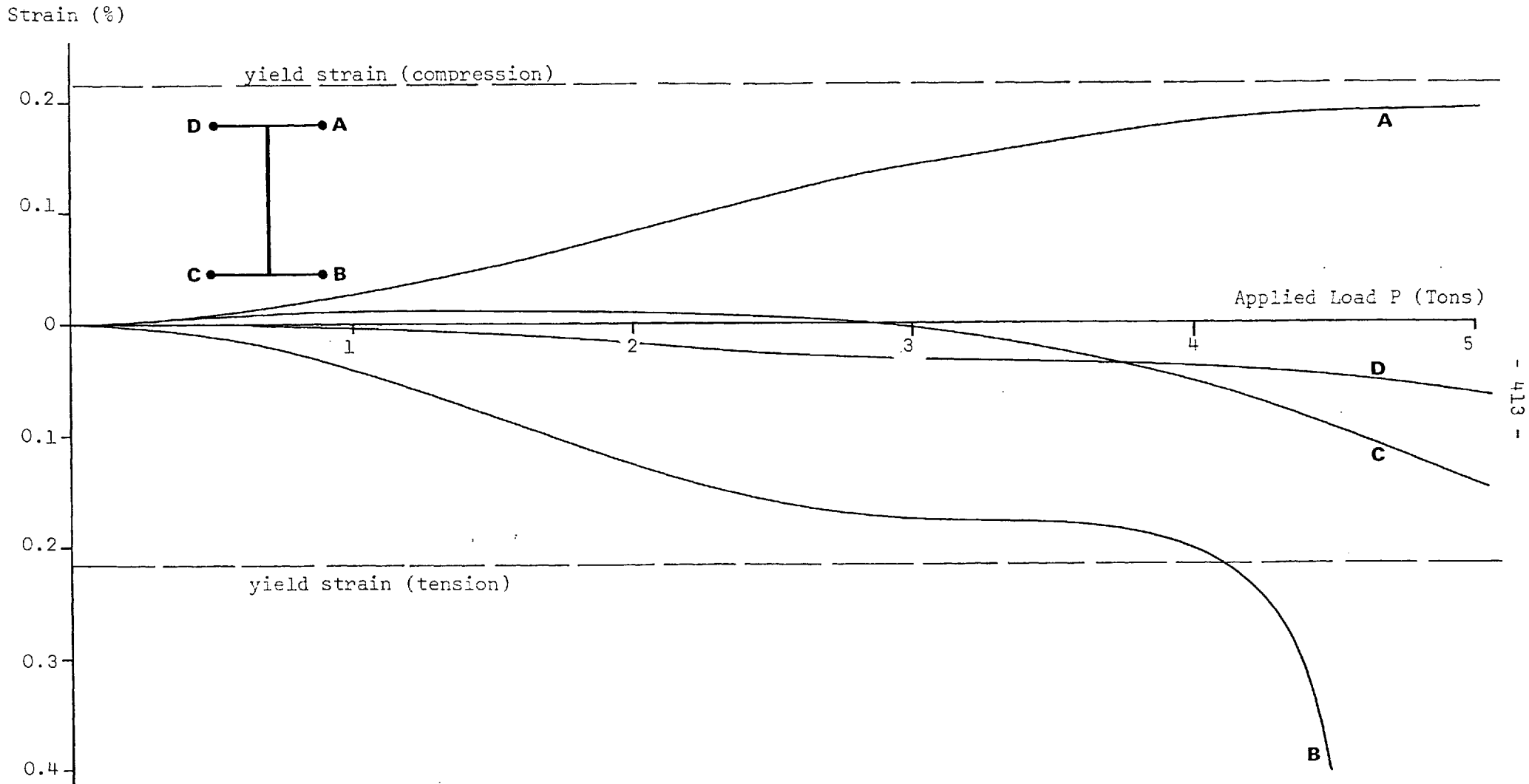
Figure 5.25 Average Longitudinal Strain in the Corner Bars of Beam II
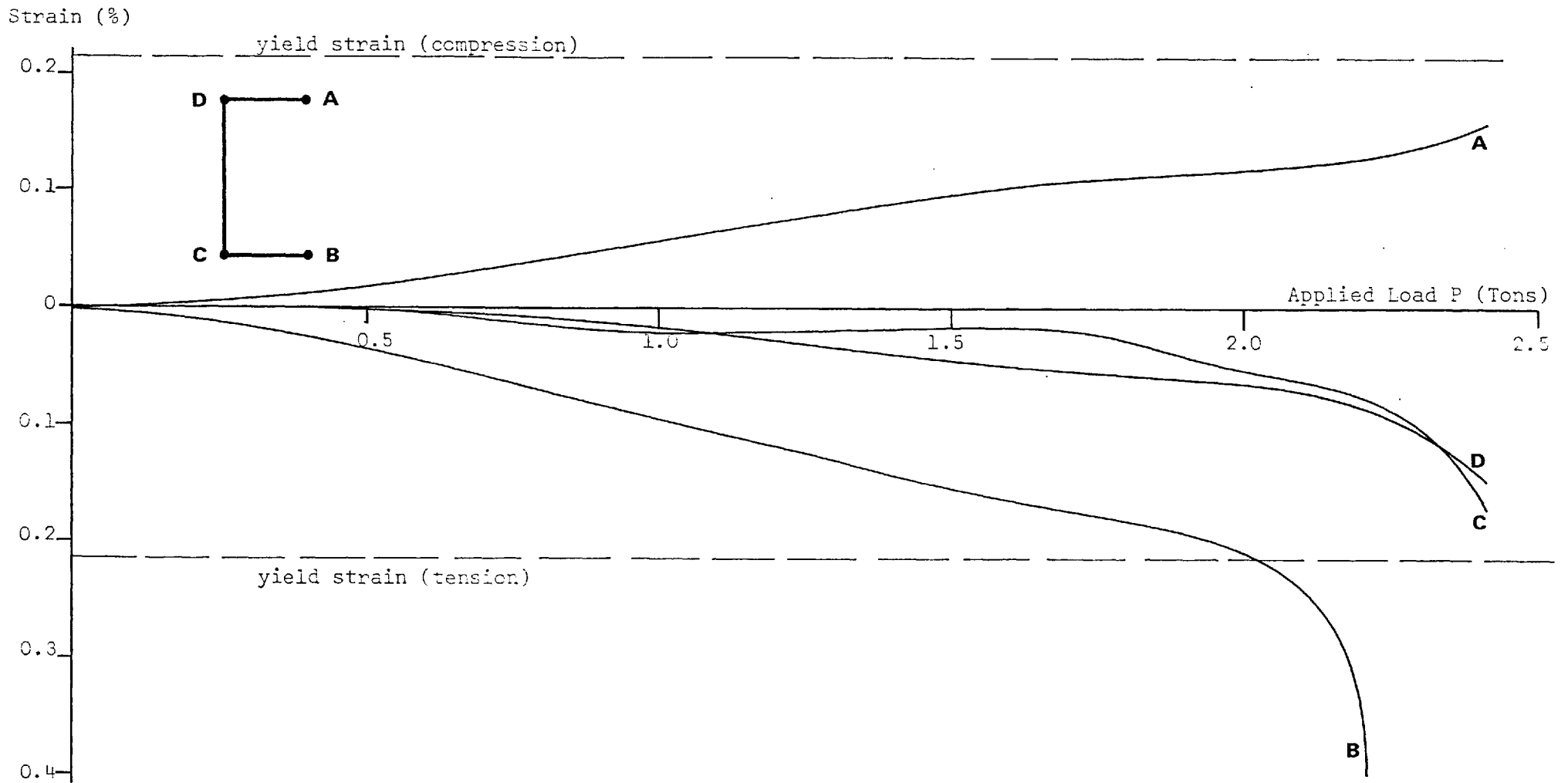
Figure 5.26 Average Longitudinal Strain in the Corner Bars of Beam III
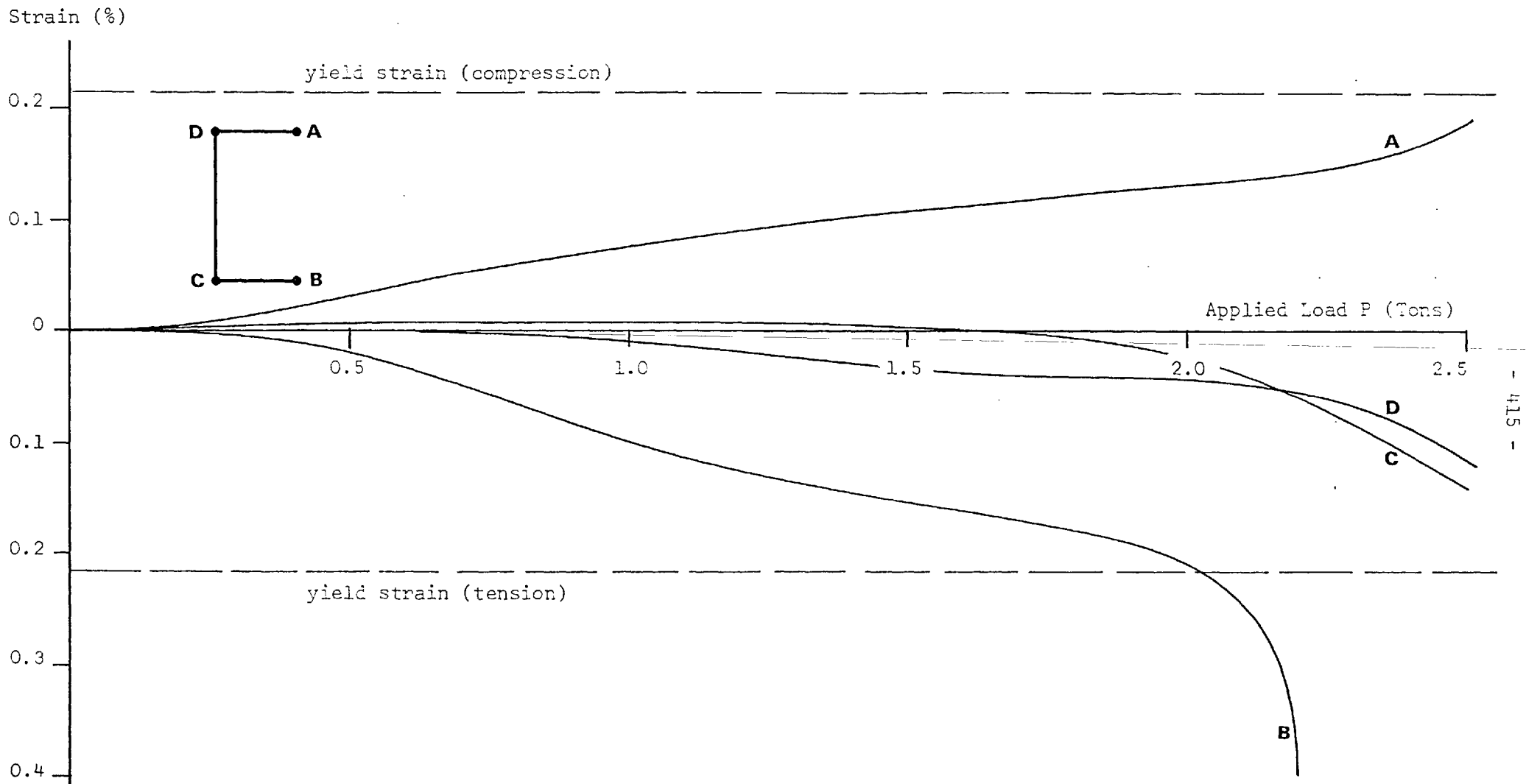
Figure 5.27 Average Longitudinal Strain in the Corner Bars of Beam IV

Behaviour at Ultimate Load

It is evident from fig. 5.23 that extensive cracking occurred at an early stage in all the tests. It is not intended to give details of crack measurements here, although the general crack patterns for beams I-IV at failure are shown in plates 5.4 - 5.7 respectively.

Substantial levels of torque and bimoment were applied to beam I by adopting a relatively large lever-arm for the test. A large number of closely spaced cracks developed without causing obvious distress, and failure was primarily due to yield of bars B and D located in diagonally opposite corners. Essentially, the torsional couple applied to this section was resisted by transverse beam action of the top and bottom flanges and, thus, two separate compression zones formed at failure. Eccentricity was considerably reduced in test II with the result that significant levels of bending moment and shear force were also applied in combination with the torque and bimoment. Collapse was initiated by yield of the main bars in corners B, C and D, followed by a secondary compression failure at corner A.

Beams III and IV were tested under almost identical arrangements of load in order to investigate the effects of the different densities of stirrup reinforcement at failure. As a result, the torque/rotation curves (fig. 5.23) and patterns of crack development (plates 5.6 and 5.7) obtained for this pair of beams were almost identical. The overall behaviour of beams III and IV was also similar to that of beam II, in all major respects, despite a torque/bending moment ratio almost three times larger (at failure). For example, the corner bar B yielded before collapse in all three tests, while bars C and D were also subject to significant tensile forces (figs. 5.26 and 5.27). However, unlike beam II, collapse of beams III and IV was primarily

due to a compression failure about corner A.   This occurred prior to

yield of either bar C or D in both tests.   The ultimate capacity of

each beam only differed by approximately 10%, the higher value being

recorded for beam IV which incorporated double stirrup reinforcement.

In addition to the central rotation about the longitudinal

axis, the displacement of both the section centre and the point of

loading were also required.   In practice, this was achieved after each

increment of load by measuring the horizontal and vertical displacement

of a single reference point located at the end of the lever-arm.

Together with the central rotation, this information enabled any other

point on the central plane to be determined by simple geometric

considerations.   In this way the relative positions of the section

centre and the point of loading have subsequently been computed for

each beam at failure.

In all cases the loading was initially applied in a direction

parallel to the vertical axis of the beam, $i.e.$ the upper loading

point on the lever-arm was always directly above the lower point of

jack fixity.   Clearly, after deformation, the effective direction of

loading is given by the angle between the line joining the upper and

lower jacking points and the initially vertical beam axis.   Further-

more, the effective lever-arm is the perpendicular distance measured

from the line joining the upper and lower jacking points to the actual

position of the assumed centre of rotation.

The initial lever-arm and recorded collapse load are presented

in Table 5.11 for each beam.   Final lever-arms and directions of

loading are also given in this table, although this has not been

possible in the case of beam I due to the premature failure of the

central inclinometer.
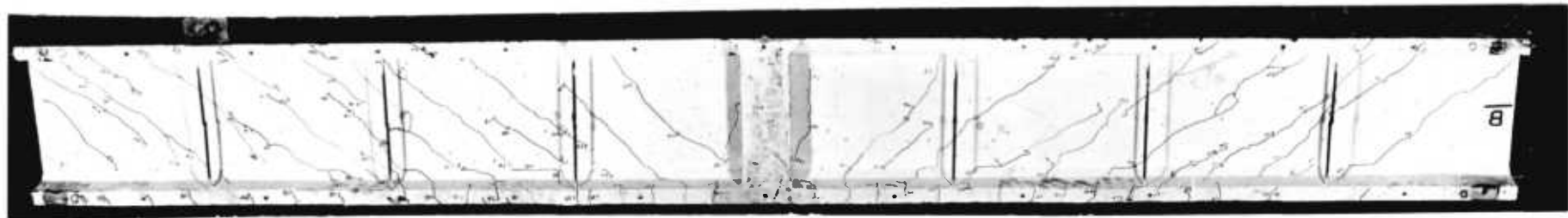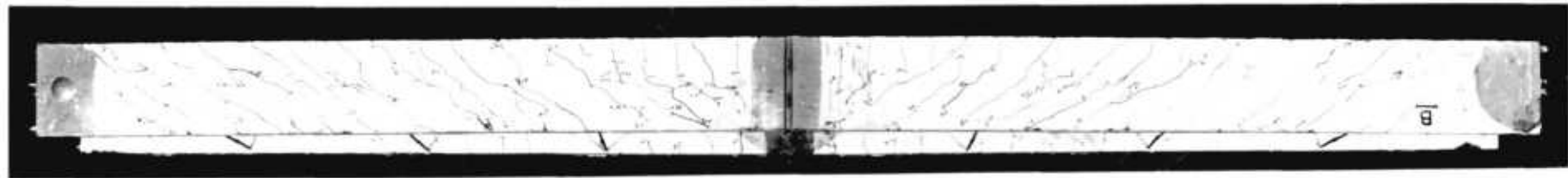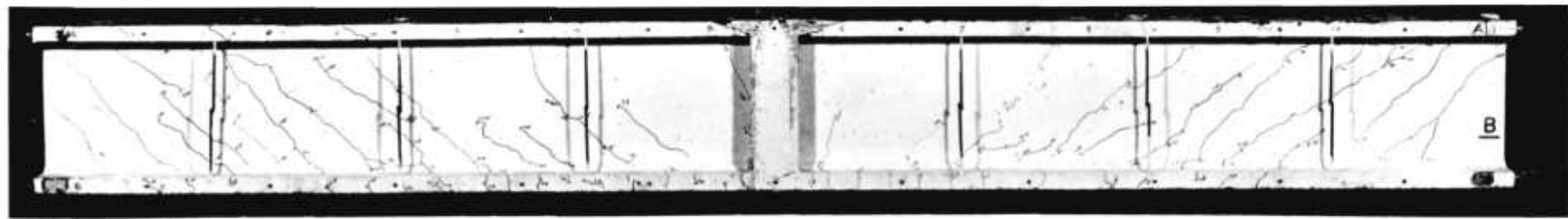
Plate 5.4   Crack Development on I-Section with Single Stirrup Reinforcement
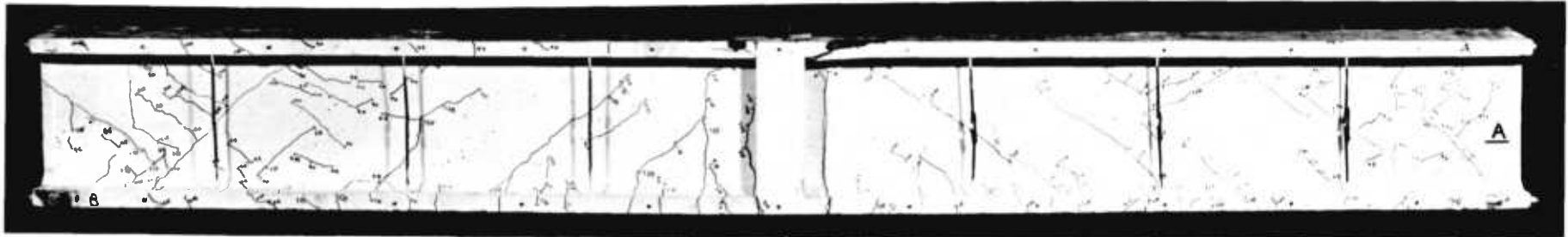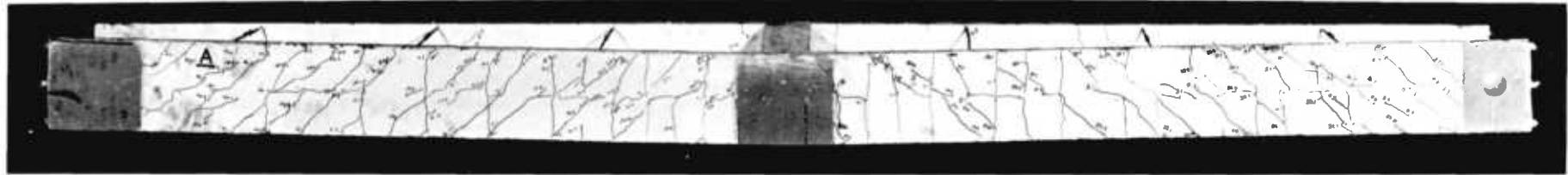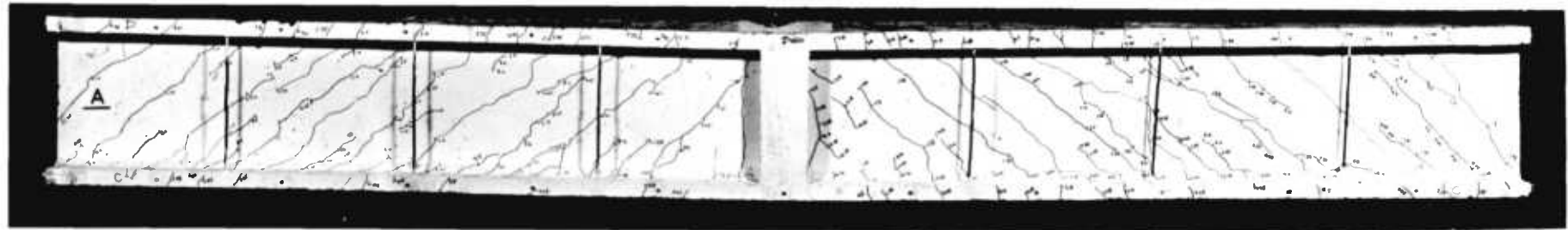
Plate 5.5   Crack Development on I-Section with Double Stirrup Reinforcement
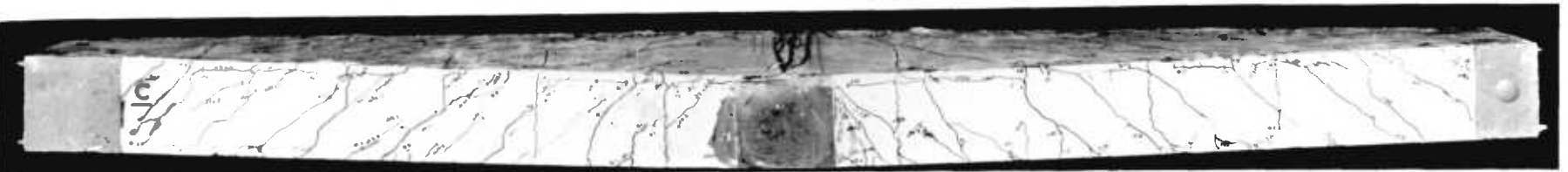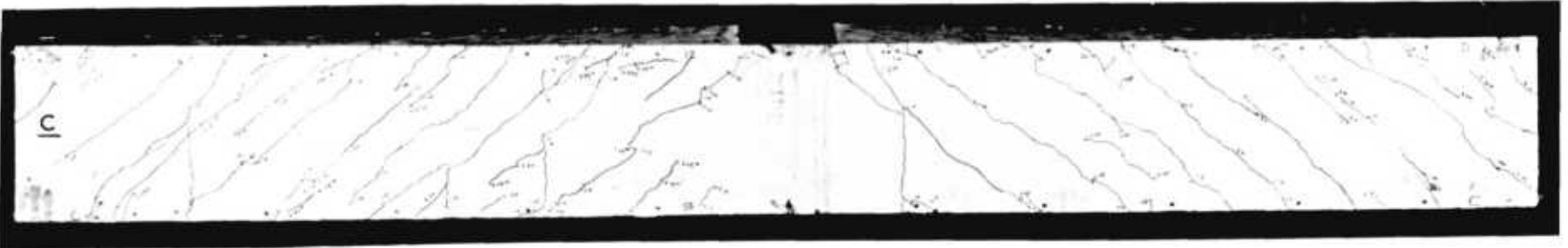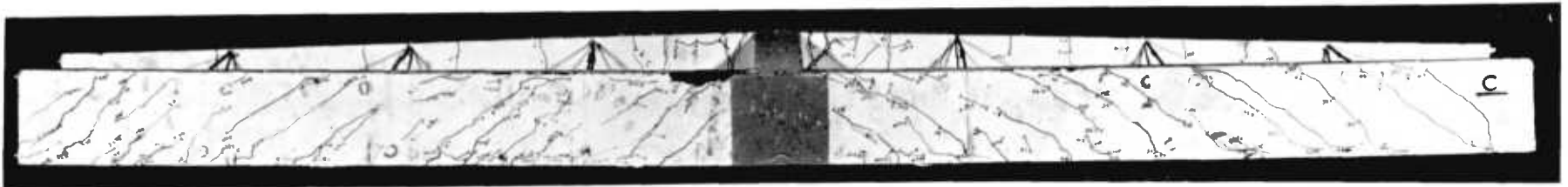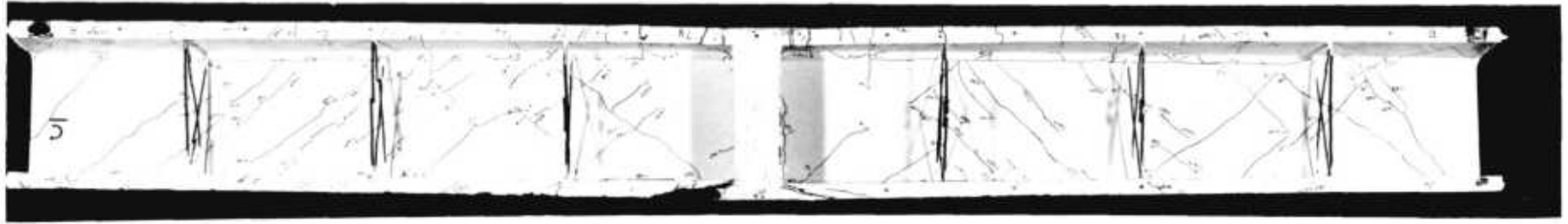
Plate 5.6   Crack Development on Channel Section with Single Stirrup Reinforcement
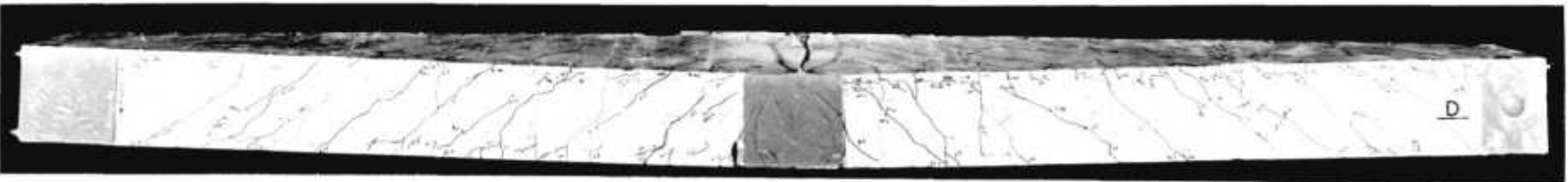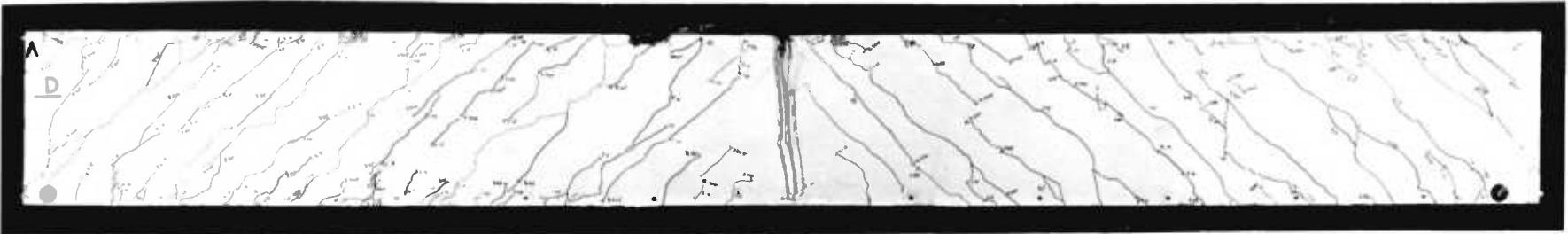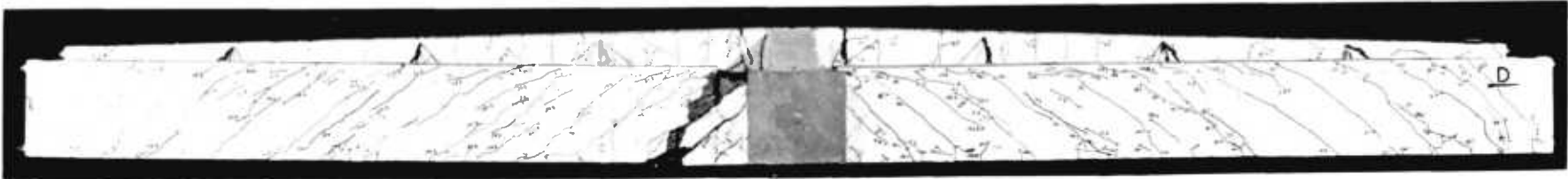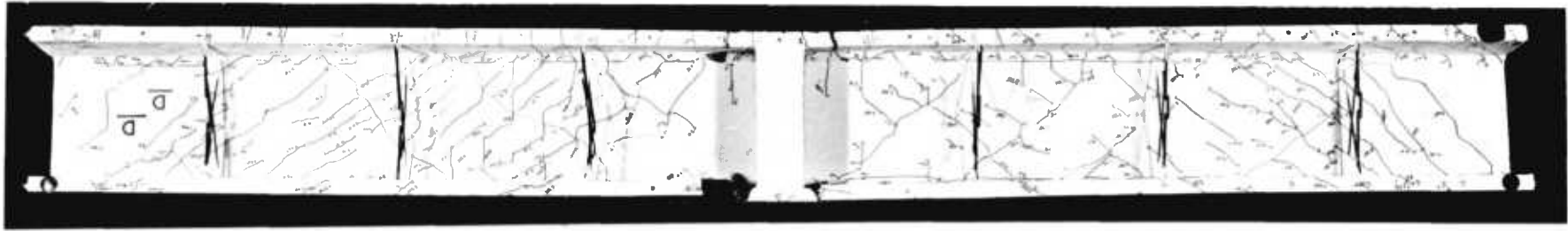
Plate 5.7   Crack Development on Channel Section with Double Stirrup Reinforcement

Measured Quantity	Beam Reference Number			
	I	II	III	IV
Collapse load (tons)	2.05	5.75	2.38	2.64
Initial lever-arm (mm)	337.0	97.0	124.0	120.0
Final lever-arm (mm)	-	45.2	154.3	153.8
Final load angle	-	13.3°	7.0°	7.7°

Table 5.11   Loading Arrangements for Beams I-IV

5.4.4   Comparison between Experiment and Theory

The Centre of Action of the Compressive Stresses at Failure

Determining the position of the compression zone at failure is relatively straightforward for beams with either solid or closed cross-sections.   A computer program developed for this purpose has previously been described in §5.3, and this is equally applicable to open sections subject to pure torsion in combination with other forms of loading.   However, when warping deformations are in any way restrained, the hypothesis of plane sections employed in the program is completely invalidated.   In general, strains will no longer be directly proportional to the perpendicular distance from the neutral axis and, thus, the position of maximum compressive strain need not necessarily correspond to that of the extreme concrete fibre.

The problem is further complicated by the fact that an infinite variety of different direct strain profiles due to warping restraint exist and, in general, these may be superimposed directly on to the strain profile due to combined bending moment and axial force. As a result, any number of permissible solutions are available for each selected orientation of the neutral (zero strain) axis.   This is a complex problem requiring further investigation and has not been considered further here.

For the simple I-beam and channel section, the centre of action of the compressive forces has, once again, been computed assuming plane sections remain plane. Clearly, while this can only be an approximation to the actual position when significant levels of bi-moment are present, it is not an unreasonable simplification for the general case of combined loading. This is because, for a particular orientation of the zero strain axis, the total compressive force in the concrete must equate with the total tensile force in the steel at all times. Thus, while the distribution of stress over the com-pression zone will undoubtedly be different when any bimoment is present, the total compressive force will not alter significantly and will result in the zero strain axis having a similar offset from the section centre as before. On the other hand, even if the offset of the zero strain axis is completely unchanged for a particular orientation, the different distribution of compressive stress will almost certainly result in a new location for the centre of action. However, since it is the locus of all these points that is required, even this is unlikely to be greatly affected by the application of moderate levels of bimoment.

Results from the computer analysis are presented in figs. 5.28 and 5.29 for the channel and I-sections, respectively. It must be emphasised, once again, that these results will only approximate the actual situation with any degree of accuracy when the structural behaviour is not predominantly governed by warping restraint effects. While this requirement is unlikely to prove a severe limitation in any practical application, it was not satisfied in the test of Beam I. In this case, it was found (from fig. 2.24 and Table 4.16) that the direct stress at each corner due to bimoment exceeded that due to bending moment by a factor of approximately eight. Clearly, the

Key:

☐ Centre of action of
the compressive forces

O Shear Centre at failure assuming
actual strain profile in the
compression zone

Δ Shear centre at failure assuming
initial elastic moduli for
elements in compression
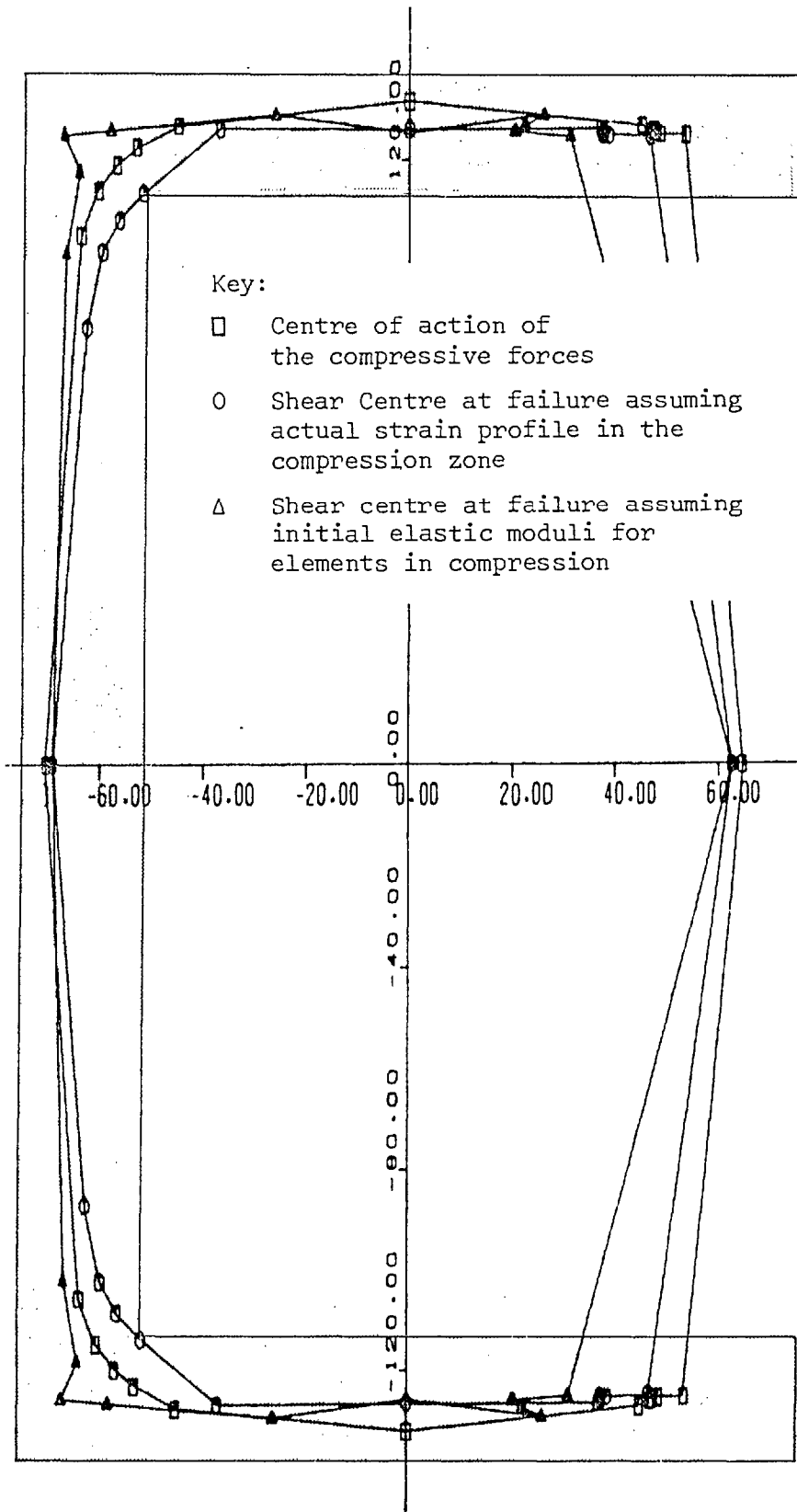
*Figure 5.28   Loci of the Centres of Action and Shear Centre
Positions at Failure (Channel Sections)*

Key:

☐   Centre of action of
    the compressive forces

O   Shear centre at failure assuming
    actual strain profile in the
    compression zone

Δ   Shear centre at failure assuming
    initial elastic moduli for
    elements in compression
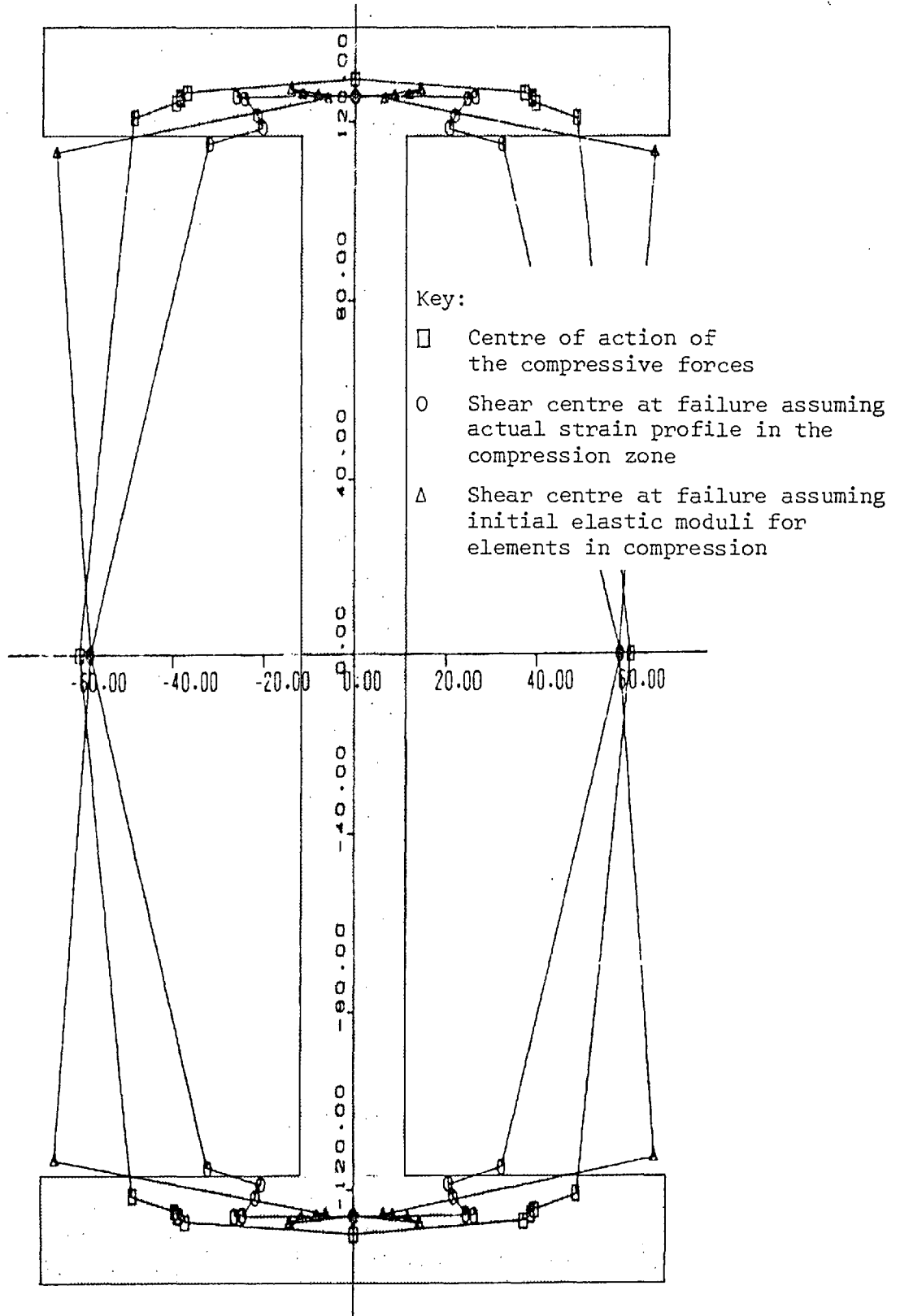
*Figure 5.29   Loci of the Centres of Action and Shear Centre
Positions at Failure (I-Beams)*

bimoment predominated the bending moment in this instance, a fact that was reflected in the mode of failure reported in §5.4.3. Indeed, the level of bimoment was such that a compression zone formed in each of two diagonally opposite corners, thus immediately invalidating the proposed theory.

The Position of the Shear Centre at Failure

Once the offset of the zero strain axis has been determined for any particular orientation, it is an easy matter to calculate the position of the shear centre at failure. This is given by the last two expressions in eqn. 5.64 which are derived in terms of the new principal co-ordinate system, X_c, Y_c. However, if required, eqn. 5.61 may subsequently be used to transform the final shear centre position into the original co-ordinate system, X, Y.

Clearly, one of the first requirements is to establish the origin and orientation of the new principal co-ordinate system. The effective modulus of the main reinforcement after yield is zero and, thus, only the unyielded steel and concrete in the compression zone contribute to the cross-sectional area and section stiffness. However, in calculating the centroid of the compression zone, the effective modulus of the various constituent elements must also be taken into consideration. For this reason, the centroid of the compression zone will not generally coincide with the centre of action of the compressive forces, the position of which has already been determined.

The computer program previously described in §5.3 has been extended to enable the new shear centre position to be established. This requires not only the determination of the origin and orientation of the principal axes at failure, but also the solution of the various integrations in eqns. 5.64 and 5.65. Furthermore, since the angle

between the cracked and uncracked principal axes is known at this stage, use has also been made of eqn. 5.61 to calculate the final shear centre position in terms of the original co-ordinate system.

Results from the computer analyses of the channel and I-sections have been presented in the form of a locus of final shear centre positions, $-e_x$, e_y, in each case. These curves are shown in figs. 5.28 and 5.29, each superimposed upon the corresponding locus of the centres of action of the compressive forces, x, y. There is, in general, good agreement between these curves. However, the eccentricity of each centre of action from the section centre is nearly always greater, by a small amount, than that of the corresponding shear centre position. This is to be expected since much of the concrete and some of the steel in the region of the extreme fibre has an effective modulus of zero and is, therefore, not included in the computation of the shear centre position. The computer program was also modified to enable the shear centre position to be calculated assuming that each constituent element of the compression zone possessed its initial elastic modulus. The resulting loci, shown in figs. 5.28 and 5.29, also compare favourably with the loci of the centres of action but are now slightly further from the section centre at nearly all positions.

A General Interaction Equation for I-Beams

It has been established that the shear centre position at failure is very nearly coincident with the centre of action of the compressive forces (apart from the change of sign in the x-co-ordinate). In view of the approximate nature of these results, due to the assumption that plane sections remain plane, it is therefore permissible to put

$$e_x = -x \; ; \quad e_y = y$$

Furthermore, the value of the constant of integration, K (defined in eqn. 5.64), has also been calculated in the computer analysis of the two sections and is closely approximated by $K = - xy$, in most instances. By substituting these terms into eqn. 5.70 and noting that for a change of axes to the computed centre of action, $\Delta_x = x$, $\Delta_y = y$, we have

$$B - x.M_x - y.M_y + xy.N + \sum_{j=1}^{n} F_j^2 \frac{s_j}{D_{jy}} (\omega_j - xy_j - x_j y + xy)$$

$$= \sum_{i=1}^{m} Z_{iy} \omega_{ci} - Z.\omega_c \qquad 5.73$$

For the two simple sections considered here

$$\omega_j = x_j y_j; \quad \omega_{ci} = x_{ci} y_{ci}; \quad \omega_c = 0$$

in which case, eqn. 5.73 takes the identical form of eqn. 5.37. This is the general interaction equation derived previously for closed sections where the warping function, W, is now replaced by the bimoment term, B.

For the idealized, doubly-symmetric I-beam, subject to the general system of loading shown in fig. 5.30a, the total shear flows in the web and in the top and bottom flanges are given by

$$\left. \begin{array}{l} F_w = V_y/h \\[2mm] F_t = T_w/bh + V_x/2b \\[2mm] F_b = T_w/bh - V_x/2b \end{array} \right\} \qquad 5.74$$

After substitution of the various shear flow terms from eqn. 5.74 into eqn. 5.73, and after much rearrangement, an interaction equation may be formed, thus:

$$\frac{B}{B_u} + \frac{M_x}{M_{xu}} + \frac{M_y}{M_{yu}} + \frac{T_w^2}{T_{wu}^2} + \frac{V_x^2}{V_{xu}^2} + \frac{V_y^2}{V_{yu}^2} - \frac{h}{y} \cdot \frac{T_w V_x}{T_{wu} V_{xu}} = 1 \qquad 5.75$$

In this expression, the ultimate load terms have the following definitions:

$$B_u = \Sigma Z_{iy}x_{ci}y_{ci}$$

$$M_{xu} = -x.\Sigma Z_{iy}x_{ci}y_{ci}$$

$$M_{yu} = -y.\Sigma Z_{iy}x_{ci}y_{ci}$$

$$T_{wu} = 2bh.\sqrt{\frac{D_y.\Sigma Z_{iy}x_{ci}y_{ci}}{8sbxy}}$$

$$V_{xu} = \sqrt{\frac{2bD_y.\Sigma Z_{iy}x_{ci}y_{ci}}{sxy}}$$

$$V_{yu} = \sqrt{\frac{hD_y.\Sigma Z_{iy}x_{ci}y_{ci}}{sxy}}$$

5.76

In all of these terms the summation is carried out over the range i = 1,m and is only effective for elements of reinforcement in tension.

a. I-Section   b. Channel Section
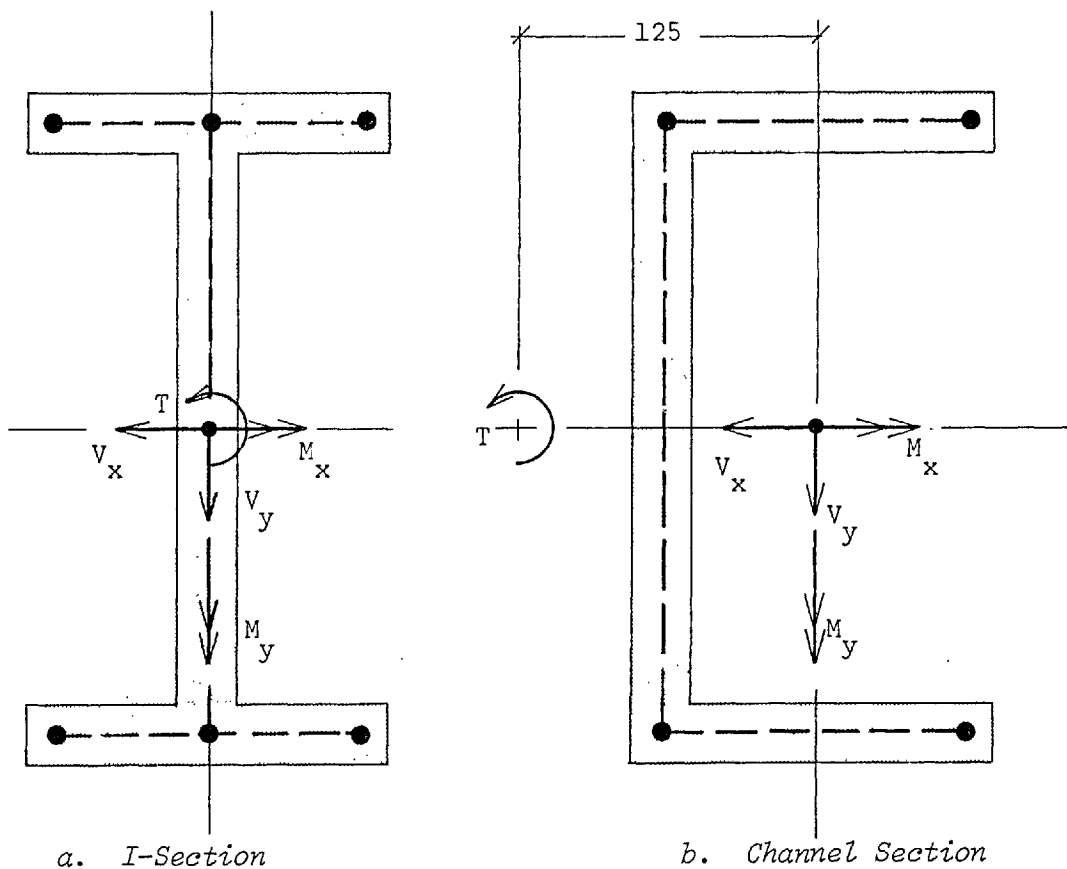
Figure 5.30   Idealizations of Open Section Beams adopted in
the Advanced Failure Method

A General Interaction Equation for Channel Sections

For the idealized, singly-symmetric channel section, shown in fig. 5.30b, the total shear flows in the web and in the top and bottom flanges are given by

$$\left. \begin{aligned} F_w &= V_y/h \\ F_t &= T_w/bh + V_x/2b + V_y/2h \\ F_b &= T_w/bh - V_x/2b - V_y/2h \end{aligned} \right\} \qquad 5.77$$

After substitution of these terms into eqn. 5.73, the general interaction equation for channel sections has the following form:

$$\frac{B}{B_u} + \frac{M_x}{M_{xu}} + \frac{M_y}{M_{yu}} + \frac{T_w^2}{T_{wu}^2} + \frac{V_x^2}{V_{xu}^2} + \frac{V_y^2}{V_{yu}^2} - \frac{h}{y} \cdot \frac{bx}{(bh+2xh+bx)} \cdot \frac{V_x \cdot T_w}{V_{xu} T_{wu}}$$

$$+ \frac{2bx}{(bh+2xh+bh)} \cdot \frac{V_x \cdot V_y}{V_{xu} V_{yu}} - \frac{h}{y} \cdot \frac{V_x \cdot T_w}{V_{xu} T_{wu}} = 1 \qquad 5.78$$

The ultimate vertical shear force, V_{yu}, is now given by

$$V_{yu} = h \cdot \sqrt{\frac{2D_y \ \Sigma \ Z_{iy} \cdot x_{ci} \cdot y_{ci}}{sy(bh + 2xh + bx)}} \qquad 5.79$$

although the remaining terms are identical to those previously defined in eqn. 5.76 for the I-section.

Theoretical Results

Since full warping restraint is provided at the centre section by the symmetrical nature of the loading, there can be no change of rotation at this point, *i.e.* $\phi' = 0$. Therefore, in accordance with eqn. 2.34, the torque applied to the centre of the beam must consist entirely of warping torsion, T_w, since $T_{sv} = 0$. Furthermore, from

Table 4.16, the bimoment at the centre section is given by

$$B = \frac{\tanh(k\ell/2)}{2k} \cdot T \qquad\qquad 5.80$$

This expression is only strictly valid for a constant value of the decay function, k, *i.e.* the ratio of warping stiffness to pure torsional stiffness is unchanged along the beam. While this is clearly the case for uncracked sections, the situation after cracking is complex and requires further investigation.

For the purposes of this analysis the initial value of k has been assumed to remain unchanged throughout the length of the beams. Thus, with the term k determined previously in §5.4.3, we have, from eqn. 5.80

$$B = 0.0967 \; T\ell \quad \text{(I-beam)}$$

and $\qquad B = 0.1253 \; T\ell \quad \text{(channel)}$

However, the quantity T used in eqn. 5.80 is the actual torque applied to the section and must take account of the horizontal change in shear centre position after cracking. Thus, with the approximation adopted earlier for e_x, we have

$$T = \frac{P}{2} \text{(lever-arm} + e_x) = \quad T_w - \frac{P}{2} \cdot x \qquad\qquad 5.81$$

On the other hand, the warping torsion, T_w, and the shear forces, V_x, V_y, are compeltely independent of the change in shear centre position. This is due to the formulation of the interaction equations in which the shear flows corresponding to these stress resultants are in full equilibrium with the applied load P.

With the effective loading angles and final lever-arms given in Table 5.11, it has been possible to determine the various components of load applied to beams II - IV as they approached failure (Table 5.12). This information is not available for beam I, due to the broken central

inclinometer, although the mode of failure also invalidates it from the subsequent analysis.

Component of Load	Beam Reference Number		
	II	III	IV
Bimoment, B	111.2(45.2-x)P	144.1(154.3-x)P	144.1(153.8-x)P
Bending Moment, M_x	0.973 Pℓ/4	0.993 Pℓ/4	0.991 Pℓ/4
Bending Moment, M_y	0.231 Pℓ/4	0.122 Pℓ/4	0.137 Pℓ/4
Torque, T_w	45.2 P/2	154.3 P/2	153.8 P/2
Shear Force, V_x	0.231 P/2	0.122 P/2	0.137 P/2
Shear Force, V_y	0.973 P/2	0.993 P/2	0.991 P/2

Table 5.12   Components of Load at Failure for Beams II-IV

The following dimensions are common for all three beams:

ℓ = 2300 mm

b = 125 mm

h = 250 mm

s =   50 mm

In addition, D_y may be obtained from fig. 5.22 and has the value of 6.58 kN for beam III (one stirrup leg), and 13.16 kN for beams II and IV (two stirrup legs). By introducing these values into eqns. 5.75 and 5.78, together with the appropriate components of load from Table 4.12, both general interaction equations may now be expressed in the following form:

$$P(k_1 + k_2.x + k_3.y) + xy.P^2(k_4 + k_5/y + k_6/x) = \sum_{i=1}^{n} Z_{iy} x_{ci} y_{ci} \qquad 5.82$$

The values of k_1 - k_6 in this expression are given in Table 4.13 for the three beams under consideration.

Multiplier	Beam Reference Number		
	II	III	IV
k_1	-5.033×10^3	-2.224×10^4	-2.216×10^4
k_2	6.708×10^2	7.151×10^2	7.140×10^2
k_3	1.328×10^2	7.015×10^1	7.875×10^1
k_4	4.284×10^{-2}	3.028×10^{-1}	1.507×10^{-1}
k_5	-7.917×10^{-1}	-3.999	-2.239
k_6	$-$	4.669	2.325

Table 5.13   Values of the Multipliers for Beams II-IV

Before a solution to eqn. 5.82 is possible, it is necessary to introduce the appropriate values of x, y, etc. for a particular beam and neutral axis orientation.   These variables are tabulated for both the channel and I-sections in Table 4.14.   Only the first quadrant has been considered since the compression zone was observed to form about this corner in all three tests.

The positive solution of eqn. 5.82 for each of the selected orientations is given in Table 4.15.   The stationary value for beam II occurs at an orientation of approximately 20°, with failure predicted at a load of 4.23 T.   Beam II was observed to fail at a load of 5.75 T (Table 4.11), representing an overload of approximately 36% with respect to the ultimate load theory proposed here.   However, in the computer analysis of the section on which this theory is based, a yield stress of 431 N/mm^2 was used for all main steel.   In practice, a significant increase in this value is possible due to work hardening effects and, in fig. 5.22, an average increase of approximately 31.5% was apparent before failure.   Since an under-reinforced section has

been assumed, the collapse load is governed completely by the physical properties of the steel. Accordingly, if the gain in strength due to work hardening effects is taken into consideration, the predicted and observed failure loads are in excellent agreement.

The predicted behaviour of the two channel sections was very similar in all major respects. From Table 4.15 a stationary value can be seen to occur at an orientation of approximately 70° in both cases. These represent local maxima and correspond to predicted failure loads of 4.43 T for beam III and 4.97 T for beam IV. However, a second stationary value occurring at an orientation of $30{-}40^{\circ}$ is also evident in each case. These are local minima with values of 4.30 T for beam III and 4.84 T for beam IV. Although the two stationary values for each beam are not greatly different, they predict failure loads exceeding those actually observed (Table 4.11) by a factor of approximately two. Moreover, if strain hardening effects are once again taken into consideration, the disparity between the observed and predicted loads is further increased.

These poor theoretical results indicate the importance of satisfying all the limiting criteria upon which the analysis is based. In particular, the beams must be fully under-reinforced and have sufficient strain capacity to permit redistribution of forces at yield of either component of steel. However, the observed modes of failure reported earlier in this section indicate that yield of all elements of reinforcement was in fact preceded by a compression failure in one corner. An additional constraint that must also be satisfied relates to the level of applied bimoment. In computing the co-ordinates of the centre of action of the compressive forces, plane sections were assumed to remain plane. This is only strictly the case in the absence

Neutral Axis Orientation	Co-ordinates of the Centre of Action (mm)				$\sum_{i=1}^{n} Z_{iy} x_{ci} y_{ci}$ $(\times 10^8 N.mm^2)$	
	I-Beam		Channel			
	x	y	x	y	I-Beam	Channel
10°	22.85	126.12	35.85	126.82	8.470	8.895
20°	25.79	125.65	37.97	125.92	9.540	9.384
30°	26.46	124.53	38.30	125.58	9.743	9.449
40°	26.62	123.55	38.34	125.40	9.758	9.450
50°	27.64	122.49	39.45	125.28	10.553	9.980
60°	30.14	121.66	41.78	125.20	12.032	11.061
70°	35.38	120.53	46.82	124.81	15.000	13.076
80°	51.85	52.85	56.67	78.87	10.118	9.312

Table 5.14   Data relating to the Centre of Action of the Compressive Forces for both Channel and I-Sections

Neutral Axis Orientation	Predicted Failure Load (T)		
	Beam II	Beam III	Beam IV
10°	2.746	4.395	4.985
20°	4.233	4.308	4.860
30°	3.791	4.296	4.842
40°	3.506	4.295	4.841
50°	3.360	4.336	4.885
60°	3.299	4.401	4.953
70°	3.267	4.434	4.971
80°	3.109	3.258	3.457

Table 5.15   Failure Loads predicted for different Orientations of the Neutral Axis

of warping stresses although significant inaccuracies are unlikely if
the level of bimoment is relatively small.   This restriction was not
satisfied in the test of beam I which was disqualified from the analysis
due to the formation of separate compression zones in two diagonally
opposite corners.   However, the level of bimoment was also substantial
at the centre sections of the channels, although only one bar was
evidently in compression in each test (figs. 5.26 and 5.27).   In both
beams III and IV, the direct stress at each corner due to bimoment
may be shown (from fig. 2.24 and Table 4.16) to exceed that due to
bending moment by a factor of approximately three.   Under this com-
bination of load, the distribution of stress across the compression zone
is likely to be significantly different from that assumed and, thus, the
accuracy with which the centre of action has been determined must be in
some doubt.

Finally, the level of bimoment adopted in the failure analysis
of each beam was calculated using the initial (uncracked) value of the
decay function, k.   Since, after cracking, this function is unlikely
to remain constant along the length of the beam, a significant error in
this term is also possible.   Clearly, before the applications and
limitations of this method can be fully assessed, an extensive programme
of research is necessary into several important aspects of the behaviour
of open section beams after cracking.

CHAPTER SIX

GENERAL DISCUSSION, CONCLUSIONS AND
RECOMMENDATIONS FOR FUTURE RESEARCH

6.1   GENERAL DISCUSSION

For concrete structures, in which self-weight contributes a
significant proportion of the design load, considerable economies can
be effected by making reductions in section thickness.   This is
particularly true in the case of box girder bridges and floating
structures.   The primary objective of this research has been to
identify those cross-sectional configurations in which large warping
displacements are likely to occur and, then, to determine the levels
of stress induced if these displacements are in any way restrained.
Most aspects of the behaviour of thin-walled concrete structures have
already been discussed at some length and, thus, it only remains to
show how this research could be best applied to practical situations.

The method of analysis adopted for a particular structure
depends, to a large extent, on the accuracy to which the solution is
required and on the computational facilities available.   Thus, with the
relatively low running costs associated with the large capacity com-
puters available to-day, there has been a tendency towards the use
of sophisticated analytical techniques.   These methods are almost
invariably based on a stiffness formulation since this provides a
degree of generality which is desirable in computer-based approaches.
One such method in which considerable experience has been gained in
the grillage analysis.   This remains popular with designers largely
due to the ease with which a structure may be idealized into an
assemblage of equivalent beam elements.   The technique is particularly

useful in the analysis of slab or pseudo-slab bridge decks, in which the transverse and longitudinal distributions of load are equally important.   Although the method has also been extended to the analysis of multi-cellular bridges, it is only truly applicable where the number of cells is in excess of four[71].

However, finite element techniques are being increasingly employed in the analysis of cellular structures due to the close resemblance between the structural idealization and the actual geometry. The use of this method is fully justifiable where warping, distortion, shear lag and local effects are likely to be important contributary factors in the final distribution of stress.   However, it has already been shown that this is frequently not the case for concrete structures, where typical wall thicknesses are such that the significance of most of these secondary effects is considerably reduced.   Indeed, for the important class of structures described in this thesis, the finite element method is entirely inappropriate.   Nevertheless, it has frequently been used due to the absence of a more suitable method in which warping restraint effects are fully considered.

The structural idealizations adopted by the grillage and finite element methods are clearly more suited to the analysis of two- and three-dimensional problems, respectively.   It is therefore only to be expected that their use in the analysis of what is essentially a one-dimensional structure would require significantly more computational effort than the alternative method described in Chapter 3.   This is demonstrated with reference to the bifurcated bridge, which has already been represented by a single beam idealization in §4.2.   The structure was originally designed by the grillage method and has also recently been analysed using finite element techniques[85].   The structural idealization adopted by both of these methods

is shown in fig. 6.1. In the case of the grillage analysis, the webs have been replaced by a series of end-connected straight beam elements which have each been assigned a proportion of the total flexural and torsional stiffness. Secondary cross-beams have also been provided in order to take account of the excellent load distribution properties of the flanges and diaphragms. No provision has been made for side cantilevers although the effects of loading in these areas is accommodated by applying appropriate fixed-end forces to the adjacent nodes.

Whereas the lines in fig. 6.1 represent beam elements in the grillage method, they also form the outline of the various plate elements in the structural idealization of the bottom flange adopted for the finite element approach. The top flange is similarly modelled but with an additional row of elements on either side to represent the cantilevers. Finally, the idealization is completed by separating the two flanges with an appropriate number of web and diaphragm elements.

The total number of elements, nodes and degrees of freedom associated with each method are also given in fig. 6.1. Computer time necessary for solution is largely governed by the total number of degrees of freedom, although storage requirements can usually be significantly reduced by taking the bandwidth of the various matrices into account. Nevertheless, a considerable disparity clearly exists between the amount of computation required for solution by the different methods. Several other advantages are also apparent in the case of the single beam method of analysis proposed here. For ex-ample, by employing a circular curved element, the solution is 'exact' in the sense that the longitudinal distributions of the various stress resultants are continuous functions and not just a series of values at

the nodal points.   Since the degree of accuracy obtained with the other methods depends entirely on the degree of refinement adopted in the initial idealization, these methods can, at best, only provide an approximation of the response of the structure.

The small amount of input data necessary to describe the structural idealization is also an important feature of the single beam method since this not only saves time but also reduces the possibility of human error.   However, input data is also required for each loading condition and, whereas this is a simple matter for both the single beam and finite element methods, in the case of the grillage analysis fixed-end forces must first be determined at each nodal position.   Further dissimilarities between the methods are also apparent after analysis due to differences in output.   In the simple beam method this takes the form of the longitudinal distributions of the various stress resultants, thus enabling the section to be designed immediately.   The grillage analysis also provides stress resultants at the end of each member but, due to the necesssary method of idealization, these must usually be combined before determining levels of reinforcement and prestressing for the section.   On the other hand, results from the finite element analysis are in the form of components of stress at each node, and these require considerable post-processing especially for the design of prestressing.

Indeed, the only real disadvantage with the single beam method is its inability to accommodate continuously varying sections.   This was apparent in the analysis of the bifurcated bridge where the junction was idealized by the three curved outer spans joining at a solid transverse diaphragm.   An attractive solution to this problem would be to perform a finite element analysis of the junction subject to a series of unit displacements at the three ends.   A stiffness matrix could then be derived for the central element and incorporated into the single beam analysis.

	Method of Analysis		
	Single Beam	Grillage	Finite Element
Number of elements	18	210	569
Number of nodes	19	136	380
Total number of degrees of freedom	67	399	2171
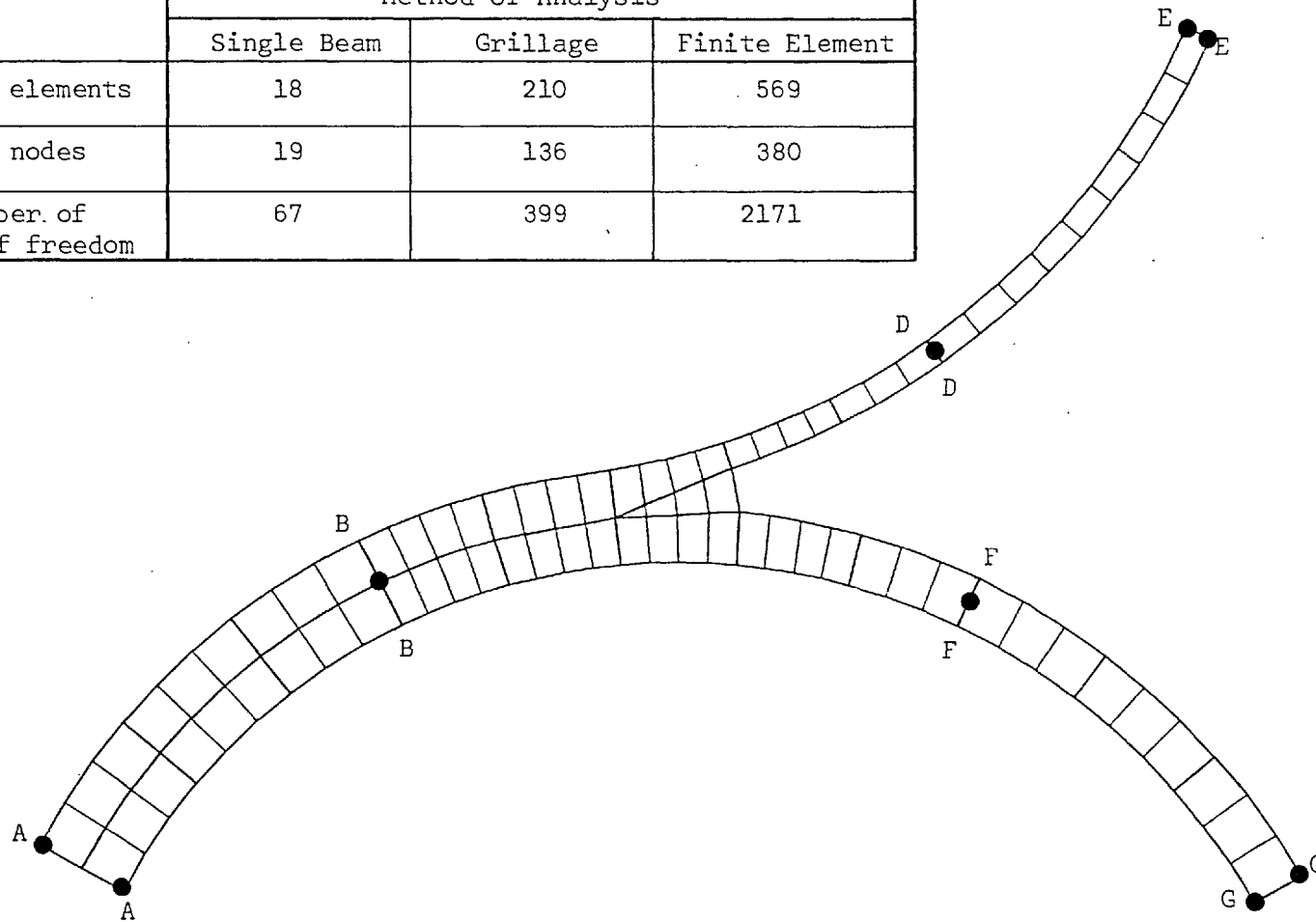
Figure 6.1   Structural Idealization of the Bifurcated Bridge

6.2   GENERAL CONCLUSIONS

1.   The tendency towards thinner walled concrete sections has reached such a point that thin-walled behaviour must now frequently be assumed.   For the important range of concrete structures considered here, cross-sectional distortion and shear lag effects are usually negligible in comparison with those due to warping restraint.

2.   Box girder bridges, even those displaying significant levels of warping, do not always fully satisfy the limiting criterion (stated in §2.1) defining thin-walled sections.   Significant variations in the transverse distribution of shear stress are apparent in such cases, although this is not usually reflected in the computed value of the resultant torsional moment.

3.   A better estimate of the importance of warping restraint, in a particular application, is given by two dimensionless terms, namely, the decay function, $k\ell$, and the warping shear parameter, μ.   These quantities have been determined for a large number of existing structures and indicate that warping is of equal importance in concrete box girder bridges as in composite bridges of similar cross-sectional configuration.

4.   For the computer analysis of structures, the stiffness methods have considerable advantages over other forms of solution. However, the finite element and grillage methods are largely inappropriate for the analysis of the one-dimensional structures considered in this thesis.   With the single beam approach proposed here, significant savings are not only possible in computer running time and storage requirements but also in the preparation of input data and in the handling of results.

5.   The member stiffness matrix for the straight beam element, incorporating the effects of warping restraint, has been derived in

explicit form.   However, this is not easily achieved in the case of

the circular curved beam and, therefore, an alternative numerical approach

has been adopted.   This involves inversion of the member flexibility

matrix and can lead to problems of ill-conditioning for members possessing

a relatively small warping stiffness.   It is therefore recommended that

thin-walled members should be treated as solid members for the purposes

of analysis when $k\ell > 30$.   However, in practice, the effects of warping

restraint are usually negligible for very much smaller values of $k\ell$.

The limiting value, $k\ell = 10$, adopted elsewhere[79], would appear to be

entirely satisfactory, although the merits of each individual case may

be easily assessed from the distributions of the various stress resultants

presented in graphical form in Chapter 3.

6.   Errors introduced into the various stiffness analyses have

been quantified for a wide range of typical sections.   However, since

it is difficult to generalize about these results, their effect has

been demonstrated in the case of a three span continuous bridge of

composite construction.   In this particular bridge, the idealization

of the central curved span as an assemblage of equivalent straight

beam elements introduced relatively small errors into the computed

values of the various stress resultants.   These were generally less

than 5% for beams subtending a central angle of approximately 30° and

were, therefore, very much smaller than those due to neglecting either

the change in the shear centre position, or the actual value of the

warping shear parameter.

7.   With reference to the continuous and bifurcated bridges,

member curvature had a negligible effect on the computed values of

the various second moments of area and, thus, did not greatly influence

the longitudinal distribution of stress.   However, the transverse

distribution of stress was significantly affected and curvature effects must therefore be fully considered in the design of the section.

8.	An advanced method of ultimate load analysis has been presented which enables a corner mode of failure to develop under certain combinations of shear, torsion and bending moment. Excellent agreement between theory and experiment apparently exists, and this has been demonstrated with reference to an extensive series of prestressed concrete beams, for which results were already available.

9.	An advanced ultimate load method has also been proposed for the analysis of open sections subject to general combinations of load including bimoment. The theory compares favourably with the result from one I-beam test but an extensive experimental programme is required in order to determine the range of application and limitations of the method.

6.3	RECOMMENDATIONS FOR FUTURE WORK

1.	Parametric surveys of existing structures are of invaluable assistance to the designer. As the trend towards thinner sections continues, information on the warping and torsional behaviour of different configurations would be highly beneficial (*e.g.* figs. 2.11 - 2.13).

2.	In the computer program described in §4.1, sub-routines were developed for determining fixed-end forces due to uniformly distributed and central point loads only. This work could be usefully extended to include more general forms of loading, thereby reducing the number of beam elements still further.

3.	The fundamental equations governing the torsional deformation of curved members include components of both bending moment

and axial force.   Since the effects of axial force are usually in-
significant in closed sections of practical proportion, this component
of load was neglected in the subsequent development of the theory.
However, in the case of open sections or in the design of prestressing
arrangements, axial force may be important and must therefore be included
in the formulation of the stiffness matrix.

4.   For asymmetrical sections or for those displaying super-
elevation, bending moment about the vertical axis must also be con-
sidered.   Furthermore, since economies in construction can often be
effected by omitting intermediate diaphragms, the range of application
of the analysis would also be greatly extended by the inclusion of
distortional effects.   The basic theory relating to both of these
structural actions already exists although, due to the additional com-
plexities, both the flexibility and stiffness matrices would be best
derived numerically

5.   The stiffness analysis proposed in this thesis incorporates
both straight and circular curved beam elements.   However, in the
design of elevated road bridges, transitional curves are invariably
used to achieve a gradual change in curvature between straight and
curved sections.   A variety of curves exists for this purpose
including the clothoid, lemniscate, cubic parabola and cubic spiral[81].
Although a solution to the fundamental equation is possible for each
of these curves, this would be difficult to achieve in explicit form
and requires a numerical solution.

6.   In the analysis of box girder bridges and shear core
structures the positions of both the centroid and the shear centre
are unlikely to differ greatly from one element to the next.   However,

where this does occur, local stress variations are possible which merit further investigation.

7.   Proposals for an advanced method of ultimate load analysis have been formulated for simple open and closed sections. For these methods to be verified and extended to the general case, rigorous upper and lower bound solutions are required based on the general theory of plasticity.

8.   No other relevant experimental evidence is available on the ultimate load behaviour of thin-walled open sections subject to significant levels of bimoment. Furthermore, in the case of solid or closed sections, subject to bending moment, torsion and shear, the large majority of existing test results were invalidated from this study due to unfavourable systems of loading or support. As a result, extensive experimental investigations are necessary in order to verify the advanced failure methods, particularly in the case of open sections.

9.   The testing of four open section beams highlighted several problems which require further study. These include theoretical and experimental investigations of (i) changes in the position of the shear centre and centroid of all stages up to failure, (ii) the transverse distribution of strain over a cross-section when bimoment is present, and (iii) variations in all the components of structural stiffness after cracking.

REFERENCES

1.   ALAM, K.M.A., HONGLADAROMP, T. and LEE, S.L.
       Curved Box Girder Bridges with Intermediate
       Diaphragms and Supports, International Association
       of Bridge and Structural Engineering Vol. 33-11, 1973

2.   AMERICAN CONCRETE INSTITUTE, Torsion of Structural Concrete
       Special Publication SP18, 1968

3.   AMERICAN CONCRETE INSTITUTE, Concrete Bridge Design,
       Special Publication SP26, 1969

4.   AMERICAN CONCRETE INSTITUTE, Analysis of Structural Systems
       for Torsion, Special Publication SP35, 1973

5.   AMERICAN CONCRETE INSTITUTE, Response of Multistorey
       Concrete Structures to Lateral Forces,
       Special Publication SP36, 1973

6.   A.S.C.E./A.A.S.H.T.O. COMMITTEE, Curved Steel Box Girder
       Bridges : Survey and State of the Art, Journal of
       the American Society of Civil Engineers, ST11,
       November 1978

7.   ARGYRIS, J.H. and DUNNE, P.C. The General Theory of
       Cylindrical and Conical Tubes Under Torsion and Bending
       Loads, Journal of the Royal Aeronautical Society
       Parts I-VI, 1947-1949

8.   BATCHELOR, B. de V. and McEWEN, W.D. Eccentrically
       Prestressed Box Girders Under Combined Bending and
       Torsion, American Concrete Institute Journal, April 1977

9.   BAZANT, Z.P. Non-Uniform Torsion of Thin-Walled Bars of
       Variable Section. International Association of Bridge
       and Structural Engineering, Vol. 25, 1965

10. BELOW, K.D., RANGAN, B.V. and HALL, A.S. Theory for Concrete
       Beams in Torsion and Bending, Journal of the Structural
       Division, Proceedings of the American Society of Civil
       Engineers, ST8, August 1975

11. BENSCOTER, S.U., A Theory of Torsion Bending for Multicell
       Beams, Journal of Applied Mechanics, Vol. 21, No, 1
       March 1954 pp 25-34

12. BILLINGTON, C.J., and DOWLING, P.J. Bifurcated Elevated
       Highways - Construction, Instrumentation and Testing
       of Four Linearly Elastic Models, Civil Engineering
       Structures Laboratory, Imperial College, Report BB1
       London, 1972

13.　BILLINGTON, C.J. and DOWLING, P.J.　Bifurcated Elevated
　　　　Highways - Model 1, Spine Beam Model Results of
　　　　Lane Loading Test,　Civil Engineering Structures
　　　　Laboratory, Imperial College, Report BB2, London 1972

14.　BILLINGTON, C.J., and DOWLING, P.J.　Bifurcated Elevated
　　　　Highways - Model 1, Spine Beam Model Results of HB,
　　　　Knife Edge and Point Loading Tests,　Civil Engineering
　　　　Structures Laboratory, Imperial College Report BB3, 1972

15.　BOMMER, C.M. and SYMONDS, D.A., Skeletal Structures. Matrix
　　　　Methods of Linear Structural Analysis Using Influence
　　　　Coefficients,　Crosby Lockwood and Son Ltd, London 1968
　　　　(not seen by this author)

16.　CERVENKA, V. and GERSTLE, K.H.　Inelastic Analysis of
　　　　Reinforced Concrete Panels :　Theory,　International
　　　　Association of Bridge and Structural Engineering,
　　　　Vol. 31-II, 1971

17.　CHEUNG, M.S., and CHEUNG, Y.K., Analysis of Curved Box
　　　　Girder Bridges by Finite Strip Method, International
　　　　Association of Bridge and Structural Engineering
　　　　Publications, Vol. 31-I, 1971

18.　CHUNG, H.W. and GARDINER, N.J.　Model Analysis of a Curved
　　　　Prestressed Concrete Cellular Bridge,　Concrete
　　　　Bridge Design, American Concrete Institute SP26, 1969

19.　COLLINS, M.P., WALSH, P.F., ARCHER, F.E. and HALL, A.S.
　　　　Ultimate Strength of Reinforced Concrete Beams
　　　　Subjected to Combined Torsion and Bending, Torsion
　　　　of Structural Concrete,　American Concrete Institute,
　　　　SP18, 1968

20.　COMITÉ EUROPÉEN DU BÉTON (CEB)　Effort Tranchant - Torsion,
　　　　Bulletin D'Information, No. 92, Final Draft, Paris, 1973

21.　CORLEY, W.G. et al,　Construction and Testing of 1/10th Scale
　　　　Micro Concrete Model of New Pontomac River Crossing,
　　　　PCA Bulletin　RD 031, OIE

22.　COULL, A.　and STAFFORD SMITH, B.　Tall Buildings,
　　　　Proceedings of Symposium on Tall Buildings and Shear
　　　　Wall Structures, Southampton University, 1966

23.　COWAN, H.J.,　Reinforced and Prestressed Concrete in Torsion
　　　　Edward Arnold, London, 1965

24.　CUSENS, A.R. and PAMA, R.P.,　Bridge Deck Analysis,
　　　　John Wiley & Sons, London, 1975

25.　DABROWSKI, R.,　Curved Thin-Walled Girders,Translation
　　　　from the German by C.V. Amerongen, Cement and Concrete
　　　　Association Publication 61.144, 1972

26. DANESI, R.F., Prestressed Concrete Box Girders of Deformable Cross-Section, Ph.D. Thesis, Imperial College, London University, 1977

27. EDWARDS, A.D. and LOVEDAY, R.W., Structural Behaviour of a Prestressed Box-Beam with Thin Webs Under Combined Bending and Shear, Concrete Structures & Technology Section, Department of Civil Engineering, Imperial College, London, 1975

28. ELFGREN, L. Reinforced Concrete Beams Loaded in Combined Torsion, Bending and Shear. A Study of the Ultimate Load-Carrying Capacity, Chalmers University of Technology (Division of Concrete Structures, Publication 71:3) Göteborg, Sweden, 1971

29. ELFGREN, L., KARLSSON, I. and LESBERG, A., Torsion/Bending/ Shear Interaction for Concrete Beams, Journal of the Structural Division, American Society of Civil Engineers, August 1974

30. GANGARAO, H.V.S., and ZIA, P., Rectangular Prestressed Beams in Torsion and Bending, Journal of the Structural Division, Proceedings of the American Society of Civil Engineers, ST1, January, 1973

31. GERWICK, B.C. (Editor), Concrete Ships and Floating Structures, Conference Proceedings, University of California, September 1975

32. GOODE, C.D., Torsion, Bending and Shear Tests on Reinforced Microconcrete Beams, Proceedings of the Joint I. Struct. E/B.R.E. Reinforced and Prestressed Microconcrete Models Seminar, 1978

33. GOODE, C.D., and HELMY, M.A., Ultimate Strength of Reinforced Concrete Beams in Combined Bending and Torsion, Torsion of Concrete Structures, American Concrete Institute SP18, 1968

34. GVOZDEV, A.A., LESSIG, N.N., and RULLE, L.K. Research on Reinforced Concrete Beams Under Combined Bending and Torsion in the Soviet Union, Torsion of Structural Concrete, American Concrete Institute SP18, 1968

35. HAMBLY, E.C., Bridge Deck Behaviour, Chapman and Hall, London, 1976

36. HAMBLY, E.C., and PENNELS, E., Grillage Analysis Applied to Cellular Bridge Decks, The Structural Engineer No. 7, Vol. 53, July 1975

37. HEIDEBRECHT, A.C., and SWIFT, R.D., Analysis of Asymmetrical Coupled Shear Walls, Journal of the Structural Division, A.S.C.E. ST5, No. 97, May 1971

38.　HEILIG, R., A Contribution to the Theory of Box Girders
　　　　of Arbitrary Cross-Sectional Shape (Translated
　　　　from German by C.V. Amerongen), Cement and Concrete
　　　　Association, Publication No. 61.145, 1971

39.　HENRY, R.L. and ZIA, P.　Prestressed Beams in Torsion,
　　　　Bending and Shear, Journal of the Structural Division,
　　　　Proceedings of the American Society of Civil
　　　　Engineers, ST5, May 1974

40.　IRWIN, A.W. and BOLTON, C.J.,　Torsion of Tall Building
　　　　Cores,　Proceedings of the Institution of Civil
　　　　Engineers, Vol. 63, September 1977

41.　IRWIN, A.W. and YOUNG, R.W.,　Tests on a Reinforced
　　　　Concrete Model Shear Wall Building,　Proceedings of
　　　　the Institution of Civil Engineers, Vol. 61, March 1976

42.　IRWIN, A.W. and ANDREW, N.　Torsional Performance of
　　　　Coupled Channels in Tall Buildings,　Proceedings of
　　　　the Institution of Civil Engineers, Vol. 61,
　　　　December 1976

43.　JACKSON, N. and ESTANERO, R.A.　The Plastic Flow Law for
　　　　Reinforced Concrete Beams under Combined Flexure
　　　　and Torsion, Magazine of Concrete Research, Vol. 23,
　　　　No. 77, December 1971

44.　JOHNSTON, D.W. and ZIA, P., Prestressed Box Beams Under
　　　　Combined Loading, Journal of the Structural Division,
　　　　Proceedings of the American Society of Civil
　　　　Engineers, ST7, July 1975

45.　JORDAAN, I.J., KHALIFA, M.M.A. and McMULLEN, A.E.
　　　　Collapse of Curved Reinforced Concrete Beams,
　　　　Journal of the Structural Division, ST11,
　　　　Proceedings of the American Society of Civil
　　　　Engineers, November 1974

46.　KARLSSON, I. and ELFGREN, L., Torsional Stiffness of
　　　　Reinforced Concrete Members Subjected to Pure Torsion,
　　　　Magazine of Concrete Research, Vol. 24, No. 80,
　　　　London, September 1972

47.　KHAN, M.A.H. and STAFFORD SMITH, B., Restraining Action
　　　　of Bracing in Thin-Walled Open Section Beams,
　　　　Proceedings of the Institution of Civil Engineers,
　　　　Vol. 59, March 1975

48.　KHAN, M.A.H. & TOTTENHAM, H.,　The Method of Bimoment
　　　　Distribution for the Analysis of Continuous Thin-
　　　　Walled Structures Subject to Torsion, Proceedings
　　　　of the Institution of Civil Engineers, Vol. 63,
　　　　December 1977

49. KNITTEL, G., The Analysis of Thin-Walled Box Girders of
       Constant Symmetrical Cross-Section, Cement and
       Concrete Association Library Translation, 1965

50. KOLLBRUNNER, C.F. and BASLER, K., Torsion in Structures -
       An Engineering Approach, Springer-Verlag,
       New York, 1969

51. KOLLBRUNNER, C.F. and HAJDIN, N., Warping Torsion of
       Thin-Walled Beams of Closed Section (in German)
       Mitteilungen der Technischen Kommission, Heft 32,
       1966 (not seen by this author)

52. KONISHI, I. and KOMATSU, S., Three Dimensional Analysis
       of Continuous Thin-Walled Sections, (in Japanese)
       Proceedings of the Japanese Society of Civil
       Engineers, No. 91, March 1963

53. KONISHI, I. and KOMATSU, S., Three Dimensional Analysis
       of Curved Girders with Thin-Walled Cross-Section,
       International Association of Bridge and Structural
       Engineering, Vol. 25, 1965

54. KRAJCINOVIC, D., Matrix Force Analysis of Thin-Walled
       Structures, Journal of the Structural Division,
       ST1, Proceedings of the American Society of Civil
       Engineers, January 1970

55. KUHN, P., Stresses in Aircraft and Shell Structures,
       McGraw Hill, New York 1956

56. KUPFER, H., Box Beam with Elastically Stiffened Cross-
       Section Under Line and Point Loadings, (in German)
       Stahlbetenbau : Berichte aus Forschung und Praxis,
       Berlin 1969 (not seen by this author)

57. KUYT, B., A Theoretical Investigation of Ultimate Torque
       as Calculated by Truss Theory and by the Russian
       Ultimate Equilibrium Method, Magazine of Concrete
       Research, Vol. 23, No. 77, London, December 1971

58. KUYT, B., A Method for Ultimate Strength Design of
       Rectangular Reinforced Concrete Beams in Combined
       Torsion, Bending and Shear, Magazine of Concrete
       Research, Vol. 24, No. 78, London, March 1972

59. LAMPERT, P., Torsion and Bending in Reinforced and
       Prestressed Concrete Members, Proceedings of the
       Institution of Civil Engineers, December 1971

60. LAMPERT, P. and THÜRLIMANN, B., Ultimate Strength and
       Design of Reinforced Concrete Beams in Torsion and
       Bending, International Association of Bridge and
       Structural Engineering, Vol. 31-I, 1971

61. LEONHARDT, F., et al, Torsion and Shear Tests on Prestressed Concrete Box Girders, (Translated from German by C.V. Amerongen), Cement and Concrete Association, London, 1968

62. LESSIG, N.N., Theoretical and Experimental Investigation of Reinforced Concrete Beams subjected to Combined Bending and Torsion, (in Russian) Design and Construction of Reinforced Concrete Structures, Moscow, 1958, (not seen by this author)

63. LIAUW, T.C., Torsion of Multi-Storey Spatial Core Walls, Proceedings of the Institution of Civil Engineers, Vol. 65, September 1978

64. LIVESLEY, R.K., Matrix Methods of Structural Analysis, Pergamon Press, London, 1964

65. LOO, Y.C., and CUSENS, A.R., Developments of the Finite Strip Method in the Analysis of Bridge Decks, Developments in Bridge Design and Construction, Crosby Lockwood & Sons Ltd, 1971

66. LYALIN, I.M., Chapter in Reinforced and Prestressed Concrete in Torsion by H.J. Cowan, Edward Arnold, London, 1965

67. McMANUS, P.S., NASIR, G.A., and CULVER, C.G., Horizontally Curved Girders - State of the Art, Journal of the Structural Division, ST5, Proceedings of the American Society of Civil Engineers, May 1969

68. McMULLEN, A.E. and WARWARUK, M., Concrete Beams in Bending, Torsion and Shear, Journal of the Structural Division, American Society of Civil Engineers, May 1970

69. MAISEL, B.I., Review of Literature Related to the Analysis and Design of Thin-Walled Beams, Cement and Concrete Association, Publication No. TRA440, July 1970

70. MAISEL, B.I. and ROLL, F., Methods of Analysis and Design of Concrete Box Beams With Side Cantilevers, Cement and Concrete Association, Publication No. 42.494, November 1974

71. MAISEL, B.I., ROWE, R.E. and SWANN, R.A., Concrete Box-Girder Bridges, The Structural Engineer, No. 10, Vol. 51, October 1973

72. MALLICK, D.V., and DUNGAR, R., Dynamic Characteristics of Core Wall Structures Subjected to Torsion and Bending, The Structural Engineer, No. 6, Vol. 55, June 1977

73. MANSUR, M.A. and RANGAN, B.V., A Lower Bound Analysis
       for Torsion in Concrete Frames, Magazine of
       Concrete Research, Vol. 29, No. 101, December 1977

74. MEGSON, T.H.G., Aircraft Structures for Engineering
       Students, Edward Arnold, London 1972

75. MICHAEL, D., Torsional Coupling of Core Walls in Tall
       Buildings, The Structural Engineer, Vol. 47,
       February 1969

76. MISIC, J. and WARWARUK, J., Strengths of Prestressed
       Solid and Hollow Beams Subjected Simultaneously
       to Torsion, Shear and Bending, Douglas McHenry
       International Symposium on Concrete and Concrete
       Structures, SP55, American Concrete Institute, 1978

77. MUKHERJEE, P.R. and WARWARUK, J., Torsion, Bending and
       Shear in Prestressed Concrete, Journal of the
       Structural Division, Proceedings of the American
       Society of Civil Engineers, ST4, April 1971

78. MÜLLER, P., Failure Mechanisms for Reinforced Concrete
       Beams in Torsion and Bending, International
       Association of Bridge and Structural Engineering,
       Vol. 36-II, 1976

79. NAKAI, H.and HEINS, C.P., Analysis Criteria for Curved
       Bridges, Journal of the Structural Division,
       ST7, Proceedings of the American Society of
       Civil Engineers, July 1977

80. NEVILLE, A.M., Properties of Concrete, Pitman & Sons Ltd.,
       London, 1968

81. OLLIVER, J.G. and GLENDINNING, J., Principles of
       Surveying, Vol. 1, Plane Surveying, 4th Edition,
       Constable, London, 1978

82. PAULAY, T., An Elasto-Plastic Analysis of Coupled Shear
       Walls, Journal ACI Vol. 67, No. 11, November 1970

83. PAULAY, T., Coupling Beams of Reinforced Concrete
       Shear Walls, Journal of the Structural Division,
       A.S.C.E. Vol. 97, March 1971

84. PEARCE, D.J. and MATTHEWS, D.D., An Appraisal of the
       Design of Shear Walls in Box Frame Structures,
       Directorate of Civil Engineering Development,
       Department of the Environment, HMSO, 1973

85. PINKNEY, M.W., Curved Box Beam Analysis with Reference
       to a 1/12th Scale Prestressed Concrete Bifurcated
       Bridge Model, Ph.D. Thesis (to be submitted)
       Imperial College, London University, 1980

86.   PIPPARD, A.J.S. and BAKER, J.F., Analysis of Engineering
          Structures, Edward Arnold, London 1968

87.   PUCHER, A., Influence Surfaces of Elastic Plates
          (in German) Third Edition, Springer, 1964
          (not seen by this author)

88.   RABBAT, B.G. and COLLINS, M.P., A Variable Angle Space
          Truss Model for Structural Concrete Members
          Subjected to Complex Loading, Douglas McHenry
          International Symposium on Concrete and Concrete
          Structures, American Concrete Institute, SP55, 1978

89.   RAUSCH, E., Berechmung des Eisenbetons gegen
          Verdrehung und Abscheren (Analysis of Torsion and
          Shear in Reinforced Concrete), Dissertation
          submitted to Technical University of Berlin, 1929
          (not seen by this author)

90.   REILLY, R.J., Stiffness Analysis of Grids Including
          Warping, Journal of the Structural Division ST7,
          Proceedings of the American Society of Civil
          Engineers, July 1972

91.   REISSNER, E., Analysis of Shear Lag in Box Beams by the
          Principle of Minimum Potential Energy, Quarterly
          of Applied Mathematics, October 1946, (not seen
          by this author)

92.   RICHMOND, B., Twisting of Thin-Walled Box Girders,
          Proceedings of the Institution of Civil Engineers,
          April 1966

93.   ROSMAN, R., Torsion of Perforated Shafts, Journal of
          the Structural Division, Journal of the American
          Society of Civil Engineers ST5, May 1969

94.   SANDEGREN, D.S. and YU, C.W., An Equilibrium -
          Compatibility Approach to the Determination of
          the Strength of Reinforced Concrete Rectangular
          Beams Under Combined Bending and Torsion,
          Magazine of Concrete Research, Vol. 30, No. 102,
          March 1978

95.   SAWKO, F., Computer Analysis of Grillages Curved in
          Plan, International Association of Bridge and
          Structural Engineers, Vol. 27, 1967

96.   SOMERVILLE, G., Roll, F. and CALDWELL, J.A.D., Tests
          on a 1/12th Scale Model of the Mancunian Way,
          Cement and Concrete Association Technical Report,
          No. 42.394, 1965

97.   SPENCE, R.J.S. and MORLEY, C.T., The Strength of
          Single-Cell Concrete Box Girders of Deformable
          Cross-Section, Proceedings of the Institution
          of Civil Engineers, Vol. 59, December 1975

98.   STAFFORD SMITH, B. and TARANATH, B.S., The Analysis
          of Tall Core-Supported Structures Subject to
          Torsion, Proceedings of the Institution of
          Civil Engineers, Vol. 53, September 1972

99.   STEINLE, A., Torsion and Cross-Sectional Distortion of
          the Single Cell Box Beam, (in German), Beton und
          Stahlbetonbau, September 1970 (not seen by this
          author)

100. SWANN, R.A. and WILLIAMS, A., Combined Loading Tests
          on Model Prestressed Concrete Box Girder Box
          Beams, Reinforced with Steel Mesh, Cement and
          Concrete Association, Publication Nos. 42.485
          and 42.486, London, 1973

101. SWANN, R.A., Construction and Testing of a 1/12th Scale
          Model for the Prestressed Concrete Superstructure
          of Section 5, Western Avenue Extension, Cement
          and Concrete Association Technical Report
          No. 42.441, 1970

102. SWANN, R.A., A Feature Survey of Concrete Box Spine
          Beam Bridges, Cement and Concrete Association
          Publication No. 42.469, June, 1972

103. TAKABA, N. and NARUOKA, M., An Analysis of Grillage
          Girder Bridges with Thin-Walled Cross-Section by
          the Deformation Method, Transactions of the
          Japanese Society of Civil Engineers, Vol. 2,
          Part 1, 1970

104. TAYLOR, H.P.J. and CLEMENTS, S.W., Tests on a 1/9th
          Scale Model of a Transverse Section of the West
          Gate Bridge, Melbourne, Cement and Concrete
          Association Technical Report No. 42.425, 1969

105. TEZCAN, S.S. and OVUNC, B., Analysis of Plane and
          Space Frameworks with Curved Members, International
          Association for Bridge and Structural Engineering,
          Vol. 25, 1965

106. TIMOSHENKO, S. and GOODIER, J.N., Theory of Elasticity,
          McGraw Hill Book Co. Inc, New York, 1951

107. TURKSTRA, C.J. and FAM, A.R.M., Behaviour Study of
          Curved Box Bridges, Journal of the American Society
          of Civil Engineers, ST3, March 1978

108. VICTOR, D.J., LAKSHMANAN, N. and RAJAGOPALAN, N.,
          Ultimate Torque of Reinforced Concrete Beams,
          Journal of the Structural Division, Proceedings
          of the American Society of Civil Engineers, ST7,
          July 1976

109. VLASOV, V.Z., Thin-Walled Elastic Beams, (Translated from the Russian), National Science Foundation, Washington, 1961

110. WALDRON, P. and PERRY, S.H., Small Scale Microconcrete Control Specimens, Proceedings of the Joint Institution of Structural Engineers/Building Research Establishment Reinforced and Prestressed Micro-Concrete Models Seminar, 1978

111. WALDRON, P., PINKNEY, M.W. and PERRY, S.H., The Construction of a 1/12th Scale Concrete Bifurcated Bridge Model, Proceedings of the Joint Institution of Structural Engineers/Building Research Establishment Reinforced and Prestressed Microconcrete Models Seminar, 1978

112. WALDRON, P., PINKNEY, M.W. and PERRY, S.H., A 1/12th Scale Prestressed Concrete Bifurcated Bridge Model - Construction, Imperial College, Department of Concrete Structures and Technology Report, London 1979

113. WEST, R., Recommendations on the Use of Grillage Analysis for Slab and Pseudo-Slab Bridge Decks, Cement and Concrete Association/Construction Industry Research and Information Association, Publication No. 46.017, 1973

114. WEST, R., The Use of a Grillage Analogy for the Analysis of Slab and Pseudo-Slab Bridge Decks, Research Report 21, Cement and Concrete Association, 1973

115. WESTERGAARD, H.M., Computation of Stresses in Bridge Slabs Due to Wheel Loads, Public Roads, Vol. 11, 1930

116. WILLIAM, K.J. and SCORDELIS, A.C., Cellular Structures of Arbitrary Plan Geometry, Journal of the Structural Division, ST7, Journal of the American Society of Civil Engineers, July 1972

117. WINOKUR, A. and GLUCK, J., Ultimate Strength Analysis of Coupled Shear Walls, Journal ACI, Vol. 65, No. 12, December 1968

118. WOODHEAD, H.R. and McMULLEN, A.E., Torsional Strength of Prestressed Concrete Beams, Journal of the Structural Division, Proceedings of the American Society of Civil Engineers, ST5, May 1974

119. YOO, C.H., EVICK, D.R. and HEINS, C.P., Non-Prismatic Curved Girder Analysis, Computers and Structures Journal, London, 1974

120. YOO, C.H. and HEINS, C.P., Plastic Collapse of
     Horizontally Curved Bridge Girders,
     Journal of the Structural Division, ST4,
     Journal of the American Society of Civil
     Engineers, April 1972

121. ZBIROHOWSKI-KOSCIA, K.F., Stress Analysis of Cracked
     Reinforced and Prestressed Concrete Thin-Walled
     Beams and Shells, Magazine of Concrete Research,
     Vol. 20, No. 65, December 1968

122. ZBIROHOWSKI-KOSCIA, K.F., Thin-Walled Beams,
     Crosby Lockwood and Sons Ltd, London, 1967

123. BRITISH STANDARDS INSTITUTION, The Structural Use of
     Concrete, Code of Practice, CP110:Part 1:1972

APPENDIX 1 — DEFINITIONS OF GEOMETRICAL AND SECTORIAL FUNCTIONS FOR THIN-WALLED, MULTI-CELLULAR SECTIONS DISPLAYING CURVATURE

Quantity	Symbol	Straight Members	Curved Members
Section Area	A	$\displaystyle\int_s \delta\,ds$	$\displaystyle\int_s \delta\,ds$
1st. Moment of Area	G_x, etc.	$\displaystyle\int_A y\,dA$	$\displaystyle R\int_A \frac{y}{\rho}\,dA$
2nd. Moment of Area	I_x, etc.	$\displaystyle\int_A y^2\,dA$	$\displaystyle R\int_A \frac{y^2}{\rho}\,dA$
Shear Strain	γ	$\left\{\dfrac{\partial w}{\partial s} + r_s\cdot\phi'\right\}$	$\left\{\dfrac{\partial w}{\partial s}\cdot\dfrac{\rho}{R} + r_s\cdot\dfrac{R}{\rho}\phi'\right\}$
Unit Shear Flow (for $\phi'=1$)	$\overline{F}_{sv}$	T/Ω	$\displaystyle T/R^2\int_s \frac{r_s}{\rho^2}\,ds$
2nd. Moment of Area for Pure Torsion	I_d	$\dfrac{\Omega^2}{\displaystyle\oint\frac{ds}{\delta}} = \overline{F}_{sv}\cdot\dfrac{\Omega}{\delta}$	$\dfrac{\overline{F}_{sv}}{\delta}\cdot R^2\displaystyle\int_s \frac{r_s}{\rho^2}\,ds$
Sectorial Co-ordinate	$\hat{\omega}$	$\displaystyle\int_o^s r_s\,ds - \int_o^s \frac{\overline{F}_{sv}}{G\delta}\,ds$	$\displaystyle R^2\int_o^s \frac{r_s}{\rho^2}\,ds - R^3\int_o^s \frac{\overline{F}_{sv}}{G\delta\rho^3}\,ds$
Warping Moment of Area	$I_{\hat{w}}$	$\displaystyle\int_A \hat{\omega}^2\,dA$	$\dfrac{1}{R}\displaystyle\int_A \rho\hat{\omega}^2\,dA$
Sectorial Shear Function	$S_{\hat{w}}$	$\displaystyle\int_o^A \hat{\omega}\,dA$	$\displaystyle R\int_o^A \frac{\hat{\omega}}{\rho}\,dA$
Reduced Sectorial Shear Function	$\overline{S}_{\hat{w}}$	$\displaystyle S_{\hat{w}} - \frac{1}{\Omega}\int_A S_{\hat{w}} r_s\,dA$	$\displaystyle S_{\hat{w}} - \int_A \frac{S_{\hat{w}} r_s}{\rho^3}\,ds \Big/ \int_A \frac{r_s}{\rho^3}\,ds$
Bimoment	B	$\displaystyle\int_A \sigma\hat{\omega}\,dA$	$\dfrac{1}{R}\displaystyle\int_A \sigma\hat{\omega}\rho\,dA$

APPENDIX 2 - FLEXIBILITY INFLUENCE COEFFICIENTS

A.2.1 - Circular Curved Beam

$$f_{11} = \frac{r}{GI_d}\left\{\frac{\beta}{2}(j^2+1-\mu\eta)+\frac{SC}{2}(j^2-1+\mu\eta(3-2\eta))+\mu\eta(1-\eta)\frac{SH}{krCH}(1-k^2r^2S^2-\frac{2krS}{SH})\right\}$$

$$f_{12} = \pm\frac{r}{GI_d}\left\{\frac{S^2}{2}(j^2-1+\mu\eta(3-2\eta)) + \mu\eta(1-\eta)\left[(krSSH+1)\frac{C}{CH} - 1\right]\right\}$$

$$f_{13} = -\frac{r^2}{GI_d}\left\{\frac{S^2}{2}(1-j^2-\mu\eta) + C - 1 + \frac{\mu\eta}{CH}\cdot(1-C(1-\eta))[SSH.kr - CCH + 1]\right\}$$

$$f_{14} = \pm\frac{1}{GI_d}\left\{\frac{(1-\eta)}{kr.CH}(SH - krS)\right\}$$

$$f_{22} = \frac{r}{GI_d}\left\{\frac{\beta}{2}(j^2+1-\mu\eta) + \frac{SC}{2}(1-j^2+\mu\eta(2\eta-3)) - \mu\eta(1-\eta)\frac{SH}{CH}\cdot krC^2\right\}$$

$$f_{23} = \mp\frac{r^2}{GI_d}\left\{\frac{\beta}{2}(\mu\eta-1-j^2) + \frac{SC}{2}(j^2-1+\mu\eta(3-2\eta)) + S(1-\mu\eta)+\mu\eta krC\frac{SH}{CH}(C-\eta C-1)\right\}$$

$$f_{24} = \frac{1}{GI_d}\left\{\frac{(1-\eta)}{CH}(C-CH)\right\}$$

$$f_{33} = \frac{r^3}{GI_d}\left\{\frac{\beta}{2}(j^2+3) + \frac{SC}{2}(1-j^2) - 2S\right\}$$

$$f_{34} = \mp\frac{r}{GI_d}\left\{\frac{\eta(C-CH) + 1 - C}{CH}\right\}$$

$$f_{44} = \frac{1}{GI_d}\cdot\frac{k}{\mu}\cdot\frac{SH}{CH}$$

A.2.2 - Circular Curved Beam (neglecting warping)

$$f_{11}' = \frac{r}{GI_d}\left\{\frac{\beta}{2}(j^2+1) + \frac{SC}{2}(j^2-1)\right\}$$

$$f_{12}' = \pm\frac{r}{GI_d}\left\{\frac{S^2}{2}(j^2-1)\right\}$$

$$f_{13}' = -\frac{r^2}{GI_d}\left\{\frac{S^2}{2}(1-j^2) + C - 1\right\}$$

$$f_{22}' = \frac{r}{GI_d}\left\{\frac{\beta}{2}(j^2+1) + \frac{SC}{2}(1-j^2)\right\}$$

$$f_{23}' = \mp\frac{r^2}{GI_d}\left\{\frac{SC}{2}(1-j^2) - \frac{\beta}{2}(j^2+1)\right\}$$

$$f_{33}' = \frac{r^3}{GI_d}\left\{\frac{\beta}{2}(j^2+3) + \frac{SC}{2}(1-j^2) - 2S\right\}$$

A.2.3 - Straight Beam

$$g_{11} = \frac{\ell}{\Psi EI_x}$$

$$g_{12} = 0$$

$$g_{13} = \frac{\ell^2}{2\Psi EI_x}$$

$$g_{14} = 0$$

$$g_{22} = \frac{\ell}{GI_d} \cdot \left(1 - \frac{\mu}{k\ell} \cdot \tanh k\ell\right)$$

$$g_{23} = 0$$

$$g_{24} = \frac{1}{GI_d} \cdot \left(\frac{1 - \cosh k\ell}{\cosh k\ell}\right)$$

$$g_{33} = \frac{\ell^3}{3\Psi EI_x}$$

$$g_{34} = 0$$

$$g_{44} = \frac{\tanh k\ell}{k \cdot EI_{\hat{w}}}$$

A.2.4. - Straight Beam (neglecting warping)

$$g'_{11} = \frac{\ell}{\Psi EI_x}$$

$$g'_{12} = 0$$

$$g'_{13} = \frac{\ell^2}{2\Psi EI_x}$$

$$g'_{22} = \frac{\ell}{GI_d}$$

$$g'_{23} = 0$$

$$g'_{33} = \frac{\ell^3}{3\Psi EI_x}$$

A.2.5 - Transformed Straight Beam

$$h_{11} = \frac{r}{GI_d}\left\{2j^2\sin\frac{\beta}{2}\cdot\cos^2\frac{\beta}{2} + 2\sin^3\frac{\beta}{2} - \frac{\mu}{kr}\cdot\frac{SH}{CH}\cdot\sin^2\frac{\beta}{2}\right\}$$

$$h_{12} = \pm\frac{rS}{GI_d}\left\{\sin\frac{\beta}{2}(j^2-1) + \frac{\mu}{2kr}\cdot\frac{SH}{CH}\right\}$$

$$h_{13} = +\frac{r^2}{GI_d}\cdot S\cdot j^2\sin\frac{\beta}{2}$$

$$h_{14} = \mp\frac{1}{GI_d}\cdot\frac{(1-CH)}{CH}\cdot\sin\frac{\beta}{2}$$

$$h_{22} = \frac{r}{GI_d}\left\{2j^2\sin^3\frac{\beta}{2} + 2\sin\frac{\beta}{2}\cdot\cos^2\frac{\beta}{2} - \frac{\mu}{kr}\cdot\frac{SH}{CH}\cdot\cos^2\frac{\beta}{2}\right\}$$

$$h_{23} = \pm\frac{r^2}{GI_d}\cdot 2j^2\sin^3\frac{\beta}{2}$$

$$h_{24} = \frac{1}{GI_d}\cdot\frac{(1-CH)}{CH}\cdot\cos\frac{\beta}{2}$$

$$h_{33} = \frac{r^3}{GI_d}\cdot\frac{8}{3}\sin^3\frac{\beta}{2}$$

$$h_{34} = 0$$

$$h_{44} = \frac{1}{GI_d}\cdot\frac{k}{\mu}\cdot\frac{SH}{CH}$$

A.2.6 - Transformed Straight Beam (neglecting warping)

$$h'_{11} = \frac{r}{GI_d}\left\{2\sin\frac{\beta}{2}\left[j^2\cos^2\frac{\beta}{2} + \sin^2\frac{\beta}{2}\right]\right\}$$

$$h'_{12} = \pm\frac{r}{GI_d}\cdot 2(j^2-1)\cdot\sin^2\frac{\beta}{2}\cdot\cos\frac{\beta}{2}$$

$$h'_{13} = \frac{r}{GI_d}\cdot 2j^2\sin^2\frac{\beta}{2}\cdot\cos\frac{\beta}{2}$$

$$h'_{22} = \frac{r}{GI_d}\left\{2\sin\frac{\beta}{2}\left[j^2\sin^2\frac{\beta}{2} + \cos^2\frac{\beta}{2}\right]\right\}$$

$$h'_{23} = \pm\frac{r^2}{GId}\cdot 2j^2\sin^3\frac{\beta}{2}$$

$$h'_{33} = \frac{r^3}{GI_d}\cdot\frac{8}{3}\cdot\sin^3\frac{\beta}{2}$$

APPENDIX 3 - STIFFNESS MATRICES FOR STRAIGHT MEMBERS

A.3.1 Torsion/Bimoment Matrix in terms of f,f'

$$
\begin{bmatrix} T_1 \\ \dfrac{B_1}{\mu} \\ T_2 \\ \dfrac{B_2}{\mu} \end{bmatrix}
= K_1
\begin{bmatrix}
kSH & & & symmetrical \\
(1-CH) & \frac{1}{k}(k\ell CH-SH) & & \\
-kSH & -(1-CH) & kSH & \\
(1-CH) & \frac{1}{k}(SH-k\ell) & -(1-CH) & \frac{1}{k}(k\ell CH-SH)
\end{bmatrix}
\begin{bmatrix} f_1 \\ f'_1 \\ f_2 \\ f'_2 \end{bmatrix}
$$

$$\text{where } K_1 = \frac{GI_d}{2(1-CH)+k\ell SH}$$

A.3.2 Torsion/Bimoment Matrix in terms of ϕ, f'

$$
\begin{bmatrix} T_1 \\ B_1 \\ T_2 \\ B_2 \end{bmatrix}
= K_2
\begin{bmatrix}
kSH & & & symmetrical \\
\mu(1-CH) & \frac{\mu}{k}(k\ell CH- SH) & & \\
-kSH & -\mu(1-CH) & kSH & \\
\mu(1-CH) & \frac{\mu}{k}(\mu SH-k\ell) & -\mu(1-CH) & \frac{\mu}{k}(k\ell CH-\mu SH)
\end{bmatrix}
\begin{bmatrix} \phi_1 \\ f'_1 \\ \phi_2 \\ f'_2 \end{bmatrix}
$$

$$\text{where } K_2 = \frac{GI_d}{2\mu(1-CH)+k\ell SH}$$

A.3.3 Bending/Shear Matrix for Open and Closed Sections

$$
\begin{bmatrix} M_1 \\ V_1 \\ M_2 \\ V_2 \end{bmatrix}
= K_3
\begin{bmatrix}
4\ell^2 & & & symmetrical \\
6\ell & 12 & & \\
2\ell^2 & 6\ell & 4\ell^2 & \\
-6\ell & -12 & -6\ell & 12
\end{bmatrix}
\begin{bmatrix} v'_1 \\ v_1 \\ v'_2 \\ v_2 \end{bmatrix}
$$

$$\text{where } K = \Psi EI_x/\ell^3$$

APPENDIX 4   -   INTEGRAL SOLUTIONS OF VARIOUS CIRCULAR AND HYPERBOLIC FUNCTIONS

$$F(\beta) \quad = \quad \int_0^\beta f(\alpha).d\alpha$$

$f(\alpha)$	$F(\beta)$
$\sin \alpha$	$1 - C$
$\cos \alpha$	S
$\sin^2\alpha$	$\beta/2 - SC/2$
$\cos^2\alpha$	$\beta/2 + SC/2$
$\sin \alpha.\cos \alpha$	$S^2/2$
$\sinh kr\alpha$	$(CH - 1)/kr$
$\cosh kr\alpha$	SH/kr
$\sinh^2 kr\alpha$	$SH.CH/2kr - \beta/2$
$\cosh^2 kr\alpha$	$SH.CH/2kr + \beta/2$
$\sinh kr\alpha.\cosh kr\alpha$	$SH^2/2kr$
$\sinh^2 kr\alpha + \cosh^2 kr\alpha$	$SH.CH/kr$
$\alpha.\sin \alpha$	$S - \beta C$
$\alpha.\cos \alpha$	$\beta S + C - 1$
$\alpha.\sinh kr\alpha$	$\beta.CH/kr - SH/k^2r^2$
$\alpha.\cosh kr\alpha$	$\beta.SH/kr - (CH-1)/k^2r^2$
$\sin \alpha.\sinh kr\alpha$	$\eta(kr.S.CH - C.SH)$
$\sin \alpha.\cosh kr\alpha$	$\eta(kr.S.SH - C.CH + 1)$
$\cos \alpha.\sinh kr\alpha$	$\eta(kr.C.CH + S.SH - kr)$
$\cos \alpha.\cosh kr\alpha$	$\eta(kr.C.SH + S.CH)$

where S = $\sin \beta$

         C = $\cos \beta$

         SH = $\sinh kr\beta$

         CH = $\cosh kr\beta$